UNIVERSITY OF SEVILLE

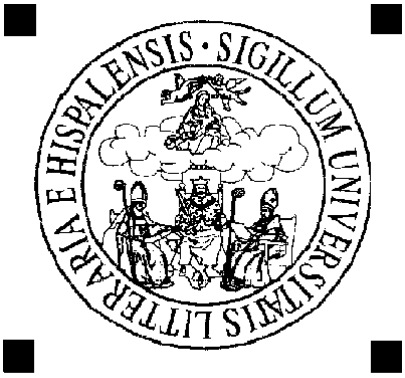

DEPARTMENT OF BUILDING STRUCTURES AND GROUND ENGINEERING

CONSOLIDATION OF SOFT SOILS IN THE PRESENCE OF BAND-SHAPED DRAINS

ELISA MARIA DE JESUS DA SILVA

JUNE 2013

UNIVERSITY OF SEVILLE

DEPARTMENT OF BUILDING STRUCTURES AND GROUND ENGINEERING

CONSOLIDATION OF SOFT SOILS IN THE PRESENCE OF BAND-SHAPED DRAINS

Thesis submitted by

Elisa Maria de Jesus da Silva

to accede to the degree of

Doctor by the University of Seville

(Doctora por la Universidad de Sevilla)

Under the supervision and guidance of:

Director:
José Luis de Justo Alpañés
(Doctor Ingeniero de Caminos, Canales y Puertos, Professor Emeritus by the University of Seville)

Co-director:
Percy Durand Neyra
(Doctor Ingeniero de Caminos, Canales y Puertos, Professor at University of Seville)

Seville, June 2013

"THERE IS ONLY ONE THING ABOUT WHICH I AM CERTAIN, AND THIS IS THAT THERE IS VERY LITTLE ABOUT WHICH ONE CAN BE CERTAIN."

WILLIAM SOMERSET MAUGHAM (1874-1965)

To

This thesis is dedicated to my mother and to my late father, as a token of my appreciation for their valuable lessons and the spirit of determination that they instilled in me. They helped me in the pursuit of my dreams and in achieving my goals. I also would like to share some special words that my father once wrote to me, which touched me, and that I keep always in my mind.

"Dreaming is good
Dreams should lead our lives
Unfortunately, life is not only made of dreams…
Nevertheless, you are always in mine!"

(Augusto José Ascensão da Silva, 27-Maio-1999)

ACKNOWLEDGMENTS

I would like to express my sincere gratitude and appreciation to Professor José Luís de Justo Alpañés from the University of Seville, Spain, for his valuable guidance, inspiration and continuous support throughout the researching of this work and for providing the data of the case study analysed in this thesis. Valuable suggestions and advice were also given by Professor Percy Durand Neyra from the University of Seville and by Professor Mário Jesus from the University of Algarve, Portugal. Their contributions were crucial to the development, organization and drafting of this document and I would like to thank them both.

I must address a special word of thanks to my former Professor, Pedro Guedes de Melo, from "*Instituto Superior Técnico*" of the Technical University of Lisbon, Portugal, for so skilfully transmitting his knowledge of soil mechanics and kindling my fascination for the field of geotechnics.

I am grateful to the University of Algarve for providing the financial support to acquire the PLAXIS software, which was vital for the development of this thesis, and to the PLAXIS Support Team, from Delft University, Netherlands, for their assistance with the numerical analysis.

Special thanks go to the "*Confederación Hidrográfica del Guadalquivir*" for allowing the publication of the monitoring results for Dikes 1 and 3 of the *Lebrija* Pond.

To the enterprise "*INPOLUKIS, Traduções*" a word of appreciation for the effort of translation and revising this thesis from Portuguese to English, in particular to Marta Aragão and Sónia Costa;

These acknowledgements would not be complete without a word of appreciation to my colleague David Pereira for his helpful advice on the graphics and for his friendship over these last years, as well as to Ângela Vairinhos for being always available in the difficult moments.

To my friends and colleagues Carolina Sousa, Paula Ribeiro and Sara Madeira, a special word of thanks for their friendship, encouragement and moral support.

Finally, with heartfelt love and an enormous debt of gratitude, I wish to thank my beloved mother, daughter Mariana and husband Fernando for their affection, support and encouragement throughout the time I devoted to this special and personal project.

ABSTRACT

This thesis focuses on the study of the consolidation of soft soil with vertical band-shaped drains, comparing real data collected in a case study (Dikes No.1 and No.3 of the Lebrija Pond) with those obtained via numerical simulation. The comparison between these results leads to the perception and understanding of the phenomena associated to these types of work and soils, also providing the possibility of intervention in equivalent scenarios.

In view of the high compressibility of the soil foundation of these dikes, they were treated with prefabricated vertical band-shaped drains and monitored since construction, allowing the gathering of relevant data. Later, the monitoring results were confronted with numerical simulations. Finite element software, which is recognized internationally among the geotechnical engineers, is used to this end. This programme offers several soil material models. In the case study, three models were applied to define the behaviour of the soft soil foundation, namely the Mohr-Coulomb, Soft Soil and Soft Soil Creep models. Special attention was paid to the last model, since it allows considering the viscosity (creep) of soft soil. A sensitivity analysis of the secondary compressibility index was also performed.

The analysis of the consolidation phenomenon, in the areas where the vertical band-shaped drains are used, is a problem of axisymmetric nature (tridimensional-3D), nevertheless it is performed in the plane strain state (two dimensional-2D). Therefore, the spatial pattern adopted in the design had to be converted into several parallel drainage screens. An equivalent degree of consolidation in both systems must be ensured. New horizontal permeability coefficients for this zone are estimated, according to several hypotheses for the diameter and reduction of the permeability in the disturbed zone around the drains (smear effect).

The flow was also incorporated in these analyses, with the purpose of introducing more realism to the numerical simulations, and with this option a better approximation between the numerical results and the monitoring data was achieved. However, a better agreement is only obtained when the numerical analyses include, in addition to the flow, the correct magnitude of the smear effect, the viscosity creep (creep) in the behaviour of the soft soil and appropriate secondary compressibility indexes.

Therefore, the confrontation of the monitoring data associated to a real case work, with numerical results allowed for the validation and gauging of methods, models and geotechnical parameters for the soft soil when prefabricated vertical band-shaped drains were used.

KEY-WORDS: Soft Soil, Soil Improvement, Vertical Band-shaped Drains, Consolidation Analysis, Material Models, Creep Behaviour, Smear Effect, *Lebrija* Pond, PLAXIS software.

RESUMEN

Esta tesis se centra en el estudio de la consolidación de suelos blandos tratados con drenes verticales prefabricados de banda, comparando datos reales recogidos en un caso de obra (Diques Nº1 y Nº3 del Embalse de *Lebrija*), con los obtenidos por simulación numérica. La comparación entre estos resultados conduce a la percepción y comprensión de los fenómenos asociados a este tipo de obras, proporcionando de igual modo la posibilidad de intervención en escenarios equivalentes.

Frente a la elevada compresibilidad de los suelos de fundación de estos diques, los mismos fueron tratados con drenes verticales prefabricados de banda y monitorizados desde su construcción, conduciendo a la obtención de datos relevantes sobre de su comportamiento. Posteriormente se validaron los resultados de la monitorización recurriendo a la simulación numérica.

En las simulaciones numéricas se utilizó un programa de elementos finitos reconocido internacionalmente en el seno de la geotecnia, el cual facilita varios modelos de comportamiento para suelos. En el caso de estudio, se aplicaron tres modelos para definir el comportamiento de los suelos blandos de la fundación, concretamente el modelo *Mohr-Coulomb*, *Soft Soil* y *Soft Soil Creep*. Especial atención recibe el modelo *Soft Soil Creep*, dado que el mismo permite traducir la fluencia viscosa (*creep*) de los suelos blandos a muy blandos, habiéndose realizado también un análisis paramétrico del índice de compresibilidad secundario.

El análisis del fenómeno de la consolidación en las zonas tratadas con drenes verticales prefabricados de banda se realiza en el estado plano de deformación (bidimensional -2D), a pesar de que se trata de un problema de naturaleza axisimétrica (tridimensional-3D). Como tal, el sistema espacial de la malla triangular se ha convertido en una pared de drenes verticales paralelos entre sí, siempre garantizando la igualdad del grado de consolidación en ambos sistemas. Se han calculado nuevos coeficientes de permeabilidad horizontal para esta zona, analizándose diversas hipótesis para el diámetro y reducción de la permeabilidad en la zona perturbada alrededor de los drenes (efecto *smear*).

Con el objetivo de dotar de mayor realismo a las simulaciones numéricas, se incorporó el flujo en estos análisis, consiguiéndose una mejor aproximación entre los resultados numéricos y los datos de la monitorización. Asimismo, tales resultados sólo se alcanzan cuando en los análisis numéricos se integran, además del flujo, la magnitud de la perturbación asociada a la ejecución de los drenes en la zona tratada (efecto *smear*), la fluencia viscosa (*creep*) en el comportamiento de los suelos blandos de fundación e índices de compresibilidad secundaria adecuados a los mismos.

De este modo, la confrontación de los datos asociados a un caso real con los resultados numéricos permitió la validación y contraste de los métodos, modelos y parámetros geotécnicos de los suelos blandos de la fundación cuando se tratan con drenes verticales de banda.

PALABRAS-LLAVE: Suelos Blandos, Mejora del Terreno, Drenes de Banda, Análisis de Consolidación, Modelos de Comportamiento, Fluencia Viscosa, *Smear*, Balsa de Lebrija, PLAXIS.

NOTATION AND ACRONYMS

The symbols and parameters referred here, are explain throughout the text, however it is convenient to present a list of the most important. Some of the following symbols have more than one meaning, so one should see the context in which they are used. Nevertheless, the author tried to keep the notation and terminology used in the bibliography of the specialties covered.

The symbols are organized by alphabetic order, beginning with Latin capital and then lowercase letters, followed by Greek capital and lowercase letters. Finally the meanings of some mathematical symbols and abbreviations are presented.

Latin Symbols	Nomenclature
A	Parameter representing the recompressibility on logarithmic strain formulation of secondary consolidation;
	Parameter used on the parabolic model for the permeability on smear zone, by Walker & Indraratna (2006)
A'	Parameter used on the linear model for the permeability on smear zone, by Walker & Indraratna (2007)
$\mathbf{A_w}$	Cross section of the drain
B	Equivalent half with consecutive parallel drains in plane strain;
	Parameter representing the part correspondent to the subtraction between compressibility and recompressibility on logarithmic strain formulation of secondary consolidation;
	Parameter used on the parabolic model for the permeability on smear zone, by Walker & Indraratna (2006)
B'	Parameter used on the linear model for the permeability on smear zone, by Walker & Indraratna (2007)
C	Parameter representing the creep, on logarithmic strain formulation, of secondary consolidation,
C	Slope representing the linear variation of smear permeability on Chai *et al.* (1997) model;
	Parameter used on the parabolic mode, for the permeability on smear zone, by Walker & Indraratna (2006)
$\mathbf{C_1}$; $\mathbf{C_2}$	Slopes representing the bi-linear variation of smear permeability on Chai *et al.* (1997) model
$\mathbf{C_B}$	Secondary consolidation coefficient
$\mathbf{C_c}$	Compression index
$\mathbf{C_d}$	Deviatoric compression coefficient in (e; $log(1+(\eta^2+M^2))$) plane
$\mathbf{C_f}$	Ratio of field and laboratory coefficient of permeability
$\mathbf{C_h}$	Coefficient of horizontal consolidation

$C_{hAx;hPD}$	Axisymmetric and plane strain equivalent horizontal coefficient of consolidation
C_{ijkl}	Elasticity Tensor
C_r	Recompression index
C_s	Swelling index
Cu	Uniformity coefficient
C_v	Coefficient of vertical consolidation
C_α	Secondary compression index
$D_{85;60;50;15;10}$	Diameter of soil particles corresponding to 85%, 60%, 50%, 15% and 10% passing
E	Young's modulus
E_{DMT}	Marchetti dilatometer modulus
E_{ref}	Young's reference modulus on PLAXIS for Mohr-Coulomb model
E_{oed}	Oedometer modulus
E_s	Soil stiffness modulus
E_u	Undrained strain modulus
E_{ur}	Unload-reload strain modulus
F_c	Influence factor on discharge capacity of prefabricated vertical drain due to drain deformation
F_{fc}	Influence factor on discharge capacity of prefabricated vertical drain due to clogging
F_t	Influence factor on discharge capacity of prefabricated vertical drain due to time
$F_{(n)}$	Drain spacing factor on consolidation analysis
$F_{(r)}$	Drain discharge capacity factor or drain hydraulic resistance factor on consolidation analysis
$F_{(s)}$	Drain smear factor on consolidation analysis
$F(\sigma)$	Yield surface function
$F(\sigma,\chi)$	Hardening or softening law
G	Shear modulus
G_s	Specific gravity of soil solid
H	Soil thickness
IP	Plasticity index
K_0	Coefficient of lateral earth pressure at rest
K_0^{NC}	Coefficient of lateral earth pressure at rest for normally consolidated soils
K_0^{OC}	Coefficient of lateral earth pressure at rest for overconsolidated soils
L_d	Drain length

M	Slope of critical state line in (p'; q) plane
N_{DP}	Dynamic Probe penetration number
N_k	Factor used for the determination of undrained cohesion obtained by Cone Penetration Test
N_{SPT}	Standard Penetration Test number
$O_{95;90;50;15}$	Size of particle which is larger than 95%, 90%, 50% and 15% of the fabric geotextil pores
OCR	Overconsolidation ratio
$P_{drain,\ eq}$	Equivalent perimeter of a prefabricated band-shaped drain
P_m	Perimeter of a mandrel
Q (σ,ζ)	Plastic potential function
S	Field spacing of drains
S*	Consecutive parallel spacing of drains in plane strain
Sr	Saturation degree
S_e	Effective saturation degree in partly saturated soils
St	Sensitivity ratio
T_h	Time factor for horizontal flow
$T_{hAx;\ hPD}$	Axisymmetric and plane strain time factor for horizontal flow
T_r	Time factor for radial flow
Tv	Time factor for vertical flow
U	Degree of consolidation
U_r	Degree of consolidation for radial flow
U_v	Degree of consolidation for vertical flow
U_z	Degree of consolidation at z depth
$U_{(z,t)}$	Degree of consolidation at z depth and t time
$\bar{U}$	Average degree of consolidation
$\bar{U}_h$	Average degree of consolidation for horizontal flow
$\bar{U}_{hAx}$	Axisymmetric average time factor for horizontal flow
$\bar{U}_{hPD}$	Plane strain average time factor for horizontal flow
$\bar{U}_r$	Average degree of consolidation for radial flow
$\bar{U}_s$	Average degree of consolidation based on settlements
$\bar{U}_v$	Average degree of consolidation for vertical flow
V	Volume
X_i	External force applied to the soil
a_v	Coefficient of compressibility

a'_v	Compressibility index
b_s	Equivalent half width of smear zone in plane strain
b_w	Equivalent half width of drain in plane strain
c	Cohesion
c'	Effective cohesion or effective shear strength
c_u	Undrained cohesion or undrained shear strength
d	Discharge length;
	Displacement
d^e	Elastic displacement
d^p	Plastic displacement
d_e	Diameter of effective influence zone of the drain
$d_{m,eq}$	/Equivalent diameter of mandrel
d_s	Diameter of smear zone
$d_{s,eq}$	Equivalent diameter of smear zone
$d_{sx;sy}$	Dimensions of smear zone
$d_{t,eq}$	Equivalent diameter of transition zone
$d_{tx;ty}$	Dimensions of transition zone
d_w	Drain diameter
d_x, d_y, d_z	Dimensions on x, y, z direction
e	Void ratio
e_0	Initial void ratio
e_c	Void ratio at the end of primary consolidation
e_{pp}	Void ratio on perfect plasticity or critical state
h	Height;
	Hydraulic head
h_w	Water height
i	Hydraulic gradient
k	Permeability coefficient;
	Adimensional parameter used on the parabolic model for the permeability on smear zone, by Walker & Indraratna (2006)
k_A	Permeability on the vicinity of the drain, for the non linear model of permeability on smear zone, by Onoue *et al.* (1991)
k_B	Permeability correspondent to the passage from smear to transition zone, for the non linear model of permeability on smear zone, by Onoue *et al.* (1991)
$k_{geotextil}$	Permeability of geotextil filter

k_h	Horizontal coefficient of permeability
k_{h0}	Initial horizontal coefficient of permeability on undisturbed zone
k_{hAx}	Axisymmetric equivalent horizontal coefficient of permeability
k_{hPD}	Plane strain equivalent horizontal coefficient of permeability
k_{hL}	Horizontal coefficient of permeability obtain in laboratory
k_{hs}	Smear zone horizontal coefficient of permeability
k_{hsAx}	Axisymmetric horizontal coefficient of permeability in smear zone
k_{hsPD}	Plane strain horizontal coefficient of permeability in smear zone
k_{ht}	Transition zone horizontal coefficient of permeability
k_s	Permeability coefficient of the soil in saturated conditions
$k_w(\psi)$	Permeability coefficient of partly saturated soils
$k_r(\psi)$	Soil permeability reduction factor with suction
k_{sL}	Smear zone horizontal coefficient of permeability obtain in laboratory
k_v	Vertical coefficient of permeability
k_{v0}	Initial vertical coefficient of permeability
k_{vL}	Vertical coefficient of permeability obtain in laboratory
k_x, k_y, k_z	Permeability in x, y, z directions
k_w	Coefficient of permeability of a prefabricated band-shaped drain
k_{wAx}	Axisymmetric coefficient of permeability of a prefabricated band-shaped drain
k_{wPD}	Plane strain coefficient of permeability of a prefabricated band-shaped drain
m	Parameter used by Chai *et al.* (1997) for the linear model of permeability on smear zone; van Guenuchten adjustment parameter for the Soil-Water Characteristic Curve
m_1; m_2	Parameters used by Chai *et al.* (1997) for the bi-linear model of permeability on smear zones
m_v	Volume coefficient of compressibility
n	Spacing ratio; Parameter used by Chai *et al.* (1997) for the linear model of permeability on smear zone van Guenuchten adjustment parameter for the Soil-Water Characteristic Curve
p	Pressure
p^{ref}	Mean effective stress of reference on PLAXIS
p'	Mean effective stress or isotropic stress
p'_c	Maximum initial preconsolidation mean effective stress

p'_f	Final mean effective stress
$p'_i = p'_0$	Initial or *in-situ* mean effective stress
p'_p	Preconsolidation mean effective stress
p'_{p0}	Initial preconsolidation mean effective stress
p'_{pc}	Preconsolidation mean effective stress at the end of primary consolidation
p'_{pp}	Mean effective stress on perfect plasticity or critical state
q	Deviator stress
q_c	Cone point resistence
q_{pp}	Deviatoric stress on perfect plasticity or critical state
q_{req}	Theoretical required discharge capacity for a prefabricated vertical band-shaped drain
q_u	Unconfined compression strength
q_w	Discharge capacity of a drain for unitary hydraulic gradient
q_{wAx}	Axisymmetric discharge capacity for a prefabricated vertical band-shaped drain for unitary hydraulic gradient
q_{wPD}	Plane strain discharge capacity for a prefabricated vertical band-shaped drain for unitary hydraulic gradient
$q_{w,min}$	Minimum discharge capacity of a drain
r	Radius
r_e	Radius of effective influence zone of the drain
r_s	Radius of smear zone
r_t	Radius of transition zone
r_w	Radius of prefabricated band-shaped drain
s	Settlement or vertical displacement;
	Smear ratio
s_{cs}	Secondary consolidation settlement
s_f	Final settlement corresponding a 25% of soil thickness
s_i	Immediate settlement
s_{pc}	Primary consolidation settlement
s_t	Settlement after a time t
s_{tot}	Total settlement
s_u	Undrained shear strength from Vane-test
$s_{u(max)}$	Maximum or peak undrained shear strength from Vane-test
$s_{u(max)}^*$	Reduced maximum undrained shear strength from Vane-test
$s_{u(residual)}$	Residual undrained shear strength from Vane-test
t	Time

t'	Time in which occurs secondary consolidation
t_c	Time at the end of primary consolidation
u	Pore pressure
u_i	Initial pore pressure
u_f	Final pore pressure
u_w	Water pressure in partly saturated soils
u_a	Air pressure in partly saturated soils
v	Specific volume
w	Width of prefabricated band-shaped drain
y	Thickness of prefabricated band-shaped drain
z	Depth

Greek Symbols	**Nomenclature**
Γ	Specific volume of critical state line when p'=1 kPa, in (*lnp'; v*) plane
Λ	Reduction factor to be applied on the Vane-Test results
N	Specific volume of isotropic normally consolidated soil when p'=1 kPa, in (*lnp'; v*) plane
K	Bulk modulus
K_{ur}	Unload-reload bulk modulus
χ	Hardening or softening parameter
χ_f	Saturated degree function for partly saturated soils
ζ	State parameter in plastic potential
Θ	Conversion coefficient between the axisymmetric and plane strain systems
α	Coefficient of secondary consolidation; Parameter used by Onoue *et al.* (1991) for the non linear model of permeability on smear zone van Guenuchten adjustment parameter for the Soil-Water Characteristic Curve
α^*	Parameter representing smear in plane strain by Indraratna & Redana (1997)
β	Parameter used by Onoue *et al.* (1991) for the non linear model of permeability on smear zone
β^*	PParameter representing smear and hydraulic resistance of the drain in plane strain by Indraratna & Redana (1997)
ε	Strain
$\varepsilon_1, \varepsilon_2, \varepsilon_3$	Axial, intermediate and minor principle strains
ε^e	Elastic strain

ε^p	Plastic strain
ε_v	Volumetric strain
ε_{v0}	Initial volumetric strain
ε_q	Deviatoric strain
ε_v^e	Elastic volumetric strain
ε_p^e	Elastic volumetric strain for mean effective stress
ε_q^e	Elastic deviatoric strain or elastic strain for deviatoric stress
ε_v^p	Plastic volumetric strain
ε_p^p	Plastic volumetric strain for mean effective stress
ε_q^p	Plastic deviatoric strain or plastic strain for deviatoric stress
ε_{kl}	Strain tensor
ε_{pc}	Strain at the end of primary consolidation
ε_v^{pcr}	Creep volumetric strain due to at the end of primary consolidation
ε_v^{scr}	Creep volumetric strain due to at the end of secondary consolidation
ε_v^{cr}	Total creep volumetric strain
ε^H	Logarithmic strain
ε_{pc}^H	Total logarithmic strain at the end of final primary consolidation
ε_{pc}^{He}	Elastic logarithmic strain at the end of final primary consolidation
ε_{pc}^{Hcr}	Creep logarithmic strain at the end of final primary consolidation
$\varepsilon_{xx;\ yy;\ zz}$	Strain on x, y, z directions
γ	Unit weight
γ_d	Dry unit weight of soil
γ_h	Moist unit weight of soil
γ_s	Unit weight of soil solids
γ_t	Moist unit weight of soil
γ_{sat}	Saturated unit weight of soil
$\gamma_{sub} = \gamma'$	Submerged unit weight of soil
γ_w	Unit weight of water
η	Stress ratio or ratio between mean effective and deviatoric stress;
η_{MAX}	Parameter used by Onoue *et al.* (1991) for the non linear model of permeability on smear zone
φ	Friction angle

φ'	Effective friction angle
φ'_{cri}	Effective friction angle on critical state
φ'_{peak}	Maximum effective friction angle
φ'_{pp}	Effective friction angle on perfect plasticity
φ_u	Undrained friction angle
κ	Slope of unloading-reloading line or recompressibility index in (*e; lnp'*) plane
κ^*	Slope of unloading-reloading line or modified recompressibility index in (ε_v; *lnp'*) plane
λ	Slope of normal compression line or compressibility index in (*e; lnp'*) plane
λ^*	Slope of normal compression line or modified compressibility index in (ε_v; *lnp'*) plane
λ_d	Deviatoric compressibility index in (e; $log(1+(\eta^2+M^2))$) plane
μ	Factor incorporating spacing, smear and drain hydraulic resistance for radial flow
μ_{Ax}	Axisymmetric factor incorporating spacing, smear and drain hydraulic resistance
μ_{PD}	Plane strain factor incorporating spacing, smear and drain hydraulic resistance
μ^*	Creep modified compression index in (ε_v; *lnp'*) plane
θ^*	Parameter representing hydraulic resistance of the drain in plane strain by Indraratna & Redana (1997)
θ_r	Residual water content
θ_s	Saturated water content
ν	Poisson's ratio
ν_{ur}	Unload-reload Poisson's ratio
σ	Stress
$\sigma_1, \sigma_2, \sigma_3$	Axial, intermediate and minor principle stresses
σ'_f	Effective final vertical stress
σ_{ij}	Stress Tensor
σ^0_{ij}	Initial stress Tensor
σ'_i ou σ'_0	*In situ* effective vertical stress or initial effective vertical stress
σ_h	Total horizontal stress
σ'_h	Effective horizontal stress
σ_v	Total vertical stress
σ'_v	Effective vertical stress

σ'_p	Effective preconsolidation vertical stress
σ'_{p0}	Initial effective preconsolidation vertical stress
σ'_{pc}	Effective preconsolidation vertical stress at the end of primary consolidation
σ_s	Principal stress in plane strain
σ_t	Maximum shear stress in plane strain
σ_y	Yielding stress
$\sigma_{xx;\ yy;\ zz}$	Stress on x, y, z directions
$\tau=\tau_{xy}$	Shear strength
τ_c	Time giving to the instant line on Bjerrum graphical representation of oedometer test
τ_f	Shear strength on partly saturated soils
ψ	Dilatancy angle; Soil suction
ω	Water content
ω_L	Liquid limit
ω_{nat}	Natural moisture content
ω_P	Plastic limit
ϑ	Ratio between secondary compressibility index and compressibility index or recompressibility index

Mathematical Symbols	**Nomenclature**
ln (...)	Natural logarithm
log (...)	Decimal logarithm
Δ	Variation or change of...
Σ	Some of...
δ	Increment of....
π	PI number
∂	Partial derivative or derivative in order to...
[...]	Matrix

Units	**Nomenclature**
m	Meter
km	Kilometer
cm	Centimeter
mm	Millimeter

m^2	Square meter
m^3	Cubic meter
Hm^3	Cubic hectometer
N	Newton
kN	Kilo Newton
MN	Mega Newton
kg	Kilogram
kPa	Kilopascal
%	Percentage

Acronyms	**Nomenclature**
AOS	Apparent Opening Size
ASCE	*American Society of Civil Engineering*
ASTM	*American Standard Testing Materials*
CC	*Cam-Clay*
CPT	Cone Penetration Test
CPTU	Cone Penetration Test with pore pressure measurements
CPVD	Cap Prefabricated Vertical Drain
CSL	Critical State Line
DP	Dynamic probe
DTM	Marchetti Dilatometer
EVD	Electric Prefabricated Vertical Drain
EXPO'98	1998 Lisbon World Exposition
HS	*Hardening Soil*
HSsmall	*Hardening Soil with small-strain stiffness*
I	Inclinometer
ISO	Isotropic Consolidation Line
LNEC	Laboratório Nacional de Engenharia Civil
MC	*Mohr-Coulomb*
MCC	*Modified Cam-Clay*
NC	Normally consolidated soil
OC	Overconsolidated soil
PL	Settlement plate
PP	Perfect plasticity
PVD	Prefabricated Vertical Drain

PZ	Piezometer
SC	Sand columns
SCP	Stone columns
SD	Sand drains
	Probing or survey
SPT	Standard Penetration Test
SS	*Soft Soil*
SSC	*Soft Soil Creep*
SWCC	*Soil-Water Characteristic Curve*
TS	Topographic stake
UC	Underconsolidated soil
USCS	Unified Soil Classification System
VCL	Virgin Compression Line
VT	Vane-Test

TABLE OF CONTENTS

LIST OF TABLES

LIST OF FIGURES

LIST OF GRAPHS

I. INTRODUCTION

I.1. BACKGROUND AND OUTLINE OF THE THESIS

The importance of soil and rocks in civil engineering is more and more accepted by civil engineers themselves since all structures are supported directly or indirectly on soil or rocks. Due to these aspects, a specialised field arose in civil engineering which is based on the study of these natural materials, on characterizing them properly and knowing their behaviour when facing external actions determined by the needs and use of Man. These factors are of vital importance for the proper sizing of civil engineering works, as engineers make their decisions based on them. The final objective is and always will be the total stability and the safety of the construction itself, seeking the optimum combination between these factors and the impact that any works presents, whether socially, economically or environmentally.

In the past, the human species has preferably occupied areas with good geotechnical characteristics, thereby avoiding hard-to-use areas, such as extensive alluvial lowlands, although the easy access to water is located near these types of lands. With the social-economic development in recent decades, there has also been a growth in the occupation of soil and the rapid expansion of urban centres created the need to occupy areas of land with geological soil properties that did not favour the construction. Faced with the occupation of these areas, constraints arise associated with the construction on soil with high compressibility, namely the difficulty in guaranteeing their safety regarding the total and slope stability, as well as the settlements, which occur slowly over time and assume high values in the long term. To deal with these constraints, over time, engineers have developed a great variety of soil improvement techniques. The choice of the solution employed depends of their major goal and greatly on the cost/benefit ratio.

In coastal, lagoon and low alluvial areas, the small particles, with origin from the erosion of rocks, are deposited and form the so-called fine soil. These areas are located in places with phreatic levels near the surface and so the soil in these conditions has high water content and degrees of saturation. These are usually classified as fine organic (wet marshland and peats) or inorganic (clays and silts) soils, with high plasticity, weak resistant characteristics, extraordinarily deformable and with very low permeability. Soils with these characteristics are usually designated as soils with high compressibility or soft soil.

When saturated and under continuous load, fine soils suffer volume reduction as the excess pore pressure dissipates. Initially, it is assumed that the water trapped in the interstices supports the entire applied load, since it is considered as an incompressible material. Over time, the water is expelled and the pressure or load is transferred to the solid skeleton of the soil, resulting in increased strength. However, the process is very slow due to the reduced permeability of this type of soils and therefore lasts for long periods.

The void reduction, associated to the water expulsion, results on ground settlements. This process is designated as primary or hydrodynamic consolidation.

Once the dissipation of excess pore pressure is almost complete, settlements increment should decrease significantly and stop. However, on soft soils the vertical strain continues to occur, which is generally associated with secondary consolidation, representing a significant part of the total settlements. Based on data monitoring of embankments founded on this type of soils, it is observed that the consolidation settlements exceed those calculated in the design phase, and extend in time beyond what has been forecast, showing a clear indication that secondary consolidation is still going on. These settlements occur at a constant pressure and are associated with the viscosity of the soil (creep). Although relevant, this phenomenon is rarely taken into account when estimating the settlements in a project design; hence, they are underestimated relative to those observed in the post-construction phase. Given the stated reasons, it is therefore essential to take into consideration, in the consolidation analyses of soft clay soils, material models where the secondary consolidation can be accounted for.

In order to minimise post-construction settlements derived from the consolidation process, it is often imperative to appeal to artificial processes in order to accelerate this phenomenon. When the construction site covers large extensions, it may be considered the use of vertical drains, associated, or not, with the application of preload embankments. Prefabricated vertical band-shaped drains (PVD) are currently a quick, economic and efficient method of ground treatment, which is applied to this type of soil. This technique allows the consolidation process to be accelerated, and also obtaining a significant increase in soil strength within a short period of time. This reduction in time depends on various factors, including: a) the drains pattern adopted (square or triangular) b) the space between the drains; c) length of the drain and drainage capacity; d) the horizontal permeability of the soil. By combining this solution with the application of preload embankments, it is also possible to minimise settlements in the post-construction phase.

Although prefabricated vertical band-shaped drains are in fact a highly effective solution in accelerating soil consolidation and improving clayed soils properties, there are some factors that affect their performance and should be considered in the design. Among them, we highlight the following: a) the permeability of the drainage blanket, which is placed over the improved soil; b) the reduction of the discharge capacity of the drain due to clogging of the geotextile filter, clogging of the drain itself, or by a high deformation of the ground; c) effect of soil disturbance adjacent to the drain due to the installation process, known as the smear effect.

The PVD drains are driven into the ground using mandrels closed at the base, thereby causing an increase in pore pressure during their installation and a reduction in both, the strength and permeability of the soil around the drain, referred to as the disturbed or smear zone (Holtz & Holm, 1973). The most significant consequence will be the decrease in the water flow to the drain and a delay in the consolidation process of the treated soil. This effect may be considered in the analysis of consolidation either by an overall reduction in the consolidation coefficient or by introducing a disturbed area around the drain, thereby reducing the permeability coefficient in this zone. If this second hypothesis is considered an adequate characterisation of the smear effect should be made, and it will be necessary to estimate not only the diameter of the disturbed area (d_s), but also the horizontal permeability of this zone (k_{hs}).

When considering the smear effect the problem lies on the determination of these values and in their correspondence between theory and practice. It has been noted that the extent and permeability of the disturbed area depends on the installation process, the size and the shape of the mandrel and the soil ground characteristics. As these parameters cannot be determined accurately, they are estimated based on field experiences, laboratory tests and theoretical considerations, or by retro-analysis of real case study results.

This research project focuses the consolidation of soft soil in the presence of prefabricated vertical band-shaped drains, and their application to the analysis of an actual worksite, namely in Dikes No.1 and No.3 of the *Lebrija* Pond, located in southern Seville, Spain.

Dikes No.1 and No.3 of the *Lebrija* Pond were founded in soils classified as clay or silty soils, with high plasticity and compressibility. Due to the reduced geotechnical properties of these soils, the initial design was revised and prefabricated vertical band-shaped drains, arranged in a triangular pattern, were applied to the soil foundation in both dikes. In the case of Dike No.1, it was also decided to place geotextile reinforcement between the dike embankment and the foundation. In addition, the dikes were properly instrumented, being subjected to monitoring from the beginning of their construction in order to control their stability and safety, as well as the efficacy of the prefabricated vertical drains. Based on data from settlement plates, piezometers and inclinometers installed in the body of the embankments and foundations of the dike, it was found that the settlements slightly exceeds those estimated in the design. Settlements are now practically stabilised, but the order of magnitude of the maximum settlements is around 7% to 11% of the total height of the dikes, indicating significant secondary settlements.

The finite element method (FEM) used in the simulation of consolidation and stability of soils treated with prefabricated vertical drain, presents a high potential, as it allows the incorporation of not only the construction phases but also reinforcement elements, when necessary. However, while the analysis of the phenomenon of soil consolidation around a drain is a problem of axisymmetric nature (3D-tridimensional), real geotechnical consolidation problems are mostly analysed in plane strain (two-dimensional-2D). So, in order to perform the simulations, some adaptations are needed. In this case, the system of the drain arrangement needs to be converted, on a wall of parallel vertical drains. The spacing of the drains and the coefficient of the permeability of the treated area must be adjusted along with the three-dimensional system, always ensuring the equality of the average degree of consolidation in both systems. The solutions currently used are those of Hird *et al*. (1992), and Indraratna & Redana (1997).

The Plaxis, a finite element method (FEM) software, was used to model and to simulate the consolidation process and several built-in material models, including the Mohr-Coulomb, Soft Soil and Soft Soil Creep were considered. Based on these numerical simulations, it was possible to evaluate the response of the soil foundation and the dikes, compare the adequacy of the material models adopted to characterise them, as well as the mechanical and permeability soil parameters. Furthermore, and by retro-analysis, and estimation for the parameters associated with the smear effect and some considerations regarding the viscosity of the soil are also made. Additionally, the program also allows accounts the flow. In this case, the soils are saturated or partially saturated depending on the location of the groundwater head, drainage conditions and time.

The most significant contribution of this thesis is focused on the analysis of consolidation of soft soils, considering simultaneously: a) the influence of the smear effect of soil treated with prefabricated vertical band-shaped drains; b) the viscosity effect (creep) of clay soils with high compressibility; c) the influence of the flow net on the foundation and dikes.

The previous paragraph raises the following important questions:

- "What is the interest in combining such diverse phenomena, as the smear, the creep and the flow, in the consolidation of soft soil in the presence of band-shaped drains?"
- "Why is it so important to incorporate a real case work on the research?"

The answer to these questions will be answer in the conclusions of this thesis, which structure will be presented in the following section.

I.2. STRUCTURE OF THE THESIS

This thesis consists of eight chapters and four appendices, being the sequence and preview of the themes, presented in the paragraphs below.

Chapter I (INTRODUCTION) has the goal of introducing the reader to the topic covered throughout the thesis, the motivations that led to its study and the way in which it is structured.

In Chapter II (CONSOLIDATION), the consolidation phenomenon will be covered, with the presentation of several analytical formulations. The introduction to the subject starts with the Terzaghi's unidirectional analytical consolidation solution, followed by the solutions considering vertical drains, and more specifically prefabricated vertical drains. Therefore, the Hansbo formulation (1979) will initially be presented for radial flow (axisymmetric problem), and subsequently its conversion to the plane strain. In the last case two analytical solutions are presented, namely those of Hird *et al*. (1992) and Indraratna & Redana (1997). Note that in the analytical solutions for vertical drains, both the discharge capacity of the drain and the effect of the disturbed area around it (smear effect) can be taken into account. In addition, a first discussion of the secondary consolidation is considered. This phenomenon occurs on fine soils at constant pressure, depends on time and on the soil viscosity (creep). This settlement is quite significant when in the presence of compressible or soft soil. This chapter ends with the presentation of the combined solution of Carrillo (1942) witch considerer the vertical and horizontal flow.

Chapter III (MATERIAL MODELS) concerns the constitutive laws that describe the soil behaviour and their response in different contexts. Therefore, and according to the previous chapter, firstly it will be presented some simple material models, progressing to ones that are more complex. The model behaviour of soft soils that considerers the viscosity (creep) will merit a special emphasis. The mathematical modelling of the behaviour of these soils is complex, yet it is essential for the correct analysis of the associated strain throughout the design. Lastly, the Mohr-Coulomb, Soft Soil and Soft Soil Creep models of Plaxis software will be presented since they were used in the modelling of dikes of the *Lebrija* Pond.

Chapter IV (VERTICAL DRAINS) is completely focused on vertical drains, their origins and how they have evolved until today. References are made to their installation process, as well as the equipment and *modus operandi*. Special attention is given to the prefabricated vertical band-shaped drains, their advantages and drawbacks. We will also present some work cases where this technique has been applied to the treatment of soil foundations.

Chapter V (SMEAR) is completely dedicated to the smear effect and to the characterisation of the parameters, which allows its consideration in the consolidation analyses. A state-of-the-art on the topic in question is presented, where it can be seen the importance of the smear in the consolidation process delay. Next, a comparative study is made between the analytical solutions of Hird *et al*. (1992) and Indraratna & Redana (1997), both for plane strain. In this stage, the intention is to demonstrate not only the differences between the two solutions, but also the influence of some parameters in the estimation of the horizontal permeability coefficient on the disturbed area (smear). This is a key point of the thesis since the case work is analysed in plane strain, and this study allows to decide which analytical solution should be adopted in the future simulations. The chapter ends with a sensitivity analysis of the smear parameters and their influence on the evolution of the degree of consolidation.

The theoretical concepts previously presented will be applied to the analysis of a specific casework, introduced in Chapter VI (DIKES NO.1 AND NO.3 OF THE *LEBRIJA* POND). In this phase, the geographic location of the dikes , it's purpose and it's integration considering the environmental and socio-economic of the region, is presented, as well as: a) the initial design project and modifications suffered during construction; b) the prospecting campaigns performed at each stage; c) geotechnical characterisation of the soil foundation, based on the results of the field and laboratory tests; d) geological-geotechnical profiles for the cross sections analysed; d) geotechnical characterisation of the materials which form the dike embankments; e) instrumentation applied for control measurements; f) analysis of the monitoring results.

In chapter VII (MODELLING OF DIKES NO.1 AND NO.3 OF THE *LEBRIJA* POND), the results of numerical simulations performed are showed and confronted to the monitoring data. However, a first step is necessary, which correspond to the estimation of the horizontal permeability coefficients to be adopted in the areas treated with PVD. In the suite, modelling of the cross sections are presented, including a description of the calculation procedure, the boundary conditions for displacements and drainage in each phase, and the generation of the initial stress state. The simulations are performed with and without the consideration of a flow net in the foundation as well as in the embankment dikes. Once this option is adopted, the software considers the soil located above the saturation streamline as partly saturated. In order to analyse the importance of material models in the soil response, the Mohr-Coulomb model is used in the initial simulations for the soil foundations; Lately, Soft Soil and Soft Soil Creep models will be given preference. A sensitivity analysis is also performed for the smear and creep parameters. Based on the results of the numerical simulations and by comparing them with the monitoring ones, the permeability coefficient will be estimated along with the diameter of the disturbed zone (smear), together with the secondary compressibility index (C_α) for the soil foundation, and the importance of considering the flow net.

Finally, the safety coefficients for the slope stability of the dikes are determined, for the phases associated to the end of the construction and the last step for the raised up of the water level in the reservoir. The objective will be to establish the efficiency of the treatment in the global stability of the dikes.

In chapter VIII the conclusions are presented, as well as some research lines to be followed in the future, regarding the topic analysed.

Finally, in Appendices I, II, III and IV, the following results will be presented:

APPENDIX I: DATA REFERENT TO DIKE NO.1 AND DIKE NO.3 OF *LEBRIJA* POND.

APPENDIX II: PREFABRICATED COLBONDDRAIN CX1000 TECHNICAL DATA SHEET.

APPENDIX III: PLAXIS SIMULATION RESULTS OF *LEBRIJA* POND DIKE NO.1.

APPENDIX IV: PLAXIS SIMULATION RESULTS OF *LEBRIJA* POND DIKE NO.3.

II. CONSOLIDATION

This chapter is dedicated to the consolidation theory, which represents an essential and fundamental theme in this thesis, and therefore it will be the first to be covered.

As mentioned in Chapter I, the vertical strains observed in fine soils, when subject to a load, are due to the consolidation phenomenon, and are prolonged over time. The factors, which control the time associated with the phenomenon in question, depend on both the location of the drainage boundaries and the permeability of the soil. In normal conditions, without the use of artificial techniques, the consolidation is treated as a vertical unidirectional problem, since the closest boundary drainage conditions are located at the top and/or the base of the stratum, and the vertical flow depends on the permeability in that direction. When vertical drains are used in the ground, the predominant flow changes since the boundary drainage conditions also changes. In this case, the consolidation around the drain is formulated as an axisymmetric problem since the dominant flow is radial and the associated parameter will be the horizontal permeability of the soil. The distance that a water particle has to travel to arrive at the vicinity of the drain is substantially reduced and consequently the acceleration of the consolidation phenomenon occurs. In the analysis of a real case, where vertical drains are used, the consolidation will be a combination of the two situations.

As the thesis includes the study of a real case work, in which the application of vertical drains was used, the analytical formulations associated with consolidation will be presented. The introduction to the theme begins with the analytical formulation of Terzaghi's unidirectional vertical consolidation, followed by the consolidation formulations taking into account the vertical drains, and more specifically the prefabricated vertical drains. Therefore, the Hansbo solutions (1979) will initially be presented for radial drainage (axisymmetric problem) followed by the solutions for plane strain analysis, namely those of Hird *et al*. (1992) and Indraratna & Redana (1997). Beware that the consolidation analytical solutions for the drains allow both the effect of the disturbed zone around it (smear effect), as well as the limitations of the discharge capacity of the drains. Lastly, the combined solution of Carrillo (1942), taking into consideration the vertical and horizontal flow, is also presented.

At the end of this chapter, a first discussion of the secondary consolidation is considered. This phenomenon occurs on fine soils at constant pressure, depends on time and on the soil viscosity (creep). This settlement is quite significant when in the presence of compressible or soft soil.

II.1. INTRODUCTION

When soil is submitted to a load that is different to that of its normal state, a vertical strain occurs, called settlement. This settlement may be significant or not; however, it must be estimated. The settlements in the soil are not elastic as they are mainly due to the reorganisation of the soil, due to both the displacement of particles and void reduction, and the fracturing of other particles at the contact points. Therefore, most settlements in soil are not recoverable after the removal of the load. The vertical displacement of the particles often implies a reduction in the voids, and this

causes a temporary increase in the pore pressure (Δu), if the soil is saturated, and negligible when dry.

Theoretically, the settlement of soil is defined as being the vertical displacement (Δs) which occurs due to a load ($\Delta\sigma$), in a soil stratum with a thickness H and with a strain module (E_s), i.e.:

$$\Delta s = \int_0^H \frac{\Delta\sigma}{E_s}\, dz = \int_0^H \varepsilon\, dz \qquad \text{(II.1)}$$

If the thickness of the layer is relatively small, and the strain module is considered constant, then the integration will be:

$$\Delta s = \varepsilon\, H \text{, being } \varepsilon \text{ the vertical strain} \qquad \text{(II.2)}$$

However, the parameter E_s is not simple to obtain, as it depends on the type of soil, it's conditions on ground, the confinement to which it is subjected and also the depth. The increase in stress ($\Delta\sigma$) at depth is also difficult to quantify, and so approximations are usually used in both cases.

When the soil is saturated or partially saturated, then the complexity of the problem increases as the settlement will not be complete until the total dissipation of the excess pore pressures has occurred. In certain soils, this process may take quite some time as the dissipation depends on the permeability of the soil. In granulated saturated soil, especially when poorly graded, drainage is practically instantaneous and so it is usual to apply the equation (II.1). In fine saturated soil, the settlements can be rather significant and delayed on time due to the low permeability coefficients (k). These types of vertical displacements, which depend on the time factor, are designated as consolidation settlements. In fine, partly saturated soils, drainage also does not occur instantaneously, and depends not only on time but also on their degree of saturation (Sr) (Bowles, 1996).

Therefore, the total settlement of the foundations are composed by three distinct parts, namely the immediate settlement (s_i), the primary consolidation settlement (s_{pc}) and the secondary or secular consolidation settlement(s_{sc}). The immediate settlement, which is low in clayed soils and higher in sandy soils, is the result of the strain of the soil at constant volume. Generally, and depending on the type of soil, it is common to have the following relations between total and immediate settlement (Soriano, 2005):

$s_i \approx$ (10% a 15%) s_{tot} for soft and very soft clays,
$s_i \approx$ (60%) s_{tot} for overconsolidated clays,
$s_i \approx$ (80%) s_{tot} for silts,
$s_i \approx$ (100%) s_{tot} for granular soils (gravels and sand).

Primary consolidation settlements are related to the dissipation of excess pore pressure generated by the application of a load, and secondary consolidation to the settlements of the soil under constant stress. Even though both phenomena are associated to time, the settlement that corresponds to the primary consolidation ends when pore pressure dissipates; however, secondary consolidation continues to occur, even though it evolves more slowly. In reality, both consolidations occur simultaneously, which complicates the analysis of the settlement results. However, it is usual to consider that secondary consolidation only occurs when the dissipation of the pore pressure has

been practically concluded (Bardet, 1997). This theme will be covered in chapter II.6 and later in chapter III.3.2, in terms of mathematical formulation.

II.2. ANALYTICAL SOLUTION – UNIDIRECTIONAL VERTICAL FLOW

As already mentioned, consolidation is a phenomenon, which is associated with fine saturated soil when submitted to a load higher than the actual stress state condition, and the effect corresponds to the vertical strain, or settlement, in time. Since the water and solid particles present reduced or no compressibility al all, then the overburden stress applied to the soil will be supported by the water and not by the solid skeleton of the soil. Only as the increased pressure in the water dissipates, which occurs due to the drainage of the water from the soil, is the load transferred to the solid skeleton of the soil. As the permeability of this soil are low, the drainage of the water particles take time, and the settlements which correspond to the dissipation of the pore pressure excess also occurs very slowly, (Coelho, 1996). These corresponds the primary consolidation or hydrodynamic settlements.

The consolidation theory was developed by Terzaghi in 1925, and is based on the following assumptions:

a) the layer of the soil is homogeneous;
b) the soil is completely saturated (Sr=100%);
c) the compressibility of the water and particles which form the soil is negligible;
d) the strains or extensions (ε) are infinitesimal, meaning that an element of the dimensions dx, dy and dz, have the same response as an element with the dimensions x, y and z;
e) the draining and compression are one-dimensional;
f) Darcy's Law is valid;
g) the properties of the soil at depth are constant;
h) the relation between the void index (e) and the stress applied (σ) is linear.

Therefore, and in accordance with this theory, the variation of volume V of a mass of soil, in a three dimensional medium and with drainage in the three directions will be:

$$\left(k_x \frac{\partial^2 h}{\partial x^2} + k_y \frac{\partial^2 h}{\partial y^2} + k_z \frac{\partial^2 h}{\partial z^2} \right) dx\ dy\ dz = \frac{\partial V}{\partial t} \qquad \text{(II.3)}$$

When h is the hydraulic head and k_x, k_y and k_z the permeability coefficients on the x, y and z directions. This expression depends on assumptions a), d) and f) of Terzaghi's theory.

For one-dimensional flow (in the vertical direction z), the two first terms disappear, and in this case, it can be assumed that $k=k_v=k_Z$ and the volumetric draining is defined as:

$$k \frac{\partial^2 h}{\partial z^2}\ dx\ dy\ dz = \frac{\partial V}{\partial t} \qquad \text{(II.4)}$$

The volumetric element is dx dy dz, and the volume of pores will be $\left(dx\ dy\ dz\right)\cdot\left(\frac{e}{1+e}\right)$, with (e) being the void ratio. Based on assumption c) of Terzaghi's theory, the variation of volume with time will be:

$$\frac{\partial}{\partial t}\left(dx\ dy\ dz\frac{e}{1+e}\right)=\frac{\partial V}{\partial t} \qquad \text{(II.5)}$$

in addition, as (dx dy dz)/(1+e) is the constant volume of a solid; the previous equation may be re-written as:

$$\left(\frac{dx\ dy\ dz}{1+e}\right)\frac{\partial e}{\partial t}=\frac{\partial V}{\partial t} \qquad \text{(II.6)}$$

Applying this in equation II.4, and cancelling the terms dx, dy and dz, we obtain:

$$k\frac{\partial^2 h}{\partial z^2}=\frac{1}{1+e}\frac{\partial e}{\partial t} \qquad \text{(II.7)}$$

Only excess pore pressure (Δu) will cause drainage and a variation in volume, and as the hydraulic head is $h=z_0+\Delta u/\gamma_w$, where γ_w is the water volume weight, then the previous expression becomes:

$$\frac{k}{\gamma_w}\frac{\partial^2 u}{\partial z^2}=\frac{1}{1+e}\frac{\partial e}{\partial t} \qquad \text{(II.8)}$$

In order to continue with the theory, it is now necessary to define the compressibility coefficient a_v and the rate of compressibility a'_v. These parameters taken from the linear part of a graphic, relates the void ratio (e), or the strain (ε) to the applied pressure or strain (σ), being:

$$a_v=\frac{\Delta e}{\Delta\sigma}=\frac{\partial e}{\partial\sigma} \qquad \text{(II.9)}$$

$$a'_v=\frac{\Delta\varepsilon}{\Delta\sigma}=\frac{\partial\varepsilon}{\partial\sigma} \qquad \text{(II.10)}$$

Before the occurrence of the pore pressure dissipation, the stress increment equals the pore pressure ($\partial\sigma=\partial u$), and therefore, $\partial e=a_v\,\partial u$. Substituting this expression in equation II.8, ones obtain:

$$\left[\frac{k\ (1+e)}{a_v\ \gamma_w}\right]\frac{\partial^2 u}{\partial z^2}=\frac{\partial u}{\partial t} \qquad \text{(II.11)}$$

The expression, which appears in square brackets, is defined as being the consolidation coefficient C_v, or in other words:

$$C_v=\frac{k\ (1+e)}{a_v\ \gamma_w} \qquad \text{(II.12)}$$

One should now introduce the volumetric compressibility coefficient m_v, in which the void ratio (e) is substituted by the initial void ratio (e_0). This coefficient is defined as:

$$m_v=\frac{a_v}{1+e_0}=a'_v \qquad \text{(II.13)}$$

Another way to present the consolidation coefficient, and normally used in numerical method applications, is the following:

$$C_v = \frac{k\ (1+e_0)}{a_v\ \gamma_w} = \frac{k}{m_v\ \gamma_w} \tag{II.14}$$

in this case, equation II.11 can be re-written as:

$$C_v \frac{\partial^2 u}{\partial z^2} = \frac{\partial u}{\partial t} \tag{II.15}$$

The analytical solution of the previous equation is not trivial, and uses the expansion of the Taylor series. This solution will be:

$$u = \sum_{n=1}^{n=\infty} \left(\frac{1}{H} \int_0^{2H} u_i\ \sin\frac{n\pi z}{2H} dz \right) \left(\sin\frac{n\pi z}{2H} dz \right) e^{\left(\frac{n^2\pi^2 C_v t}{4H^2} \right)} \tag{II.16}$$

being H the thickness of the layer. This is the general solution and is applied to any initial hydrostatic pressure u_i in the stratum, thickness of the compressible stratum, and for any depth z. This last parameter is measured from the top to bottom.

As the consolidation coefficient C_v is considered constant, and time t is a multiple of C_vH, then one can introduce a time factor, dimensionless, defined as:

$$Tv = \frac{C_v\ t}{d^2} \tag{II.17}$$

where d is the drainage length. Substituting the previous expression in equation II.16, then it becomes:

$$u = \sum_{n=1}^{n=\infty} \left(\frac{1}{H} \int_0^{2H} u_i\ \sin\frac{n\pi z}{2H} dz \right) \left(\sin\frac{n\pi z}{2H} dz \right) e^{\left(\frac{n^2\pi^2 Tv}{4} \right)} \tag{II.18}$$

If the fine soil is between two permeable layers, such as two layers of sand (Figure II.1a), then the drainage length will be d=H/2. Otherwise, the drainage is only processed in one direction (Figure II.1b), and then the drainage distance will be equal to H.

The progress of consolidation, both time t and depth z, is given by the equation:

$$U_{(z,t)} = \frac{u_i - u_{(z,t)}}{u_i} = \frac{\Delta\sigma'_{(z,t)}}{\Delta\sigma} \tag{II.19}$$

where $U_{(z,t=0)}$=0 at the start of the consolidation and $U_{(z,t=\infty)}$=1 at the end of the consolidation. However, the most common procedure to determine the average degree of consolidation of a soil layer, for a given time t, is based on the expression:

$$\overline{U} = \frac{1}{H} \int_0^H U_z\ dz \tag{II.20}$$

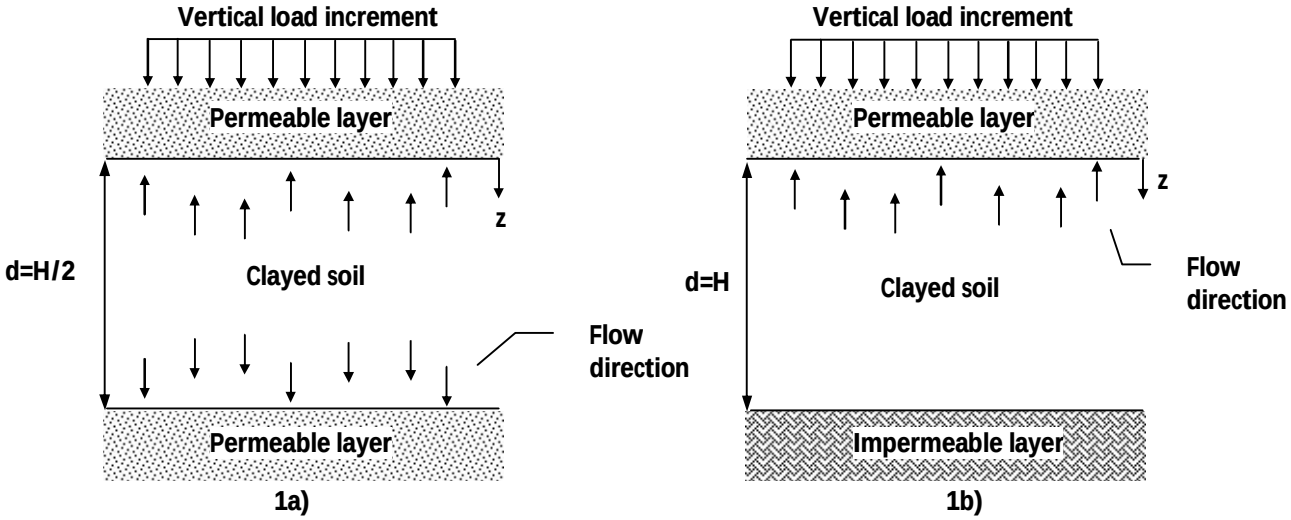

Figure II.1 – Unidirectional vertical flow: 1a) in both ways; 1b) only in one way

Substituting the expression II.18 in this last, we obtain:

$$\bar{U} = 1 - \frac{8}{\pi^2} \sum_{n=1}^{\infty} \frac{e^{\left(\frac{-n^2\pi^2 Tv}{4}\right)}}{n^2} \qquad \text{(II.21)}$$

Based on approximations and simplifications, equation II.21 will be sub-divided into two, depending on the time factor (Bardet, 1997). The most common are those proposed by Fox, in 1948, being:

$$\bar{U}_{(Tv)} = \sqrt{\frac{4Tv}{\pi}} \text{, for } Tv < 0.2827 \qquad \text{(II.22)}$$

$$\bar{U}_{(Tv)} = 1 - \frac{8}{\pi^2} e^{\left(-\frac{\pi^2 Tv}{4}\right)} \text{, for } Tv \geq 0.2827 \qquad \text{(II.23}$$

In turn, the variation of the time factor Tv with the average degree of consolidation may also be approximately determined, based on the following expressions (Das, 1999):

$$Tv = \frac{\pi}{4}\left(\frac{\bar{U}_{[\%]}}{100}\right)^2 \text{, for } \bar{U} < 60\% \qquad \text{(II.24)}$$

$$Tv = 1{,}781 - 0{,}933 \ln(100 - \bar{U}_{[\%]}) \text{, for } \bar{U} \geq 60\% \qquad \text{(II.25)}$$

Sivaram & Swamee (1977) developed an empirical relationship (equation II.26) which relates these two parameters, and this is valid for any value of the average degree of consolidation.

$$Tv = \frac{\frac{\pi}{4}\left(\frac{\bar{U}_{[\%]}}{100}\right)^2}{\left[1 - \left(\frac{\bar{U}_{[\%]}}{100}\right)^{5,6}\right]^{0,357}} \text{ for } 0\% \leq \bar{U} < 100\% \qquad \text{(II.26)}$$

In simple terms, one can also estimate the average degree of consolidation of a layer based on the relationship between the settlements, namely:

$$\bar{U}_s = \frac{s_t}{s_{pc}} \qquad \text{(II.27)}$$

in which s_t is the settlement in a given time t, and s_{pc} is the maximum settlement using primary consolidation.

Regarding the determining of the maximum settlement of a clay layer, using primary or hydrodynamic consolidation, associated with unidirectional vertical drainage, this value can be estimated based on the generic expression:

$$s_{pc} = \frac{H}{1+e_0}\left(C_s \log\frac{\sigma'_p}{\sigma'_0} + C_c \log\frac{\sigma'_f}{\sigma'_p} \right) \qquad \text{(II.28)}$$

where the final vertical effective stress is given by $\sigma'_f=\sigma'_0+\Delta\sigma$, and the parameters e_0, C_c, C_s, σ'_P are determined on the oedometer test (one-dimensional conventional consolidation test), whose laboratory curve, once corrected, is presented in the form of a diagram in figures II.2a and II.2b.

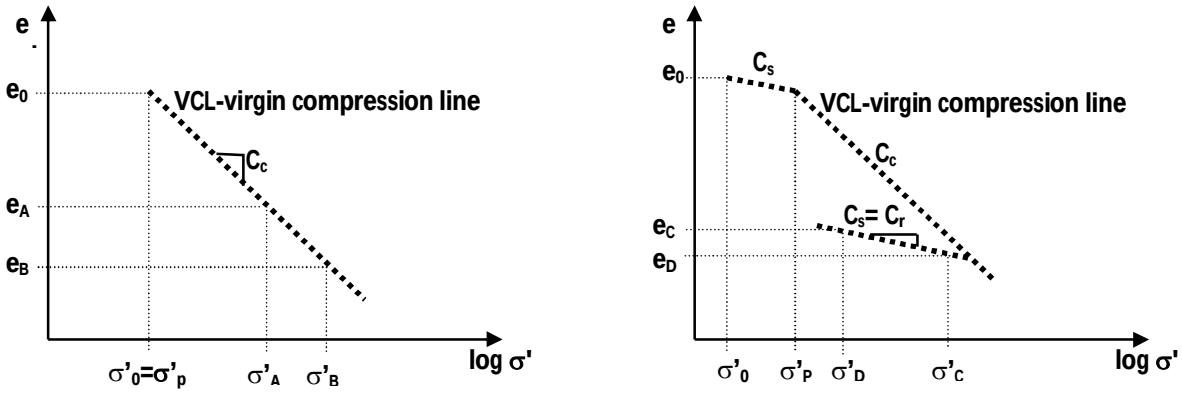

Figure II.2 – Oedometer test curve, after correction, for normally consolidated soil 2a) and overconsolidated soil 2b).

The compressibility index C_c and the recompressibility C_r or expansion index C_s of the soil will be given, respectively, by equations II.29 and II.30.

$$C_c = \frac{e_A - e_B}{\Delta \log\sigma'} = \frac{e_A - e_B}{\log(\sigma'_B) - \log(\sigma'_A)} = \frac{e_A - e_B}{\log\frac{\sigma'_B}{\sigma'_A}} \qquad \text{(II.29)}$$

$$C_r = C_s = \frac{e_C - e_D}{\Delta \log\sigma'} = \frac{e_C - e_D}{\log(\sigma'_D) - \log(\sigma'_C)} = \frac{e_C - e_D}{\log\frac{\sigma'_D}{\sigma'_C}} \qquad \text{(II.30)}$$

Points A and B are located on the virgin compression line (VCL) while points C and D are located on the unload (expansibility of the soil) and reload (recompressibility of the soil) line. Note that, contrary to the volumetric compressibility coefficient, the compressibility and the recompressibility indexes do not depend on the state of the stress, and therefore are adopted in the calculations, instead of the parameter m_v.

The pre-consolidation soil stress σ'_p will correspond to the maximum vertical effective stress already applied to the soil, from the depth which the sample was taken. Based on this value and on the initial vertical effective stress, at this same depth, one can determine the overconsolidation ratio (OCR). This parameter is given by the ratio between these stresses before the application of the additional load, according to the expression:

$$OCR = \frac{\sigma'_P}{\sigma'_0} \tag{II.31}$$

Based on this parameter and depending on its numerical value, the clay and fine soils in general, are classified as:

a) Normally consolidated soil if OCR=1 (NC);
b) Overconsolidated soil if OCR>1 (OC);
c) Underconsolidated soil if OCR<1 (UC).

Depending on the stress state, the settlements can be estimated by three different expressions, in accordance to the initial and final effective vertical stress, whereby:

a) The soil is under consolidated or normally consolidated ($\sigma'_0=\sigma'_p$). In this situation, whatever the increment load $\Delta\sigma$, the final vertical effective stress will be greater than the preconsolidation stress ($\sigma'_f>\sigma'_p$), the variation of the voids will always correspond to the points located on the virgin compression line (Figure II.3a) and the settlement will be:

$$s_{pc} = \frac{H}{1+e_0} C_c \log \frac{\sigma'_f}{\sigma'_0} \tag{II.32}$$

b) The soil is overconsolidated ($\sigma'_p>\sigma'_0$), however the load increment $\Delta\sigma$ is not sufficient for the final vertical effective stress to exceed the preconsolidation stress ($\sigma'_f\leq\sigma'_p$). When this occurs, the soil will respond following the recompression line, but not reaching the virgin compression line (Figure II.3b), and the settlement value is given by:

$$s_{pc} = \frac{H}{1+e_0} C_s \log \frac{\sigma'_f}{\sigma'_0} \tag{II.33}$$

c) The soil is overconsolidated ($\sigma'_p>\sigma'_0$), but the load increment $\Delta\sigma$ is sufficient for the final vertical effective stress to exceed the preconsolidation stress ($\sigma'_f>\sigma'_p$). In this case, the settlement will correspond to the sum of two parts. One corresponds to the void reduction in the recompression line (Δe_1), until the preconsolidation stress is reached, and the other part corresponds to void reduction (Δe_2) following the virgin compression line (Figure II.3c). The total settlement value is given by equation II.28.

Many of the numerical calculation programmes, using the finite element method, determine the consolidation or the degree of consolidation, based on the expression:

$$U=1-\frac{\text{Pore pressure diagram area for a given time t}}{\text{Initial pore pressure diagram area}} \tag{II.34}$$

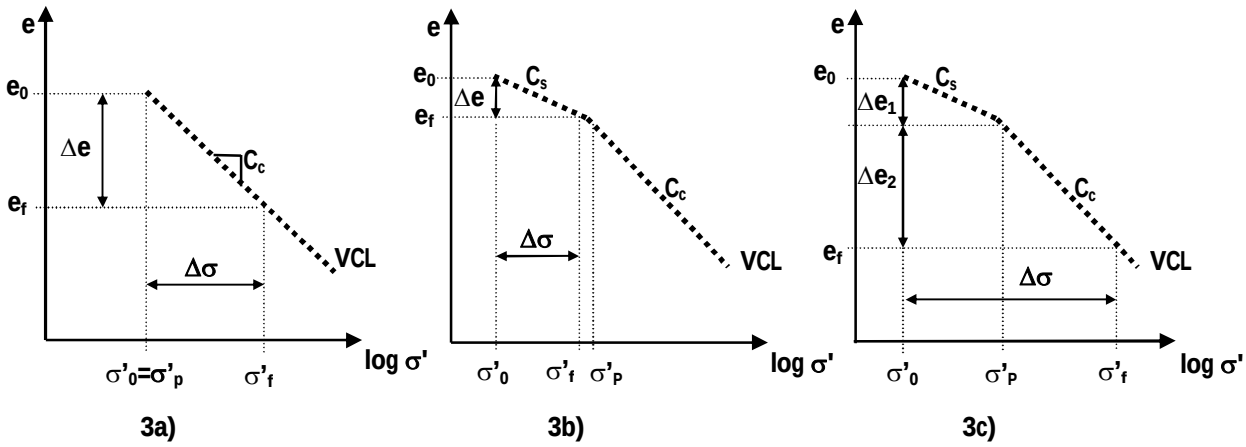

Figure II.3 – Void ratio decrease for the different situations of initial and final vertical effective stress applied to the soil, when it is normally consolidated 3a) or overconsolidated 3b) and 3c).

Since these pore pressure diagrams are not constant in depth, the areas in question are determined by numerical integration (Sridharam & Rao (1981); Sridharam & Prakash (1985)). In Figure II.4, some schemes of the hypotheses used for the variation in pore pressure (Δu) are presented.

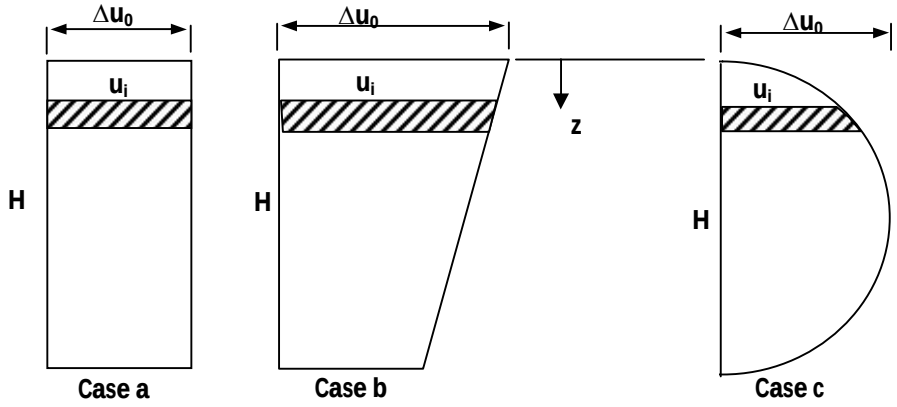

Figure II.4 - Distribution of the pore pressures for case a) (constant variation - rectangular), b) (trapezoidal variation) and c) (sinusoidal variation) (Taylor, 1948)

All the expressions of the Terzaghi's theory are for one-dimensional drainage, usually vertical, and consequently all the parameters used in the expressions represent the soil characteristics in this direction. Additionally, this theory does not consider the secondary consolidation settlements, as they do not depend on the dissipation of the excess pore pressure (already mentioned before).

II.3. ANALYTICAL SOLUTION - RADIAL FLOW (AXISYMMETRIC ANALYSIS)

Terzaghi's theory was later adapted for radial flow by Rendulic (1935). However, in 1944 Barron was the first researcher to analyse the influence of the vertical drains in the consolidation of clays. His solution, for cylindrical sandy drains, presented in his PhD, was based on the simplified theory of the one-dimensional consolidation proposal from Terzaghi's under the assumption of the validity of Darcy's law. Two distinct solutions were presented regarding the vertical strain on the soil, namely:

a) Free vertical strains: in this case the vertical stresses on the surface remain constant during the consolidation process, but the displacements on the surface are not uniform;

b) Equal vertical strains: in this solution vertical displacements on the ground surface are constant and uniform, however the vertical stresses are not.

These solutions also combined the radial flow in the drain direction and the vertical drainage within the drain. However, when the ratio between the length of the drains and the spacing between them is high, the radial flow can be considered predominant, and so the consolidation may be treated as a unidirectional horizontal flow problem (Figure II.5).

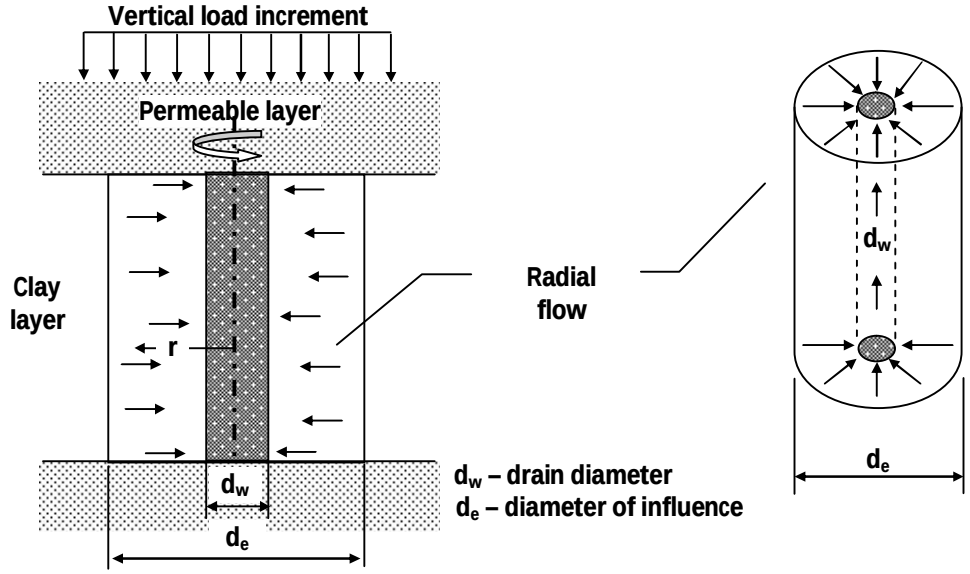

Figure II.5 – Radial flow in a soil layer in the presence of vertical drains

In this case, the dissipation of the pore pressures with time, is governed by the equation:

$$\frac{\partial u}{\partial t} = C_h\left[\frac{1}{r}\frac{\partial u}{\partial r} + \frac{\partial^2 u}{\partial r^2}\right] \qquad \text{(II.35)}$$

where C_h is the horizontal consolidation coefficient of the soil. Resolving equation II.34 for a soil cylinder with a cylindrical vertical drain, in which the pore pressure in the vicinity of the drain is null, and for the condition of equal vertical strains (Barron, 1948), the average degree of consolidation for the layer is:

$$U_r = 1 - e^{\left(-\frac{8T_r}{F(n)}\right)} \qquad \text{(II.36)}$$

in which T_r is the time factor for the radial drainage, and given by:

$$T_r = \frac{C_h\, t}{d_e^{\,2}} \qquad \text{(II.37)}$$

$F_{(n)}$ is a function of the quantity and density of the drains (equation II.39), also depending on the ratio between the influence diameter of the drain (d_e), and the diameter of the drain itself (d_w) (equation II.38).

$$n = \frac{d_e}{d_w} \tag{II.38}$$

$$F_{(n)} = \left[\frac{n^2}{(1-n)}\right]\left[\ln(n) - \frac{3}{4} + \frac{1}{n^2}\right] \tag{II.39}$$

For typical values of drain spacing and drain diameter, the ratio (n) equals or exceeds 20, and in these cases, the $F_{(n)}$ factor is simplified to:

$$F_{(n)} = \ln\left(\frac{d_e}{d_w}\right) - \frac{3}{4} \tag{II.40}$$

The vertical drains are installed according to a square or triangular pattern, spaced between axes at a constant distance (S). Knowing that each drain has an influence diameter d_e, with a corresponding area of ($\pi\ d_e^2/4$), and matching this to:

a) Quadrangular geometric area for the square pattern (Figure II.6a);

b) Hexagonal geometric area for the triangular pattern (Figure II.6b);

ones obtain:

Square pattern

$$\frac{\pi d_e^2}{4} = S^2 \quad \Leftrightarrow \quad d_e = S\sqrt{\frac{4}{\pi}} \approx 1{,}1284\ S^2 \tag{II.41}$$

Triangular pattern

$$\frac{\pi d_e^2}{4} = \frac{\sqrt{3}}{2}S^2 \quad \Leftrightarrow \quad d_e = S\sqrt{\frac{2}{\pi}\sqrt{3}} \approx 1{,}050\ S^2 \tag{II.42}$$

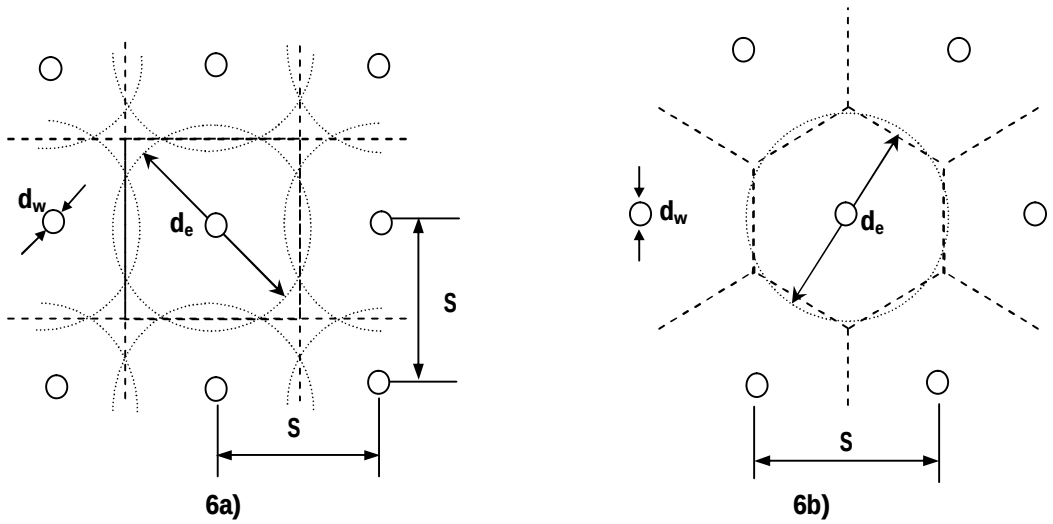

6a) 6b)

Figure II.6 – Spacing between the drains (S) and the influence diameter or equivalent diameter of a drain (d_e), for square pattern 6a) and triangular pattern 6b) (Rixner *et al*., 1986)

Barron also solved the equation II.35 for free vertical strains, but realise that in the case of n>5, the two solutions were very close. Therefore, he recommended the equal vertical strains solution due to its simplicity. Later, in 1948, he included, in his initial solution, the effect of soil disturbance caused by the drain installation process (smear effect) and the reduction of discharge capacity of drains (hydraulic resistance of the drain).

In 1979, Hansbo introduced some approximations and modified the equations developed by Barron, in order to adapt them for prefabricated drains, obtaining a solution for the degree of consolidation at a given depth, for radial flow, and considering equivalent vertical strains. He also highlighted that the free and equivalent vertical strain solutions are rather similar (Hansbo, 1979 and 1981a). However, when considering both the radial and the vertical flow contributions, for the analysis of the final degree of consolidation, the solution is not exact. A solution is considered exact when the equations, in the boundary conditions, are mathematically satisfied.

In 1974, Yoshikuni & Nakamodo presented an exact solution considering both flows and the discharge capacity of the drain, excluding the smear effect. In 1978, Runesson drew a comparison between Barron's initial solutions for free vertical strains and the associated exact solution; however, the differences were not significant. A thorough compilation of these solutions are presented by Magnan (1983a), who carried out a retro-analysis of the consolidation results analyses for several solutions (1983b).

Therefore, according to Hansbo, who considers a disturbed zone around the drain with reduced permeability (Figure II.7), reduction of discharge capacity of the drains, and equivalent vertical strains during the entire consolidation process, the average degree of consolidation is given by:

$$\overline{U}_r = 1 - e^{\left(-\frac{8T_r}{\mu}\right)} \qquad \text{(II.43)}$$

being μ a factor which expresses three effects, namely the spacing between the drains $F_{(n)}$, the smear effect $F_{(s)}$ and the hydraulic resistance of the drain $F_{(r)}$.

$$\mu = F_{(n)} + F_{(s)} + F_{(r)} \qquad \text{(II.44)}$$

The $F_{(n)}$ factor continues to be determined by the expression II.39 or II.40 and the $F_{(s)}$ factor will be determined by the equation:

$$F_{(s)} = \left[\left(\frac{k_h}{k_{hs}}\right) - 1\right] \ln\left(\frac{d_s}{d_w}\right) \qquad \text{(II.45)}$$

in which d_s is the diameter of the disturbed zone around the drain, k_{hs} is the coefficient of the horizontal permeability in this zone, and k_h or k_{h0} is the coefficient for the initial horizontal soil permeability.

Lastly, and since the prefabricated drains can also suffer a reduction on discharge capacity, it will be necessary to determine the hydraulic resistance of the drain, according with expression II.46, assuming that Darcy's law may also be applied to the vertical flow within the drain.

$$F_{(r)} = \pi (L_d - z) z \frac{k_h}{q_w} \qquad \text{(II.46)}$$

z is the distance considered from the top of the drain, L_d is the length of the drain and q_w is the drain discharge capacity for a unitary hydraulic gradient (i=1), given by:

$$q_w = k_w i A_w = k_w A_w \qquad \text{and} \qquad A_w = \pi r_w^2 \qquad \text{(II.47) and (II.48)}$$

where k_w is the coefficient of permeability of the drain and A_w the cross-section of the drain.

Finally, considering the sum of the three previous factors, and for $n \geq 20$, the μ will be:

$$\mu = \ln\left(\frac{d_e}{d_s}\right) + \left(\frac{k_h}{k_{hs}}\right) \ln\left(\frac{d_s}{d_w}\right) - \frac{3}{4} + \pi (L_d - z) z \frac{k_h}{q_w} \qquad \text{(II.49)}$$

yet:

$$\mu = \ln\left(\frac{n}{s}\right) + \left(\frac{k_h}{k_{hs}}\right) \ln(s) - \frac{3}{4} + 4 (L_d - z) z \frac{k_h}{k_w d_w^2} \qquad \text{(II.50)}$$

where the parameter (s) is the ratio between the diameter of the smear zone (d_s) and the diameter of the drain (d_w):

$$s = \frac{d_s}{d_w} \qquad \text{(II.51)}$$

If the drain flow is limited at the end, then L_d=H, becoming only half of this value (L_d=H/2) if the drainage can occur at both ends of the drains.

The Hansbo (1979) solution is generalised, and is the most used, due to its simplicity. The results obtained based on this solution do not differ much from the results obtained using more sophisticated solutions, determined using the finite element method (Onoue, 1988; Lo, 1991).

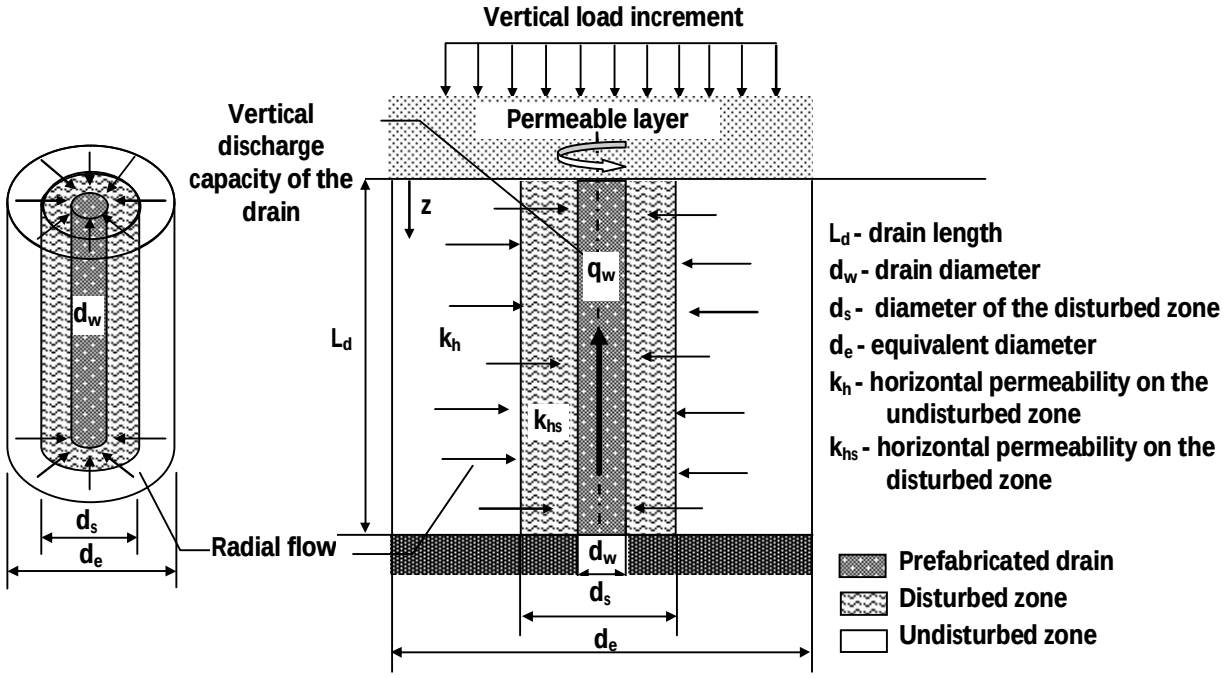

Figure II.7 – Exemplifying outline of the drain, of the disturbed zone (smear) and radial drainage

The validity of Darcy's law was questioned by several researchers, namely Silfverberg (1947), Hansbo (1960 and 1997a), Miller & Low (1963), and Dubin & Moulin (1986). In 1960, Hansbo adopted an exponential flow law in the theory for the consolidation of soil treated with vertical drains, and later, in 1986, Dubin & Moulin solved the solution for the vertical consolidation of a one-dimensional problem. Later, based on real scale field tests, performed in Sweden in 1960, Hansbo observed that the settlements calculated with an exponential flow law gave closer results to the measured data, although alerting that this may not be the only explanation, also referring the possible reduction in the consolidation coefficient throughout the consolidation process (Hansbo, 1997a).

II.4. ANALYTICAL SOLUTION - HORIZONTAL DRAINAGE (PLANE STRAIN ANALYSIS)

The finite element method (FEM) used for the analysis of soil consolidation including prefabricated vertical drains, with or without the application of preload embankments or others type of loads, are an unquestionable powerful tool if well employed. It allows the incorporation, not only of the construction phases gradually, but also the reinforcement elements if needed (Hird *et al.*, 1992). Its application in this type of analysis was study and investigated by Zeng *et al.* (1987 and 1989), Kumamoto *et al.* (1988), Sanchez & Sagaseta (1990), Cheung *et al.* (1990), Hird *et al.* (1992), followed by Indraratna & Redana (1997) and Chai & Miura (1999), among others.

The analysis of the phenomenon of the consolidation of the soil around a drain is a problem of an axisymmetric nature (three-dimensional 3D), however in real case works, and using two-dimensional (2D) software, the problem is considered in the plane strain state. This is an extremely important topic for designers and researchers, since appropriate adaptations are necessary in order to obtain an equivalent average degree of consolidations in both systems. In a two-dimensional analysis, the water flow in the soil is considered horizontal and not radial, and so it is necessary to convert the spatial system of the drains, on a wall of parallel vertical drains (Figure II.8) (Shinsha *et al.*, 1982). So, the spacing of the drains and the permeability coefficient in the area, where the drains were incorporated, must be adjusted for the plane strain. In a very simplified manner, a ratio between the two systems can be expressed by the equation II.52; however, the solutions currently used are those of Hird *et al*. (1992) and Indraratna & Redana (1997), which will also be presented in detail.

$$\frac{k_{hPD}}{k_{hAx}} = \Theta \frac{B^2}{r_e^2} \qquad \text{(II.52)}$$

where: k_{hPD} - Permeability coefficient in the plane strain;

k_{hAx} - Axisymmetric permeability coefficient;

Θ - Conversion coefficient between the two systems;

B - Half the width between two parallel and consecutive drains (axis to axis);

r_e - Equivalent radius of the drain influence diameter (related to the original pattern).

In 1992, Hird *et al*., proposed a method to incorporate the vertical drains in the analysis of problems in plane strain and, in 1995, presented new studies in which they confirmed the adequacy of this method.

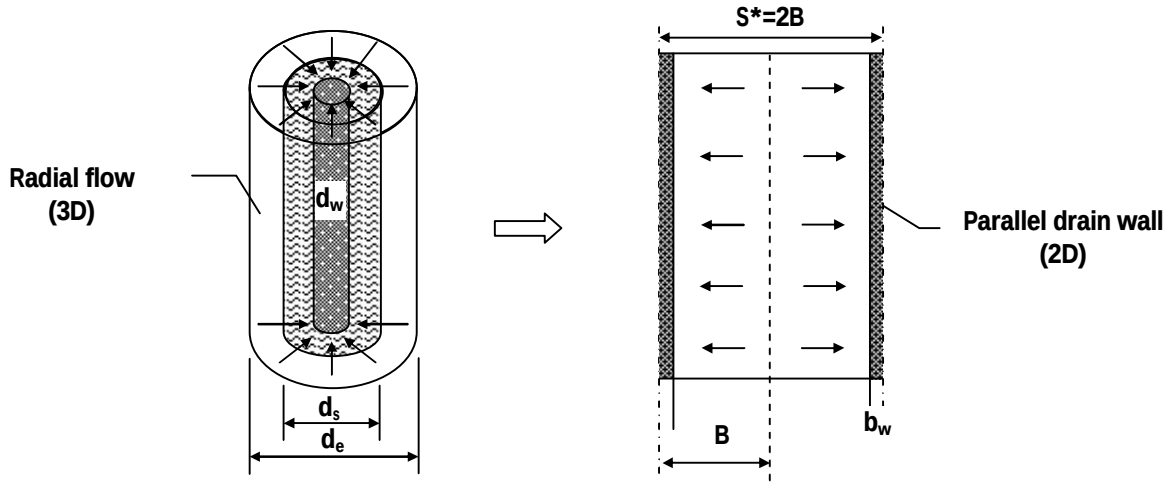

Figure II.8 – Conversion of the radial flow in a vertical drain for a wall of vertical drains, with geometric consideration of a disturbed zone, only in the axisymmetric system.

These researchers presented an analytical solution for the plane strain identical to Hansbo's solution for the axisymmetric consolidation of a soil cylinder in the surrounding of a vertical drain. This solution considerers both the effect of the disturbance of the ground due to the drain installation process, but also the discharge limitation of the drains. According to them, the average degree of consolidation in both system, plane strain (PD) and axisymmetric state (Ax), as to be equal, at any time and for each load level (Hird *et al*., 1995). Therefore:

$$\bar{U}_{hAx} = \bar{U}_{hPD} \qquad \text{(II.53)}$$

with:

$$\bar{U}_{hAx} = \bar{U}_r = 1 - e^{\left(-\frac{8T_{hAx}}{\mu_{Ax}}\right)} \quad \text{and} \quad \bar{U}_{hPD} = 1 - e^{\left(-\frac{8T_{hPD}}{\mu_{PD}}\right)} \qquad \text{(II.54) and (II.55)}$$

consequently, for the same time t, the match is obtained if:

$$\frac{8T_{hAx}}{\mu_{Ax}} = \frac{8T_{hPD}}{\mu_{PD}} \Leftrightarrow \frac{C_{hAx}t}{d_e^2\mu_{Ax}} = \frac{C_{hPD}t}{S^{*2}\mu_{PD}} \Leftrightarrow \frac{C_{hAx}}{4r_e^2\mu_{Ax}} = \frac{C_{hPD}}{4B^2\mu_{PD}} \Leftrightarrow \frac{k_{hAx}}{m_v\gamma_w r_e^2\mu_{Ax}} = \frac{k_{hPD}}{m_v\gamma_w B^2\mu_{PD}} \Leftrightarrow$$
$$\Leftrightarrow \frac{k_{hPD}}{k_{hAx}} = \frac{B^2}{r_e^2}\frac{\mu_{PD}}{\mu_{Ax}} \qquad \text{(II.56)}$$

Once again, the parameters μ_{PD} and μ_{Ax} express the effects associated with the spacing between the drains $F_{(n)}$, the smear effect $F_{(s)}$ and the hydraulic resistance of the drain $F_{(r)}$, for both plane strain and an axisymmetric state. The parameter μ_{Ax} will be given by the expression II.49 or II.50 (Hansbo, 1979), and the μ_{PD} parameter will be given by the equivalent expression, but for the plane strain (equation II.57).

$$\mu_{PD} = \frac{2}{3} + 2\left(L_d z - z^2\right)\frac{k_{hPD}}{Bq_{wPD}} \qquad \text{(II.57)}$$

Since no delimitation of the smear zone was considered in plane strain scheme, between the parallel drains, this means that, even though smear effect is considered in both systems, it is not geometrically represented in the drain parallel wall (Figure II.8).

Consequently the new horizontal coefficient of permeability calculated is extends to the entire area between parallel drains. Therefore, substituting the parameters μ_{Ax} and μ_{PD} in equation II.56, the relation between permeability coefficients is given by:

$$\frac{k_{hPD}}{k_{hAx}}=\frac{B^2}{r_e^2}\frac{\left[\frac{2}{3}+2\left(L_d z-z^2\right)\frac{k_{hPD}}{Bq_{wPD}}\right]}{\left[\ln\left(\frac{d_e}{d_s}\right)+\left(\frac{k_{hAx}}{k_{hsAx}}\right)\ln\left(\frac{d_s}{d_w}\right)-\frac{3}{4}+\pi\left(L_d z-z^2\right)\frac{k_{hAx}}{q_{wAx}}\right]} \qquad \text{(II.58)}$$

which is equivalent to:

$$k_{hPD}r_e^2\left[\ln\left(\frac{d_e}{d_s}\right)+\left(\frac{k_{hAx}}{k_{hsAx}}\right)\ln\left(\frac{d_s}{d_w}\right)-\frac{3}{4}+\pi\left(L_d z-z^2\right)\frac{k_{hAx}}{q_{wAx}}\right]=k_{hAx}B^2\left[\frac{2}{3}+2\left(L_d z-z^2\right)\frac{k_{hPD}}{Bq_{wPD}}\right] \qquad \text{(II.59)}$$

alternatively, even to:

$$k_{hPD}r_e^2\left[\ln\left(\frac{n}{s}\right)+\left(\frac{k_{hAx}}{k_{hsAx}}\right)\ln(s)-\frac{3}{4}+\pi\left(L_d z-z^2\right)\frac{k_{hAx}}{q_{wAx}}\right]=k_{hAx}B^2\left[\frac{2}{3}+2\left(L_d z-z^2\right)\frac{k_{hPD}}{Bq_{wPD}}\right] \qquad \text{(II.60)}$$

being: q_{wPD} - Discharge capacity of a drain in plane strain;

q_{wAx} - Discharge capacity of a drain in axisymmetric state;

k_{hsAx} - Permeability coefficient in the disturbed zone for axisymmetric state.

The compatibility between both the systems is ensured, as long as there is equivalence or correspondence, either in the discharge capacity of the drains (II.61) and in the soil consolidation (II.62).

$$\frac{k_{hPD}\pi r_e^2 k_{hAx}}{q_{wAx}}=\frac{k_{hAx}2B^2k_{hPD}}{Bq_{wPD}}\Leftrightarrow\frac{\pi r_e^2}{q_{wAx}}=\frac{2B}{q_{wPD}} \qquad \text{(II.61)}$$

$$k_{hPD}r_e^2\left[\ln\left(\frac{n}{s}\right)+\left(\frac{k_{hAx}}{k_{hsAx}}\right)\ln(s)-\frac{3}{4}\right]=\frac{2B^2}{3}k_{hAx} \qquad \text{(II.62)}$$

Replacing, in the equation II.61, the drain discharge capacities for a unitary hydraulic gradient, and adopting identical permeability in both systems ($k_{wPD}=k_{wAx}$), then b_w is given by:

$$q_{wPD}\pi\frac{d_e^2}{4}=S^*q_{wAx}\Leftrightarrow\ 2b_w.i.k_{wPD}\pi\frac{d_e^2}{4}=S^*\pi r_w^2.i.k_{wAx}\Leftrightarrow b_wk_{wPD}\frac{d_e^2}{2}=S^*r_w^2k_{wAx}\Leftrightarrow$$

$$\Leftrightarrow b_w=\frac{2S^*r_w^2}{d_e^2}\frac{k_{wAx}}{k_{wPD}}\Leftrightarrow b_w=\frac{2S^*r_w^2}{d_e^2} \qquad \text{(II.63)}$$

when particularizing for square and triangular patterns, the values are estimated by:

$$\text{square pattern: } b_w\approx\frac{2S^*r_w^2}{(1{,}128\,S)^2}\approx\frac{2S^*r_w^2}{1{,}2724\,S^2}\approx1{,}57\frac{S^*r_w^2}{S^2} \qquad \text{(II.64)}$$

triangular pattern: $$b_w \approx \frac{2S^* r_w^2}{(1{,}05\ S)^2} \approx \frac{2S^* r_w^2}{1{,}1025\ S^2} \approx 1{,}814 \frac{S^* r_w^2}{S^2} \quad \text{(II.65)}$$

To satisfy the equation II.62, three distinct methods can be applied, corresponding to:

a) 1st Hypothesis: Geometric correspondence - This is determined by assuming that the permeability coefficients in both systems are equal ($k_{hPD}=k_{hAx}$), and so the distance between drains on the plane strain depends on the real distance between the drains (II.66):

$$B^2 = \frac{3}{2} r_e^2 \left[\ln\left(\frac{n}{s}\right) + \left(\frac{k_{hAx}}{k_{hsAx}}\right) \ln(s) - \frac{3}{4} \right] \quad \text{(II.66)}$$

b) 2nd Hypothesis: Permeability correspondence - This is determined by assuming that the spacing between drains, in both systems are equal ($2B=d_e$), and the permeability coefficient in plane strain is (II.67):

$$k_{hPD} = k_{hAx} \frac{2}{3\left[\ln\left(\frac{n}{s}\right) + \left(\frac{k_{hAx}}{k_{hsAx}}\right) \ln(s) - \frac{3}{4} \right]} \quad \text{(II.67)}$$

c) 3rd Hypothesis: Combination of the two previous hypotheses - In this case a given spacing between drains is allowed for the plane strain and then the corresponding coefficient of permeability is calculated so that the equality of the systems is ensured (II.68).

$$k_{hPD} = \frac{B^2}{r_e^2} \frac{2}{3\left[\ln\left(\frac{n}{s}\right) + \left(\frac{k_{hAx}}{k_{hsAx}}\right) \ln(s) - \frac{3}{4} \right]} k_{hAx} \quad \text{(II.68)}$$

This last hypothesis is a more complex solution, nevertheless it guarantees greater equality between the two systems.

In 1997, Indraratna & Redana, incorporated the smear zone geometrically in the plane strain (Figure II.9), as well as also in the analytical solution.

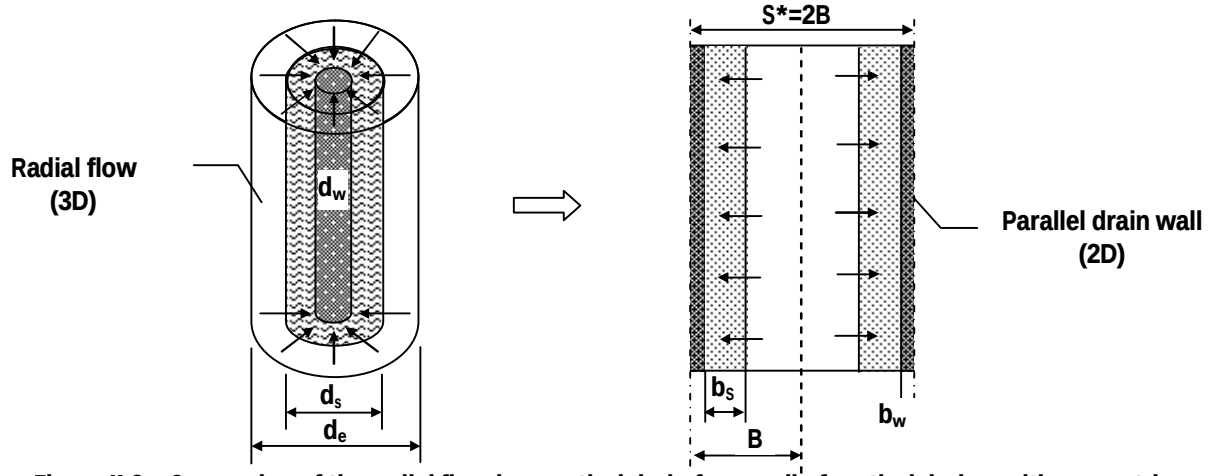

Figure II.9 – Conversion of the radial flow in a vertical drain for a wall of vertical drains, with geometric consideration of a disturbed zone, in both systems.

The base assumptions are kept, however the μ_{PD} parameter will be defined by the following equation (Indraratna & Redana, 1997):

$$\mu_{PD} = \alpha^* + \beta^* \left(\frac{k_{hPD}}{k_{hsPD}} \right) + \theta^* \left(L_d z - z^2 \right) \tag{II.69}$$

with: $$\alpha^* = \frac{2}{3} - \frac{4b_s^3}{3B^3} + \frac{2b_s^2}{B^2} - \frac{2b_s}{B} \tag{II.70}$$

$$\beta^* = -\frac{b_s^3}{3B^3} - \frac{2b_w^3}{3B^3} + \frac{b_w^2 b_s}{B^3} + \frac{b_s^2}{B^2} + \frac{b_w^2}{B^2} - \frac{2b_w b_s}{B^2} \tag{II.71}$$

$$\theta^* = \frac{2k_{hPD}^2}{Bq_{wPD}} - \frac{2b_w k_{hPD}^2}{B^2 q_{wPD}} \tag{II.72}$$

moreover, k_{hsPD} is the coefficient of permeability in the disturbed zone, in plane strain conditions.

Considering the μ_{PD} factor, defined by Indraratna & Redana (equation II.69), in equation II.56, then the general analytical solution to the problem, according to these researchers, will be:

$$k_{hPD} = k_{hAx} \left(\frac{\alpha^* + \beta^* \left(\frac{k_{hPD}}{k_{hsPD}} \right) + \theta^* \left(L_d z - z^2 \right)}{\ln\left(\frac{d_e}{d_s} \right) + \left(\frac{k_{hAx}}{k_{hsAx}} \right) \ln\left(\frac{d_s}{d_w} \right) - \frac{3}{4} + \pi \left(L_d z - z^2 \right) \frac{k_{hAx}}{q_{wAx}}} \right) \frac{B^2}{r_e^2} \tag{II.73}$$

which is equivalent to:

$$k_{hPD} = k_{hAx} \left(\frac{\alpha^* + \beta^* \left(\frac{k_{hPD}}{k_{hsPD}} \right) + \theta^* \left(L_d z - z^2 \right)}{\ln\left(\frac{n}{s} \right) + \left(\frac{k_{hAx}}{k_{hsAx}} \right) \ln(s) - \frac{3}{4} + 4z(H - z) \frac{k_{hAx}}{k_{wAx} d_w^2}} \right) \frac{B^2}{r_e^2} \tag{II.74}$$

on the other hand, even to:

$$k_{hPD} r_e^2 \left[\ln\left(\frac{n}{s} \right) + \left(\frac{k_{hAx}}{k_{hsAx}} \right) \ln(s) - \frac{3}{4} + \pi \left(L_d z - z^2 \right) \frac{k_{hAx}}{q_{wAx}} \right] = k_{hAx} B^2 \left[\alpha^* + \beta^* \left(\frac{k_{hPD}}{k_{hsPD}} \right) + \theta^* \left(L_d z - z^2 \right) \right] \tag{II.75}$$

If the discharge capacity is high, this parameter can be disregarded and the solution is simplified to:

$$k_{hPD} = k_{hAx} \left(\frac{\alpha^* + \beta^* \left(\frac{k_{hPD}}{k_{hsPD}} \right)}{\ln\left(\frac{n}{s} \right) + \left(\frac{k_{hAx}}{k_{hsAx}} \right) \ln(s) - \frac{3}{4}} \right) \frac{B^2}{r_e^2} \tag{II.76}$$

On the other hand, ignoring the smear effect but including the discharge capacity, the solutions turns out:

$$k_{hPD} = k_{hAx}\left(\frac{\left(\frac{2}{3}-\frac{4b_w^3}{3B^3}+\frac{2b_w^2}{B^2}-\frac{2b_w}{B}\right)+\theta^*\left(L_d z-z^2\right)}{\ln(n)-\frac{3}{4}+4z(H-z)\frac{k_{hAx}}{k_{wAx}d_w^2}}\right)\frac{B^2}{r_e^2} \qquad \text{(II.77)}$$

as $k_{hsAx}=k_{hAx}$, $k_{hsPD}=k_{hPD}$, $b_s=b_w$, $r_s=r_w$, which implies that s=1 and ln(s)=0.

When none of the previous effects are taken into account, then estimations of the plane strain permeability coefficient is considerably simplified (II.78).

$$k_{hPD} = k_{hAx}\left(\frac{\left(\frac{2}{3}\right)}{\ln(n)-\frac{3}{4}}\right)\frac{B^2}{r_e^2} \Leftrightarrow \quad k_{hPD} = \frac{2k_{hAx}}{3\left[\ln(n)-0,75\right]}\frac{B^2}{r_e^2} \qquad \text{(II.78)}$$

II.5. ANALYTICAL SOLUTION - COMBINED DRAINAGE

When vertical drains are used, one must consider the vertical drainage direction in addition to the horizontal drainage direction. The simultaneous occurrence of the two drainages is called combined flow. This phenomenon was studied by Carrillo (1942), whom applied the separation of variables method. Therefore, the average degree of consolidation of a soil layer will be given by:

$$(1-\bar{U}) = (1-\bar{U}_v)(1-\bar{U}_r) \qquad \text{(II.79)}$$

The contribution of vertical drainage in this type of solution is significant for compressible soil layers with thicknesses of less than 10 metres (Vertematti *et al.*, 2004; Vairinhos, 2013).

II.6. VISCOSITY OF FINE SOILS

The viscosity of fine soils (creep) is a factor, which must be considered in the analysis of consolidation over time, and the corresponding strains are designated as secondary consolidation settlements. Generally, it is assumed that secondary consolidation settlement may correspond to a percentage of the primary consolidation settlement. Therefore, soil that has high values for hydrodynamic consolidation will have significant settlements associated to creep, hence, it is extraordinarily important to consider this aspect in the consolidation analyses.

This phenomenon may be observed in oedometer tests, as long as the evolution of the settlements during the 24 hours, in which a given increase in stress is applied, is carefully measured. Given the small thickness of the samples, it is usual that almost all of the primary consolidation occurs in the first hours, even in soil with very low permeability. Therefore, during the remaining time, the settlements correspond to phenomenon of consolidation under creep effect, even if one does not have this perception. In these tests, the relation of the strain with time only becomes obvious when the primary consolidation ends (Figure II.10); however, this does not mean that the phenomenon has not initiated before the conclusion of the primary consolidation (Bjerrum, 1967).

According to Mesri (1973), secondary consolidation settlement s_{sc} may be estimated based on the expression:

$$s_{sc} = \frac{H}{1+e_0} \cdot \left(C_\alpha \log \frac{t'}{t_c} \right) \tag{II.80}$$

where: t_C - is the time that corresponds to the end of the primary consolidation;

t'- is the time that corresponds to real time of the secondary consolidation;

C_α- is the secondary compressibility index, obtained based on the oedometer test.

The C_α parameter represents the slope of the curve on the graph (*e; log t*) for a given load increment, once it has been considered that the "total" dissipation of the excess pore pressure has occurred (primary consolidation), and given by:

$$C_\alpha = \frac{\Delta e}{\Delta \log(t)} = \frac{e_E - e_F}{\log(t_F) - \log(t_E)} = \frac{e_E - e_F}{\log \frac{t_F}{t_E}} \tag{II.81}$$

The magnitude of this settlement will depend on C_α and also on the ratio between t'/ t_C.

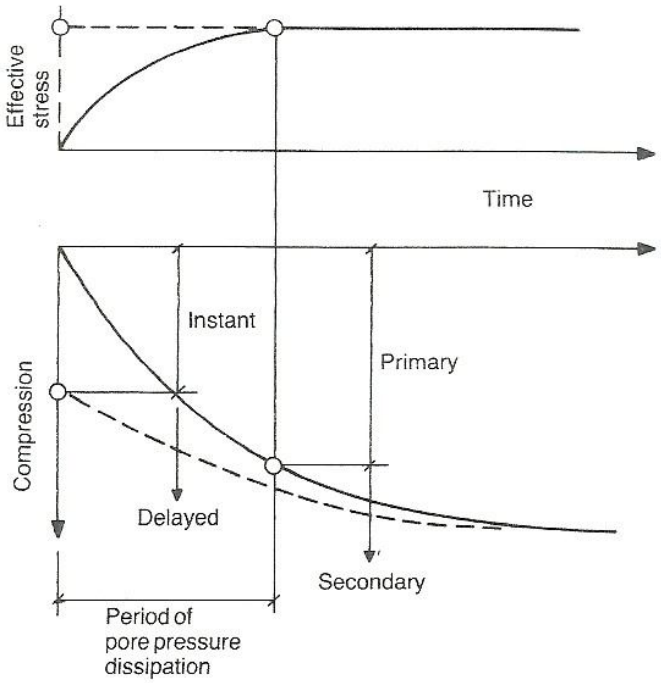

Figure II.10 – Definition of instantaneous settlement, primary settlement and secondary settlement, for a constant load (Bjerrum,1967)

Mesri & Godlewski (1977) observed that, for any loading stage, the ratio between the secondary compressibility index (C_α) and compressibility index (C_c), as well as between secondary compressibility (C_α) and recompressibility (C_r), were constant. According to them, the magnitude and the soil behaviour in the secondary consolidation phase are directly related to the magnitude of C_c and C_r, and with the ratio between the final effective vertical stress and the effective preconsolidation stress. Therefore, C_α remains constant, decreases or increases with time, to a given

final effective vertical stress value (σ'_f), in accordance with its positioning on the graph (*e; log*σ'), which means that there is a dependency or a ratio between these parameters. The positioning of the final effective vertical stress, in relation to the effective preconsolidation stress (σ'_p), is crucial and determines this evolution. In consequence, the three scenarios can occur:

a) When σ'_f is located on the recompression curve ($\sigma'_f / \sigma'_p < 0,7$), the time of the primary consolidation (t_c) is small, as it is C_r, and the secondary settlements will not be significant, being $C_\alpha = \vartheta C_r$;

b) When σ'_f is close to the effective preconsolidation stress σ'_p, the time of the primary consolidation may also be small, but in this case there is a transition from the recompressibility curve to the primary compression curve (passage from C_r to C_c), and so there are two secondary compressibility indexes, with $C_{\alpha 1} = \vartheta C_r$ and $C_{\alpha 2} = \vartheta C_c$. As a result the settlements for secondary compression become significant (Mesri *et al.*, 1997);

c) When σ'_f is on the primary compression curve, the secondary consolidation settlements will be very significant, since C_α will also be very high since it only depends on the value of the compressibility index C_c, or in other words $C_\alpha = \vartheta C_c$.

The ratios between the secondary compressibility index and the compressibility or recompressibility indexes, for geotechnical materials, are given in table II.1.

Table II.1 – Parameter ϑ for several types of soil (Terzaghi *et al*., 1996)

Type of soil	$\vartheta = C_a/C_r = C_a/C_c$
Gravels and sand	0.02± 0.01
Schist and mudstone	0.03± 0.01
Inorganic clays and silts	0.04± 0.01
Organic clays and silts	0.05± 0.01
Peat	0.06± 0.01

The compressibility concept described above is, for simplification purposes, denominated by ratio C_α versus C_c or C_r, as these ratios are constant, both in the compression phase and in the recompression phase. In 1992, Fox *et al*. also analysed this concept, applying it to peat.

Special attention must be given to secondary settlements in the analysis of dams and dikes founded in this type of soft soil, and also in foundations. Even in overconsolidated soils, once the final effective vertical stress exceeds the preconsolidation vertical stress, then the situation described above occurs. The primary consolidation settlement value is small, but the secondary consolidation settlement may be high (Soriano, 2005; PLAXIS 2D-V11.02, 2012). Such cases are very dangerous as there is no significant primary consolidation settlement before, which might indicate the settlement, which follows (PLAXIS 2D-V11.02, 2012).

Buisman (1936) was the first researcher to propose a constitutive law, taking into account the creep phenomenon of soft clay soils, after observing that the settlements of compressible soils were not fully explained by the classic consolidation theory. This law was developed for problems with

unidirectional flow, such as the Terzaghi's theory, being continued by Bjerrum (1967), Garlanger (1972), Mesri & Godlewski (1977) and Leroueil (1977) some decades later.

Mesri & Godlewshi, in 1977, mentioned that there is no logical reason to separate the consolidation phenomena into the mechanisms of volume variation, due to the change in the effective vertical stress, from the volume variations at constant load over time. According to Hawlader *et al*. (2002), primary consolidation should be viewed as the load phase during which the hydrodynamic effect overlaps the creep effect. In a second phase, consolidation due to the hydrodynamic effect decreases substantially, and settlements are due to the creep effect with time. Hansbo (1997b) also recommends that the creep effect be considered in the primary consolidation phase.

In 1981, Pilot mentioned that the creep effect in clayed soil was often ignored in the analyses of consolidation incorporating vertical drains, in spite of the fact that it was a phenomenon already well known. In 2002, Hawlader *et al.* led a study on soil treated with prefabricated vertical drains, considering both the creep and the smear effect, concluding that the influence of creep in the consolidation of clayed soil has greater significance when the drains are quite far apart, and is much lower when the drains are relatively close. However, during this study, it was observed that the consideration of the creep effect is significant even if the drains are relatively close.

Constitutive models, which include creep in the primary consolidation, were developed by (Kabbaj *et al.*, 1986; Murakani, 1988; Yin & Graham, 1989; Kutter & Sathialingam, 1992). Some were formulated based on time and others on the strain rate.

The PLAXIS V02.2011 software also provides a material model that considers the viscosity or creep of the soft soil, which will be presented in the following chapter.

III. MATERIAL MODELS

This chapter is dedicated to the material models and the constitutive laws used to describe the soil behaviour, and their response towards several solicitations.

With the advances in computer science and the computational resources available, the numerical calculation methods evolved, being used more and more. Their main purpose is to anticipate the response of the materials and structures, and therefore optimise the engineering construction techniques as well as the design methods, analyse accidents or incidents occurred in the construction or pos-constructive phases, exceed the limits of approximate calculation methods and also exceed the limits of the exact methods which do not cover complex situations. For these reasons, software, which uses the finite elements method (FEM), were developed and enhanced in the recent years, with increased application on geotechnical design. The FEM allows the consideration of geometries that are more complex, non-linear elastic, elastoplastics, viscoelastics or viscoplastics models, to traduce the soil behaviour, and other phenomena, such as time, water seepage or dynamic actions.

For the reasons given, this method is currently considered as the one, which provides greater reliability in the forecasting of the global behaviour of structures. This statement is correct as long as the following conditions are met: a) suitable characterisation of the materials, namely their strength, strain and permeability parameters; b) adequate geometric discretization of the problem, with well-defined boundary conditions and restrictions; c) representation of the discontinuities and heterogeneities of the medium; d) adoption of material models which can traduce the soils response reasonably well; e) correct characterisation of the drainage and flow conditions, in the presence of water.

Among the various finite element programmes currently available on the market, some are especially suitable for geotechnical purposes, allowing the modelling of both laboratory and *in-situ* tests, and geotechnical problems, being PLAXIS one of them. This software was developed by Delft University, in the Netherlands, and it has been updated and optimised since then. The work developed in this thesis was carried out using the second 2D version of 2011, which was released in May 2012.

Due to the aspects mentioned above, and following the theme covered previously (consolidation), this chapter will begins with the presentation of some simple constitutive laws, later moving onto more complex ones. Greater emphasis will be given to the material models, which are able to traduce the response of fine saturated soils, facing problems of primary and secondary or creep consolidation settlements. The mathematical modelling of the behaviour of these soils is complex, yet it is essential for the correct analysis of the associated deformations, since it is usual to found on these types of soils.

Therefore, the main objective will be to present some of the models available in the Plaxis software, namely the Mohr-Coulomb, Soft Soil and Soft Soil Creep models, as they will be used in the modelling of the *Lebrija* Pond Dikes No.1 and No.3.

III.1. INTRODUCTION

The soil is considered a particulate medium, composed of solid, liquid and gas phases, and for this reason its behaviour presents additional complexity, conferred by its nature and origins. Therefore, the laboratory and in-situ test are, and will always be, an important base to describe the behaviour of geotechnical materials. In more complex situations, such as those observed in real cases, the model considered for a specific soil should be supported by laboratory tests, such as oedometer and triaxial test. Therefore, and based on these same tests, one can establish a set of mathematical relations in order to describe the soil response, called constitutive laws, whose variables and constants indicate physical soils aspects and parameters, which are measurable or deductible.

Nowadays, on geotechnical problems, it is common to use stress-strain analyses in addition to stability analysis, in order to avoid the limitation of confining the design analysis to ultimate limit states, i.e., soil rupture (Mateus da Silva, 1996). In this perspective more complex mathematical models continue to be investigated and developed, with the purposes of traducing the soil behaviour more accurately. However, the models used to define the behaviour of materials must always find a commitment between the response capacity of the model, and the number of parameters needed to define it; in other words, it is not worth using more advanced models if the parameters are too theoretical or difficult to determine.

III.2. BEHAVIOUR MODELS

III.2.1. ELASTIC BEHAVIOUR

An elastic response of a material is easier to describe and to understand than a plastic response. In the first one, the material can recover to the initial state, while on the second one the material may suffer irrecoverable strains. This is the reason why the linear elastic model was the first to be developed, and was the most used, until the development of hardware and software, which allowed the current use of more demanding mathematical models.

The linear elastic model defines a bi-univocal relation between the stress and the strain, so there is no dependency between the history of the stress or strain and the response of the material. This relation, designated by Hooke's generalised law, describes the capacity of a body to recover its original shape when the action that caused the deformation ceases, which defines the elasticity of a material (Tovar de Lemos, 1990). Mathematically, and in general, the model can be traduced by:

$$\sigma_{ij} = C_{ijkl} \cdot \varepsilon_{kl} + \sigma^{o}_{ij} \qquad \text{(III.1)}$$

where σ_{ij} and ε_{kl} represent, respectively, the stresses and strains tensors, σ^{o}_{ij} the initial stresses tensors and C_{ijkl} a 4^{th} order tensor called elasticity tensor.

If the initial condition of the material body is the neutral state, meaning that it is free from stress when not subjected to any strain, the Hooke's model will be given by:

$$\sigma_{ij} = C_{ijkl} \cdot \varepsilon_{kl} \qquad \text{(III.2)}$$

For the simplest case, meaning for a homogenous and isotropic material, the number of parameters independent of the elasticity tensor is reduced to only two elastic constants, namely the Young or Elasticity (E) modulus and the Poisson coefficient (ν). In this case, when performing an analysis on the xy plane, the soil strains would be determined by the equations below:

$$\varepsilon_{yy} = \frac{\sigma_{yy}}{E} \qquad \text{and} \qquad \varepsilon_{xx} = \nu \cdot \varepsilon_{yy} \qquad \text{(III.3) and (III.4)}$$

These constants are easily understood as they can be deduced from experimental observation (Figure III.1a); however, in many cases, is preferable to use the alternative pair, volumetric strain modulus (K) and distortional strain modulus (G), this last one called in a simplified form as distortional modulus. These last two parameters allow the decomposing of the elastic strain on a purely volumetric part, a variation of the volume maintaining the original shape (Figure III.1b), and in another part purely distortional, a change in shape without volume change (Figure III.1c).

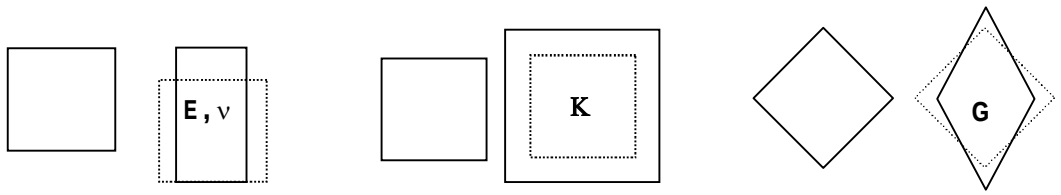

Change in shape and in volume **1a)**

Constant shape with change in volume **1b)**

Constant volume with change in shape **1c)**

Figure III.1 Schematic representation of the Young module (E) and the Poisson coefficient (ν), of the volumetric strain module (K) and the distortion module (G) (Wood, 1990)

The relations between the volumetric strain modulus and the distortion modulus with the Young modulus and the Poisson coefficient are given by expressions III.5 and III.6:

$$K = \frac{E}{3(1-2\nu)} \quad , \qquad G = \frac{E}{2(1+\nu)} \qquad \text{(III.5) and (III.6)}$$

The benefit of using the volumetric strain and distortion modulus becomes more evident on the elastic behaviour of saturated soil in undrained conditions, since the strain is especially related to the soil strain at constant volume, meaning that there is only purely distortional strain (change in shape without a variation in the volume). This occurs because water is considered an incompressible material, meaning ν=0.5.

III.2.2. PLASTIC BEHAVIOUR

The need to consider, behaviours more realistic and adequate to other type of materials, associated with the incapacity of the elastic models, to describe conveniently the behaviour of the materials, especially in situations close to failure, inevitably lead to the formulation of more complete models.

Even the non-linear elastic models, such as the K-G model and the hyperbolic model, which have allowed significant improvement in describing the soil behaviour, do not allow, for example, the permanent strains, which occur when a structure is discharged after being subjected to a load above a certain limit. In addition to this, the elastic models cannot describe the soil response for high stress levels, thereby invalidating their application in the analysis of ultimate limit states.

New models, plastic and elastoplastic, were developed in order to incorporate some characteristics which get much closer to the real materials. The complexity of these models may not be much greater than those of certain elastic models, but are sometimes more intuitive. The formulation of a theory with plastic behaviour is based on three fundamental concepts, yielding, hardening and flow.

III.2.2.1. YIELDING AND YIELD FUNCTION

Yield is observed when a material body reaches a state where irreversible strains occur, called plastic strains. Before plastic strain occurs, the material may present a linear or non-linear elastic behaviour or rigid. The practical observation of the yield stress may be obtained based on several compression tests, in which the load is applied to the body and the resulting strains measured. The body is then submitted to an unload-reload process and it is then possible to measure the plastic strain component and the yielding value corresponding to the previous stress state. The start of the yielding is determined through a function of yield. The yield function is a scalar function which depends on the stress state (invariant stresses, principal stresses and stress components) and which indicates the beginning of the appearance of permanent strains, i.e. plastic strains (Figure III.2). This function may be symbolically described as $F(\sigma)=0$ (Naylor *et al*., 1981).

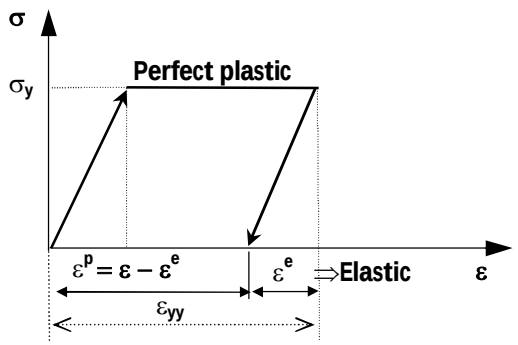

Figure III.2 - Stress-strain relation for a perfect elastoplastic material

If this function is represented in a spatial stress state, one obtains a surface which is called the yield surface; inside this surface the material behaviour is elastic - referred as the elastic domain - $F(\sigma)<0$, while by convention positive values are not allowed- $F(\sigma)>0$ (Figure III.3). In this last situation, and since it is impossible to have a stress state exterior to the yield surface, then this suffers an "expansion" in order to embrace this new stress state, causing what is called the hardening of the yield surface.

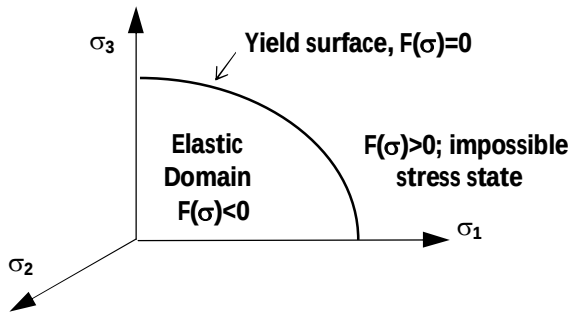

Figure III.3 - Representation of the yield surface in the spatial stress space

Regarding the yield functions, in Soil Mechanics, it is common to use the following criteria (Naylor *et al.*, 1981):

Tresca Criterion – Yield function of cohesive type. Suitable for materials whose yield behaviour is regarded as purely cohesive, as the typical cases of saturated clay soils in undrained conditions, and depends only on the undrained cohesion (c_u). The yield criteria occur when the Mohr circle, which represents the stress state applied to the soil, is tangential to the Tresca yielding surface (Figure III.4).

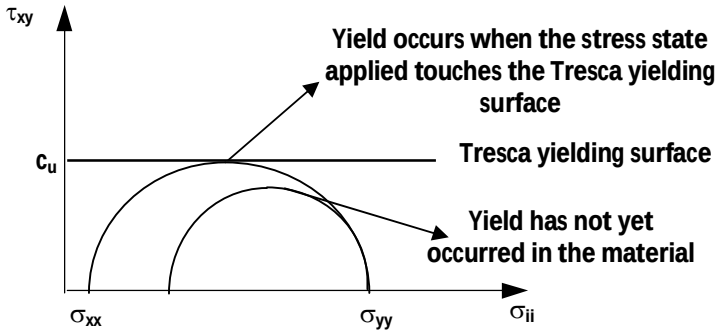

Figure III.4 – Yield function for cohesive materials (Tresca Criterion)

The yield function may be described, for a plane strain and in terms of the stress components, in the following manner:

$$F\left(\sigma_{xx},\sigma_{yy},\tau_{xy}\right)=\sqrt{\left(\sigma_{xx}-\sigma_{yy}\right)^2+4\tau_{xy}{}^2}-2c_u=0 \qquad \text{(III.7)}$$

moreover, considering them expressed according to the stress invariants for the plane strain (σ_s and σ_t), they change into:

$$F\left(\sigma_s,\sigma_t\right)=\sigma_t-2c_u=0 \qquad \text{(III.8)}$$

where:

$$\sigma_s=\frac{\sigma_1+\sigma_3}{2} \text{ is the principal stress in a plane strain;} \qquad \text{(III.9)}$$

$$\sigma_t=\sigma_1-\sigma_3 \text{ is the maximum shear stress in a plane strain.} \qquad \text{(III.10)}$$

Mohr-Coulomb Criterion – Yield function of frictional type. Suitable for materials whose yield behaviour is considered as frictional and cohesive, and thus depending on the internal friction angle of the soil (φ) and its cohesion (c). The yield criterion occurs when the stress state is such, that the Mohr circle touches the Mohr-Coulomb yielding surface or failure condition (Figure III.5).

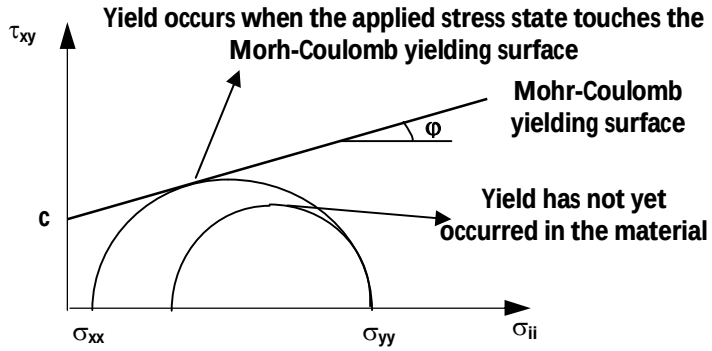

Figure III.5 – Yield function for frictional and cohesive materials (Mohr-Coulomb Criterion)

In this case, the yield criterion may be described, for a plane strain, as:

$$F\left(\sigma_{xx},\sigma_{yx},\tau_{xy}\right)=\sqrt{\left(\sigma_{xx}-\sigma_{yy}\right)^2+4\tau_{xy}{}^2}-\left(\sigma_{xx}+\sigma_{yy}\right)\cdot\sin\varphi-2c\cdot\cos\varphi=0 \qquad \text{(III.11)}$$

being also possible to express it base on the stress invariants, according to:

$$F\left(\sigma_s,\sigma_t\right)=\sigma_t-2\sigma_s\cdot\sin\varphi-2c\cdot\cos\varphi=0\,, \qquad \text{(III.12)}$$

One of the limitations of these criteria is related to the fact that one cannot consider the influence of the intermediate stress (σ_2).

III.2.2.2. HARDENING LAW

The yield causes changes to the microstructure that are macroscopically traduced by changes in the measurable variables, namely the combination of stresses that determine the start of the yield process. The phenomenon that leads to the change in this stress combination is called hardening. The relation between the plastic strains and the increase of the yield stress is designated as hardening law. This relation is a function of the type $F(\sigma,\chi)=0$; once again if $F(\sigma,\chi)< 0$ then the material response is elastic, and when $F(\sigma,\chi)> 0$ the stress condition is considered impossible (Maranha das Neves & Guedes de Melo, 1975). χ is a parameter that expresses the hardening or softening of the soil.

As for the evolution of the yield stress with the increase of plastic strains, three different situations may occur (Figure III.6):

a) Increase in the yield stress $\Rightarrow$ Elastoplastic law with hardening;

b) Reduction in the yield stress $\Rightarrow$ Elastoplastic law with softening;

c) Yield stress at a constant value $\Rightarrow$ Perfect elastoplastic law.

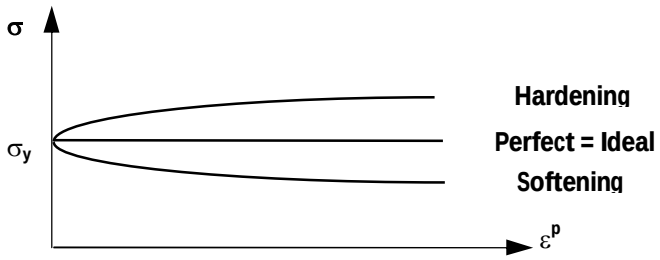

Figure III.6 – Representation of the variation of the yield stress with plastic strain

When a material as associated a yield function of the hardening type, then there is an increase in the zone where the response is elastic; the materials with a softening yield function presents the opposite behaviour. In both situations, this kind of yield functions implies a modification in the material behaviour, increasing or reducing the stress state associated to the yielding.

III.2.2.3. FLOW RULE

The flow rule for the plastic material gives the ratios of the plastic strain increments when the material is yielding in a particular stress state, as well as theirs direction or orientation for each stage. Therefore, the calculation of plastic strain increments depends on this rule, which is given by the mathematical equation III.13.

$$\delta\varepsilon^{p} = \chi \cdot \frac{\partial Q(\sigma,\zeta)}{\partial\sigma}, \qquad \text{(III.13)}$$

where $\delta\varepsilon^{p}$ represents the plastic strain increments, Q is the plastic potential function and ζ the parameter, which controls the size or dimension of the surface of the plastic potential. If the previous equation is plotted in the principal stress space, it can be seen that the vector, which defines the direction of these increments in plastic strain, is normal to the plastic potential surface (Brito & Gunn, 1987).

For many materials, it is observed that the yield function and the plastic potential function are equal, being the direction of the plastic strain increments also normal to the yield function. When this happens then it is often said that the "normality condition" holds, and the flow rule is called as an "associated" (Figure III.7a). In this case, the expression of the flow rule becomes:

$$\delta\varepsilon^{p} = \chi \cdot \frac{\partial F(\sigma,\chi)}{\partial\sigma}, \qquad \text{(III.14)}$$

If the yield function and the plastic potential function are not the same, then the flow rule is called as a "non-associated" flow rule, and the plastic strains increments are just normal to the plastic potential function (Figure III.7b).

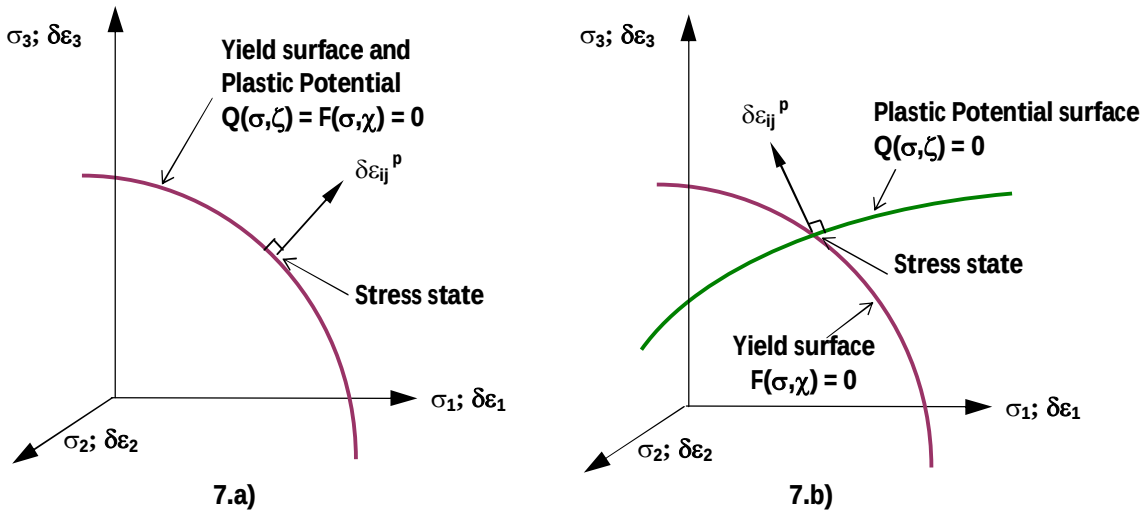

Figure III.7a) – Representation of an "associated" flow rule and the "normality condition";
III.7b) – Representation of a "non-associated" flow rule and the "normality condition".

III.2.2.4. EQUILIBRIUM: STABILITY AND INSTABILITY

It is extremely important not to confuse Drucker's principle of normality with Drucker's principle of stability (1954, 1966) which says that, for a material subjected to a given state of stress, imposed by an external agent, the work produced by this agent, in the corresponding displacement (d), must be positive or equal to zero. However, it must be noted that the principle of stability implies the existence of normality, even though the opposite is no longer true (Wood, 1990).

Taking, for example, a saturated soil sample, subject to a load-unload cycle, and observing the relation between the load increments and the respective displacements for different conditions, the following situations may occur:

a) The OP path described in figure III.8a represents the slow application of a load increment δX_i, which leads to a slow compression, thereby allowing the absence of excessive pore pressure of the soil sample. The OP path represents, in turn, the slow removal of the same load, and the occurrence of a slow expansion of the soil is observed. It is clear that in P, the external agent slowly transferred a quantity of work equal to $\frac{1}{2}\delta X_i \cdot d$ to the system, and that at the end of the OPO cycle this work was fully recovered;

b) In contrast, the OQ path indicated in figure III.8b represents the fast application of a load increment δX_i, thereby an excess of pore pressure (Δu) is registered. This excess gradually dissipates and when it reaches R, it is null. During the QR transition, the work transferred by the system is $\delta X_i \cdot d$, with half being dissipated in the system by trying to accelerate the outflow of water from the soil (OQR area) and the other half is stored in the sample (ORS area). The RS path represents a fast removal of the load increment. In this phase a negative gradient pore pressure is observed, which quickly sucks the remaining water from the sample and, at the end of the cycle, the work which was temporarily stored has been completely dissipated;

c) The most common case is represented in figure III.8c, in which permanent strains occur. In this case, the total displacement is separated in an elastic component (d^e), which corresponds to the part that is recovered after the removal of the load, and in a plastic component (d^p), which corresponds to the permanent displacement. If the soil presents a rigid behaviour, then $d^e=d^p=0$ and no change occurs. If the soil presents an elastic behaviour, then $d^p=0$ and all the displacements are recoverable without the occurrence of work transference to the system. If the soil does not completely recover from the displacements suffered at the start, or in other words $d^p>0$ (in the case of material with plastic behaviour), then the quantity of the work transferred to the system is given by the OUT area (Schofield & Wroth, 1968).

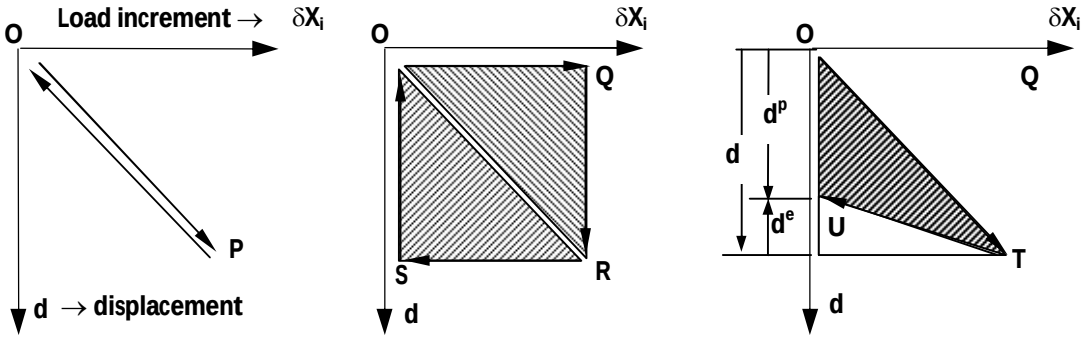

Figure III.8 - Work carried out during the load-unload cycle for saturated soil (Schofield & Wroth, 1968)

In any of these three hypotheses, the system always verified the stability criterion, or in other words, Drucker's stability principle (1954). This is mathematically represented by the expression:

$$\sum \delta X_i \cdot d_i^p \geq 0 \qquad \text{(III.15)}$$

in which d_i^p is the increment in plastic strain, associated with the respective load increment δX_i. Therefore, it is possible to define three distinct types of responses, respectively:

a) Stable System - whenever the condition $\sum \delta X_i \cdot d_i^p > 0$ is satisfied;

b) Unstable System - whenever the condition indicated in equation III.15 is not verified;

c) Neutral System - whenever the condition $\sum \delta X_i \cdot d_i^p = 0$ is assured;

III.2.3. ELASTOPLASTIC BEHAVIOUR

The soil generally presents behaviours that correspond, in good measures, to the standards described by the elastoplastic models. To fully describe the stress-strain relations for an elastoplastic material, it is necessary to consider and specify the four conditions previously introduced. Now it is only necessary to group them in order to obtain the relation between the stresses and strains, or between their increments:

a) The elastic behaviour, i.e., the elastic parameters which describe the elastic relation between stress and strain (Wood, 1990);

b) The yield function and the definition of the stress state correspondent to the beginning of plastic strains ;

c) The flow rule;

d) The hardening law.

The strains corresponding to this type of material behaviour, are separate into elastic plastic terms, meaning:

$$\varepsilon_{kl} = \varepsilon_{kl}^{e} + \varepsilon_{kl}^{p} \tag{III.16}$$

Considering that the formulation is made from the point of view of the incremental strains, then the anterior expression is formulated as:

$$\delta\varepsilon_{kl} = \delta\varepsilon_{kl}^{e} + \delta\varepsilon_{kl}^{p} \tag{III.17}$$

with the elastic and plastic component of the strain given, respectively, by:

$$\delta\varepsilon_{kl}^{e} = C_{ijkl}^{e} \cdot \delta\sigma_{ij} \tag{III.18}$$

$$\delta\varepsilon_{kl}^{p} = C_{ijkl}^{p} \cdot \delta\sigma_{ij} \tag{III.19}$$

The determination of the elastic strains increments are performed based on the elasticity theory, already described, and the strain corresponding to the plastic part is obtained in accordance with the expression III.13, which can be re-written as:

$$\delta\varepsilon_{kl}^{p} = \chi \cdot \frac{\partial Q(\sigma,\zeta)}{\partial\sigma_{ij}}, \tag{III.20}$$

being necessary to known the hardening or softening parameter value (χ).

The determination of χ is done for the yield condition, taking into consideration expression III.17 and III.20, and that the stress increment $\delta\sigma_{ij}$ must always result in the condition of $F(\sigma,\chi)=0$, as the stress state cannot be exterior to the yield surface. According to the procedure indicated by Naylor *et al.* (1981) and by Mateus da Silva (1996), the expression that allows one to know the value of the scalar χ with the strain increment $\delta\varepsilon_{kl}$, is:

$$\chi = \frac{\dfrac{\partial F}{\partial\sigma_{ij}} + \left(\dfrac{3K-2G}{6G}\right)\delta_{ij}\left(\dfrac{\partial F}{\partial\sigma_{ij}}\delta_{ij}\right)}{\left(\dfrac{3K-2G}{6G}\right)\left(\dfrac{\partial Q}{\partial\sigma_{mn}}\delta_{mn}\right)\left(\dfrac{\partial F}{\partial\sigma_{ij}}\delta_{ij}\right) + \dfrac{\partial Q}{\partial\sigma_{ij}}\dfrac{\partial F}{\partial\sigma_{ij}}}\delta\varepsilon_{kl} \tag{III.21}$$

Now introducing the concept of mean effective stress or isotropic stress (p′) and distortional or deviator stress (q), which represents the stress invariants and are given by the expressions:

$$p' = \frac{\sigma_1' + \sigma_2' + \sigma_3'}{3} \tag{III.22}$$

$$q = \sigma_1' - \sigma_3' \tag{III.23}$$

and applying this same procedure, but in terms of the stress invariants increments $\delta p'$ and δq, it is demonstrate bellow, how to obtain the plastic stress-strain increments, dependent of the plastic potential and yield functions. The corresponding irreversible strains or plastic strains increments, will be designated by $\delta\varepsilon_p^p$ and $\delta\varepsilon_q^p$.

Assuming that the yield function is described by:

$$F(p', q, p'_0) = 0 \tag{III.24}$$

where p'_0 is the parameter that indicates the increase of the yield surface. If represented in a differential form, it becomes:

$$\frac{\partial F}{\partial p'}\delta p' + \frac{\partial F}{\partial q}\delta q + \frac{\partial F}{\partial p'_0}\delta p'_0 = 0 \tag{III.25}$$

If it is assumed that the size of the yield surface, i.e., the increase of p'_0, is related to both plastic strain increments, in accordance with the hardening law:

$$\delta p'_0 = \frac{\partial p'_0}{\partial \varepsilon_p^p}\delta\varepsilon_p^p + \frac{\partial p'_0}{\partial \varepsilon_q^p}\delta\varepsilon_q^p \tag{III.26}$$

that the plastic potential function is defined by:

$$Q(p', q, \zeta) = 0 \tag{III.27}$$

and that the flow rule may be represented as:

$$\delta\varepsilon_p^p = \chi\frac{\partial Q}{\partial p'} \qquad \text{and} \qquad \delta\varepsilon_q^p = \chi\frac{\partial Q}{\partial q} \tag{III.28) and (III.29}$$

in which χ is the parameter that expresses the hardening or softening of the soil, given by the expression:

$$\chi = -\frac{\dfrac{\partial F}{\partial p'}\delta p' + \dfrac{\partial F}{\partial q}\delta q}{\dfrac{\partial F}{\partial p'_0}\left(\dfrac{\partial p'_0}{\partial \varepsilon_p^p}\dfrac{\partial Q}{\partial p'} + \dfrac{\partial p'_0}{\partial \varepsilon_q^p}\dfrac{\partial Q}{\partial q}\right)} \tag{III.30}$$

then, once the parameter χ has been found, the determination of the partial plastic strain increments and consequently, the total plastic strain, is obtained by the sum of equations (III.28) and (III.29). Therefore, mathematically the relation between the mean effective stress (p') and deviator stress (q) increments, with the plastic strain increments, can be described, in a matrix, in the following manner:

$$\begin{Bmatrix}\delta\varepsilon_p^p \\ \delta\varepsilon_q^p\end{Bmatrix} = \frac{-1}{\dfrac{\partial F}{\partial p'_0}\left(\dfrac{\partial p'_0}{\partial \varepsilon_p^p}\dfrac{\partial Q}{\partial p'} + \dfrac{\partial p'_0}{\partial \varepsilon_q^{pp}}\dfrac{\partial Q}{\partial q}\right)}\begin{bmatrix}\dfrac{\partial F}{\partial p'}\dfrac{\partial Q}{\partial p'} & \dfrac{\partial F}{\partial q}\dfrac{\partial Q}{\partial p'} \\ \dfrac{\partial F}{\partial p'}\dfrac{\partial Q}{\partial q} & \dfrac{\partial F}{\partial q}\dfrac{\partial Q}{\partial q}\end{bmatrix}\begin{Bmatrix}\delta p' \\ \delta q\end{Bmatrix} \tag{III.31}$$

In the case of an associated flow rule, then the plastic potential function $Q(\sigma, \zeta)$ coincides with the yield function $F(\sigma,\chi)$, and so the determination of the plastic multiplier becomes simpler and the matrix is symmetrical.

III.2.4. CRITICAL STATE MODEL

The unification of the deformation and strength concepts is due largely to the work undertaken by the University of Cambridge, and from which the formulation of a model that incorporated the concept of critical states was derived. The model was initially used to predict the response of remoulded saturated clay, when subjected to triaxial compression tests, since this one of the most widely used test for obtaining the soil strength parameters. As such, this model incorporates the principal soils parameters used to describe the soil resistance of these types of soils, but it can also be applied to other types of materials. This model was originally developed under the leadership of Roscoe, between the 50's and the 60's, and was presented in 1958 by Roscoe *et al*., and later in 1968 by Roscoe & Burland. However, only in 1968 did Schofield & Wroth make the theory accessible with the launching of their book; even today this book is a reference for the understanding of the model.

The model unifies different concepts accepted in soil mechanics that are usually seen in a separated way, this being one of the main innovations introduced by the method, which combines the concepts of failure criterion, load and plastic potential, volume variation as well as its relation with effective stresses (Maranha das Neves & Guedes de Melo, 1975).

The presentation of this concept is important, since the Soft Soil and Soft Soil Creep models of PLAXIS, used in the numerical simulations, are somewhat based on the Modified Cam Clay model. Therefore, there will be a first approach to the critical states model, followed by a brief reference to the Original Cam-Clay model and lastly the Modified Cam-Clay.

The description of soil behaviour in the critical state model is done in a three-dimensional space, in which two axes represents the stress invariants, isotropic (p′) and distortional (q) stresses, and the other represents the variations in the specific volume (v), i.e. the overall volume occupied by the unit volume of solids, or the void ratio. The stress invariants were already defined, but the specific volume still needs to be specified (v). This last parameter will be given by:

$$v = 1 + e \tag{III.32}$$

The critical state concept postulates the existence of an ideal material, which behaves as a frictional fluid at a specific constant volume, when p' and q satisfies the equations:

$$q = M \cdot p' \tag{III.33}$$

$$\Gamma = v + \lambda \cdot \ln p' \Leftrightarrow \Gamma = v + \lambda \cdot \log_e p' \tag{III.34}$$

where M, Γ and λ represents basic soil properties. In fact, when the planes defined by these two equations intersect, it results in a line that represents the failure at the triaxial tests, called as the critical state line (CSL) (Figure III.9). Therefore, regardless of the stress trajectory, once the critical

state line is reached, the material will suffers distorcional strains at p′, q and v constants in drained conditions, or in the case of undrained conditions to pore pressure (u).

Mathematically, these conditions can be described in the following manner:

$$\frac{\partial v}{\partial \varepsilon_q} = 0 \qquad \frac{\partial q}{\partial \varepsilon_q} = 0 \qquad \text{and} \qquad \frac{\partial p'}{\partial \varepsilon_q} = 0 \qquad \text{(III.35) (III.36) and (III.37)}$$

being the volumetric strain and the distortional strain, respectively, equal to:

$$\varepsilon_v = \varepsilon_1 + \varepsilon_2 + \varepsilon_3 \qquad \text{(III.38)}$$

$$\varepsilon_q = \frac{2}{3}(\varepsilon_1 - \varepsilon_3) \qquad \text{(III.39)}$$

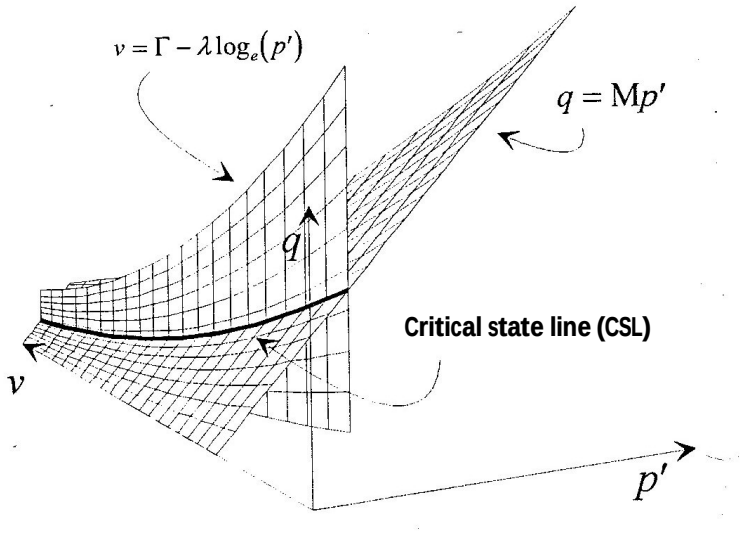

Figure III.9 – Spatial representation of the critical state line (Mateus da Silva, 1996)

However, and in order to better understand the concept associated with critical states, a brief description of the stresses trajectories or paths for the triaxial compression tests, both drained and undrained, will be given.

When a triaxial compression test is conducted, a stress-strain relationship is obtained. Based on these curves, it is possible to determine the parameters of the shear strength, using Mohr circle representation. With three different test results, associated to three different stress confinement of the specimen, the Mohr-Coulomb failure criterion or yield surface can be estimated. The correspondent procedure is plotted in figure III.10 for normally consolidated soil, and in figure III.11 for over-consolidated soil. The stresses used to obtain the Mohr-Coulomb envelope correspond to the yielding stress state in the triaxial tests.

When in the presence of overconsolidated soil, it presents a maximum stress value or a peak value, then reducing to a residual value, which is designated as the critical state baseline or perfect plasticity.

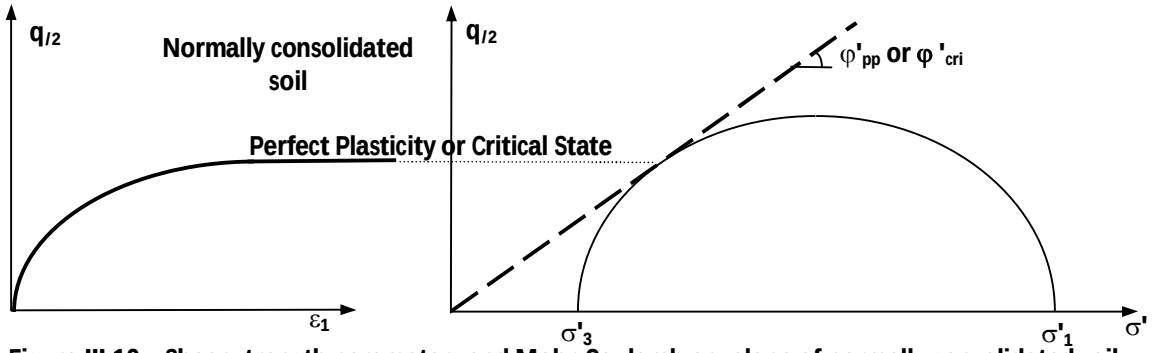

Figure III.10 – Shear strength parameters and Mohr-Coulomb envelope of normally consolidated soils

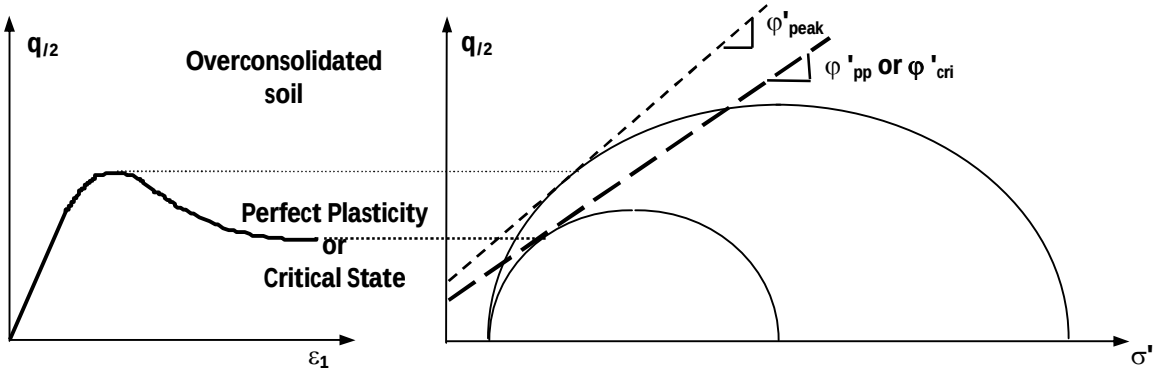

Figure III.11 – Shear strength parameters and Mohr-Coulomb envelope of overconsolidated soils

The critical state can also be represented in a (*p'; q*) plot as a straight line q=Mp', being the yielding stress state obtained by the interception of this same line with the one which defines the stress path of the triaxial test, both drained or undrained. Associated to these yielding stress states there is also a void ratio, designated as critical void ratio (Biarez & Hicher, 1994). The M parameter is determined based on equation III.40.

$$M = \frac{6 \cdot \sin\varphi'_{pp}}{3 - \sin\varphi'_{pp}} \qquad \text{(III.40)}$$

However, the representation of the stress paths in the (*p'-q*) plot is not unique, depending on the type of triaxial test performed (Da Silva, 1999). Therefore:

- For the isotropic consolidation phase, in which $\sigma'_1=\sigma'_2=\sigma'_3$ and $\Delta\sigma'_1=\Delta\sigma'_2=\Delta\sigma'_3$, then p'>0 and q=0, and the corresponding stress trajectory is a horizontal line which coincides with the x-axis (Figure III.12).

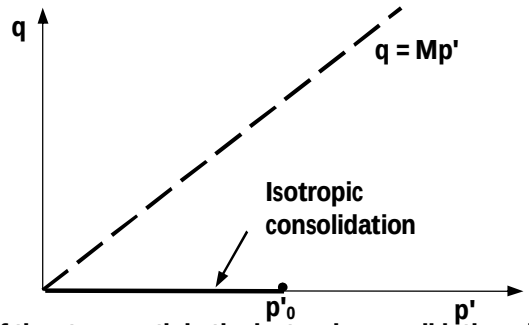

Figure III.12- Representation of the stress path in the isotropic consolidation phase of the triaxial test, in the (*p'; q*) plot (Da Silva, 1999)

- For the conventional triaxial test, where $\sigma'_2=\sigma'_3$ and $\Delta\sigma'_2=\Delta\sigma'_3$, the slope of the stress path is of 1/3, starting at p'_0; so, the trajectory equation will be $p'=p'_0+q/3$ (Figure III.13).

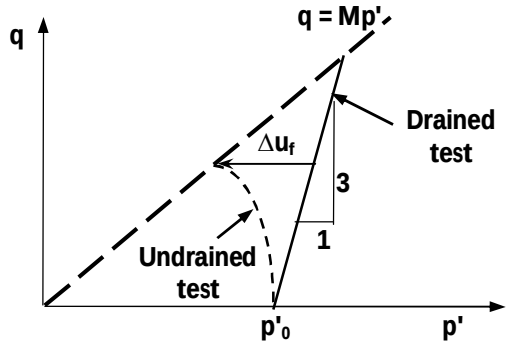

Figure III.13 - Representation of the stress path in the compression phase of the triaxial test, in the (*p'; q*) plot (Da Silva, 1999)

- For the triaxial test with $\sigma'_1+\sigma'_2+\sigma'_3=c^{te}$, which means that $\Delta\sigma'_1+\Delta\sigma'_2+\Delta\sigma'_3=0$, or in other words $p'=c^{te}$ and $q>0$, the stress path is described by a vertical line which starts at p'_0 (Figure III.14).

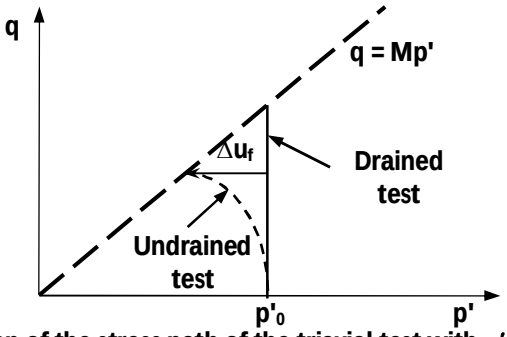

Figure III.14 - Representation of the stress path of the triaxial test with $\sigma'_1+\sigma'_2+\sigma'_3=c^{te}$, in the (*p'; q*) plot (Da Silva, 1999)

- In the case of undrained tests, the trajectory of the total stresses will be equal to that of the drained test; however, in order to obtain the mean effective stress path, the pore pressure must be subtracted to the total stress, with the distortional stress remaining constant, or in other words ($p'=p-u$ and $q'=q$) (Figure III.13) and (Figure III.14).

In addition, it is also necessary to observe the rate of the specific volume v in the (*p'; v*) plot, in accordance with the Cambridge notation (Britto & Gunn, 1987). Following the same procedure as mentioned for the (*p'; q*) plot, current triaxial tests ($\sigma'_2=\sigma'_3$) performed on remoulded clay, begins with an isotropic stress state ($\sigma'_1=\sigma'_2=\sigma'_3$) or ($p'>0$; $q=0$), which is characterised in the (*e; ln p'*) plot by the isotropic consolidation line (ISO) and whose slope is given by λ. This course is similar to the virgin compression line (VCL) obtained in the oedometer test in the (*e; log p'*) plot, being the slope characterised by the compressibility index C_c. The same type of similarity in the progress of the curves or lines is observed when there is a release of the stress on the soil followed by a new load. In this case we observe that the expansibility or recompressibility index C_s obtained in the oedometer test is replaced by the κ parameter (Figure III.15).

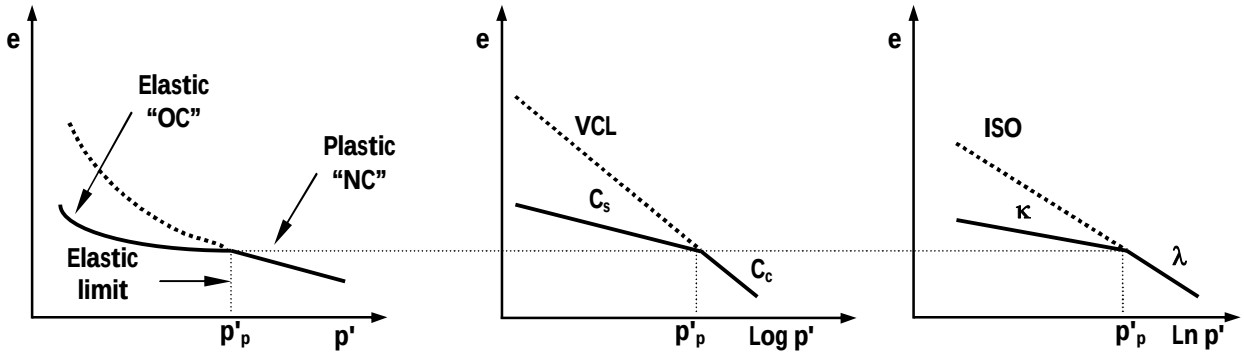

Figure III.15 – Representation of the variation of the void ratio with mean effective stress in the (*e; p'*), (*e; ln p'*) and (*e; log p'*) plots (Da Silva, 1999)

The relation between the parameters λ and C_c, as well as between κ and C_s, are given by:

$$\lambda = \frac{1}{\ln 10} C_c = \frac{C_c}{2,3} \tag{III.41}$$

$$\kappa = \frac{1}{\ln 10} C_s = \frac{C_s}{2,3} \tag{III.42}$$

The rate of the specific volume with the mean effective stress, in isotropic consolidation phase, for load and unload-reload cycles, can be described, respectively, by the equations III.43 and III.44.

$$v = v_\lambda - \lambda \cdot \ln\left(\frac{p'}{p'_0}\right) \tag{III.43}$$

$$v = v_\kappa - \kappa \cdot \ln\left(\frac{p'}{p'_0}\right) \tag{III.44}$$

The value of v_λ is usually substituted by the parameter N. Conventionally, this parameter is attributed with the value of the specific volume, which corresponds to the mean effective stress equal to the unit $v_{(p'=1)}$, hence, the value of p'_0 is omitted, and then equation III.43 can be re-write as:

$$v = N - \lambda \cdot \ln p' \tag{III.45}$$

Once the isotropic consolidation of the soil has been concluded, a load increment is applied to the sample, and the soil yields once it reaches the yield surface, correspondent to the critical state line (CSL) or "perfect plasticity" (PP). In the (*e; ln p'*) plot the critical state line is parallel to the virgin compression line. It is important to indicate that during the undrained tests, the soil sample does not suffer volumetric variation, which is why the specific volume value of perfect plasticity is equal to the specific volume after the isotropic consolidation phase.

In Figure III.16 and figure III.17 both ISO or VCL and the PP or CSL lines are plotted, as well as the trajectories in the (*e; lnp'*) plot, for the conventional drained and undrained compression triaxial tests, respectively for normally consolidated soil and overconsolidated soil.

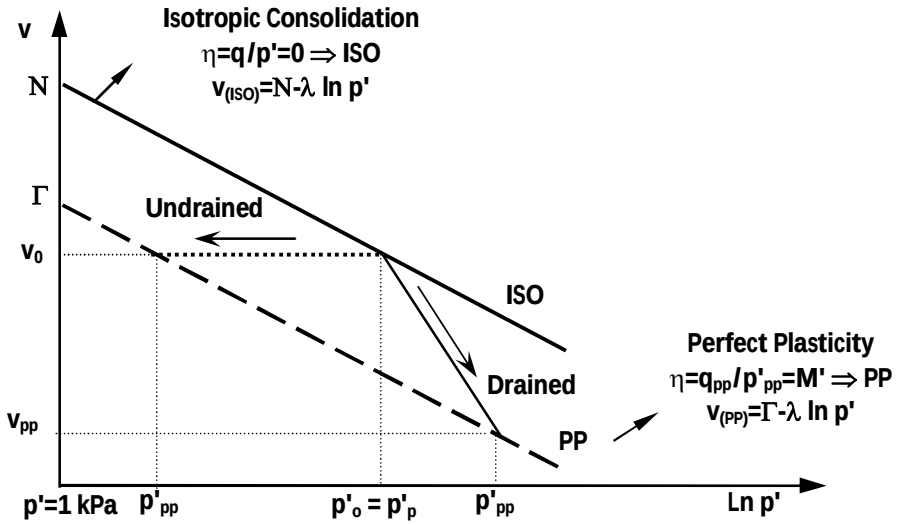

Figure III.16 – (ISO) and (PP) lines in the (*e; lnp'*) plot, as well as specific volume path for drained and undrained triaxial test of normally consolidated soils (Da Silva, 1999)

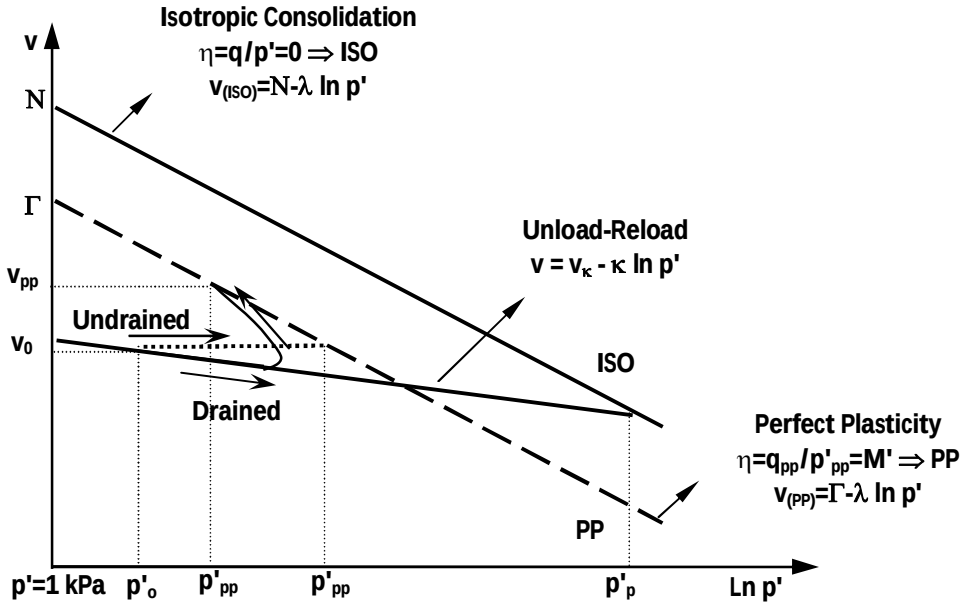

Figure III.17 – (ISO) and (PP) lines in the (*e; lnp'*) plot, as well as specific volume path for drained and undrained triaxial test of overconsolidated soils (Da Silva, 1999)

The variation of the void ratio for the triaxial test at constant mean effective stress ($p'=c^{te}$), can also be plotted against different relations, as it is presented in figure III.18 (Biarez & Hicher, 1989; Saïm, (1996 and 1997)).

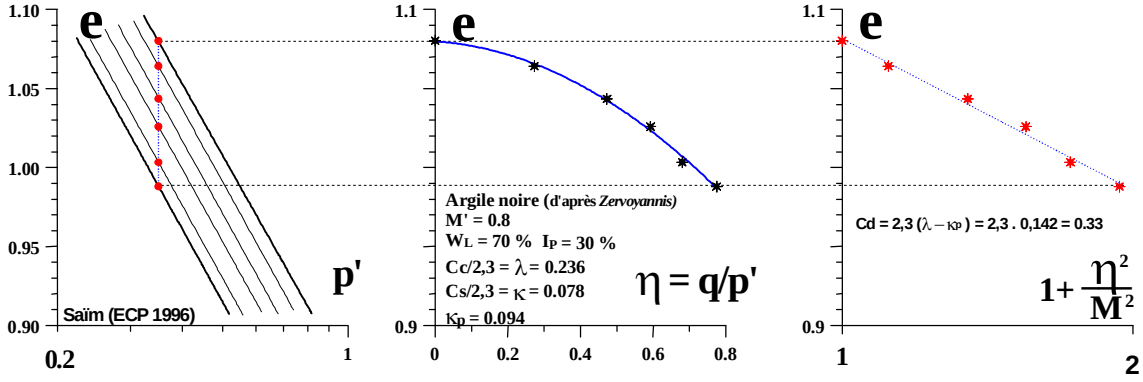

Figure III.18 – Triaxial test for p^{ct} – Representation in the (*e; logp'*), (*e;*η) and (*e; 1+(η²+M²)*) plots (Biarez & Hicher, 1989; Saïm, (1996 and 1997) – Zervoyannis data, 1982)

In these types of tests, and during the compression phase, it is possible to see that the deviator stress causes a volume decrease. This ratio is defined by equation III.46.

$$e = e_0 - C_d \cdot \log\left(1 + \frac{\eta^2}{M^2}\right) \qquad \text{(III.46)}$$

C_d is the distortional compression index, and it correspondent to the slope of the straight line, which relates the void ratio to the decimal logarithm of the expression $1+(\eta^2/M^2)$. If the same ratio is given by the natural logarithm, then the parameter C_d turns into λ_d, where $\lambda_d=(\lambda - \kappa_p)$, being κ_p different from κ.

Lastly, it is worth mentioning that the trajectory for triaxial test with $\sigma'_2=\sigma'_3$, for normally consolidated soil ($\varepsilon > 10^{-2}$), are represented in the surface expressed by equation III.47 (Roscoe *et al.*, 1958; Schofield & Wroth, 1958), which only needs parameters M, λ and λ_d (natural logarithm) or M, C_c and C_d (decimal logarithm) for its definition.

$$e = e_{pp} - \lambda \cdot \ln\left(\frac{p'}{p'_{pp}}\right) + \lambda_d \cdot \ln\left(\frac{2}{1 + \frac{\eta^2}{M^2}}\right) \qquad \text{(III.47)}$$

This expression can also be re-written according to the initial values of the void ratio and mean effective stress, as it is indicated in equation III.48, since the critical state values are difficult to obtain before the tests are concluded.

$$e = e_0 - \lambda \cdot \ln\left(\frac{p'}{p'_0}\right) + \lambda_d \cdot \ln\left(\frac{1}{1 + \frac{\eta^2}{M^2}}\right) \qquad \text{(III.48)}$$

The Original Cam-Clay model was the first model where the concept of critical state was used, and later on updated to Modified and Revised Cam-Clay models. For decades, it was the model which was most adopted to describe the behaviour of fine soils, with low strength characteristics, and consequently presenting significant deformations (Ortigão, 1993).

III.2.4.1. ORIGINAL CAM-CLAY MODEL

To recap, the basic hypothesis or concepts of the critical states model or Cam-Clay are respectively:

a) Critical State - When the stress state touches the critical state line, the model allows for the occurrence of distortion without an alteration in the effective stress or volume (or pore pressure in the case of undrained conditions). This is the essence of the critical state concept;

b) Void ratio: Relation with the effective stress - This is considered in the hardening law;

c) Characteristics of plastic strains - Once again these are considered both in the hardening law and in the flow rule;

d) Mohr-Coulomb failure criterion - This criterion is considered to represent the yield surface, and is a function of two well-known soil parameters, namely c′and φ'.

The Original Cam-Clay model, considers that the equality between the work performed by the interior forces and the dissipated work, in the critical state, is expressed in the following manner:

$$p'\delta\varepsilon_p^p + q\delta\varepsilon_q^p = Mp'\delta\varepsilon_q^p \qquad \text{(III.49)}$$

Re-writing equation III.49, so that the plastic strain increments are separated from the stress, the flow rule will be:

$$\frac{\delta\varepsilon_p^p}{\delta\varepsilon_q^p} = M - \frac{q}{p'} = M - \eta \qquad \text{(III.50)}$$

Knowing, in turn, that the condition of associated flow rule implies that the directions of the plastic strains increments are normal for the yield surface, then:

$$\frac{\delta\varepsilon_p^p}{\delta\varepsilon_q^p} = -\frac{\partial q}{\partial p'} \qquad \text{(III.51)}$$

and combining equation III.50 with III.51, it results:

$$\frac{\partial q}{\partial p'} = \eta - M \qquad \text{(III.52)}$$

Integrating this last expression, and taking in consideration that in the yield, $q_{pp}=Mp'_{pp}$, then the yield function can is determine. For this model the yield function is given by:

$$\frac{q}{Mp'} + \ln\left(\frac{p'}{p'_{pp}}\right) = 1 \qquad \text{or} \qquad q = Mp'\ln\left(\frac{p'}{p'_c}\right) \qquad \text{(III.53); (III.54)}$$

Equation III.54 results from equation III.53, since the maximum pre-consolidation stress is equal to $p'_c=2.72\ p'_{pp}$.

Once the yield function has been determined, the governing relations between the plastic strains increments and stress increments can also be obtained. The description of the model is therefore complete, and the elastic and plastic response of the soil can be traduced by the following matrices:

$$\begin{Bmatrix} \delta\varepsilon_p^e \\ \delta\varepsilon_q^e \end{Bmatrix} = \begin{bmatrix} \dfrac{\kappa}{v\cdot p'} & 0 \\ 0 & 0 \end{bmatrix} \begin{Bmatrix} \delta p' \\ \delta q \end{Bmatrix} \tag{III.55}$$

$$\begin{Bmatrix} \delta\varepsilon_p^p \\ \delta\varepsilon q \end{Bmatrix} = \frac{(\lambda-\kappa)}{v\cdot p' M} \begin{bmatrix} (M-\eta) & 1 \\ 1 & \dfrac{1}{(M-\eta)} \end{bmatrix} \begin{Bmatrix} \delta p' \\ \delta q \end{Bmatrix} \tag{III.56}$$

III.2.4.2. MODIFIED CAM-CLAY MODEL

The Modified Cam-Clay model is developed with the goal of overcoming some limitations and insufficiencies in the base model, i.e., the Original Cam-Clay model. The main difference between these two models is based on the formulation assumed for work dissipation, which will have implications on the flow rule, yield function and consequently on the stress-strain governing equations (Roscoe & Burland, 1968).

In the Modified Cam-Clay model, the energy equation considers, in the part correspondent to the dissipated work in the critical state, another term related to the dissipation of energy in the plastic volumetric strain, becoming:

$$p'\delta\varepsilon_p^p + q\delta\varepsilon_q^p = p'\sqrt{\left(\delta\varepsilon_p^p\right)^2 + \left(M\delta\varepsilon_q^p\right)^2} \tag{III.57}$$

By performing the exact same procedure indicated for the case of the Original Cam-Clay, the flow rule and yield surface equations are:

$$\frac{\delta\varepsilon_p^p}{\delta\varepsilon_q^p} = \frac{M^2-\eta^2}{2\eta} \tag{III.58}$$

$$q = Mp'\sqrt{\left(\frac{2\cdot p'_{pp}}{p'}\right)-1} \qquad \text{or} \qquad q = Mp'\sqrt{\left(\frac{p'_c}{p'}\right)-1} \tag{III.59}; \ \text{(III.60)}$$

in which equation III.60 is no more than equation III.59 re-written in terms of the maximum pre-consolidation stress p'_c, which, in this case, is equal to $2\cdot p'_{pp}$.

The relations between the stress and strain increments, respectively for the elastic and plastic soil behaviour, are mathematically described by the matrixes:

$$\begin{Bmatrix} \delta\varepsilon_p^e \\ \delta\varepsilon_q^e \end{Bmatrix} = \begin{bmatrix} \dfrac{\kappa}{v\cdot p'} & 0 \\ 0 & \dfrac{1}{3G'} \end{bmatrix} \begin{Bmatrix} \delta p' \\ \delta q \end{Bmatrix} \tag{III.61}$$

$$\begin{Bmatrix}\delta\varepsilon_p^p\\ \delta\varepsilon_q^p\end{Bmatrix}=\frac{(\lambda-\kappa)}{v\cdot p'\left(M^2+\eta^2\right)}\begin{bmatrix}\left(M^2-\eta^2\right) & 2\eta\\ 2\eta & \dfrac{4\eta^2}{\left(M^2-\eta^2\right)}\end{bmatrix}\begin{Bmatrix}\delta p'\\ \delta q\end{Bmatrix} \qquad \text{(III.62)}$$

Matrixes III.56 and III.62 are only used when the material (soil) suffers plastic strains, which always occurs when the new stress state exceeds the yield surface, i.e., $F(\sigma)>0$. It should be noted that the matrixes for these equations are symmetrical, a fact related to the consideration of an "associated" flow rule (existence of "normality condition"), as has already been mentioned.

For simplification purposes, some of the equations associated to each of the models are synthesize in table III.1.

Table III.1 – Equations from the Original and Modified Cam-Clay Model

	Original Cam-Clay	**Modified Cam-Clay**
Energy equation (read note)	$p'\delta\varepsilon_p^p+q\delta\varepsilon_q^p=Mp'\delta\varepsilon_q^p$	$p'\delta\varepsilon_p^p+q\delta\varepsilon_q^p=p'\sqrt{\left(\delta\varepsilon_p^p\right)^2+\left(M\delta\varepsilon_q^p\right)^2}$
Yield Surface	$q=Mp'\ln\left(\dfrac{p'}{p_c'}\right)$	$q=Mp'\sqrt{\left(\dfrac{p_c'}{p'}\right)-1}$
Volumetric strain increment	$\delta\varepsilon_p^e=\dfrac{\kappa\cdot\delta p'}{(1+e)p'}$	$\delta\varepsilon_p^e=\dfrac{\kappa\cdot\delta p'}{(1+e)p'}$
	$\delta\varepsilon_q^p=\dfrac{\delta\varepsilon^p}{(1+e)}=\dfrac{\lambda-\kappa}{(1+e)}\left(\dfrac{\delta p'}{p'}+\dfrac{\delta\eta}{M}\right)$	$\delta\varepsilon_q^p=\dfrac{\delta\varepsilon^p}{(1+e)}=\dfrac{\lambda-\kappa}{(1+e)}\left(\dfrac{\delta p'}{p'}+\dfrac{2\eta\delta\eta}{M^2+\eta^2}\right)$
Distortional strain increment	$\delta\varepsilon_q^e=0$	$\delta\varepsilon_q^e=\dfrac{\delta q}{3G}$
	$\delta\varepsilon_q^p=\dfrac{\delta\varepsilon_p^p}{M-\eta}$	$\delta\varepsilon_q^p=\dfrac{2\eta\cdot\delta\varepsilon_p^p}{M^2-\eta^2}$
Pore pressure increment	$\delta u=p_0-p+\dfrac{q}{3}$	$\delta u=p_0-p+\dfrac{q}{3}$
Axial strain	Drained: $\varepsilon_1=\varepsilon_q^{\text{total}}+\dfrac{\varepsilon_p^{\text{total}}}{3}$	Drained: $\varepsilon_1=\varepsilon_q^{\text{total}}+\dfrac{\varepsilon_p^{\text{total}}}{3}$
	Undrained: $\varepsilon_1=\varepsilon_q^{\text{total}}$	Undrained: $\varepsilon_1=\varepsilon_q^{\text{total}}$

Note: It can be observed that the energy equation for both models verifies Drücker's stability postulate, meaning $p'\delta\varepsilon_p^p+q\delta\varepsilon_q^p\geq 0$.

Representing the respective yield functions in the stress plane (*p'; q*) and the critical state line, then it is possible to see that the latter divides the interior space of the yield surfaces in two zones, each one being associated to distinct soil behaviour (Figure III.19).

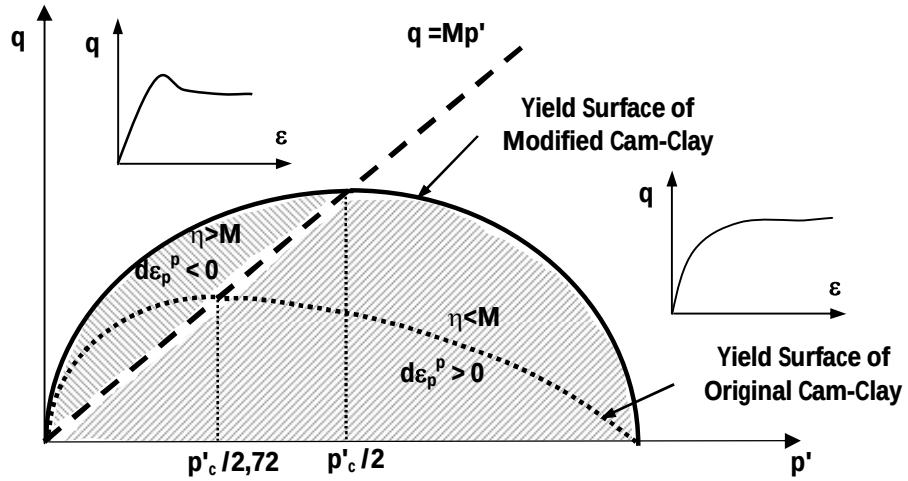

Figure III.19 – Yielding surfaces for the Original and Modified Cam-Clay model (Da Silva, 1999)

Therefore, when the stress state defined by p′ and q corresponds to a point on the interior of the surfaces, then the soil only presents elastic behaviour and as such, the volumetric strains or variations are reversible. In situations where the stress state exceeds, or is located on the yield surfaces, in the zone below the perfect plasticity line (critical state line), or in other words with $\eta<M$, then plastic compression volumetric strains (drained test) or positive pore pressures increments (undrained test), are generated. In the opposite case, meaning for $\eta>M$, expansion or dilation volumetric plastic strains (drained test) or negative increments in pore pressure (undrained test), are generated. The first situation is typical of normally consolidated soil (NC) and the second is associated to overconsolidated soils (OC). When $\eta=M$, the plastic volumetric strains will be null, as the plastic volume remains constant (Naskos, 1985) and (Britto & Gunn, 1987).

III.3. PLAXIS MATERIAL MODELS

The material models available on PLAXIS are, in most cases, suitable for soils and rocks. Nevertheless, the linear elastic model (*Hooke's* model) is also available, allowing the use of other types of materials in the geotechnical problems. One must not forget that the design engineer must select the model which best describes the behaviour of the materials in question, and also the values which will be attributed to the parameters required by the programme, according to the model adopted.

Often extremely complex and sophisticated models are used, in order to obtain predictions and results of high quality; however, this procedure will only bring benefits if the values attributed to the parameters are also reliable (Da Silva, 2009).

Next, and before presenting the Soft Soil and Soft Soil Creep model with more detail, some of the material models available for soils, on PLAXIS 2D-V11.02, will be briefly introduced. As already indicated, only three models were used in the simulation analysis of the case study presented in the next chapters; so the aim of this models description is done only to elucidate of the options eligible on PLAXIS.

- *Mohr-Coulomb* model (MC) – This is the well-known linear elastic perfectly plastic model, with non-associated flow rule. This model is recommended as a first approximation of soil the behaviour, and so is more suitable for a preliminary analysis, regardless the problem in question. Average constant soil stiffness is adopted, and, as such, the computations tend to be much quicker in comparison to others. In addition to this, a first order of magnitude, associated to the deformations expected, can be obtained.
- Hardening Soil model (HS) - The current HS model is an advanced model applicable to various type of soils, ranging from stiff soils such as gravels and sand, to very soft soil, such as clay and silt. It is an elastoplastic model of the hyperbolic type, formulated in the framework of shear hardening plasticity. When the soil is under primary compression conditions, the model calculates irreversible plastic strains and hardening compression is considered. Therefore there is an increment in the stiffness of the medium according to the stress state. The HS model, although suitable for any type of soil, does not consider the creep effect.
- Hardening Soil with small-strain stiffness model (HSsmall) - This model results from a modification to the HS model, incorporating dependency between stiffness modulus with strains, thereby allowing the simulation of soil reactions for different states of strain (from low strain levels ($\varepsilon<10^{-5}$), usually associated with vibrations, to large strain levels ($\varepsilon>10^{-3}$), typically imposed by engineering works). When applied to dynamic situations, it can also model the hysteresis of the material damping.
- Soft Soil model (SS) – This is a Cam-Clay type model, suitable to simulate the behaviour of normally consolidated clay soil or soils with degrees of consolidation ranging one (OCR=1), in primary compression situations. Even though the Hardening Soil model has surpassed this one, it continues to be used quite often, as it is a reliable model, one that is easy to understand and its entry parameters are obtained based on well-known tests. For all these reasons, PLAXIS users are comfortable using the SS model, for soils with the previously mentioned characteristics.
- Modified Cam-Clay model (MCC) - Based on the Cam-Clay critical states model which is well known, this model arose from the original, with the objective of overcoming some limitations and insufficiencies which existed in the base model. The model assumes a logarithmic relationship between volumetric strains and the mean effective stress. This model, according to the PLAXIS manual, sometimes has convergence problems in some stress trajectories, and so it is not recommended for some practical applications.
- Soft Soil Creep model (SSC) - This is a model formulated on the framework of soil viscoplasticity. It allows the simulation of the behaviour of compressible soil, such as very soft to soft soils (clay soil and peats) or normally consolidated soils, accounting for primary and secondary soil consolidation or compression, being this last one due to creep phenomena. This model is relatively recent and was specially developed to analyse the foundation settlement of very compressible soils, embankments and others. However, it should be noted that, for analyses involving unloading, or the removal of loads, such as tunnels or large excavations, it is preferable to use the MC model.

All these models are elastoplastic. The interesting particularity of some of these elastoplastic models is the consideration of the dilatancy angle (ψ) as one of the soil behaviour parameters. This parameter is very important in sandy soil or medium to dense soils, as well as on overconsolidated clayed soils, since it allows the description of the dilatancy phenomenon and therefore the progress of the void ratio with the strain more realistic.

Regarding the initial stress state of the soil, which plays a fundamental role in the study of geotechnical problems, this one is calculated based on the consideration of a suitable coefficient of earth pressure at rest (K_0).

Despite the attempts to improve, in each version, both the code associated with the computational methods of the finite elements, as well as the material models which simulates the soil behaviour, there are still some limitations. Although some of them are of analytical nature, others are related to models themselves. Thus, for each of the models mentioned before, and in accordance with the PLAXIS 2D-V11.02 (2012) manual, the limitations associated to the models are now described:

- Mohr-Coulomb model (MC) – This model includes only a limited number of features that soil behaviour shows in reality. Although the increase of stiffness with depth can be taking into account, the model does not incorporate either the stress-dependency, or the stress-path dependency of stiffness, or the anisotropy of the soil. In general, the Mohr-Coulomb failure criterion describes well the behaviour in drained conditions, considering the effective stress parameters. However, in undrained conditions, and since the effective stress path followed in the model may not be realistic, the resulting shear stress may be incorrect. This situation is worse in soft soil such as normally consolidated clay, as well as very dense, stiff, or highly overconsolidated soils.
- Hardening Soil model (HS) - This model does not account the softening of the soil due to the dilatancy phenomenon. It is an isotropic hardening model that does not consider the hysteretic and cyclic loading or anisotropy behaviour. Its greatest disadvantage is that the calculation time is excessive as the stiffness matrix is formed at each step of the calculation.
- Hardening Soil with small-strain stiffness model (HSsmall) – This model incorporates the loading history of the soil and a strain-dependent stiffness. It can be used to simulate cyclic loads, but is not suitable for cyclic problems in which softening plays an important role. As the anterior model, this model does not account the softening of the soil due to the dilatancy phenomenon. The HSsmall model presents a calculation time even greater than that of the HS model, thus only advisable for special cases.
- Soft Soil Creep model (SSC) - The limitations of the HS model are also applied in this model. Furthermore the range of elastic soil behaviour is over-estimated in this model, especially when in the presence of excavation problems, including tunnelling.
- Soft Soil model (SS) - Not recommended for problems with large excavations, and should be limited to problems which involve primary consolidation settlements.
- Modified Cam-Clay model (MCC) - Due to the characteristics of this model, the shear stresses for overconsolidated soils are very high and unrealistic, if the stress path crosses the critical state line. Furthermore, the model may give softening behaviour for such stress trajectories.

Still, in accordance to the PLAXIS manual, both the Hardening Soil and the Soft Soil models estimate relatively well, the primary consolidation settlements, however, they do not consider the creep effect and so are not suitable for soils with high compressibility.

III.3.1. SOFT SOIL MODEL

Soft Soil is a behaviour model adequate for soil which has considerable compressibility values, such as clays, clayey silts and peats. According to the PLAXIS 2D-V11.02 (2012) manual, some features of this model are:

a) Stress dependent stiffness (compression behaviour of the logarithmic type);
b) Distinction between the primary loading and unloading-reloading;
c) Memory of the pre-consolidation stress;
d) Failure behaviour according to the Mohr-Coulomb criterion.

III.3.1.1. STRESS AND STRAIN ISOTROPIC STATE ($\sigma'_1=\sigma'_2=\sigma'_3$)

This model assumes the existence of a logarithmic relation between the volumetric strain (ε_v) and the mean effective stress (p'), according to expression III.63.

$$\varepsilon_v - \varepsilon_{v0} = -\lambda^* \cdot \ln\left(\frac{p'_f}{p'_p}\right) \quad \text{, with } p'_f > p'_p \qquad \text{(III.63)}$$

During isotropic unloading-reloading, different path is followed, and the elastic volumetric strains can be formulated as:

$$\varepsilon_v^e - \varepsilon_{v0}^e = -\kappa^* \cdot \ln\left(\frac{p'}{p_0}\right) \quad \text{, with } p' \le p'_p \qquad \text{(III.64)}$$

These equations differ from those defined in the Cam-Clay models since the soil compressibility of is defined in terms of the volumetric strain and not the void ratio (Figure III.20). Therefore, λ^* and κ^* will be, respectively, the modified compressibility index and the modified recompressibility or expansibility index. The relationship between these modified parameters to those defined by Burland (1967), can be expressed as:

$$\lambda^* = \frac{\lambda}{(1+e)} \qquad \text{and} \qquad \kappa^* = \frac{\kappa}{(1+e)} \qquad \text{(III.65) and (III.66)}$$

However, the ratio between λ^*/κ^*, is the same as the ratio λ/κ.

The elastic behaviour is simulated by Hooke's model and equation III.64 implies a linear dependency between the stress and the volumetric strain module (K_{ur}), i.e.:

$$K_{ur} = \frac{E_{ur}}{3\,(1-2\,\upsilon_{ur})} = \frac{p'}{\kappa^*} \qquad \text{(III.67)}$$

in which "ur" means unload-reload.

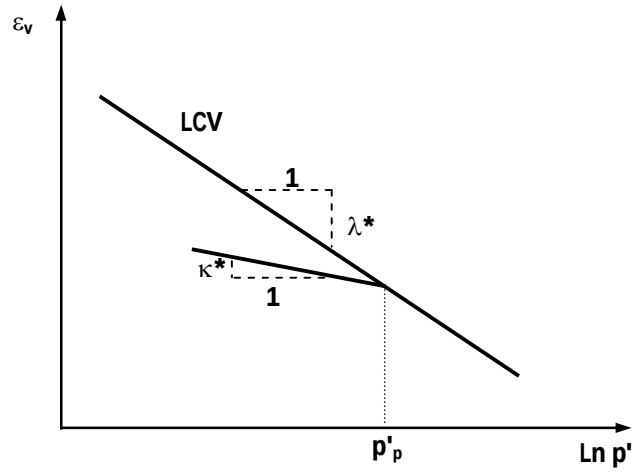

Figure III.20 – Logarithmic relation between volumetric strain and mean effective stress for the SS model (PLAXIS 2D-V11.02, 2012)

It should be emphasised that the soil parameters are defined in terms of effective stress instead of total stresses (undrained), therefore neither the strain modulus E_{ur}, nor the volumetric strain modulus K_{ur}, are considered. In contrast, and to define the elastic component of the soil, ν_{ur} and κ^* parameters are required.

The pre-consolidation stress p'_p defines the stress state value from which the irreversible volumetric strains start to occur (plastic state). Thus, in an unload-reload phase and while the pre-consolidation stress is not reached, the strains will only be elastic, but as soon as they exceed this stress state, the soil follows the virgin consolidation line and so, for each load increase the pre-consolidation stress will increase, leading to an increment in the plastic strains.

III.3.1.2. YIELD FUNCTION FOR THE COMPRESSION TRIAXIAL STATE ($\sigma'_2=\sigma'_3$)

The SS model is able to simulate the behaviour of the soil for several stress states; however, and only to obtain a better understanding of the model, it will presented the case of the triaxial compression test, where $\sigma'_2=\sigma'_3$. For this stress state, the yield function is defined as:

$$F=\left[\frac{q^2}{M^2\left(p'+c\cdot\cot g\varphi\right)}+p'\right]-p'_p \qquad \text{(III.68)}$$

being the pre-consolidation stress dependent of the plastic strain, and given by the equation:

$$p'_p=p'_{p0}\exp\left(\frac{-\varepsilon_v^p}{\lambda^*-\kappa^*}\right) \qquad \text{(III.69)}$$

This yield function describes an ellipse in the (*p'; q*) plot, as shown in figure III.21. This ellipse, where M indicates the height of the ellipse, has the same format as the Modified Cam-Clay model, and is responsible for the relationship between the vertical stress and the horizontal stress in primary compression, meaning that the M parameter is related to the value of K_0^{NC}. This assumptions differs

slightly from the Cam-Clay model, since it is different from the original concept of the critical state line and does not only depend on the friction angle of the soil, but also of the soil cohesion; however, it ensures that the value assumed for K_0^{NC} is correct. Therefore, in the SS model, the failure is not necessarily related to the concept of the critical state model, being the failure criterion defined by the Mohr-Coulomb criterion, and by the parameters (c' e φ'). The slope of the failure line in the SS model is smaller than the slope of the critical state line or M-line. Although the failure line is fixed, the cap may increase in primary compression.

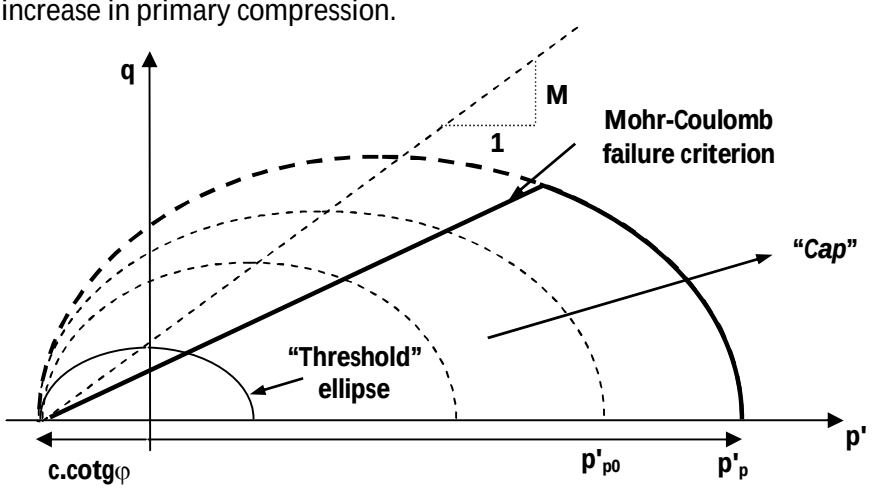

Figure III.21 – Yield function for the Soft-Soil model in the (*p'; q*) plot (PLAXIS 2D-V11.02, 2012)

The isotropic stress of pre-consolidation p'_p, indicates the length of the ellipse along the p' axis. During the load, there is an infinite number of ellipses, each one corresponding to a given value of p'_p. In traction, i.e.: for p'<0, the ellipse extends to c.cotg(φ). In order to make sure that the hand side of the ellipse (i.e. the "cap") is always located on the compressed side (p'>0), then a minimum value for c.cotg(φ) is adopted. Hence there is a "threshold" ellipse as illustrated in figure III.21.

In summary, this model considers a yield function which is defined by equation III.68, which describes the irreversible volumetric strains (plastic) in primary compression, and which delimits superiorly the yield zone (the top=cap). The Mohr-Coulomb failure criterion is adopted, being noted that this line is below the M-line in the (*p'; q*) plot (Figure III.21). The final contour of the yield or yield limit, in the elastic state, will then be given by the "cap" lines, being variable and increasing with primary compression, even though the failure line is fixed (Mohr-Coulomb). Stress paths within these limits only cause elastic strains, but as soon as the limits are crossed the soil presents both plastic and elastic strains. The final contour, described in the space of the principal stresses, is given in Figure III.22.

III.3.1.3. SOFT SOIL MODEL PARAMETERS

In addition to the initial void ratio (e_0), the model needs another 5 basic parameters, namely:

a) Modified compressibility index (λ*);
b) Modified recompressibility index (κ*);
c) Cohesion (c);
d) Internal effective friction angle (φ');
e) Dilatancy angle (ψ).

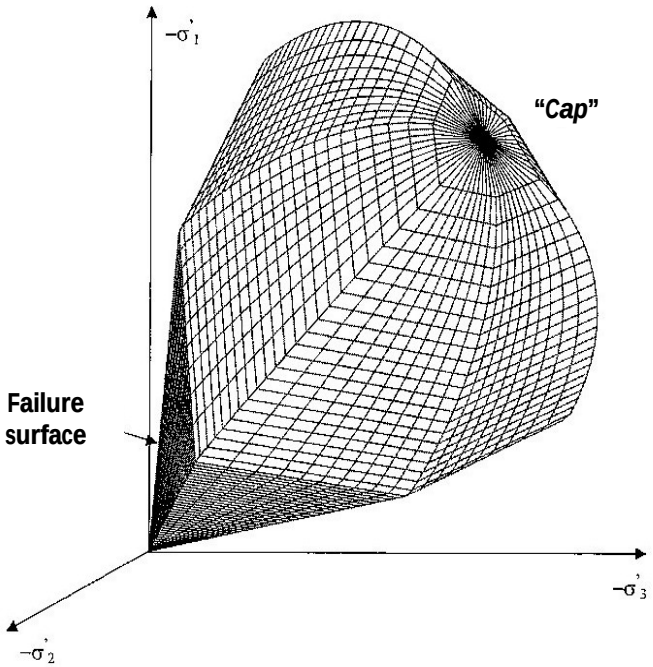

Figure III.22 – Representation of the yield surface of the Soft Soil model, in the principal stress space (PLAXIS 2D-V11.02, 2012)

The first two parameters will define the soil stiffness, which and can be determined based on the isotropic compression test. The ratios between $\lambda^*$and λ, as well as between κ^* and κ, have already been indicated in equations III.65 and III.66. The ratio between λ^*/κ^* will be equal to λ/κ, and usually range from 2.5 to 7, for most soils. Alternatively, the compressibility C_c and recompressibility or expansibility C_s indexes may also be used, if the one-dimensional compression test is performed (oedometer test). If the latter is considered, then the ratios between λ^* and κ^*, with the internationally standardised and most used parameters will be:

$$\lambda^* = \frac{C_c \log e}{1+e_0} \simeq \frac{C_c}{2{,}3(1+e_0)} \qquad \text{and} \qquad \kappa^* \approx \frac{2C_s \log e}{1+e_0} \approx \frac{2C_s}{2{,}3(1+e_0)} \qquad \text{(III.70) and (III.71)}$$

Regarding these parameters, the following comments are yet to be made:

a) It is assumed that the void ratio used on the previous equations are constant, however, they change in the course of a compression test. Nevertheless this variation is considered very small and, so the initial void ratio, or the average void ratio after the test has been concluded, may be considered. The first situation is more commonly used;

b) The ratio between the modified recompressibility index κ^* and the recompressibility index C_r is not exact, as the ratio between the horizontal and vertical stress changes in the unloading of the one-dimensional test. By approximation, it is considered that the average stress state during the unloading will be an isotropic stress state, meaning that the horizontal and vertical stresses will then be the same.

In addition to these, there are also advanced parameters, namely:

a) The Unload-reload Poisson's ratio (ν_{ur}). In this model, ν_{ur} is a purely elastic constant, in contrast to the pseudo-elastic behaviour used in linear elastic perfectly plastic models. Their value may vary between 0.1 and 0.2, and 0.15 is the value adopted by default. This parameter has little expression in normally consolidated soil, in compression. However, in the unloading phase, and since this value is very small, the reduction in the lateral stress will be less than the vertical stress applied in this phase, leading to an increase of the ratio between the horizontal and vertical stress; this phenomenon is associated with overconsolidated soils. For this reason, it is advisable to determine this value based on oedometer tests, in the unloading and reloading phase and not on the value of K_0^{NC}.

b) The lateral earth pressure coefficient for the normally consolidated state (K_0^{NC});

c) The "M" parameter. This is automatically calculated by the programme after entering the value of the coefficient of lateral earth pressure for the normally consolidated state K_0^{NC}, depending also on the unload-reload Poisson's ratio ν_{ur}, and also on the ratio λ^*/κ^*, even though the first parameter is dominant. According to Brinkgreve, in 1994, it will be given by:

$$M = 3\sqrt{\frac{\left(1-k_0^{NC}\right)^2}{\left(1+2k_0^{NC}\right)^2}+\frac{\left(1-k_0^{NC}\right)\left(1-2\upsilon_{ur}\right)\left(\frac{\lambda^*}{\kappa^*}-1\right)}{\left(1+2k_0^{NC}\right)\left(1-2\upsilon_{ur}\right)\left(\frac{\lambda^*}{\kappa^*}\right)-\left(1-k_0^{NC}\right)\left(1+\upsilon_{ur}\right)}} \qquad \text{(III.72a)}$$

or more simply, by $M \approx 3-2.8k_0^{NC}$ (III.72b)

For these parameters, it is recommended to use the default values assumed in the PLAXIS manual.

The Soft Soil parameters are introduced in effective stresses, even though undrained type analyses may also be performed. In this case, the programme transforms the data entered into undrained parameters and performs the calculations in total stress, but always considering the excess pore pressure.

III.3.2. SOFT SOIL CREEP MODEL

The Soft Soil Creep model is suitable to simulate the behaviour of soft to very soft soil, with a high degree of compressibility, taking in consideration the plastic strains due to creep, which depends on time, designated by secondary or secular consolidation. As already mentioned, secondary consolidation corresponds to the re-arranging of the soil particles at a constant pressure. This value may be negligible in stiff and dense soil, bust usually very high for soft to very soft soils. This last situation is generally associated with soil that also presents high settlements due to primary consolidation.

The model's features are the same of the SS model, including the consideration of the secondary compression (time dependent behaviour).

This model is also an elastoplastic model, with un-associated flow law. One of the surfaces is defined by the Mohr-Coulomb rupture criterion and fixed in the stress space, and another is variable depending on the isotropic stress of pre-consolidation, which delimits superiorly the yield zone (the top=*cap*), as treated in the SS model. The representation in the main stress space is equal to that of figure III.22. The mathematical modelling of Soft Soil Creep is duly detailed and described in the PLAXIS manual, however, for a better understanding of the work carried out in this study, it will be presented.

III.3.2.1. ONE-DIMENSIONAL CREEP

Normally, on oedometer tests, one is focused on the soil response related to step loading, even thought natural loading processes tend to continue in nature. Buisman, in 1936, was probably the first to considerer such phenomenon, associated to the creep behaviour. According to Buisman's formulation, the strain of soil under constant effective stress is given by:

$$\varepsilon = \varepsilon_{pc} - C_B \cdot \log\left(\frac{t}{t_c}\right) \quad \text{, for } t>t_C \tag{III.73}$$

where:

ε_{pc} - is the strain at the end of the primary consolidation;
t - is the time measured from the beginning of loading, and must be greater than t_C;
t_C - is the time correspondent to the end of the primary consolidation;
C_B - is a constant of the soil, determined in the phase correspondent to creep behaviour, and it is given by:

$$C_B = \frac{s(t_1) - s(t_2)}{s_{tot}} \cdot \log\left(\frac{t_1}{t_2}\right) \tag{III.74}$$

As PLAXIS does not follow the conventional methodology for soil mechanics in which the compressions are considered positive, then the equation III.73 must be re-written in the following manner:

$$\varepsilon = \varepsilon_{pc} + C_B \cdot \log\left(\frac{t_c + t'}{t_c}\right) \text{, for } t'>0 \tag{III.75}$$

with $t'= t-t_C$, and corresponding to time in which secondary compression occurs, also designated as the effective creep time.

In 1972, Garlanger, based on the works of Bjerrum from 1967 related to secondary consolidation, proposed that this should be a function of the void ratio, as indicated:

$$e = e_c - C_\alpha \cdot \log\left(\frac{\tau_c + t'}{\tau_c}\right) \tag{III.76}$$

where C_α represents the secondary compressibility index. This last is related to C_B by:

$$C_\alpha = C_B\left(1 + e_0\right) \text{ ,for } t'>0 \tag{III.77}$$

The differences between both formulations are modest, with strain ε being substituted by the void ratio, and time t_c by parameter τ_C.

It should be noted that τ_C is not the time of the primary consolidation t_c. Time τ_C is not a parameter of the material but instead a factor which does not only depend on consolidation, but also on the geometry of the samples tested (Alves, 2011). If it is considered that $\tau_C=t_c$ then the equations III.75 and III.76 will be entirely identical. The exact value of τ_C is difficult to calculate; however, the difference between these last two parameters disappears as the time of creep t' increases, it then being possible to consider equality between both. According to PLAXIS 2D-V11.02 (2012), the determination of t_c and τ_C will depend on the evolution of the response from the soil, and is distinct for each soil type.

Another way to describe secondary consolidation was given by Butterfield, in 1979, using the logarithmic strain ε^H, as it is showed in equation III.78.

$$\varepsilon^H = \varepsilon^H_{pc} - C \cdot \ln\left(\frac{\tau_c + t'}{\tau_c}\right) \qquad \text{(III.78)}$$

The logarithmic strain is not currently used in terms of engineering, and was originally adopted by Hencky. This strain is defined by:

$$\varepsilon^H = \ln\left(\frac{V}{V_0}\right) = \ln\left(\frac{1+e}{1+e_0}\right) \qquad \text{(III.79)}$$

For small displacements, the logarithmic strains ε^H are approximately equal to conventional strains ε, and thus it results:

$$C = \frac{C_\alpha}{(1+e_0)\ln 10} = \frac{C_B}{\ln 10} \qquad \text{(III.80)}$$

Janbu, in 1969, has developed a graphical construction to evaluate the parameters C and τ_c, having separated equation III.78 in terms of time and dropping the term (H) to simplify the notation (Figure III.23b). Both the traditional method represented in figure III.23a), and the Janbu method can be used to determine parameter C.

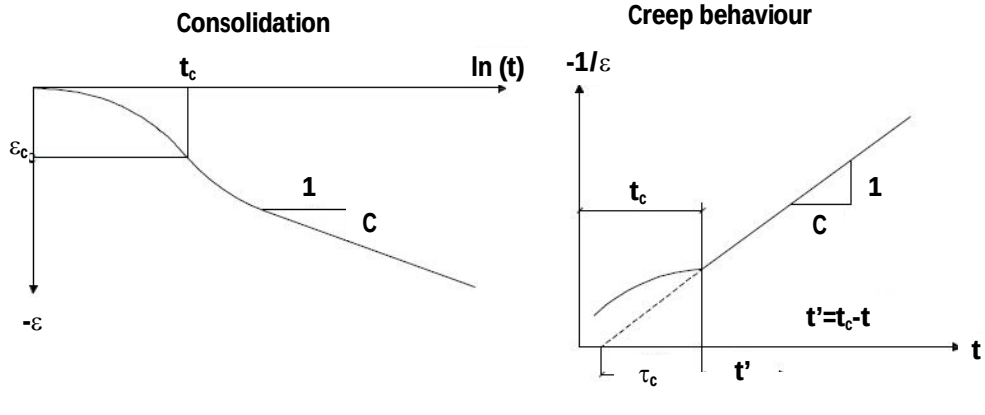

Figure III.23 – Representation of consolidation in a standard oedometer test

However, the Janbu method is more attractive, as it also allows the obtaining of parameter τ_c, which corresponds to the interception of the straight creep line with the time axis (non-logarithmic). The linear curve of the graph, for $t<t_c$, is due to the primary consolidation of the sample (Alves, 2011).

According to the same author, primary consolidation strains are calculated based on the expression:

$$\varepsilon_{pc}^{H} = \varepsilon_{pc}^{He} + \varepsilon_{pc}^{Hcr} = -A \cdot \ln\left(\frac{\sigma'_f}{\sigma'_0}\right) - B \cdot \ln\left(\frac{\sigma'_{pc}}{\sigma'_{p0}}\right) \quad \text{(III.81)}$$

meaning that the elastic and viscoplastic strains are equal to:

$\varepsilon_{pc}^{He} = A \cdot \ln\left(\frac{\sigma'_f}{\sigma'_0}\right)$ - elastic strains at the end of primary consolidation;

$\varepsilon_{pc}^{Hcr} = B \cdot \ln\left(\frac{\sigma'_{pc}}{\sigma'_{p0}}\right)$ - viscoplastic strains at the end of primary compression;

where: σ'_f – final effective vertical stress;

σ'_0 – initial effective vertical stress;

σ'_{p0} – initial effective vertical pre-consolidation stress;

σ'_{pc} – effective vertical pre-consolidation stress at the end of primary consolidation.

The total strain is obtained by adding secondary consolidation in equation III.81, resulting:

$$\varepsilon^{H} = -A \cdot \ln\left(\frac{\sigma'_f}{\sigma'_0}\right) - B \cdot \ln\left(\frac{\sigma'_{pc}}{\sigma'_{p0}}\right) - C \cdot \ln\left(\frac{t_C + t'}{t_C}\right) \quad \text{(III.82)}$$

With the last term corresponding to the viscoplastic strains during the secondary consolidation. Parameters A, B and C are related to parameters C_c, C_r and C_α in the following manner:

$$A = \frac{C_r}{(1+e_0)\ \ln 10} \quad \text{(III.83)}$$

$$B = \frac{(C_c - C_r)}{(1+e_0)\ \ln 10} \quad \text{(III.84)}$$

$$C = \frac{C_\alpha}{(1+e_0)\ \ln 10} \quad \text{(III.85)}$$

The strains associated with the three terms of equation III.82 are plotted in figure III.24.

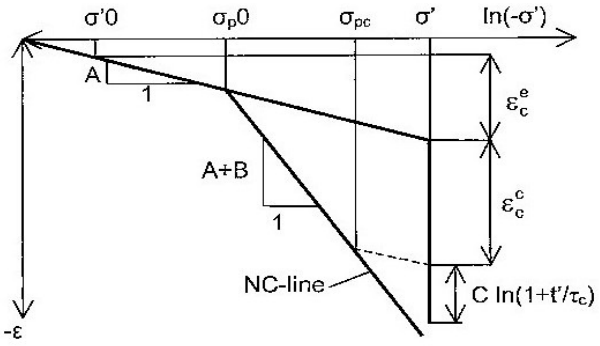

Figure III.24 – Elastic and plastic strains, in primary and secondary consolidation, with effective vertical stress (PLAXIS 2D-V11.02, 2012)

III.3.2.2. INTRODUCTION OF CREEP IN THE MODEL

Introducing the previously defined concepts, and being the Soft Soil Creep model an extension of the Soft Soil, then the upgrade will be the addition of the creep phenomenon to the latter model, meaning the deformation associated to secondary compression. For this, adapting equation III.82 for volumetric strains instead of hyperbolic, and adding to the equations III.63 and III.64 of model SS, the creep effect, it becomes:

$$\varepsilon = \varepsilon_v^e + \varepsilon_v^{pcr} + \varepsilon_v^{scr} = \kappa^* \cdot \ln\left(\frac{p'_f}{p'_0}\right) + \left(\lambda^* - \kappa^*\right) \cdot \ln\left(\frac{p'_{pc}}{p'_{p0}}\right) + \mu^* \cdot \ln\left(\frac{\tau_c + t'}{\tau_c}\right) \qquad \text{(III.86)}$$

each term corresponding to:

$\varepsilon_v^e = \kappa^* \cdot \ln\left(\frac{p'_f}{p'_0}\right)$ - elastic strains at the end of primary consolidation;

$\varepsilon_v^{pcr} = \left(\lambda^* - \kappa^*\right) \cdot \ln\left(\frac{p'_{pc}}{p'_{p0}}\right)$ - viscoplastic strains at the end of primary consolidation;

$\varepsilon_v^{scr} = \mu^* \cdot \ln\left(\frac{\tau_c + t'}{\tau_c}\right)$ - viscoplastic strains at the end of secondary consolidation;

where: p'_f – final mean effective stress ;

p'_0 – initial mean effective stress;

p'_{p0} – initial mean effective pre-consolidation stress;

p'_{pc} – mean effective pre-consolidation stress at the end of primary consolidation.

Figure III.25 and figure III.26 helps to understand the three different component of the total strain in the SSC model. As one can observed, when creep behaviour is considered, at the end of the primary consolidation, the isotropic compression line has not yet been reached. To reach the ISO line the creep strains have to be accounted for. Furthermore p'_{pc} is not equal to p'_p, since the latter is considered as the mean effective stress at the end of primary consolidation taking into account the creep phenomenon. For t'+tc=1 day, one arrives precisely on the ISO or NC-line.

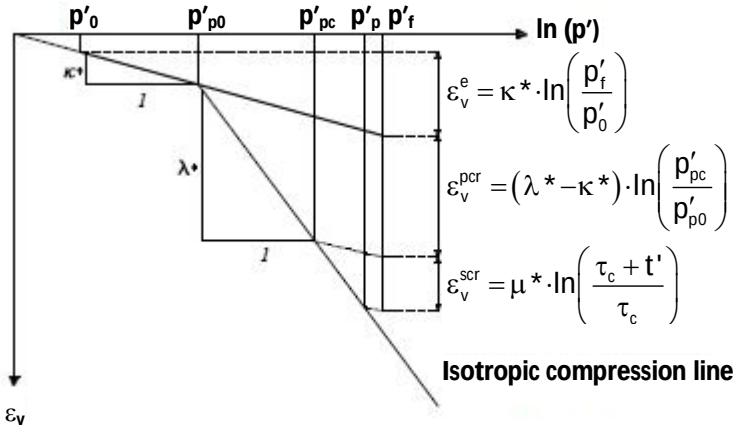

Figure III.25 – Division of the strain increments into elastic and creep components, in the mean effective stress-strain plot (Neher *et al.*, 2000).

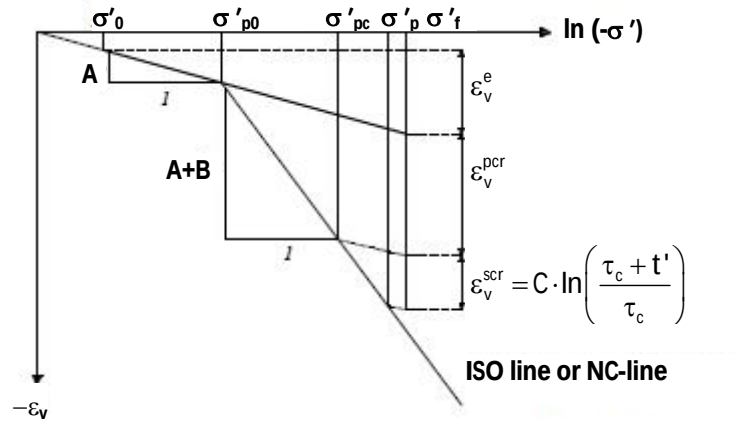

Figure III.26 – Idealised stress-strain curve from oedometer test, with division of the strain increments into elastic and creep components (PLAXIS 2D-V11.02, 2012).

Equation III.86 is valid for constant mean effective stresses, as it is the case of the oedometer test, where constant load increments are applied during a period of one day.

According to the Bjerrum concept (1967), which assumes that pre-consolidation stress is totally dependent on the deformation accumulated over the time in which the soil is subjected to a load, then equation III.86 can be written in the following manner (Neher *et al.*, 2000):

$$\varepsilon_v = \kappa^* \cdot \ln\left(\frac{p'_f}{p'_0}\right) + \left(\lambda^* - \kappa^*\right) \cdot \ln\left(\frac{p'_p}{p'_{p0}}\right) \qquad \text{(III.87)}$$

Consequently, the component corresponding only to the viscoplastic strains will then be:

$$\varepsilon_v^{cr} = \left(\lambda^* - \kappa^*\right) \cdot \ln\left(\frac{p'_p}{p'_{pc}}\right) + \mu^* \cdot \ln\left(\frac{\tau_c + t'}{\tau_c}\right) \qquad \text{(III.88)}$$

Therefore, and based on figure III.25 or III.26, as well as on equations III.87 and III.88, the following can be observed (Alves, 2011):

a) If the creep effect is not considered, i.e. $\mu^*=0$, then $p'_p=p'_{pc}$, which means that the soil initially responds with an elastic stiffness (κ^*), and later with a plastic stiffness (λ^*), a behaviour which corresponds to the traditional elastoplastic model;

b) For intermediate values of creep, the soil initially has an elastic response according to a κ^* stiffness. Once the initial pre-consolidation stress p'_{p0} is reached, a plastic response will follows, with an intermediate stiffness between λ^* and k*, until the end of the primary consolidation. Lastly, creep strains take place;

c) As the creep behaviour gains importance, p'_{pc} reduces to a minimum value equal to p'_{p0}. The soil response is initially elastic with stiffness k*, until the average effective stress p'_f is achieved, and then followed only by creep strains.

III.3.2.3. SOFT SOIL CREEP MODEL PARAMETERS

For the Sof Soil Creep model, besides the initial void ratio (e_0) and the five parameters already stated for the Soft Soil model (λ^*; κ^*; c; φ'; ψ), one last parameter is required, namely the modified creep index (μ^*).

Alternatively, and for the soil stiffness definition, the compressibility index C_c and the recompressibility index C_r may also be considered, as mentioned for the Soft Soil model. For the creep, the secondary compressibility index C_α may also be adopted, according to the expression:

$$\mu^* = \frac{C_\alpha \log e}{1+e_0} = \frac{C_\alpha}{2{,}3(1+e_0)} \tag{III.89}$$

These three parameters can be related to the A, B and C parameters, as indicated below:

$$\lambda^* = B + \kappa^* \tag{III.90}$$

$$\kappa^* \approx 2A \tag{III.91}$$

$$\mu^* = C \tag{III.92}$$

As already mentioned, according to the PLAXIS manual (PLAXIS 2D-V11.02, 2012), the ratio λ^*/κ^* should be comprehended between 2.5 and 7, and for the ratio λ^*/μ^*, the values ranges between 15 and 25. Regarding the remaining parameters, meaning the ν_{ur}, K_0^{NC} and the "M" parameter, designated in PLAXIS as the advanced parameter, the indications given for the SS model are maintained for the SSC model.

Manviannan (2005), based on a data collection from other researchers works, presented a table with the ratios between the parameters λ^*, κ^* and α (Table III.2). This last parameter is given by C_α/ln(10).

Table III.2 – Values of λ^*, κ^*, α and ratio (λ^*-κ^*/α) (Manivannan, 2005)

References	Soil type	λ^*	κ^*	α	(λ^*-κ^*)/α
Mesri & Godlewski (1977)	Organic silty clay, from New Haven	0.33	0.041	0.01737	16.64
Kavazanjian (1978)	Muddy remoulded clay, from San Francisco Bay	0.28	0.043	0.02171	10.91
Hermann *et al*. (1981)	Kaolin	0.151	0.018	0.00604	22.03
Adachi *et al*. (1985)	Alluvial clay, from Osaka	0.372	0.054	0.01481	21.47
Yin & Graham (1989a)	Reconstituted illite clay	0.21	0.084	0.00838	15.03
Gnanendran (1993), Rowe & Hinchberger (1998)	Organic silty clay, from Sackville	0.154-0.242	0.021-0.055	0.0045-0.0094	20.0
Hinchberger & Rowe (1998)	Silty clay with high plasticity, from Gloucester	0.32-1.35	0.025	0.0098-0.0442	30.0
Yin & Zhu (1999b)	Marine deposits, from Hong Kong	0.205	0.047	0.00649	24.35
Yin & Zhu (1999a)	Clay, from Tarsiut Island	0.064-0.121	0.003-0.013	0.0087-0.0121	7.05-8.93
Zhu *et al*. (2001)	Surface marine clay, from Hong Kong	0.40	0.025	0.0175	21.43
	Surface alluvium, from Hong Kong	0.15	0.025	0.0080	15.63
	Deep marine clay, from Hong Kong	0.25	0.035	0.0074	29.05

Lastly, and to validate the ratios proposed in the PLAXIS manual, for the λ^* and κ^* parameters, in table III.3 the values obtained for the ratio λ^*/κ^* are presented, as well as the current values of the secondary compressibility index (C_α) for highly compressible soils.

These values and ratios were fundamental to the development of this thesis, especially in the estimation of the creep parameter for this type of soils, in the case studied. In fact, and as it will be presented in Chapter VI, parameter C_α obtained from the oedometer test performed on the foundation soils of the *Lebrija* Pond dikes, were rather lower than the expected.

Table III.3 – Ratio (λ^*/κ^*) and C_α values for several highly compressible soils

References	Soil type	λ^*/κ^*	$C_\alpha = \alpha \ln(10)$
Mesri & Godlewski (1977)	Organic silty clay, from New Haven	8.0	0.039996
Kavazanjian (1978)	Muddy remoulded clay, from San Francisco Bay	6.5	0.049989
Hermann *et al*. (1981)	Kaolin	8.4	0.013908
Adachi *et al*. (1985)	Alluvial clay, from Osaka	6.9	0.034101
Yin & Graham (1989a)	Reconstituted illite clay	2.5	0.019296
Gnanendran (1993), Rowe & Hinchberger (1998)	Organic silty clay, from Sackville	7.3	0.010362 - 0.021644
Hinchberger & Rowe (1998)	Silty clay with high plasticity, from Gloucester	12.8	0.022565 - 0.101774
Yin & Zhu (1999b)	Marine deposits, from Hong Kong	4.4	0.014944
Yin & Zhu (1999a)	Clay, from Tarsiut Island	11.6	0.020032 - 0.027861
Zhu *et al*. (2001)	Surface marine clay, from Hong Kong Surface alluvium, from Hong Kong Deep marine clay, from Hong Kong	16.0 16.0 6.0	0.040295 0.040295 0.018421

The following chapter is dedicated to vertical drains. This one begins with a brief introduction to its origins and development, as well as the several types of vertical drains available nowadays in the market. After that, greater emphasis in given to the prefabricated vertical drains (PVD), their physical characteristics and application methodology, equipment required to the execution process, as well as their advantages and disadvantages. Some work cases, where this technique of soil improvement was used, are also presented.

IV. VERTICAL DRAINS

This chapter is dedicated to the vertical drains, their origins, and how they evolved until today. Special attention is given to the prefabricated vertical band-shaped drains, mentioning their advantages as well as their disadvantages. The installation process, equipment used to place these types of elements in to the ground, and the method of execution are presented. Lastly, some work cases, where this technique has been applied, are referred, though summarized.

In recent decades, it has become very common to construct on highly compressible soils due to the growth and expansion of the urban areas in the coastal and lagoon regions. Generally, these soils present significant void ratios, high liquid limits and plasticity indexes, and consequently are considered as weak soils, with low shear strength and very low permeability. In this case, the dissipation of the excess pore pressure is slow and ground settlements extend for long periods. Consequently, civil engineering faced with new challenges, namely the construction of more complex and demanding structures, in less time, but located on areas with worse geotechnical characteristics, having to assure the safety in short and long-term analysis.

The vertical drains emerge as a solution to this problem; they can be applied to improve soil foundations consisting of extraordinarily deformable fine soil, with limited resistance and low permeability, such as peats and sludge, lagoon areas, fine organic soil, or very plastic inorganic soil (Coelho, 1996). These drains are significantly more permeable than the improved soils, and are therefore used when the consolidation of soil needs to be accelerated, in order to achieve a significant increase in shear strength more rapidly, or to minimize post-construction settlements. The drains allow the dissipation of the excess pore pressure to be processed more quickly, as the course of the drainage is reduced when they are used, since the water moves towards the drain, and then is guided from out of the foundation. In fact, not only the drainage path to the drain is minimal when compared to thick layer, but also the horizontal permeability of fine soils is, usually, higher than the vertical permeability, and consequently the consolidation process is accelerated. The benefits, in terms of time and degree of consolidation, when using the vertical drains, depends on the thickness of the compressible layer, the drain pattern adopted and the distance between drains, and also the horizontal coefficient of permeability of the soil. This advantage is lower when this technique is applied to thin layers or to soils with high consolidation coefficients.

If stability of the soil foundations is not at stake and the engineer has the time for it, this technique should be combined with the application of preload embankments (Figure I). The combining of the drains and the embankment surcharge will allow even greater acceleration of consolidation, thereby reducing the primary and secondary consolidation settlements in the post-construction phase.

When the stability of the foundation is an issue, this technique is further improved with the application of reinforcement geotextile between the foundation soil and the embankment, together with the execution of berms (Justo, 2000a; Da Silva, 2010a; Alves, 2011).

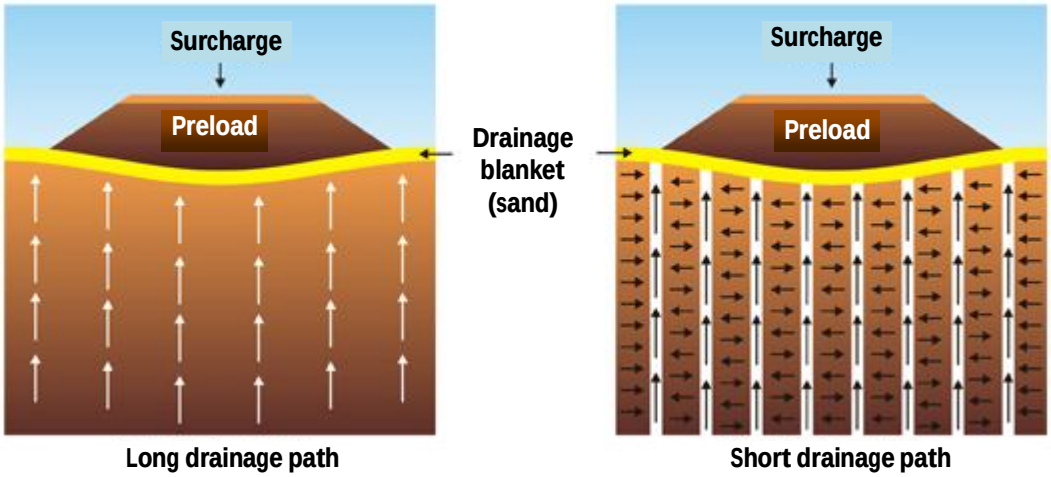

Figure IV.1 – Water seepage in a homogeneous stratum, subject to consolidation, without drains and with vertical drains (image taken from http://www.retech.in/prefa.html, in January of 2013)

It is important to highlight that the vertical drains do not reduce the settlements when a given load is applied; they only accelerate them.

IV.1. HISTORICAL SYNOPSIS

At the start of the 20th century, more specifically in 1925, Daniel E. Moran, presented and suggested, for the first time, the application of vertical drains for the stabilisation of marshland soil foundation at the San Francisco-Oakland Bay, for the construction of a road embankment (Hansbo, 1977). These drains consisted of vertical boreholes filled with sand and the aim was to improve the characteristics of the soft compressible soil. This suggestion was not used in the project; however, between 1933 and 1934, the California Division of Highways performed laboratory and field tests to check the behaviour of these drains.

With time, the sand drains were substituted by prefabricated vertical drains (PVDs). Kjellman drain, in 1939, was the first prefabricated vertical drain used, and was driven in the soil. It was made from a porous cardboard, attached to a corrugated board membrane, with vertical canals for water circulation. The geometry of these drains was approximately 3 to 4mm thick and 100mm width, being considered less voluminous, much lighter, and so they were more practical, quicker to execute and more economical. This drain was developed in one of Kjellman's first works, for a construction in Sweden, which required foundation improvement. It was found that the required distance between drains was very small and so, the use of sand drains was a very expensive and difficult solution to perform. So, this new type of drain was presented as a better solution. They are still used today due to their low cost; however, they are not advised due to their weak mechanical resistance and conservation in time (Coelho, 1996).

In 1981, Atkinson & Eldred confirmed that most vertical drains used, from those first installed in California until the early 70s, were large vertical sand drains. However, due to the high cost of purchasing large quantities of sand for this type of drains, there was a need for the development of a new product. Due to the advance in the techniques for the manufacture of filters, another new type

of prefabricated vertical, appear on the market, designated as band-shaped drain. According to some specialists, the relative efficiency of the prefabricated drains and the sand drains, as long as the latter ones are properly executed, are equivalent, although some see advantages for those made of sand, in spite of the associated high cost and greater complexity in execution, while others have the opposite opinion.

Today, polymer-based drains are the most commonly used and there is a great variety available. There are the band-shaped or wick type drains with a rectangular or circular cross-section, although this last one is less used. These drains can reach a depth of 20m to 30m.

Regarding the historical evolution of design and consolidation analysis of compressible soil under the influence of these elements, we have included a very brief summary below since this theme was covered in chapter II. Thus, in 1935 Rendulic was the first researcher to analyse the influence of vertical drains in the consolidation of clay, based on the simplified one-dimensional consolidation Terzaghi's theory in 1925, with the assumption that Darcy's law was valid, and considering a sand drain with cylindrical geometry. Later, in 1944, Barron continues with this theme, and only in 1948 considers, for the first time, the effects of the soil disturbance near the drains, caused by their installation and known as the smear effect. At the same time he also regards the limitations of the drain's discharge capacity (hydraulic resistance), on his solution.

In 1974, Yoshikuni & Nakamodo presented a thorough solution for the consolidation problem with vertical drains considering both vertical and radial flows, and the hydraulic resistance of the drain, excluding the smear effect.

In 1979, Hansbo introduced some approximations and modified the equations developed by Barron (1948) for prefabricated drains. The Hansbo solution is widespread, and it is the most used, due to its simplicity. The results obtained based on this solution do not differ much from the results obtained using more sophisticated solutions, determined using the finite element method (Onoue, 1988; Lo, 1991).

In 1991, Cheung *et al.* presented an analytical solution to determine the average degree of consolidation considering the problem in plane strain, i.e. transposing the radial drainage solution (three-dimensional) to horizontal drainage (two-dimensional), and taking in consideration only the limitation of the drain discharge capacity. Hird *et al.*, in 1992, and Indraratna & Redana, in 1997, presented, respectively, analytical solutions for the analysis of consolidation in plane strain, incorporating the smear effect and the hydraulic resistance of the drain. Although the Indraratna & Redana (1997) analytical solution is more complete, it is also more complex; however, its results do not present significant differences compared to the Hird *et al*. (1992) solution, as will be shown in the course of the present work.

IV.2. TYPES OF DRAINS

Vertical drains can be divided into two large groups, namely vertical circular drains and vertical wick or wick drains, commonly designated by band-shaped drains.

Within the group of circular drains, there are the traditional sand drains, Sandwicks drains, and Wrapped flexible drains. The prefabricated drains are included on the second group, whose shapes are usually rectangular and can be made from various materials (McGown & Hughes, 1981).

IV.2.1. CIRCULAR DRAINS

Traditional circular drains are made by opening a borehole on the ground and fill it with sand (Sand Drain), with minimum and maximum diameters of 15cm and 45cm. Usually the diameters varies between 18cm and 30cm, being noted that smaller diameters may lead to continuity problems in the sand drains, and therefore are not advisable. Larger diameters do not present additional advantages that justify the higher cost. Spacing between sand drains go from 2.5m to 5m, approximately (axes to axes) (Purushothama Raj, 1999).

In 1948, Stanton mentioned the importance and care that should be taken in selecting the material used to fill the sand drains. Whenever possible, the filter conditions must be respected so that the water is drained without dragging fine particles into the drain, thereby avoiding clogging. When this situation is not possible, the use of clean, poorly graded sand is recommended. The vertical permeability of the sand drains should be around 10^{-2}cm/s (Coelho, 1996).

The Sandwick drains consist on a filter, set into a previously opened borehole, or placed in the ground using a mandrel, and then filled with sand (Hughes & Chalmers, 1972). These combine the technologies of prefabricated drains with those of sand drains, hence the reason for being called also as prefabricated sand drains (Figure IV.2). These drains, in addition to being more economical in terms of the quantity of the sand needed, may be installed in two ways: driven or using vibration, with a continuous auger or hollow continuous auger. They can support significant ground movements, due to the flexibility of the geotextile sleeve (Bell, 2004).

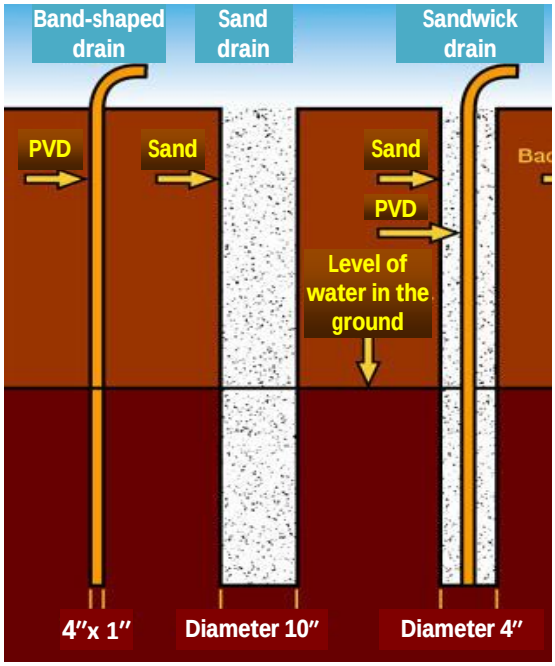

Figure IV.2 – Sand drain, Sandwick or prefabricated vertical drain and band-shaped drain (image taken from http://www.barriergeocon.com/services drains.htm, in January of 2013)

Wrapped flexible drains are made up of flexible, circular corrugated plastic tubes, which are wrapped by both a layer of natural fibre and a geotextile sleeve similar to those in prefabricated sand drains (Figure IV.3). These can be installed using several methods; however, they are usually driven with a circular cross-section mandrel.

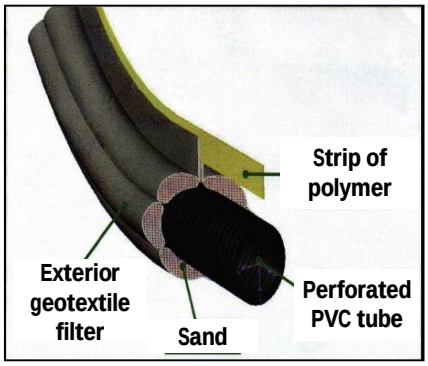

Figure IV.3 – Wrapped flexible drains
(image taken from http://cleanculverts.com/ products.htm, in January 2013)

IV.2.2. PREFABRICATED BAND-SHAPED VERTICAL DRAINS

The group of wick drains or band-shaped prefabricated drains includes several types (Table IV.1). Since all of them as is origins from the cardboard drain developed by Kjellman, their sizes are practically similar. For greater longevity of the exterior filters, when made from paper, they are soaked in chemical products in order to prevent their deterioration.

Table IV.1 – Characteristics supplied by the manufacturer of band-shaped prefabricated vertical drains, according to McGown & Hughes (1981)

Type of drain	Approximate sizes		Nominal diameter	Materials		Permeability of the filter
	Width	Thickness		Core	Filter	[cm/s]
Kjellman	100 mm	3.0 mm	66 mm	card	card	1×10^{-5}
Mebra						
Paper filter	95 mm	3.2mm	63 mm	polyethylene	treated paper	6×10^{-7}
Polypropylene	95 mm	3.4mm	63 mm	polyethylene	polypropylene	2×10^{-2}
Polyester	95 mm	3.4mm	63 mm	polyethylene	polyester	2×10^{-2}
Geodrain	95 mm	4.0 mm	63 mm	polyethylene	treated paper	6×10^{-7}
Colbond						
Initial	300 mm	4.0 mm	194 mm	non-woven polyester KF650		3×10^{-2}
Alidrain	100 mm	7.0 mm	68 mm	plastic	cellulosic	3×10^{-4}
Castle Drain Boards	94 mm	2.6 mm	62 mm	polyolefin	non-woven	2×10^{-2}

Based on table IV.1, only the initial Colbond drain presents a larger width compared to the others; Nowadays, the Colbond drain width is similar to the other prefabricated vertical band-shaped drains for issues related to the drilling equipment.

The prefabricated vertical drains (PVDs) are currently made up of a plastic core, wrapped in a geotextile filter, as it can be seen in the images (Figures IV.4a, IV.4b, IV.4c, IV.4d) or schemes (Figures IV.5a, IV.5b), and they presents a high discharge capacity which corresponds to 70% of the total area of the drain (Figures IV.6a, IV.6b).

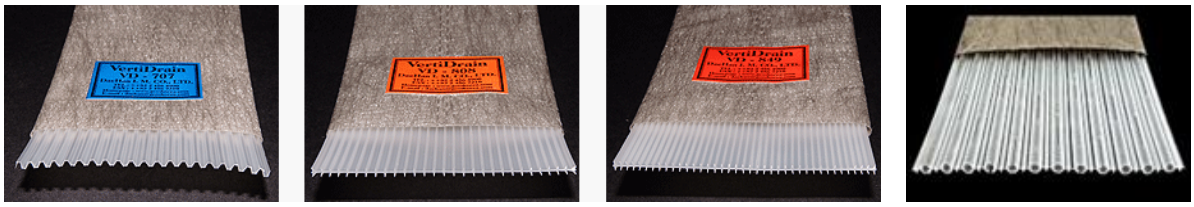

4a) 4b) 4c) 4d)

Figure IV.4 – Prefabricated vertical band-shaped drains (images token from http://www.geosko.com/en/sub2/wick-drain.php, in January of 2013)

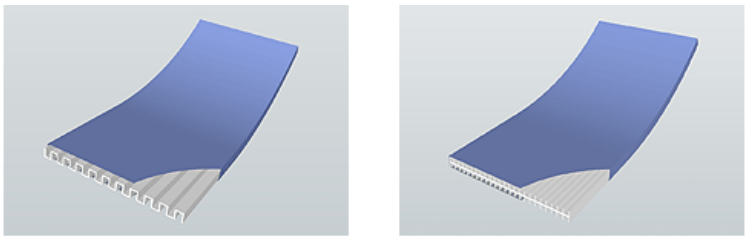

5a) 5b)

Figure IV.5 – Schemes of prefabricated vertical band-shaped drains (images token from http://www.geosko.com/en/sub2/wick-drain.php, in January of 2013)

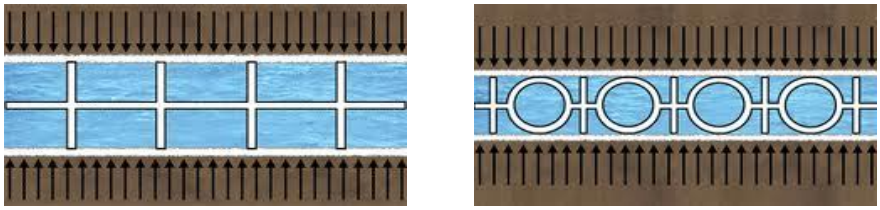

6a) 6b)

Figure IV.6 – Drainage of prefabricated vertical band-shaped drains (images token from http://www.gobizkorea.com/blog/..., in January of 2013)

Although the PVD drains present some advantages over the sand drains, they do not withstand large ground deformations. These two issues are covered in more detail in the following subchapters.

IV.3. INSTALLATION METHODS

The main recommendations for the use of prefabricated band-shaped drains concern their installation method. For sand drains and Sandwick drains, the main issue if related to the drilling method used to open the borehole, or the driven method used to install the tube or pipe into the ground. The installation of the drains has a huge influence on the future behaviour of the set, due to the disturbances caused around the drain (Calderon, 1992).

According to Coelho (1996) and Purushothama Raj (1999), the boreholes made for the installation of the sand drains are relatively cheap, but the drain itself is expensive because they need sandy material with specific hydraulic and filter properties. Although the procedure associated with the execution of this type of drain is always the introduction of a steel tube into the ground, which is later removed as the sand is inserted from the top of the hole, the methods used to do this may be distinct, namely:

a) Driving a tube closed at the end, with a mandrel, using a cover-hinge-valve, with vibration or percussion (dynamic), being the sand introduced into the borehole as the tube is extracted. This method has the inconvenience of causing a high disturbance to the adjacent soil, with a subsequent increase in pore pressure, and reduction in the permeability in the zone surrounding the drain, in addition to a decrease in the shear strength;

b) Sinking of the steel tube on the soil due to its own proper weight. This is possible when water is injected under pressure ("*lançage*") into the ground, causing the disaggregation of the soil. The soil comes out of the borehole with the flow of ascending water, and filling is made at the same time as the equipment is removed, already with a very low injection pressure. The inconvenience of this method is the high quantity of water needed to put it into practice, and the pollution of the work platform due to the disaggregated material returning to the surface. This method causes less disturbance to the adjacent soil;

c) Rotary drilling with continuous flight auger, if the soil near the borehole can stand vertically during the extraction of the equipment and also the filling with sand, or with a hollow auger for the supply of sand, thereby allowing the self-sustaining of the borehole walls to be dispensed. This method has the same inconvenience regarding the disturbance of the soil in the zone around the borehole;

d) Opening of the borehole only by washing. This method may form boreholes with an irregular format and doubts or uncertainties may arise regarding their diameter. Often the diameter is larger than the expected and its performance exceeds the estimated results. In addition to this, sand columns with a large diameter tend to increase the resistance of the soil and the settlements of the surrounding soil change. The costs associated with this process are high due to the large volumes of sand needed to fill the borehole, as well as the possibility of cavities forming during the filling stage, and their later collapse. It is a very slow method and so is not suitable when it involves large areas, or when the lengths of the drains are extensive.

Regarding prefabricated vertical drains, these are installed using the static driving methods. The vibrating or dynamic driving of the soil must be avoided. The drive of the mandrel always causes displacements and disturbances to the surrounding and adjacent soil; however, there is less displacement with this methods and type of drains due to their reduced volume. Their installation is very simple and quick, with reduced costs, making it a more desirable technique than vertical sand drains (Rathmayer & Saari, 1983). According to Purushothama Raj (1999), these may be inserted up to a depth of 45m with the application of a static force of 200kN and with speeds that varies between 0.3 and 0.6m/sec. However, in 1987, Folque indicated that the drains might be installed up to a depth of 60m and with an installation speed of 1m/sec.

In table IV.2, and according to McGown & Hughes (1981), the installation methods and processes of the vertical drains are summarised.

Table IV.2 – Methods currently used for the installation of vertical drains, according to McGown & Hughes (1981)

Group description	Specific methods	Remarks
Displacement methods	▪ Dynamic driving; ▪ Vibration; ▪ Static driving; ▪ Washing; ▪ Combination of several.	For any of the methods, a mandrel is used, with or without a disposal shoe at the end.
Drilling or perforation methods	▪ Rotary drill with or without a casing; ▪ Rotary auger, including continuous standard and hollow flight augers; ▪ Percussion (shell and auger) methods, with or without casing; ▪ Hand auger.	
Washing methods	▪ Rotary wash jet; ▪ Washed open ended casing; ▪ Weighted wash jet head on flexible hose.	Methods in which sand is washed through the jet pipe are not suitable for prefabricated drains.

IV.4. CONSTRUCTIVE SEQUENCE OF THE FOUNDATION TREATMENT WITH BAND-SHAPED DRAINS

Since vertical drains are an efficient and very common method applied to highly compressible soils, then their bearing capacity is often insufficient to support the equipment used for their installation. In that case, and if this type of soil is located very close the surface, then the application of a reinforcement geotextile is recommended, before the application of the drainage sand blanket. This sand layer will allow the flow of the water to outside of the area under intervention (Figure IV.7). The global aim is to ensure the local stability of the foundation soil under surcharge, whether caused by the machinery during the installation phase of the drains, or by the overloads to which it will later be subjected (Lorenzo *et al*. 2004; Vertematti *et al.* 2004).

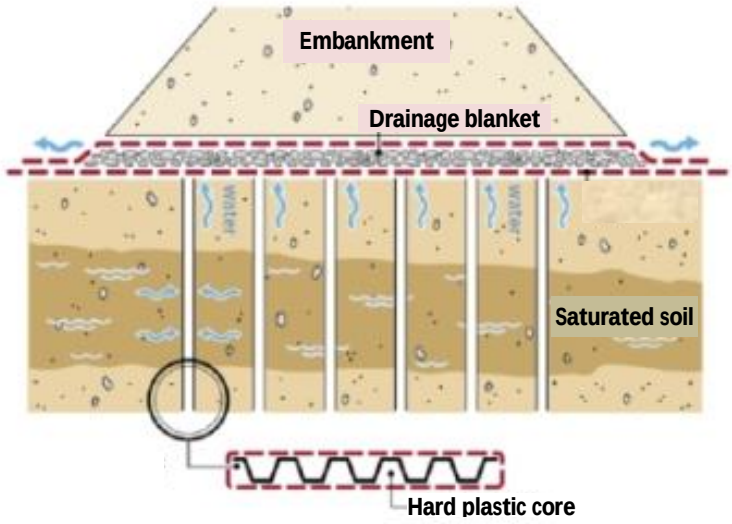

Figure IV.7 – Sand drainage blanket sand placed above the intervened area (image taken from http://www.americanwick.com/products/..., in January of 2013)

Another possibility is the construction of drainage mats forming strips or bands of sand, if the drains are concentrated in specific zones, as indicated in figure IV.8.

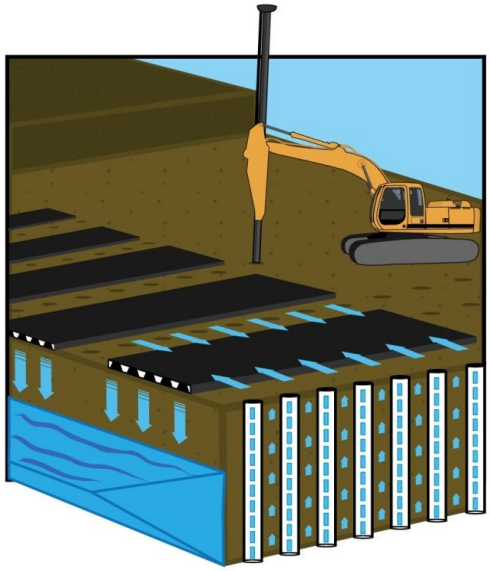

Figure IV.8 – Layer of sand placed in a restricted area, forming a drainage mat or mattress above the area treated with drains (image taken from http://www.americanwick.com/products/..., in January of 2013)

When the vertical band-shaped drains are distributed according to straight-line alignments, or are not far apart, as an alternative, they can be connected at the top to horizontal drains designated as Stripdrains (Figure IV.9a) and redirected to drainage trenches (Figure IV.9b).

9a)

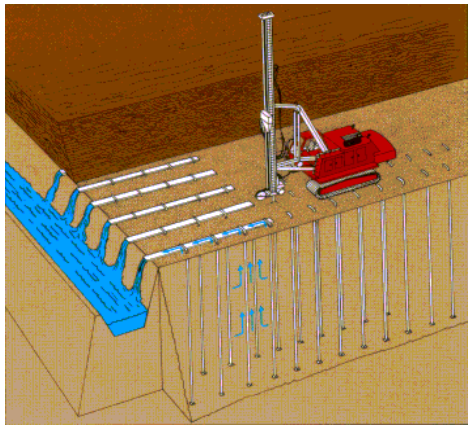

9b)

Figure IV.9 – Connection of the vertical band-shaped drains to the Stripdrain type drains
9a) image taken from http://www.ceteau.com/Products and Services /CeTeau Stripdrain, in January of 2013
9b) image taken from http://www.geotechnics.com/vertical.htm, in January of 2013

After the sand blanket is concluded, the next step corresponds to the drain installation. They should cross, preferably, the entire thickness of the compressible layer. In stratified foundations is advisable to cross at least the most compressible soil. In 1985, Runesson *et al*., performed studies on the efficiency of the drains when they do not completely cross the compressible layers.

The placing of the prefabricated drains in the ground is done through the driving of a steel mandrel, with a hollow cross-section, where the draining wick or band is placed. This should present a cross-sectional as small as possible to minimize the disturbance to the surrounding soil, but at the same time, it must be able to withstand the driving forces. For prefabricated drains, driving mandrels were developed with specific formats and sizes (Figures IV.10a and IV.10b).

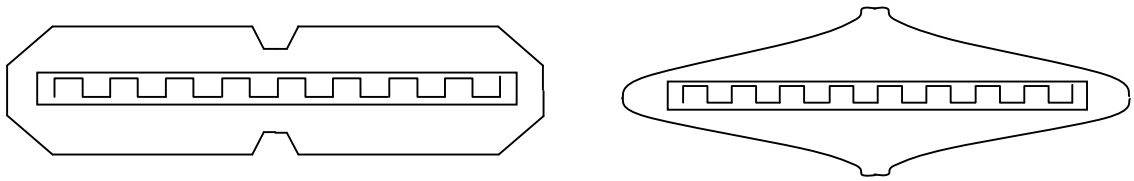

10a) **10b)**

Figure IV.10 - Steel mandrel with specific formats for driving PVD drains

At the end of the driving equipment, the band-shaped drain is connect it to a steel plate, called an anchoring or fixing plate (Figures IV.11a, IV.11b and IV.11c), which will anchor the drain to the ground. This has the double role of preventing the entry of material into the equipment during the driving, and, maintaining the drain at the depth desired during withdraws of the mandrel (Figures IV.12a and IV.12b).

11a) **11b)** **11c)**

Figure IV.11 – Steel hollow mandrel where the band is placed, and anchor steel plate
11a) image taken from http://www.fundesp.com.br/..., in January of 2013
11b) image taken from http://www.solotrat.com.br/..., in January of 2013
11c) image taken from http://www.geosyntheticsworld.com, in January of 2013

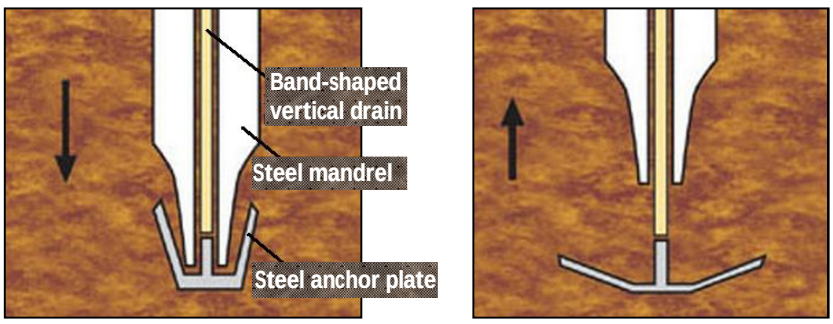

12a) **12b)**

Figure IV. 12 – Anchoring the band-shaped drain to the ground (images token from http://www.fundesp.com.br/..., in January of 2013)

Once the total withdraws of the mandrel is complete, the band-shaped drain is cut about 15cm to 20cm above the ground surface (McGown & Hughes, 1981) (Figures IV.13a and IV.13b).

13a)

13b)

Figure IV.13 – Cutting of the prefabricated band-shaped drain, after their complete installation (images token from http://www.ceteau.com/..., in January of 2013)

The methodology of the prefabricated vertical band-shaped drains execution is outlined in Figure IV.14.

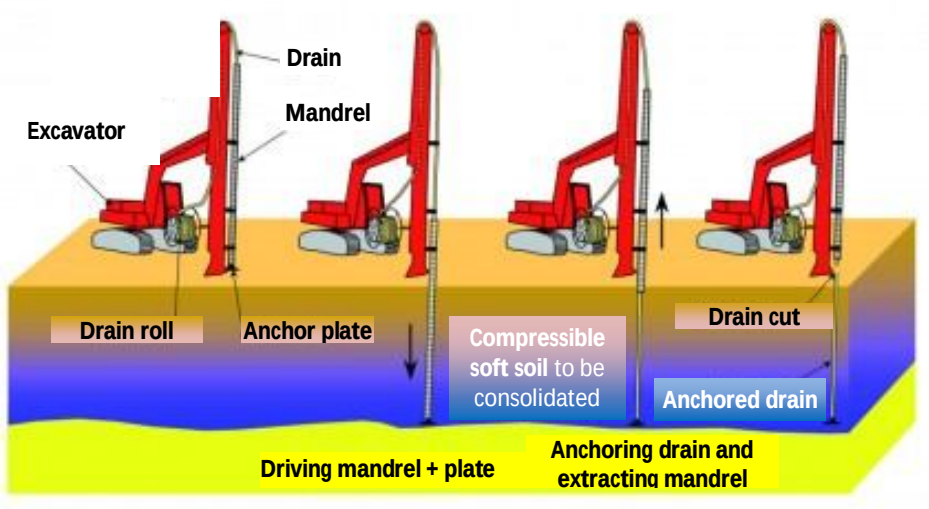

Figure IV.14 – Execution methodology of the prefabricated vertical band-shaped drains (image taken from http://www.vibromenard.co.uk/techniques/vertical-drains, in January of 2013)

Figures IV.15a and IV.15b present the machinery used for the execution of this type of drains.

15a)

15b)

Figure IV.15 – Equipment used for the installation of prefabricated vertical band-shaped drains (image taken from http://www.fundesp.com.br/..., in January of 2013)

Generally, this equipment can cross sandy layers, superficial or deep, with some consistency (Coelho, 1996). Figure IV.16a shows a panoramic sky view of a zone treated with prefabricated vertical drains, and figure IV.16b is a 3D representative scheme of it.

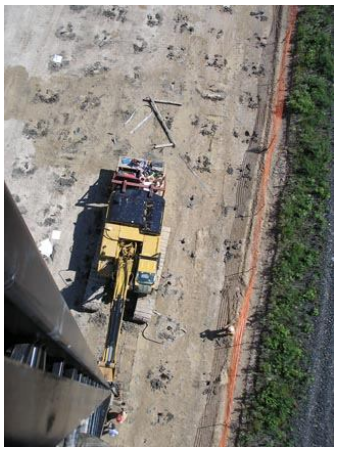

16a)

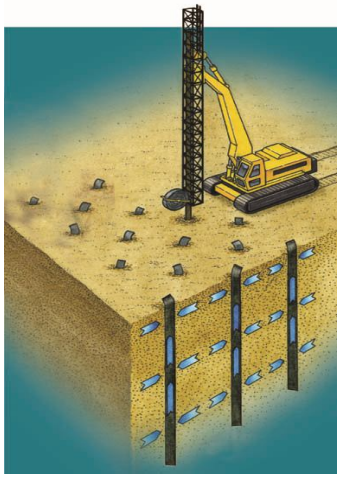

16b)

Figure IV.16 – Panoramic view of a zone treated with prefabricated vertical band-shaped drains

16a) image taken from http://www.layfieldenvironmental.com/pages/Products/..., in January of 2013

16b) image taken from http://www.admir-geo.com/Consolidation_Acceleration-Vertical_Drains, in January of 2013

As already mentioned, this technique is often combined with the construction of temporary preload embankments (Figure IV.17). The combination of the embankment surcharge with the drains, allows the anticipation of the consolidation, and a substantial part of the foundation settlements take place during the construction and the time just after it (Holtz, 1987). At the toe of the slope embankment is usual to place stabilising berms, especially when soil foundation stability is a major concern (Alves, 2011).

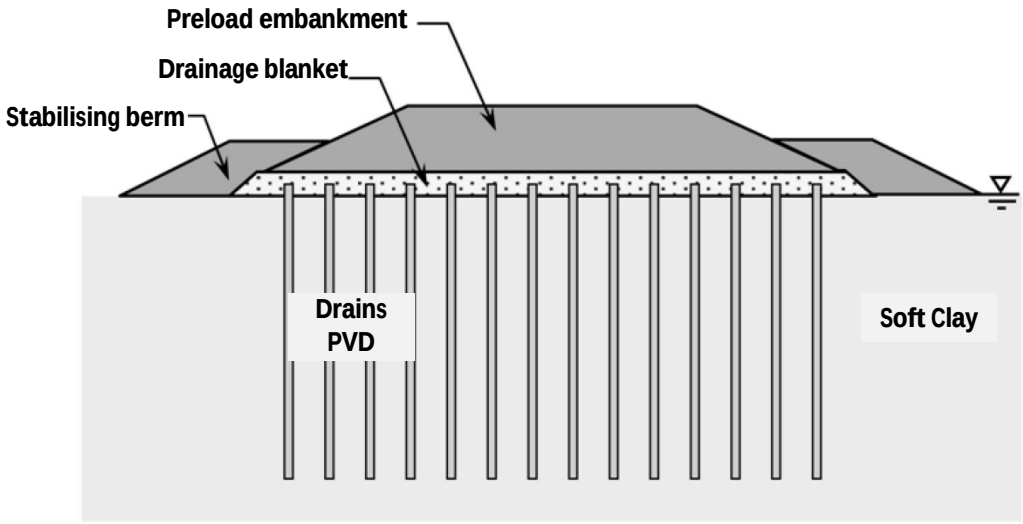

Figure IV.17 – Preload embankment combined with vertical drains and stabilising berms (Alves, 2011)

According to Nagaraj & Miura (2001), this preload must be greater than the one, which will be applied in the final phase. The excess load must only be removed when there are settlements of a similar magnitude to those estimated in the design. When combined with preload embankments, the area covered or treated with drains should extend a little the out limits of the embankment (Abrantes, 2008).

The construction rate of the embankment must also be controlled in the presence of soft to very soft soil, even when geotextile reinforcement has been used, in order to prevent the rupture of the soil foundation (Hughes & Chalmers, 1972).

A design project is only complete if an adequate survey plan is proposed. So the construction works are only concluded, after the installation of monitoring equipment, both in the soil foundation and embankment. This is essential to control the rating of settlements and excess pore pressure dissipation on this type of geotechnical projects. Settlement plates, topographic stake marks and inclinometers are recommended to measure the soil displacements, as well as piezometers to control the excess pore pressure dissipation. Readings should be taken periodically, and the results measured *in loco* should be confronted with the estimated in design. Doing so, ones can verify the efficacy and adequacy of the vertical drains and the soil behaviour.

In resume, the main advantages associated with prefabricated vertical drains are their low cost, quick installation, clean work place, and lighter installation equipment, high permeability of the drain and drainage discharge capacity, and minimum disturbance on the surrounding soil.

IV.4.1. BAND-SHAPED DRAINS WITH VACUUM (CPVDS)

Associated with this technique, the vacuum consolidation method may also be applied. Kjellman proposed this for the first time in 1952 (Chai *et al.,* 2008). The vacuum allows a decrease on pore pressures for constant total stresses, thereby leading to an increase in effective stresses, with a consequent improvement in soil strength. Due to a hydraulic gradient created by the vacuum, the water flow is forced and then accelerated. The original technique, developed by Kjellman, consisted on placing an impermeable membrane on the surface, sealing the tips in the ground, followed by applying the vacuum (dragging out the air from it) (Figure IV.18).

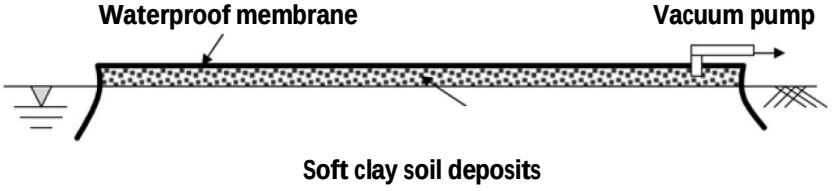

Figure IV.18 – Application of the vacuum to the clay deposit layer

The efficiency of this method depends mostly on the vacuum pump power and on the good conditions of the impermeable membrane placed on the surface. Damages on this membrane must be avoided so that the vacuum pressures are not annulled. Its employment is advisable in soft soil where the application of a load may cause instability to the foundation (Rathmayer & Saari, 1983).

Recently this technique was complemented with the introduction of vertical drains, and therefore, a new method has been developed, combining the application of vacuum to the drains elements, called Cap-drains (CPVDs). The new CPVD's consists of prefabricated vertical band-shaped drains, all connected to horizontal pipelines where the vacuum is applied. The connection system is designated as cap, giving the name to this method (Figure IV.19).

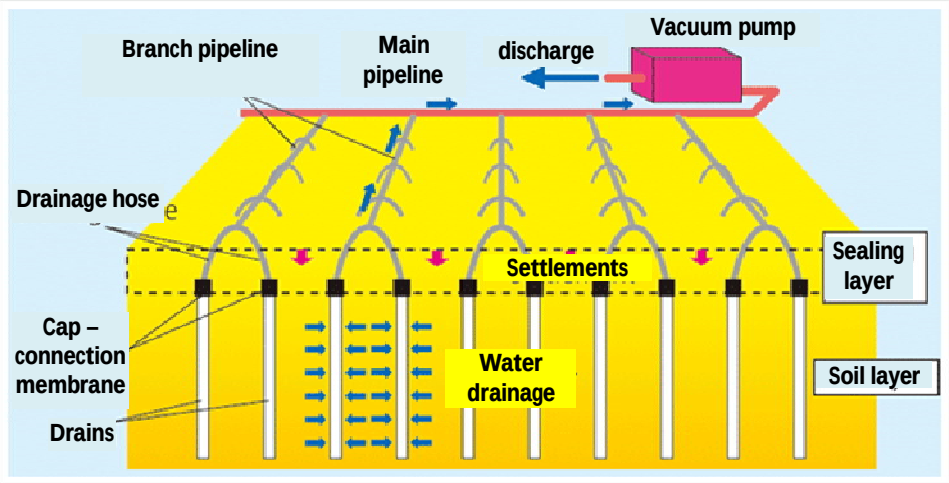

Figure IV.19 – Methodology applied to the Cap-drains (image taken from http://www.penta-ocean.co.jp/english//business/civil/vacuum_drain.html, in January of 2013)

In this technique, the vacuum is directly applied to the drains, thereby creating a pressure and stress state different to the one produced by the original technique. The pressure envelop for single and double drainage boundary are shown in figures IV.20a and IV.20b (Chai *et al.*, 2010). If this technique is used on clayed soils intercalated by sand, layers, than the CPVD drains must be sealed when in contact with the sand, in order to prevent the loss of pressure (ensure close system).

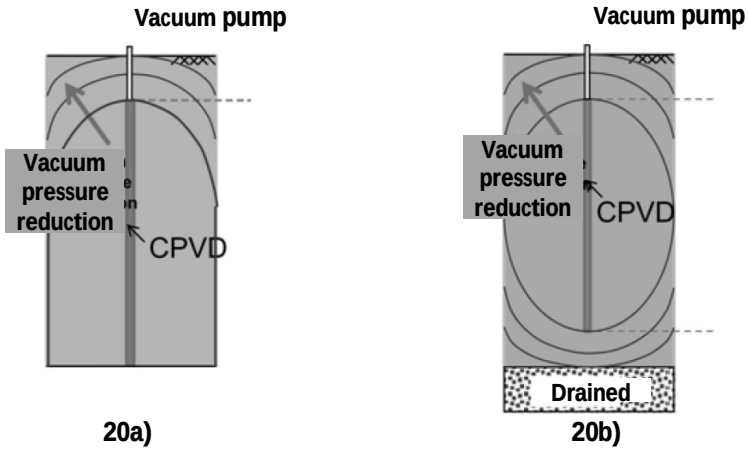

Figure IV.20 – Pressure envelop for single and double drainage boundary (Chai *et al.*, 2010)

One of the advantages of combining the drains with the vacuum is that nowadays, submerged soft soil can be consolidated more quickly, something that would be very difficult to do only with vacuum traditional method (Chai *et al.*, 2008). More recently, several researchers have developed analytical formulations which integrates this effect in the consolidation with drains (Indraratna *et al*., 2004; Indraratna *et al*., 2005; Indraratna *et al*., 2007; Chai *et al*., 2008; Saowapakpiboon *et al*., 2010).

IV.4.2. ELECTRICAL BAND-SHAPED DRAINS (EVDS)

Another recent technique was developed by the University of Singapore using electro-osmosis associated with the prefabricated vertical band-shaped drains. The concept behind electro-osmosis consists on the application of an electric current to the soil, causing the flow on water particles (Van Impe, 1989). The clay particles are naturally negatively charged, which is balanced by the positive charges of water. By passing this electric current through the soil, the water ions (OH- and H+) are attracted to the electrodes with opposite charges, i.e., the OH- ions are attracted to the anode and H+ ions to the cathode, triggering a water flow. The water flows from the anode to the cathode (Chew *et al.*, 2004; Alves, 2011). As it happen with vacuum consolidation, this technology is also combined with the introduction of PVD drains in the soil. In this case, an electric current is passed through geodrain conductors (EVD's). Compared with the methods, which use the classic PVD drains, electro-osmosis is much more effective since it does not depend only of the hydraulic gradient and external loads (Chew *et al.*, 2004; Alves, 2011).

IV.5. SPACING BETWEEN DRAINS AND EQUIVALENT DIAMETER

The drains are usually arranged according to a square or triangular pattern (Figure IV.21a and 21b). The designer is responsible for defining the pattern adopted, as well as the spacing between them (S). Prefabricated vertical band-shaped drains are closely to each other since they are smaller is

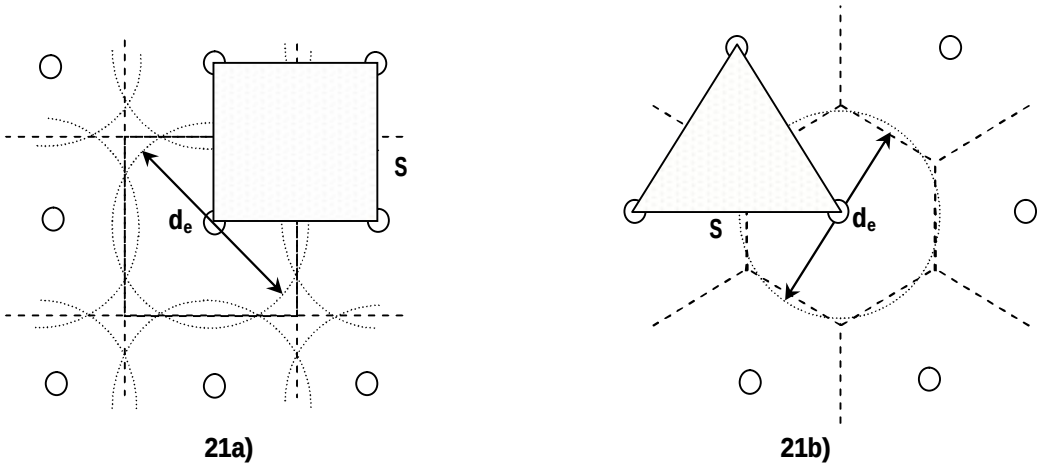

21a) **21b)**

Figure IV.21 – Vertical drain patterns adopted in the design

Traditional sand drains, Sandwicks or Wrapped flexible drains, have a circular cross-section diameter designated as d_w, which is easily determined. However, regarding prefabricated drains, and because they have rectangular dimensions, a transformation into an equivalent circular cross-section which produces the same consolidation as band-shaped drain is required (Figure IV.22).

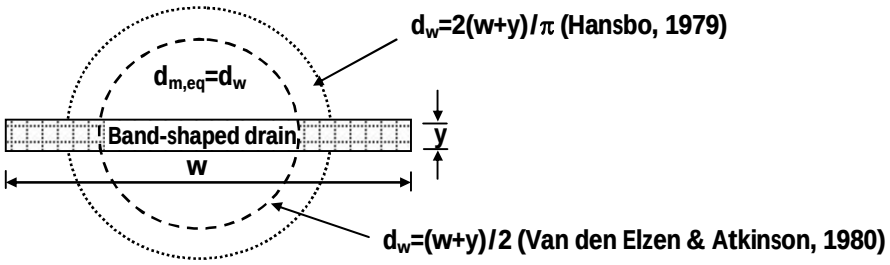

Figure IV.22 –Dimensions of a prefabricated band-shaped drain and equivalent diameter of the drain

Kjellman (1948) suggested that the equivalent diameter of a band-shaped drain, $d_{m,eq}$, would be estimated based on the mandrel perimeter. Hansbo (1979) adopted the same hypothesis. Therefore, being the perimeters equal to:

$$P_m = 2(w+y) \quad \text{and} \quad P_{dreno,\,eq} = \pi\, d_{m,\,eq} \qquad \text{(IV.1) and (IV.2)}$$

where w is the width and y is the thickness of the prefabricated PVD drain. Considering equality between the perimeter of the rectangular section of the PVD drain, and the supposed equivalent circular drain, then the result is:

$$P_m = P_{dreno,\,eq} \Leftrightarrow 2(w+y) = \pi \cdot d_{m,\,eq} \Leftrightarrow d_{m,\,eq} = \frac{2(w+y)}{\pi} \qquad \text{(IV.3)}$$

As the effect of the corners causes a decrease in the presupposed drainage perimeter of the drains, in 1980, Van den Elzen & Atkinson proposed a reduction of the equivalent PVD drain diameter by $\pi/4$, i.e.:

$$d_{m,\,eq} = \frac{(w+y)}{2} \qquad \text{(IV.4)}$$

For a typical drain of (100x4)mm, the equivalent diameter given by equation IV.3 from Hansbo (1979) gives approximately 66mm. Applying equation IV.4 from Van den Elzen & Atkinson, the equivalent diameter is reduced to 52mm. Rixner *et al.* (1986), based on the retro-analysis of real case works, performed using finite elements, achieved results which were identical to those in expression IV.4. This principle was later used in other studies by Chai & Miura (1999). However, Davies & Humpheson (1981), also based on the retro-analysis of the field results, propose that the equivalent diameter of a typical (100x4)mm drain should be 50mm. According to Atkinson & Elred (1981), and in spite of the significant differences between the diameters given by equations IV.3 and IV.4, observed that its effect on the rate of the degree of consolidation was about only 2%, i.e., this is not a factor of great relevance in the analyses of consolidation with band-shaped drains.

The majority of prefabricated vertical band-shaped drains have equivalent diameters that range between 50mm and 75mm, and the use of drains with d_w less than 50mm is not advisable (Rixner *et al*., 1986).

IV.6. FACTORS WHICH INFLUENCE DRAINS PERFORMANCE

The drains performance, both sand and band-shaped prefabricated drains, are affected by different factors, namely:

a) Permeability of the drainage blanket located above the treated soil;
b) Limitation of the vertical discharge capacity of the drain;
c) Effect of the disturbance of the soil adjacent to the drain due to its installation.

In the following paragraphs, some considerations regarding the first two aspects are presented. The third factor, the smear effect, will be looked at in a chapter dedicated exclusively to this specific theme.

IV.6.1. PERMEABILITY OF THE DRAINAGE BLANKET

As already mentioned, a layer of sand is always placed above the treated soil, with the aim of forwarding the water collected in the drains to drainage tranches. The thickness of this layer should be greater than 50cm, and the percentage of fine soil should never exceed 5%, so that the discharge capacity of this blanket will not be compromised. Chai & Miura (1999) concluded that the permeability of the sand must be higher than 10^{-4}m/s, so that it does not interfere in the drainage process and in the consolidation of the soil foundation.

IV.6.2. LIMITATION OF THE DISCHARGE CAPACITY OF THE DRAINS

The discharge capacity of a band-shaped drain, for hydraulic gradient equal to one, is defined by the product of the longitudinal permeability by the cross-section of the drain. These values are indicated in the drain technical data sheet, but it is common to find different values for the same drain, due to the different standard testing used by the manufacturers (Bo, 2004).

Hansbo analysed several methods to determine the discharge capacity of the prefabricated drains in laboratory, and concluded that the results obtained are generally greater than those observed in the field, since it is difficult to reproduce the exact filtering conditions and the effects of the installation process in the laboratory test. He also mentioned that the discharge capacity of a drain depends on the effective lateral stress that the soil exerts against the filter sleeve, deforming it and reducing the drainage section (Hansbo, 1981b). This reduction will be more significant for long drains, i.e. drains longer than 20m. In addition to this, he observed that the drainage also decreased with time, as the filter always allows the infiltration of fine soil particles to the drain core, causing a global cutback of the cross-section, or even its complete clogging. Another problem is the clogging of the filter sleeve, hence his permeability must take into account the characteristics of both the soil and the drain.

These factors are more important in the long term, having Holtz *et al.* (1987) and Chai *et al.* (2004) noted that the reduction in the drain discharge capacity (q_w) presents little influence on the consolidation rate, even for long drains, if this value is greater than $100m^3$/year. Besides that, they referred that the geotextile filter itself should allow this flow; otherwise, the discharge capacity becomes a critical design property.

Miura *et al.* (1998) investigated the theme, alerting for important factors, which causes the reduction on the discharge capacity of the drains. The study was based on laboratory tests, and on the compilation of other previous researches. The conclusions for PVD drains, are:

a) Clogging of the geotextile sleeve over time. This has a filtering role, so it must present not only high permeability but simultaneously, as to prevent the entry of fine soil particles inside the drain (Manivannan, 2005). When the fine soil particles pass through the filter and arrive at the drain core, the probability of drain clogging is high. Furthermore, it may also origin the piping phenomenon in the soil. Therefore, when choosing a geotextile filter for the drain, the particle size distribution of soil and its permeability must be taken into consideration. Kellner *et al*., in 1983, also suggested that the chemical properties of the soil and of the geotextile fibres should be considered in the criterion used for selecting the filters. The most common filter criteria for the soil/geotextile filter systems are based on correlations between the apparent sizes of the opening of the geotextile filter (Apparent Opening Size - AOS) and the diameters of the soil particles, as well as on the permeability of the geotextile sleeve and soil, according to:

- Regarding the ratios between the soil particles diameters and the apparent opening sizes of the geotextile, the criteria and ratios proposed by several researchers are presented in table IV.3:

Table IV.3 – Criteria proposed for PVD geotextile filters (Bergado *et al*., 1996c)

References	Criteria	Remarks
Calhoun (1972)	$O_{95}/D_{85} \leq 2$ to 3	Suitable for geotextile filters with a high percentage of wide pores
Ogink (1975)	$O_{90}/D_{90} \leq 1.8$	Type of soil not specified
Sweetland (1977)	$O_{15}/D_{85} \leq 1$	Soils with Cu=1.5 e Cu=4
Shober & Teindl (1979)	$O_{90}/D_{50} \leq 1.7$ to 3	Considered too conservative
Rankilor (1981)	$O_{50}/D_{85} \leq 1$ $O_{50}/D_{50} \leq 25$ to 37 $O_{15}/D_{15} \leq 1$	Soils with $0.02 \leq D_{85} < 0.25$ mm Cohesive soil Soils with $D_{85} > 0.25$ mm
Carroll (1983)	$O_{95}/D_{85} \leq 2$ to 3	O_{95} <0.50 mm to 0.75mm
Christopher & Holtz (1985)	$O_{95} \leq 1.8\ D_{85}$	Soil with more than 50% of particles passing on the 75μm sieve
Chen & Chen (1986)	$O_{90}/D_{85} \leq 1.2$ to 1.8 $O_{50}/D_{50} \leq 10$ to 12	
Holtz & Christopher (1987)	$O_{95} \leq 0.5$, $D_{85} \leq 0.3$ mm	Suitable for silt and clay
Bergado *et al.* (1992)	$O_{90}/D_{85} \leq 2$ to 3 $O_{50}/D_{50} \leq 18$ to 24	Suitable for clay

where:

∴ O_{95}, O_{90}, O_{50} and O_{15} - represents the apparent opening sizes of the filter for 95%, 90%, 50% and 15%, of the pores with smaller sizes than these. The AOS is determined on the basis of standard ASTM D 4751;

∴ D_{85}, D_{50} e D_{15} – represents the soil particles with sizes smaller than 85%, 50% and 15% of passing material, obtained in the grain-size distribution curve;

∴ $Cu=D_{60}/D_{10}$ – is the uniformity coefficient of the soil.

The ratio O_{50}/D_{50} ensures that the seepage forces in the filter are relatively small. The maximum value of 12 attributed to the ratio O_{50}/D_{50} is to prevent the infiltration of fine particles into the drain core (Bergado *et al*., 1993a). $O_{95} \leq 0.0075$mm is often specified for prefabricated drains (Chu *et al.*, 2004).

- Regarding the geotextile filter permeability, this value must always be greater than the soil permeability, namely $k_{geotextile} \geq 10k_s$ (Holtz, 1987). Bergado *et al.* (1996c) suggest, for the Bangkok soft soil clays, the ratio of $k_{geotextile} \geq 2k_s$.

b) Reduction of the drain core area available for flow, sometimes termed as the free volume, due to the infiltration of fine particles of soil to the drainage system;

c) Deformation of the drain with depth, due to the increase of lateral earth pressure. In reality, it is the exterior geotextile sleeve that suffers the deformation, leading to the reduction of the drainage area in the drain (Figure IV.23);

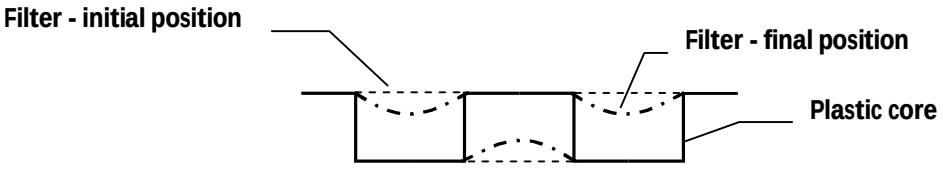

Figure IV.23 – Deformation of the geotextile filter due to lateral earth pressure

d) Possible folding, bending and crimping of the drain, due to large consolidation settlements or slope instability. The soils where the PVD drains are applied generally exhibit high settlements, and consequently the drains are subjected to these deformations. If the thickness of the layer is relatively large and uniform, then the deformations of the drain will present a less pronounced curvature. On the other hand, on the presence of stratified foundation, some layers may present weaker strength characteristics and, subsequently drain deformation are higher in these zones, so the angles formed are more accentuated and may cause a considerable decrease in the drain discharge capacity (Bergado *et al*. 1996b). Possible deformation modes of band-shaped drains, as the result of ground movements, is presented in figures IV.24a, IV.24b for homogeneous soils, and in figures IV.25a, IV.25b, and IV.25c for stratified foundations, according to Lawrence & Koerner (1988).

Figure IV.24 – Possible deformation modes of PVD drains, due to ground movements, for homogeneous soils (Lawrence & Koerner, 1988)

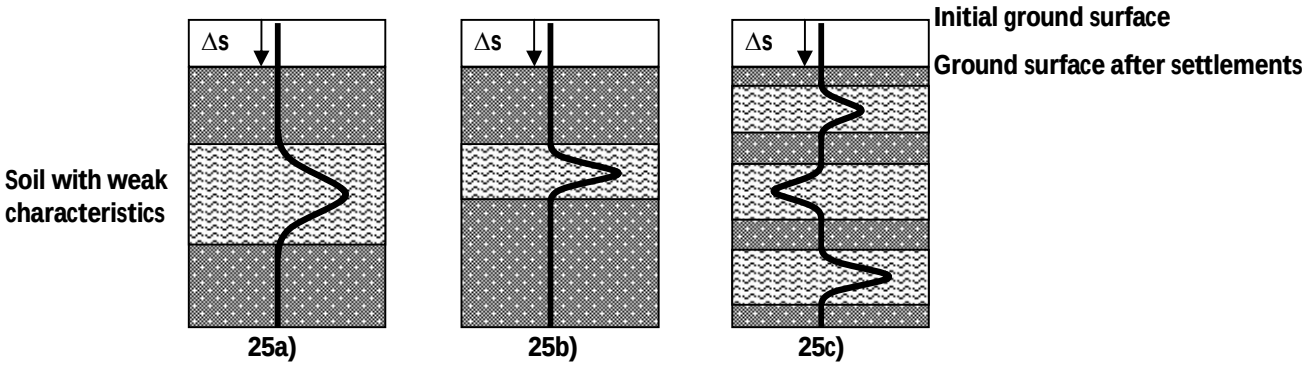

Figure IV.25 – Possible deformation modes of PVD drains, due to ground movements, for stratified foundations (Lawrence & Koerner, 1988)

Kremer (1983) concluded that the bending of the drains, associated to the foundation settlements may reduce the drainage capacity of a PVD drain to zero if the settlements reach 15% of the thickness of the compressible layer. Thus, in the design phase, the required value for the discharge capacity should be evaluated with more care, since the type of drain will be chosen based on this result. Therefore, the theoretical discharge capacity required (q_{req}) for a prefabricated band-shaped drain, considering the consolidation of a soil cylinder mass with a diameter d_e, and drain length L_d, can be estimated using the expression defined by Kamon *et al.* (1984).

$$q_{req} = s_f . \bar{U}_{10} . L_d \frac{\pi C_h}{4 T_h} \qquad \text{in m}^3\text{/year} \qquad \text{(IV.5)}$$

where:

s_f - Final settlement of the soft clay layer, equivalent to 25% of the total depth of the layer to be improved with PVD drains;

$\bar{U}_{10}$ - Time associated to 10% of the average degree of consolidation;

C_h - Horizontal consolidation coefficient of the soil;

T_h - Time factor for the horizontal consolidation.

Furthermore, in order to consider the factors that might affect and reduce the discharge capacity, this parameter must be increased by three reduction factors (Bergado *et al.*, 1996b). Therefore, the proposed minimum drain discharge capacity is given by:

$$q_{w,min} \geq F_t . F_c . F_{fc} . q_{req} \qquad \text{in m}^3\text{/year} \qquad \text{(IV.6)}$$

where:

F_t - Reduction factor associated to time;

F_c - Reduction factor associated to drain deformation;

F_{fc} - Reduction factor associated to drain and filter clogging, in the long term.

According to the authors, the values associated with these reduction factors are approximately 1.5, 2.0 and 3.5 respectively, thus:

$$q_{w,min} \geq 1.5 x 2.0 x 3.5 x q_{req} \geq 10,5 q_{req} \qquad \text{in m}^3\text{/year} \qquad \text{(IV.7)}$$

In 1985, Fellenius & Castonguay published the following results related to the drain deformation factor (F_c):

a) Drains with a hard plastic core presents reduction factors in the drain discharge capacity of around 5 to 15;
b) Drains with more flexible plastic cores present more moderate reduction factors, ranging between 1.5 and 2.

According to Hansbo (1997b), the prefabricated vertical drains present a higher drainage capacity when compared to sand drains; therefore, the hydraulic resistance of the drain may be neglected in consolidation analyses, as long as the previous conditions are respected.

IV.7. CASE STUDIES

There are many reports from work cases performed with sand drains and PVD drains. The majority of them are extremely extensive, since they were used as case studies, on researches developed for Masters and PhD theses.

However, the compilation of the results that Justo presented in 1966, in his research study, concerning the application of sand drains is highlighted. He detailed, with great precision, 116 work cases, indicating:

a) Name of the project and construction start date;
b) Characteristics of the improved soil, including soil consolidation coefficient and thickness of the layer;
c) Characteristics of the sand drains (diameter, depth, spacing and pattern adopted) and installation methods;
d) Thickness of the drainage blanket;
e) Characteristics of the preload embankment (height of the embankment, % of the load applied in comparison to the definitive load and application time);
f) Settlements obtained;
g) Excess pore pressure dissipation over time.

Among these cases we have works in Brazil, Italy, England, France, India, Sweden, New Zealand, Norway, Germany, Japan, Belgium, Puerto Rico and America (Connecticut, Los Angeles, Texas, Illinois, Washington, Salt Lake City, New Jersey, Chicago, California, Ontario, Oregon, Hawaii, New York, Norfolk, Seattle, Boston, San Francisco), and others (Justo, 1966). Although the sand drains are not the scope of the research in question, it is always interesting to consult and analyse the characteristics of these works, especially given their detail.

From the bibliography consulted, the works with greatest projection in terms of international publications and references, which subsequently led to many research studies, are those where the field tests were conducted in a real scale. Among them, we have the following works:

I. Ska-Edeby airport, west of Stockholm, Sweden (Hansbo *et al*., 1981);
II. Motorway connecting Örebro to Gothenburg, Sweden (Hansbo *et al*., 1981);
III. Refinery expansion in Trieste, Italy (Hansbo *et al*., 1981);

IV. New industrial zone in the west Port of Amsterdam in Aziëhaven, Netherlands (Hansbo et al., 1981);
V. Elevation of the railway line in Hemspoor, near Amsterdam, Netherlands (Hansbo et al., 1981);
VI. Thermo-electric plant in Porto Tolle, Italy (Hansbo et al., 1981); Pothiraksanon et al., 2010);
VII. Tha Chang Bridge in Bangkok, Thailand (Bergado et al., 1993a);
VIII. Asian Institute of Technology in Bangkok, Thailand (Bergado et al., 1993a; Bergado & Long, 1994b);
IX. Pom Prachul Naval Dock, Thailand (Bergado et al., 1993a);
X. New Bangkok International Airport, Thailand (Bergado et al., 1993a; Balasubramanian et al., 1997; Bergado et al., 2002);
XI. Storage tanks for petroleum products in Valencia, Spain (Calderon & Romana, 1997);
XII. Highway in Belfast, Northern Ireland (Davies & Humpheson, 1981);
XIII. Road and rail conjunction in Queenborough, Isle of Sheppey, UK (Nicholson & Jardine, 1981).

Many of the results observed in these case studies and sites, were used by researchers all over the world, and some of the theories and empirical expressions presented previously are based, tested and compared to them. Field tests in real scale are extremely important, since various scenarios can be experimented, namely different types of drains, with different spacing and patterns, applying several construction methods, and so on. It is also important to point out that the foundation soil, in these case studies, is generally extremely well characterised, based on “in-situ” and laboratory tests results. Additionally, all of these experimental real case studies were monitored, at each phase of the construction. All the cases mentioned above are available in the bibliography of this thesis.

The use of vertical drains are often used in port construction sites, and are mostly combined with preload embankments as the loads supported are usually very high (heavy cranes, warehouse zones, container loading and unloading zones, among others), and so, minimum deformation in the work platform is required. The choice of the improvement methods to be applied on these areas depends greatly on the characteristics of the ground foundation, the magnitude of the loads, which the soil will be subjected, the dimension of the area where the intervention is needed and finally the cost associated to each scenario.

To give an idea of the importance of the vertical drains in these type of construction work, in the next tables are presented the compilation results of several works cases, made by the Group of Port Experts from the Republic of Korea, in 2002. They studied three port construction sites located in their own country, as well as three other cases in Australia and five in Japan (Tables IV.4, IV.5a, IV.5b, and IV.6). In all of them, the soil foundation was improved using sand drains (SD), either Sandwick drains, prefabricated band-shaped drains (PVD), sand columns (SC) or stone columns (SCP).

Table IV.4 – General characteristics of the Ports where vertical drains were applied, according to the Port Expert Group - APEC 20*th* *TPT-WG* (2002)

Name of the Port	Type of Port	Location	Total Area of the Port [m^2]	Construction Period	
				Start	Conclusion
Port of Brisbane	----	Bishop Island, Australia	5 000 000	1980	----
Sakai-Senboku	Industrial Port	Sakai-2, Japan	3 500 000	1997	2008
Amagasaki-Nishinomiya-Ashiya	Industrial Port	Amagasaki, Japan	40 000	1987	2003
Sakai	Commercial Port	Gaiko -7.5G, Japan	3 900	1986	1995
Sakai	Commercial Port	Gaiko -14G, Japan	12 900	1995	2003
Hiroshima	Commercial Port	Dejima -14G, Japan	26 400	1993	2002
Gamman	Commercial Port	Busan, Korea	310 000	1997	2002
Kwangyang-1	Commercial Port	Kwangyang, Korea	596 664	1996	2001
Kwangyang-2	Commercial Port	Kwangyang, Korea	597 910	1999	2003

Table IV.5a – Geotechnical characteristics of the soil foundations, according to the Port Expert Group - APEC 20*th* *TPT-WG* (2002)

Name of the Port	Type of soil and thickness		Strength	Characteristics of consolidation	
	Description	Thickness of the layer [m]		OCR	Miscellaneous properties
Port of Brisbane	Marine sand	7.1	φ_{cu} = 32° to 34°		
	Marine clay	6.0	s_u = 6 kPa		
	Sandy clay	1.0	s_u = 80 kPa		
	Sandy silt	9.0	φ_{cu} = 33°		
	Silty clay	18.0	s_u = 150 kPa		
Sakai-Senboku	Clay	14.0	c_u=1.8z-12.7(kN/m^2) z:depth(m)	1	m_v=0.22P-1.04 C_v=40(cm^2/ day) γ_t=1.5tf/m^3
	Sand	0.6			
	Clay	4.0	c_u=17.8z-365.7(kN/m^2) z:depth(m)		m_v=0.22 P-0.04 C_v=70(cm^2/day) γ_t=1.7 tf/m^3
Amagasaki-Nishinomiya-Ashiy	Sand	10-11	N_{SPT} = 4-13		
	Clay	14-19	q_u=-0.7+0.2z (tf/m^2) z: depth(m)		C_c=0.58-1.17 C_v=50-1200(cm^2/ day) w_n = 59.1-95.6 %
Sakai-7.5G	Clay	30.0	s_u=2.35+0.13z(tf/m^2) z:depth(m)	1	C_c=0.49-2.42 C_v=232(cm^2/ day) w_n=40-85%
Sakai-14G	Clay	25.0	s_u=2.73+0.16z(tf/m^2) (z=0.0 up to 13m)	1	C_c=0.25-1.01 C_v=518(cm^2/ day) w_n=30-90%
Hiroshima-14G	Clay	20.0	s_u=0.18+0.14z(tf/m^2) (z = 0.0 up to 12 m)	1	C_c= 0.89-1.80 C_v = 167 (cm^2/ day) w_n = 40-140 %
Gamman	Clay	17.1	s_u=0.40 kgf/cm^2		C_c= 0.71 C_v = 43 (cm^2/ day) w_n = 62 %

Table IV.5b – Geotechnical characteristics of the soil foundations, according to the Port Expert Group - APEC 20*th* *TPT-WG* (2002)

Name of the Port	Type of soil and thickness		Strength	Characteristics of consolidation	
	Description	Thickness of the layer [m]		OCR	Miscellaneous properties
Kwangyang-1	Clay	14.0	s_u=0.48 kgf/cm^2	1	C_c= 0.71 C_v = 43 (cm^2/ day) ω_n = 62 %
	Clay	21.0	s_u=0.78 kgf/cm^2	1	C_c= 0.71 C_v = 43 (cm^2/day) ω_n = 62 %
Kwangyang-2	Clay	3-14	s_u=0.15 kgf/cm^2	1	C_c= 0.71 C_v = 43 (cm^2/ day) ω_n = 62 %
	Clay	6.5-18.5	s_u=0.13 kgf/cm^2	1	C_c= 0.71 C_v = 43 (cm^2/ day) ω_n = 62 %

s_u - undrained shear strength obtained from the Vane-Test; q_u – unconfined compression strength; c - cohesion; φ_{cu} - friction angle obtained from the triaxial (Consolidated-Undrained) test; C_c - compressibility index; C_v - vertical consolidation coefficient; m_v - volumetric compressibility coefficient; ω_n - natural water content; γ_t - total volumetric weight; N_{SPT} – number of blows from the Standard Penetration Test

Table IV.6 – Type of vertical drains used, area of intervention and height of the embankment, according to the Port Expert Group - APEC 20*th* *TPT-WG* (2002)

Name of the Port	Type of drain	Improved area [m^2]	Embankment height [m]	Thickness of the layer [m]	Length of the vertical drains [m]	Degree of consolidation required [%]	Consolidation time	
							Estimated	Real
Port of Brisbane	SCP	80 000	4 (approx.)					
	SC	-	-	6.0	6.0	-	3 months	3 months
Sakai-Senboku	SD	44 517	10.5-17.2	14.2	14.2-16.1	90 %	12 months	??
Amagasaki-Nishinomiya-Ashiy	SCP/SD	484	3.8-4.2	30.6	SCP = 18.4 SD = 12.2	90 %	7 months	31 months
	PVD	792	4.2-5.1	32.2	32.2$_{(media)}$	90 %	7 months	31 months
Sakai-7.5G	SD	5 200	1.9	15.5	14.5	90 %	33 months	89 months
Sakai-14G	SD	4 600	1.9	22.6	10.0	80 %	1 month	??
Hiroshima-14G	SD	8 900	4.8	15.3	12.0	90 %	6 months	??
Gamman	Sandwicks/ PVD/SD	227 000	9.4	17.1	28.0	96 %	8 months	7.7 months
Kwangyang-1	Sandwicks	255 000	8.0-8.3	14.0	19.5	90 %	12 months	12 months
	Sandwicks	330 500	2.0-5.5	21.0	23.8	90 %	15 months	15 months
Kwangyang-2	Sandwicks (1.2×1.2)	182 066	1.5-9.5	3.0-14.0	7.0-18.0	92.5-96.9%	287 days	293 days
	Sandwicks (1.2×0.8)	156 182	6.0-6.4	13.5-18.5	16.5-21.5	84.0-92.7%	353 days	357 days
	Sandwicks (0.9×0.9)	179 851	2.8-3.8	6.5-13.5	9.5-16.5	88.0-96.0%	355 days	306-333 days

Based on the data presented above, in table IV.6, most of the improvement technique used the sand drains and the Sandwicks drains. Although these methods have associated higher costs, it is believed that they were chosen due to the dimensions of the improved areas, and in some cases the depth. Furthermore, since the soils foundations presented high compressibility and the expected settlements were significant, then the risk of prefabricated drains suffered relevant deformations was a factor to be considered. In addition to this, the sand drains, sand columns and stone columns, brings additional resistance to the soil foundation, since the weaker clay soils are substituted by materials with better characteristics.

In order to add new work cases to those already referred, five recent works undertaken in Portugal will be presented. These had less international visibility and projection, but were published in congresses and specialised Portuguese magazines. Finally, some aspects related to the case study for the new Ota airport are indicated. They are presented in chronological order.

IV.7.1. WORKS CASES IN PORTUGAL

IV.7.1.1. DOCK NO.4, *LEIXÕES* PORT

According to Furtado (1995), the Administration of the *Douro* River and *Leixões* Ports decided, in mid-1987, to install a container terminal on an embankment adjacent to the designated South Quay of Dock No.4 of the Port of *Leixões*, located in the North of Portugal, near the River *Leça* (Figure IV.26).

Figure IV.26 – Container terminal of Dock No.4, *Leixões* Port (image taken from http://www.bing.com/maps/..., in November of 2012)

In the geological characterisation of the site, a thick layer of alluvial silt, filling the fossil valley of the River *Leça*, was observed. Therefore, the soil was characterised as having low shear strength, high compressibility and consequently low permeability. The combination of these factors resulted in the prediction of major settlements in long term, and so, the Port Authorities decided to undertake works that promoted the preconsolidation of the silty soils.

The area to be consolidated was divided into four areas, each one of them treated with vertical prefabricated drains and using a preload embankment. The embankment surcharge represented the future demands of the project and its construction was carried out in steps. The goal was to obtain, in three months, 90% of the estimated total settlement, which was achieved satisfactorily.

The characteristics of the clay stratum profile considered in the analyses represented the average soils conditions. The in-situ test included 28 CPT tests and 24 boreholes, in which SPT and Vane Tests were performed, with re-mixed samples being collected. Laboratory tests were also performed, including Atterberg limits, grain-size distribution analysis, specific soil weight, water content, triaxial compression and oedometer tests with vertical drainage and radial drainage. The estimated values for the silty layer, based on the results from the tests performed, were (Table IV.7):

Table IV.7 – Average characteristics of the silty layer of the Dock no. 4, *Leixões* Port (Furtado, 1995)

Parameters	West Area	East Area
m_v	$3x10^{-2}$ cm^2/kg	$5x10^{-2}$ cm^2/kg
C_v	$4x10^{-4}$ cm^2/s	$4x10^{-4}$ cm^2/s
C_r	$16x10^{-4}$ cm^2/s	$25x10^{-4}$ cm^2/s

Based on these values, and only in three months, 80% to 90% of the estimated settlements were achieved, correspondent to a value of approximately 80cm. The prefabricated vertical drains used were the MEBRADRAIN 7407 type, with an equivalent diameter of 5cm, for a triangular pattern with a spacing of 1.40m.

During the execution of the drains and of the loading embankment, their behaviour was constantly monitored by settlements plates, piezometers and inclinometers. The control and measurement continued until the complete stabilisation of the settlements.

IV.7.1.2. EAST EXPANSION OF THE *BEIROLAS* LANDFILL

The 1998 World Exposition, also known as EXPO ' 98, or, by 1998 Lisbon International Exhibition, took place in Lisbon-Portugal. The area chosen for the construction of this important exposition covered a big area at the eastern boundary of the city of Lisbon, near the River Tagus, currently designated as *Parque das Nações* (Figure IV.27a). Studies conducted in the southern part of *Parque das Nações*, identified the presence of high hydrocarbon levels, above the accepted values for residential land, as indicated in the approved Urbanisation Plan. However, the results of these studies were encouraging, as it was possible to confirm that the geological characteristics of the site (a layer of low permeability clay was identified) served as a natural barrier to the migration of the contaminants in depth. The depth up to which the contamination of the soil was identified did not exceed 2 metres, estimating approximately 250 000m^3 of the soil volume needed to be treated and/or removed. Therefore, most of this contaminated soil was removed and sent to the *Beirolas* landfill, located at the far North end of *Parque das Nações*, between the River *Trancão* and the *Beirolas* water waste power plant treatment.

In order to house all the contaminated soil, removed from the construction site, three additional cells were built (Figure IV.27b), and occupying a rectangular area of approximately 7.5 hectares and stretching to the side adjacent to the east slope of the landfill. In June 1995, a large landslide affected this east slope.

27a)

27b)

Figure IV.27 – Area of the EXPO 98 where the contaminated soil were removed, and the cells of the Beirolas landfill where they were deposited (images taken from http://www.google.com)

At the request of *Parque EXPO'98*, the National Laboratory of Civil Engineering (LNEC) of Portugal analysed the causes of the landslide and concluded that the insufficient resistance of the silty soil of the foundation had caused the accident. Based on tests, it was observed that, as an effect of the landslide, the silt suffer an important loss of strength, and so it was decided to carry out a treatment of the foundation ground with prefabricated vertical drains in the zone, together with the application of an overload platform. With this solution, the shear strength of the soil foundation should increase due to the acceleration of the consolidation process, under the load of the existing embankment and the new overload.

The zone for which the treatment with vertical drains was planned was located between the cells for the contaminated soil at the East extension of the landfill and the bank of the River Tagus, forming a strip of about 60m wide, in front of cells 2 and 3, and 40m in front of cell 1. Drains could not be installed inside the cells because of the impermeable geomembranes located at the base of the cells. They cannot be perforated in order to ensure that no leakage occurs. The plastic vertical drains (geodrains) were installed between December 1996 and January 1997, forming a triangular pattern with spacing of 2m (area per drain of 3.46m^2), and with a length of between 30 and 35m from the ground surface. The installation of drains in the entire area was not possible due to the thickness and consistency of the superficial layers in some locations.

Prior to the installation of the vertical drains, in the first months of 1996, re-profiling of the slope in the improved area was carried out, as a corrective measure of the June 1995 landslide. With this re-profiling, which covered the zone of cells 2 and 3, from the slope of the landfill up to the river, and also the area between cell 1 (empty) and the river, the ground surface was also levelled and its inclination was softened. The sunken areas, located between the East berm of the cells and the river, were filled with sand. A sand blanket with a minimum thickness of 50cm was also applied in the areas to be improved with PVD drains.

After the installation of the drains, an overload embankment was built with a maximum height of approximately 1.75m. A geotextile was placed between the sand blanket and the embankment. Considering the information available of the soil characteristics, with a horizontal consolidation coefficient of C_h of $7x10^{-8}m^2/s$, 75% of the consolidation would be achieved within 11 months and 90% in 19 months.

Once again, the area was instrumented in order to control the evolution of the consolidation degree of the soil foundation. It was necessary to considered that, between the date of installation of the drains and the placement of the embankment, some important settlements possibly occurred because the soils were underconsolidated. The final consolidation settlement values were estimated, and corresponded to 0.69m and 1.14m for the zones where the settlement plates were applied. From the analysis of the settlement measurement plates, it was possible to verify the efficacy of these drains in the increment of the shear strength of the silty soil. The cells are currently sealed, and its final appearance is that presented in figure IV.28.

Figure IV.28 – Sealed landfill located near the *Beirolas* water waste powerplant treatment (image taken from http://www.google.com, in March of 2013)

All the information referred here was taken from De Santayanna & Fernando (1997).

IV.7.1.3. PEDESTRIAN FOOTPATH ON THE TAGUS WATERFRONT, EXPO'98

In approximately 1996, it was decided to build a pedestrian footpath with about 700m in length along the right bank of the River Tagus, in the EXPO'98 intervention zone, north of the *Vasco da Gama* panoramic tower (Figure IV.29).

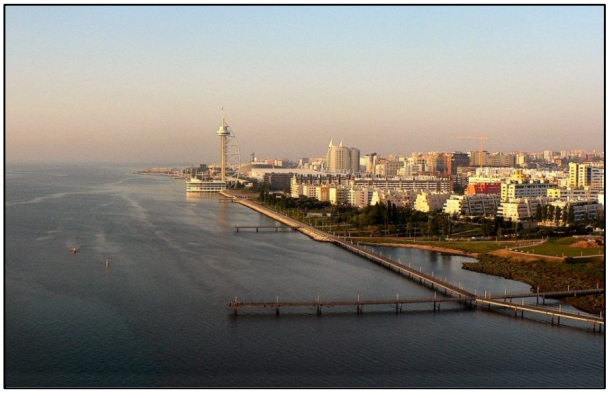

Figure IV.29 – Pedestrian footpath along the right bank of the River Tagus, EXPO'98 (image taken from http://es.wikipedia.org, in March of 2013)

An embankment was built between the river and the immersed area located just in the surroundings, with the aim of creating a leisure area and a nice quiet and green space, where people could take a walk at the end of the day, or ride a bicycle or even run. The pedestrian footpath is located along the riverside, on the extreme of this embankment. At the same time, there was the need of protecting this area against floods caused by the tides, as well as to prevent the action of erosion from the waves generated by the wind. Therefore, a rock fill prism was placed on the limit of this embankment. The remaining area was covered with embankments, which are laid on silty foundations with very low consistency, with a reduced bearing capacity and consequently presenting high deformations.

The main problem was the instability of the rock fill prism, therefore the treatment of the ground with stone columns was proposed using a vibro-substitution technique, as well as the application of prefabricated vertical drains under the embankment.

The lithological formation of the soil foundation is constituted by silty soils with a depth of 23 metres. A horizontal consolidation coefficient (C_h) of $10^{-7}m^2/s$ was considered for the entire layer. The parameters of the undrained shear strength adopted for this formation were obtained not only from Vane Tests results, but also from Cone Penetration Tests (CPT) based on empirical correlations. Table IV.8 shows the average values for the undrained cohesion (c_u).

Table IV.8 – Average characteristics of the soil foundation layer on the south zone of the Tagus waterfront, EXPO'98 (Cristóvão, 1997; Pinto & Da Silva, 2000)

Depth [m]	Undrained cohesion (c_u) [kN/m^2]
0 - 6	22.5
6 - 10	25.0
10 - 14	28.0
14 - 18	36.0
18 - 22	39.0

The prefabricated vertical drains were applied with a spacing of 1.5m between axes and distributed hexagonally (triangular mesh). The drains were applied in the zone where the embankment was placed, to reduce the consolidation time as well as the post-construction settlements. The depth of the PVD drains varied between 15m and 23m.

Once the drain installation was complete, the embankment was constructed gradually, in order to guarantee a suitable level of safety of the bearing capacity of the foundation. Then the stone columns were executed, and afterwards the work platform was removed, allowing the constructing of the rock fill.

Regarding the settlements observed, they achieved approximately 2m, ranging the magnitude expected in the design project. This value corresponds to 75% of the degree of consolidation for 6 months, after the application of the preload embankment. Cristóvão describes this work case in 1997, as well as Pinto & Da Silva, in 2000.

IV.7.1.4. *Caldas da Rainha / Marinha Grande*

In mid-2011, the company Geotest – Structural and Geotechnical Consultant, Lda, carried out the monitoring for the implementation of an embankment between PK 3+690 and 4+130, in the scope of the works for the construction of the A8 -motorway *Caldas da Rainha / Marinha Grande* Subsection. In this section of the motorway, the maximum height of the road embankment was about 12m and the foundation terrain crossed was formed of alluvial soils with defective mechanical features.

Based on this data, Geotest decided on the application of prefabricated vertical drains in the foundation terrain, thereby accelerating the consolidation process of the alluvial soil, and consequently reducing the construction time of the embankment.

The solution consisted of driving the drains from sand blankets with a maximum thickness of 1.4m, placed on a geotextile mat. In most of the area, the distribution of the drains was done on a triangular mesh with a spacing of 1.1m between them and with lengths of 20m. On the side edges of the treated area, as the compressible terrain was not as thick, the length of the drains used was 10m with a triangular mesh arrangement and spacing of 2m. Due to the weak resistance characteristics of the foundation terrain, the construction of the embankment at height had to be done in stages to avoid the occurrence of the rupture of the foundation terrain.

Based on laboratory tests, it was found that the foundation soils were classified as CL-Thin clay and CL-Thin clay with sand, which corresponded to the continuous penetration test results with the measurement of the pore pressure (CPTU). The liquid limit (ω_L) varied between 23% and 47%, with an average value of 40%. The plasticity index (IP) presented an average value of 15%, ranging between 7% and 24%. The vertical consolidation coefficient value (C_v) was around $0.5x10^{-3}cm^2/s$ to $5x10^{-3}cm^2/s$, with the designer having adopted the average value.

Based on Vane Tests carried out during the prospecting campaign, a ratio between the undrained shear strength and the actual stress given by $c_u=0.206\sigma'_v+14.04$ was adopted. However, looking at the laboratory test results, and based on the Skempton proposal, with a value of IP=15%, it can be seen that $c_u/\sigma'_v=0.11+(0.0037xIP)$.

The maximum settlement expected in the design was 1.43m, considering a maximum thickness of compressible soil of 22m, and considering a maximum embankment height of 12m. In the observation campaigns, the largest settlement recorded has a maximum value of 1.40m. However, for the section with an embankment height of 12m, the settlement observed was 1.38m, which corresponds to 96% of what had been calculated**.** Due to the results observed, the treatment was considered as adequate (Carvalho *et al.*, 2002).

IV.7.1.5. STUDY FOR THE DESIGN PROJECT OF NEW *OTA* AIRPORT

The future Lisbon Airport is expected to be constructed at *Ota*, which is located in the region of the lower Tagus River valley. The viability study and design associated to this project was performed by the FCG Consortium and publish in 2004.

Based on the geotechnical survey performed in the area, a layer of alluvium, which constituted the most recent geological unit, should be divided into two distinct zones, with clearly differentiated geotechnical behaviours. Therefore, horizon (a1) was identified as a fine soil, predominantly clay silts with layers of sandy clays, and horizon (a2) consists of medium to coarse sand with gravel and rolled stones interlayered with fine silty sands.

The vertical zoning of the alluvial layer indicates the preferential occurrence of the horizon (a1) in the top and middle of the stratum, with progressively worst characteristics and higher thickness in the downstream floodplains. The alluvial sandy and coarser horizon (a2) is distributed preferentially at the base of the alluvial layer.

Due to the unfavourable geomechanical characteristics and hydrological conditions of the clay-silt horizon (a1), it is not adequate to construct these types of projects, on this type of foundations, without the adoption of stabilizing solutions. The maximum thickness of the alluvial material was about 19.5m. The number of blows in the standard penetration test (SPT) ranged from zero to four, with a large predominance of zero values, indicating a very soft consistency, typical of muddy soils. From the *in-situ* and laboratory geotechnical tests results, being these last performed at LNEC, the following geotechnical parameters are:

- moist soil weight: γ=16kN/m³
- undrained cohesion: c_u=20kN/m²
- "pseudo-elastic" modulus: E=850kN/m²
- vertical consolidation coefficient: C_v=5x10^{-9}m²/s a 1x10^{-8}m²/s
- horizontal consolidation coefficient: C_h=1x10^{-7}m²/s
- compressibility index: C_c=0.68
- initial void index: e_0=1.58

For the horizon (a2), consisting of medium and coarse sand with rolled stones , the SPT values ranged between 10 and 50 blows for the penetration of the 30cm. Its geomechanical behaviour is indicated through the following geotechnical parameters:

- moist soil weight: γ=19kN/m³
- effective internal friction angle: ϕ'=35º
- effective cohesion: c'=0kN/m²
- "pseudo-elastic" stifness modulus: E_s=40 000kN/m²

The new airport will involve the construction of embankments, with a maximum height of approximately 18m, over these silty and clayed soils, posing stability problems due to the loading of the embankments in question. In light of these restrictions, several improvement soil solutions were studied; however, only the solution that included the application of prefabricated vertical band-shaped drains will be presented.

In order to evaluate the applicability of this method, for a soil thickness of 16m to 20m, characterised by a horizontal consolidation coefficient (C_h) value of 10^{-7}m^2/s, embankments with 11m to 16m were consider, in order to obtain 90% of the consolidation degree. This degree of consolidation was obtained after 12 months for a drain square pattern, distanced of 1.5m, axis to axis.

For the soil thickness of 16m to 20m, the value of the settlement estimated by the software used in the design, and confirmed by the PLAXIS finite elements method, was of approximately 5m. So, at the end of this period, the same height must be added to the embankment, due to the settlement predicted, in order to achieve the same crest level. In these circumstances, the thickness of the drainage blanket should be such that, after the settlement, the horizontal drainage still functions and remains above the phreatic level.

If one regards only the estimated deadlines for the 90% degree of consolidation, these would be acceptable within the global context of the works. However, regarding the amplitude of the settlements, it is believed that the 5m of vertical displacements would have serious implications, especially when the take off and runaway tracks are founded on these embankments. In addition to the settlements issue and the consolidation time, there is the problem regarding the stability of the foundation soil and embankments. Considering the undrained cohesion values in the calculation of slope stability, safety factors of FS=0.85 and 0.88 were obtained with the band-shaped solutions and for 90% of the consolidation achieved. Therefore, the solution based only on prefabricated vertical drains, without the use of other resistance elements, was considered inadequate.

IV.7.1.6. *LEZÍRIA* PARK, *FORTE DA CASA*

This work case is very interesting and is fully detailed in De Melo (2007), being a synthesis of the same presented here.

Lezíria Park, which consists of 11 industrial warehouses, is located within a set of endeavours at *Forte da Casa*, located between Lisbon and *Alverca*, near the River Tagus (Figure IV.30).

Figure IV.30 – Industrial area *Forte da Casa* - *Lezíria* Park (image taken from http://www.bing.com/maps, in March of 2013)

The construction of these warehouses occurred from 2005 to 2006, consisted on two phases: first the construction of six industrial warehouses and later the construction of the remaining five. In the construction site, a layer of organic soil with low shear strength and high compressibility was detected. To deal with the weak mechanical characteristics of the foundation, it was decided to install prefabricated vertical band-shaped drains in a triangular layout and crossing the entire formation.

Together with the drains, preload embankments were also constructed with the objective of achieving a considerable degree of consolidation prior to the construction of the warehouses.

In 2002, a prospecting campaign was carried out, which included SPT tests, vane tests, sieve analyses, Atterberg limits, oedometric and triaxial compression tests. Based on the results, a detailed geological-geotechnical report was elaborated with the characterisation of the foundations, served as a base for the embankment design. Therefore, the magnitude of the preloads embankments and the spacing of the drains installed were adapted according to the use of the plot, namely the zones destined to the warehouses, circulation and parking. In the zone of the warehouses, a drain spacing of 1.5m was adopted with a preload of approximately 20kN/m^2, corresponding to an embankment of 1m height. On the parking area of the heavy transport vehicles, for loading and unloading the products to the warehouses, the drains spacing was the same as the one mentioned above, but the design preload reached the 45kN/m^2, associated to an extra embankment height of 2.3m. In the area located near the railway line and on the plot limit, the drains were placed more nearly (1.3m between axis) but with a preload charge of only 10kN/m^2, corresponding to a 0.5m height embankment. With these solutions, the designer intended to attempt a 90% of the consolidation degree before the start of the industrial construction works.

The construction sequence of the embankments involved various stages, including:

a) Levelling the ground surface;
b) Placing of drainage layer above the surface foundations, improved with vertical prefabricated drains, with a thickness of approximately 0.8m;
c) Installation of the vertical band-shaped drains, from the top of the drainage layer, crossing the compressible soils;
d) Construction of the preload embankments.

In 18 months, the average degree of consolidation of the compressible soil was approximately achieved. Note that in the consolidation analysis, the smear effect was considered.

This is last effect is precisely the topic of the next chapter, with the presentation of several studies performed by different researchers, as well as a sensitivity analysis of the parameters characterising the smear effect. Some considerations were are also taken, regarding the solutions proposed for plane strain analysis, by Hird *et al.* in 1992, and Indraratna & Redana in 1997.

V. SMEAR

Chapter V is entirely dedicated to the smear effect and to the characterisation of the parameters that allow it to be accounted in the consolidation analyses. It is presented an extensive summary of the studies performed by several researchers, related to this subject, due to the importance of the phenomenon on the consolidation process. Immediately thereafter, a comparative study is made between the solutions of Hird *et al*. (1992) and Indraratna & Redana (1997), both for plane strain conditions, in order to demonstrate not only the differences between them, but also the influence of some parameters on the estimation of the horizontal permeability coefficient of the disturbed area (smear). This is a key point of the work undertaken since the practical work case is analysed in plane strain and this comparison allowed to decide which solution should be adopted in future analyses. The chapter ends with a sensitivity analysis of the smear parameters and their influence on the evolution of the consolidation degree. In this phase, the consolidation analytical formulations will be applied taking into account the prefabricated vertical drains, already described in chapter II, for both the axisymmetric strain and the plane strain conditions.

V.1. INTRODUCTION

As has already been mentioned, the drains installation in the ground creates a disturbance in the surrounding soil adjacent to them, designated by disturbed zone. Usually, PVD drains are installed using mandrels closed at the base and driven in the ground, thereby causing an increase in pore pressure and a reduction in both the strength and permeability of the soil in the disturbed zone, usually known as smear effect (Holtz & Holm, 1973). The most significant consequence will be the decrease in the water flow to the drain and a delay in the consolidation process of the improved soil. This effect can be considered in the consolidation analyses in two distinct manners:

a) Through the global reduction in the consolidation coefficient (C_h and C_v);
b) Through the introduction of a disturbed area around the drain, with a reduction in the coefficient of permeability in this zone.

Adopting the second hypothesis, two parameters will still be needed to be able to characterise the smear effect properly, these being:

a) The diameter of the disturbed zone (d_s);
b) The horizontal permeability of the disturbed zone (k_{hs}).

Regardless of the method used, the problem lies in the determination of these parameters and in their correspondence between theory and practice. It has been noted that the extent and permeability of the disturbed zone vary depending on the installation process, the size and the shape of the mandrel and the characteristics of the soils. As these parameters cannot be determined accurately, they are attributed based on field experiences, laboratory tests, and theoretical considerations, or by means of retro-analyses of real case results (Hird & Moseley, 2000).

V.2. DIAMETER OF THE DISTURBED ZONE

The extension of the disturbed zone or width of the smear was studied by several researchers and numerous relationships were suggested between the diameter of the disturbed zone (d_s) and the diameter of the drain (d_w), or between the corresponding areas, including:

a) $d_s \approx (1 \text{ to } 4)d_w$, by Hotz & Holm (1973), Jamiolkowski *et al.* (1983), Hansbo (1987, 1997b), Bergado *et al.* (1991, 1993b), Onoue *et al.* (1991), Holtz (1991), Mesri *et al.* (1994), Madhav *et al.* (1993), Chai & Miura (1999), Indraratna & Redana (1998);

b) Other studies led by Akagi (1979), Jamiolkowski & Lancelota (1981), *Bergado et al.* (1994a and 1996a), Hansbo (1987, 1997b), Chai & Miura (1999), and also Hird & Moseley (2000), recommend that $d_s \approx (1.6 \text{ to } 3)d_w$;

c) Chai & Miura (1999), advise the use of $d_s \approx 3d_w$ if there are no elements/tests which allow for the evaluation of the extension of the disturbance;

d) McDonal (1985), Aboshi & Inoue (1986) suggest the adoption of $A_s \approx A_{m,eq}$;

e) Basu & Prezzi, in 2007, considered that the extension or equivalent diameter of the disturbed zone is given by:

$$d_s = d_{s,\,eq} = \sqrt{\frac{4(d_{sx} + d_{sy})}{\pi}} \qquad \text{(V.1)}$$

where d_{sx} and d_{sy} correspond to the dimensions of the disturbed zone (Figure V.1) for a PVD drain, fixed by a rectangular mandrel. These dimensions are determined in accordance with expressions V.2 and V.3:

$$d_{sx} = w + (\rho - 1)y \quad \text{and} \quad d_{sy} = \rho y \quad \text{, with } 2 \le \rho \le 3 \qquad \text{(V.2) and (V.3)}$$

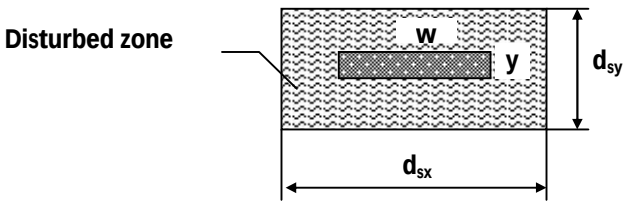

Figure V.1 – Dimensions of the mandrel/drain and disturbed zone

In addition to this disturbed zone, some researchers also consider a transition zone between the smear zone and the undisturbed zone. The diameter of this transition zone (d_t) is also given according to the diameter of the drain (d_w), or the dimensions of the mandrel. Therefore, we have:

a) Onoue *et al.* (1991) and Indraratna & Redana (1998), based on experimental results concluded that $d_t \approx (6 \text{ to } 7)d_w$;

b) Xiao (2001) obtained $d_t \approx (10 \text{ to } 15)d_w$;

c) Madhav *et al.* (1993) and Jamiolkowski *et al.* (1983), reached for d_t values expressed on the basis of the maximum dimension of the mandrel, obtaining respectively, 12w and 20w;

d) Bazu & Prezzi (2007), followed the same principle as they used to defined the smear zone, adopted the following expressions for the transition zone:

$$d_t = d_{t,\,eq} = \sqrt{\frac{4(d_{tx} + d_{ty})}{\pi}}\,, \qquad \text{admitting that:} \tag{V.4}$$

$$d_{tx} = w + (\rho - 1)y \quad \text{and} \quad d_{ty} = \rho y \quad , \text{with } 6 \le \rho \le 12 \tag{V.5) and (V.6}$$

Hawlader *et al.*, in 2002, also considered the existence of two distinct zones; however, instead of calling them smear zone and transition zone, they named them smear zone I (of a smaller size and immediately adjacent to the drain) and smear zone II (larger and surrounding the previous zone). These same researchers refer that it is the disturbed zone closer to the drain, which controls and dominates the progress of the consolidation process. Even zones with small smear diameter may significantly delay consolidation, being the degree of disturbance far more important than the extension of this zone, as other researchers had already reported.

In this case, the degree of disturbance refers to the reduction in the horizontal coefficient of permeability in the disturbed zone. In fact, this is the conditioning parameter, as it will be seen in the sensitivity analysis presented in subchapters V.4 and V.5. However, this finding is hardly surprising as consolidation is extraordinarily dependant on the soil permeability.

V.2.1. OVERLAPPING OF DISTURBED ZONE DIAMETERS

As the technology for soil foundation improvement, based on PVD drains becomes economically more accessible, it has been observed a tendency to place the drains increasingly closer, or in other words, with less distance between axes, always with the objective of accelerating the consolidation process of fine soils (Chu *et al.*, 2004). However, based on experimental field tests, Saye (2001) has noticed that there is a minimum limit for the distance between drains; once this limit is attained, there is no advantage on the consolidation rate. Walker & Indraratna (2007) explained this phenomenon with the possible overlapping of the disturbed zone of the drains (Figure V.2). Additionally, taking into account only one smear zone with a linear variation of k_{hs}, they concluded that there is no overlapping of the disturbed diameter, if the ratio $r_e / r_s \ge 0.6$ is respected.

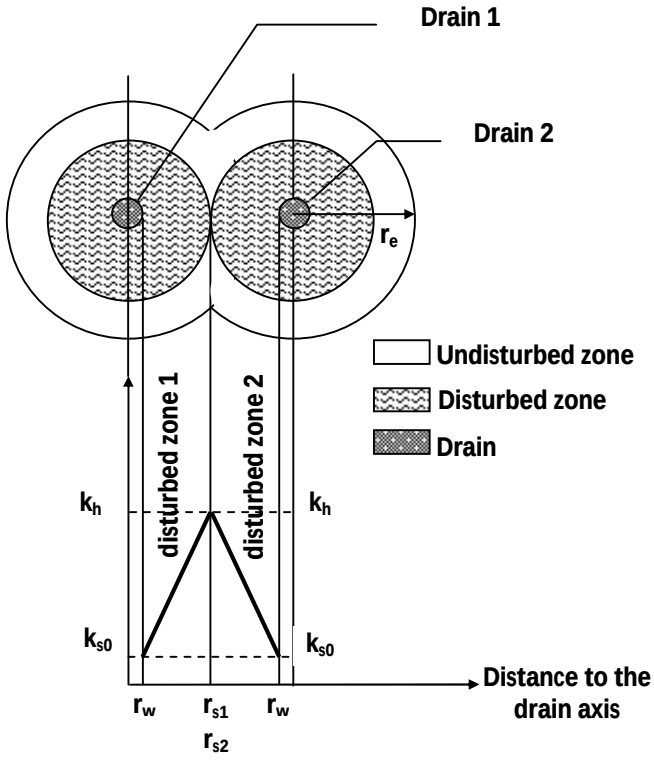

Figure V.2 – Overlapping of the disturbed zone of the drains (Walker & Indraratna, 2007)

V.3. HORIZONTAL PERMEABILITY IN THE DISTURBED ZONE

The degree of disturbance is expressed by the ratio between the horizontal permeability in the disturbed (k_{hs}) and undisturbed ($k_{h0}=k_h$) zones, being this value inferior to one $\left(k_{hs}/k_{h0}<1\right)$. Several researchers have studied the theme, having proposed the following values for the ratio k_{hs}/k_{h0}:

a) Bergado *et al.* (1991) and Onoue *et al.* (1991), based on laboratory tests, estimate that this value varies between 0.5 and 0.66;

b) Madhav *et al.* (1993), from samples collected in the field, obtain a ratio equal to 0.2;

c) Later, Bergado *et al.* (1993a, 1993b), Hansbo (1987, 1997b), Madhav *et al.* (1993) and Hird & Moseley (2000), based on field data, laboratory tests and numerical simulations, obtained, for this ratio, values ranging between 0.1 and 0.33.

If the ratio is calculated with the horizontal coefficient of permeability in the disturbed zone k_{hs} and the undisturbed vertical coefficient of permeability (k_v), then the values varied between:

a) $0.9 \le k_{hs}/k_v \le 1.42$ for natural clayed soils, where k_v is determined with the conventional oedometer test, and $1.2 \le k_{hs}/k_v \le 1.3$ for the "Matagani Varved clay", according to Tavenas *et al.* (1983);

b) Hansbo, in 1987, suggests that $k_{hs}/k_v \approx 1$ for relatively large disturbed areas;

c) Bergado *et al.* (1991), concluded that $k_{hs} \approx k_v$ for the Bangkok soft clay;

d) $0.9 \le k_{hs}/k_v \le 1.3$, with an average value of 1.15, according to Indraratna & Redana (1998);

e) Chai & Miura (1999), propose that $k_h/k_{hs} = \left(k_h/k_s\right)_L . C_f$, where k_{hL} and k_{sL} are the horizontal coefficients of permeability determined in the laboratory, associated with the undisturbed and disturbed zone, and C_f a dimensionless parameter that relates the permeability in the field and in the laboratory, this latter being, generally, greater than the unit. This correction factor is related to the disturbance of the sample and with the scale effect, and it may be considered, in some cases, $k_{sL}=k_{vL}$. It should be point out that the soil samples collected in the field, in order to determine their permeability in the laboratory, must be collected on the drain border.

Even though the analytical solutions of consolidation with drains proposed by Barron (1948), Yoshikuni (1979) and Hansbo (1979) consider a constant coefficient of permeability in the disturbed zone, experimental tests confirm a variation in this parameter with the radial distance from the drain (Onoue *et al.*, 1991; Madhav *et al.*, 1993; Bergado *et al.*, 1996a; Indraratna & Redana, 1998). Next, an overview of the proposals for the evolution of this parameter in the disturbed zone, and their respective equations, are presented. However, due to the complexity of implementing them in the numerical simulations, the engineer should verified if the gain in precision, on the rate of the consolidation is significant, or if it would be preferable to maintain more simplified solutions.

a) Barron (1948) and Hansbo (1979) - Scheme for k_{hs} constant

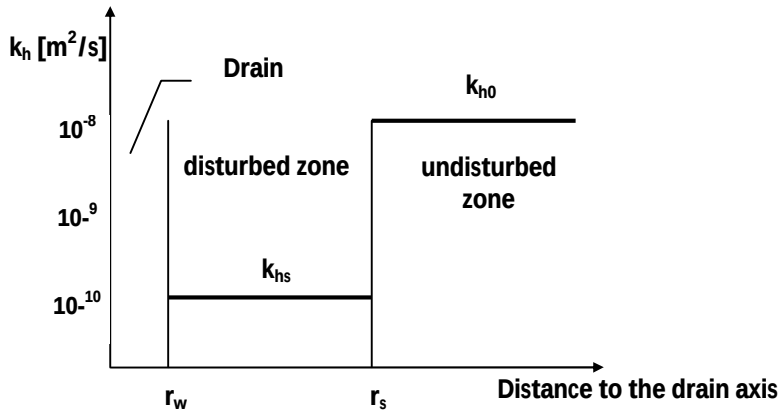

Figure V.3 – Model proposed by Barron (1948) and Hansbo (1979)

b) Onoue *et al.* (1991) - Scheme for k_{hs} with non-linear variation

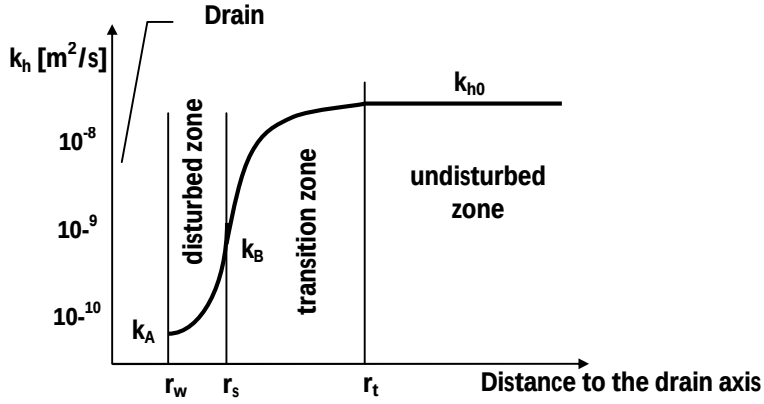

Figure V.4 – Non-linear model proposed by Onoue *et al.* (1991)

For $r_w \le r \le r_s$:

$$k_{hs} = \frac{k_{h0}}{\eta_{MAX}} \left(\frac{r}{r_t}\right)^{\alpha} \left(\frac{r}{r_w}\right)^{\beta} \quad \text{, if } r=r_w \Rightarrow k_{hs}=k_A \tag{V.7}$$

For $r_s \le r \le r_t$:

$$k_{ht} = k_{h0} \left(\frac{r}{r_t}\right)^{\alpha} \quad \text{, if } r=r_s \Rightarrow k_{hs}= k_{ht} =k_B \quad \text{and} \quad \text{if } r=r_t \Rightarrow k_{ht}=k_{h0} \tag{V.8}$$

where α is a function of the void ratio, η_{MAX} represents the remoulded effect and β is given by:

$$\beta = \alpha + \frac{\log \eta_{MAX}}{\log\left(\frac{r_s}{r_w}\right)} \tag{V.9}$$

c) Chai *et al.* (1997) - Scheme for k_{hs} with linear variation and k_{hs} with bi-linear variation

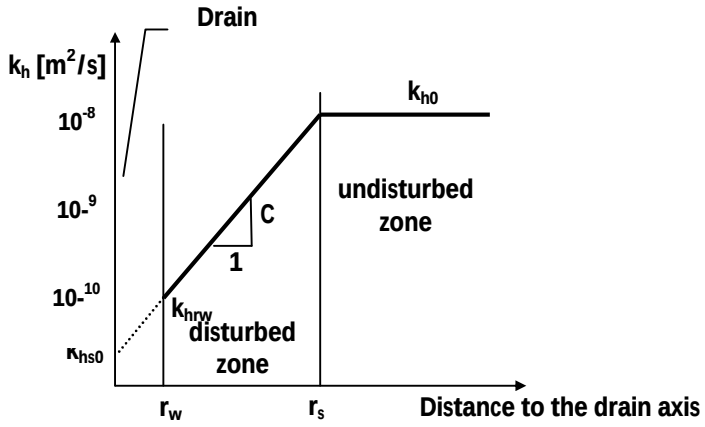

Figure V.5 – Linear model proposed by Chai *et al.* (1997)

For $r_w \le r \le r_s$, the variation of the permeability coefficient in the disturbed zone, will be given by:

$$k_{hs} = k_{hs0}\left(C \cdot r\right) \quad \text{, if } r=r_w \Rightarrow k_{hs}=k_{hrw} \quad \text{and} \quad \text{if } r=r_s \Rightarrow k_{hs}=k_h \qquad \text{(V.10)}$$

being k_{sh0} the imaginary permeability at the centre of the drain and C a positive constant. Although the model is linear, these researchers defined three distinct constants values for k_{hs}, in order to compare their results with Hansbo's solution (1979). The equations correspondents to these three distinct hypotheses are:

1st hypothesis: Permeability coefficient in the disturbed zone given by the average weighted value defined by the area:

$$k_{hs1} = k_{hs0} + \frac{2}{3}k_{hrw}\frac{s^2+s+1}{s^2-1}\left(\frac{k_{h0}}{k_{hrw}}-1\right) \qquad \text{(V.11)}$$

2nd hypothesis: Permeability coefficient in the disturbed zone defined by the simple average value:

$$k_{hs2} = \frac{k_{hrw}+k_{h0}}{2} \qquad \text{(V.12)}$$

3rd hypothesis: Permeability coefficient in the disturbed zone which gives the same smear result as the linear variation hypothesis:

$$k_{hs3} = \frac{k_{hs0}\ln(s)}{\ln(s)-(1-m^2)^2\ln\left[\left(m+\frac{s}{n}\right)\Big/\left(m+\frac{1}{n}\right)\right]+\frac{s-1}{n}m\cdot(m^2-2)} \qquad \text{(V.13)}$$

where the parameter s, n and m are defined as:

$$s = r_s/r_w\ ,\ n = r/r_w \ \text{ and } \ m = k_{hs0}/\left(C \cdot r\right) \qquad \text{(V.14), (V.15) and (V.16)}$$

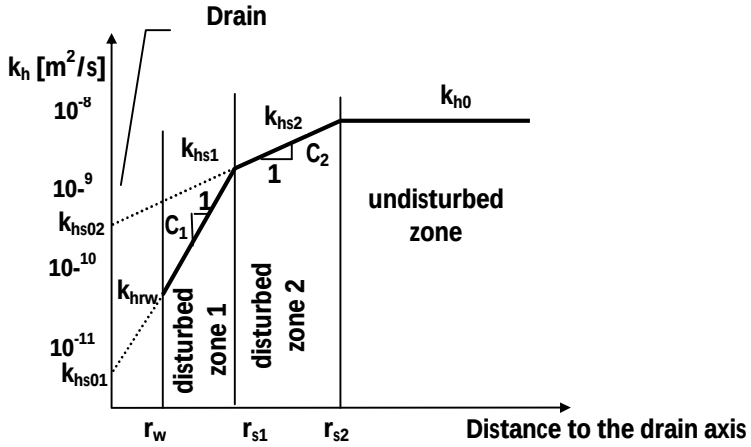

Figure V.6 – Bi-linear model proposed by Chai *et al.* (1997)

The bi-linear model will be identical to the previous model, with the slope of disturbed zone 1 being more accentuated than that of zone 2, which means that $C_1 > C_2$, both being positive constants. Therefore, we have for $r_w \le r \le r_{s1}$ and for $r_{s1} \le r \le r_{s2}$, respectively:

$$k_{hs1} = k_{hs01}(C_1 \cdot r) \quad \text{, if } r=r_w \Rightarrow k_{hs1}=k_{hrw} \tag{V.17}$$

$$k_{hs2} = k_{hs02}(C_2 \cdot r) \quad \text{, if } r=r_{s1} \Rightarrow k_{hs2}=k_{hs1} \text{ and if } \quad r=r_{s2} \Rightarrow k_{hs2}=k_{h0} \tag{V.18}$$

Developing these equations to take into account the evolution of the average degree of consolidation, the dimensionless parameters s_1, s_2, m_1 and m_2 will be needed, being determined by the following equations (Chai *et al*., 1997):

$$s_1 = r_{s1}/r_w \quad \text{and} \quad s_2 = r_{s2}/r_w \tag{V.19) and (V.20}$$

$$m_1 = k_{hs01}/(C_1 \cdot r) \quad \text{and} \quad m_2 = k_{hs02}/(C_2 \cdot r) \tag{V.21) and (V.22}$$

d) Hawlader *et al.* (2002) - Scheme for k_{hs} constant or linear

These researchers used the non-linear model by Onoue *et al.* (1991) as the base of their formulation; however, instead of considering two zones with a non-linear variation of permeability, they admitted two distinct disturbed zones, designating the zone adjacent to the drain as interior disturbed zone (zone I), and the transition zone as exterior disturbed zone (zone II). In addition to this, they considered four distinct scenarios for the permeability coefficients for each zone, three of them with k_{hs} constant, and one with a linear variation.

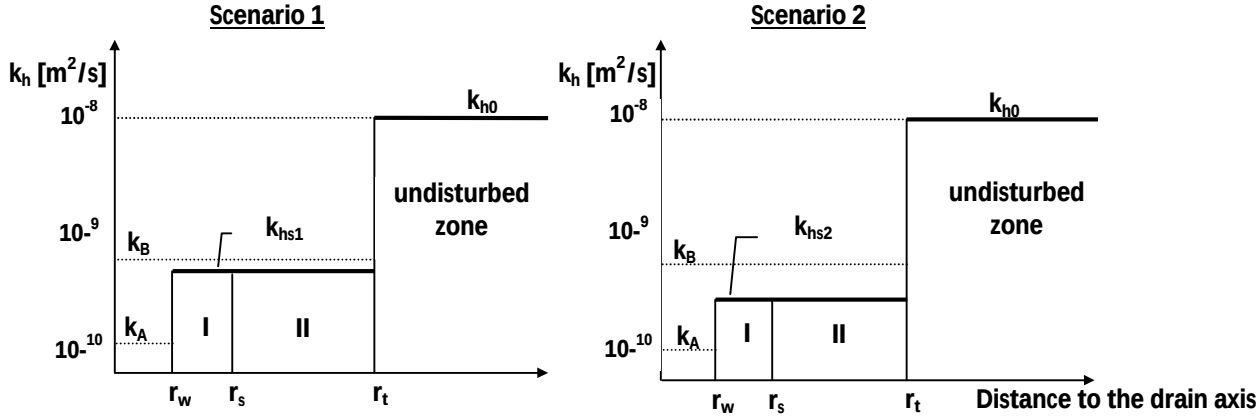

Figure V.7 – Hawlader *et al*. (2002) model, with constant permeability in zone I and II

For scenario 1, and with $r_w \leq r \leq r_t$, the permeability is given by:

$$k_{hs1} = \frac{\sum(k_s \cdot \Delta r)}{r_t - r_w} \tag{V.23}$$

For scenario 2, and with $r_w \leq r \leq r_t$, the permeability coefficient changes to:

$$k_{hs2} = \frac{k_{r=r_w} + k_{r=r_t}}{2} \tag{V.24}$$

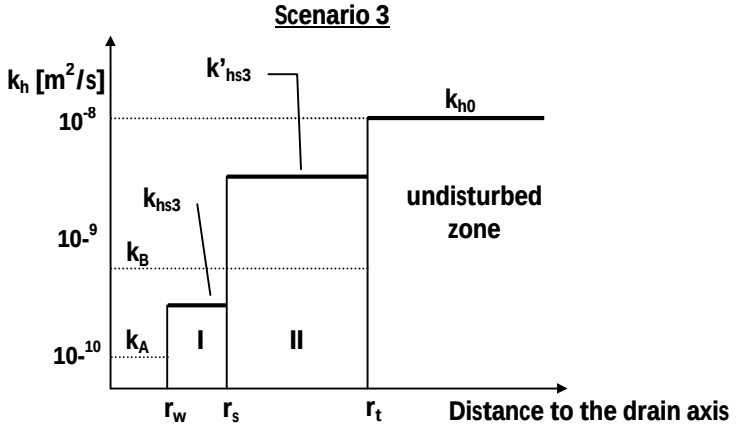

Figure V.8 – Hawlader *et al*. (2002) model, with constant permeability in the disturbed zone, although $k_{hsII} > k_{hsI}$

For scenario 3, the permeability value in the disturbed areas remains constant, although different from each other. So, and for the zone adjacent to the drain (zone 1), with $r_w \leq r \leq r_s$, the permeability coefficient will be:

$$k_{hs3} = \frac{k_{r=r_w} + k_{r=r_s}}{2} \tag{V.25}$$

In the exterior disturbed zone (zone II), with the radius r varying between r_s and r_t, the permeability coefficient will correspond to:

$$k'_{hs3} = \frac{k_{r=r_s} + k_{r=r_t}}{2} \tag{V.26}$$

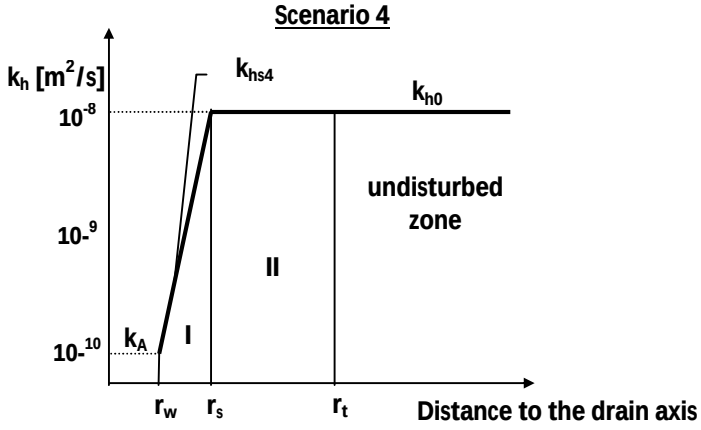

Figure V.9 – Linear model proposed by Hawlader *et al*. (2002)

For the fourth scenario, corresponding to the linear variation, when $r=r_w$, than the permeability coefficient will be k_A value, indicated by Onoue *et al.* (1991), in their non-linear model. For $r=r_s$, the permeability coefficient will corresponds to the undisturbed soil (k_{h0}), and it will remains constant and equal to k_{h0} from there on.

e) Walker & Indraratna (2006) - Scheme for k_{hs} with parabolic variation

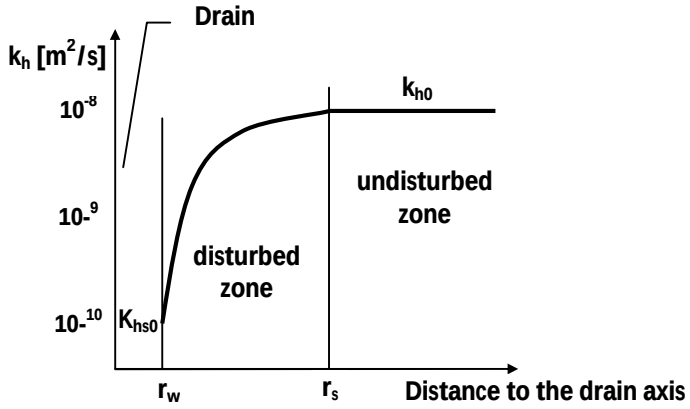

Figure V.10 – Parabolic model proposed by Walker & Indraratna (2006)

For $r_w \leq r \leq r_s$, the variation of the permeability coefficient in the smear zone for this model is given by:

$$k_{hs} = k_{hs0}\,(k-1)\left(A - B + C\frac{r}{r_w}\right)\left(A + B - C\frac{r}{r_w}\right) \qquad \text{(V.27)}$$

being parameters k, A, B and C obtained from the expressions presented below and s from equation V.19:

$$k = \frac{k_{h0}}{k_{hs0}},\ A = \sqrt{\frac{k}{k-1}},\ B = \frac{s}{s-1} \text{ and } C = \frac{1}{s-1} \qquad \text{(V.28), (V.29), (V.30) and (V.31)}$$

f) Walker & Indraratna (2007) - Scheme for k_{hs} with linear variation

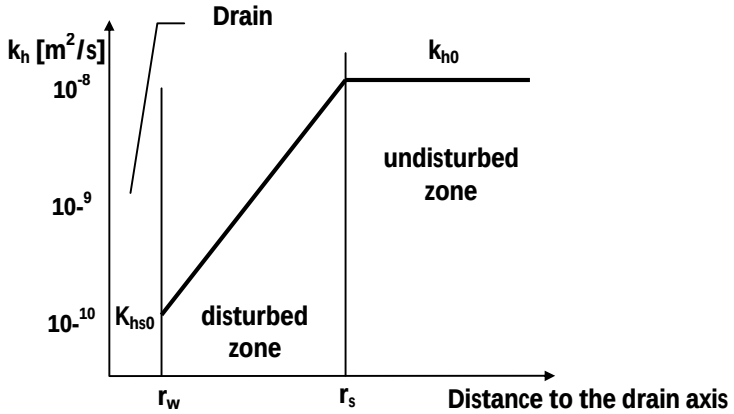

Figure V.11 – Linear model proposed by Walker & Indraratna (2007)

In this case, and for $r_w \leq r \leq r_s$, the evolution of the permeability coefficient in the smear zone will be defined by the equation:

$$k_{hs} = k_{hs0}\left(\frac{A'}{r_w}r + B'\right) \qquad \text{(V.32)}$$

In which the dimensionless parameter k is given by the equation V. 28, being A′ and B′ equal to:

$$A' = \frac{k-1}{s-1} \quad \text{and} \quad B' = \frac{s-k}{s-1} \qquad \text{(V.33) and (V.34)}$$

g) <u>Basu & Prezzi (2007) - Scheme for k_{hs} constant and k_{ht} with linear variation</u>

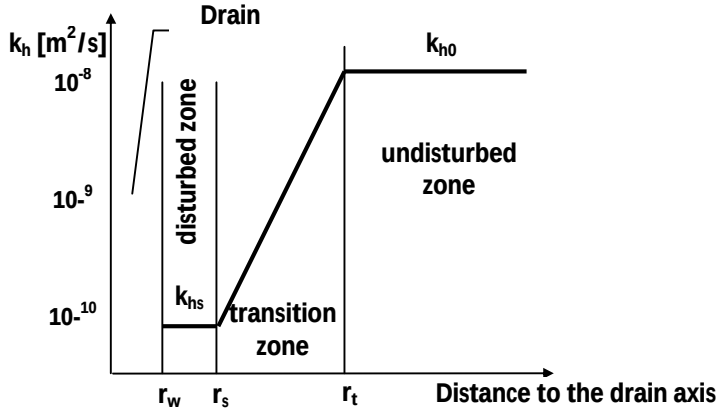

Figure V.12 – Linear model for the transition zone proposed by Basu & Prezzi (2007)

Lastly, the Basu & Prezzi (2007) model is presented, which considers a constant permeability coefficient in the disturbed zone and equal to k_{hs}, and a linear variation in the transition zone expressed by:

$$k_{ht} = k_{hs} + (k_{h0} - k_{hs})\left(\frac{2r - d_s}{d_t - d_s}\right) \qquad \text{(V.35)}$$

This equation, contrary to the previous ones, is expressed according to the diameters of the smear zone and the transition zone, not the radius.

All the permeability models briefly presented in this chapter are well detailed in the correspondent bibliography.

As a closure, the most important considerations and remarks made by several researchers, regarding this subject, are now presented:

a) Bergado *et al.* (1996a) reported that the area of the disturbed zone, in the field, is greater than that obtained in laboratory tests;

b) In turn, Hird & Moseley (2000) demonstrated that the decrease of permeability in the disturbed zone, is more accentuated in a distance of $3r_w$, and the exterior disturbed zone (transition) may extend up to $6.5r_w$;

c) Hawlader *et al.* (2002), in light of the results from the analyses, demonstrate that the calculated consolidation degree, using the linear model, is quite close to the non-linear model of Onoue *et al.* (1991). On the other hand, they state that the disturbance effect is underestimated considering any other hypothesis with a constant k_s value. These results confirm the observations made previously by Chai *et al*. (1997), without taking into account the creep effect;

d) The use of distinct or different permeability coefficients, on the boundary of two adjacent zones, may create problems during the numerical analyses, due to the discontinuity in the interfaces. Madhav *et al.* (1993) solved this problem by creating additional assumptions for the nodes located in these interfaces, and thereby allowing the use of constant values for permeability in the numerical simulations.

It should be noted that in the numerical simulations of the case study, performed in chapter VII, a constant horizontal permeability was considered, as well as just one disturbed zone. This option was due to fact that PLAXIS software does not allow the variation of this parameter with the distance from the drain. This aspect will also be taken into account in the determination of the smear effect and on the sensitivity analysis presented in the following subchapters.

V.4. SENSITIVITY ANALYSIS ON THE HORIZONTAL PERMEABILITY IN THE DISTURBED ZONE

In the modelling of a real problem, when one moves from an analysis in axisymmetric to plane strain conditions, there are always parameters which must be attributed and others which will have to be determined based on the criteria defined in the theoretical formulations described previously in chapter II. Indraratna *et al*., in 2003, performed an evaluation of the efficiency of the numerical modelling and its benefits to the design of this type of work cases.

Regarding the geometric characteristics in the plane strain, both the distance between two consecutive drains (S*), and the drain diameter (b_w), are parameters admitted by the designer. In the limit case, the improved zone can be modelled only by two drain walls; however, this solution is inadvisable, since the accuracy and approximation of the calculation method to the real problem is higher, as the distance between the consecutive drain walls are closer. Furthermore, the simplest computer solution corresponds to the adoption of b_w=0m, and the most complex and exact one will considered the radius of the drain being equal in both systems (Cheung *et al.* 1991). Regarding the characteristics of the smear zone, firstly, estimation of the diameter d_s and of the horizontal permeability coefficient K_{hsAx} is required in axisymmetric conditions. Once these values are adopted, then they must be transposed for the plane strain analyses (PD). In order to do that, and for prefabricated vertical band-shaped drains, two formulations or solutions can be used, namely the model proposed by Hird *et al.* (1992) or by Indraratna & Redana (1997). All these choices falls upon the engineer and so all the decisions must be well weighted and justified.

Therefore, in the first phase, a sensitivity analysis for the horizontal permeability coefficient in plane strain conditions was performed, varying some parameters, namely:

a) Diameter of the disturbed zone in axisymmetric conditions (d_s);
b) Reduction in the permeability in the disturbed zone in axisymmetric state (k_{hsAx});
c) Spacing between the parallel drains in the plane strain conditions (S^*).

For these analysis the real permeability and geometry of the drains, used in the case study of the *Lebrija* Pond Dikes, were considered, as well as the spacing between their axes. However, though the drains are placed in a triangular pattern, it was also decided to study the influence of the arrangement in a quadrangular pattern. As such, the data and hypotheses considered were:

1) Drains with the dimensions ($w_x y$) of 10cm by 4mm, with drain spacing of S=1.5m (axis to axis), and arranged according to a triangular or a quadrangular pattern;
2) Calculation of the equivalent diameter of the drain according to the Hansbo (1979) expression $\Rightarrow d_w=(w+y)*(2/\pi)=0,06621m$;
3) The permeability of the geotextile filter of the prefabricated drain is inferior to the discharge capacity of the drain, limiting the drainage of the band-shaped drains; therefore $k_{wAx}=k_{geotextile}=0,07m/s$;
4) In both systems, the drains present the same permeability, meaning $k_{wAx}=k_{wPD}=0,07m/s$;
5) In both systems, the permeability in the disturbed zone is considered equal, meaning $k_{hsAx}=k_{hsPD}$ (applied in the analytical solution of Indraratna & Redana, 1997);
6) The determination of b_s and b_w obeys to the same equivalence criterion between the systems, and so, if $b_w=(B.d_w^2)/d_e^2$, then $b_s=(B.d_s^2)/d_e^2$ (applied in the analytical solution of Indraratna & Redana, 1997).

Respecting all the expressions defined previously and the equations presented in chapter II for the analytical solution of Hird *et al.* (1992), and Indraratna & Redana (1997), the values for the new horizontal permeability coefficient for plane strain conditions are indicated in tables V.I to V.6. It is worth recalling that the main difference between the solutions is the geometrical delimitation of a smear zone in the plane strain for Indraratna & Redana (1997). Even though the solution proposed by these authors is the most correct from a geometric point of view, and easy to model for a few drains, it becomes difficult to implement when in the presence of a real case in which there are many drains. This occurs for two reasons, namely:

a) difficulty in defining the diameter of the disturbed zone since it has only a few centimetres, as it depends on the drain diameter, varying between $1.5d_w \leq d_s \leq 6.0d_w$;
b) divergence errors in the numerical resolution of the problem, due to the distortion of the elements that will constitute the finite element mesh in these zone.

If a greater distance between drains in the plane strain analysis were adopted (S*), the smear diameter in the zone adjacent to the drain it would become easier to considered. However, this solution may lead to a bigger difference between the real spacing (S) and the adopted spacing (S*), and consequently the disturbed horizontal permeability coefficient will result on unrealistic values, as can be seen in tables V.5 and V.6.

Table V.1 - Triangular pattern: Influence of the diameter of the disturbed zone d_s

S [m]	S*=2B [m]	$s=d_s/d_w$	$K_{h0}=k_{hAx}$ [m/s]	k_{hsAx}/k_{h0}	k_{hPD} [m/s]	k_{hPD}/k_{h0} [%]	k_{hPD} [m/s]	k_{hPD}/k_{h0} [%]
					Hird *et al.*		Indraratna & Redana	
1.5	3	**1.5**	$7.01x10^{-10}$	0.33	**$5.23x10^{-10}$**	74.58	**$5.17x10^{-10}$**	73.69
1.5	3	**2.0**	$7.01x10^{-10}$	0.33	**$4.43x10^{-10}$**	63.20	**$4.34x10^{-10}$**	61.87
1.5	3	**3.0**	$7.01x10^{-10}$	0.33	**$3.65x10^{-10}$**	52.01	**$3.48x10^{-10}$**	49.59
1.5	3	**4.0**	$7.01x10^{-10}$	0.33	**$3.24x10^{-10}$**	46.21	**$2.98x10^{-10}$**	42.46
1.5	3	**6.0**	$7.01x10^{-10}$	0.33	**$2.80x10^{-10}$**	39.93	**$2.31x10^{-10}$**	32.99

Ax – Axisymmetric; PD- Plane strain

Table V.2 - Quadrangular pattern: Influence of the diameter of the disturbed zone d_s

S [m]	S*=2B [m]	$s=d_s/d_w$	$K_{h0}=k_{hAx}$ [m/s]	k_{hsAx}/k_{h0}	k_{hPD} [m/s]	k_{hPD}/k_{h0} [%]	k_{hPD} [m/s]	k_{hPD}/k_{h0} [%]
					Hird *et al.*		Indraratna & Redana	
1.5	3	**1.5**	$7.01x10^{-10}$	0.33	**$4.43x10^{-10}$**	63.19	**$4.39x10^{-10}$**	62.58
1.5	3	**2.0**	$7.01x10^{-10}$	0.33	**$3.77x10^{-10}$**	53.72	**$3.70x10^{-10}$**	52.78
1.5	3	**3.0**	$7.01x10^{-10}$	0.33	**$3.11x10^{-10}$**	44.36	**$2.99x10^{-10}$**	42.59
1.5	3	**4.0**	$7.01x10^{-10}$	0.33	**$2.77x10^{-10}$**	39.47	**$2.57x10^{-10}$**	36.71
1.5	3	**6.0**	$7.01x10^{-10}$	0.33	**$2.40x10^{-10}$**	34.17	**$2.03x10^{-10}$**	28.98

Ax – Axisymmetric; PD- Plane strain

Table V.3 - Triangular pattern: Influence of the permeability reduction in the disturbed zone k_{hsAx}

S [m]	S*=2B [m]	$s=d_s/d_w$	$K_{h0}=k_{hAx}$ [m/s]	k_{hsAx}/k_{h0}	k_{hPD} [m/s]	k_{hPD}/k_{h0} [%]	k_{hPD} [m/s]	k_{hPD}/k_{h0} [%]
					Hird *et al.*		Indraratna & Redana	
1.5	3	3	$7.01x10^{-10}$	**0.10**	**$1.38x10^{-10}$**	19.65	**$1.31x10^{-10}$**	18.74
1.5	3	3	$7.01x10^{-10}$	**0.20**	**$2.49x10^{-10}$**	35.49	**$2.37x10^{-10}$**	33.84
1.5	3	3	$7.01x10^{-10}$	**0.33**	**$3.65x10^{-10}$**	52.01	**$3.48x10^{-10}$**	49.59
1.5	3	3	$7.01x10^{-10}$	**0.50**	**$4.82x10^{-10}$**	68.75	**$4.59x10^{-10}$**	65.54
1.5	3	3	$7.01x10^{-10}$	**0.66**	**$5.68x10^{-10}$**	81.01	**$5.41x10^{-10}$**	77.23

Ax – Axisymmetric; PD- Plane strain

Table V.4 - Quadrangular pattern: Influence of the permeability reduction in the disturbed zone k_{hsAx}

S [m]	S*=2B [m]	$s=d_s/d_w$	$K_{h0}=k_{hAx}$ [m/s]	k_{hsAx}/k_{h0}	k_{hPD} [m/s]	k_{hPD}/k_{h0} [%]	k_{hPD} [m/s]	k_{hPD}/k_{h0} [%]
					Hird *et al.*		Indraratna & Redana	
1.5	3	3	$7.01x10^{-10}$	**0.10**	**$1.19x10^{-10}$**	16.92	**$1.14x10^{-10}$**	16.25
1.5	3	3	$7.01x10^{-10}$	**0.20**	**$2.13x10^{-10}$**	30.42	**$2.05x10^{-10}$**	29.21
1.5	3	3	$7.01x10^{-10}$	**0.33**	**$3.11x10^{-10}$**	44.36	**$2.99x10^{-10}$**	42.59
1.5	3	3	$7.01x10^{-10}$	**0.50**	**$4.09x10^{-10}$**	58.34	**$3.93x10^{-10}$**	56.02
1.5	3	3	$7.01x10^{-10}$	**0.66**	**$4.80x10^{-10}$**	68.51	**$4.61x10^{-10}$**	65.78

Ax – Axisymmetric; PD- Plane strain

Table V.5 - Triangular pattern: Influence of the spacing between the parallel drains S^*

S [m]	S*=2B [m]	$s=d_s/d_w$	$K_{h0}=k_{hAx}$ [m/s]	k_{hsAx}/k_{hAx}	k_{hPD} [m/s]	k_{hPD}/k_{h0} [%]	k_{hPD} [m/s]	k_{hPD}/k_{h0} [%]
					Hird *et al.*		Indraratna & Redana	
1.5	**1.5**	3	$7.01x10^{-10}$	0.33	**$9.11x10^{-11}$**	13.00	**$8.69x10^{-11}$**	12.39
1.5	**2.0**	3	$7.01x10^{-10}$	0.33	**$1.62x10^{-10}$**	23.12	**$1.54x10^{-10}$**	22.03
1.5	**3.0**	3	$7.01x10^{-10}$	0.33	**$3.65x10^{-10}$**	52.01	**$3.48x10^{-10}$**	49.59
1.5	**4.5**	3	$7.01x10^{-10}$	0.33	**$8.20x10^{-10}$**	117.02	**$7.83x10^{-10}$**	111.64
1.5	**6.0**	3	$7.01x10^{-10}$	0.33	**$1.46x10^{-09}$**	208.04	**$1.39x10^{-09}$**	198.63

Ax – Axisymmetric; PD- Plane strain

Table V.6 - Quadrangular pattern: Influence of the spacing between the parallel drains S*

S [m]	S*=2B [m]	$s=d_s/d_w$	$K_{h0}=k_{hAx}$ [m/s]	k_{hsAx}/k_{h0}	k_{hPD} [m/s]	k_{hPD}/k_{h0} [%]	k_{hPD} [m/s]	k_{hPD}/k_{h0} [%]
					Hird *et al.*		Indraratna & Redana	
1.5	**1.5**	3	$7.01x10^{-10}$	0.33	**$7.77x10^{-11}$**	11.09	**$7.46x10^{-11}$**	10.64
1.5	**2.0**	3	$7.01x10^{-10}$	0.33	**$1.38x10^{-10}$**	19.71	**$1.33x10^{-10}$**	18.93
1.5	**3.0**	3	$7.01x10^{-10}$	0.33	**$3.11x10^{-10}$**	44.36	**$2.99x10^{-10}$**	42.59
1.5	**4.5**	3	$7.01x10^{-10}$	0.33	**$7.00x10^{-10}$**	99.80	**$6.72x10^{-10}$**	95.87
1.5	**6.0**	3	$7.01x10^{-10}$	0.33	**$1.24x10^{-09}$**	177.43	**$1.20x10^{-09}$**	170.54

Ax – Axisymmetric; PD- Plane strain

Analysing the results obtained from the two methods, it can be seen that the horizontal permeability for the plane strain, calculated with the analytical solution of Indraratna & Redana, are slightly inferior to the results obtained by Hird *et al.*, even though very similar. However, the analytical formulation proposed by Indraratna & Redana may also be directly compared to the Hird *et al.*, as it allows one to take into consideration the smear effect in the axisymmetric strain, without representing it, in the plane strain.

In addition, based on the sensitivity analysis it was observed that the horizontal permeability coefficients for the plane strain are:

a) More influenced by the reduction in the coefficient of permeability in the disturbed zone k_{hsAx}, than its diameter d_s. This conclusion is taken from observing the values in the last columns of tables V.1 to V.4. While a variation of $s=d_s/d_w$ of 1.5 to 6.0 (diameter of the smear zone 4 times greater), means a reduction in permeability from 73.7% to 33%, a variation in horizontal permeability in the disturbed zone from $0.66k_{hAx}$ to $0.1\ k_{hAx}$ means a reduction in permeability from 77.2% to 18.7% (triangular pattern);

b) Always smaller when the spatial pattern of the drains is quadrangular. This result allows one to conclude that the analytical formulation of triangular pattern presents fewer errors and will therefore translate the real problems more adequately;

c) Extraordinarily affected by the spacing considered for the parallel drain walls (S*), in the geometry of the two-dimensional problem. Therefore, and for the example presented, the distance between two consecutive drain walls cannot exceed 3 times the real distance between the drains axis. If this relation is exceeded, the horizontal permeability values in the plane strain will always overcome the initial permeability values (> 100%), thereby losing considerable precision in the results, as it is indicated in table V.5 and V.6.

In a second phase, another sensitivity analysis was performed to take into account the influence of the smear effect and the discharge capacity of the drain. In this case, the distance between the drains in the plane strain (S*) was kept constant and equal to 3 metres. The analysis was only performed for triangular pattern, but varying the spacing (S) according to the real scenarios of the soil foundation improvement of the *Lebrija* Pond Dikes, and considering the analytical formulation of Indraratna & Redana (1997). In table V.7, and for the same characteristics of the drains already presented, the results of the analytical calculations for the different scenarios have been indicated, according, namely:

a) Considering the smear effect and its geometrical representation, as well as the discharge capacity of the drains, in both systems (axisymmetric and plane strain)(1);

b) Considering the smear effect and its geometrical representation, but without accounting for the discharge capacity of the drains, in both systems (2);

c) Considering the smear effect in both systems, but without representation of this zone in the plane strain even though it exists in the axisymmetric conditions, and also considering the hydraulic resistance of the drains in both systems (3) – Comparable to the solution of Hird *et al*. (1992);

d) Without considering the smear effect, but taking into account the discharge capacity of the drains, in both systems (4);

e) Without considering the smear effect, neither the discharge capacity of the drains, in both systems (5).

Table V.7 - Triangular pattern: Influence of the discharge capacity of the drains and smear effect, considering the analytical formulation of Indraratna & Redana (1997)

S [m]	S*=2B	$s=d_s/d_w$	$K_{h0}=k_{hAx}$ [m/s]	k_{hsAx}/k_{h0}	k_{hPD}/k_{h0} [%] (1)	(2)	(3)	(4)	(5)
1.50		**2**			27	27	28	100	100
1.75		**2**			20	20	20	69	69
2.00		**2**			15	15	15	50	50
1.50		**3**			19	19	20	100	100
1.75	3	**3**	$7.01x10^{-10}$	**0.10**	14	14	14	69	69
2.00		**3**			11	11	11	50	50
1.50		**4**			15	15	16	100	100
1.75		**4**			11	11	12	69	69
2.00		**4**			9	9	9	50	50
1.50		**2**			62	62	63	100	100
1.75		**2**			44	44	45	69	69
2.00		**2**			33	33	33	50	50
1.50		**3**			50	50	52	100	100
1.75	3	**3**	$7.01x10^{-10}$	**0.33**	36	36	37	69	69
2.00		**3**			27	27	28	50	50
1.50		**4**			42	42	46	100	100
1.75		**4**			31	31	33	69	69
2.00		**4**			23	23	25	50	50
1.50		**2**			85	85	87	100	100
1.75		**2**			60	60	61	69	69
2.00		**2**			44	44	44	50	50
1.50		**3**			77	77	81	100	100
1.75	3	**3**	$7.01x10^{-10}$	**0.66**	55	55	57	69	69
2.00		**3**			40	40	42	50	50
1.50		**4**			71	71	77	100	100
1.75		**4**			51	51	54	69	69
2.00		**4**			38	38	40	50	50

Ax – Axisymmetric; PD- Plane strain

Based on the values in Table V.7, it is seen that:

a) The values of the discharge capacity of the drains in question are rather high and consequently they may be considered ideal (comparison between the results given in the columns (1) and (2), as well as at the columns (4) and (5) for the k_{hPD}/k_{h0} ratio);

b) On the other hand, the consideration of the smear effect implicates significant reductions in the horizontal permeability coefficient in the plane (comparison between the results given in the columns (1) and (4), as well as at the columns (2) and (5) for the k_{hPD}/k_{h0} ratio);

c) Once more it is observed that the reduction of the horizontal permeability in the disturbed zone (K_{hsAx}) has greater impact than the extension of this zone (d_s) (comparison of k_{hPD}/k_{h0} obtained for different K_{hs} and kipping d_s constant, with the opposite scenario, i.e., varying d_s and K_{hs} being constant);

d) When comparing the results obtained between columns (1) and (3), is the same thing as comparing the Indraratna & Redana (1997) solution with the Hird *et al*. (1992) solution, for the same smear conditions. Based on the values calculated for the K_{hPD} parameter, it can be seen that they do not differ greatly. At the most, there is a variation of 6%, which corresponds to the extreme smear conditions of having a relationship of k_{hsAx}/k_{h0}=0.66 and d_s/d_w=4. For the situations which correspond to the more common cases of smear, defined by several researchers as having k_{hsAx}/k_{h0}=0.33 and d_s/d_w=3, the difference in the results between both solutions is around 2%.

Based on this last statement, as well as on the results of the tables presented above, it was decided to consider the analytical solution of Indraratna & Redana for the determination of the disturbed horizontal permeability coefficient in the plane strain analysis, in the numerical simulations of the case study. Nevertheless, the conditions assumed correspond to the same as the Hird *et al*. solution, i.e., the account for the smear effect in both systems, but without the discretization of these zones in the plane strain, even though they were considered in the axisymmetric conditions.

V.5. SENSITIVITY ANALYSIS OF THE CONSOLIDATION DEGREE WITH PREFABRICATED VERTICAL DRAINS

In order to check the influence of PVD drains on the evolution of the consolidation degree of clay layer, as well as its variation with the smear effect parameters, the following scenarios were considered for axisymmetric analysis with triangular distribution of the PVD drains:

a) Drain spacing constant and equal to 1.5m between them, with K_{hsAx} fixed for each analysis, and varying d_s;
   - with S=1.5m, k_{hsAx}=0.10k_{h0} and varying d_s (d_s=1.5d_w; d_s=3d_w; d_s=6d_w)
   - with S=1.5m, k_{hsAx} =0.33k_{h0} and varying d_s (d_s=1.5d_w; d_s=3d_w; d_s=6d_w)
   - with S=1.5m, k_{hsAx} =0.66k_{h0} and varying d_s (d_s=1.5d_w; d_s=3d_w; d_s=6d_w)

b) Drain spacing constant and equal to 1.5m between them, with d_s fixed for each analysis and varying k_{hsAx};
   - with S=1.5m, d_s=1.5d_w and varying k_{hsAx} (k_{hsAx}=0.10k_{h0}; k_{hsAx}=0.33k_{h0}; k_{hsAx}=0.66k_{h0})
   - with S=1.5m, d_s=3d_w and varying k_{hsAx} (k_{hsAx}=0.10k_{h0}; k_{hsAx}=0.33k_{h0}; k_{hsAx}=0.66k_{h0})
   - with S=1.5m, d_s=6d_w and varying k_{hsAx} (k_{hsAx}=0.10k_{h0}; k_{hsAx}=0.33k_{h0}; k_{hsAx}=0.66k_{h0})

c) Drain spacing (S) varying, with and without the consideration of the smear effect;

d) Ideal drain ($F_{(r)}$=0) and non-ideal drain ($F_{(r)}$>0), considering (d_s=3d_w and K_{hsAx}=0.33K_{h0}).

The thickness of the clay layer considered is 13 metres, presenting drainage only at the top and the drains cross the entire stratum. The characteristics of the drain are listed in the previous sensitivity analysis, and those of the soil are as follows (Table V.8):

Table V.8 – Properties of the clay soil for the analysis in question

Type of soil	γ_h [kN/m^3]	γ_{sat} [kN/m^3]	K_{h0} [m/s]	K_{v0} [m/s]	C_h [m^2/s]	C_v [m^2/s]	e_0	C_c	C_r=C_s
Soft clay	14.60	16.00	7.01E-10	2.69E-10	7.44E-08	2.85E-08	1.422	0.544	0.148

Therefore, and considering the axisymmetric analytical formulation, the following results were obtained:

a) Drain spacing constant or equal to 1.5m between them, with K_{hsAx} fixed for each analysis, and varying d_s (Graphs V.1, V.2 and V.3)

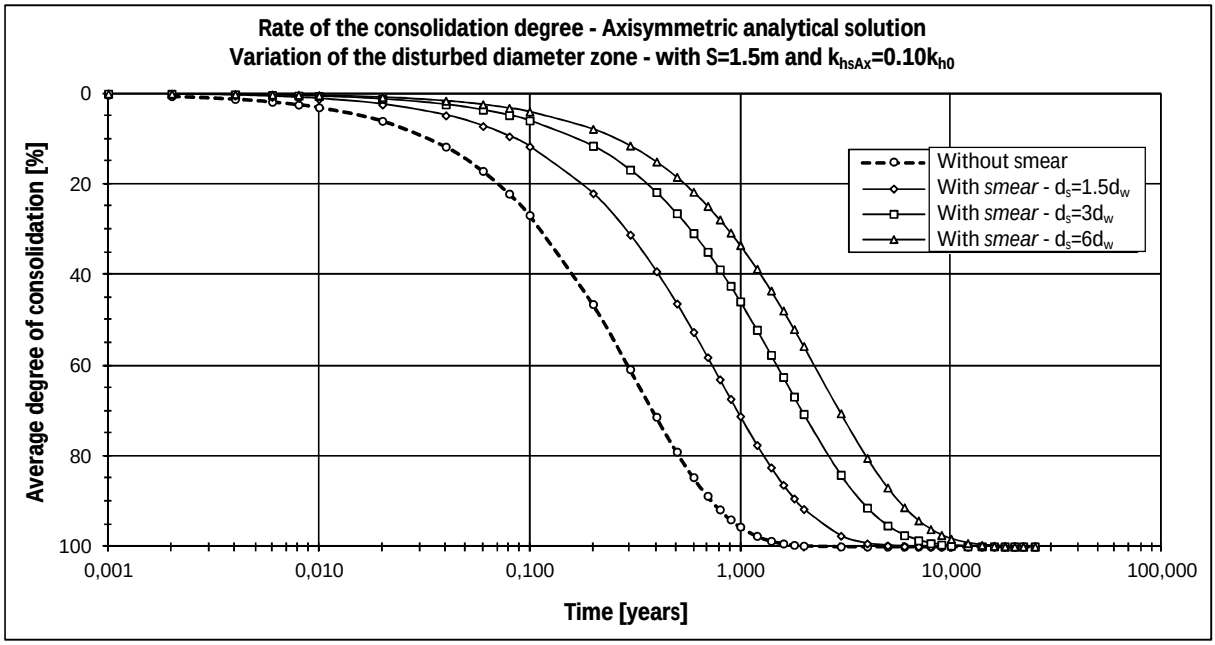

Graph V.1 - Rate of the consolidation degree, in axisymmetric analysis, with S=1.5m, $k_{hsAx}=0.10k_{h0}$ and varying d_s ($d_s=1.5d_w$; $d_s=3d_w$; $d_s=6d_w$)

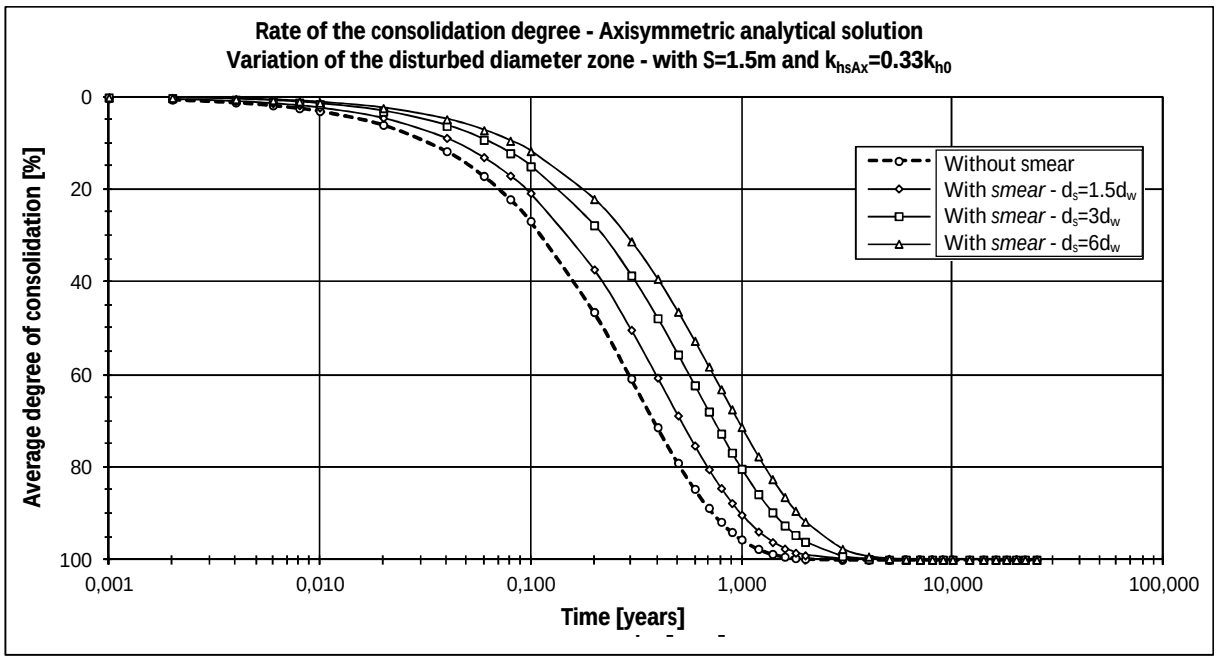

Graph V.2 - Rate of the consolidation degree, in axisymmetric analysis, with S=1.5m, $k_{hsAx}=0.33k_{h0}$ and varying d_s ($d_s=1.5d_w$; $d_s=3d_w$; $d_s=6d_w$)

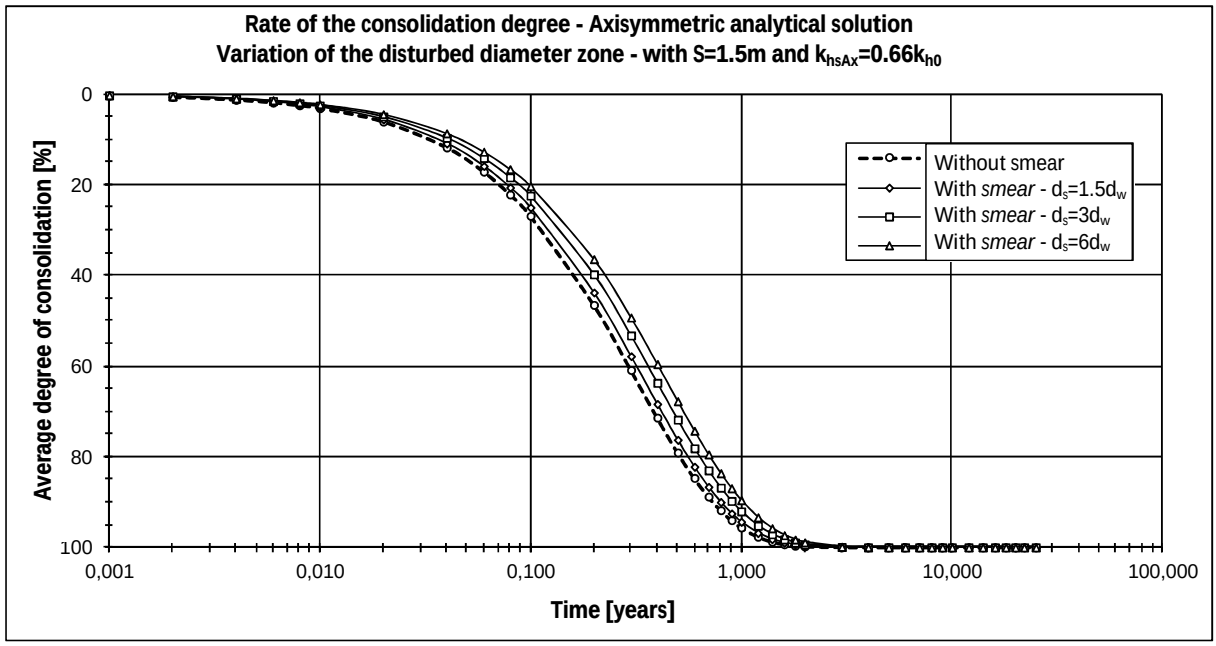

Graph V.3 - Rate of the consolidation degree, in axisymmetric analysis, with S=1.5m, $k_{hsAx}=0.66k_{h0}$ and varying d_s ($d_s=1.5d_w$; $d_s=3d_w$; $d_s=6d_w$)

According to the curves represented from graphs V.I to V.3, the average consolidation degree will take longer, as the diameter of the disturbed zone is larger. Additionally, one can have already a glimpse of the importance of the permeability in the disturbed zone, since the consolidation degree curve for low reduction of the disturbed horizontal permeability coefficient, gets closer to the curve without taking into account the smear effect.

b) Drain spacing constant and equal to 1.5m between them, with d_s fixed for each analysis and varying k_{hsAx} (Graphs V.4, V.5 and V.6)

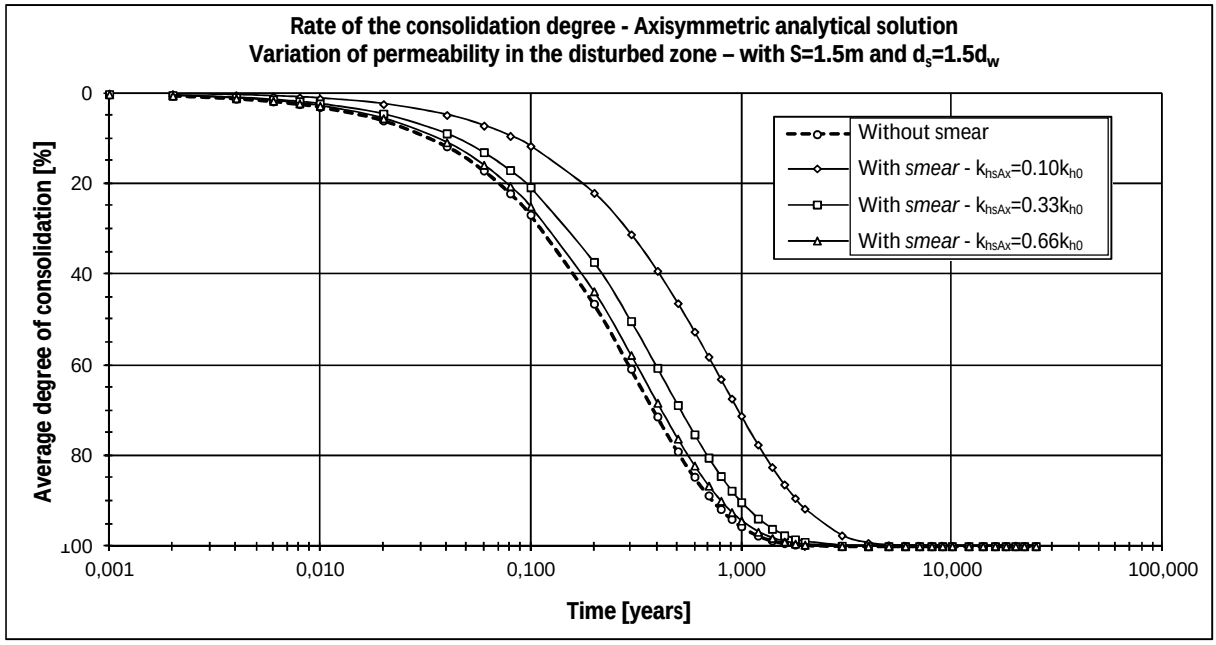

Graph V.4 - Rate of the consolidation degree, in axisymmetric analysis, with S=1.5m, $d_s=1.5d_w$ and varying k_{hsAx} ($k_{hsAx}=0.10k_{h0}$; $k_{hsAx}=0.33k_{h0}$; $k_{hsAx}=0.66k_{h0}$)

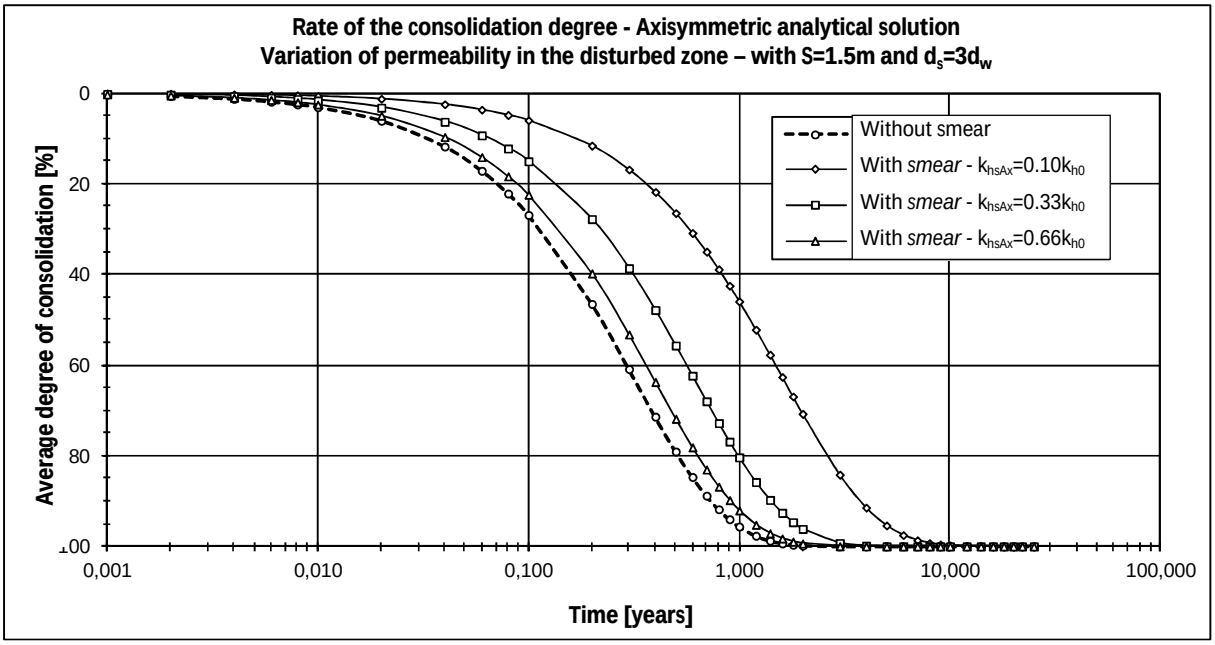

Graph V.5 - Rate of the consolidation degree, in axisymmetric analysis, with S=1.5m, $d_s=3d_w$ and varying k_{hsAx} ($k_{hsAx}=0.10k_{h0}$; $k_{hsAx}=0.33k_{h0}$; $k_{hsAx}=0.66k_{h0}$)

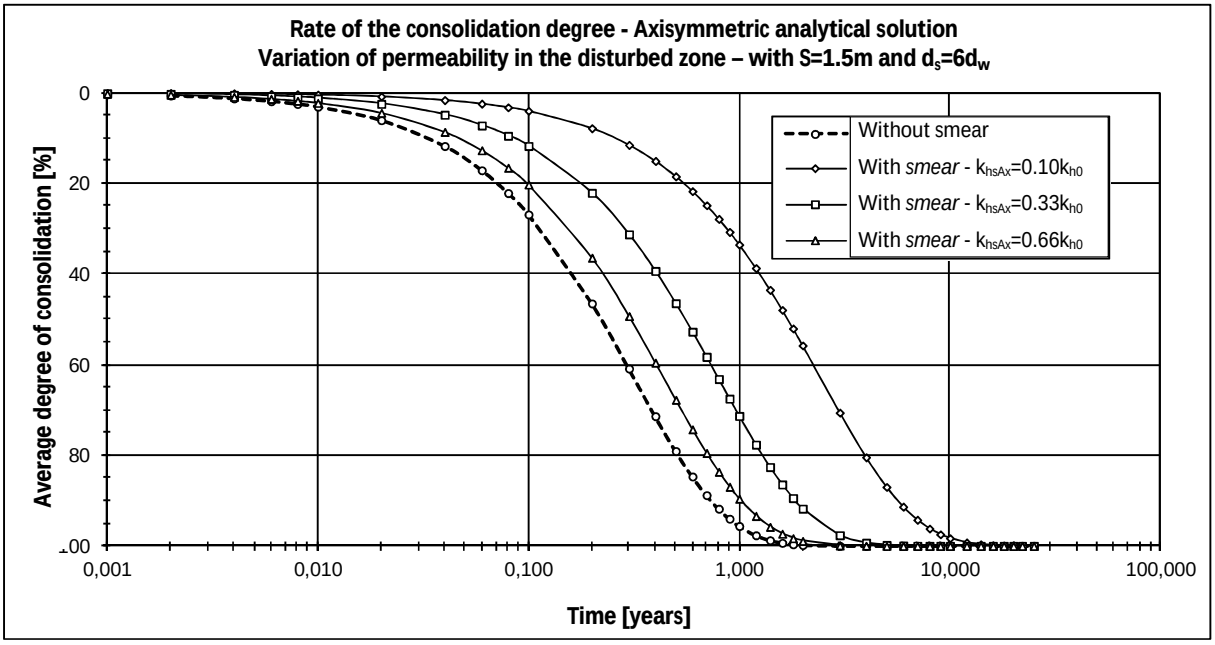

Graph V.6 - Rate of the consolidation degree, in axisymmetric analysis, with S=1.5m, $d_s=6d_w$ and varying k_{hsAx} ($k_{hsAx}=0.10k_{h0}$; $k_{hsAx}=0.33k_{h0}$; $k_{hsAx}=0.66k_{h0}$)

Again, based on the results from the previous graphs, the importance of the reduction in permeability in the disturbed zone is perceptible. In fact, for the same diameter of the disturbed zone, the consolidation process takes longer as the horizontal permeability coefficient in the disturbed zone is smaller. Furthermore, comparing the results of graphs V.1 to V.6, the k_{hsAx} parameter presents undoubtedly greater influence over the d_s parameter.

c) Drain spacing (S) varying, with and without the consideration of the smear effect (Graph V.7)

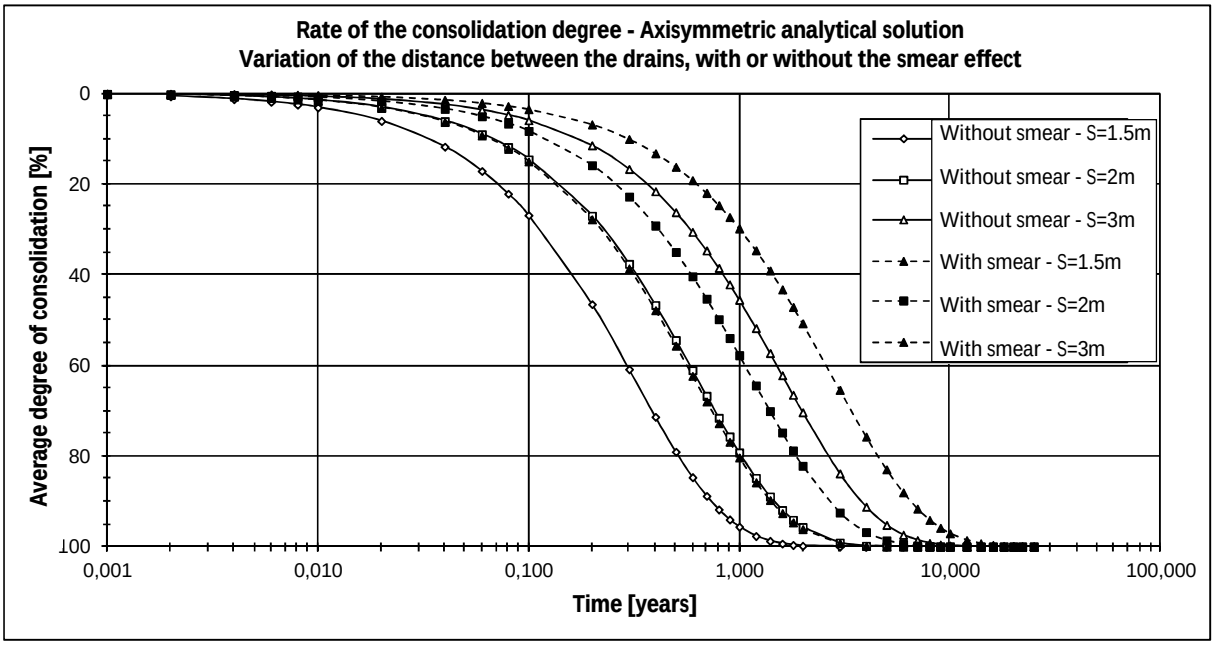

Graph V.7 - Rate of the consolidation degree, in axisymmetric analysis, varying S, without smear and with smear ($d_s=3d_w$ y $K_{hsAx}=0.33K_{h0}$)

In graph V.7, the average degree of consolidation curves are relatively parallels to each other for the hypotheses considered, being notice that the smear effect substantially slows the consolidation rate and delays the time associated to the conclusion of the process. In turn, and as expected, the greater the distance between the drains, the longer the soil takes to reach the same degree of consolidation.

d) Ideal drain and non ideal drain, considering ($d_s=3d_w$ and $K_{hsAx}=0.33K_{h0}$) (Graph V.8)

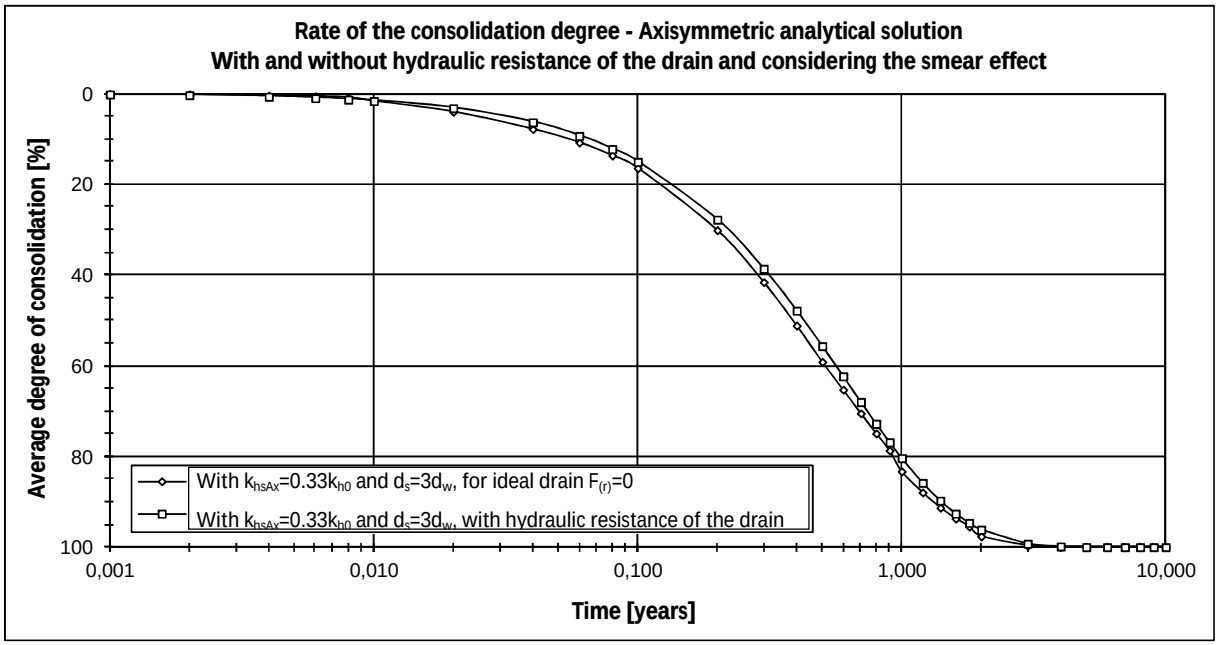

Graph V.8 - Rate of the consolidation degree, in axisymmetric analysis, with ideal drain and non ideal drain, considering the smear effect ($d_s=3d_w$ y $K_{hsAx}=0.33K_{h0}$)

The drain in question may be considered as an ideal drain in light of the results presented in table V.7, which compares the permeability in plane strain whether one considers the hydraulic resistance of the drain or ignores it. However, hydraulic resistance was always considered in the analysis in this subchapter, or in other words, the parameter $F_{(r)}$ was always greater than zero. Graph V.8 shows the minimum differences, almost insignificant, between the consolidation rate for an ideal drain and for the real drain used in these sensitivity studies.

To end this chapter, another interesting comparison concerning the rate of the consolidation degree is performed. In this case, the following scenarios were studied:

a) Terzaghi's consolidation analytical solution (vertical flow);
b) Hansbo's consolidation analytical solution (radial flow);
   - Without considering the smear effect and ideal drain;
   - Considering the smear effect and real drain parameters;
c) Carrilo's consolidation analytical solution (combined flow):
   - Without considering the smear effect and ideal drain;
   - Considering the smear effect and real drain parameters;

Graph V.9 represents the curves obtained for the analytical solutions in the axisymmetric analysis, considering vertical flow, horizontal flow and the combined solution. For these last calculations, the drains were taken as ideal, and regarding the smear two hypothesis were adopted, namely without smear or with smear given by ($d_s=3d_w$ and $K_{hsAx}=0.33K_{h0}$). The vertical coefficient of permeability used in the calculations was the one indicated in table V.8.

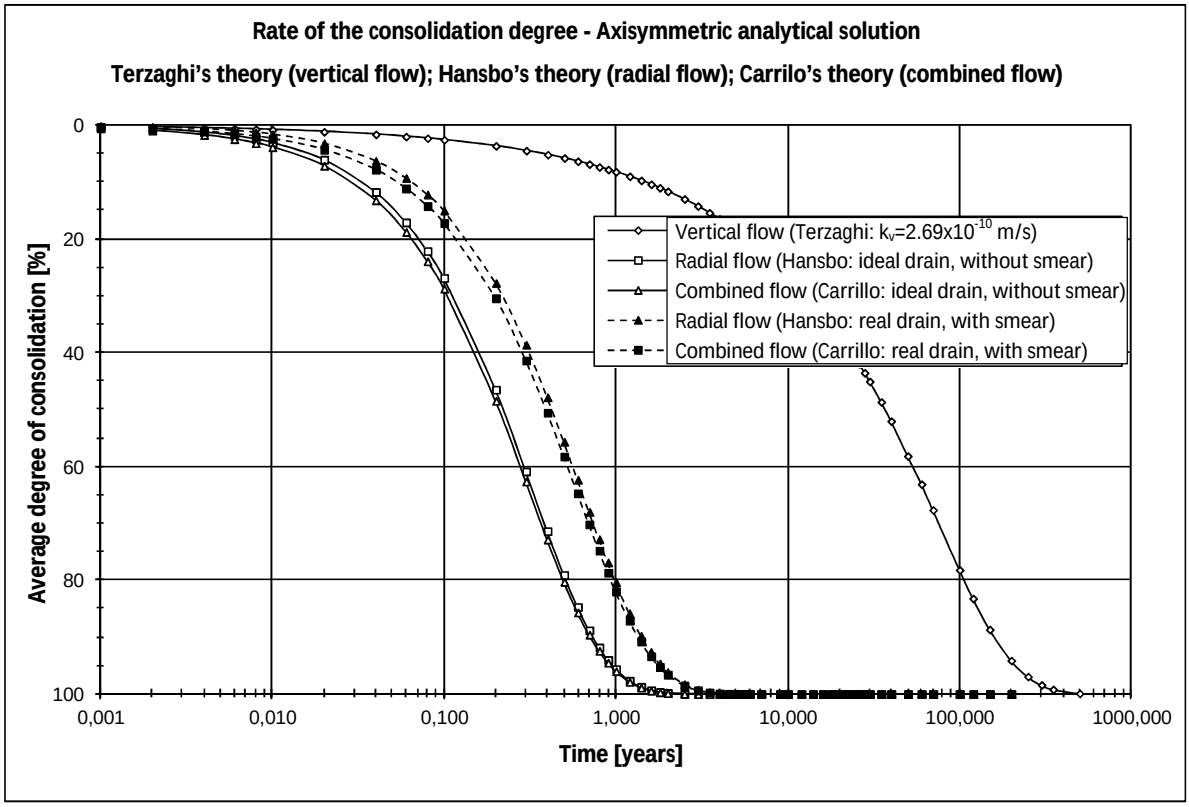

Graph V.9 - Rate of the consolidation degree, in axisymmetric analysis, for various drainage conditions (vertical, radial and combined)

Based on the results obtained, and for the example studied, the foundation treatment, or improvement, with PVD drains will be fundamental on the acceleration of the consolidation process. According to Vairinhos (2013), the consolidation curves for radial and combined flow becomes closer, when the vertical permeability coefficient is much lower than the horizontal. In addition to this, Vairinhos (2013) also performed a sensitivity analysis related to the thickness of the layer in the presence of PVD drains, seeing that the contribution of the vertical drainage is minimal for layers with thicknesses greater than 10m, as suggested by other researchers, since the radial flows will definitely dominates the consolidation rate.

Lastly, a comparison between the rate of the consolidation degree between the solutions of Hird *et al.* (1992) and of Indraratna & Redana (1997) are made, for plane strain analysis, adopting the same smear conditions and spacing between the drains (Graph V.10). As one can see, the results are quite similar, as they coincide, and therefore they can be considered equivalent. This result was already expected in light of the values indicated in table V.7.

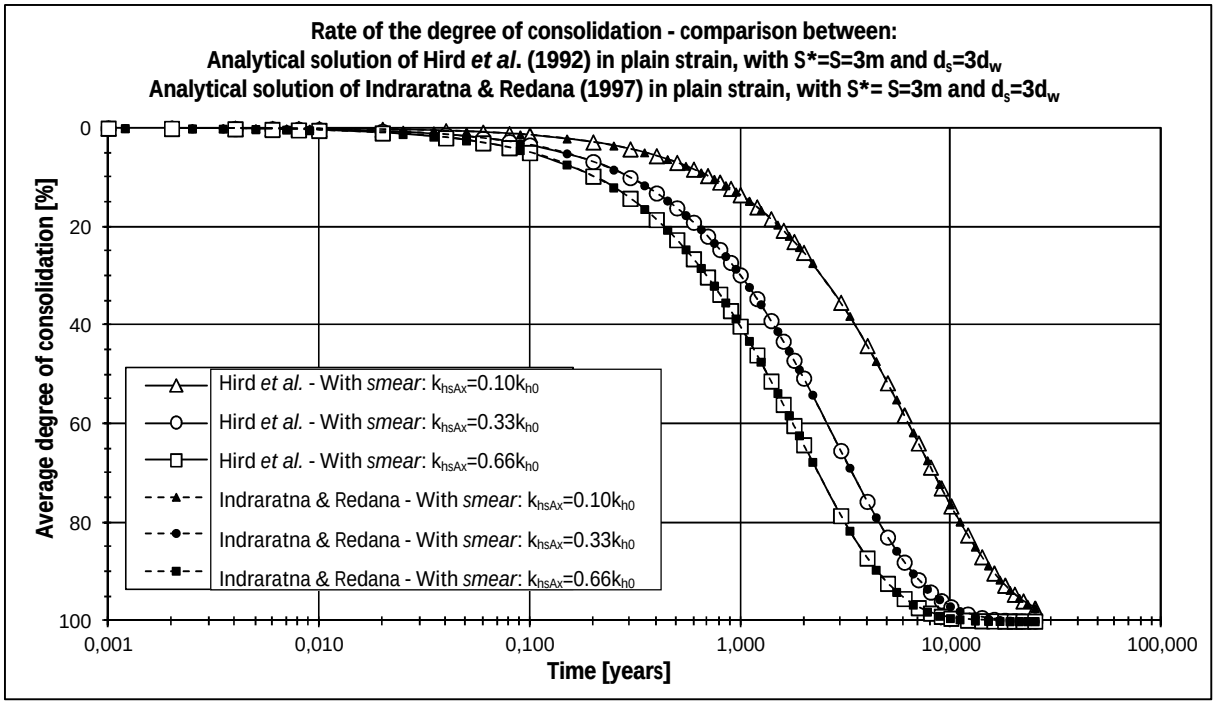

Graph V.10 - Rate of the consolidation degree, in plane strain analysis, for Hird *et al.* (1992) and Indraratna & Redana (1997) analytical solutions, with smear and hydraulic resistance of the drain, considering the distance between drains equal in both systems (S*=S=3m)

After reviewing the theoretical concepts, concerning:

a) the consolidation of fine soil treated with prefabricated vertical band-shaped drains, and how to transform an axisymmetric problem into a plane strain analysis (chapter II);
b) the material models which are suitable for compressible clay soils, and can simultaneously considered the primary and secondary consolidation settlements (chapter III);
c) the account of the smear parameters and discharge capacity of the drains (chapter V);

it remains the characterisation of the soil foundation of Dikes No. 1 and No.3 of the *Lebrija* Pond, and their geometry and materials used in the embankment. These subjects will be addressed and presented on the next chapter (chapter VI).

VI. DIKES NO.1 AND NO.3 OF THE *LEBRIJA* POND

The theoretical concepts previously presented will be applied to the analysis of a specific work case study, introduced in this chapter, namely the *Lebrija* Pond dikes, with special emphasis being given to Dikes No.1 and No.3. These are the two tallest dikes, and due to the high estimated settlements in the initial phase of their design, as well as the extremely reduced slope stability safety factors associated, they were revised in the early stage of their construction.

Therefore, the chapter will begin with a brief introduction of the *Lebrija* Pond, its geographical location and geological mapping of the zone in which it is located, its primary function and the environmental and socioeconomic impact of this pond in the region. Later, the more technical issues related to Dikes No.1 and No.3 will be covered, including:

a) The results from the *in-situ* subsoil exploration, as well as the laboratory tests and the geotechnical characterisation of the soil foundation;
b) The geotechnical foundation profiles of Dike No.1 and Nº.3**;**
c) The results from the geotechnical characterisation of the dikes materials, namely the rip-rap upstream slope protection, the drainage blanket, filters and finally the soil used in the embankment dike.
d) The modifications proposed to the initial design of the dikes, after being reviewed, and the final cross-section profiles correspondent to the highest sections of these dikes;
e) Instrumentation equipments placed in the foundations and dike embankments, their position and chronological order of application;
f) Data processing of the monitoring results from the beginning of the construction, until 2008, and their analysis.

VI.1. GEOGRAPHICAL LOCATION

The *Lebrija* Pond, also known as the *Don Meledon* Pond is geographically located at Northeast of *Lebrija* village, South of Seville, and in the East side of the *Guadalquivir* River. The pond has the double role of regularising and storage the water needed to irrigate 14600 hectares of agriculture land, belonging to the Irrigators Community of Sector B-XII of the Low *Guadalquivir*. The *Guadalquivir* Canal, made exclusively to feed the *Lebrija* Pond, stats at the *Peñaflo*r Dam and it has 148km long. This canal runs parallel to the *Guadalquivir* River, although at a higher level.

Designed for an initial capacity of 8.2Hm^3, the pond allowed water use to be rationalised, ensuring farming capacity to supply vegetables to the largest nearby population centres, namely Seville and Cádiz. Additionally, the impact on nature was significant, since an arid region turned out into a more refreshing and green zone. This can be seen in the flyer presentation (Figure VI.1), as this zone is a nesting and hibernation area for several species of migratory birds, representing a benefit in terms of the environment (Figures VI.2a and VI.2b). It is also relatively close to other humid areas of great ecological value, located on the southwest of the *Guadalquivir* River, such as the *Doñana* Park.

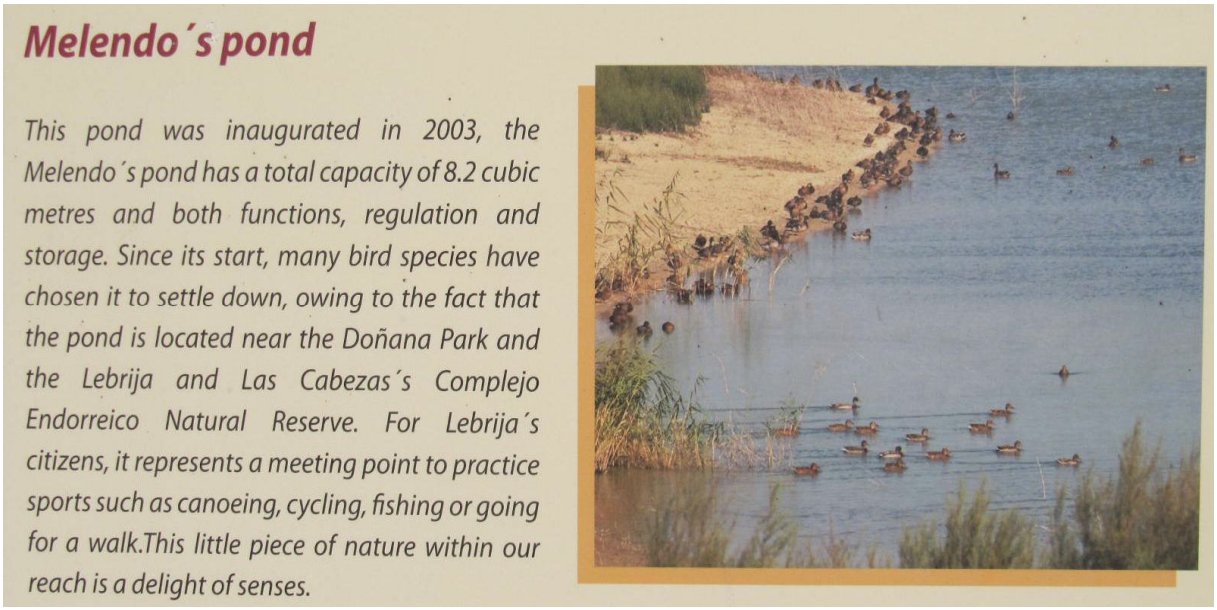

Figure VI.1 – Flyer presentation of *Lebrija* or *Don Melendon* Pond

2a) **2b)**

Figure VI.2-a) Ducks and other birds in the *Lebrija* Pond (Photo of Paco Infante, in 2007);
b) Reservoir of *Lebrija* Pond (Photo of Elisa Silva in February 2013)

The topography of the region allowed the use of a natural depression in the area, which is geologically known as the large hydrographical basin depression of the *Guadalquivir*, to storage the water in question. The construction of four homogenous dikes in specific zones, designated as Dikes No.1, No.2, No.3 and No.4 of the *Lebrija* Pond, assured the enclosure of the water in this area (Figures VI.3 and VI.4).

According to the initial design, the four homogenous dikes had a height over foundation up to 11.17m, 6.19m, 9.04m and 4.998m, respectively for Dike No.1, No.2, No.3 and No.4.

Figure VI.3 - Aerial view of *Lebrija* Pond - location of the four dikes (image taken from Google Maps in January 2013)

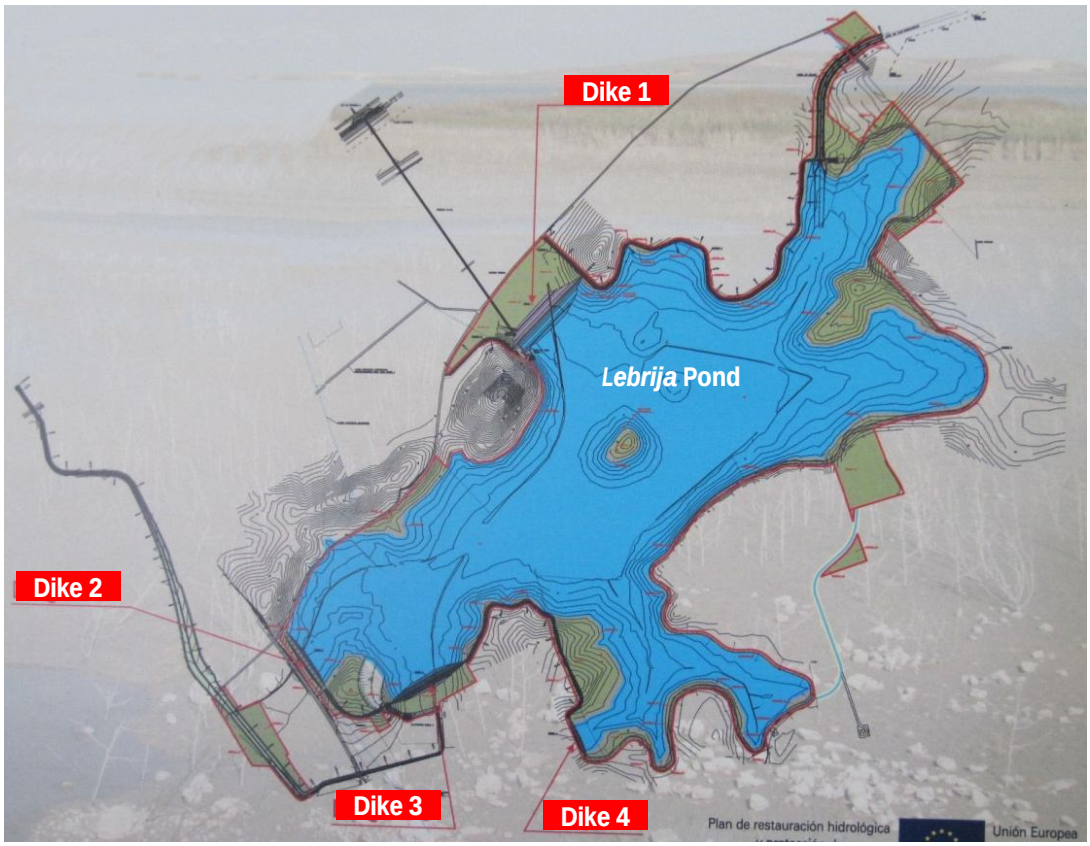

Figure VI.4 – Topographic implantation of the *Lebrija* dikes (Photo of Elisa Silva in February 2013)

VI.2. GEOLOGICAL-GEOTECHNICAL CHARACTERISATION

According to the local geology, the lower *Guadalquivir* hydrographical basin consists of marine deposits, which were later covered by sediment of continental origin, from the Pliocene or Quaternary era (meaning marshland deposits). Two major stratigraphic groups can be distinguished in the zone. In the first, with large representation in the area of the pond, are the grey and white marls with sandy levels. This marly layer consists on clay soils with high plasticity. Regarding the second group, the dominant material corresponds to the blue-grey clays (Upper Miocene and Pliocene era) with unknown and very irregular thicknesses. These soils are composed of clay or silt, with considerable high plasticity, and covered by quaternary sediments (Saura Martinez et al. 2004). Dikes No.1, No.2 and No.3 are founded precisely on the highly compressible soils of the second group.

The characterisation of the soil foundation was based on three site investigations, carried out in different phases of the design and construction works.

Initially a conventional site investigation consisting of Dynamic Probe (DP) tests and Standard Penetration Test (SPT) were carried out, as well as laboratory tests such as grain-size analysis, Atterberg limits, determination of the natural moisture content and specific gravity of soils solid, oedometer tests, direct shear strength and unconfined compression tests, was performed. The results from this first site survey, allowed the identification of several layers of soft to very soft soils, due to their low mechanical characteristics, since:

a) The liquid limits (ω_L) are quite high (ranging between 56% and 96%);

b) The plasticity indexes (IP) are comprehended between 29% and 62%;

c) The SPT number, in some cases, are less than 5 (N_{SPT}<5 blows);

d) The initial void ratios (e_0) are high and the compressibility indexes C_c vary between 0.36 and 0.75. Consequently the oedometer modulus (E_{oed}) are extremely low, varying between 765kN/m^2 and 2590kN/m^2, with an average value of about 1250 kN/m^2;

e) The vertical permeability coefficient of the foundation soil, obtained from the oedometer tests, ranges between 1.32x10^{-10}m/s and 4.08x10^{-10}m/s;

f) The shear strength values, in undrained conditions, are between 20kPa and 25kPa, sometimes falling to 10kPa (Saura Martínez *et al.*, 2004).

In the beginning of the construction of Dike No.1, and due to the soil foundation weak resistence, the works had to be interrupted at the very start, in order to perform more prospecting campaigns. Therefore, a second geotechnical site investigation was realized, and a revision of the initial design of the dikes took place. During that time, piezocono tests (PZC) were performed in the area where Dike No.1 was to be built. Based on this type of tests, the undrained cohesion (c_u) and the horizontal consolidation coefficient (C_h) were determined with more reliability. This last parameter was found to be 3 to 4 times higher than the vertical consolidation coefficient, obtained from the oedometer tests for Dike No.1 (Justo *et al*., 2003).

The results confirmed, once more, the low stiffness of the soils and also the reduced shear strength of some layers. Based on these values, for Dike No.1 the settlements estimated ranged the 72cm (Justo, 2002). Other problem concerned the slope stability of the dike in the central zone (PK0+240). According to Justo (2001), the safety factor obtained for this section of Dike No.1, was about 0.29.

Lastly, a third prospecting exploration was carried out in boreholes opened to place inclinometers. At this stage, undisturbed soil samples, of very good quality, were taken in order to perform new triaxial tests. In addition to these, Vane-Tests (VT) and *Marchetti* dilatometer tests (DMT) were also conducted in the area where Dikes No.1 and No.3 were to be founded (Justo *et al*., 2003; Soriano, 2005).

The plan of the geotechnical site investigation performed for both Dike No.1 and Dike No.3, are plotted in Figures VI.5 and VI.6. The test results were carefully analysed during the research study, aiming not only the layout of the geotechnical profiles of the subsoil (longitudinal and transversal) for both dikes, but also the geotechnical characterisation of the soils. The corresponding results(*) are presented in Appendix I, in several tables. The compilation of the values arranged and grouped according to each soil type, allows the determination of the correspondent average values for the parameters. Nevertheless, these average values should be determined with special care, as it will be indicated latter on.

Therefore, based on the site investigation results, the subsoil in the zone were Dike No.1 and No.3 will be founded, can be specified, from top to bottom, as:

Soil A: Top soil (to be removed in the construction phase)

Soil B': High liquid limit, organic clay and silt, slightly overconsolidated.

Soil B: Blue-grey organic clay and silt, with extremely high liquid limits, normally consolidated, considered as medium to soft soils, and sometimes very soft soils;

Soil C: Yellowish clay, with high liquid limits and overconsolidated (from medium to very stiff clay);

Soil D: Greenish marly clay, with high consistency (very stiff to hard clay).

Furthermore, it was observed that the soils in layers B and C showed slight variations in terms of mechanical strength given by field tests results. This same distinction was confirmed by the results from the oedometer tests for stratum B, since different values of stiffness were obtained, as well as important differences in the overconsolidation ratios. Based on these facts reasons, the layers in question where sub-divided and split into B1+B2+B3 and C1+C2 soils, respectively.

The geotechnical longitudinal profiles of Dikes No.1 and No.3 are plotted in figures VI.7 and VI.8. These include the original level of the ground surface, as well as the dikes crest level and the excavation needed to reach the foundation of the dikes cut-off. As it was previously mentioned, the top soil will be completely removed, being the dikes founded directly on the B' layer.

(*) The data from the tests was supplied by Professor José Luís de Justo Alpañés.

According to the tests, it was observed that in the zone of Dike No.1, the B soil layer presents a maximum thicknesses of around 15 metres in section PK0+240, reaching the level -13.00m. For Dike No.3, the maximum thickness of this layer is approximately 11 metres in section PK0+0140, reaching the level -10.50m. Regarding the position of the phreatic level, it was found that fluctuations occur. However, on average, it is assumed that the phreatic level is approximately 1.83m for the highest section of the zone of Dike No.1 and 1.35m for the zone of Dike No.3.

Although the test results of the soils foundations of Dikes No.1 and No.3 are compiled in Appendix I, they will be analysed in the next subchapter, in order to obtain the representative geotechnical parameters of these soils for both the prospected areas. Therefore, in a first phase, the values indicated correspond to the averages obtain in each test and for each soil type and zone. No critical analysis is made regarding the test results, with the exception of the values determined from the oedometer tests. In a second phase, a comparative analysis of some geotechnical parameters is made, either determined from distinct tests or estimated based on well-known empirical correlations, which depend on easy-to-determine parameters. These analyses will allow the determination of the values to be used in the numerical simulations performed for the case study, and covered in chapter VII.

VI.2.1. GEOTECHNICAL CHARACTERISATION OF THE SOILS FOUNDATION OF DIKE NO.1

As already mentioned, the main goal of this section regards the geotechnical characterization of the soils where Dike No.1 will be founded. These are obtained directly from the compilation of the test results presented in Appendix I. Hence, the average representative values, of the sub-soils parameters in this zone, corresponding to the several tests performed, are listed in tables VI.1, VI.2 VI.3, VI.4, VI.5, VI.6 and VI.8.

Table VI.1 – Dike No.1: Average test results: Grain-size analysis, *Atterberg* limits, moist unit weight, specific gravity of soil solid and unified soil classification system (USCS)

Soils	< #200 [%]	*Atterberg* limits			γ_t [kN/m^3]	G_s	USCS Soil Classification
		ω_L [%]	ω_P [%]	IP [%]			
A	97.0	66.5	32.5	34.0	17.6	2.63	MH
B'	99.2	77.4	28.8	48.6	15.9	2.74	CH
B1	96.1	61.1	26.8	34.3	17.4	2.63	MH; CH
B2	96.4	56.2	24.0	32.2	16.2	2.66	MH-OH; CH
B3	97.7	63.7	34.6	29.2	18.4	2.85	MH
C1	90.8	63.5	18.3	45.2	16.1	---	CH
C2	95.7	60.4	34.8	25.6	18.1	---	MH
D	96.1	58.1	34.5	23.6	18.4	---	MH

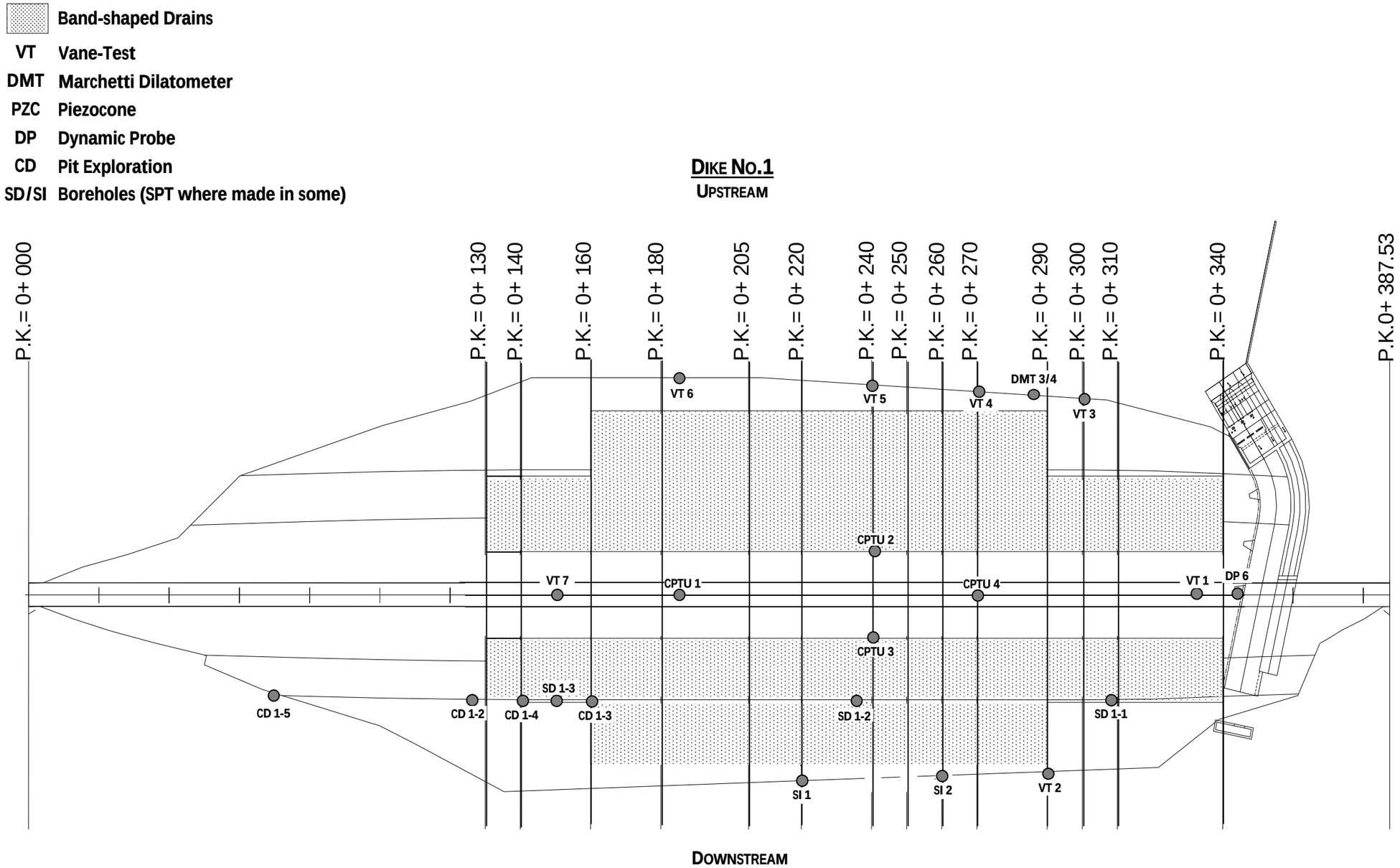

Figure VI.5 – Plan showing the geotechnical site investigation made in Dike No.1.

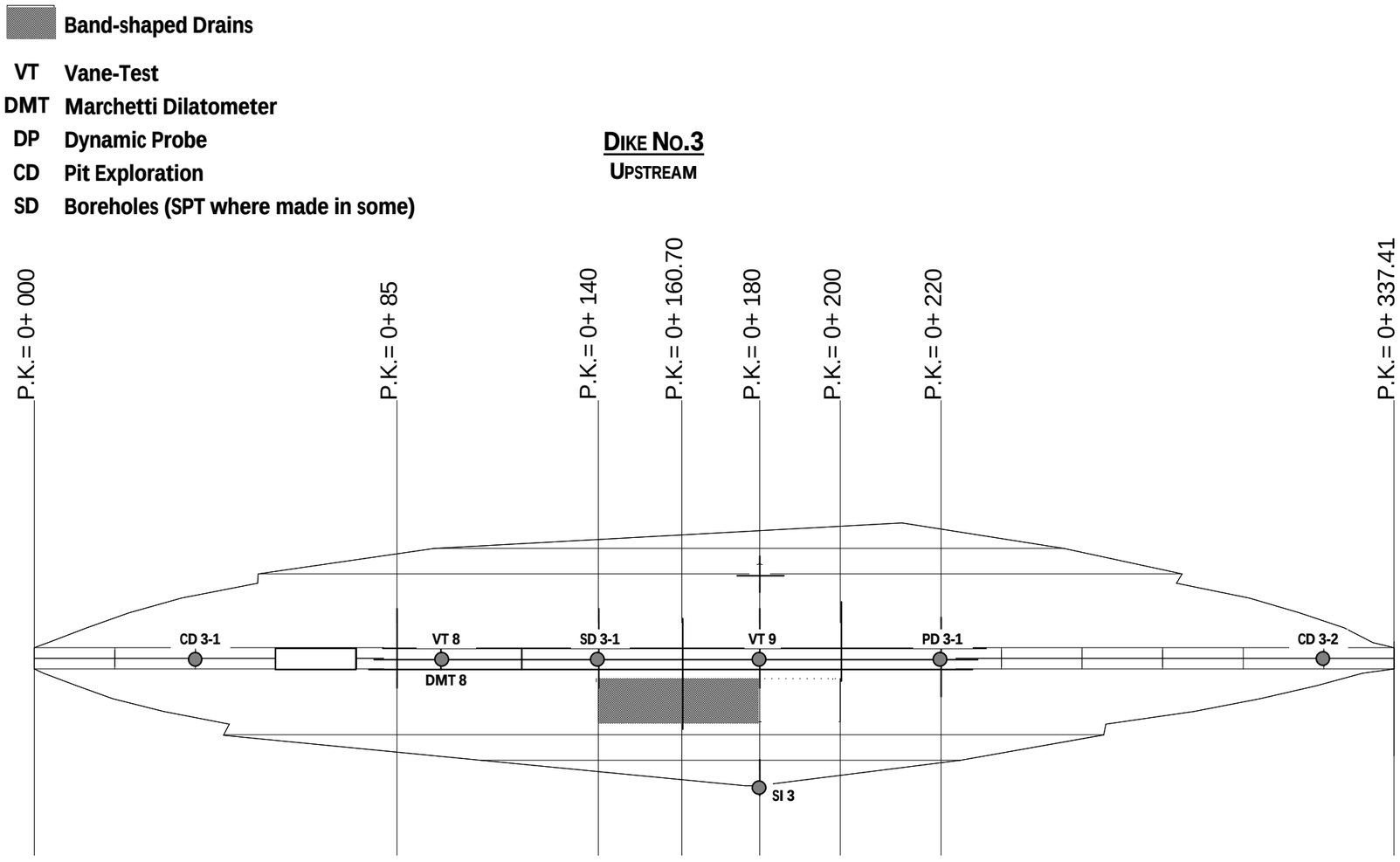

Figure VI.6 – Plan showing the geotechnical site investigation made in Dike No.3.

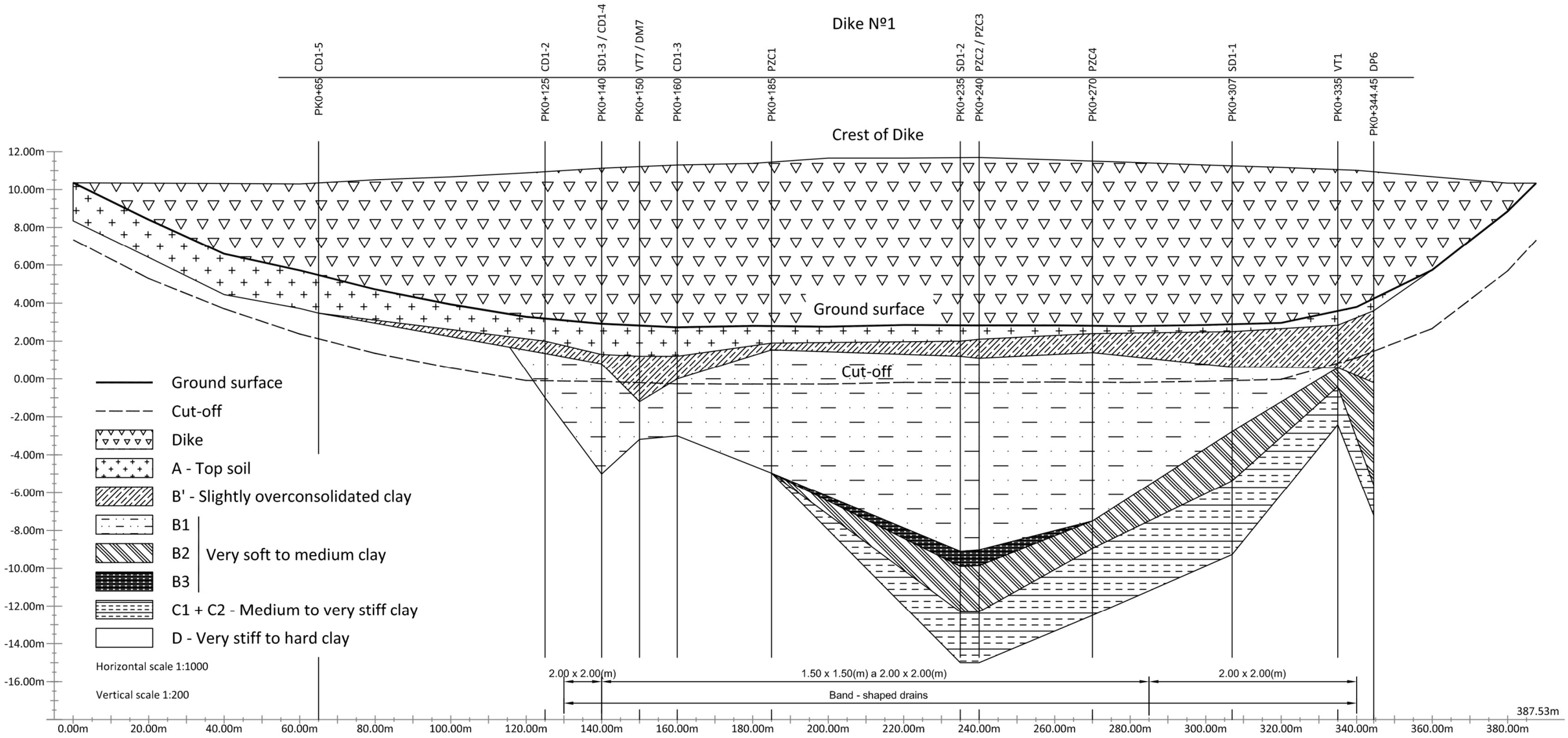

Figure VI.7 – Geotechnical foundation profile on Dike No.1, including level of initial ground surface, crest dike, and cut-off.

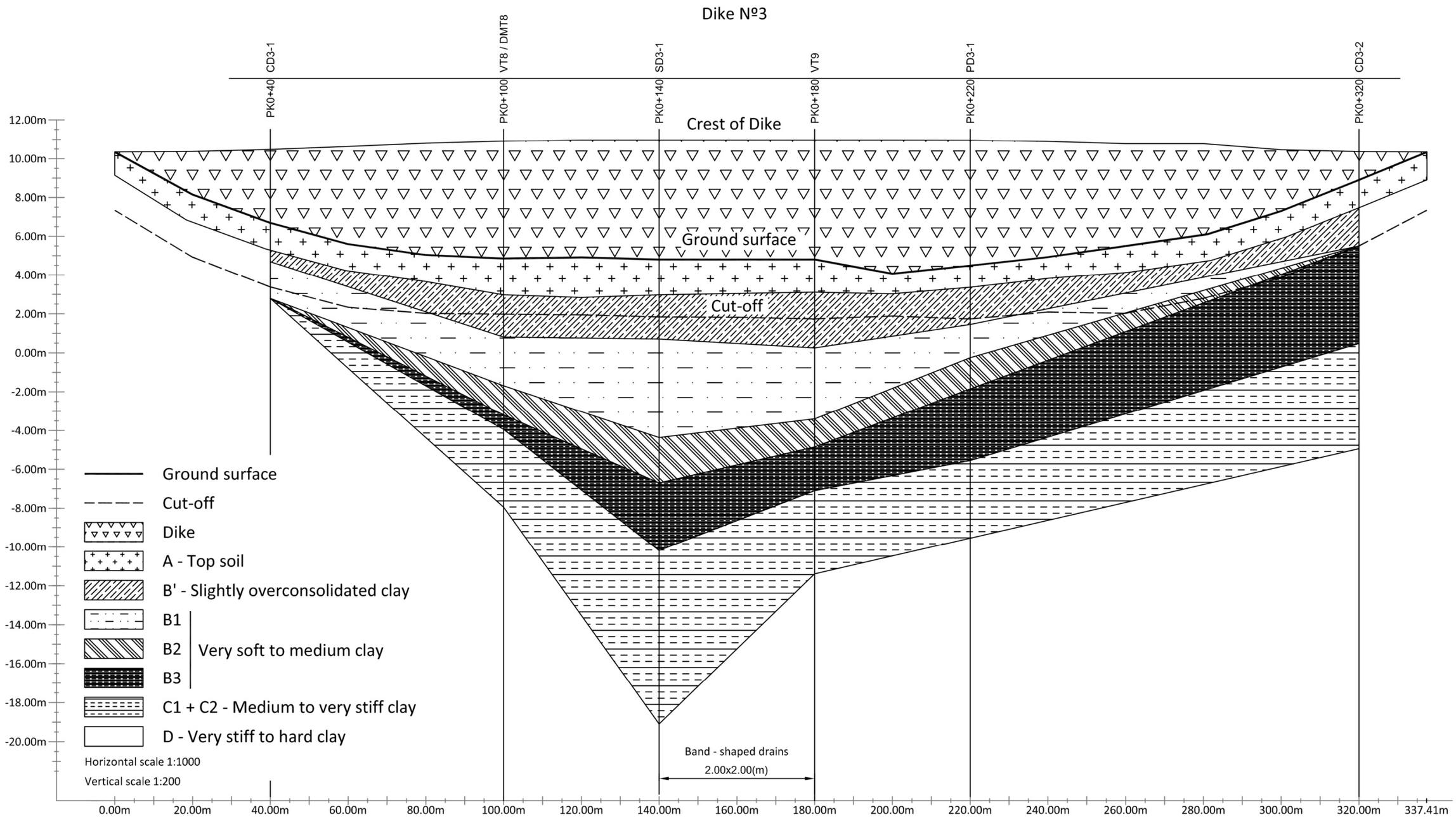

Figure VI.8 – Geotechnical foundation profile on Dike No.3, including level of initial ground surface, crest dike, and cut-off.

Table VI.2 – Dike No.1: Average results of dynamic probe tests (DP), standard penetration test (SPT), direct shear tests and unconfined compression tests

Soils	$N_{DP(20cm)}$	N_{SPT}	Direct shear test				Unconfined compression test	
			c' [kN/m²]	φ' [º]	c_{cu} [kN/m²]	φ_{cu} [º]	q_u [kN/m²]	c_u [kN/m²]
A	---	---	---	---	---	---	274.7	137.4
B'	11	---	10.8	12.4	---	---	14.7(*)	7.4(*)
B1	---	1 to 5	---	---	---	---	16.7(*)	8.4(*)
B2	---	---	---	---	12.3	17.9	---	---
B3	9	3 to 6	11.8	16.7	---	---	---	---
C1	19	13 to 17	---	---	8.8	26.7	87.4	43.7
C2	57	27	41.2	18.1	---	---	143.2	71.6
D	82 to 136	36 to 60	---	---	147.2	24.6	394.4	197.2

(*) Low values. Need to be confirmed by to other tests results

Table VI.3 – Dike No.1: Average results of piezocono tests (PZC) and Vane-Test

Soils	PZC			$C_{h(PZC)}/C_{v(OED)}$	Vane-Test		
	c_u [kN/m²]	OCR	C_h 10^{-8} [m²/s]		$s_{u(max)}$ [kN/m²]	$s_{u(residual)}$ [kN/m²]	St(*)
A	---	---	---	---	169.3	49.4	3.42
B'	34.3	> 2.0	7.44	---	30.7	22.5	1.37
B1	17.6	1.0 to 1.7	7.44	3.91	18.1	14.5	1.40
B2	27.0	1.0	13.60	2.96	26.4	17.8	1.48
B3	37.3	1.0 to 1.5	13.60	3.89	39.3	29.5	1.33
C1	51.0	1.0 to 2.0	---	---	52.9	7.7	6.83
C2	---	---	---	---	83.5	37.5	2.22
D	176.6	10.0	10.20	---	207.9	87.1	1.96

(*) Clay sensitivity - $St=s_{u(max)})/s_{u(residual)}$

Table VI.4 – Dike No.1: Average results of *Marchetti* dilatometer tests and triaxial test

Soils	Triaxial				*Marchetti* dilatometer				
	c' [kN/m²]	φ' [º]	c_{cu} [kN/m²]	φ_{cu} [º]	c_u [kN/m²]	E_{DMT} [kN/m²]	φ [º]	OCR	K_0
A	---	---	---	---	160 to 180	> 6800	42 to 46	> 10.0	3.4 to 4.0
B'	---	---	---	---	10 to 24	3150 to 6350	---	3.5 to 6.0	1.1 to 1.4
B1	13.8	23.3	8.8	18.8	16 to 24	1350 to 4550	---	1.0 to 1.8	0.5 to 0.65
B2	18.3	18.7	---	---	21 to 38	1150 to 2700	---	0.7 to 1.0	0.45 to 0.5
B3	---	---	---	---	28 to 40	1800 to 6800	---	0.6 to 1.0	0.38 to 0.5
C1	---	---	2.0	28.8	40 to 46	7700 to 11800		0.75 to 1.0	0.45 to 0.5
C2	---	---	---	---	---	---	---	---	---
D	---	---	---	---	215 to 260	26300 to 30850	---	15.0	2.0

Table VI.5 presents the results obtained from the oedometer tests performed on seven undisturbed samples. These were compiled and presented by Soriano, in 2005. Although the values of the initial void ratio (e_0), compressibility index (C_c), recompressibility and/or expansibility index ($C_r = C_s$) and effective pre-consolidation stress (σ'_p) are equal to those defined by Soriano (2005), the overconsolidation degree (OCR) presented here is slightly different. This is due to the fact of having used the volumetric weights presented in Table VI.1 for the determination of the initial effective vertical stress, instead of those proposed by Soriano (2005).

Table VI.5 – Dike No.1: Initial void ratio, compressibility index, recompressibility index and effective preconsolidation stress (Soriano, 2005); Initial effective vertical stress and OCR value (Da Silva, 2009)

Soils	Borehole	e_0	C_c	$C_s=C_r$	σ'_p [kN/m^2]	σ'_0 [kN/m^2]	σ'_f [kN/m^2]	OCR=σ'_p/σ'_0
A (1.5 -2.1)	SD 1.3	0.862	0.315	0.067	79.4	30.3	182.5	2.6
B'(1.5 -2.1)	SD 1.1	1.480	0.570	0.137	68.0	19.9	177.6	3.4
B'(1.0 -1.6)	SD 1.2	1.364	0.518	0.158	77.0	16.9	182.3	4.6
B' average	----	1.422	0.544	0.1475	----	----	----	4.0
B1 (3.75 -4.35)	SD 1.2	1.508	0.748	0.132	70.0	34.3	202.4	2.0
B2 (3.5 -4.1)	SD 1.1	1.652	0.811	0.153	38.7	30.7	190.0	1.3
B2 (6.5 -7.1)	SD 1.2	1.439	0.471	0.097	47.0	52.5	220.9	0.9
B2 average	----	1.546	0.641	0.125	----	----	----	1.1
B3 (3.7 -4.3)	SD 1.3	1.558	0.473	0.121	58.3	46.7	215.1	1.3

The average values of the initial vertical permeability coefficient (k_{v0}), of the oedometer modulus (E_{oed}), and also the secondary compressibility index (C_α), were determine applying equations VI.4, VI.5, and VI.6, respectively. Regardless the loads used on the oedometer tests exceed the final vertical stress applied in the soil foundation, the values presented for the parameters in questions, where only determined taking into account the results correspondent to the final vertical stress, which the foundation will be subjected after the construction of Dike No.1. The final effective vertical stress is obtained accordingly to:

$$\sigma'_f = \sigma'_0 + \Delta\sigma \qquad \text{(VI.1)}$$

The initial effective vertical stress (σ'_0) and the load increment ($\Delta\sigma$) due to the construction of the dike are, respectively:

$$\sigma'_0 = (\gamma_h \cdot h) + (\gamma_{sat} - \gamma_w) \cdot h_w \qquad \text{(VI.2)}$$

$$\Delta\sigma = (\gamma \cdot h)_{dique} \qquad \text{(VI.3)}$$

where: γ_h is the moist unit weight of the foundation soil and h the respective height;

γ_{sat} is the saturated unit weight of the soil and h_w the height up to the water level;

γ_{dike} is the embankment unit weight and h_{dike} its height.

Thus, the vertical permeability coefficient (k_v) is calculated based on the geometric average:

$$k_v = \sqrt[n]{(k_{v1} \cdot k_{v2} \cdot \ldots \cdot k_{vn})} \qquad \text{(VI.4)}$$

For the determination of the average oedometer modulus (E_{oed}) it was used the expression:

$$E_{oed} = \left(\frac{\frac{1}{E_{oed1}} + \frac{1}{E_{oed2}} + \ldots + \frac{1}{E_{oedn}}}{n} \right)^{-1} \quad \text{(VI.5)}$$

Lastly, the secondary compressibility index (C_α) is obtained based on the arithmetic average:

$$C_\alpha = \frac{C_{\alpha 1} + C_{\alpha 1} + \ldots + C_{\alpha n}}{n} \quad \text{(VI.6)}$$

The horizontal permeability coefficient may (k_h) be estimated using the expression VI.7 or VI.8, in which the horizontal consolidation coefficient (C_h) is the one resulting from the piezocono test. Both the vertical permeability coefficient and the oedometer modulus are determined based on the previous expressions.

$$k_h = \frac{C_h \times \gamma_w}{E_{oed}} \quad \text{(VI.7)}$$

$$k_h = \frac{C_h}{C_v} k_v \quad \text{(VI.8)}$$

In spite of these two possibilities, due to the very low values of E_{oed}, it was decided to use the expression VI.8 for the determination of the horizontal permeability coefficient, and to consider the ratio between the horizontal and vertical consolidation coefficients indicated previously in table VI.3.

The secondary compressibility index (C_α) also showed very low results, when all the load levels were considered up to the final effective stress, since this value gave zero for low load levels. Consequently, it was decided to calculate this average only for the load levels that correspond to the final stress applied to the soil foundation. The value thus determined is indicated as $C_{\alpha mod}$. Despite this is slightly higher than the value calculated by equation VI.6 for all the load levels, it continues to be very low in comparison to the clayed soil in question. Table VI.6 show the values for the soil foundation of Dike No.1.

Table VI.6 – Dike No.1: Secondary compressibility index, consolidation coefficient and permeability coefficients (vertical and horizontal)

Soils	E_{oed} [kN/m^2]	C_α	$C_{\alpha mod}$	k_{v0} [m/s]	k_{h0} [m/s]	$C_{v\ (Oedometer)}$ [m^2/s]	$C_{h\ (PZC)}$ [m^2/s]	C_h/C_v
B' average	1282	0.00476	0.01195	2.69×10^{-10}	7.01×10^{-10}	2.85×10^{-8}	7.44×10^{-8}	2.61
B1 (3.75 -4.35)	1314	0.00694	0.00938	1.83×10^{-10}	7.17×10^{-10}	1.90×10^{-8}	7.44×10^{-8}	3.92
B2 average	1178	0.00400	0.00390	4.08×10^{-10}	1.21×10^{-9}	4.60×10^{-8}	1.36×10^{-7}	2.96
B3 (3.7 -4.3)	1267	0.00766	0.01282	1.49×10^{-10}	5.79×10^{-10}	3.50×10^{-8}	1.36×10^{-7}	3.89

Lastly, the ratios between the compressibility, recompressibility and modified secondary compressibility indexes were determined, with the objective of determining whether they correspond to the limits defined and expected for the compressible clayed soil. According to the PLAXIS 2D-V11.02 (2012) manual, and for the Soft Soil and Soft Soil Creep models, the ratio between λ^*/κ^* should be comprehended between 2.5 and 7, and between 15 and 25 for the ratio of λ^*/μ^*.

Calculating the parameters λ^*, κ^* and μ^*, based on the indexes C_c, C_r and $C_{\alpha mod}$, the values in table VI.7 were obtained. It can be seen that, though the results for the ratio $\lambda^*/\kappa^*$are acceptable, the same cannot be said regarding the ratio λ^*/μ^*, with indications that the secondary compressibility indexes obtained in the oedometer test, even for $C_{\alpha mod}$, are extremely low. In light of this, and in order to have an idea of the expected values for the secondary compressibility index for these clays and silts, it was decided to use the Terzaghi *et al.* (1996) expression. So, and according to these researchers, the ratio C_α/C_c is 0.04 for non-organic clays and silts and 0.05 for organic clays and silts. Considering the average value for the soils of the B stratum, i.e. C_α/C_c=0.045, then the new values for the secondary compressibility index of the soils are indicated in table VI.8.

Table VI.7 – Dike No.1: Initial relationship between $\lambda^*/\kappa^*$and λ^*/μ^* based on edometer test results

Soils	λ^*	κ^*	λ^*/κ^*	μ^*	λ^*/μ^*
B' average	0,0975	0,0529	1.8	0,00214	45.5
B1 (3.75 -4.35)	0,1295	0,0457	2.8	0,00163	79.7
B2 average	0,1094	0,0427	2.6	0,00067	164.3
B3 (3.7 -4.3)	0,0803	0,0411	2.0	0,00218	36.9

Table VI.8 – Dike No.1: New C_α, considering the expression proposed by Terzaghi *et al.* (1996), and new values for the ratio λ^*/μ^*

Soils	$C_{\alpha Terzaghi}$	μ^*	λ^*/μ^*
B' average	0.02448	0.00439	22.2
B1 (3.75 -4.35)	0.03366	0.00583	22.2
B2 average	0.02885	0.00492	22.2
B3 (3.7 -4.3)	0.02129	0.00361	22.2

With these new values of $C_{\alpha Terzaghi}$, the ratio between λ^*/μ^* is already ensured. In the numerical simulations analysis for this case study, both the values will be used, being their results compared.

VI.2.2. GEOTECHNICAL CHARACTERISATION OF THE SOILS FOUNDATION OF DIKE NO.3

In this section, and regardless the site investigation test results for the soils foundation of Dike Nº3, are presented in Appendix I, the average values of the most important parameters will be summarised in tables VI.9, VI.10 and VI.11. It should be mention that neither triaxial tests nor piezocono tests were performed at the site of this dike.

Table VI.9 – Dike No.1: Average test results: Grain-size analysis, *Atterberg* limits, moist unit weight, specific gravity of soil solid and unified soil classification system (USCS)

Soils	< #200 [%]	*Atterberg* limits			γ_t [kN/m^3]	Gs	USCS Soil Classification
		ω_L [%]	ω_P [%]	IP [%]			
A	62.0	88.0	37.1	50.9	17.0	2.55	CH
B'	98.8	96.0	47.1	48.9	16.2	2.56	MH
B1	98.8	62.0	32.8	29.2	17.0	---	CH
B2	83.4	72.2	30.9	41.3	16.2	2.47	MH
B3	99.6	107.5	45.7	61.8	16.5	2.60	---
C1	---	---	---	---	---	---	---
C2	96.7	62.2	43.7	18.5	17.9	---	MH
D	88.6	83.9	47.7	36.1	18.0	---	MH

Table VI.10 – Dike No.3: Average results of dynamic probe tests (DP), standard penetration test (SPT), direct shear tests and unconfined compression tests

Soils	N_{DP}	N_{SPT}	Direct shear test				Unconfined compression test	
			c' [kN/m^2]	φ' [º]	c_{cu} [kN/m^2]	φ_{cu} [º]	q_u [kN/m^2]	c_u [kN/m^2]
A	---	---	---	---	---	---	202,0	101,0
B'	4	5	11.8	19.3	---	---	101,0	50,5
B1	2	2	---	---	14.7	10.5	---	---
B2	9	---	---	---	---	---	17,6	8,8
B3	---	---	---	---	---	---	43,2	21,6
C1	22	---	---	---	---	---	---	---
C2	46	28	---	---	---	---	51,0	25,5
D	62 to 126	---	---	---	---	---	225,2	112,6

Table VI.11 – Dike No.3: Average results of *Marchetti* dilatometer tests (DMT) and Vane-Test

Soils	Vane-Test			*Marchetti* dilatometer				
	$s_{u(max)}$ [kN/m^2]	$s_{u(residual)}$ [kN/m^2]	St(*)	c_u [kN/m^2]	E_{DMT} [kN/m^2]	φ [º]	OCR	K_0
A	---	---	---	---	12700 to 16350	36 to 45	---	1.6 to 4.5
B'	43.8	16.0	2.75	25 to 30	2250 to 4550	---	2.0 to 3.5	0.8 to 1.1
B1	19.0	7.8	2.44	---	---	---	---	---
B2	25.7	9.5	2.82	22 to 26	1800	---	1.0	0.6
B3	43.1	---	---	32 to 44	5450	---	1.8	0.7
C1	---	---	---	---	---	---	---	---
C2	---	---	---	60	5450 to 14500	---	2.1	0.8
D	---	---	---	>100	29000		4.5	1.2

(*)Clay sensitivity - $St=s_{u(max)})/s_{u(residual)}$

Based on what was mentioned before for the oedometer tests, and according to the results presented by Da Silva (2009), then the parameters for Dike No.3 are those indicated in tables VI.12 and VI.13.

Table VI.12 – Dike No.3: Initial void ratio, compressibility index, recompressibility index, effective preconsolidation stress, initial effective vertical stress and OCR value (Da Silva, 2009)

Soils	Boreholes	e_0	C_c	$C_s=C_r$	σ'_p [kN/m^2]	σ'_0 [kN/m^2]	σ'_f [kN/m^2]	OCR=σ'_p/σ'_0
A $_{(1,5\ -2,1)}$	SD 3.1	1.184	0.360	0.116	152.9	25.7	155.1	6.0
B'$_{(3,5\ -4,1)}$	SD 3.1	1.621	0.588	0.181	147.1	39.5	171.0	3.7
B2	SD 3.1	1.521	0.550	0.118	33.8	55.5	203.3	0.6
B3	SD 3.1	1.475	0.573	0.l66	171.6	88.1	219.5	2.0

Table VI.13 – Dike No.3: Secondary compressibility index, consolidation coefficient and permeability coefficients (vertical and horizontal)

Soils	E_{oed} [kN/m^2]	C_α	$C_{\alpha mod}$	k_{v0} [m/s]	k_{h0} [m/s]	$C_{v\ (Oedometer)}$ [m^2/s]	$C_{h\ (PZC)}$ [m^2/s]	C_h/C_v
A $_{(1,5\ -2,1)}$	2686	0.00077	0.00153	$1.32\text{x}10^{-10}$	$5.46\text{x}10^{-10}$	$1.80\text{x}10^{-8}$	$7.44\text{x}10^{-8}$	4.13
B'$_{(3,5\ -4,1)}$	2368	0.00432	0.00620	$1.81\text{x}10^{-10}$	$4.99\text{x}10^{-10}$	$2.70\text{x}10^{-8}$	$7.44\text{x}10^{-8}$	2.76
B2	765	0.01259	0.01868	$1.78\text{x}10^{-10}$	$1.73\text{x}10^{-9}$	$1.40\text{x}10^{-8}$	$1.36\text{x}10^{-7}$	9.71
B3	2516	0.00175	0.00323	$3.78\text{x}10^{-10}$	$7.67\text{x}10^{-10}$	$6.70\text{x}10^{-8}$	$1.36\text{x}10^{-7}$	2.03

Analysing, once more, the ratios between the parameters λ^*, κ^* and μ^*, based on the C_c, C_r and $C_{\alpha mod}$ indexes, for the B soils of Dike No.3, unacceptable values are obtained for the ratio λ^*/μ. The values of λ^*/κ^* are also slightly lower than the desired (Table VI.14). In light of these results, the Terzaghi *et al*. (1996) relation was again applied to estimate the secondary compressibility index of the B soils. The new values for the secondary compressibility index are shown in table VI.15.

Table VI.14 – Dike No.3: Initial relationship between $\lambda^*/\kappa^*$and λ^*/μ^* based on edometer test results

Soils	λ^*	κ^*	λ^*/κ^*	μ^*	λ^*/μ^*
A $_{(1,5\ -2,1)}$	0.0716	0.0461	1.6	0.00030	235.1
B'$_{(3,5\ -4,1)}$	0.0925	0.0600	1.5	0.00103	90.0
B2	0.0947	0.0407	2.3	0.00322	29.5
B3	0.1005	0.0583	1.7	0.00057	177.7

Table VI.15 – Dike No.3: New C_α, considering the expression proposed by Terzaghi *et al.* (1996), and new values for the ratio λ^*/μ^*

Solo	$C_{\alpha Terzaghi}$	μ^*	λ^*/μ^*
A $_{(1,5\ -2,1)}$	0.01620	0.00322	22.2
B'$_{(3,5\ -4,1)}$	0.02511	0.00416	22.2
B2	0.02475	0.00426	22.2
B3	0.02579	0.00452	22.2

VI.2.3. ANALYSIS AND COMPARISON OF THE GEOTECHNICAL PARAMETER RESULTS

Notwithstanding the average values presented in the previous tables, based on the direct results of field and laboratory tests, some of them must be corrected. So, in this phase of the study, these corrections will be explained and performed. Other interesting analysis is the comparison of the same parameter, obtained from different tests, as well as the comparison between the tests results with the values determined based on empirical relationship.

- *Correction of the maximum or peak undrained shear strength result of the Vane-Test ($s_{u(max)}$)*

According to several researchers, the values obtained from this test need correction, when performed on soil with high plasticity, since this last parameter affects the final result, overestimating it. As such, and according to Bjerrum (1972), Jimenez, *et al.* (1981) and Morris & Williams (1994), these must be corrected, according to the expressions:

Bjerrum (1972):

$$\Lambda = 1.7 - 0.54 \log(IP) \qquad \text{(VI.9)}$$

Jimenez, *et al.* (1981):

$$\Lambda = 0.92 - 0.25 \log(IP) + 0.27\left[\log(IP)\right]^2 \qquad \text{(VI.10)}$$

Morris & Williams (1994):

$$\Lambda = 1.18 \cdot e^{-0.08 \cdot IP} + 0.57 \qquad \text{(VI.11)}$$

$$\Lambda = 7.01 \cdot e^{-0.08 \cdot \varpi_L} + 0.57 \qquad \text{(VI.12)}$$

Applying these expressions to the Vane-Test results, both for Dike No.1 and Dike No.3, the new undrained shear strength results are indicated in tables VI.16 and VI.17.

Table VI.16 – Dike No.1: Maximum undrained shear strength correction for the Vane-Test

Soils	*Atterberg* limits			Vane-Test	$s_{u(max)}$*= Λx$s_{u(max)}$		$s_{u(max)}$*= $s_{u(max)}$ / Λ		$s_{u(max)}$*= Λx$s_{u(max)}$		$s_{u(max)}$*= Λx$s_{u(max)}$	
	ω_L [%]	ω_P [%]	IP [%]	$s_{u(max)}$ [kN/m^2]	Λ f=(IP)	$s_{u(max)}$*	Λ f=(IP)	$s_{u(max)}$*	Λ f=(IP)	$s_{u(max)}$*	Λ f=(IP)	$s_{u(max)}$*
					Bjerrum (1972)		Jimenez *et al.* (1981)		Morris & Williams (1994)		Morris & Williams (1994)	
A	66.5	32.5	34.0	169.3	0.87	**147.8**	1.17	**144.7**	0.65	**109.7**	0.60	**102.3**
B'	77.4	28.8	48.6	30.7	0.79	**24.2**	1.27	**24.2**	0.59	**18.2**	0.58	**17.9**
B1	61.1	26.8	34.3	18.1	0.87	**15.7**	1.17	**15.4**	0.65	**11.7**	0.62	**11.3**
B2	56.2	24.0	32.2	26.4	0.89	**23.4**	1.16	**22.8**	0.66	**17.4**	0.65	**17.1**
B3	63.7	34.6	29.2	39.3	0.91	**35.8**	1.13	**34.7**	0.68	**26.9**	0.61	**24.1**
C1	63.5	18.3	45.2	52.9	0.81	**42.6**	1.25	**42.4**	0.60	**31.8**	0.61	**32.4**
C2	60.4	34.8	25.6	83.5	0.94	**78.5**	1.10	**75.7**	0.72	**60.3**	0.63	**52.3**
D	58.1	34.5	23.6	207.9	0.96	**199.2**	1.09	**191.5**	0.75	**155.6**	0.64	**132.4**

Observing the corrected maximum undrained shear strength, the results for the Bjerrum (1972) and Jimenez *et al*. (1981) expressions, are very close. For this last case, the average decrease gave approximately 86% for Dike No.1 and 81% for Dike No.3.

Table VI.17 – Dike No.3: Maximum undrained shear strength correction for the Vane-Test

Soils	*Atterberg* limits			Vane-Test	Bjerrum (1972) $s_{u(max)}^* = \Lambda x s_{u(max)}$		Jimenez *et al.* (1981) $s_{u(max)}^* = s_{u(max)} / \Lambda$		Morris & Williams (1994) $s_{u(max)}^* = \Lambda x s_{u(max)}$			
	ω_L [%]	ω_P [%]	IP [%]	$s_{u(max)}$ [kN/m^2]	Λ f=(IP)	$s_{u(max)}^*$ [kN/m^2]	Λ f=(IP)	$s_{u(max)}^*$ [kN/m^2]	Λ f=(IP)	$s_{u(max)}^*$ [kN/m^2]	Λ f=(ω_L)	$s_{u(max)}^*$ [kN/m^2]
A	88.0	37.1	50.9	---	---	---	---	---	---	---	---	---
B'	96.0	47.1	48.9	43.8	0.79	**34.5**	1.27	**34.6**	0.59	**26.0**	0.57	**25.1**
B1	62.0	32.8	29.2	19.0	0.91	**17.3**	1.13	**16.8**	0.68	**13.0**	0.62	**11.8**
B2	72.2	30.9	41.3	25.7	0.83	**21.3**	1.22	**21.1**	0.61	**15.8**	0.59	**15.2**
B3	107.5	45.7	61.8	43.1	0.73	**31.6**	1.34	**32.2**	0.58	**24.9**	0.57	**24.6**
C1	---	---	---	---	---	---	---	---	---	---	---	---
C2	62.2	43.7	18.5	---	---	---	---	---	---	---	---	---
D	83.9	47.7	36.1	---	---	---	---	---	---	---	---	---

Considering the expressions of Morris & Williams (1984), the reduction of the undrained shear strength is rather significant. When the factor Λ is based on the plasticity index, the decrease is about 66% for Dike No.1 and of 62% for Dike No.3. If the reduction factor Λ is calculated based on the liquid limit, then the values will fall down to 62% and 59%, respectively for Dike No.1 and No.3.

In light of this, the values from Jimenez *et al.* (1981) were considered for the future numerical simulation analysis, since it allows a reduction in the undrained shear strength, without being too conservative. These were found to be more reasonable values, with a reduction of around 14% to 19% of the field test results.

- *Comparison between the results from the SPT test and the Dynamic Probe*

According to Dahlberg (1974) equality was allowed between the results of the SPT test and the dynamic probe (DP), when the values do not exceed the 8 to 12 blows. From this point on, the values obtained from the dynamic probe are greater than those from the SPT (Jimenez *et al.*, 1981). According to Escario (1974), for values greater than these, the same proposed that the ratio between both tests may be given by $N_{SPT}=0.7N_{DP}$.

Table VI.18 – Dike No.1 e No.3: Comparison between SPT and DP results

Soils	Dike No.1				Dike No.3			
	N_{DP}	N_{SPT}	$N_{SPT}=0.7N_{DP}$	$N_{SPT}=0.45N_{DP}$	N_{DP}	N_{SPT}	$N_{SPT}=0.7N_{DP}$	$N_{SPT}=0.6\ N_{DP}$
A	---	---	---	---	---	---	---	---
B'	11	---	---	---	4	5	---	---
B1	---	1 to 5	---	---	2	2	---	---
B2	---	---	---	---	9	---	---	---
B3	9	3 to 6	---	---	---	---	---	---
C1	19	**13 to 17**	13	**15**	22	---	---	---
C2	57	**27**	40	**26**	**46**	28	32	**21**
D	82 to 136	**36** to **60**	57 to 95	**37** to **61**	62 to 126	---	---	---

Comparing the results obtained for the *Lebrija* Pond soils foundation (Table VI.18), it can be seen that the ratio $N_{SPT}=0.7N_{DP}$ is too high. For the soil in question, the ratio between the two tests is only comparable when applying $N_{SPT}=0.45N_{DP}$ to Dike No.1 and $N_{SPT}=0.60N_{DP}$ to Dike No.3, for values greater than 12 blows. This difference may be related to the energy of the equipment used in the tests (Escario, 1974; Dahlberg, 1974).

- *Comparison of the undrained shear strength obtained in the unconfined compression tests, Standard Penetration Test, Cone Penetration Test, Marchetti Dilatometer and the Vane-Test*

Tables VI.19 and VI.20 show the average results of the undrained shear strength for Dike No.1 and Dike No.3 sub-soils, based on several field tests as well as on the unconfined compression test.

Table VI.19 – Dike No.1: Summary of several undrained shear strength results

Soils	N_{SPT}	q_u - correlations with (N_{SPT})		Unconfined compression test		PZC	DMT	Vane-Test	
		q_u [kN/m^2]	c_u [kN/m^2]	q_u [kN/m^2]	c_u [kN/m^2]	c_u [kN/m^2]	c_u [kN/m^2]	$s_{u(max)}$ [kN/m^2]	$s_{u(max)}$* Jimenez *et al.* [kN/m^2]
A	---	---	---	274.7	**137.4**	---	160 a 180	169.3	**144.7**
B'	---	---	---	14.7(*)	7.4(*)	34.3	**10 to 24**	30.7	**24.2**
B1	1 to 5	10 to 50	5 to 12.5	16.7(*)	8.4(*)	17.6	**16 a 24**	18.1	**15.4**
B2	---	---	---	---	---	27.0	**21 a 38**	26.4	**22.8**
B3	3 to 6	30 to 60	15 to 30	---	---	37.3	**28 a 40**	39.3	**34.7**
C1	13 to 17	130 to 170	65 to 85	87.4	**43.7**	51.0	**40 a 46**	52.9	**42.4**
C2	27	350	175	143.2	**71.6**	---	**---**	83.5	**75.7**
D	36 a 60	> 400	> 200	394.4	**197.2**	176.6	215 to 260	207.9	**191.4**

(*) Extremely low values when compared to other test results for the same soil type.

Table VI.20 – Dike No.3: Summary of several undrained shear strength results

Soils	N_{SPT}	q_u - correlations with (N_{SPT})		Unconfined compression test		PZC	DMT	Vane-Test	
		q_u [kN/m^2]	c_u [kN/m^2]	q_u [kN/m^2]	c_u [kN/m^2]	c_u [kN/m^2]	c_u [kN/m^2]	$s_{u(max)}$ [kN/m^2]	$s_{u(max)}$* Jimenez *et al.* [kN/m^2]
A	---	---	---	202.0	101.0	---	---	---	---
B'	5	50	25	101.0	50.5	---	**25** to **30**	43.8	**34.6**
B1	2	25	12.5	---	---	---	**---**	19.0	16.8
B2	---	---	---	17.6	8.8	---	**22** to **26**	25.7	**21.1**
B3	---	---	---	43.2	21.6	---	**32** to **44**	43.1	**32.2**
C1	---	---	---	---	---	---	---	---	---
C2	28	360	180	51.0	25.5	---	60	---	---
D	---	---	---	225.2	112.6	---	>100	---	---

From the values shown in the tables above, it is observed that, in general, the results from the PZC, DMT and Vane-Tests are mutually coherent and uniform. Nevertheless, the following aspects should be noted:

a) The results from the undrained shear strength based on the PZC test, for Dike No.1, are very similar to those obtained from the Vane-Test prior to correction;

b) After correction of the Vane-Test results, adopting the Jimenez *et al.* (1981) expression, the reduced undrained shear strength becomes closer to the results obtained based on the *Marchetti* dilatometer, for both dikes;

c) Regarding the values of the undrained shear strength determined from the unconfined compression test, the similarity with the other test results occurs only for overconsolidated soil. As it can be seen in table VI.19, the values obtained for the A, C1, C2 and D soils of Dike No.1, are almost coincident to the Vane-Test results corrected with the Jimenez *et al*. (1981) factor reduction. For the soils of the B layer, the unconfined shear strength is lower than the remaining tests. This behaviour indicates that, for normally consolidated and slightly overconsolidated soils, the soil sample cannot support the same load without being confined, reaching failure for lower values;

d) The undrained shear strength estimated based on the SPT results, is not very accurate. The values for this parameter are only similar, for very low results of the SPT. From there on, it is observed a very large discrepancy. Thus, the use of this empirical relationship is not recommended for medium to high values from the SPT test.

Once again, the reduction criteria proposed by Jimenez *et al*. (1981), for the maximum undrained shear strength of the Vane-Test, is the one which seems to give greater proximity with other test results, namely with the *Marchetti* dilatometer and the unconfined compression test for overconsolidated soil.

- *Comparison of the overconsolidation ratio determined from the Oedometer test, the Marchetti Dilatometer and the Piezocono Test*

Before presenting and comparing the overconsolidation degrees (OCR) obtained from the oedometer test, dilatometer and piezocono tests, it is important to understand the influence of the empirical methods used to determine this parameter from the PZC test results.

The parameters indicated in table VI.3 and in Appendix I, associated to the piezocono test performed on the foundation soil of Dike No.1, took into consideration the *Baligh et al*. (1981) and *Campanella et al.* (1982) corrections for the cone point resistance (q_c). The undrained cohesion was determined according to equation VI.13, where N_k=16.

$$c_u = \frac{q_c - \sigma_v}{N_k} = \frac{q_c - \sigma_v}{16} \qquad \text{(VI.13)}$$

However, according to Mayne & Kemper (1988), the undrained cohesion and consolidation degree may be estimated from expressions VI.14 and VI.15, with N_k =15 for electric cones:

$$c_u = \frac{q_c - \sigma_v}{N_k} = \frac{q_c - \sigma_v}{15} \quad \text{and} \quad OCR = 0.37\left(\frac{q_c - \sigma_v}{\sigma'_v}\right)^{1.01} \qquad \text{(VI.14) and (VI.15)}$$

In 1957, Hansbo suggested that the overconsolidation degree should be obtained based on the following ratio (equation VI.16):

$$OCR = \frac{(c_u/\sigma'_v)_{PZC}}{(c_u/\sigma'_v)_{Hansbo}} \qquad \text{(VI.16)}$$

where $(c_u/\sigma'_v)_{PZC}$ is the value obtained from the PZC test, and the value $(c_u/\sigma'_v)_{Hansbo}$ is calculated using equation VI.17, only being valid for normally consolidated clay with liquid limits less than 65%.

$$\left(\frac{c_u}{\sigma'_v}\right)_{Hansbo} = 0.45\frac{\omega_L}{100} \quad \text{, with } \omega_L \text{ entering in \%} \qquad \text{(VI.17)}$$

Table VI.21 shows the values from the four static penetration tests performed in the zone of Dike No.1, taking into account the previous expressions.

Table VI.21 – Dike No.1: Overconsolidation ratio obtained from PZC tests, according to Hansbo (1957) and Mayne & Kemper (1988)

Soils	Test	ω_L [%]	σ'_v [kN/m^2]	q_c-σ_v [kN/m^2]	c_u obtained with N_k=16			Hansbo (1957)		Mayne & Kemper (1988)	
					c_u/σ'_v	c_u [kN/m^2]	OCR	c_u/σ'_v	OCR	c_u [kN/m^2]	OCR
B'	CPT1	77.4	22.3	534.4	1.50	33.4	**> 1**	0.35(*)	**4.3**	35.6	**9.2**
	CPT2		26.0	**----**	1.36	35.3	**> 1.5**		**3.9**	----	**----**
	CPT3		26.0	**----**	1.51	39.2	**> 2**		**4.3**	----	**----**
	CPT4		23.5	**----**	1.46	34.3	**> 2**		**4.2**	----	----
B1	CPT1	61.1	58.8	235.2	0.25	14.7	**1.0 to 1.7**	0.27	**0.9**	15.7	**1.5**
	CPT2		98.0	313.6	0.20	19.6	**1**		**0.7**	20.9	**1.2**
	CPT3		98.0	313.6	0.20	19.6	**1**		**0.7**	20.9	**1.2**
	CPT4		62.8	251.2	0.25	15.7	**1**		**0.9**	16.7	**1.5**
B2	CPT2	56.2	147.0	470.4	0.20	29.4	**1**	0.25	**0.8**	31.4	**1.2**
	CPT3		122.5	392.0	0.20	24.5	**1**		**0.8**	26.1	**1.2**
B3	CPT2	63.7	130.7	627.2	0.30	39.2	**1**	0.29	**1.0**	41.8	**1.8**
	CPT3		141.2	564.8	0.25	35.3	**1.5**		**0.9**	37.7	**1.5**
C1	CPT2	63.5	152.5	878.4	0.36	54.9	**1**	0.29	**1.3**	58.6	**2.2**
C1	CPT3		140.3	785.6	0.35	49.1	**2**		**1.2**	52.4	**2.1**
C1	CPT4		98.2	785.6	0.50	49.1	**2**		**1.7**	52.4	**3.0**
D	CPT1	58.1	98.1	2825.6	1.80	176.6	**10**	0.26	6.9	188.4	**11.0**

(*) These values were calculated for moisture contents greater than 65%

Finally, the comparison of the overconsolidation degrees for the oedometer, dilatometer and piezocono tests are shown in table VI.22. From their analyses, it can be seen that:

a) The overconsolidation degree determined from Hansbo (1957) expression are much lower than the others, for the soils of the stratum B, with exception of the B' soil;

b) The overconsolidation degree calculated by the oedometer test are similar to the ones obtained from the original piezocono tests;

c) The OCR result obtained with the Mayne & Kemper (1988) equations, for the B' soil is extraordinarily high when compared to the others. This could mean, therefore, that this soil belongs to the top soil A, instead of being a B' soil, or that the value calculated makes no sense, since as it was calculated for a liquid limit greater than 65%.

Table VI.22 – Dike No.1: Comparison between the overconsolidation ratios calculated based on oedometer tests, *Marchetti* dilatometer tests and piezocono tests

Soils	PZC			Oedometer	DMT
	OCR	OCR Hansbo (1957)	OCR Mayne & Kemper (1988)	OCR	OCR
A	**----**	**----**	**----**	3.0	> 10.0
B'	> 2.0	3.9 to 4.3	9.2(*)	4.0	3.5 to 6.0
B1	1.0 to 1.7	0.7 to 0.9	1.2 to 1.5	1.8	1.0 to 1.8
B2	1.0	0.80	1.20	1.1	0.7 to 1.0
B3	1.0 to 1.5	0.9 to 1.0	1.5 to 1.8	1.3	0.6 to 1.0
C1	1.0 to 2.0	1.2 to 1.7	2.1 to 3	**----**	0.75 to 1.0
C2	**----**	**----**	**----**	**----**	**----**
D	10.0	6.9	11.0	**----**	15.0

(*) Extraordinarily high value in comparison to the others results

The comparisons and considerations presented here had the purpose of checking the appropriateness of certain empirical relationships, in order to obtain geotechnical parameters. Furthermore, since the main issue is the consideration of adequate values for future numerical analysis, the similarities between those geotechnical parameters, obtained from different test and correlations, gave a sense of greater accuracy and safety.

Thus, the major considerations taken from this section are the following:

a) The undrained shear strength adopted for the soils foundation are those obtained from the Vane-Test, reduced according to Jimenez *et al.* (1981) factor, in undrained analyses;

b) The effective shear strength parameters adopted in drained analyses, correspond to the results of the triaxial tests;

c) The compressibility and recompressibility indexes, void ratios and overconsolidation degrees are the ones calculated based on the oedometer test results. For the secondary compressibility index, will be exception. For this parameter, it will be considered not only the values determined from the oedometer test, but also the values estimated according to Terzaghi *et al*. (1996) relation.

VI.2.4. GEOTECHNICAL CHARACTERISATION OF THE DIKES

According to Justo (2000a), the geotechnical properties of the soils used on Dikes No.1 and No.3, namely the embankment, the rip-rap upstream slope protection, the chimney drain and the horizontal drainage mats, are listened in table VI.23.

Table VI.23 – Average soil parameters for the *Lebrija* Pond dikes (Justo, 2000a)

Soils	c' [kPa]	φ' [º]	ψ [º]	k_h [m/s]	k_v [m/s]	γ_h [kN/m^3]	γ_{sat} [kN/m^3]
Embankment body	47.6	20.2	0.0	$5.20x10^{-10}$	$1.04x10^{-10}$	16,7	18.1
Rip-rap	0.0	40.0	10.0	$1.04x10^{-02}$	$1.04x10^{-02}$	17.6	20.6
Chimney drain and Drainage mat	0.0	35.0	5.0	$2.31x10^{-04}$	$2.31x10^{-04}$	17.0	20.0

For the embankment body, the effect of the permeability anisotropy was taken in consideration, since the soils usually suffer horizontal stratification, due to the compaction procedure during construction.

VI.3. DIKES STANDARD CROSS-SECTION PROFILE

Information will now be given about the geometry and cross-sectional profiles of the dikes, both in the initial phase of the design, and also after its revision. In fact, the dikes design underwent some significant alterations, when it became evident that the geotechnical characteristics of the soils foundation were worse than those, which had been defined, in the initial design. The extremely low soil stiffness and shear strength of some soil layers, more specifically the B1 and B2 soils, made it foreseeable that there could be extremely high settlements of the soil foundation, as well as the slope instability of the dikes, in particular for Dike No.1. In fact, preliminary stability calculations, based upon a conventional site investigation, indicated that the short-term factor of safety at the central part of Dike No.1 was 0.29 (Justo *et al*., 2009). So, Dike No.1 and No.3 were the most affected due to their location and height, and were therefore studied with greater detail. Thus, in addition to the list of alterations proposed for each of these dikes, two standard cross-sectional profiles will also be presented, corresponding to their final design.

VI.3.1. INITIAL DESIGN

The four dikes for the *Lebrija* Pond are homogeneous, and were initially design with a horizontal downstream drain, located immediately after the cut-off, and with a rip-rap protection in the upstream slope. The maximum heights over foundation, corresponding to the central section of the dikes in the initial design, were of 11.17m for Dike No.1, 6.19m for Dike No.2, 9.04m for Dike No.3 and 5.00m for Dike No.4. The crest dikes as a width of 5 metres.

The inclination of the upstream and downstream slopes was, respectively, of 3.5(H):1(V) and 3.0(H):1(V). For Dikes No.1 and No.3, 2.5m wide berms at level 6.00 were preview. From that level down, both for the upstream and the downstream slopes presented a slope gradient of 6.0(H):1(V) (Figure VI.9). The dikes were founded at a depth of 1m and the cut-off at 3m. The width of the cut-off, at the dike foundation level, was about 13 meters with slopes of 2.0(H):1(V).

In terms of longitudinal length, Dikes No.1 and No.3 are the longest, with a total of 387.5 metres and 337.4 metres, respectively.

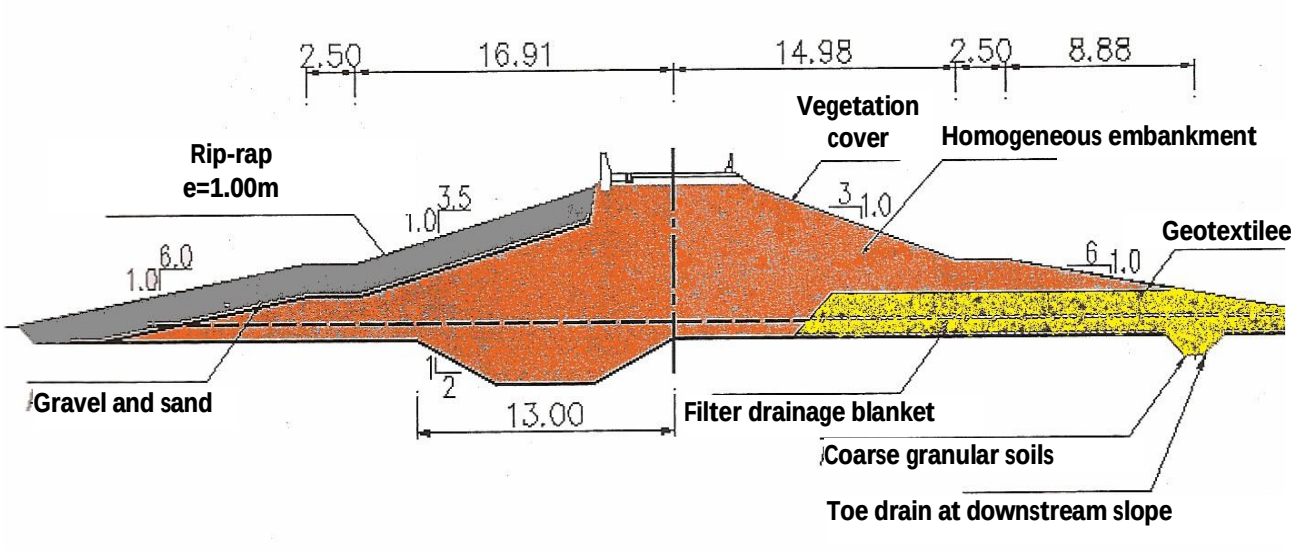

Figure VI.9 – Standard initial design of the *Lebrija* Pond dikes (Saura Martínez *et al*., 2004)

VI.3.2. REVISION OF DIKES NO.1 AND NO.3

When the excavation works started, for the implementation of the cut-off and the foundation of the dikes, it was detected that the geotechnical characteristics of the soils had to be checked, in order to guarantee the safety of the construction works and pos-constructive works. Due to this, it was decided to carry out an improved site investigation based upon piezocono, Vane-Test, and *Marchetti* dilatometer tests, and excellent piston samples. With better parameters, the safety factor of Dike No.1, assuming cracking of the embankment, was still below 1. As a result of this study, the initial design of Dikes No.1 and No.3 had to be reviewed, and it was also decided to improve and reinforce the soils foundation of these dikes (Figures VII.10 and VII.11). Therefore, it was decided to take the following steps (Cea Azañedo *et al*., 2005):

a) Creation of a chimney drain, with 2 metres wide, connected to the horizontal downstream drain of 1 metre thick;

b) Reinforcement of the Dike No.1 embankment base with the application of a geotextile Stabilenka 1000 with a stiffness of 8333 kN/m and a strength of 1000 kN/m;

c) Increment of the Dike No.1 crest width, from 5m to 6m, the berms from 2.5m to 12.5m at both sides, and enlargement of the cut-off base up to 15m. For Dike No.3, the 5m crest width was maintained, as well as the 2.5m width for the berms and the 6m at the cut-off base;

d) Installation of band-shaped drains of the Colbonddrain CX1000 type, placed in a triangular pattern, in both dikes. The drains dimensions are 10cm width by 4mm thickness, with a discharge capacity of 140ml/s (for a hydraulic gradient of 0.1). For further information and details, the technical datasheet supplied by the manufacturer can be consulted in Appendix II; The areas covered range from PK0+130 to PK0+340 in Dike No.1, and from PK0+140 to PK0+180 in No.3;

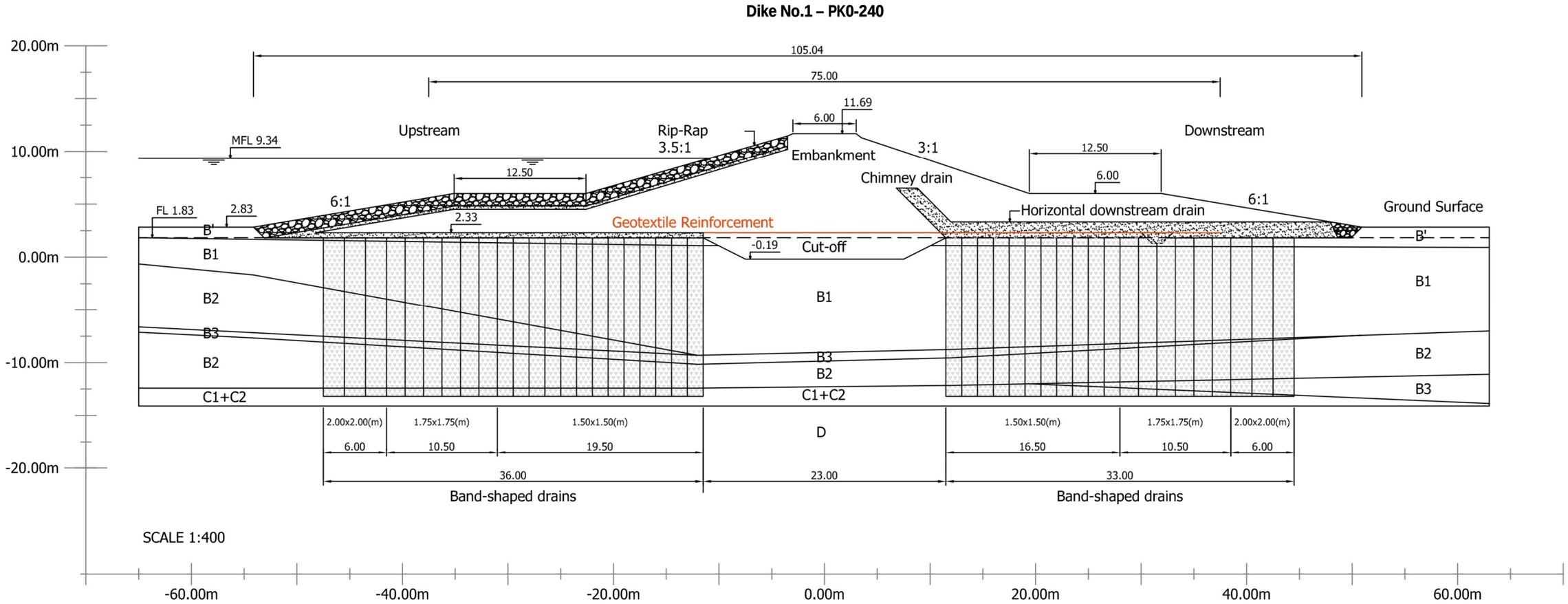

Figure VI.10 – Final design of Dike No.1, showing reinforcement geotextile, band-shaped drains and clay layers.

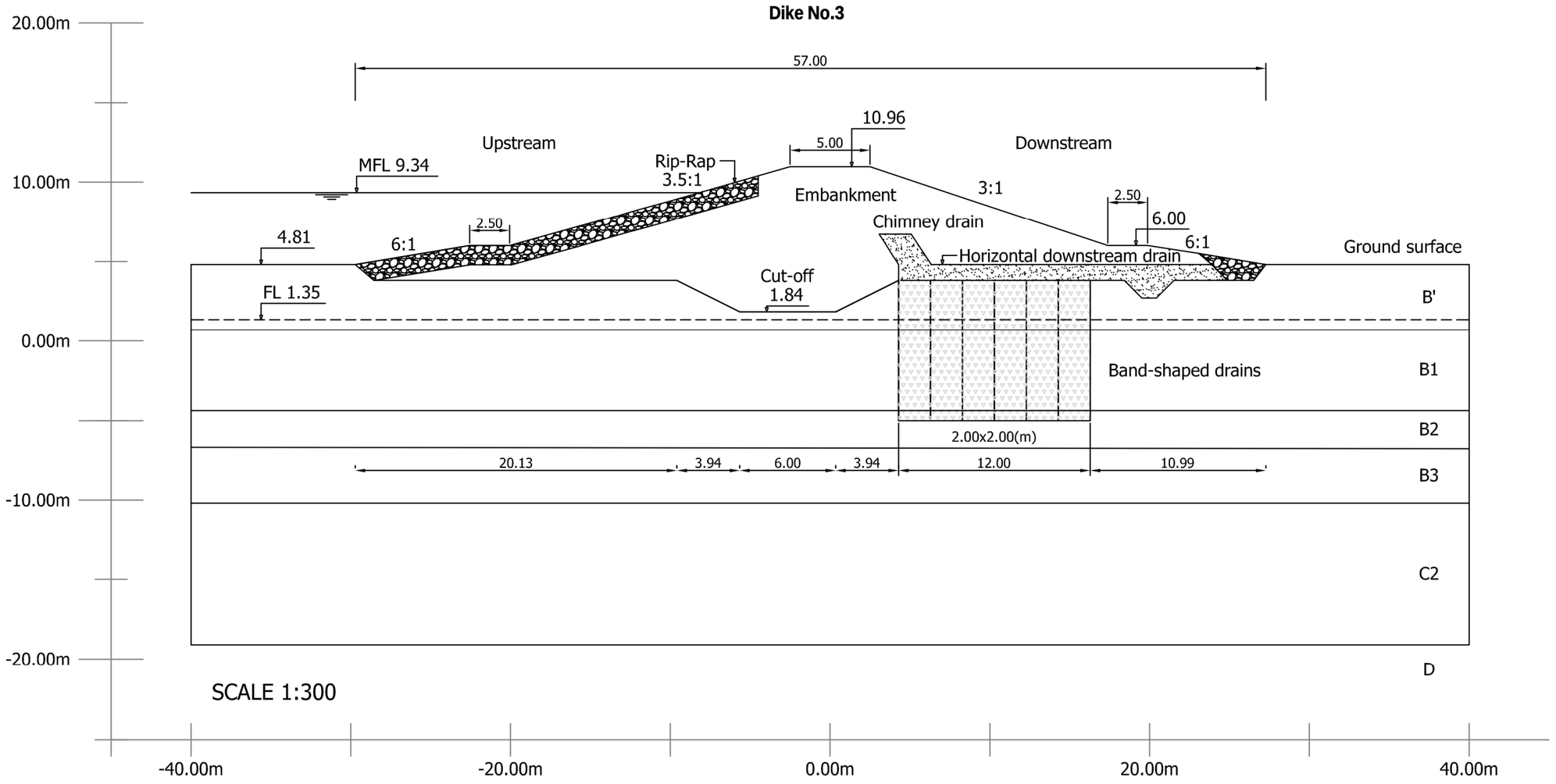

Figure VI.11 – Final design of Dike No.3, showing band-shaped drains and clay layers.

a) For Dike No.1, the drains spacing are variable, being of 1.50mx1.50m in the central zone, 1.75mx1.75m in the intermediate zone and finally 2.00mx2.00m in the limits of the dike. The adoption of gradual spacing's was to prevent the cracking of the embankment due to differential settlements. The drains have 13 metres long, and were applied in the upstream and downstream sides of the cut-off;

b) For Dike No.3, the drains were only installed in the downstream side of the cut-off. Since the area covered is relatively small, it was decided to adopt a spacing of 2.00mx2.0mm. In this case the drains length are not constant, varying from 8.8m long in the cross-section PK0+140, to 6.8m at the PK0+180;

c) Application of sand blankets with 1m thickness above the improved area, i.e., between the foundation and the dike embankment, to ensure the drainage of the water captured in the drains;

a) Installation of monitoring equipments in the embankments and foundation, in order to control the behaviour of the dikes.

The dikes are founded 1m deep in the natural ground, with the exception of the cut-off, which reaches a depth of 3m, as it was already previewed in the original design.

Settlements, as well as the pore pressures and stability analysis were recalculated. Due to these new estimated maximum settlements of 72cm and 38cm for Dikes No.1 and No.3, an over-elevation of the dike crest in the central zones were considered. As such, these dikes present, in the tallest cross-sections, the total height of 11.892m and 9.22m (Justo *et al*., 2003).

Additionally, when Dike No.1 reached level 6.00, a maximum construction rate plan was established, in order to allow the dissipation of the excess pore pressure of the foundation. So, it was established that the works should be interrupted during the winter or in more rainy periods, that each embankment layer should have a maximum thickness of 20cm, and their application would respect the following intervals:

- every 3 days until the embankment reached 2 metres above the ground level;
- every 2 days from this level up to the crest;

The raising of the water in the reservoir began immediately after the conclusion of the dikes, respecting the load plan defined in article 28 of the Safety of Dams and Reservoirs Technical Recommendations, used in Spain. These rules must be strictly respected, since they are fundamental to ensure the stability and safety of these types of structures. Therefore, and according to these recommendation, it was imposed a maximum daily rising rhythm of 7.5cm up to a level of 6.00m, and of only 3cm per day above this. The water in the reservoir reached a level of 7.15m in a relatively continuous manner. In addition to these safety measures, the capacity of the reservoir was also reduced to 7.91Hm^3 (Cea Azañedo *et al.,* 2005).

Figures VI.12a and VI.12b shows the water level in the reservoir in February 2013, and both upstream slopes of Dikes No.1 and No.3.

12a)

12b)

Figure VI.12 – a) Dike No.1 of *Lebrija* Pond (Photo of Elisa Silva, in February of 2013)
b) Dike No.3 of *Lebrija* Pond (Photo of Elisa Silva, in February of 2013)

VI.4. INSTRUMENTATION OF THE *LEBRIJA* POND DIKES

The instrumentation of the embankment dikes, as well as its foundation, is essential to control the displacements and pore pressures, developed during the construction and post-construction phases. Thus, the performances of the dikes are revealed by the analysis of these parameters, allowing not only the observation of the soil behaviour, but also the confirmation of the adequacy of the reinforcement measures. Special attention is usually given to the phase correspondent to the first filling of the reservoir. A list of the equipments used is listened below:

a) Settlement plates; these were placed in the base of the cut-off or in the embankment dike and they measure the vertical displacements (settlements);
b) Topographic stakes; these are located on the crest and along the downstream slope, and they were used to measure the settlements on the embankment dike surface;
c) Electric Piezometers; these were placed in different zones of the embankments and on the foundation, in the downstream and upstream side of the cut-off, in order to control the evolution of the pore pressures;
d) Inclinometers; these were applied in the crest of the dikes, on the downstream berms, as well as near the downstream toe drain, allowing the observation of horizontal displacements with depth.

Both dikes have being monitored almost since the beginning of the construction works. Dike No.1 has been monitored since April of 2000 and Dike No.3 has been monitored since May 2001. The readings were taken at short time intervals during construction and in the initial phase of the first filling of the reservoir. Up to now, there is a total of 2921 days of settlement readings available for analyses.

The quantification of the instrumentation used in each dike is presented in table VI.24. As it can be seen, Dike No.1 is extremely well monitored, with a total of 59 devices. Nest is Dike No.3 with 14 devices, and finally only 4 for Dike No.2. Dike No.4 has none.

Table VI.24 – Instrumentation equipments used for survey of the *Lebrija* Pond dikes

Dikes	Settlement plates	Piezometers	Inclinometers	Topographic stakes	Total of equipments
No.1	8	22	7	22	59
No.2	2	0	0	2	4
No.3	6	2	2	4	14
No.4	0	0	0	0	0

The exact location of these equipments, for each dike and cross-section, will be indicated in the next tables and figures, as well as the dates associated of their installation.

VI.4.1. DIKE NO.1 INSTRUMENTATION

In Table VI.25, the quantification of the monitoring devices installed in each cross-section of Dike No.1, is presented.

Table VI.25 – Instrumentation on each cross-section of Dike No.1 – from PK0+130 to PK0+340

Instrumentation	PK0+130	PK0+135	PK0+140	PK0+180	PK0+205	PK0+220	PK0+222	PK0+240
Settlement plates	---	---	2	---	---	---	---	**2**
Topographic stakes	1	---	---	---	1	---	---	**6**
Piezometers	---	1	---	2	---	---	2	**11**
Inclinometers	---	---	---	---	---	3	---	**1**
Total	1	1	2	2	1	3	2	**20**
Instrumentation	**PK0+250**	**PK0+258**	**PK0+260**	**PK0+270**	**PK0+300**	**PK0+310**	**PK0+340**	**Total**
Settlement plates	---	---	---	---	2	---	2	8
Topographic stakes	6	---	6	1	---	1	---	22
Piezometers	---	2	2	---	1	---	1	22
Inclinometers	---	---	3	---	---	---	---	7
Total	6	2	11	1	3	1	3	59

According to these numbers, cross-section PK0+240, which is the highest section of the dike, is the most instrumented, with 20 devices among the 59 existent. Other interesting aspect is the number of piezometers in this section. From the 22 installed in this dike, 11 are placed on the PK0+240. Due to the quantity of information which can be obtained from monitoring this section, this presents, undoubtedly, great interest and relevance to the analysis of the Dike No.1 performance. Consequently, this was the section chosen to represent Dike No.1 in the numerical simulation analysis.

Other extremely important aspect concerns the installation date of the equipments, therefore, in Tables IV.26a and IV.26b for Dike No.1, they are listened in chronological order. Regarding their positioning, it is considered that 0.00 corresponds to the axis of the dike, the negative values indicates that the device is located on the upstream side, and the positive values on the downstream side. They can also be placed at the base of the cut-off, inside or at the top of the embankment, or in the foundation.

Table VI.26a – Exact location of each instrumentation equipment on Dike No.1 and installation date

Instrumentation	Cross-section	Application date	Δt * [days]	Level	Location [m]	Depth [m]	Remarks
PL 300-2	PK 0+300	26-04-2000	25	-0.11	3.00	---	upstream
PL 140-2	PK 0+140	12-06-2000	72	-0.18	3.00	---	downstream
PZ 240-1	PK 0+240	25-07-2000	115	0.00	-7.50	---	upstream
PZ 240-2	PK 0+240	25-07-2000	115	0.00	7.50	---	downstream
PZ 135-1	PK 0+135	25-07-2000	115	0.00	0.00	---	at the axis
PZ 180-1	PK 0+180	25-07-2000	115	0.00	-7.50	---	upstream
PZ 180-2	PK 0+180	25-07-2000	115	0.00	7.50	---	downstream
PZ 260-1	PK 0+260	25-07-2000	115	0.00	-7.50	---	upstream
PZ 260-2	PK 0+260	25-07-2000	115	0.00	7.50	---	downstream
PZ 300-1	PK 0+300	25-07-2000	115	0.00	0.00	---	at the axis
PZ 340-1	PK 0+340	25-07-2000	115	0.00	0.00	---	at the axis
PL 340-2	PK 0+340	27-07-2000	117	1.12	3.00	---	downstream
PL 300-1	PK 0+300	06-07-2001	461	2.89	-3.00	---	downstream
PL 140-1	PK 0+140	10-07-2001	465	2.92	-3.00	---	upstream
PL 240-1	PK 0+240	11-07-2001	466	2.83	-3.00	---	upstream
PL 240-2	PK 0+240	11-07-2001	466	2.84	3.00	---	downstream
PZ 240-3	PK 0+240	22-07-2001	477	3.00	-7.50	---	upstream
PZ 240-4	PK 0+240	22-07-2001	477	3.00	0.00	---	at the axis
PZ 240-5	PK 0+240	22-07-2001	477	3.00	7.50	---	downstream
PZ 240-6A	PK 0+240	28-08-2001	514	-2.00	-23.25	---	upstream
PZ 240-6B	PK 0+240	28-08-2001	514	-7.00	-23.25	---	upstream
PZ 240-6C	PK 0+240	28-08-2001	514	-10.40	-23.25	---	upstream
PZ 240-7A	PK 0+240	28-08-2001	514	-2.00	29.00	---	downstream
PZ 240-7B	PK 0+240	28-08-2001	514	-7.00	29.00	---	downstream
PZ 240-7C	PK 0+240	28-08-2001	514	-10.40	29.00	---	downstream
I 260-2	PK 0+260	07-09-2001	524	3.50	42.00	18.50	toe drain
PZ 222-A	PK 0+222	07-02-2002	677	5.00	-4.00	---	upstream
PZ 222-B	PK 0+222	07-02-2002	677	1.00	-4.00	---	upstream
PZ 258-A	PK 0+258	07-02-2002	677	5.00	-4.00	---	upstream
PZ 258-B	PK 0+258	07-02-2002	677	1.00	-4.00	---	upstream
I 220-1	PK 0+220	19-02-2002	689	11.69	-3.00	35.50	upstream side crest
I 240-1	PK 0+240	19-02-2002	689	6.00	19.40	30.50	downstream berm
I 260-1	PK 0+260	19-02-2002	689	11.57	-3.00	35.50	upstream side crest
I 220-2	PK 0+220	19-02-2002	689	4.00	42.50	19.00	toe drain
PL 340-1	PK 0+340	05-04-2002	734	4.12	-3.00	---	upstream
TS 205	PK 0+205	09-08-2002	860	11.69	---	---	upstream side
TS 270	PK 0+270	09-08-2002	860	11.39	---	---	downstream side
TS 130	PK 0+130	09-08-2002	860	11.02	---	---	downstream side
TS 310	PK 0+310	09-08-2002	860	11.24	---	---	upstream side

Table VI.26b – Exact location of each instrumentation equipment on Dike No.1 and installation date

Instrumentation	Cross-section	Application date	Δt * [days]	Level	Location [m]	Depth [m]	Remarks
TS 240-1	PK 0+240	02-06-2004	1523	11.37	---	---	upstream side crest
TS 240-2	PK 0+240	02-06-2004	1523	11.16	---	---	downstream side
TS 240-3	PK 0+240	02-06-2004	1523	8.51	---	---	downstream slope
TS 240-4	PK 0+240	02-06-2004	1523	6.54	---	---	downstream pre-berm
TS 240-5	PK 0+240	02-06-2004	1523	5.46	---	---	downstream pro-berm
TS 240-6	PK 0+240	02-06-2004	1523	4.19	---	---	drain toe
TS 250-1	PK 0+250	02-06-2004	1523	11.37	---	---	upstream side crest
TS 250-2	PK 0+250	02-06-2004	1523	11.14	---	---	downstream side crest
TS 250-3	PK 0+250	02-06-2004	1523	8.91	---	---	downstream slope
TS 250-4	PK 0+250	02-06-2004	1523	6.56	---	---	downstream pre-berm
TS 250-5	PK 0+250	02-06-2004	1523	5.51	---	---	downstream pro-berm
TS 250-6	PK 0+250	02-06-2004	1523	4.23	---	---	drain toe
TS 260-1	PK 0+260	02-06-2004	1523	11.32	---	---	upstream side crest
TS 260-2	PK 0+260	02-06-2004	1523	11.09	---	---	downstream side crest
TS 260-3	PK 0+260	02-06-2004	1523	8.68	---	---	downstream slope
TS 260-4	PK 0+260	02-06-2004	1523	6.487	---	---	downstream pre-berm
TS 260-5	PK 0+260	02-06-2004	1523	5.60	---	---	downstream pro-berm
TS 260-6	PK 0+260	02-06-2004	1523	4.22	---	---	drain toe
I 220-1 (bis)	PK 0+220	14-06-2004	1535	---	-3.00	35.50	upstream side crest
I 260-1 (bis)	PK 0+260	14-06-2004	1535	---	-3.00	35.50	upstream side crest

(*) After the beginning of the construction works on Dike No.1, in 01-04-2000
PL – Settlement Plate; PZ - Piezometer; I - Inclinometer; TS – Topographic stake mark

The plan showing all the instrumentation installed in Dike No.1 is plotted in figure VI.13, and figure VI.14 shows the exact location of the monitoring devices installed only in the PK0+240 profile.

VI.4.2. DIKE NO.3 INSTRUMENTATION

With respect to the instrumentation equipments installed in Dike No.3, they are all listened in table VI.27, and plotted in Figure VI.15. In this dike there are a total of 14 devices, although only 2 piezometers in section PK0+180, 2 inclinometers in PK0+220, and 6 settlement plates in three distinct cross-sections, namely in PK0+140, PK0+170 and PK0+200.

Table VI.27 – Instrumentation on each cross-section of Dike No.3 – from PK0+085 to PK0+220

Instrumentation	PK0+085	PK0+135	PK0+140	PK0+170	PK0+180	PK0+200	PK0+220	Total
Settlement plates	---	---	2	2	---	2	---	6
Topographic stakes	1	1	---	1	---	--	1	4
Piezometers	---	---	---	---	2	---	---	2
Inclinometers	---	---	---	---	---	---	2	2
Total	1	1	2	3	2	2	3	14

For Dike No.3, the positioning of the monitoring devices and installation dates can be consulted in table IV.28. Again, 0.00 corresponds to the axis of the dike, the negative values to the upstream side, and the positive values to downstream side.

Table VI.28 – Exact location of each instrumentation equipment on Dike No.3 and installation date

Instrumentation	Cross-section	Application date	Δt * [days]	Level	Location [m]	Depth [m]	Remarks
I 220-2	PK 0+220	04-04-2001	-27	3.00	29.00	30.00	toe drain
PL 200-1	PK 0+200	27-05-2001	26	3.40	-3.00	---	upstream
PL 200-2	PK 0+200	27-05-2001	26	3.40	3.00	---	downstream
PL 170-1	PK 0+170	28-06-2001	58	3.79	-3.00	---	upstream
PL 140-1	PK 0+140	20-06-2001	50	3.84	-3.00	---	upstream
PZ 180-1A	PK 0+180	30-08-2012	486	0.00	-21.00	---	upstream
PZ 180-1B	PK 0+180	30-08-2012	486	-5.00	-21.00	---	upstream
PL 170-2	PK 0+170	21-11-2001	204	4.63	3.00	---	downstream
PL 140-2	PK 0+140	21-11-2001	204	4.81	3.00	---	downstream
I 220-1	PK 0+220	19-02-2002	294	10.90	-2.50	16.00	upstream side crest
TS 085	PK 0+085	09-08-2002	465	10.78	2.50	---	downstream side crest
TS 135	PK 0+135	09-08-2002	465	10.93	2.50	---	downstream side crest
TS 170	PK 0+170	09-08-2002	465	10.93	2.50	---	downstream side crest
TS 220	PK 0+220	09-08-2002	465	10.95	2.50	---	downstream side crest

(*) After the beginning of the construction works on Dike No.3, in 01-05-2001
PL – Settlement Plate; PZ - Piezometer; I - Inclinometer; TS – Topographic stake mark

The location of the plates, piezometers and inclinometers inside the dike, for sections PK0+140, PK0+170, PK0+180, PK0+200 and PK0+220, is plotted in figures VI.16, VI.17, VI.18, VI.19 and VI.20, respectively.

The monitoring results of Dike No.3 are also important, because, in this case, there are measurements from settlements in zones improved with and without drains. This enables a comparison between the areas covered with and without the band-shaped drains, and their effect on the soil consolidation acceleration (Da Silva *et al.,* 2010a; Da Silva *et al.,* 2010c). Unfortunately, there were placed only two piezometers on the foundation, and both below the upstream berm, meaning that it is impossible to compare directly the dissipation of the excess pore pressure, in zones where there are no drains and zones where drains were installed.

In the case of Dike No.1, the settlement plates are always located between the zones improved with drains, and so are the piezometers, although some are located inside the dike and others in the foundation. However, these devices are either located, in the drains zone or near the axis of the dike, but always between the upstream and downstream zones treated with drains. Consequently, it is difficult to draw conclusions related to the effect of the drains in the excess pore pressure dissipation, using only the measurements taken from Dike No.1, since they are inside of the zone in question, or in the middle of it (Da Silva *et al.,* 2012). Therefore, in order to draw conclusions regarding the effect of the drains and their efficiency, both monitoring results must be analysed.

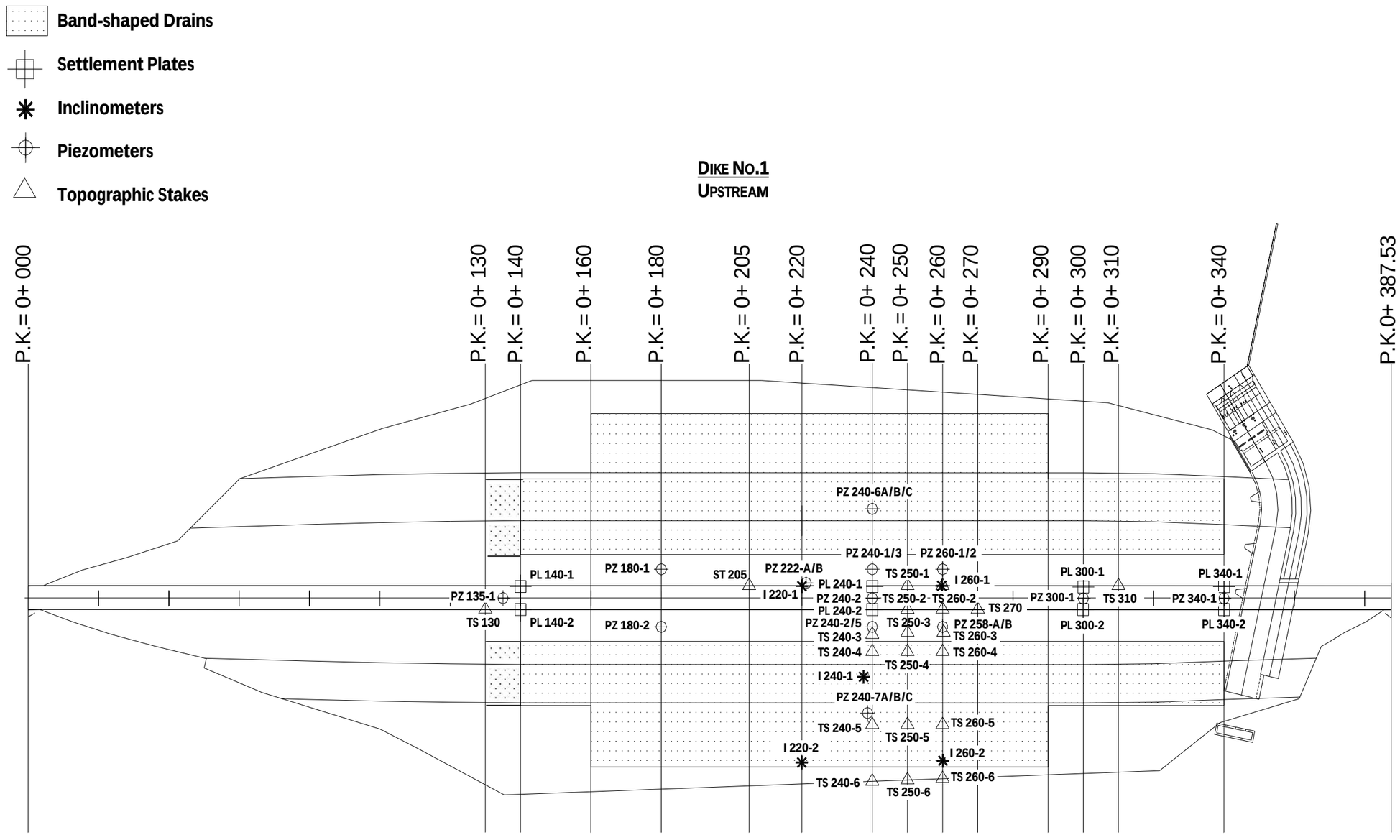

Figure VI.13 – Plan showing all the instrumentation in Dike No.1.

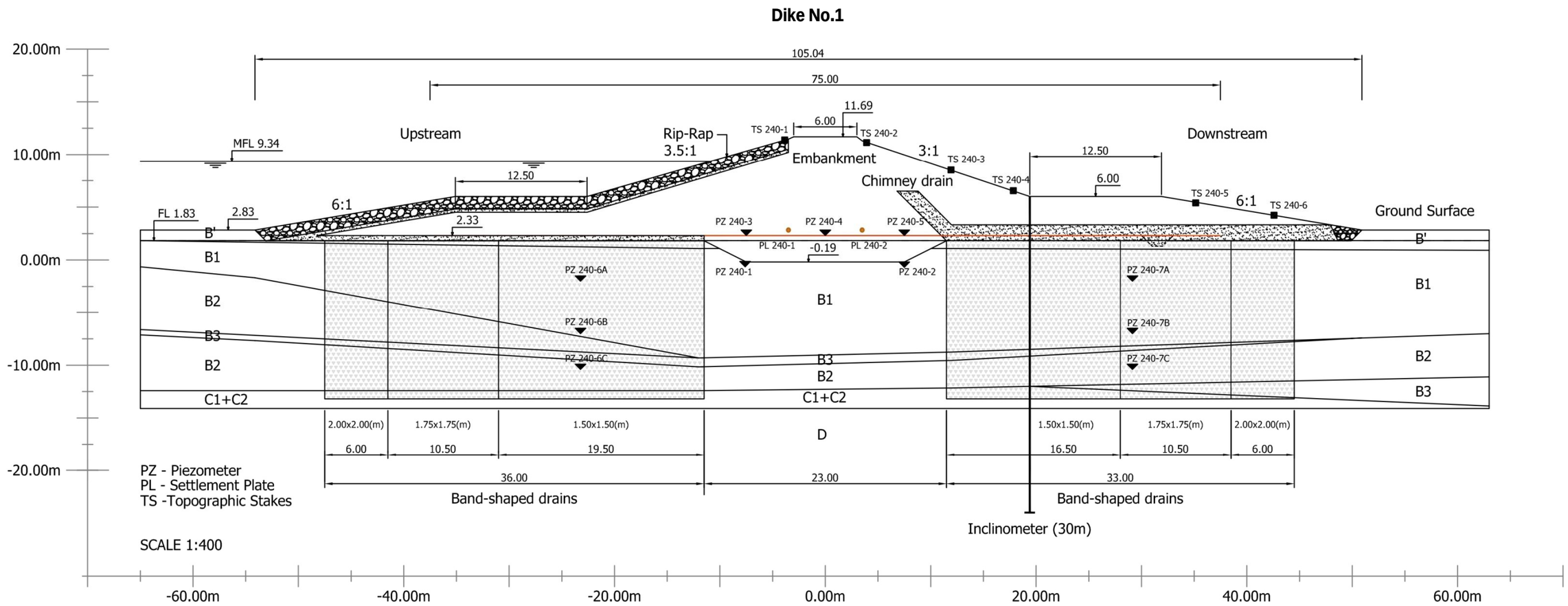

Figure VI.14 – Final design of Dike No.1 (PK0+240), showing settlement plates, topographic stake marks, piezometers and inclinometers.

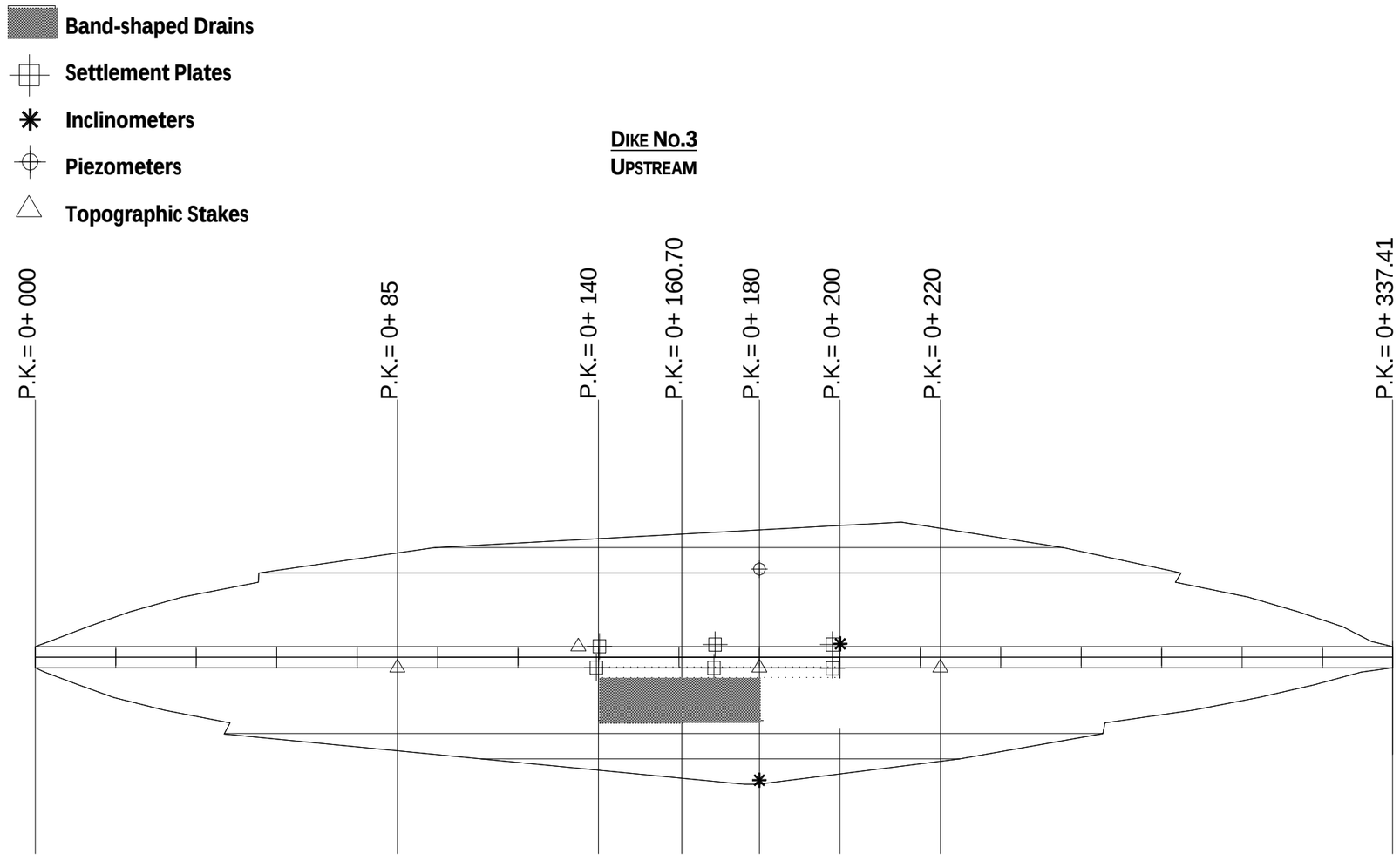

Figure VI.15 – Plan showing all the instrumentation in Dike No.3.

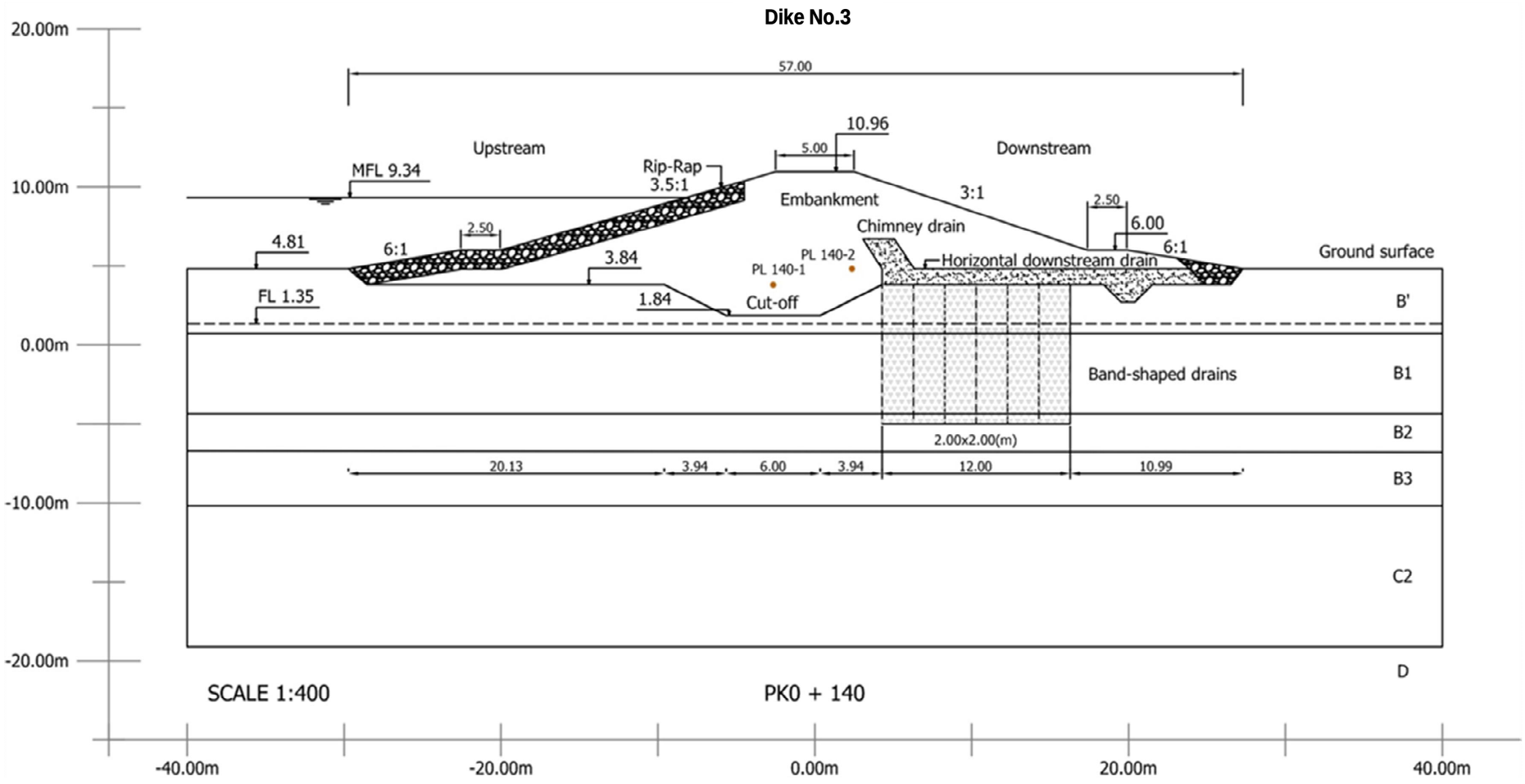

Figure VI.16 – Position of the settlement plates PL 140-1 and PL 140-2 on Dike No.3

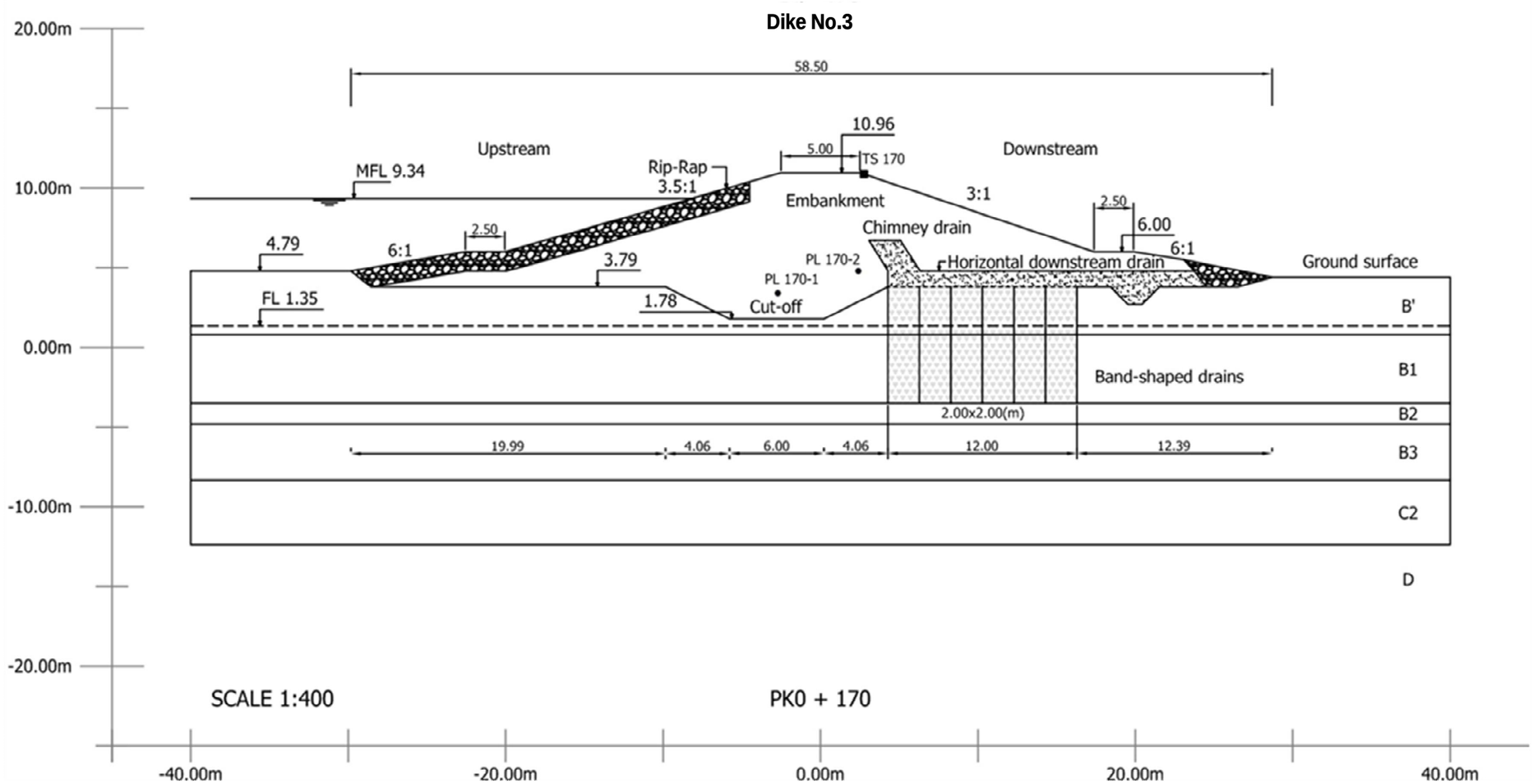

Figure VI.17 – Position of the settlement plates PL 170-1 and PL 170-2 on Dike No.3

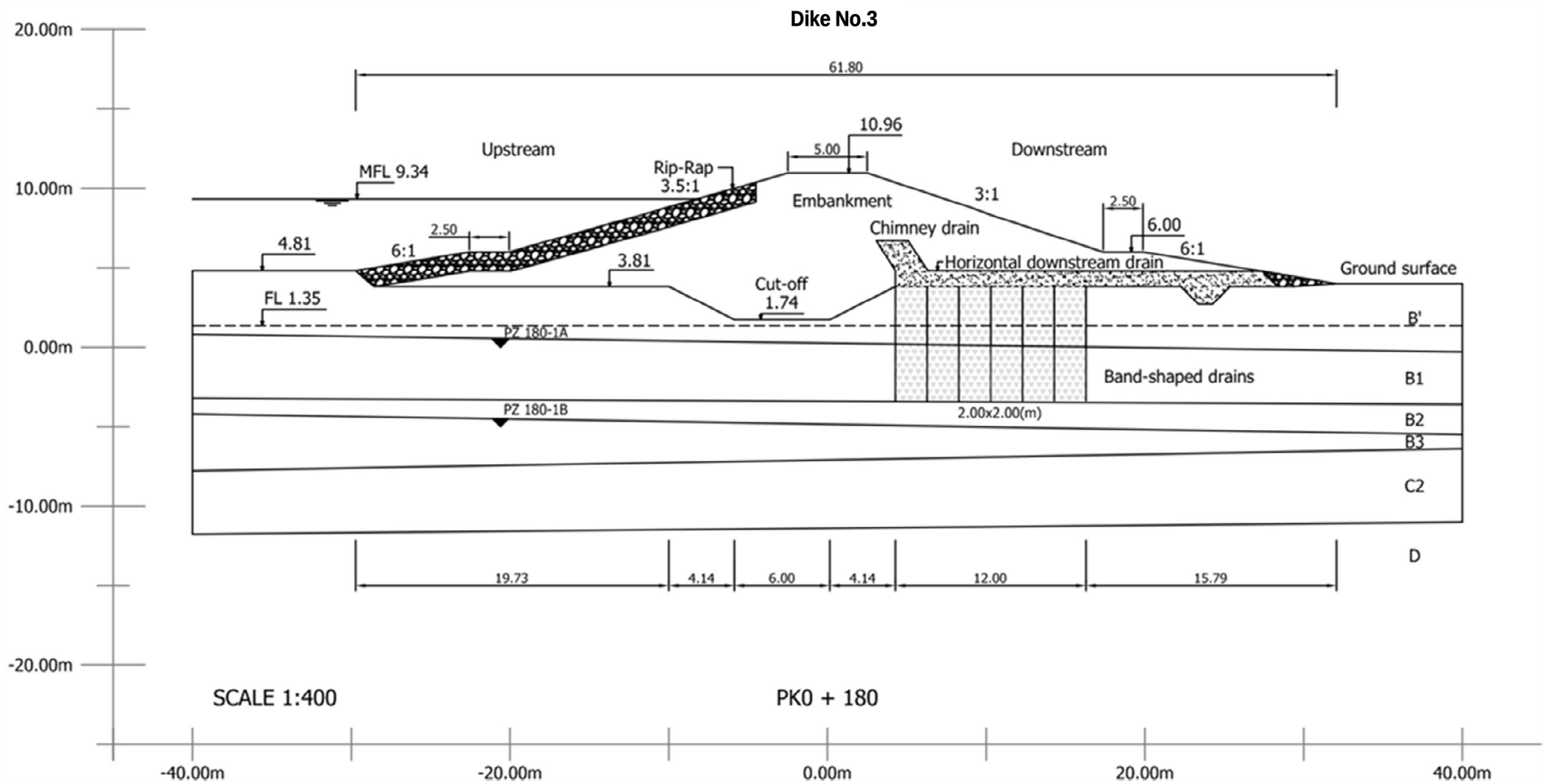

Figure VI.18 – Position of the piezometers PZ 180-1 and PZ 180-2 on Dike No.3

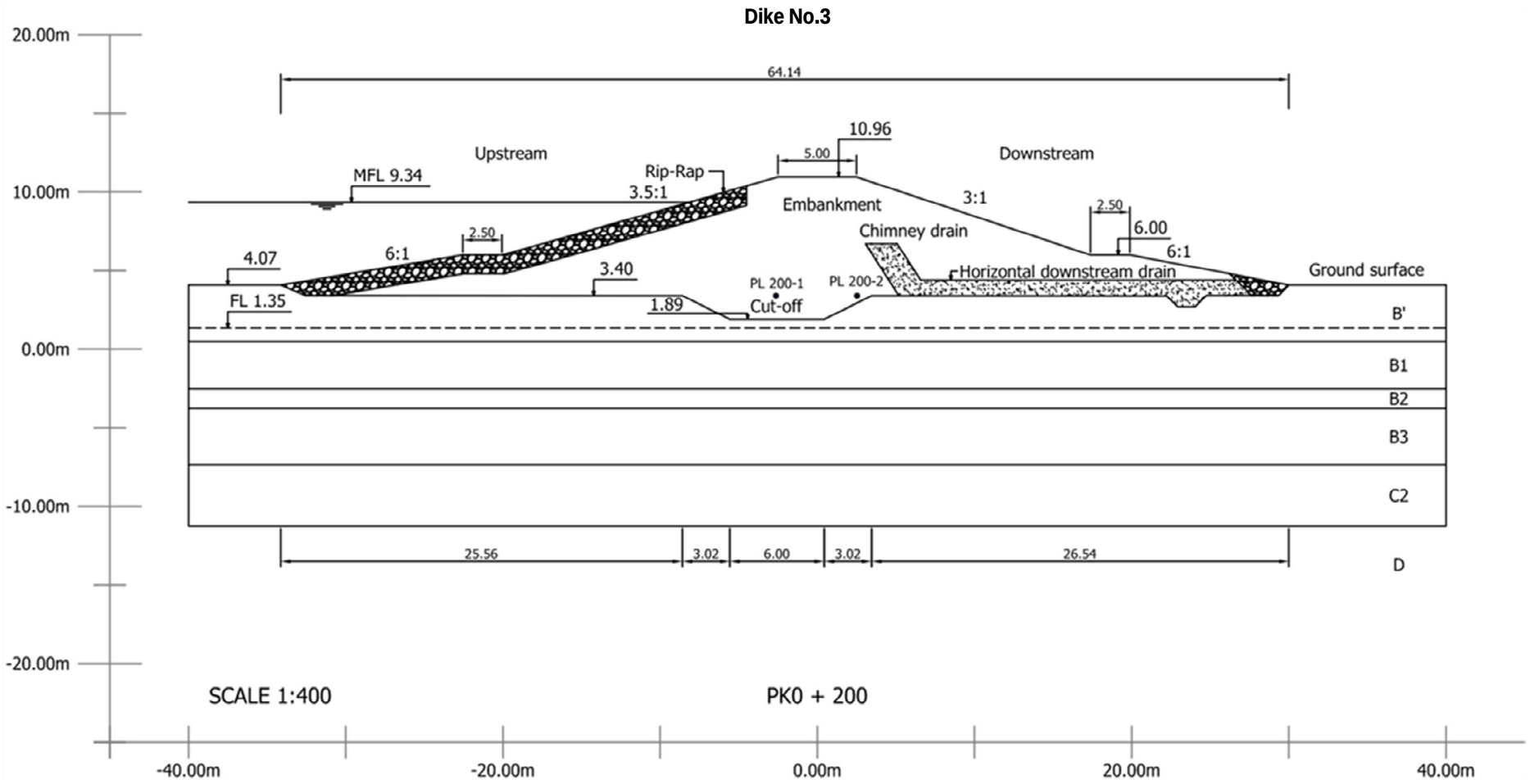

Figure VI.19 – Position of the settlement plates PL 200-1 and PL 200-2 on Dike No.3

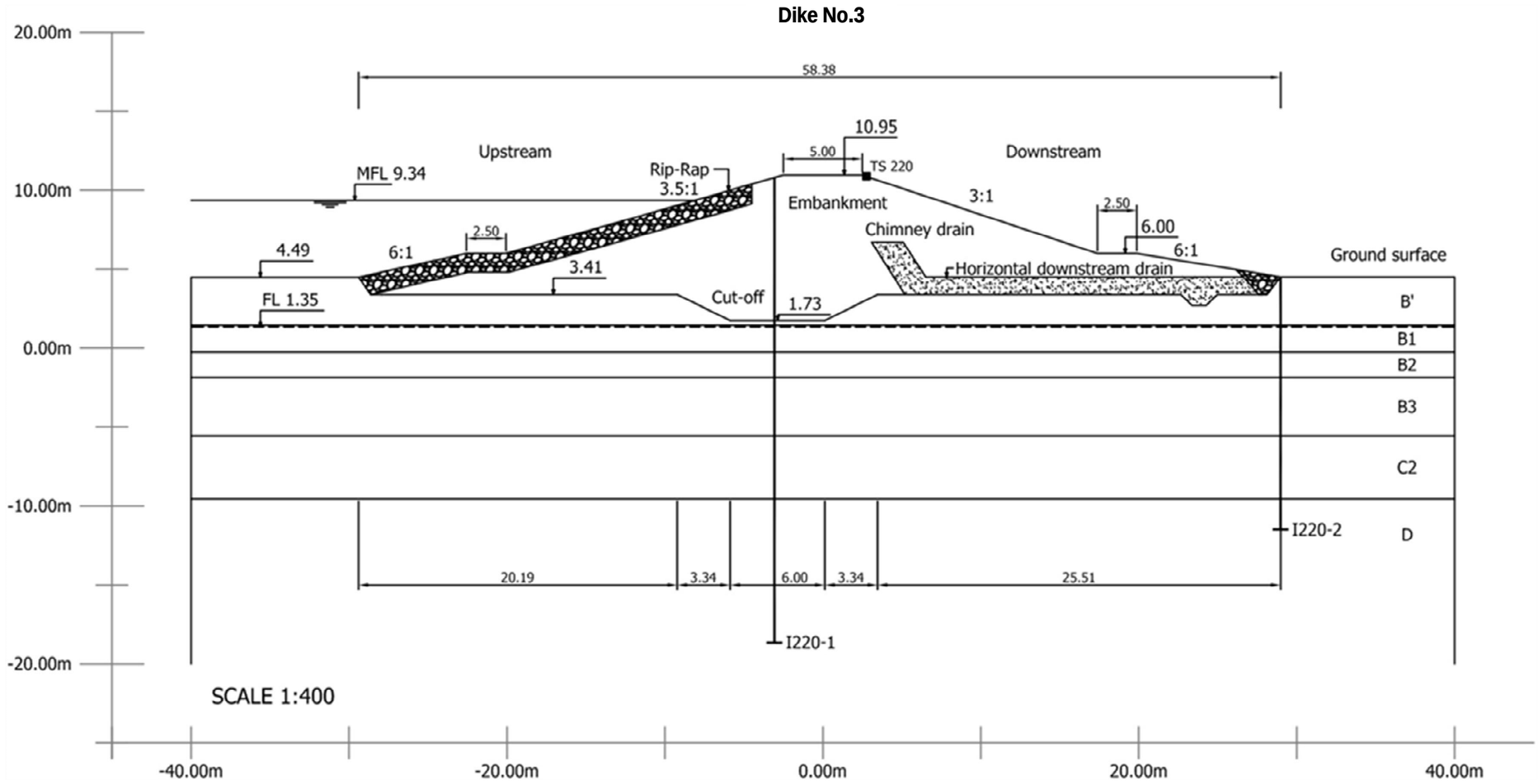

Figure VI.20 – Position of the inclinometers I 220-1 and I 220-2 on Dike No.3

Some of the instrumentations devices installed at the crest of Dike No.1 are shown in figures VI.21a), VI.21b), VI.21c) and VI.21d).

21a)

21b)

21c)

21d)

Figure VI.21 – Instrumentation devices installed on the *Lebrija* Pond Dike No.1: a) Topographic stake mark on the upstream side of the crest; b) Topographic stake mark on the downstream side of the crest; c) Piezometer; d) Inclinometer (Photos of Elisa Silva, in February of 2013)

VI.5 – CONSTRUCTION TIMELINE OF DIKES AND RESERVOIR FILLING

The phases associated to the construction works are extremely important in the analysis of the soil foundation behaviour as well as the embankment itself. The rhythm undertaken for the embankment compaction is of vital importance, being imposed maximum construction rates. The same was applied for the rose up of the water level in the reservoir. Base on these rates one can define the load increments and the surcharges applied to the foundation, during the construction and post-construction phases. Therefore, it is necessary to present the timeline regarding the construction steps for the two dikes, including the installation dates of the instrumentation equipments, before analysing the results from the monitoring (Da Silva *et al.,* 2010b).

This is also a crucial aspect, which must be taken into consideration on the numerical simulation of the dikes, since the numerical results will be later compared to the measured ones. Hence, it is important to be as precisely as possible, in the definition of the construction stages of the dikes and in the reservoir filling.

VI.5.1. DIKE NO.1 CONSTRUCTION STAGES

The construction steps and timeline of Dike No.1, as well as the rise up of the water level in the reservoir, are indicated in Table VI.29, being the values associated to the PK0+240 profile.

Table VI.29 – Timeline of construction stages of Dike No.1, for PK0+240, and rise up of reservoir

Timeline of construction stages and rise up of reservoir	Ground level [m]	Date	Δt [days]	Water level [m]
Beginning of construction works (surface ground level at 2.83)	2.83	01-04-2000	0	1.83
Ground excavation up to level 1.83 (-0.19 on the cut-off); Piezometer installation PZ 240-1 and PZ 240-2 at level 0.00	-0.19	25-07-2000	115	1.83
Cut-off compaction up to level 1.83	1.83	22-08-2000	143	1.83
Embankment reaches level 2.33; Drains and geotextile installation	2.33	17-09-2000	169	1.83
Embankment reaches level 2.83; construction interrupted (winter of 2000)	2.83	02-10-2000	184	1.83
Woks resumption; Settlement plates installation PL 240-1 and 240-2	2.83	11-07-2001	466	1.83
Embankment reaches level 3.70; Piezometer installation PZ 240-3. PZ 240-4 and PZ 240-5 at level 3.00	3.70	22-07-2001	477	1.83
Embankment reaches level 4.71	4.71	08-08-2001	494	1.83
Embankment reaches level 6.00; Piezometer installation PZ 240-6A/6B/6C and PZ 240-7A/7B/7C	6.00	28-08-2001	514	1.83
Embankment reaches level 10.29	10.29	12-11-2001	590	1.83
Embankment reaches level 10.97; construction interrupted (winter of 2001)	10.97	10-12-2001	618	1.83
Inclinometer installation I 240-1	10.97	19-02-2002	689	1.83
Construction works resumption (level 10.97)	10.97	10-05-2002	769	1.83
Embankment reaches level 11.695; Conclusion of Dike No.1	11.69	28-06-2002	818	1.83
Installation of topographic stakes TS 205 and TS 270	11.69	09-08-2002	860	2.30
Rise up of reservoir: water level at 3.00	---	21-08-2002	872	3.00
water level at 4.86	---	05-11-2002	948	4.86
water level at 6.00	---	29-11-2002	972	6.00
water level at 7.15	---	20-01-2003	1024	7.15
water level at 7.30	---	30-04-2003	1124	7.30
water level at 6.90	---	27-05-2003	1151	6.90
water level at 7.80	---	09-06-2003	1164	7.80
water level at 6.05	---	11-07-2003	1196	6.05
water level at 7.25	---	15-09-2003	1262	7.25
water level at 6.50	---	14-10-2003	1291	6.50
water level at 7.25	---	23-12-2003	1361	7.25
water level at 6.81	---	17-02-2004	1417	6.81
water level at 7.22	---	08-03-2004	1437	7.22
Installation of topographic stakes TS 240-1 to 240-6	---	02-06-2004	1523	7.22
water level at 8.01	---	10-09-2004	1623	8.01
water level at 6.71	---	15-12-2004	1719	6.71
water level at 8.04	---	27-07-2005	1943	8.04
water level at 7.80 – last survey measurements	---	31-03-2008	2921	7.80

VI.5.2. DIKE NO.3 CONSTRUCTION STAGES

In the case of dike No.3, the construction steps for cross-sections PK0+140, Pk0+170, Pk0+180 and Pk0+200 will be indicated in the next tables. However, and despite of the different steps and times associated to the dike construction, once this is concluded and the filling of the reservoir starts, the timeline is always the same for all cross-sections. As a result, only the complete timeline for section PK0+140 is presented here (Table VI.30).

Table VI.30 – Timeline of construction stages of Dike No.3, for PK0+140, and rise up of reservoir

Timeline of construction stages and rise up of reservoir	Ground level [m]	Date	$\triangle$t [days]	Water level [m]
Beginning of construction works (surface ground level at 4.81)	4.81	01-05-2001	0	1.35
Ground excavation up to level 3.84 (1.84 on the cut-off)	3.84	10-05-2001	9	1.35
Cut-off compaction up to level 3.84; Settlement plate installation PL 140-1	3.84	20-06-2001	50	1.35
Embankment reaches level 4.34; Drains installation	4.34	30-06-2001	60	1.35
Embankment reaches level 4.81; Settlement plate installation PL 140-2	4.81	21-07-2001	81	1.35
Embankment reaches level 8.15; Construction interrupted	8.15	30-10-2001	182	1.35
First measure taken for settlement plate PL 140-2	8.15	21-11-2001	204	1.35
Construction works resumption (level 8.15)	8.15	03-12-2001	216	1.35
Embankment reaches level 8.50; Construction interrupted	8.50	20-12-2001	233	1.35
Construction works resumption (level 8.50)	8.50	10-01-2002	254	1.35
Embankment reaches level 8.69	8.69	18-01-2002	262	1.35
Embankment reaches level 10.1	10.06	15-02-2002	290	1.35
Embankment reaches level 10.39	10.39	15-03-2002	318	1.35
Embankment reaches level 10.63	10.63	30-04-2002	364	1.35
Embankment reaches level 10.96; Conclusion of Dike No.3	10.96	10-07-2002	435	1.35
Installation of topographic stake TS 135	10.96	09-08-2002	465	2.30
Rise up of reservoir: water level at 3.00	---	21-08-2002	477	3.00
water level at 4.86	---	05-11-2002	553	4.86
water level at 6.00	---	29-11-2002	577	6.00
water level at 7.15	---	20-01-2003	629	7.15
water level at 7.30	---	30-04-2003	729	7.30
water level at 6.90	---	27-05-2003	756	6.90
water level at 7.80	---	09-06-2003	769	7.80
water level at 6.05	---	11-07-2003	801	6.05
water level at 7.25	---	15-09-2003	867	7.25
water level at 6.50	---	14-10-2003	896	6.50
water level at 7.25	---	23-12-2003	966	7.25
water level at 6.81	---	17-02-2004	1022	6.81
water level at 7.22	---	08-03-2004	1042	7.22
water level at 8.01	---	10-09-2004	1228	8.01
water level at 6.71	---	15-12-2004	1324	6.71
water level at 8.04	---	27-07-2005	1548	8.04
water level at 7.80 - last survey measurements	---	31-03-2008	2526	7.80

It should be emphasised that a peculiar situation occurs with the installation date of the settlement plates PL 140-2 and PL 170-2 and the date of their first readings. Settlement plates PL 140-2 and PL170-2 were placed at the level 4.81 and 4.63, respectively; however, their first readings were taken when the embankment reached level 8.15, corresponding to a time lag of 123 days for the PL 140-2 and 120 days for PL 170-2, as it is can be observed in tables VI.30 and VI.31.

Table VI.31 – Timeline of construction stages of Dike No.3, for PK0+170, and rise up of reservoir

Timeline of construction stages and rise up of reservoir	Ground level [m]	Date	Δt [days]	Water level [m]
Beginning of construction works (surface ground level at 4.79)	4.79	01-05-2001	0	1.35
Ground excavation up to level 3.79 (1.78 on the cut-off)	3.79	10-05-2001	9	1.35
Cut-off compaction up to level 3.79; Settlement plate installation PL 170-1	3.79	28-06-2001	58	1.35
Embankment reaches level 4.30; Drains installation	4.30	15-07-2001	75	1.35
Embankment reaches level 4.63; Settlement plate installation PL 170-2	4.63	24-07-2001	84	1.35
Embankment reaches level 7.93; Construction interrupted	7.93	30-10-2001	182	1.35
Construction works resumption (level 7.93)	7.93	16-11-2001	199	1.35
Embankment reaches level 8.15; construction interrupted; First measure taken for settlement plate PL170-2	8.15	21-11-2001	204	1.35
Construction works resumption (level 8.15)	8.15	03-12-2001	216	1.35
Embankment reaches level 8.32; Construction interrupted	8.32	20-12-2001	233	1.35
Construction works resumption (level 8.32)	8.32	18-01-2002	262	1.35
Embankment reaches level 8.90	8.90	01-02-2002	276	1.35
Embankment reaches level 10.02	10.02	01-03-2002	304	1.35
Embankment reaches level 10.66	10.66	30-04-2002	364	1.35
Embankment reaches level 10.96; Conclusion of No.3	10.96	10-07-2002	435	1.35
Installation of topographic stake TS 170	10.96	09-08-2002	465	2.30
Rise up of reservoir: water level at 3.00	3.00	21-08-2002	477	3.00
(*)	-----	-----	-----	-----

(*) From this date forward, the timeline and water level in the reservoir are equal to those indicated for cross-section PK0+140, on table VI.30.

Table VI.32 shows the construction sequence for section PK0+180 in Dike No.3 This section only has two piezometers, both being placed below the upstream berm, with no device of this type on the downstream side of the cut-off, or in the area where the band-shaped drains were installed.

Finally, in table VI.33 are listened the construction timeline of section PK0+200. Plates PL240-1 and PL240-2 are practically at the same level and the settlements measurements started immediately after their installation.

Table VI.32 – Timeline of construction stages of Dike No.3, for PK0+180, and rise up of reservoir

Timeline of construction stages and rise up of reservoir	Ground level [m]	Date	Δt [days]	Water level [m]
Beginning of construction works (surface ground level at 4.81)	4.81	01-05-2001	0	1.35
Ground excavation up to level 3.81 (1.74 on the cut-off)	1.74	10-05-2001	9	1.35
Embankment reaches level 3.40	3.40	20-06-2001	50	1.35
Cut-off compaction up to level 3.81	3.81	28-06-2001	58	1.35
Embankment reaches level 4.30; Drains installation	4.30	15-07-2001	75	1.35
Embankment reaches level 5.90; Piezometer installation PZ 180-1A and PZ 180-1B	5.90	30-08-2001	121	1.35
Embankment reaches level 6.00	6.00	19-09-2001	141	1.35
Embankment reaches level 7.80	7.80	13-11-2001	196	1.35
Embankment reaches level 8.10; Construction interrupted	8.10	03-12-2001	216	1.35
Construction works resumption (level 8.10)	8.10	28-01-2002	272	1.35
Embankment reaches level 8.75	8.75	08-02-2002	283	1.35
Embankment reaches level 10.96; Conclusion of Dike No.3	10.96	10-07-2002	435	1.35
Rise up of reservoir: water level at 3.00	3.00	21-08-2002	477	3.00
(*)	-----	-----	-----	-----

(*) From this date forward, the timeline and water level in the reservoir are equal to those indicated for cross-section PK0+140, on table VI.30.

Table VI.33 – Timeline of construction stages of Dike No.3, for PK0+200, and rise up of reservoir

Timeline of construction stages and rise up of reservoir	Ground level [m]	Date	Δt [days]	Water level [m]
Beginning of construction works (surface ground level at 4.07)	4.07	01-05-2001	0	1.35
Ground excavation up to level 3.40 (1.89 on the cut-off)	3.40	10-05-2001	9	1.35
Cut-off compaction up to level 3.40; Settlement plates installation PL 200-1 and PL 200-2	3.40	27-05-2001	26	1.35
Embankment reaches level 4.65	4.65	02-08-2001	93	1.35
Embankment reaches level 6.00	6.00	29-08-2001	120	1.35
Embankment reaches level 7.80; Construction interrupted	7.80	30-10-2001	182	1.35
Construction works resumption (level 7.80)	7.80	16-11-2001	199	1.35
Embankment reaches level 8.10; Construction interrupted	8.10	21-11-2001	204	1.35
Construction works resumption (level 8.10)	8.10	18-01-2002	262	1.35
Embankment reaches level 8.75	8.75	01-02-2002	276	1.35
Embankment reaches level 9.99	9.99	15-03-2002	318	1.35
Embankment reaches level 10.46	10.46	30-04-2002	364	1.35
Embankment reaches level 10.96; Conclusion of Dike No.3	10.96	10-07-2002	435	1.35
Rise up of reservoir: water level at 3.00	3.00	21-08-2002	477	3.00
(*)	-----	-----	-----	-----

(*) From this date forward, the timeline and water level in the reservoir are equal to those indicated for cross-section PK0+140, on table VI.30.

VI.6. MONITORING RESULTS OF DIKES NO.1 AND NO.3

All the monitoring results from the settlement plates, topographic stake marks, piezometers and inclinometers installed in Dikes No.1 and No.3 will be presented in this section, performing a total of 2921 days and 2526 days, respectively. Based on these data, some conclusions can be drawn regarding the settlements, pore pressures and horizontal displacements observed in the embankments dikes and foundation, during the construction and pos-constructive stage.

The sequence adopted for the presentation and interpretation of the results will start with the pore pressures measured in the piezometers, followed by the settlement plates and topographic stake marks, ending with the horizontal displacements observed in the inclinometers. This is because the settlements are directly related to the excess pore pressure dissipation, which is caused by the surcharge associated to the embankment construction, and also by the rising of the water in the reservoir. As such, analysing first the results measured in the piezometers, a better understanding can be achieve for the future settlement analyses. Nevertheless, this correspondence between settlements and pore pressures can be only performed, when the same cross-section includes results from piezometers and plates that are located relatively close to one another. This is the case in section PK0+240 of Dike No.1 for PZ 240-3, PZ 240-4, PZ 240-5 and plates PL 240-1 and PL0240-2. In Dike No.3, it is not possible to do these types of analyses, as there is no section with both piezometers and plates. Notwithstanding, the results from Dike No.3 are precious, since they allow the comparison of the foundation settlements with and without band-shaped drains, as plates were placed in improved zones and in areas where the drains were not used.

VI.6.1. PORE PRESSURES IN THE FOUNDATION AND IN DIKE NO.1

Dike No.1 construction works started in the beginning of April 2000. Meanwhile, at the same time of the ground excavation works, further site investigation was performed, and it was decided to place prefabricated vertical band-shaped drains in the foundation, on the upstream and downstream side of the cut-off, as well as a reinforcement geotextile with 75 metres long, at level 2.33. In early October, the embankment reached level 2.83 and construction was interrupted immediately after, not re-starting until mid-July 2001. From then on, construction progressed slowly, in accordance with the rate construction plan stipulated in the revised design, and stopped again in mid-December 2001 and mid-May 2002, already in an advanced phase of construction (level10.97). At the end of June 2002, Dike No.1 was concluded and the rising of the water in the reservoir began at the end of July. On 21 August 2002, the water reached level 3.00m; on 29 November 2002, the level 6.00m; and, on 20 January 2003, it had finally achieved the level 7.15. It maintained this level for one month, later suffering some fluctuations, until it attained level 7.80m on 9 June 2003. From then on, it underwent some increases and decreases with the minimum water level registered being 6.05m and the maximum 8.04m.

The pore pressures measured in the piezometers vary according to the construction of the dike and to the water level in the reservoir, as would be expected. Due to this, it was decided to present both the results from the monitoring of the pore pressure and the overloads corresponding to the construction of the dike and the hydraulic load associated with the rising of the water level in the reservoir in the same graph, in order always to have a reference.

The piezometers located approximately at the base of the cut-off trench (level 0.00m), namely, PZ 180-1, PZ 240-1, PZ 260-1 in the upstream side, PZ 135-1, PZ 300-1, PZ 340-1 at the axis of the dike and PZ 180-2, PZ 240-2, PZ 260-2 in the downstream side, installed in the initial phase of the construction, registered high increments in hydrostatic overpressure during the stage construction (Graphs VI.1, VI.2 and VI.3). These values were expected as the foundation clayed soils present undrained behaviour; consequently, in an initial phase, the load is totally supported by the water particles trapped in the soil voids. Yet, due to the presence of the drains, it can be seen that the hydrostatic overpressure in the piezometers is less than the overload associated to the embankment. Base on these results, it is possible to indicate that the drains carry out their function immediately after their installation, along with the embankment construction, allowing the excess pore pressures dissipation and speed up the consolidation. The overload correspondent to the maximum weight of the embankment, at the axis of the dike, is approximately 188kN/m^2. The differences between this overload and the overpressure increments, obtained in the piezometers, are approximately the following:

- x=-7.50m from the axis (upstream): 112kN/m^2 for PZ 180-1;
  47kN/m^2 for PZ 240-1;
  132kN/m^2 for PZ 260-1;
- x=0.00m (at the axis): 110kN/m^2 for PZ 135-1;
  110kN/m^2 for PZ 300-1;
  90kN/m^2 for PZ 340-1;
- x=7.50m from the axis (downstream): 90kN/m^2 for PZ 180-2;
  7kN/m^2 for PZ 240-2;
  132kN/m^2 for PZ 260-2.

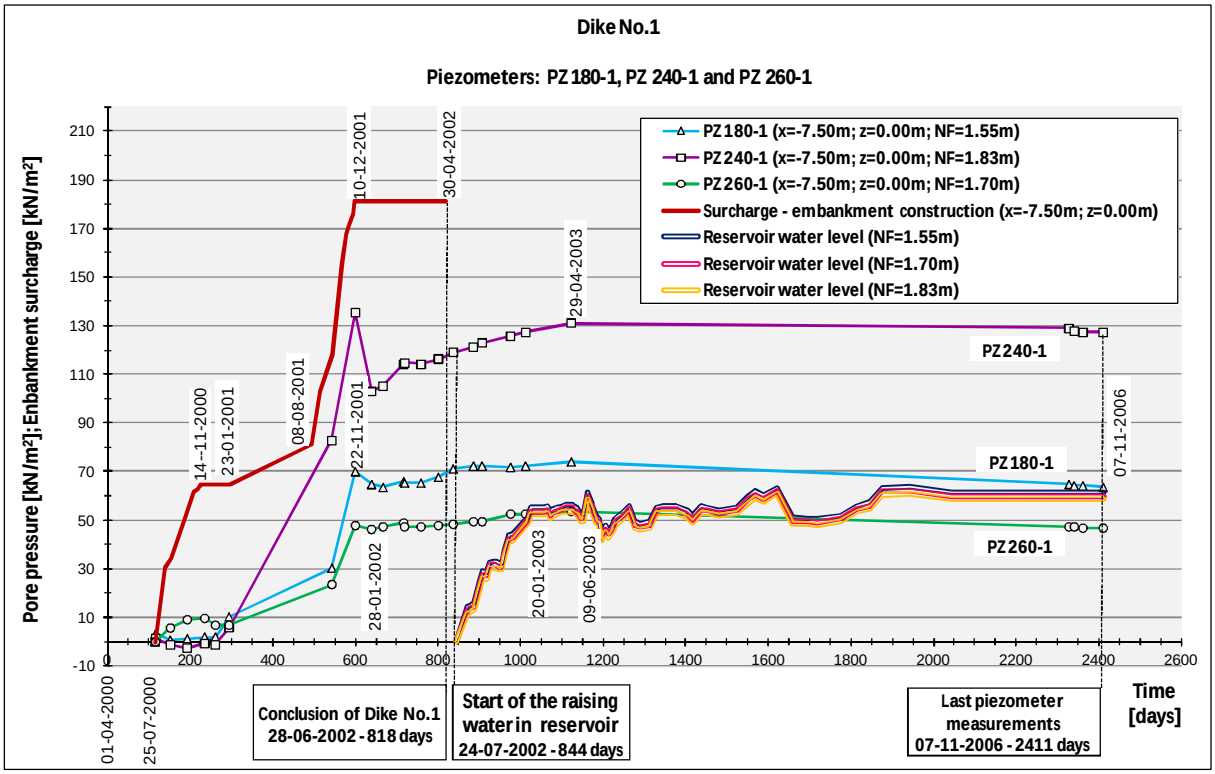

Graph VI.1 – Dike No.1: Pore pressure readings in piezometers PZ 180-1, PZ 240-1 and PZ 260-1

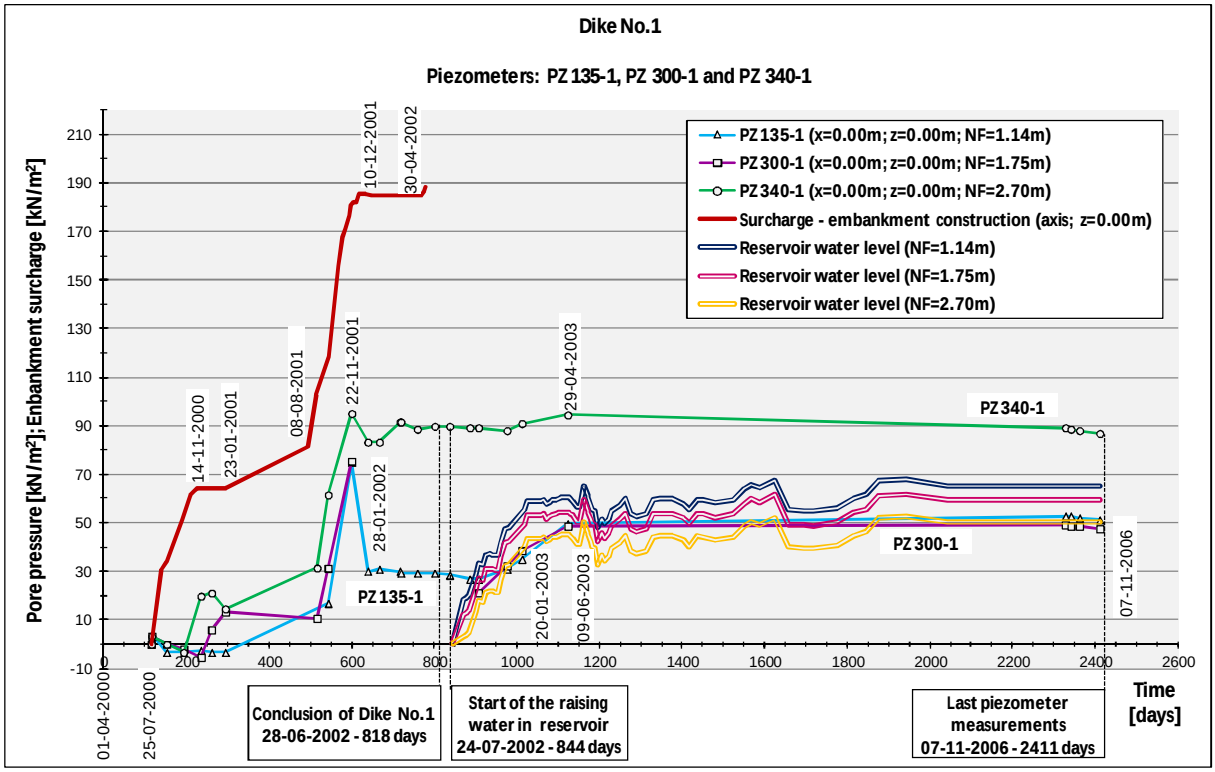

Graph VI.2 – Dike No.1: Pore pressure readings in piezometers PZ 135-1, PZ 300-1 and PZ 340-1

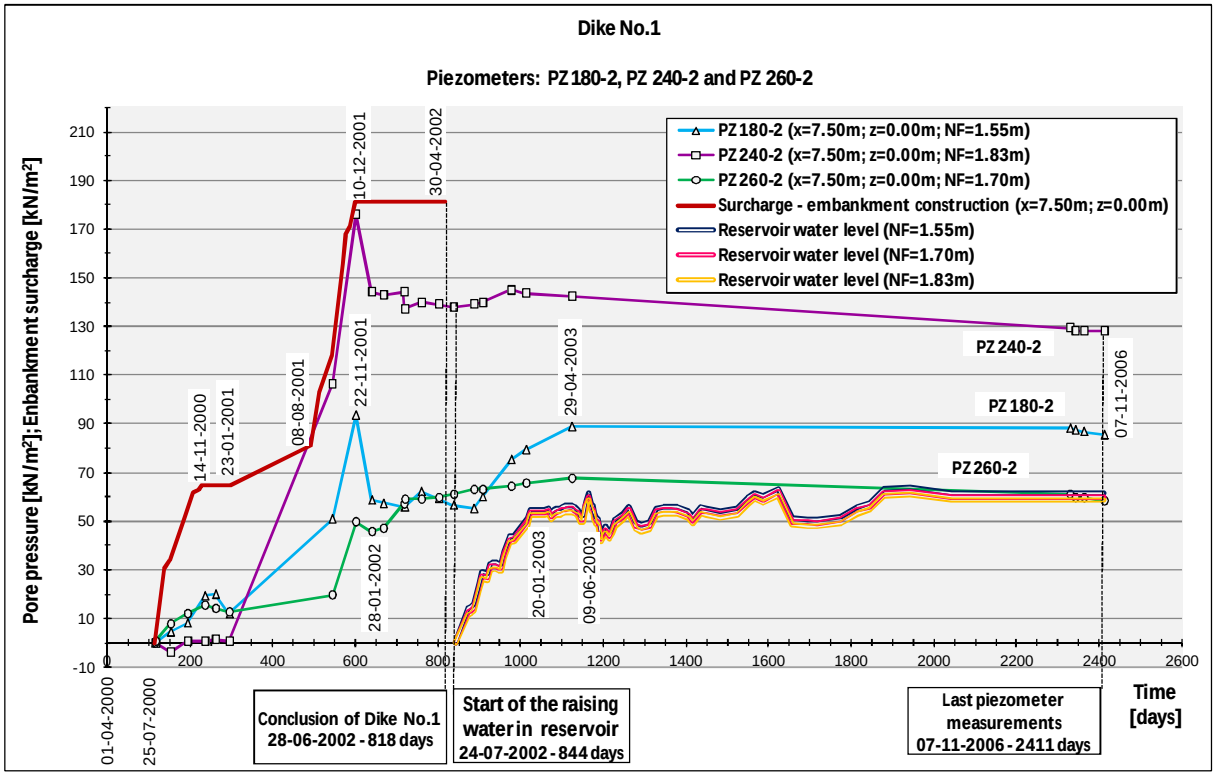

Graph VI.3 – Dike No.1: Pore pressure readings in piezometers PZ 180-2, PZ 240-2 and PZ 260-2

The piezometers PZ 240-1 and PZ 240-2, located at the cut-off base, are those were the overload of the dike is almost totally supported by the water, especially in the case of the last piezometer, being the difference of 47kN/m^2 for the first piezometer, and only of 7KN/m^2 for the second one. In fact,

these results shows that the drains nearby are not function as it was expected, since the dissipation of the pore pressure is minimal. Regarding the other piezometers, the differences range from 90kN/m^2 to 132kN/m^2, though values over 110kN/m^2 predominate.

As soon as embankment construction work are interrupted (from 10 December 2001 to 10 May 2002), an abrupt drop in the overpressure of almost all the piezometers, is observed, especially in those which presented higher values of pore pressure. Such results indicate the correct functioning of the drains, allowing the progressing of the excess pore pressure dissipation. In this phase, the differences rises to:

- x=-7.50m from the axis (upstream): 117kN/m^2 for PZ 180-1;
  82kN/m^2 for PZ 240-1;
  136kN/m^2 for PZ 260-1;

- x=0.00m (at the axis): 155kN/m^2 for PZ 135-1;
  100kN/m^2 for PZ 340-1;

- x=7.50m from the axis (downstream): 134kN/m^2 for PZ 180-2;
  40kN/m^2 for PZ 240-2;
  137kN/m^2 for PZ 260-2;

The exception happens in piezometers PZ 180-1, PZ260-1 and PZ0260-2, given the fact that they already registered low increments of pore pressure in the construction stage. The measure taken from piezometer PZ 135-1 represents the major drops in overpressure. Unfortunately, piezometer PZ 300-1 stopped functioning during this period.

During this interruption of the works, and after a substantial reduction in the pressures on the piezometers, they stabilized, with the exception of PZ 240-1 and PZ 260-2, which indicate a slight increase. Construction was re-established at the beginning of May 2002 and completed at the end of June 2002, after which the reservoir began to be filled. In the initial stages and during the gradually and controlled rise up of water in the reservoir, up to level 7.15m, the piezometers readings shows and increase of overpressure. Nevertheless, these values are lower than the ones observed during the construction of the embankment. The increment of the pore pressure inside the dike is associated to the establishment of a flow network, due to the reservoir filling, and also the saturation of the materials. The maximum overpressure corresponding to this stage occurred on 29 April 2003, 279 days after the beginning of the reservoir filling, and 99 days ($\pm$ 3 months) after the water attained level 7.15m. The minimum measured values for this stage, ranged the 49kN/m^2 to 54kN/m^2 for PZ 135-1, PZ 300-1 and PZ 260-1, being the maximum values associated to PZ 240-1 and PZ 240-2, with 131kN/m^2 and 142kN/m^2, respectively. The pore pressures in the other piezometers, varied between 70kN/m^2 and 95kN/m^2.

From here on, the pore pressure began stabilising and as time passed on a slightly decrease is noticed. Even when the water level rises up to level 8.00m, no overpressure is measured in the piezometers.

Both piezometers PZ 222-A and PZ 258-A, placed at level 5.00m, as well as PZ 222-B and PZ 258-B located at level 1.00m, were installed in the embankment body, almost in the final phase of the construction. As a result, they show extraordinarily low increments of overpressure associated with the construction phase, as the overload above the level of these devices is almost insignificant, especially for the piezometers located at level 5.00m. In this case, the increment of the pore pressure is much more significant with the raising of the water level in the pond (Graph VI.4).

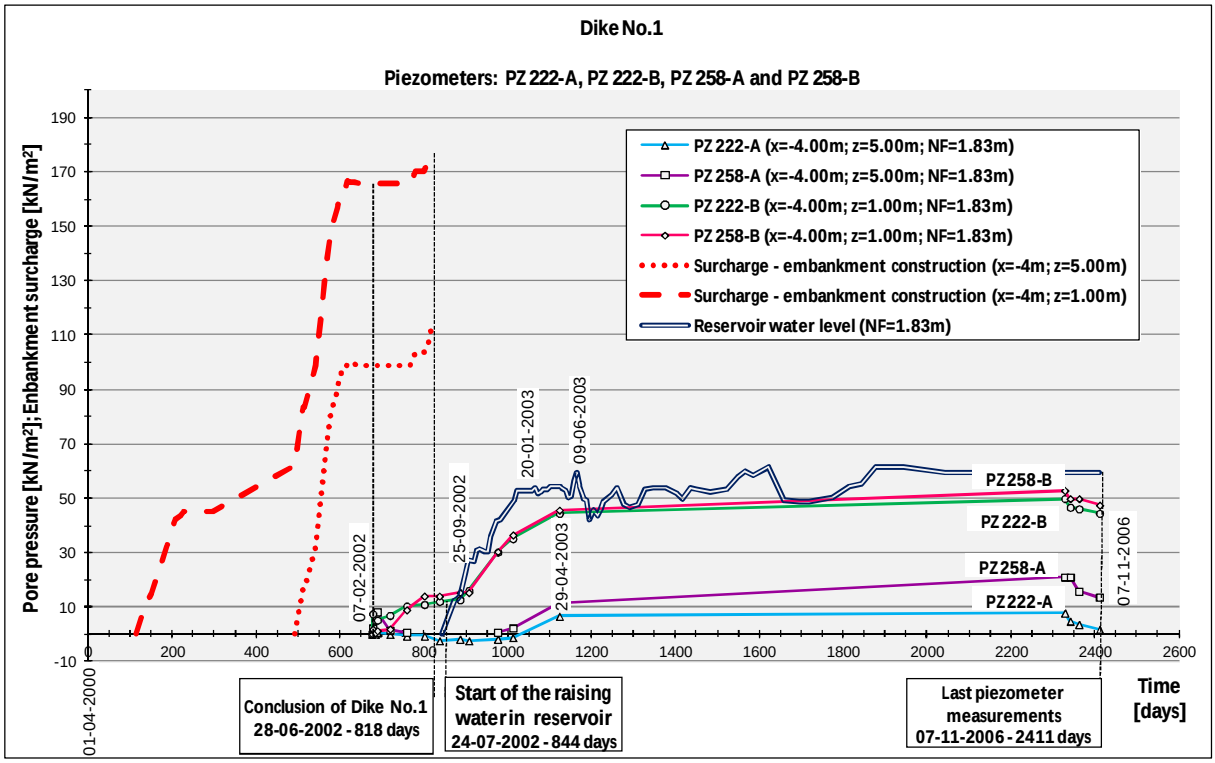

Graph VI.4 – Dike No.1: Pore pressure readings in piezometers PZ 222-A/B and PZ 258-A/B

A similar situation occurs with piezometers PZ 240-3/4/5, all placed at level 3.00m, although PZ 240-4 is located on the axis of the dike, PZ 240-3 on the upstream side and PZ 240-5 on the downstream side. These last two piezometers are aligned vertically with piezometers PZ 240-1 and PZ 240-2, but 3 metres above them, and relatively close to the upstream and downstream horizontal drains. The piezometers in question were installed immediately the re-establishment of the constructions works, being associated to the higher construction rate of the embankment (Graph VI.5). However, the piezometers readings are very low for the stage associated with the construction of the dike, indicating that the drainage system is functioning in good conditions, allowing a significant dissipation of the excess pore pressure during this phase and at this level.

As the water rises in the pond, an increment of the pore pressure is observed in these three piezometers, being the most significant measured in PZ 240-3. This result is expected since it is very near the upstream drainage sand mat, which is connected to the rip-rap slope protection. Therefore, any increase in water level in the reservoir, is strongly felt in a piezometer that is place nearby. The pore pressure measurements in the other piezometers are smaller, decreasing progressively with the distance from the reservoir, which is also associated to the establishment of the percolation network inside the dike.

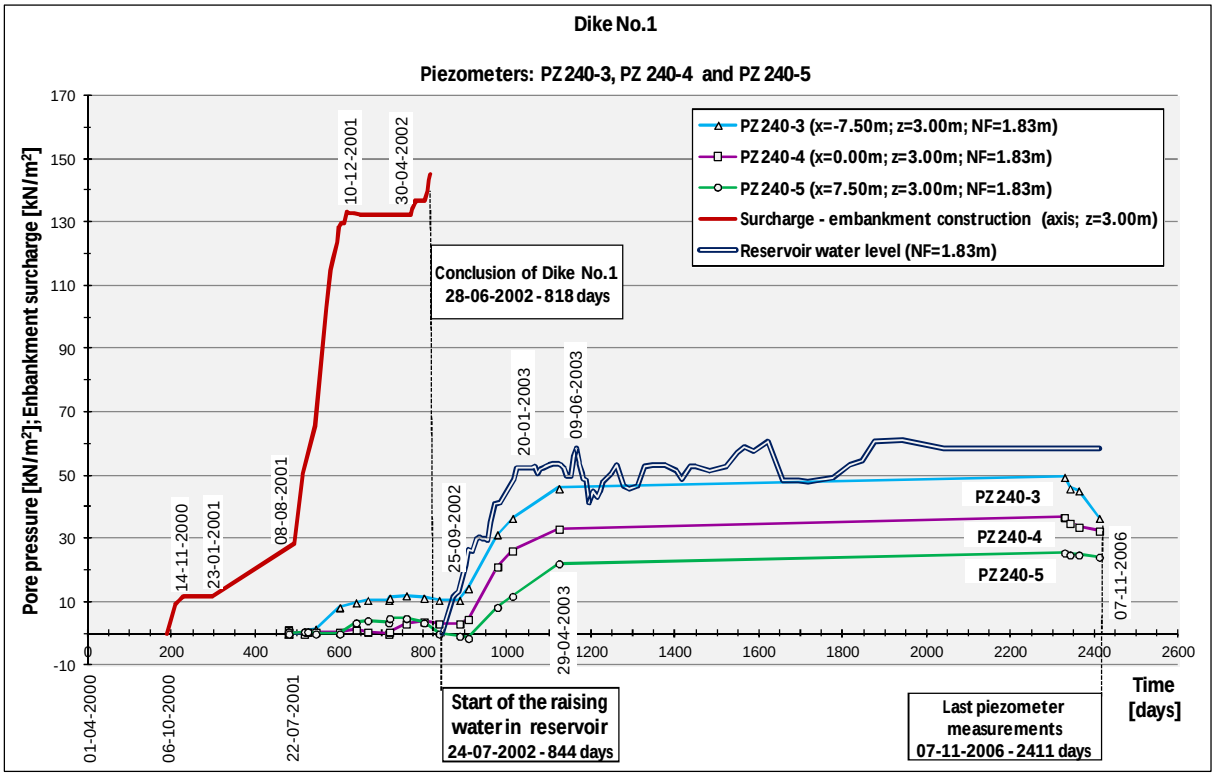

Graph VI.5 – Dike No.1: Pore pressure readings in piezometers PZ 240-3, PZ 240-4 and PZ 240-5

The piezometers installed in the foundation, below the upstream berm (PZ 240-6A/6B/6C) and downstream berm (PZ 240-7A/7B/7C), in the areas covered with band-shaped drains, shows similar tracings at different depths, which means that the effect of the embankment overload is felt simultaneously in all the piezometers. Overlaying the results from these piezometers (Graph IV.6) it can be seen that the overpressure associated with the construction phase of the dike is very similar for the piezometers placed at the same level, on the upstream and downstream sides. In this case, the maximum overload due to the weight of the dike soil, from its foundation until the berm level (6.00m), is about 67kN/m^2. In addition, for each piezometer, the hydrostatic pressure corresponding to the difference between the piezometer level and the phreatic level must be considered. Therefore, initially, the total stress above the piezometers is about 105kN/m^2, 156kN/m^2 and 187kN/m^2, respectively for the piezometers located at -2.00m (PZ 240-6A/7A), -7.00m (PZ 240-6B/7B) and -10.40m (PZ 240-6C/7C). The differences between the calculated values and the piezometers readings, after their installation and stabilisation, are approximately of:

- z=-2.00m: 49kN/m^2 for PZ 240-6A;
  46kN/m^2 for PZ 240-7A;
- z=-7.00m: 57kN/m^2 for PZ 240-6B;
  56kN/m^2 for PZ 240-7B;
- z=-10.40m: 49kN/m^2 for PZ 240-6C;
  47kN/m^2 for PZ 240-7C.

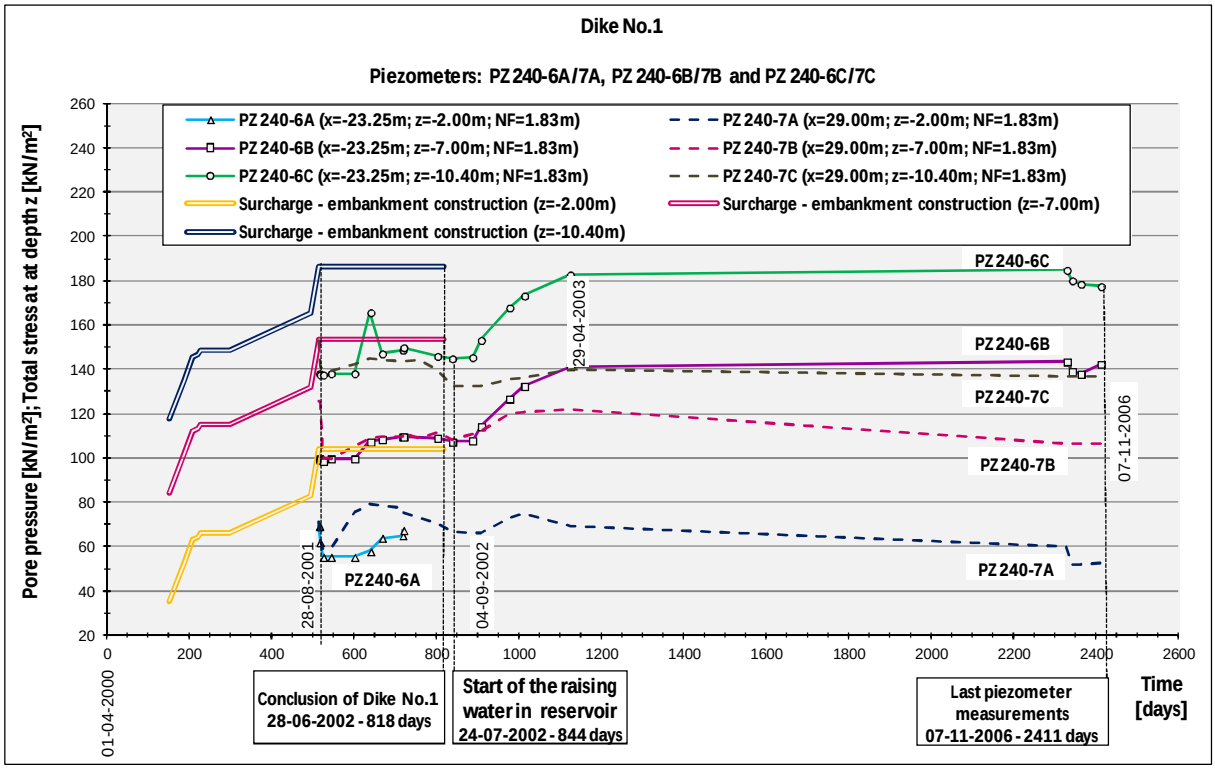

Graph VI.6 – Dike No.1: Comparison of pore pressure readings in piezometers PZ 240-6A/6B/6C and PZ 240-7A/7B/7C

From graph VI.6, it can be seen that the drains fulfil their function, being able to dissipate a significant part of the 67kN/m^2 of embankment overload up to the berm level. Both upstream and downstream piezometers show this same behaviour. In the meantime, with the on-going construction of the dike, there is a slight increase in the piezometers measurements. Although no load is applied above the berm, the effect of the construction of the dike is felt in the piezometers, since these are located inside the body embankment. This increase is little in the final construction steps, indicating that the drains continue to perform their function properly.

The main difference in the readings of the piezometers located on the upstream and downstream sides, occurs with the rised up of the water in the pond, with a significant increase of pore pressure in the upstream piezometers, contrary to what happens in those placed downstream. In the latter, i.e., in PZ 240-7A/7B/7C, there is a slight increase in an initial phase, followed by a reduction in the pore pressure. The latest measurements in the piezometers upstream and downstream correspond to the following values:

- z=-2.00m: 53kN/m^2 for PZ 240-7A;
- z=-7.00m: 143kN/m^2 for PZ 240-6B;
  107kN/m^2 for PZ 240-7B;
- z=-10.40m: 178kN/m^2 for PZ 240-6C;
  137kN/m^2 for PZ 240-7C;

being the differences between PZ 240-6B/7B and PZ 240-6C/7C, of 36kN/m^2 and 41kN/m^2.

According to Graph VI.7, the pressures in piezometers PZ 240-6B and PZ 240-6C follow the evolution of the hydraulic level in the reservoir. Thought it seems odd, in fact this behaviour is coherent, since the drains placed on the upstream side of the cut-off are connected to the above drainage blanket, and in turn, this is connected to the reservoir, through the rip-rap slope protection. For a water level rise up, from 1.83m to 7.15m, the associated hydrostatic pressure is 52.2kN/m^2. Nevertheless, the maximum differences obtained in the piezometers, since the beginning of the reservoir filling, are lower than this value, since they are approximately of 38kN/m^2 to 40kN/m^2, which correspondents to a dissipation of approximately 12KN/m^2 to 14KN/m^2.

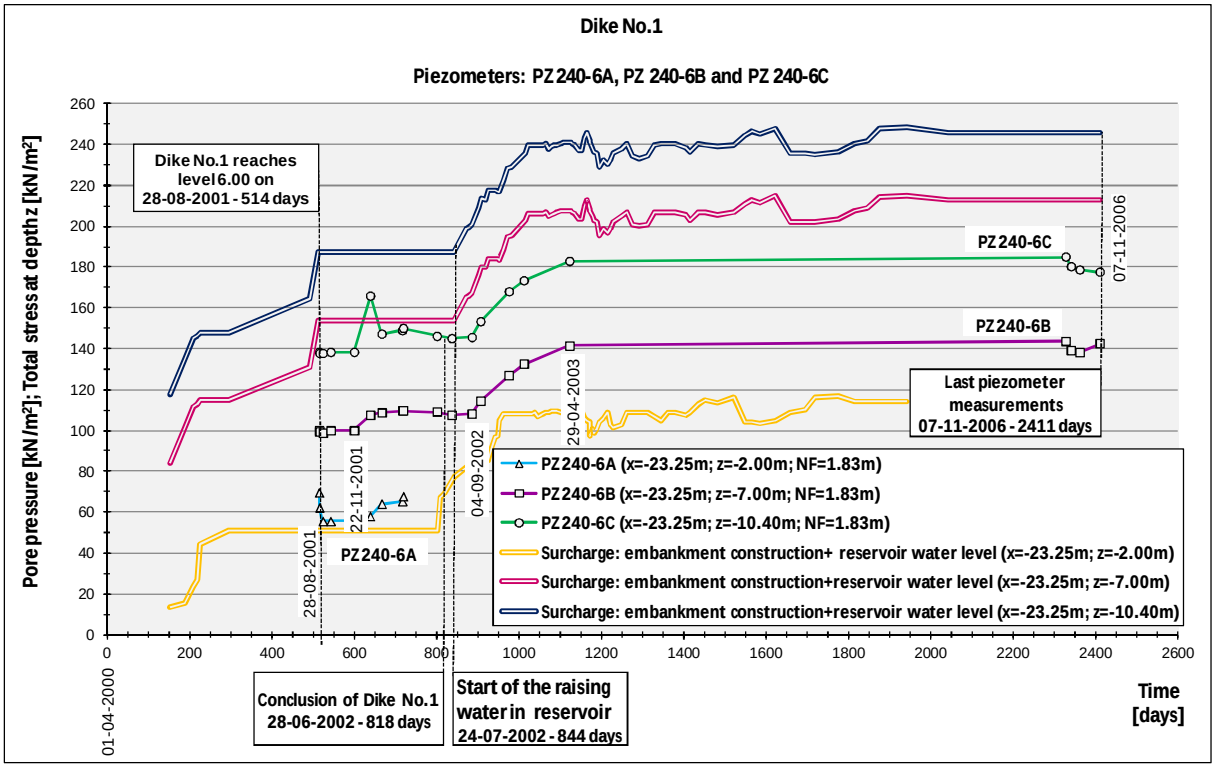

Graph VI.7 – Dike No.1: Pore pressure readings in piezometers PZ 240-6A, PZ 240-6B and PZ 240-6C

VI.6.2. PORE PRESSURES IN THE DIKE NO.3 FOUNDATION

Dike No.3 construction works started in early May 2001, being interrupted several times for short-time periods between October 2001 and January 2002, and was finalized in mid-July 2002. The reservoir began to be filled immediately after, as in the case of the Dike No.1. For Dike No.3 the monitoring results available totalize 2526 days.

Regarding the pore pressure measurements of Dike No.3, few considerations can be taken since there are only two piezometers (PZ 180-1A and PZ 180-1B), both being located in the foundation and below the upstream berm, in a zone with no drains. Howsoever, the PK0+180 profile presents an area treated with band-shaped drains, but they are located downstream of the cut-off. Unfortunately, there are no piezometers in that zone.

Regarding the construction of Dike No.3, it is known that on 29 August 2001, the embankment achieved the berms level (6.00). On 30 August 2009, piezometers were installed, with PZ 180-1A placed at 0.00 and PZ 180-1B at level -5.00m.

As it had already happened in Dike No.1, these piezometers also present similar tracings, though they are placed at different depths. The greatest difference between these two piezometers readings occurs right at the start, ranging 40kN/m^2. In the final stage, the difference between them is constant and approximately of 30kN/m^2 (Graph VI.8). On average, this difference is about 35kN/m^2. However, and given the differences of 5 meters depth between them, it was also expected a separation of 50kN/m^2 in their measurements. Due to the difference of the initial pressures measured between PZ 180-1A and PZ 180-1B, which gave 40kN/m^2 instead of the estimated 50kN/m^2, a doubt arises concerning their exact position. Apparently, they are placed with a difference of 4 and not 5 meters.

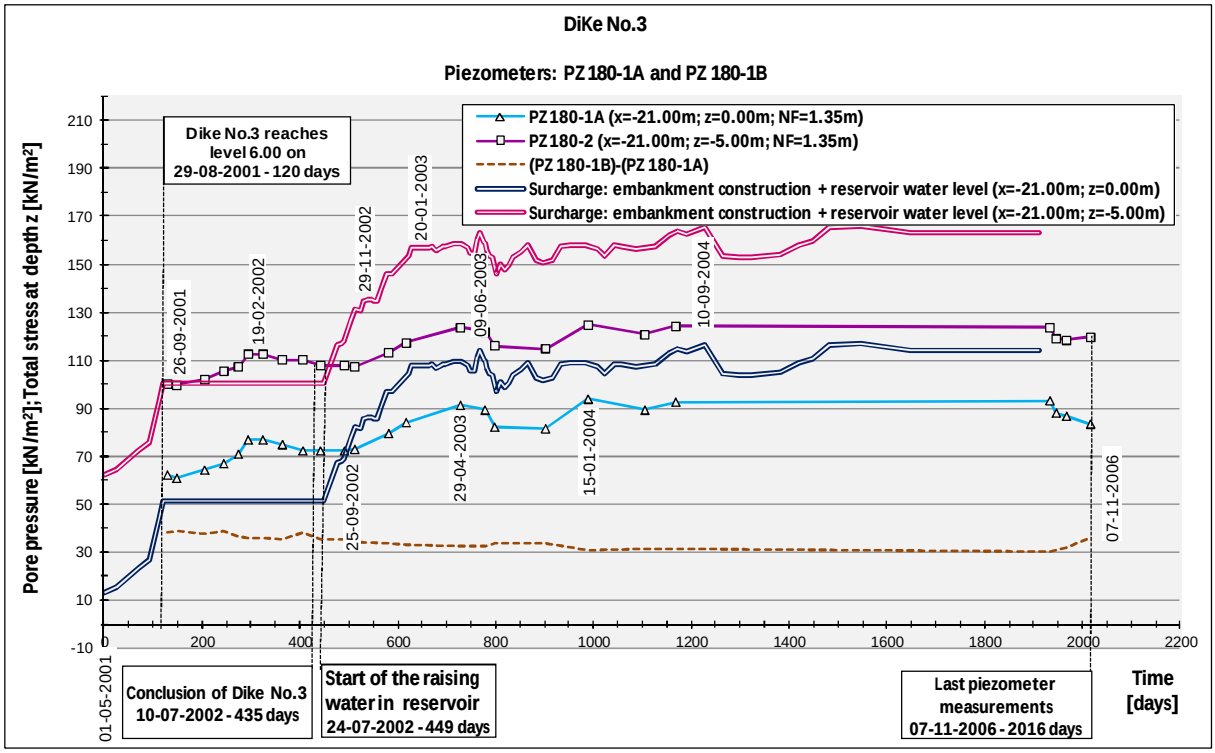

Graph VI.8 – Dike No.3: Pore pressure readings in piezometers PZ 180-1A and PZ 180-1B

The overload associated with the embankment weight up to the berms level, is approximately of 38kN/m^2. Being the phreatic level located at 1.35m and the piezometers at 0.00m and -5.00m, then the expected values of the initial total pressure at that depth, would give 51kN/m^2 and 100kN/m^2, respectively for PZ 180-1A and PZ 180-1B. Analysing the results, there is a match between the calculated and the measured values for PZ 180-1B; however in PZ 180-1A there is a difference of 10kN/m^2. In the meantime, the pressure on the piezometers continues to rise, due to the embankment construction, though the phreatic level remains constant as well as the embankment weight above the piezometers. Once again, this effect is associated with the embankment surcharge above the berms level. The increments measured in the piezometers from 30 August 2001 to 19 February 2002 were only of 16kN/m^2 and 13kN/m^2. The higher value was observed in the piezometer closest to the surface, i.e. PZ 180-1A.

In the meantime, there was a slight decrease of around 4kN/m^2 to 5kN/m^2, until 25 September 2002. Although there are no drains in this zone, this decrease indicates that the dissipation of the excess pore pressure process is in course. The filling of the reservoir had begun two months before this date, though the effect was not immediately reflected in the piezometers. From here on, and during the first phase of the reservoir filling, the pore pressure rises again, reaching another maximum on 29 April 2003, three months after the reservoir level stabilised at 7.15m. Although the hydraulic overpressure associated to the water level in the pond is around 60kN/m^2, the increments observed varied between 19kN/m^2 for the piezometer closer to the surface, and of 16kN/m^2 for the other. The accumulation of these small differences in the increases and decreases on the piezometers readings causing a rapprochement of the final result between PZ 180-1A and PZ 180-1B, going from the initial 40kN/m^2 to the final 30kN/m^2.

Lastly, regarding the differences between the values calculated and those measured, from 15 January 2004, these are approximately of 31kN/m^2 for PZ 180-1A and 44kN/m^2 for PZ 180-1B. In spite of the slight fluctuations, it can be considered that the pressure in the piezometers remains relatively constant from this moment on, with no significant reduction being seen, with the exception of the last three readings. However, there is no continuity and therefore no conclusion can be taken regarding the reduction in the excess of the pore pressures with time.

VI.6.3. SETTLEMENTS IN THE FOUNDATION AND IN DIKE NO.1

According to graph VI.9, it can be seen that the settlement curves for several plates, placed upstream and downstream of the axis, presents an identical progression even for different cross-sections. The higher settlement value occurs in section PK0+240, followed by section PK0+300, PK0+140 and lastly by section PK0+340. The maximum values were registered for the highest profile and the minimum in the lowest one, which makes sense. However, the comparison of the results itself are difficult, since the plates were placed at distinct levels and on dates. The only plates to be installed at the same level (2.83m) and on the same date (11 July 2001), i.e., 466 days after the beginning of the dike construction, were the settlement plates PL 240-1 and PL 240-2.

Cross-section PK0+240 is the highest. It is normal, therefore, that the maximum values occur precisely in this zone. Additionally, these plates are located between piezometers PZ 240-3, PZ 240-4 and PZ 240-5, which have showed extremely low overpressures caused by the construction of the dike. This means that most of the excess pore pressure associated with the construction stage was dissipated straight away in this phase, and so the consolidation settlements are high. The values measured in both the plates at the end of the construction of Dike No.1 (818 days) were around 47.5cm, raising up to the 96.5cm for PL 240-1 and 100.2cm for PL 240-2, in the final readings (2921 days), substantially exceeding the 72cm previewed in the design. In terms of percentage, at the end of the construction these settlements correspond to 5.4% of the total height of the embankment above the plates level, reaching a maximum of 10.9% and 11.3% for plates PL 240-1 and PL 240-2 (Graph VI.10). These results are extremely high, although coherent in comparison to the low characteristics of the foundation soil, more specifically stratum B.

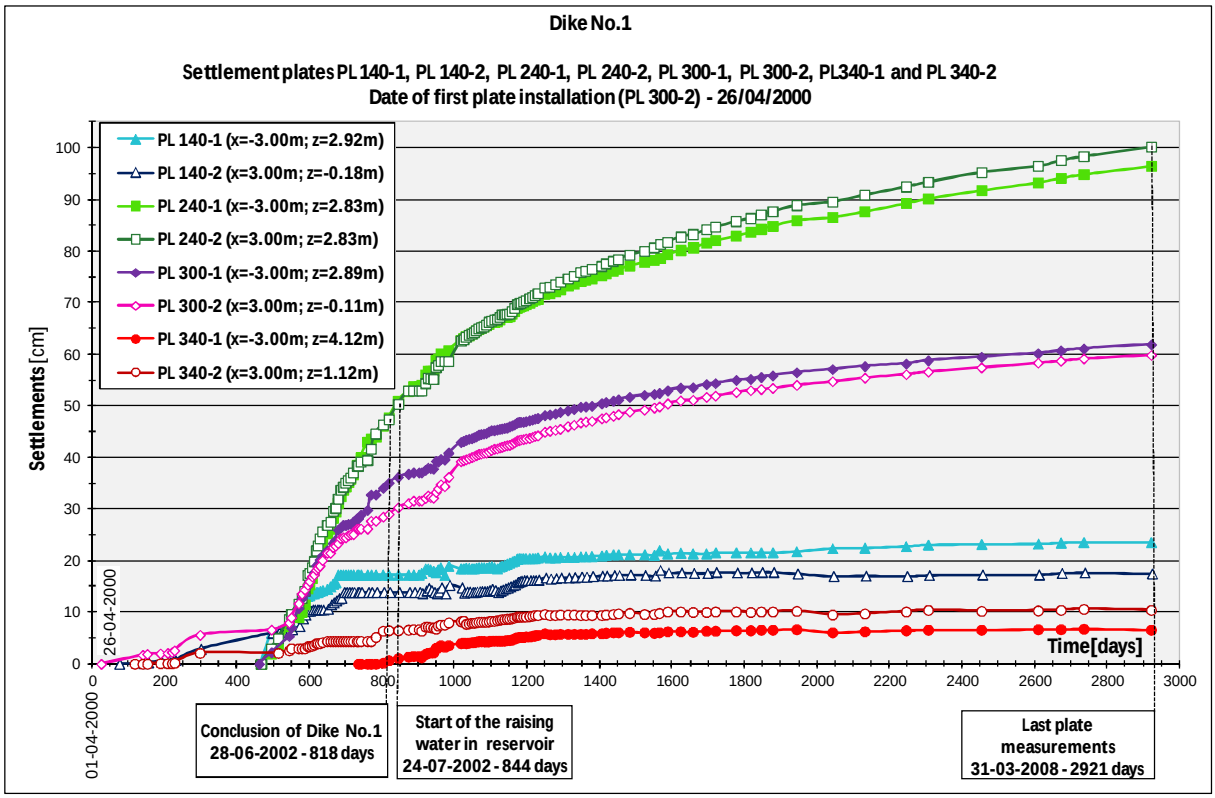

Graph VI.9 – Measurements of all settlements plates of Dike No.1

The interruption of the construction works is the reason why the settlements measured on plates PL 140-2, PL 300-2 and PL 340-2 are low and remain almost constant up to 466 days after the start of construction. These three plates are placed at the level of the cut-off base (3 metres from the axis on the downstream side), and during this phase the plates were subjected to little overload. These initial settlements correspond to the recompression phase of the soil, as the compaction of the embankment above these plates never exceed the initial height of the ground before excavation, thereby the values did not exceed 6.6cm. Once the dike works restarted, the settlements rose significantly in plate PL 300-2, with lower values in plates PL 140-2 and PL 340-2, with maximums of 60.0cm, 17.7cm and 10.6cm respectively.

Plates PL 140-1, PL 300-1 and PL 340-1 were placed at natural ground level, i.e. approximately 3 metres above those mentioned before, although on the inside of the dike (3 metres from the axis on the upstream side), such as the plates in section PK0+240. The first two were installed when construction of the dike restarted, however settlement plate PL 340-1 was only applied in an advanced phase of the works.

According to graph VI.9, apparently the settlements for both the plates of the PK0+300 and PK0+140 profiles, are quite similar; however, looking at graph VI.10, a significant difference is observed between the plates PL01401 and PL140-2, as well as between PL300-1 and PL300-2. This result indicates that there was a gaining of strength of the soil foundation during the period in which the works stopped (soil hardening), in spite of the little overload applied and the low settlement measured. If the opposite were true, the percentages would have been identical.

Although the smaller settlements occurred on the plates in cross-section PK0+340, and being this located on the fringe of the improved zone with band-shaped drains, an attempt could be made to draw some conclusions of the drains effect on the consolidation. However, due to the fact that these plates were installed much latter than the others, and since the embankment height in this profile is small, it is not advisable to used these results to compared and withdraw conclusions regarding the effect of the drains on the consolidation.

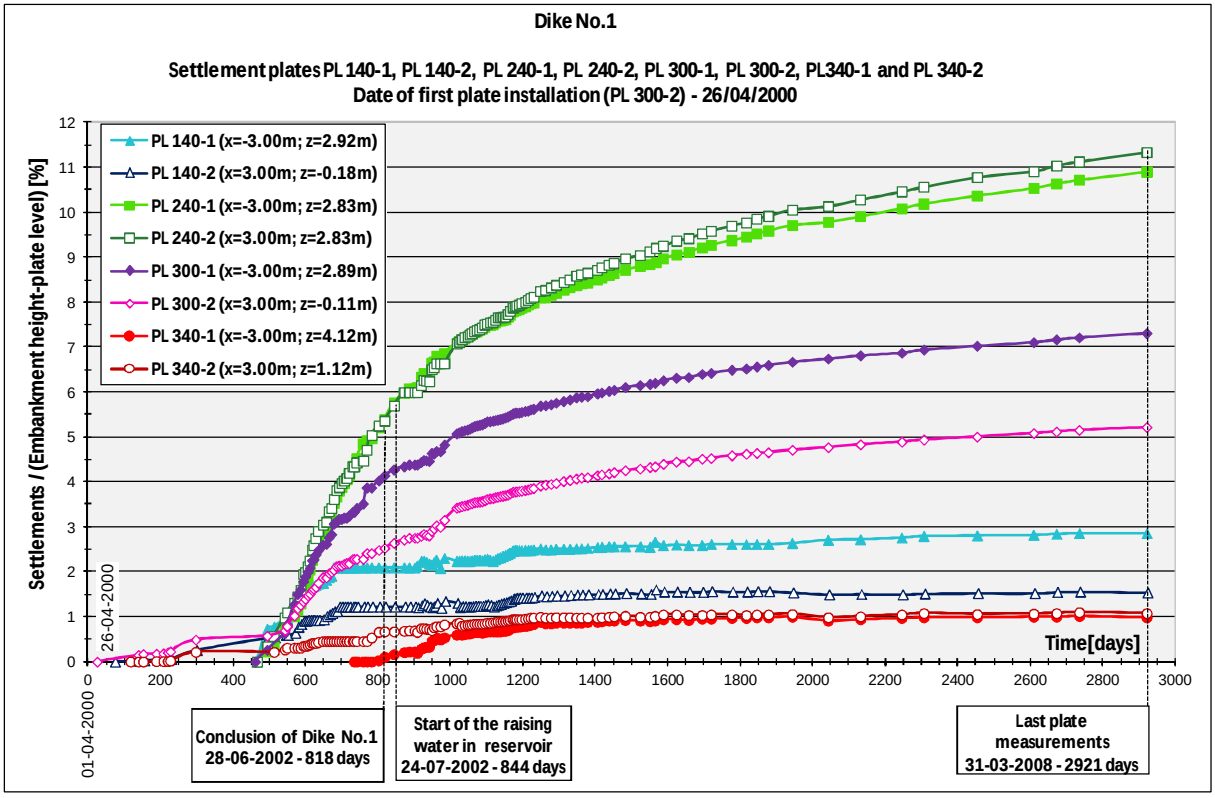

Graph VI.10 – Dike No.1: Ratio between settlements and embankment height above the correspondent plate (in percentage)

Graph IV.11 shows the time evolution of the settlement and as well as the settlement rate, for plates PL 240-1 and PL 240-2, during the construction and post-construction stages of Dike No.1. The settlement rate increases during the construction phase, slowing down in December 2001, when the works were interrupted for a few months, but already very near to the conclusion of the embankment.

With the raising of the water level in the pond, the settlement rate shows a slightly increase, reaching another maximum when the water rises up to level 6.00m. Latter, it is observed a substantial reduction on the rate, with only a slight increase when the water rises to 7.80m. From this point, the reservoir empties gradually until reaches level 6.50m, after which the settlement rate stabilises, in spite of the later variations in the water level of the reservoir. This stabilisation occurs almost one year after the conclusion of the dike construction (1200-818=382 days).

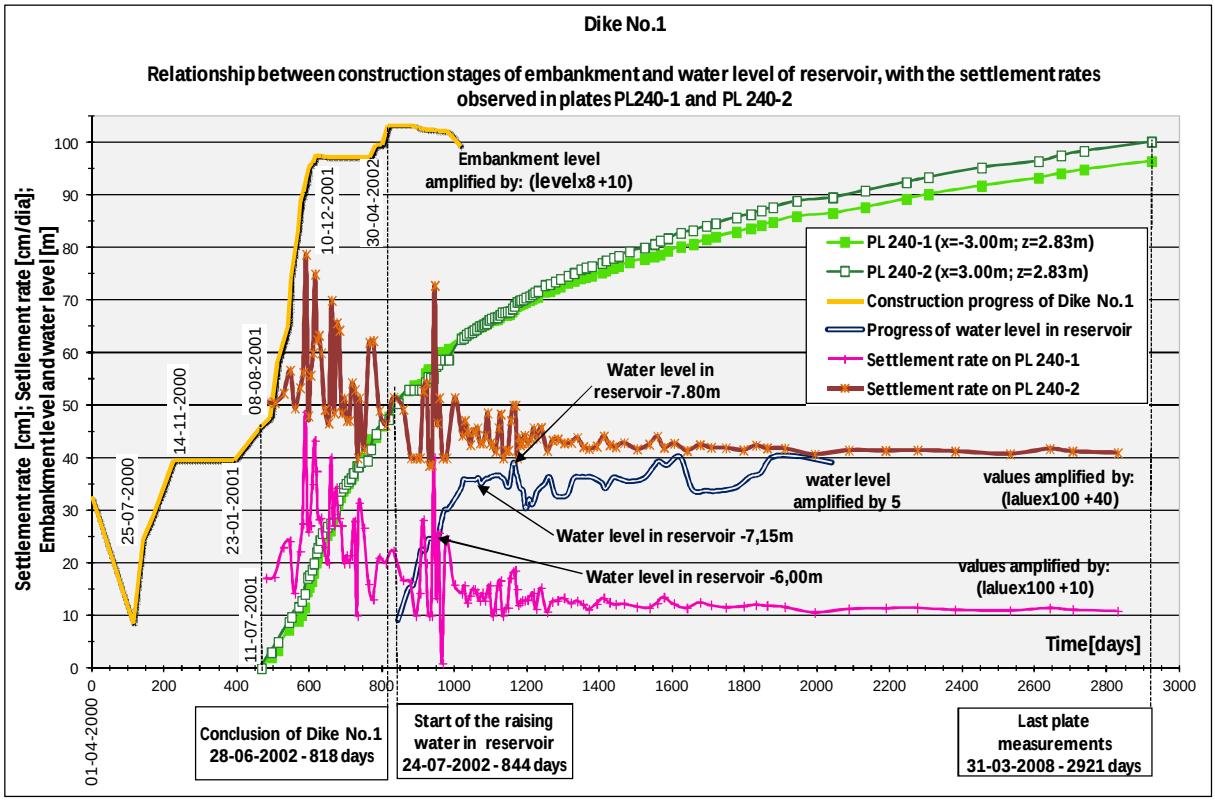

Graph VI.11 – Dike No.1: Relationship between construction stages of embankment and water level of reservoir, with the settlement rates observed in plates PL240-1 and PL 240-2

Regarding the settlements of the topographic stake marks, two types of comparisons were performed. Firstly, the settlements curves of the topographic stake marks placed only at the crest of the dike, were compared with the settlements plates placed below, for the same profile, or in nearby cross-sections. In graph VI.12 are plotted the settlements curves of topographic stakes (TS 205, TS 240-1/2, TS 250-1/2, TS 260-1/2 and TS 270) and the settlement curves of plates PL 240-1/2. Graph VI.13 shows the settlement results of topographic stake mark TS 310, as well as the settlement curves of plates PL 3001-/2. Based on these two graphs, it is possible to verified that the settlements curves of the topographic marks follows the plates results, being the difference between the two readings quite similar and constant over time, showing only a slight increment in the final measurements. This behaviour denotes that the settlement of the topographic stake marks placed at the surface of the dikes corresponds mostly to the foundation settlements, as the curves are practically parallel to each other. The fact that the measured results on this two type of devices, start to show a little difference at the end of the readings, may indicate that the embankment soil itself is consolidating and that the foundation settlement is stabilising.

On a second phase, the results of the topographic stake marks placed on each profile were analysed. The settlements of all the topographic stake marks installed in the cross-sections PK0+240, PK0+250 and PK0+260, located at the crest and on the downstream slope of Dike No.1 is plotted in graphs VI.14, VI.15 and VI.16. As expected, the devices with higher settlements readings are those placed at the crest dike, followed by that placed at lower levels. In some devices placed at lower levels, a great dispersion is observed, with the evolution being neither constant nor linear in time.

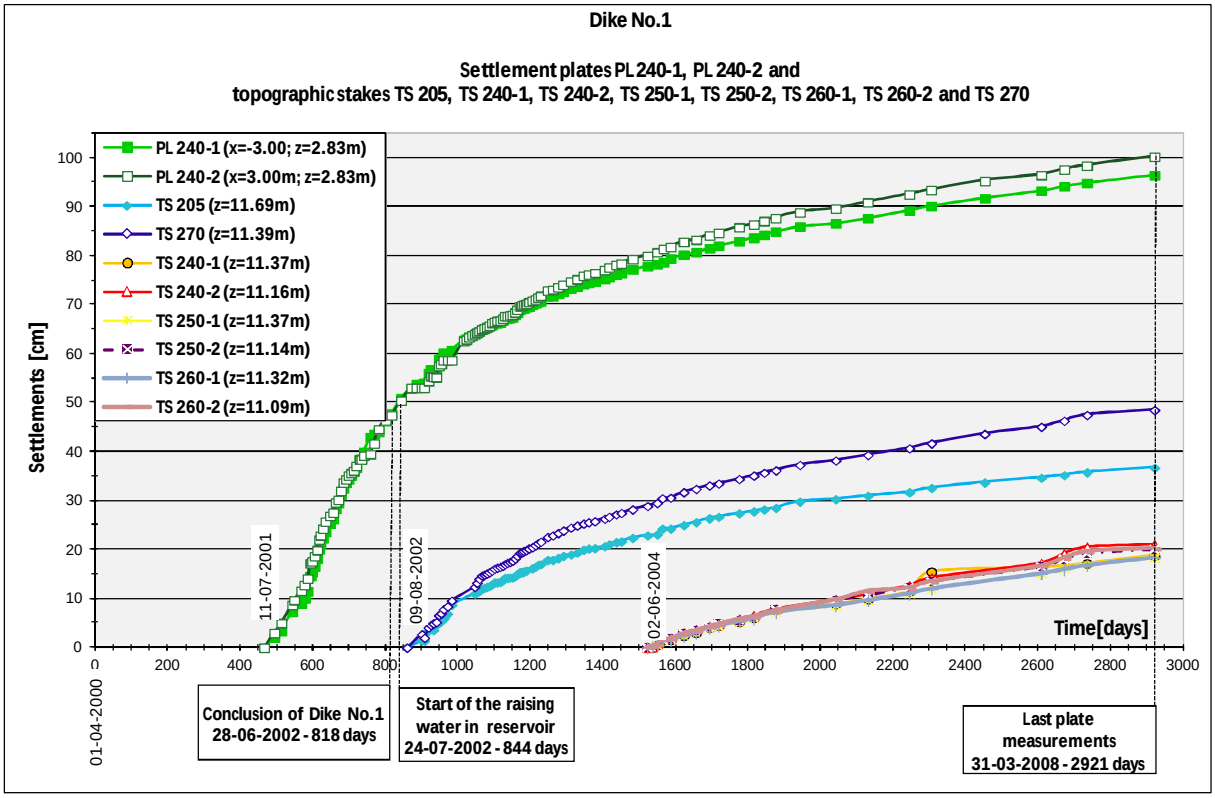

Graph VI.12 – Dike No.1: Readings of settlement plates PL 240-1, PL 240-2 and topographic stakes TS 205, TS 240-1, TS 240-2, TS 250-1, TS 250-2, TS 260-1, TS 260-2 and TS 270

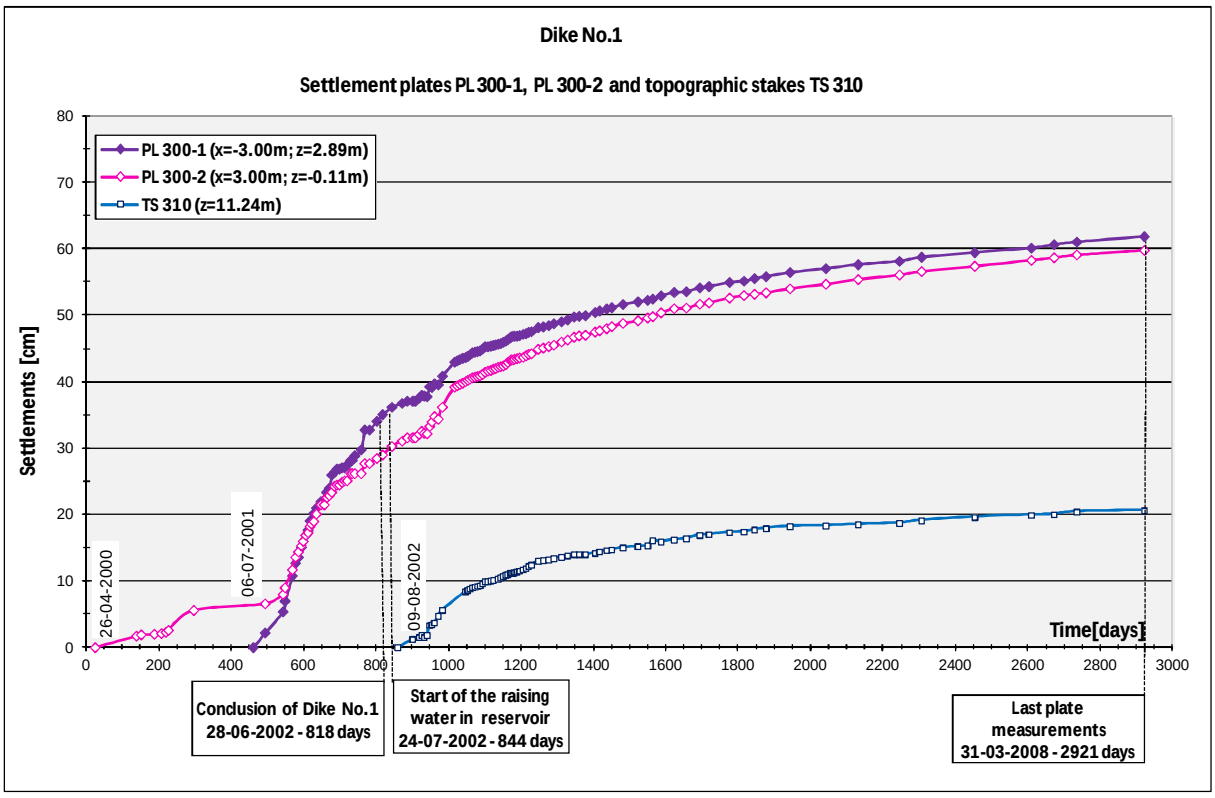

Graph VI.13 – Dike No.1: Readings of settlement plates PL 300-1, PL 300-2 and topographic stake TS 310

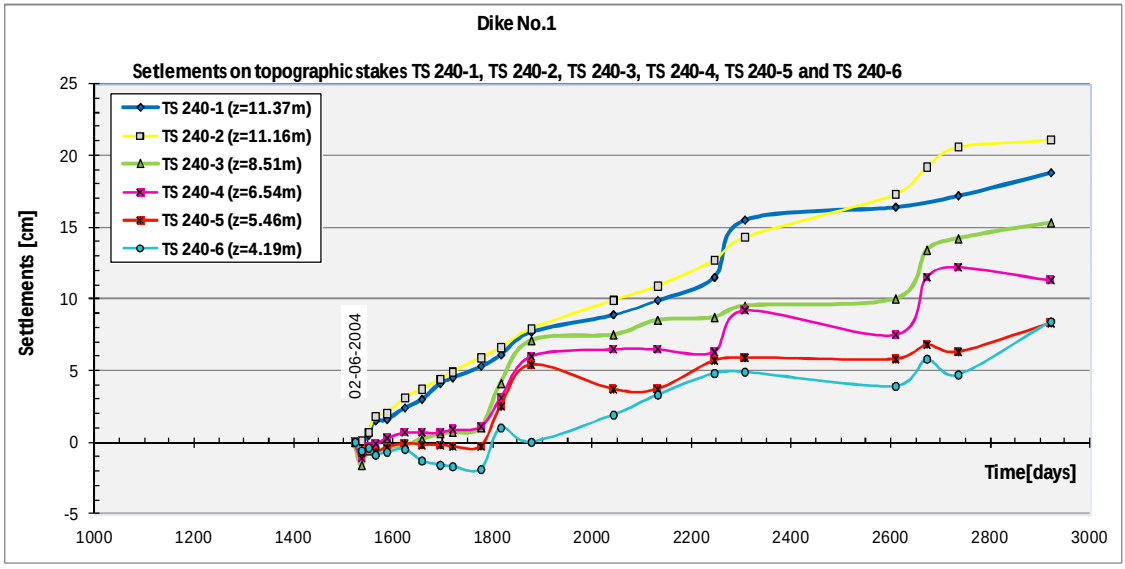

Graph VI.14 – Dike No.1: Measurements on topographic stakes TS 240-1 to TS 240-6

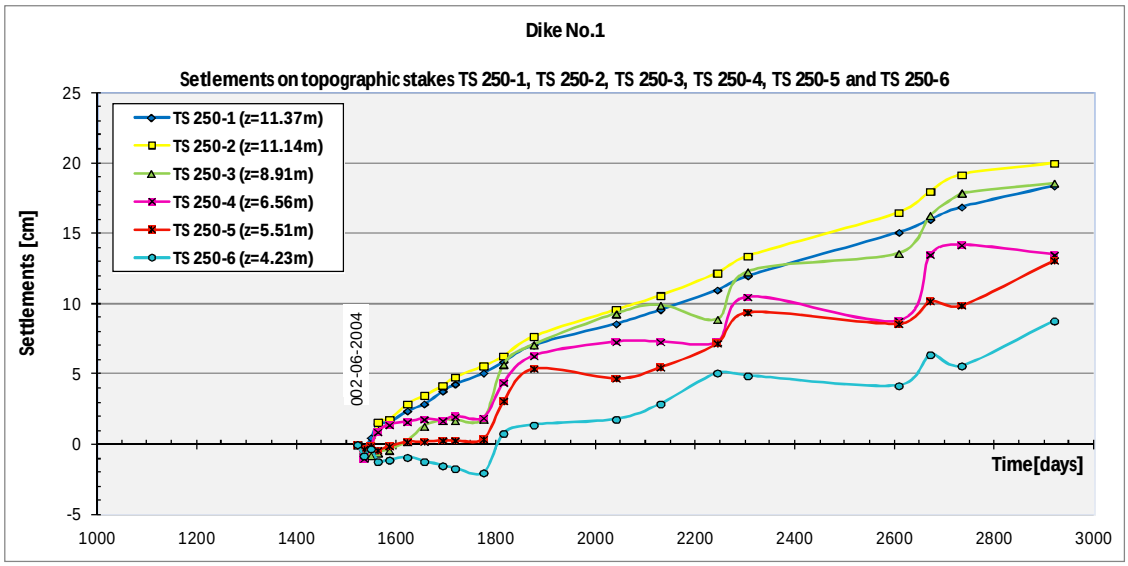

Graph VI.15 – Dike No.1: Measurements on topographic stakes TS 250-1 to TS 250-6

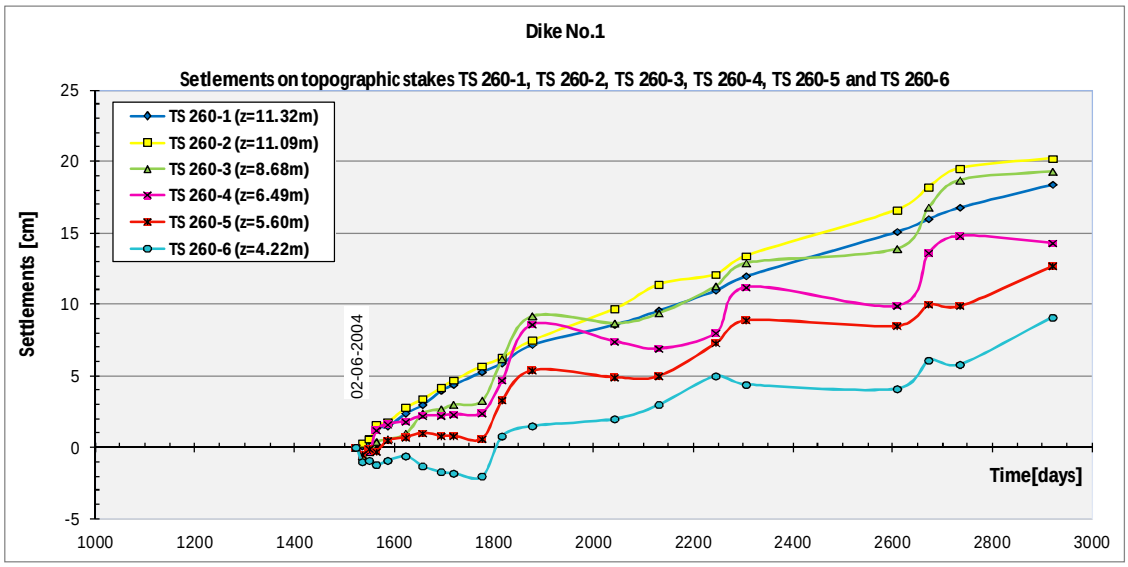

Graph VI.16 – Dike No.1: Measurements on topographic stakes TS 260-1 to TS 260-6

VI.6.4. SETTLEMENTS IN THE FOUNDATION AND IN DIKE NO.3

Before analysing the results from the settlement plates placed on Dike No.3, it is worth remembering that all of the plates are located in the interior of the embankment, and none at the level of the cut-off base. Additionally, profile PK0+140 is located on the fringe of the improved area with the band-shaped drains, cross-section PK0+170 is in the middle of the zone where the band-shaped drains were installed on the ground foundations, however section PK0+200 is located outside of the treated zone.

Graph VI.17 shows the evolution of the settlements over time for all the plates. For the same cross-section, the plates that are located at lower levels, such as PL 140-1 and PL170-1 present higher settlements, as it was expected since the overload embankment is higher for them. According to the final measurements, the settlements for these two plates are 45.7cm and 44.6cm. On the other hand, the settlements for plates PL 140-2 and PL 170-2 are around 40.1cm and 40.6cm, respectively. In the case of plates PL 200-1 and PL200-2, placed at the same level in the embankment, there is a very similar evolution of the settlements, with the final values being 31.4cm and 31.7cm. These last two plates were placed only 4cm below plates PL 140-1 and PL 170-1, and so, to analyse the efficiency of the band-shaped drains, the results of these four plates should be compared.

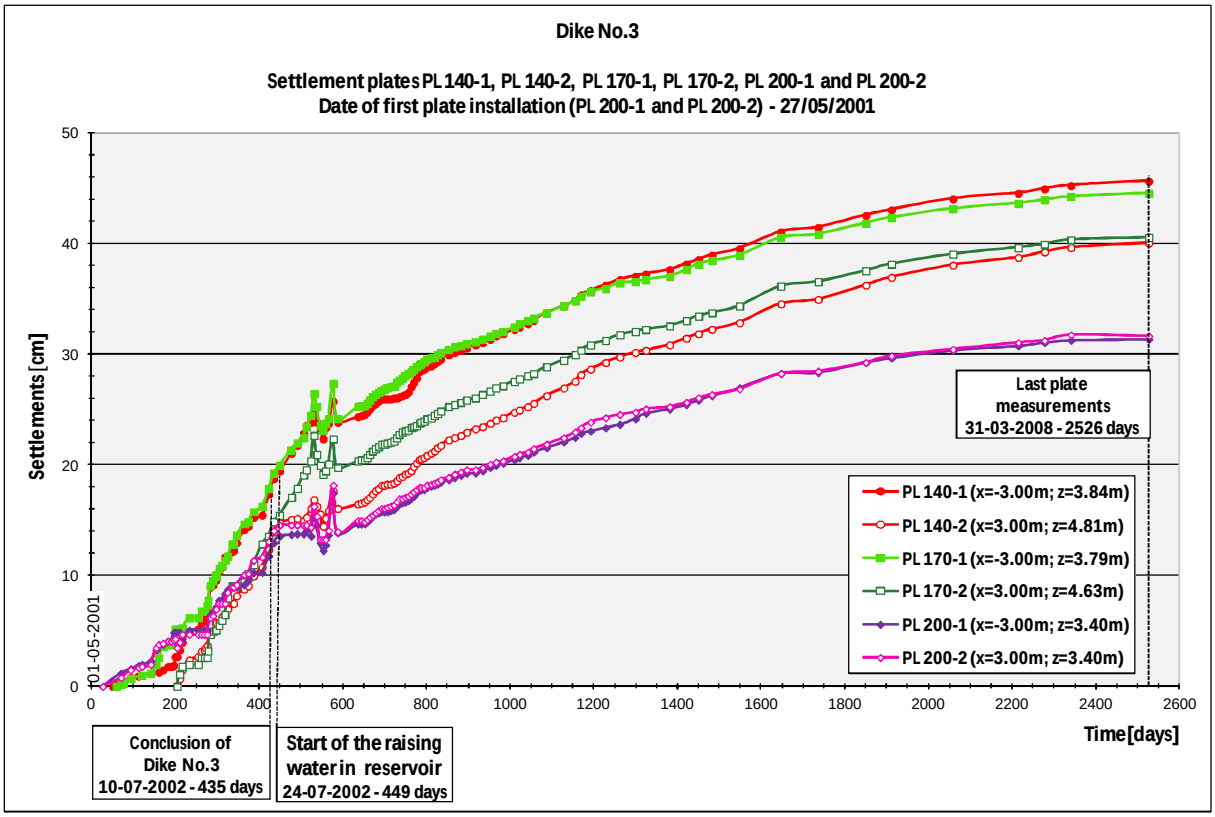

Graph VI.17 – Settlements measured on all the plates of Dike No.3

In spite of the settlement differences between the plates located in the same cross-section at different levels, it is interesting to see what happens when the settlements are normalise taking into account the height of the dike above the level plates.

These curves and percentages are plotted in graph VI.18, showing that the final value is higher for the plates located in the areas improved with band-shaped drains. In the Pk0+200, located in a zone not treated with drains, this percentage drops to one third of the final value of the other plates, being the measures of both plates quite the same. Thus, based on the results of this graph, it is seen that:

a) When the foundation soil has been improved with the band-shaped drains, the last measures of the settlement percentage (2526 days after beginning of dike construction), ranges from 6.2% to 6.5% of the embankment height above the level plates. In the final stage of the dike's construction (435 days after beginning of its construction), these values correspond only to 2.6% to 2.8%;

b) When there are no drains installed in the foundation, then the settlement readings drops to 1.7% for the end of the dike construction, and to 4.2% in the last plate measurements.

As a result, the effect of the drains on the acceleration the consolidation rate is well noticed, since the settlements in the improved zones are must higher. The biggest difference is around 14.5cm between PL 140-1 and PL 200-1, for the last reading, falling to 5.8cm in the phase corresponding to the end of construction.

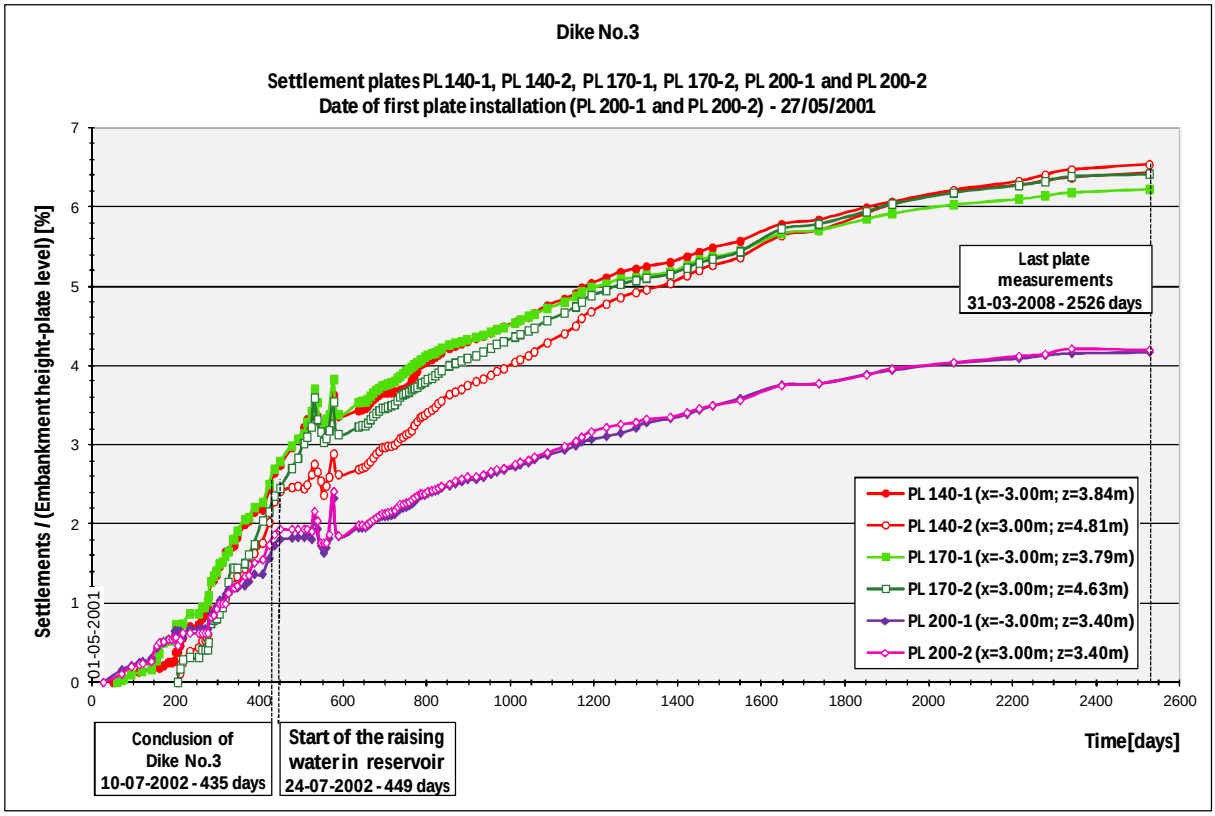

Graph VI.18 – Dike No.3: Ratio between settlements and embankment height above the level plate

Concerning the determination of the settlement rates, in the case of Dike No.3, only the results of PL 140-1 and PL200-1 where used, in order to compared two different situations (Graph VI.19). Once more, the settlement rate is higher in the construction phase and with the reservoir filling, slowing down significantly one year after the conclusion of the dike (800-435=365 days), thought a little bit earlier in the sections with drains. Between water levels from 4.50m to 6.00m, there was an anomaly in the plate readings; consequently, the settlement rate was not calculated for this period.

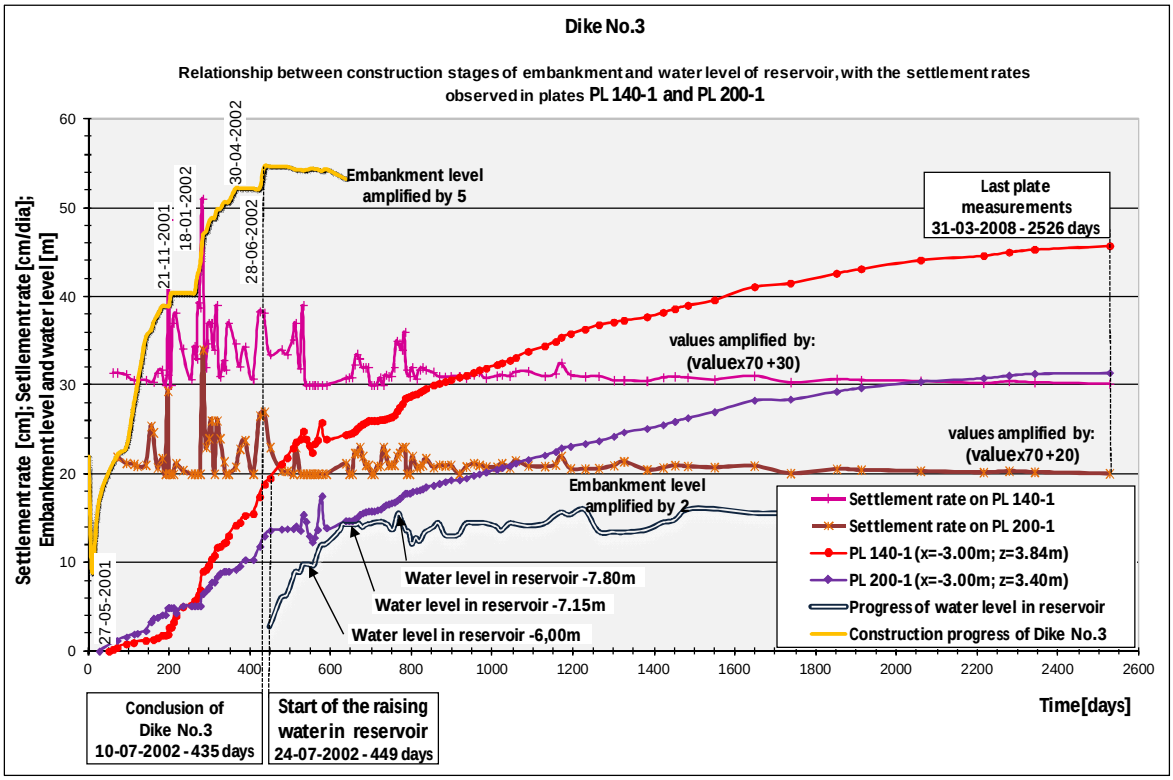

Graph VI.19 – Dike No.3: Relationship between construction stages of embankment and water level of reservoir, with the settlement rates observed in plates PL140-1 and PL 200-2

Regarding the settlements of the topographic stake marks in Dike Nº3, only the curves for TS 135 and TS 170 were plotted, since these were the only ones that could be compared to the results of the plates located in sections PK0+140 and PK0+170 (Graph VI.20).

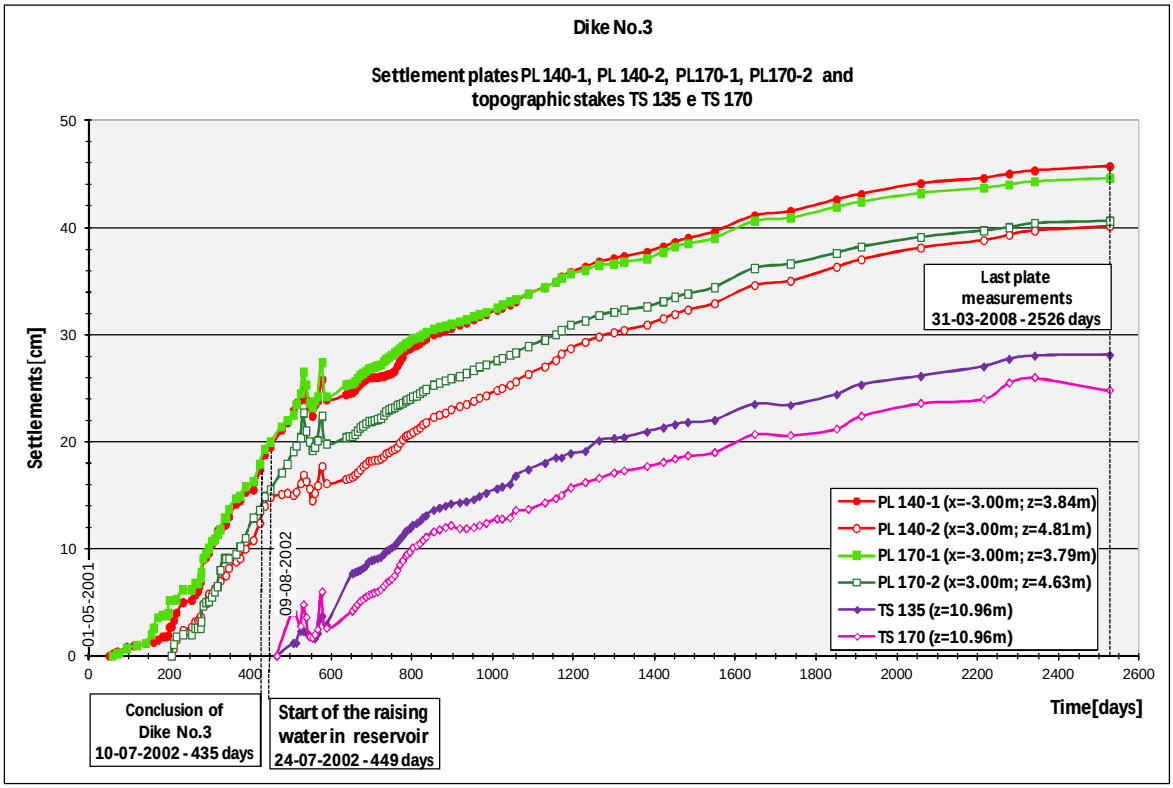

Graph VI.20 – Dike No.3: Readings of settlement plates PL 140-1, PL 140-2, PL 170-1, PL 170-2 and topographic stakes TS 135 and TS 170

Comparing the topographic settlement curves, placed at the crest, with the plates settlement curves placed inside the dike, the tracings are quite similar and relatively parallel. This was already observed for Dike No.1, indicating that the settlement observed at the surface of the embankment, until the moment, is associated to the foundation consolidation.

VI.6.5. HORIZONTAL DISPLACEMENTS ON DIKE NO.1

The inclinometers are used in order to measure the horizontal displacements along their length, i.e., with depth. They also allow withdrawing measurements in both directions. In the case studied, the horizontal displacements with more interest are the ones correspondent to axis A(0+)-A(180-), which are associated with the movements observed in the transversal profiles. Besides, the most precious information taken from this device, is the possibility of detecting if a failure surface, associated to the slope instability is in course, and locating its position. In the case of the dikes, and depending on the location of the inclinometer, this analysis is done both in the dike embankments and in the foundation.

The inclinometers I 220-1 and I 260-1, both installed in the Dike No.1 crest, with a length of 35.5 metres, presents their maximum horizontal displacements on the top, with respectively 11.6cm and 13.5cm. At a depth of around 15 metres, i.e. when they penetrate nearly 3.5 metres into the foundation soil, their values attenuate substantially, registering only to 2.0cm and 3.0cm (Graphs VI.21 and VI.22).

The inclinometers I 220-2 and I 260-2, with 19.0 and 18.5 metres long, are located at the downstream drain, in the limit of the area treated with the band-shaped drains. Although their maximum horizontal displacements occur at the same depth, the values are quite distinct. In inclinometer I 220-2 a maximum value of 9.3cm was registered at the top, followed by a slightly decrease, and then rising again and achieving the same value, but at a depth of about 5.0 to 5.5 metres (level -1.00m to -1.50m) (Graph VI.23). The readings from me 260-2 are quite different from the previous ones, although the maximum value occurs at a depth of between 4.5 and 5.0 metres, also corresponding to a level of -1.00m to -1.50m. For this inclinometer, the maximum horizontal displacement is 22.7cm (Graph VI.24). The depth where these maximum values are measured match to the layer with high compressibility and low strength characteristics. When these equipments reaches a depth of 13 metres, they penetrates the stiffness stratum, C, and the displacements are minimal.

The inclinometer I 240-1, located at the downstream berm, at level 6.00m, has its maximum displacement of 20.0cm in the clay stratum B1, at a depth of 8 metres, i.e. at a level of -2.00m. From this depth, the values attenuate until they reaches the soil layer B2 at 16 metres (level -10.00m) and become nil in stratum C, at a depth of 19 metres (level -13.00m) (Graph VI.25). This device was placed in an area with vertical drains all around.

Special attention should be giving to the position in the ground foundation, where the maximum displacements are registered, since it seems to have a pattern, being around level -1.00m to -2.00m. This is speciality important when the measured values are already significant.

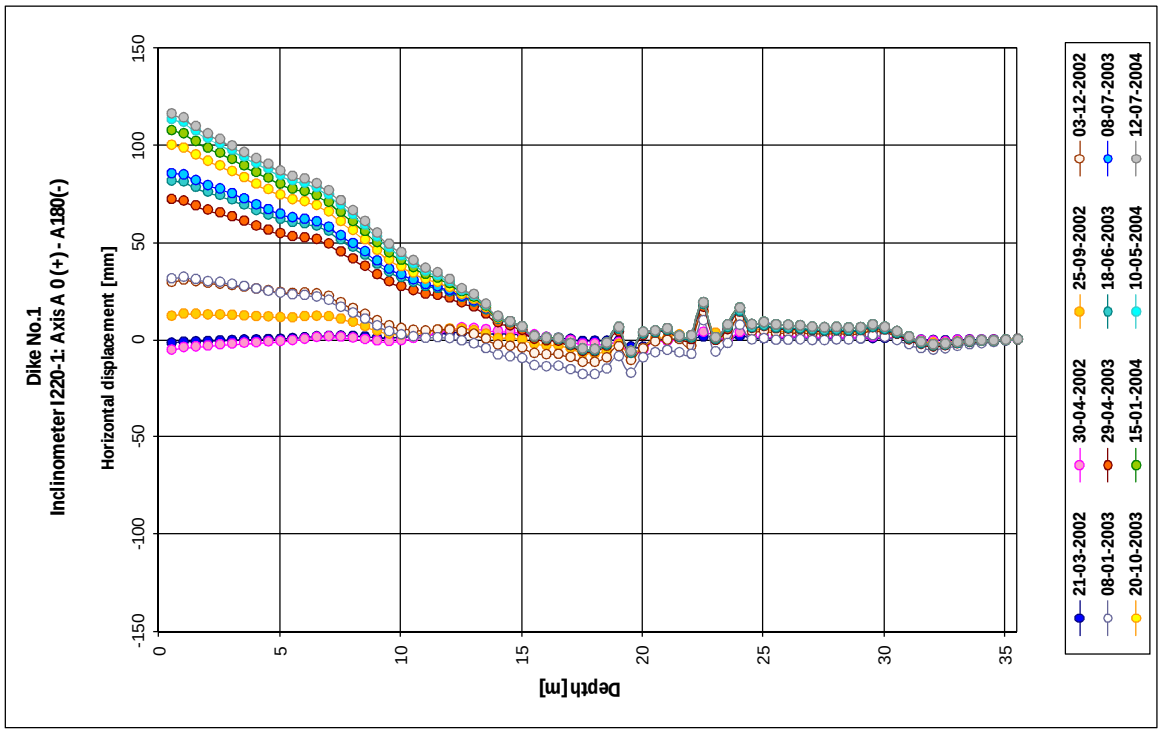

Graph VI.21 – Dike No.1: Horizontal displacements measured on I 220-1 - axis A0(+)-A180(-)

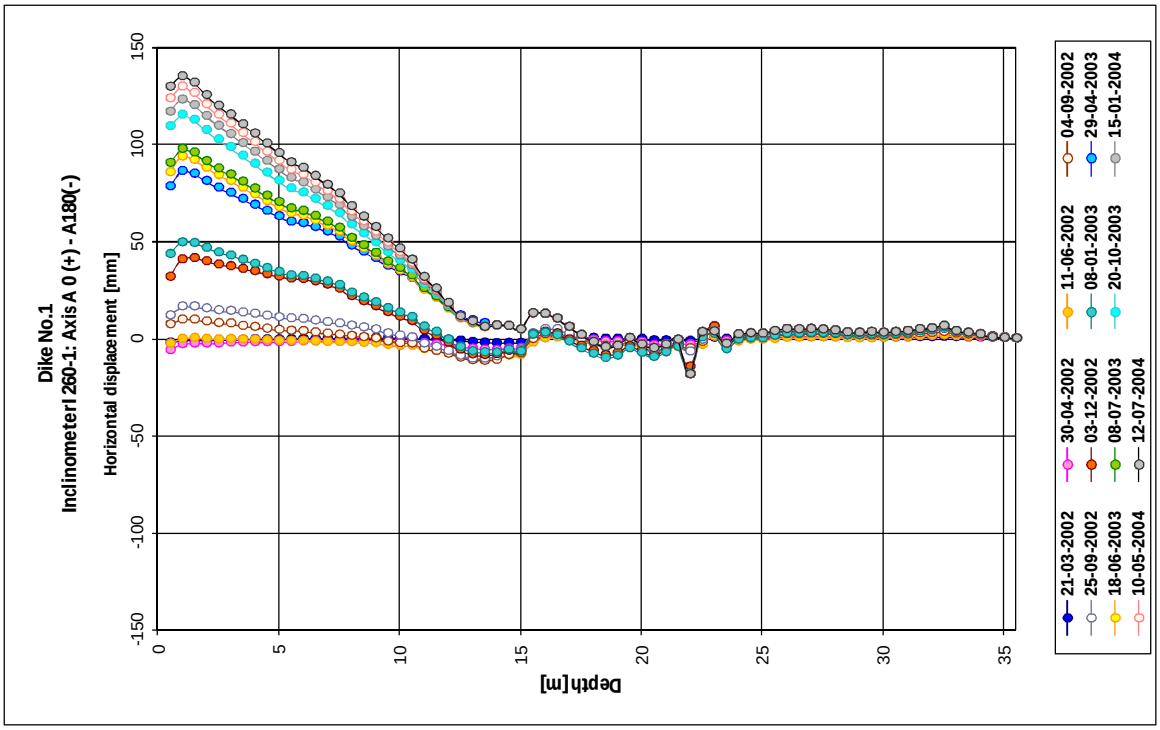

Graph VI.22 – Dike No.1: Horizontal displacements measured on I 260-1 – axis A0(+)-A180(-)

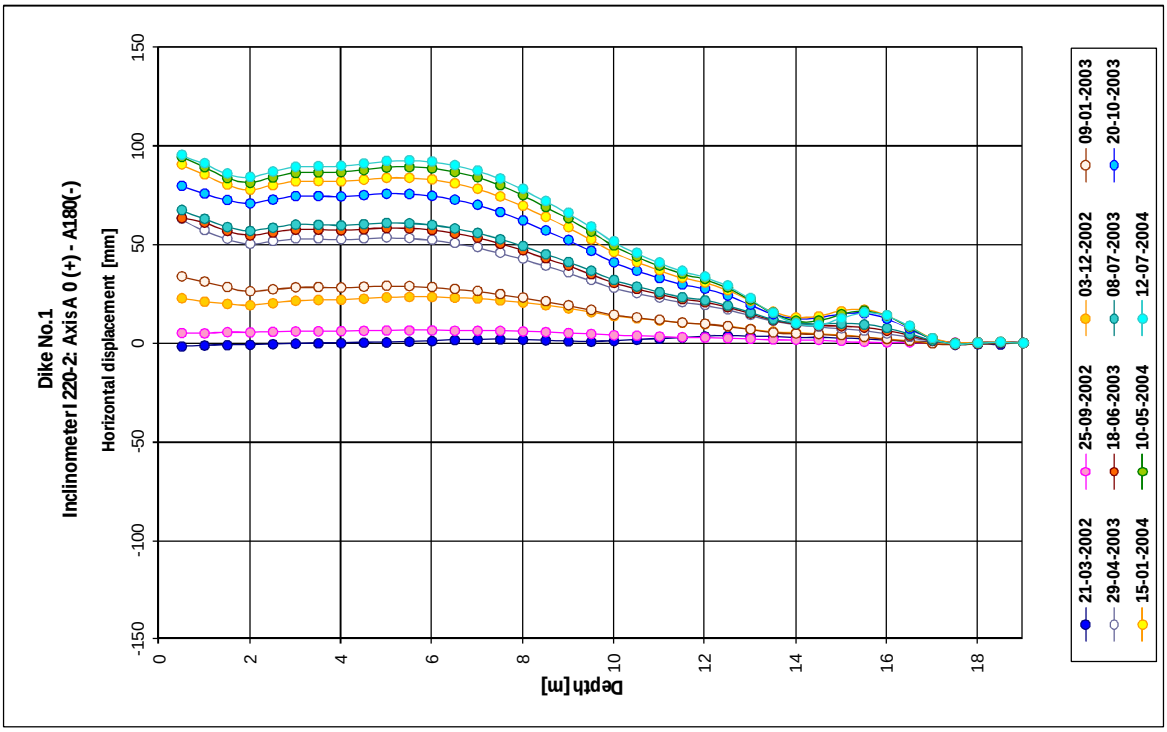

Graph VI.23 – Dike No.1: Horizontal displacements measured on I 220-2 – axis A0(+)-A180(-)

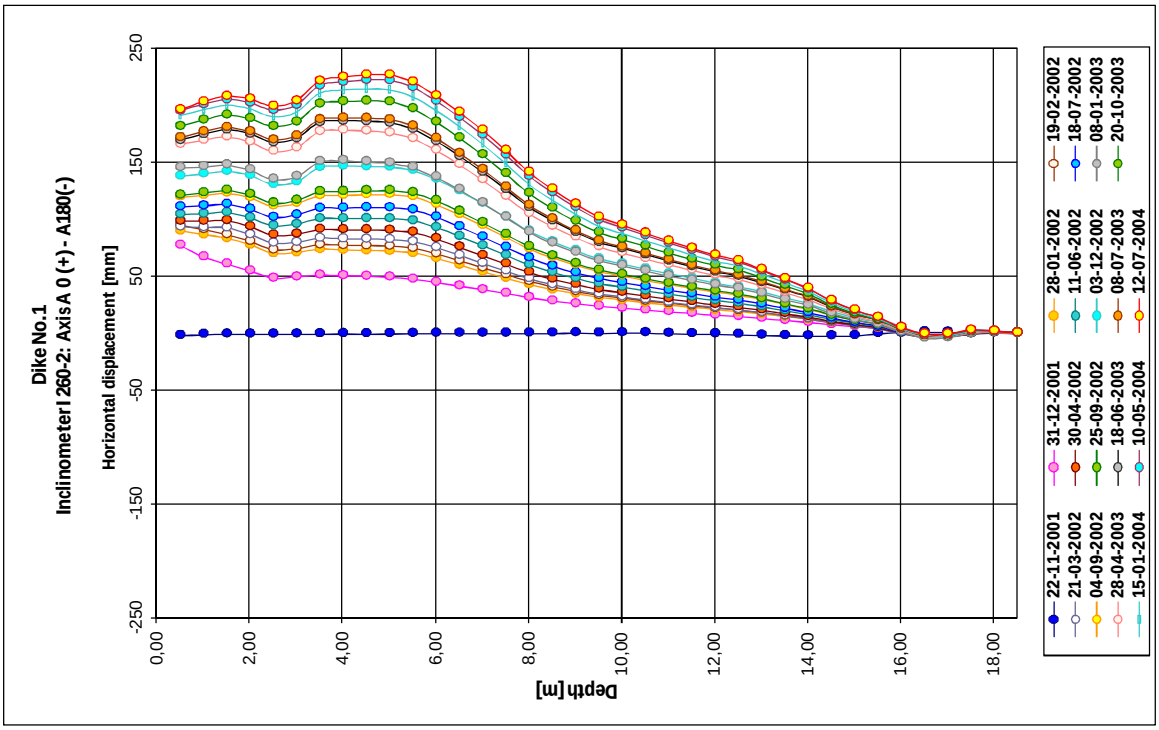

Graph VI.24 – Dike No.1: Horizontal displacements measured on I 260-2 - axis A0(+)-A180(-)

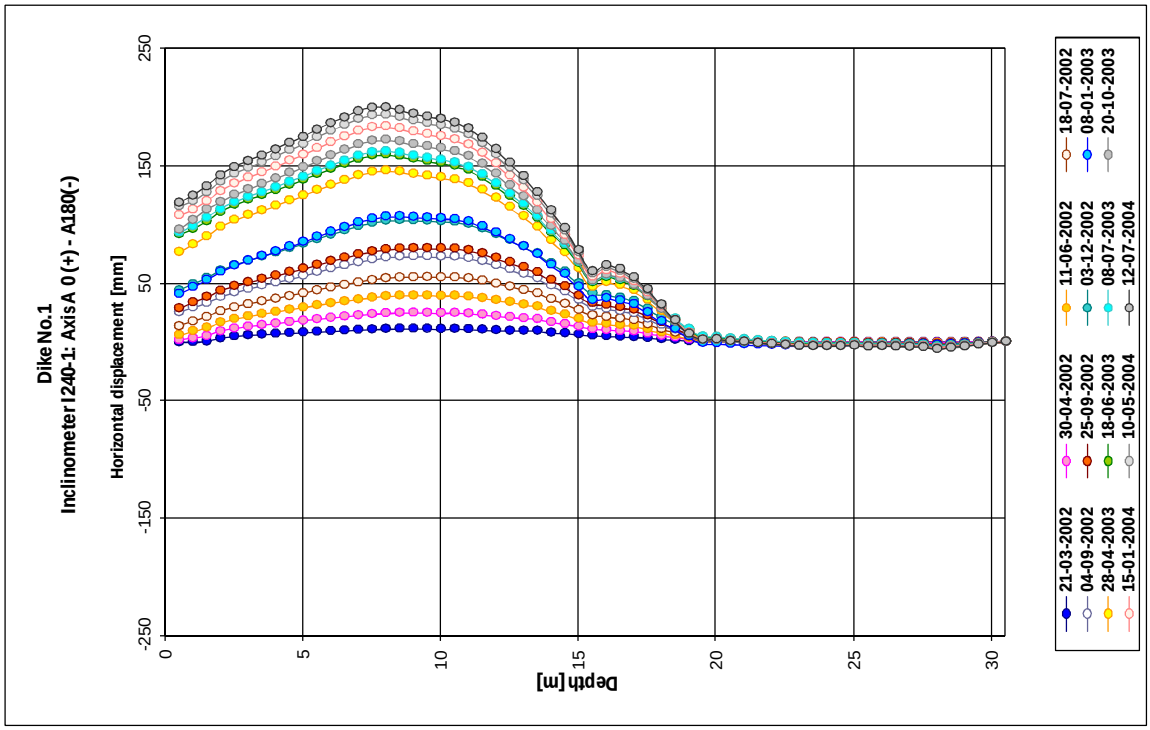

Graph VI.25 – Dike No.1: Horizontal displacements measured on I 240-1 - axis A0(+)-A180(-)

In graph VI.26, the maximum displacements of all the inclinometers placed in Dike No.1 are plotted in terms of their evolution over time, being possible to observe their behavior during the construction, and with the raising of the water level in the reservoir.

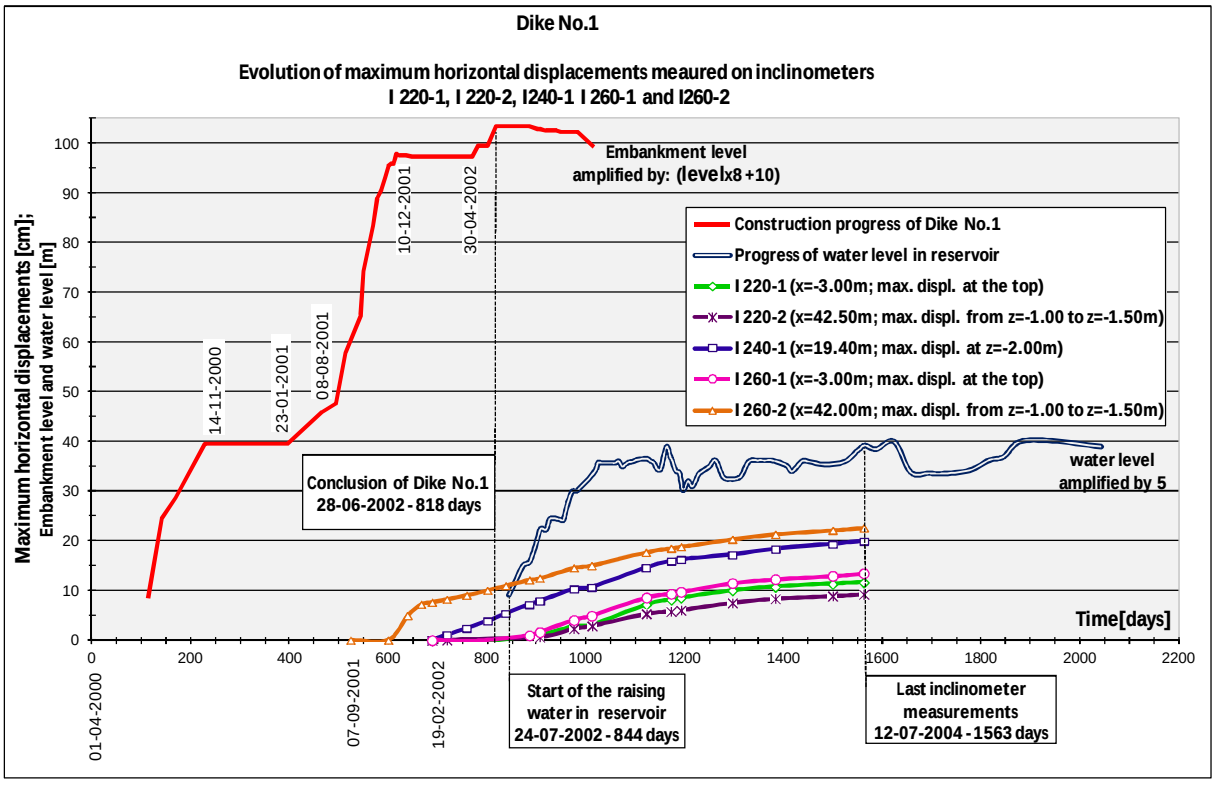

Graph VI.26 – Dike No.1: Maximum horizontal displacements on all inclinometers - axis A0(+)-A180(-)

With the results plotted in this format, one can perform other kind of comparisons and observations, namely:

a) In inclinometer I 260-2, the highest rate observed in the evolution of the maximum horizontal displacements, take place in the initial phase, being associated with the construction stage of the dike between August and December 2001. After this initial high increment, the rate decreases but still presents a gradual evolution over time. The same behaviour continues with the raising of the water in the pond;

b) Inclinometer I 240-1 also presents high horizontal maximum displacements, although lower than I 260-2, since this device was installed later. It can be seen that the layout of the displacement curves, for these two devices, remain more or less parallel from the conclusion of the dike's construction up to the latest readings. In addition to this, these maximum displacements occur in the same type of soil and at practically the same level, such as the case with the measures from I 220-2;

c) The inclinometers placed at the dike crest, I220-1 and I 260-1, present smaller horizontal maximum displacements. Besides, movements were only detected when the water in the reservoir started to rise;

d) All the displacements occurred on the downstream side direction.

VI.6.6. HORIZONTAL DISPLACEMENTS ON DIKE NO.3

In Dike No.3 there are only two inclinometers, both located at the PK0+220 cross-sections, in a zone without band-shaped drains. I 220-1, with 30 meters long, was placed on the crest, at level 10.90m, being installed on 19 February 2002. I 220-2, with 18 metres long, was placed near the downstream drain, at level 3.00m, in the initial stage of the dike construction works. Looking at the results displayed on graphs VI.27 and VI.28, the horizontal displacements are relatively small when compared to values measured in Dike No.1.

I 220-1 shows a maximum displacement of 3.6cm, 3 metres above the top, i.e., at level 7.90m. On the other hand, the maximum displacement of I 220-2 is even smaller (approximately 1cm), registered at a depth of 4 to 5 metres (between level -1.00m and -2.00m). These values are insignificant, indicating that the stability is not an issue in this section of the dike.

In the readings obtained from the inclinometer I 220-1, it was detected that, at the depths comprehended between 12 and 14 metres, which corresponds to the entry of the device into stratum C, the horizontal displacements show an unexpected inflection in the results. The same happens when the displacements in the longitudinal direction are also analysed, i.e., axis B(0+)-B(180-) (Graph VI.29).

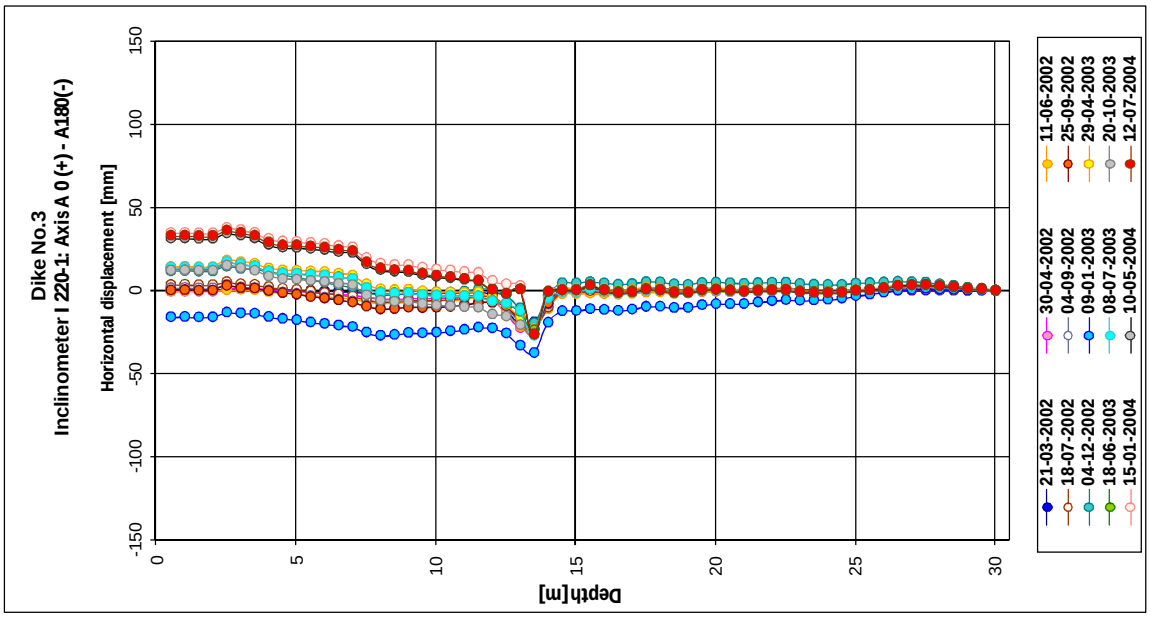

Graph VI.27 – Dike No.3: Horizontal displacements measured on I 220-1 - axis A0(+)-A180(-)

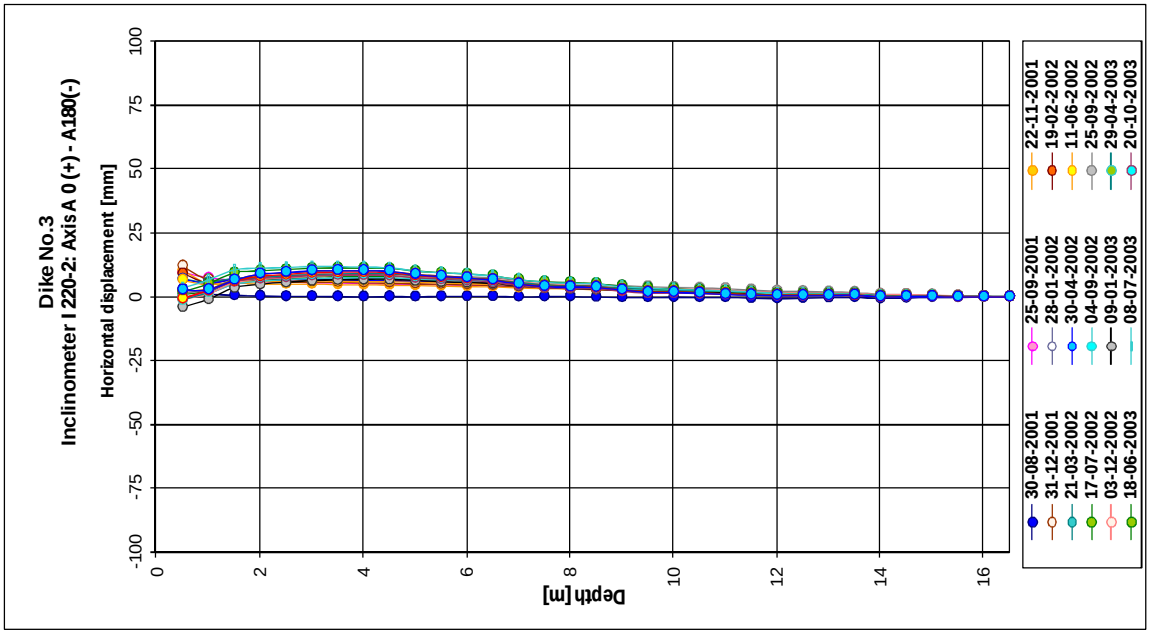

Graph VI.28 – Dike No.3: Horizontal displacements measured on I 220-2 - axis A0(+)-A180(-)

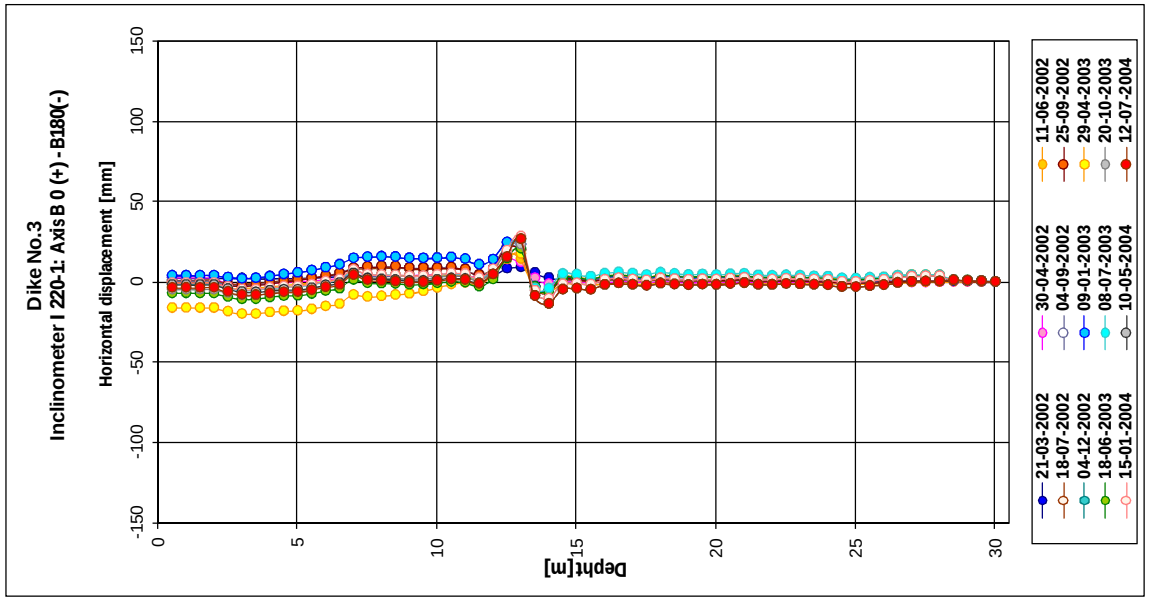

Graph VI.29 – Dike No.3: Horizontal displacements measured on I 220-1 - axis B0(+)-B180(-)

Plotting only the maximum horizontal displacements with time, this time for Dike No.3 (Graph VI.30), an interesting behaviour is observed in inclinometer I 220-1. From its readings, it is noted an inconstancy of the direction associated to the maximum values, with fluctuations between the upstream and downstream sides. After the complete construction of the dike, and before the raising of the water in the reservoir, the inclinometer moves towards the upstream side, indicating that the slope stability surface is also on this side. With the reservoir already full and the water level stabilized, an inversion of the inclinometer sense is watched, since it moves downstream. This does not occur with inclinometer I 220-2, where there is an initial increment correspondent to the construction phase, and then a very gradual evolution, even in the reservoir-filling phase.

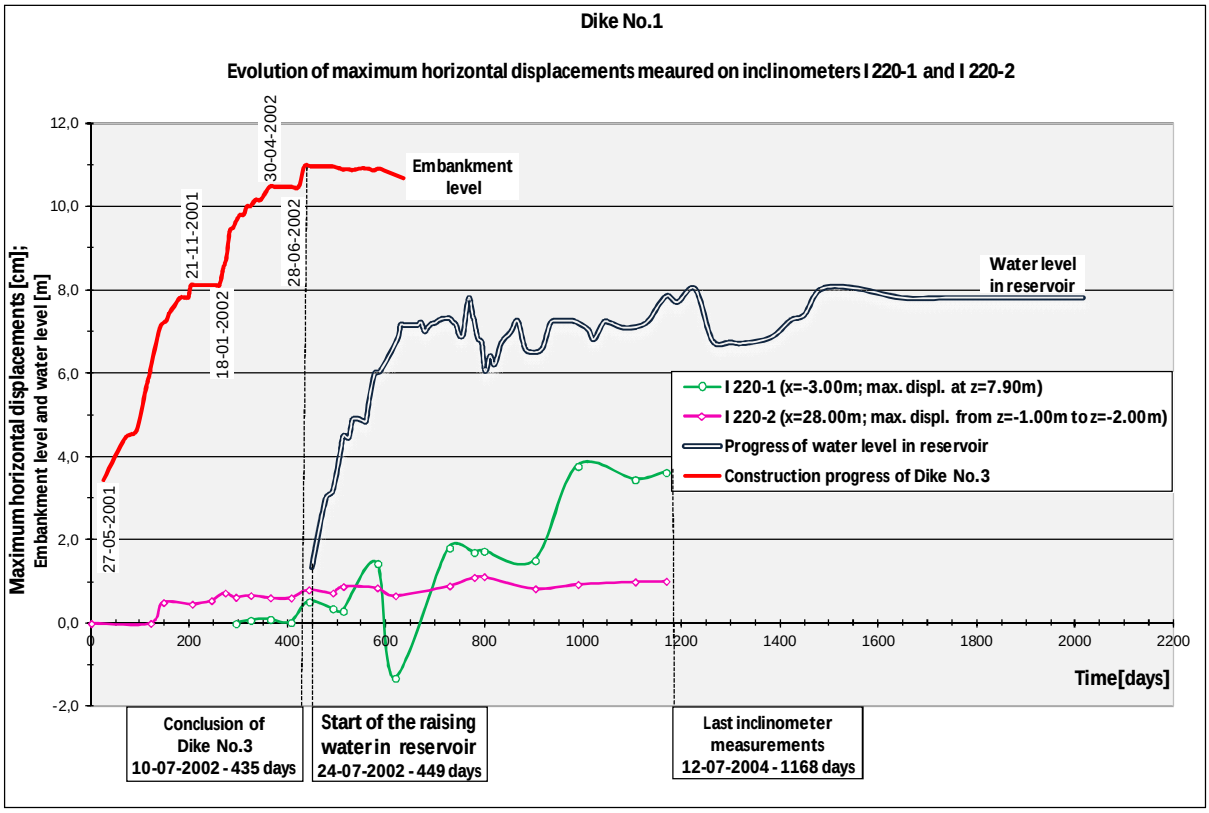

Graph VI.30 – Dike No.3: Representation of maximum horizontal displacements measurements, with time, for I 220-1 and I 2002-2 - axis A0(+)-A180(-)

Due to the extraordinary low values measured in both inclinometers, as well as the hardly adequate profile selection to place these devices, their interest regarding the dike stability analysis is small. Indeed, this cross-section do not correspondent to the maximum dike height, and no drains were installed here; additionally the results cannot be compared with others, since there are no more inclinometers in this dike. In 2009, Da Silva, presented some results associated with the modelling of this section and stated that there was no correspondence between the results measured and those calculated numerically, considering various models of soil behaviour.

VI.6.7. SUMMARY OF MONITORING RESULTS AND RECOMMENDATIONS

In light of the monitoring results and after analysing same, it can be mentioned that the recommended measures proposed for Dike No.1 and Dike No.3 and in the revision phase of the design, were adequate. The dikes stability was ensured, both during its construction, as well as in the first phase of the reservoir filling, until the present moment, thereby meeting the safety criteria. Regardless the excellent results concerning the stability, the settlements estimated in the design phase were underestimated as they correspond to about 75% of those observed until now.

In the profilePK0+240 of Dike No.1, corresponding to the highest cross-section, the maximum settlement measures reached 100.2cm, exceeding substantially the 72.0cm estimated in the design. In percentage, this result corresponds, respectively, to 11.3% of the total height of the embankment above the level plate PL 241-1. At the end of the construction phase, 5.4% of the settlement had already token place. Although these results are extremely high, they are coherent with the extremely high compressibility and low strength characteristics of the soil foundation, more specifically to the B1 and B2 soil layers. Concerning this aspect, and as a comparison term, the following cases are quoted: the Shellmouth (10%), Santa Helena (8.5%), Fresno (10%) and La Esperanza (5%) dams (Cea Azañedo *et al*., 2005).

Despite the previous statement, a direct comparison of the drains effect in the consolidation rate increment and in the associated settlements cannot be made only based on the results from the plates placed in Dike No.1, since these are always located in areas where drains were applied in the ground foundation. To do so, it is necessary to compare them with the settlements measured in several sections of Dike No.3, as some were placed in zones with and without bad-shaped drains. Therefore, for Dike No.3, the maximum settlement attained in zones with drains reached 46cm (6.5% of the total height of the dike above the level plate); in a zone without drains, the value reaches 31.5cm (4.2%). The same trend is observed in the phase correspondent to the end of the construction of Dike No.3, although the difference is less, with results of 2.8% and 1.7%, respectively.

It is important to emphasise that Dike No.1 has drains on the upstream and downstream side of the cut-off, while on Dike No.3 the drains were only placed on the downstream side of the cut-off. Off course that this is an extremely important aspect, in order to understand the differences between the 11.3% and 6.5% obtained on the highest profiles of both dikes, besides their difference of height itself.

From a comparative analysis of the settlements readings in the plates and topographic stake marks, it is noted that the vertical displacements at the dikes surface are mostly due to the consolidation of the ground foundation.

The stabilisation of the settlements occurs one year after the conclusion of the dikes, therefore confirming the efficiency of the drains in the speed up of the consolidation phenomena. The same is corroborated by the results obtained in piezometers PZ 240-3, PZ 240-4 and PZ 240-5.

Regarding the pore pressures, it can be seen an increment during the construction phase of the dike, followed by a decrease when the construction works are interrupted in the raining season. Later, with the rise up of the water level in the pond, the pore pressure also rises, although very variable, depending of the piezometers location. Once the water level stabilises in the pond, a drop can be seen in almost all of the piezometers located on the downstream side, and in some of those located in the body of the embankment and at lower levels. This behaviour suggests not only that the drains are functioning, but also that they are also having an effect in the reduction of the excess pore pressures as it was expected.

In Dike No.1, the pores pressures measured are in most cases considerably lower than the overpressures values estimated analytically, because of the drains disposed on both upstream and downstream sides, which enables the dissipation of the excess pore pressures immediately. The exception takes place for PZ 240-1 and PZ 240-2, since they indicate extremely high values in comparison to the others, reaching, in the case of PZ 240-2, a value of hydrostatic overpressure identical to that estimated, for the phases associated to the embankment construction.

Concerning the piezometers of Dike No.3, they were installed underneath the upstream berm and in a zone without drains, though they exist on the downstream side of the cut-off. Therefore, there is a relatively large concordance between the values measured in these two piezometers and those estimated based on the analytical calculations, for the phase associated to the embankment construction up to the level of the berm. With the reservoir filling, although an increment of hydrostatic pressure is noted in both piezometers, it is considerably less than the overpressure caused by the hydraulic head due to the water level rise up. This was to be expected, since the interstitial pressures depend of the flow net established on the foundation. Besides, based on the values measured and on the analytical calculations, it is suspected that piezometers PZ 180-1A and PZ 180-1B are place with a difference of 4 metres instead of 5 meters.

Accordingly, to the recommendations of the Bureau of Reclamation (1987) for dams founded in soft soil, it is mentioned that a dam's stability analysis should be carried out at the end of its construction, considering undrained conditions, being required a minimum safety factor of 1.5. It refers that this analysis is more severe than the one associated to the phase of reservoir already full, or even for the phase of quick drop of water level in the reservoir (quick emptiness of the pond in case of emergence). It also points out that the type of material used in the body of the homogeneous dams, or in the shoulder embankment of the zoned dams, is not significant for the stability analysis, since this is constrained by the type of soil foundation characteristics. This same entity recommends the use of vertical drains when in the presence of high compressible soils, in order to accelerate the consolidation phenomenon, and in these cases, special attention must be given to their study and design. It should be noted that this option is not recommended for small dams (total height <15m), unless the SPT number gives less than 4 blows for a depth inferior or equal to the total embankment height. The case study, i.e., the *Lebrija* Pond Dikes No.1 and No.3, falls in this category. Lastly, other advice includes the installation of horizontal drainage mats between the foundation and the embankment itself, both upstream and downstream of the cut-off trench. These coarse layers also enable the control of the pore pressure during the operational phase.

In Justo (2000a) technical report of the *Lebrija* dikes stability, he refers to Sherard *et al.* (1963), mentioning that according to these researchers a conservative posture would be to ignore the influence of the embankment soil strength, when stability analysis of embankments founded in silty and clayed soils are in question.

Another factor, which is important to highlight, is the slope stability analysis of these type of geotechnical structures, founded in high plasticity clayed soils, when undrained strength characteristics are given by the Vane-Test results. The safety factors obtained with these values are usually high, as they are overestimated, mainly for clays with high plasticity indexes (IP). This phenomenon is related to the rotation speed imposed during the test. Thus, when performing this type of calculation, the undrained shear strength obtained from this field test must be reduced, taking into account its plasticity index (Jiménez *et al.*, 1981).

Hereupon, in the following chapter, the numerical simulation performed for these two dikes will be presented, including the calculation procedure, such as:

- the soils characteristics used in each of the models adopted to describe the behaviour of the foundation soil and dikes;
- the boundary conditions associated to the calculation stages;
- the definition of the initial stress state;
- the definition of the construction rate and steps, as well as the water level rises up, among others.

The monitoring results will be compared to the numerical calculations, in order to check the soil stiffness, strength and permeability, as well as their influence on the consolidation rate process. So several hypotheses are considered, for the next parameters:

- the width of the smear zone;
- the reduction in the horizontal permeability in this disturbed zone;
- the influence of secondary compressibility and the value of the secondary compressibility index on clay foundation soil;

in addition other factors were studied, namely:

- the material model used for the soil foundation;
- the influence of the flow net on the pore pressures measured in the embankment and foundation.

The safety factors associated to the conclusion of the dikes construction, as well as for the final calculation step, regarding the slope stability of the dikes will also be calculated and presented.

VII. MODELLING OF DIKES NO.1 AND NO.3 OF THE *LEBRIJA* POND

In this chapter, the procedure associated to the modelling and numerical simulation of the cross-sections PK0+240 of Dike No.1, and PK0+140, Pk0+170, Pk0+180, PK0+200 of Dike No.3, of the *Lebrija* Pond, will be describe, as well as the results obtained. The specifications of each of the sections, regarding their final geometry, the additional elements considerer with respect to the ground improvement and their location in the dikes, the monitoring equipment adopted, their position and installation date, as well as the construction rate and reservoir filling steps, have already been indicated in the previous chapter, along with the monitoring results obtained since its construction. The reasons which lead to the selection of these profiles have also already been point it out. Therefore, chapters VI and VII are interconnected and cannot be dissociated.

The software chosen to model the dikes is the PLAXIS programme. Based on the finite element method, this software was developed at the Deft University, in Netherlands, and is specific for problems of a geotechnical nature.

From the comparisons between the monitoring data results presented before, and the simulation results conducted throughout this chapter, it will be possible to withdraw conclusions relating to:

a) The smear parameters which can traduce more realistically the smear effect for the case study, namely the permeability and diameter of the disturbed zone around the drain;

b) The most adequate material model to describe the behaviour of the soil foundation;

c) The values of the secondary compressibility index, associated with the creep phenomenon of the high compressible soils, which can enables a better correspondence between the real and the calculated results;

d) The influence of the flow, both in the foundation and in the body of the dike embankments.

In this last case, the programme takes into consideration the establishment of a flow net according to the soils permeability and boundary conditions. The programme itself allows that soils above the phreatic level may be partially saturated, becoming saturated as the water level rises in the pond and the flow network is created.

To achieve the abovementioned objective, several parametric and sensitivity studies had to be performed. They will be presented in detail during this chapter, nevertheless is important to make a brief introduction, in order to understand the structure followed in this chapter.

Thus, and for the study of the smear effect, several distinct hypotheses were considered for the diameter and for the horizontal permeability coefficient in the disturbed zone, namely:

a) $K_{hsAx}=0.10K_{h0}$ and $ds=2d_w$; $K_{hsAx}=0.10K_{h0}$ and $ds=3d_w$; $K_{hsAx}=0.10K_{h0}$ and $ds=4d_w$;

b) $K_{hsAx}=0.33K_{h0}$ and $ds=2d_w$; $K_{hsAx}=0.33K_{h0}$ and $ds=3d_w$; $K_{hsAx}=0.33K_{h0}$ and $ds=4d_w$;

c) $K_{hsAx}=0.66K_{h0}$ and $ds=2d_w$; $K_{hsAx}=0.66K_{h0}$ and $ds=3d_w$; $K_{hsAx}=0.66K_{h0}$ and $ds=4d_w$;

Later on, these values were converted into horizontal permeability coefficients for the plane strain analysis (K_{hPD}), being adopted the Indraratna & Redana (1997) analytical formulation.

Notwithstanding the analytical solution chosen, several hypotheses have been used to determine K_{hPD}. So, after an exhaustive analytical study, it was decided to use the same assumptions as the Hird *et al*. (1992) solution, since it brings important benefits and simplicity in the modelling procedure of the area improved with the band-shaped drains, without a loss of accuracy. Additionally, the hydraulic resistance of the drain was taken into account in these calculations, although it was concluded that for the case study, this value has no expression in the final results (see subchapters V.4 and V.5). In the parametric analysis performed in the numerical simulations, to investigate the influence of the diameter and the permeability coefficient in the disturbed zone, only some of the above hypotheses were considered.

With respect to the material models, several models were initially considered for the soil foundation, including the Mohr-Coulomb, Soft Soil and Soft Soil Creep models. For soils of the dikes, i.e., the sands of the horizontal downstream drain, chimney filter and drainage blanket, the Rip-rap protection of the upstream slope and downstream toe drain, and the clay soil of the embankment body, the Mohr-Coulomb model was the one selected. This model is simpler than the others, and requires a smaller number of geotechnical parameters which are easily determined based on field or laboratory testing. Besides they are relatively suitable for coarse soils. By contrast, although the Soft Soil and Soft Soil Creep models are more suitable for clayed soft soils, they require further parameters, which are obtained from specific tests such as the oedometer test.

After analysing the simulations results, it was observed that the Soft Soil Creep model used on the high compressible soils of the foundation, allowed greater adjustment to the curves obtained from the monitoring results. Such behaviour was expected and was not surprising, since it is the only model that permits to consider the viscosity effect (creep) of the clayed soils, and consequently the secondary consolidation phenomenon and settlements. According to the parametric analysis on the secondary compressibility index (C_α), this value has a huge influence in the final settlements curves results. The ultimate goal of this study was to estimate the parameter in question, by retro-analysis. As such, three different secondary compressibility index values are used for the B', B1, B2 and B3 soil foundation of the dikes. For the first hypothesis, the values used are those obtained from the oedometer test; in the second hypothesis, the Terzaghi *et al*. (1996) relation was considerer; and in the third and final hypothesis, the ratios suggested in the PLAXIS manual (PLAXIS 2D V11.02, 2012) were applied to the soils. The values associated with the first two situations are presented in subchapter VI.2, meanwhile the values for the last hypothesis are calculated and presented in the course of this chapter.

In order to complement this study, and bring more realism to the numerical simulations, the flow was considered in the analysis. In this case, after the generation of the initial hydrostatic pressures in a first step, the flow is then always taken into account at every phase of the calculations. Initially, before the water rises in the dam, the flow occurs only in the foundation and is associated with different permeability between layers, as well as the existence of drains in the improved areas and the differences of overload due to the dike construction. As the water level rises in the pond, the difference of the hydraulic head between the upstream and downstream and the water flows within the body of the dike embankment as well as on the foundation. This depends on several factors, including the location of boundary conditions, the difference in hydraulic head and the soil permeability, among others.

With the purpose of studying the influence of the reinforcement geotextile and the ground improvement with the band-shaped drains, without considering the smear effect in the last ones, the following scenarios were also considered for Dike No.1, in addition to the abovementioned analyses:

a) Soil foundation without drains, nor geotextile reinforcement at the base of the dike embankment;
b) Soil foundation without drains, but considering geotextile reinforcement at the base of the dike embankment;
c) Soil foundation improved with drains (without smear effect), but without geotextile reinforcement at the base of the dike embankment;
d) Soil foundation improved with drains (without smear effect), but considering geotextile reinforcement at the base of the dike embankment.

In the final part of this chapter, the safety factors associated with the dikes stability are also presented. These were calculated for two different stages, the first corresponding to the embankment conclusion, and the second associated to the date of the last measurements results, i.e., after the water level at the reservoir stabilise at 7.80m. Once again, the main purposes is to determine the influence and effect of the following aspects in the stability, namely, the reinforcement geotextile, the treatment of the foundation with the band-shaped, the smear effect, the material model used in the soils, the filling of the dam and the flow.

VII.1. PLAXIS PROGRAMME – GENERAL FEATURES

The PLAXIS finite element programme was initially developed at the Technical University of Delft under Professor Vermeer coordination, and has been available since the latest 1980s. The Programme has undergone several upgrades and improvements since then. It is divided into three sub-programmes, which are: the introduction of data and geometry (Input); follow by the calculations steps and procedures (Calculations); and, finally, the access to the results (Output).

In a first phase, even before defining the geometry, one must defined the input units for the parameters of length (L), time (t), force (F), and gravity, as well the type of problem to be analysed (axisymmetric or plane strain). When setting the geometry of a given problem, the PLAXIS programme considers triangular elements. These triangular elements may comprise 6 nodes (Figure VII.1a) or 15 nodes (Figure VII.1b). The latter permit greater precision and accuracy on the results of displacements and stresses.

Figure VII.1 – Triangular elements with 6 nodes (1a) and 15 nodes (1b)

According to the PLAXIS manual, it is important to adopt the 15 nodes triangular element in axisymmetric problems, since they provide, in this type of application, exceptionally good results, not only when predicting the rupture mechanisms, but also the stresses distribution. The results of these elements, in relation to the stress evolution, is smoother, as they are calculated at 12 points, located inside the element (Figure VII.2a) and designated as stress points. In the 6 nodes triangular element, there are only 3 stress points (Figure VII.2b), which is why these elements are rarely used.

Figure VII.2 – Stress points for triangular elements with 6 nodes (2a) and 15 nodes (2b)

The PLAXIS also allows, during calculations, to update the finite element mesh, or in other words the position of the nodes according to the deformations suffered during the calculations (Update mesh). This is also possible for the water pressure (Update water pressures). This procedure, although optional, enables updating the mesh, displacement and water pressure in each step, according to the position of the nodes. This option should be activated whenever in the presence of geotechnical problems with high levels of deformation (greater than 10%).

The reliability of the results obtained depends on various factors; some of them associated with the resolution of numerical problems and, as such, are intrinsic to the software. However, others depend on the user, their capacity to transpose the problem into a computational format. The following factors are highlighted:

a) Geometric characteristics of the problem (Input);
b) Mechanical properties of the materials (strength and stiffness) (Input);
c) Permeability characteristics of the materials (Input);
d) Material models adequate to the material type, and if applicable, indication of the conditions (drained or undrained) (Input);
e) Displacements constraints (Input);
f) Indication of the element or mesh dimensions, and its generation (Input);
g) Generation of the initial stress state based on the lateral earth pressure coefficient at rest, or in the overconsolidation ratio (Calculations);
h) Definition of the phreatic level and the initial hydrostatic pore pressures, as well as the boundary conditions (Calculations);
i) Definition of the construction steps, and the type of exterior load applied (static or dynamic). In each calculation step it is possible to change the soil characteristics, water level and boundary conditions (Calculations);

j) Consideration of flow, when applicable (Calculations);
k) Updating of the finite element mesh in light of the displacements suffered during the calculation (Calculations);
l) Selection of the analysis or calculation type (consolidation, stability, seismic, etc.) (Calculations);
m) Selection of the control points (nodes or stress points), which are to be followed during the calculation (Calculations);

The control points must be chosen accordingly with the parameter in question; so, if displacements results are required, the control points must correspond to nodes; whenever stresses are important for the problem in question, then one must select stress points, located inside the triangular element.

VII.2. MODELLING THE DIKES WITH PLAXIS

In the Dikes No.1 and No.3 of the *Lebrija* Pond, triangular elements of 15 nodes were used in their modelling, thereby guaranteeing greater precision and detail in the results. With respect to the units, the length was considered in metres [m], time in days [days] and force in kiloNewton [kN]. The acceleration of gravity is $9.81 m/s^2$ and consequently the volumetric weight of the water is $9.81 KN/m^3$.

In Dike No.1 only section PK0+240 was studied and modelled, since it is the highest cross-section and also the more instrumented. In Dike No.3 several profiles where modelled, such as PK0+140, PK0+170, PK0+180 and PK0+200. Section PK0+220 of Dike No.3 was left out from the simulations, due to the low interest of the inclinometer results (see chapter VI.6.6).

VII.2.1. DEFINITION OF THE DIKES GEOMETRY

During the definition of the dikes geometry, for the several cross-sections studied, some apparently meaningless lines appear; in reality, however, they are associated with the dikes construction process and will be essential latter on.

For each profile, a geometry is outlined, which must take into consideration the initial level of the ground surface, the levels of the excavation for the dikes foundation and cut-off trenches, the levels corresponding to the evolution of the embankment construction and of the water in the pond, the instrumentation, as well as the band-shaped drains and geotextile, where applicable. The vertical drains are modelled with the element “Drain” of PLAXIS. These are represented by vertical lines which start at the drainage blanket and cross the foundation to a given depth. The soil foundation of the cross-section PK0+240 of Dike No.1 has drains both on the upstream and downstream sides of the cut-off trench (Figure VII.3), while profiles PK0+140, PK0+170 and PK0+180 of Dike No.3 only have drains on the downstream side (Figures VII.4, VII.5 and VII.6). On the foundation of cross-section PK0+200 there are no drains (Figure VII.7). The geotextile applied in Dike No.1 is a “Geogrid” type element.

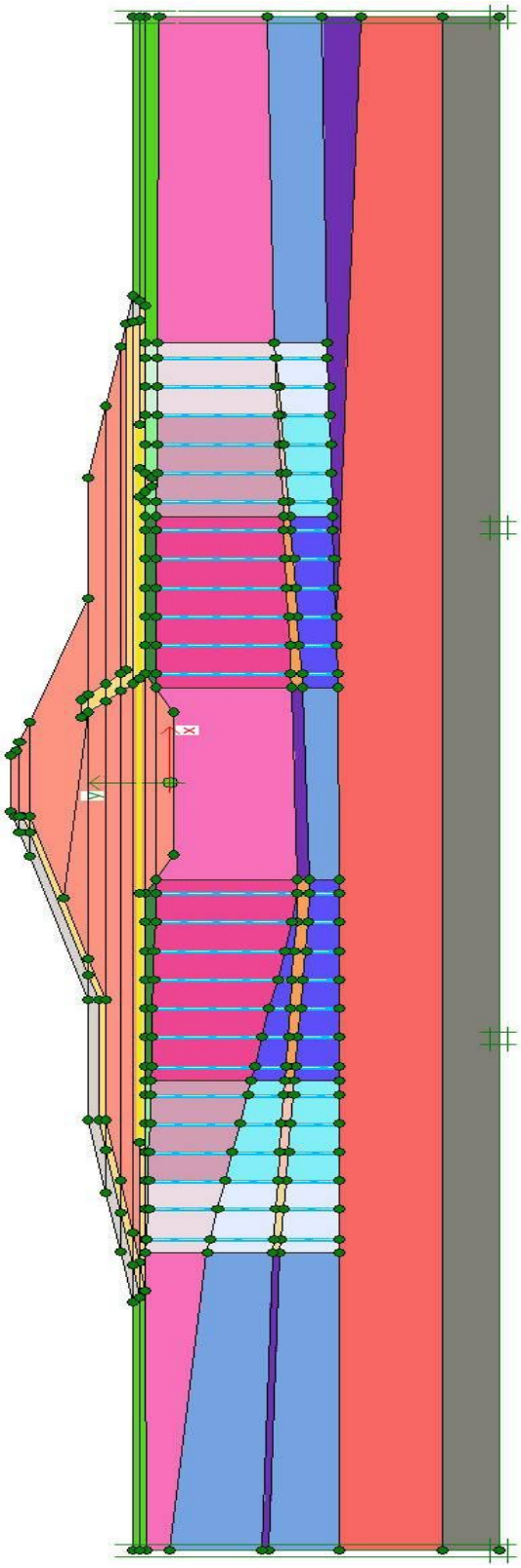

Figure VII.3 – Geometric model used for the cross-section PK0+240 of Dike No.1, including drains and geotextile

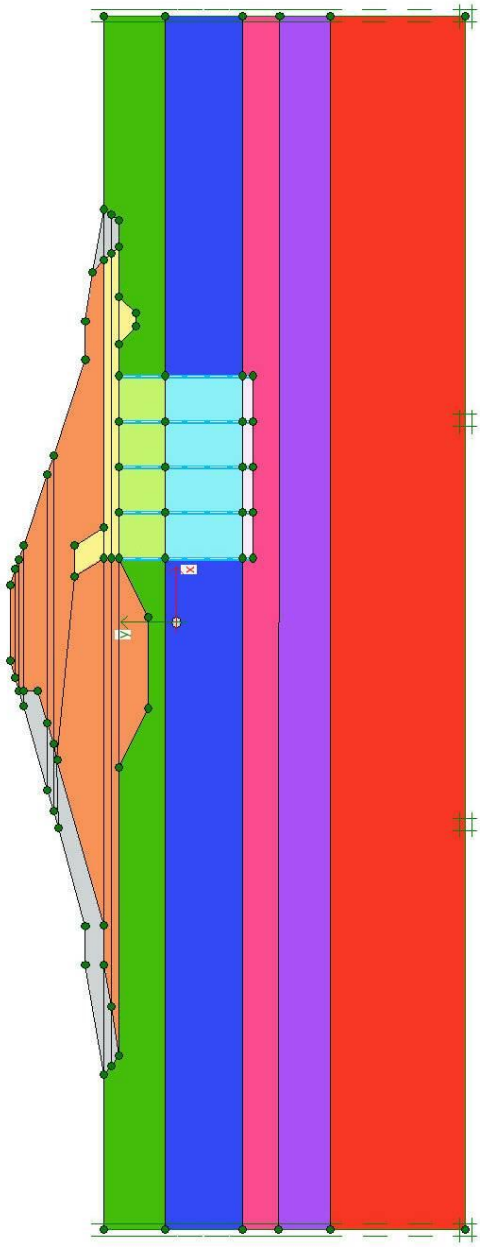

Figure VII.4 – Geometric model used for the cross-section PK0+140 of Dike No.3, including drains

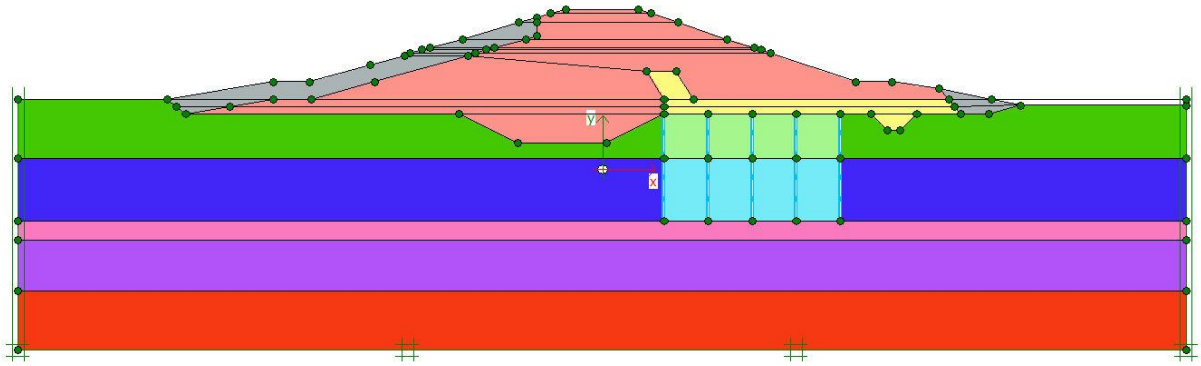

Figure VII.5 – Geometric model used for the cross-section PK0+170 of Dike No.3, including drains

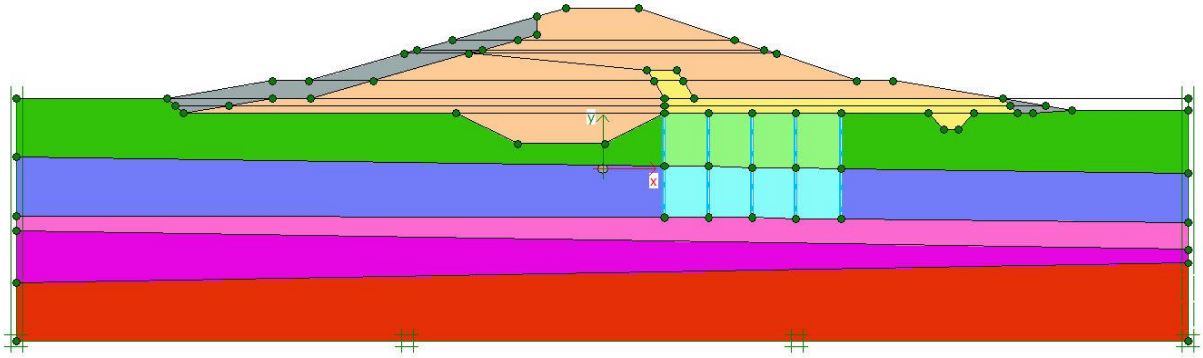

Figure VII.6 – Geometric model used for the cross-section PK0+180 of Dike No.3, including drains

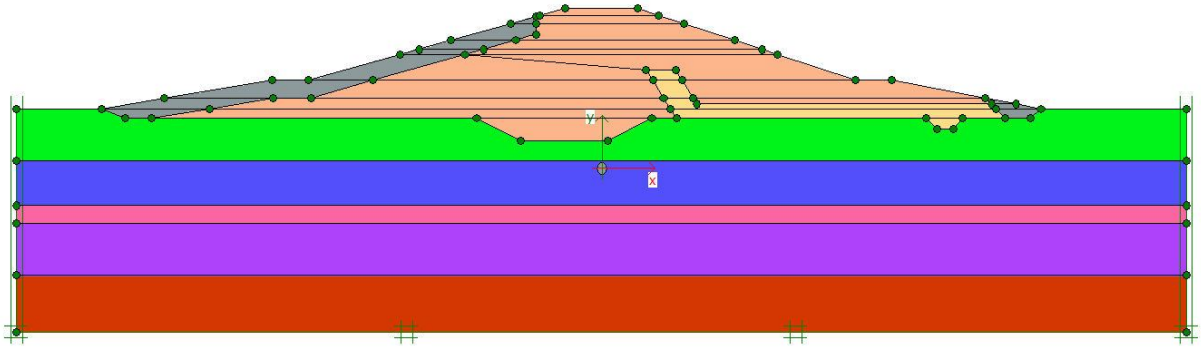

Figure VII.7 – Geometric model used for the cross-section PK0+200 of Dike No.3

The displacements constraints are imposed before the generation of the finite element mesh. In this study, it was considered that the ground foundation base displacements are completely restrained, i. e., no movements are allowed; relatively to the lateral displacement conditions, the soil foundation can only move vertically.

The dimension or size of the finite elements is indicated by the user, who may choose between a coarse, medium, fine and very fine mesh. In this case, a very fine mesh was chosen, since the geometric models contain certain zones where the "lines" are very close to each others. If other size was adopted, then the quality of the triangular elements mesh would not be so good, and the accuracy of the results could be compromised. So, combining the very fine mesh with the adoption of 15 nodes triangular elements, the precision and accuracy in the final results is very good, although it requires more memory and more time to carry out the calculations.

The finite element mesh associated with the modelling of Dike No.1 - PK0+240 is presented in figure VII.8, while figure VII.9 shows the quality of the mesh. The latter is given by the programme and traduces what was explained in the previous paragraph. Green coloured elements means excellent quality, whereas red means that the elements are slightly distorted (the element is no longer an equilateral triangle). The latter situation is to be avoided; however due to the thickness of certain layers, the drains spacing, and construction rate of the dikes, it was difficult to eliminate it altogether.

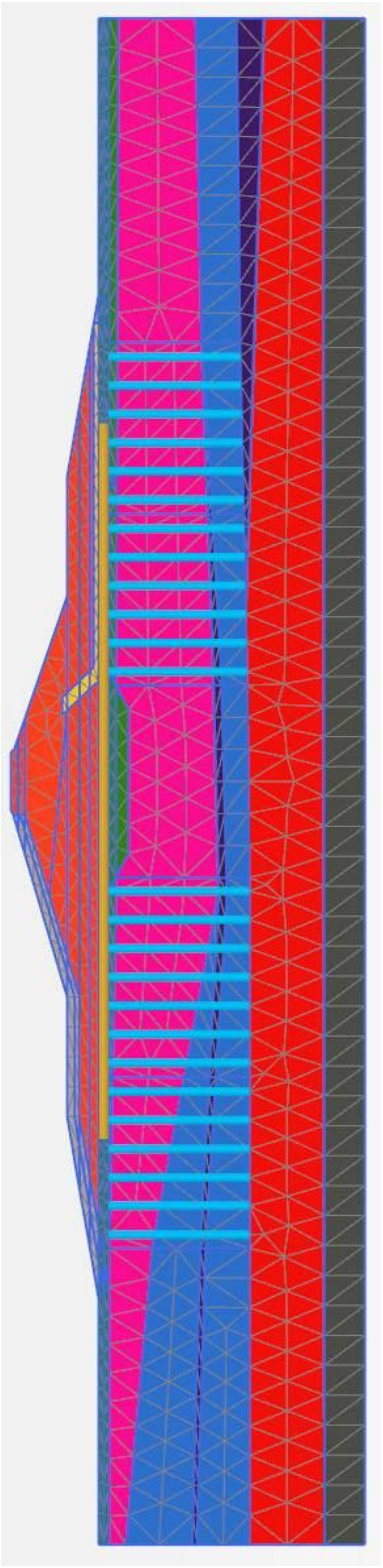

Figure VII.8 – Finite element mesh used on modeling the cross-section PK0+240 of Dike No.1

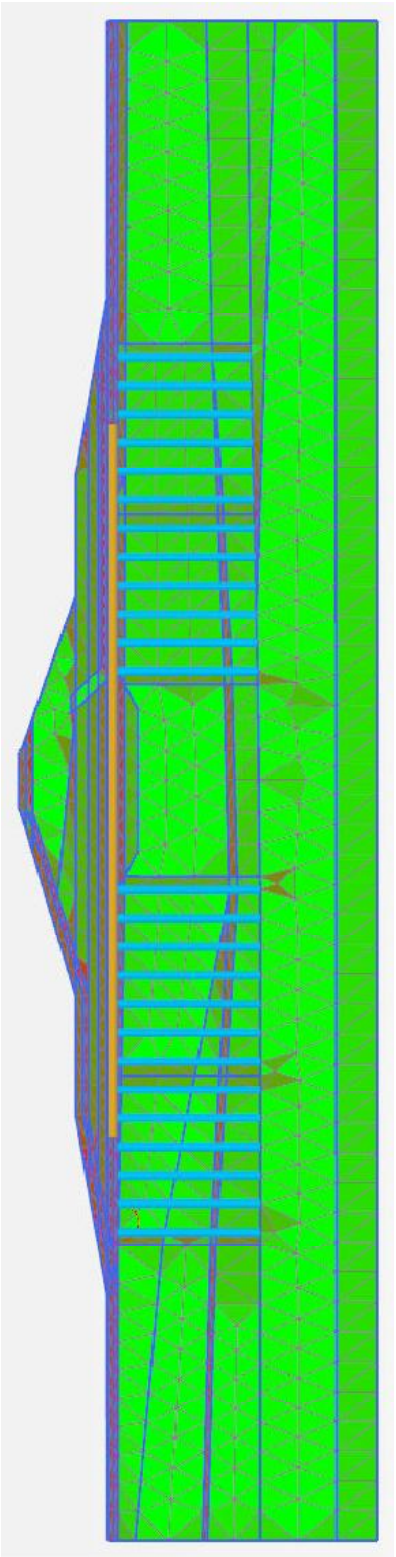

Figure VII.9 – Finite element mesh quality - cross-section PK0+240 of Dike No.1

VII.2.2. DEFINITION OF THE MATERIALS PROPERTIES

The soil properties requested by PLAXIS depend on the material models selected. For the materials used of the embankments of the dikes, rip-rap protection, chimney drain, horizontal downstream drain and drainage blanket, the Mohr-Coulomb model was applied. However, for the soil foundation, a first approached was made with the Mohr-Coulomb model, followed by the Soft Soil and Soft Soil Creep models.

All these models have already been presented in chapter III, and the Soft Soil Creep model is known to be the most suitable for soil with high compressibility, as it allows both the primary and secondary consolidation to be taken into consideration. Notwithstanding, a comparison between these models was performed, for the same conditions, in order to determine the main differences in the settlements and pore pressures results.

When considering the Mohr-Coulomb model, another extremely important step, is the choice of the drainage condition of the soil; this may vary between drained and undrained analysis. The drained behaviour is adequate for soils above the phreatic level, or which present a high drainage capacity even when saturated. Granular soil, such as gravel and sand, in general, presents high permeability and therefore meets these conditions. A drained analysis can also be performed on saturated clay soil, as long as the loads are applied gradually and slowly, allowing the soil to drain. With this type of analysis, excess pore pressures are not generated.

The undrained behaviour is very important in fine saturated soil, when the rate of loading is high, since its permeability is low and so the overloads are not transferred to the solid skeleton of the soil, but to the water trapped in the interstices. As a result, excess pore pressures are built up. In PLAXIS, the modelling of undrained behaviour may be done in three distinct schemes or methods, namely:

a) Undrained effective stress analysis with effective stiffness and strength parameters (Method A)
   In this case, the undrained calculation is performed as an effective stress analysis, since effective stiffness (E_{ref} ; ν) and effective strength (c ; φ') parameters are used. PLAXIS assumes a volumetric strain modulus for the water and for the soil and transforms the drained parameters (E_{ref} ; ν) into undrained (E_u ; ν_u). Therefore, any volumetric strain in the plastic phase will cause an excess pore pressure and consequently the pore pressure also increases. Similarly, if the resistance parameters are considered in effective stress (c' ; φ'), then the increase in the shear strength due to the excess pore pressure dissipation will also be taken into account. However, it is necessary to be careful with this method since the shear strength of the soil may be overestimated. In fact, the development of the pore pressure plays a crucial role in providing the right effective stress path that leads to failure at a realistic value of undrained shear strength; however, most soil models are not capable of providing the right effective stress path in undrained conditions. The pore pressures generated in the process may be inaccurate, and so they will produce a wrong undrained shear strength (c_u or S_u). The value which is considered for the Poisson coefficient (ν) should not exceed 0.35 (PLAXIS 2D-V11.02 Manual, 2012);

b) Undrained effective stress analysis with undrained strength parameters (Method B)
This hypothesis is often used for soft soils, once effective strength parameters are not available. In fact, in the presence of soft soil, the values resulting from the "in-situ" tests are measured in undrained conditions, therefore the parameters of c_u and S_u are directly obtained. So, this method uses the undrained strength parameters, although still applying the effective parameters for the soil stiffness (E_{ref} ; ν). As in method A, the undrained calculation is performed as an effective stress analysis, but in this case the undrained shear strength is an input parameter and not a calculated one. Therefore, there is no increase in the shear strength of the soil with the pore pressure dissipation, and consequently it is not adequate to consolidation analysis. Nevertheless, the excess pore pressure generated by the load increments continues to be calculated, but it may be highly inaccurate (PLAXIS 2D-V11.02 Manual, 2012);

c) Undrained total stress analysis with undrained parameters (Method C)
In this case, the undrained calculation is performed as a total stress analysis. All the parameters, both stiffness and strength, are considered undrained, i.e. (E_u ; ν_u ; c_u ; φ_u=0º). The Poisson coefficient allowed ranged between 0.495 and 0.499, as the exact value of 0.5 leads to singularity of the stiffness matrix. As is to be expected, this method does not allow the generation of excess pore pressures as it does not make the distinction between effective and total stress. Consequently, it does not take the increase in strength into consideration, and as the method B, it is not suitable for consolidation analysis (PLAXIS 2D-V11.02 Manual, 2012).

The values of the parameters considered in the simulations, according to the material models chosen for the different soils, are indicated below. Some of these parameters have already been presented in chapter VI, but new ones will appear, as is the case with the reference stiffness modulus E_{ref} from the Mohr-Coulomb mode, and the horizontal permeability coefficients in the improved zones with the band-shaped drains, for the plane strain analysis.

VII.2.2.1. SOILS USED ON DIKES NO.1 AND NO.3

Due to the high permeability of the rip-rap protection of the upstream slope, the downstream toe drain, the chimney filter, downstream horizontal drain and drainage blanket, the Mohr-Coulomb model was adopted. This model was also considered for the soil of the embankment, even though its permeability is much lower when compared to the others. These soils are common to both dikes and the values attributed to the parameters are indicated in Table VII.1.

Table VII.1 – Average soil parameters for the *Lebrija* Pond Dikes No.1 and No.3 (Justo, 2000a)

Soils	γ_h [kN/m^3]	γ_{sat} [kN/m^3]	k_h [m/day]	k_v [m/day]	e_0	ν	c' [kN/m^2]	φ' [º]	ψ [º]	E_{ref} [kN/m^2]	Model	Analysis
Embankment	16,7	18.1	$4.50x10^{-5}$	$9.00x10^{-6}$	0.953	0.35	47.6	20.2	0.0	28000	MC	D/UD
Rip-rap	17.6	20.6	$9.00x10^{2}$	$9.00x10^{2}$	0.454	0.30	0.1	40.0	10.0	10000	MC	D
Filters (sands)	17.0	20.0	$2.00x10^{1}$	$2.00x10^{1}$	0.569	0.30	0.1	35.0	5.0	20000	MC	D

MC - *Mohr-Coulomb*, D - Drained; UD - Undrained

VII.2.2.2. DRAINS AND GEOTEXTILE REINFORCEMENT

The drains are modelled with the "*Drain"* element available on PLAXIS. According to this software, they are considered as ideal drains, meaning they have a high discharge capacity and no associated diameter. Therefore, and in spite of the characteristics of the band-shaped drains presented in table VII.2, these will only be taken into consideration in the determination of the new horizontal permeability coefficients, for the area where they were installed.

Table VII.2 – *Colbonddrain CX1000* band-shaped drains characteristics (see Appendix II)

Soils	w [m]	t [m]	d_w [(i)] [m]	q_w [(ii)] [l/s]	$k_{geotextile}$ [(iii)] [m/s]
Drains	0.100	0.004	0.06621	0.14	0.07

(i) Equivalent drain diameter was calculated according to the Hansbo expression (1979), where $d_w=(w+y)*(2/\pi)$;
(ii) Drainage discharge capacity for a hydraulic gradient of 0.1;
(ii) Geotextile filter permeability of the band-shaped drain.

The *Stabilenka 1000* reinforcement geotextile, placed between the Dike No.1 embankment and the foundation, is an isotropic and elastoplastic "*Geogrid*" element, where EA defines the elastic stiffness of the geotextile and N the maximum tensile axial force that the geotextile withstands. In the present case, this element has the following characteristics (Table VII.3):

Table VII.3 – *Stabilenka 1000* geotextile characteristics (Justo, 2000a)

Soils	EA [kN/m]	N [kN/m]
Geotextile	8333	$10x10^3$

VII.2.2.3. SOIL FOUNDATION

The geotechnical characteristics of the soil foundation have already been given in chapter VI. However, as the Mohr-Coulomb model was used to simulate the behaviour of these soils, the effective Young modulus $E'=E_{ref}$ needs to be estimated. For the soil foundation of Dikes No.1 and No.3, only methods A and B were applied to the undrained analyses. Method C was not used since it does not calculate the pore pressure excess, nor considers the strength increment with the consolidation. This last situation also happens in the method B.

According to Justo *et al*. (2006), when adopting the method A of the Mohr-Coulomb model, i.e., considering undrained effective stress analysis with effective parameters, then the Young effective modulus (E_{ref}) may be estimated based on the relation:

$$E_{ref} = E' = 75.c_u \qquad \text{(VII.1)}$$

In addition to this hypothesis, it is also possible to estimate the Young effective modulus from the oedometer modulus (E_{oed}), as follows:

$$E_{ref} = E' = E_{oed}\frac{(1+\nu).(1-2\nu)}{(1-\nu)} \qquad \text{(VII.2)}$$

Considering the undrained effective stress analysis with undrained strength parameters and effective stiffness parameters (Method B), Justo *et al*. (2006) propose other empirical expression for estimating the Young effective modulus, which is:

$$E_{ref} = E' = 170.c_u \qquad \text{(VII.3)}$$

Still, in this model, and for methods A and B, two distinct analyses are conducted. Firstly, the undrained strength considered is the one obtained directly from the Vane-Test, but on a second analysis, the parameter in question is reduced according to the soils plasticity index (IP) (Jiménez *et al*., 1981). In this last case, the values considered are the ones indicated in tables VI.16 and VI.17 of chapter VI. Therefore, in terms of strength and stiffness, the parameters considered for the analysis with Mohr-Coulomb model, are summarised in tables VII.4 and VII.5 for Dike No.1 and tables VII.6 and VII.7 for Dike No.3.

Table VII.4 – Parameters and values considered for the soil foundation of Dike No.1, using *Mohr-Coulomb* model with method A, in the simulation analysis

Soils	γ_h [kN/m^3]	γ_{sat} [kN/m^3]	e_0	v	IP [%]	c_u [kN/m^2]	c_u*$^{(i)}$ [kN/m^2]	E_{ref}=75c_u [kN/m^2]	E_{ref}*=75c_u* [kN/m^2]	E_{ref}=f(Eoed) [kN/m^2]	c' [kN/m^2]	φ' [º]	K_0
B'	14.6	15.9	1.422	0.35	48.6	30.7	24.2	2303	1818	799	10.8	12.4	1.25
B1	----	17.4	1.508	0.35	34.3	18.1	15.4	1358	1158	819	13.8	23.3	0.60
B2	----	16.2	1.546	0.35	32.2	26.4	22.8	1980	1711	734	18.3	18.7	0.50
B3	----	18.4	1.558	0.35	29.2	39.3	34.7	2948	2600	789	11.8	16.7	0.50
C1+C2	----	17.1	1.175	0.33	35.4	68.2	57.8	5115	4333	------	41.2	18.1	0.65

(i) c_u*= c_u/Λ, where Λ is the reduction coefficient proposed by Jimenez, *et al.* (1981) (see Table VI.16).

Table VII.5 – Parameters and values considered for the soil foundation of Dike No.1, using *Mohr-Coulomb* model with method B, in the simulation analysis

Soils	γ_h [kN/m^3]	γ_{sat} [kN/m^3]	e_0	v	IP [%]	c_u [kN/m^2]	c_u*$^{(i)}$ [kN/m^2]	E_{ref} [kN/m^2]	E_{ref}* [kN/m^2]	φ_u [º]	K_0
B'	14.6	15.9	1.422	0.35	48.6	30.7	24.2	5219	4121	0.0	1.25
B1	----	17.4	1.508	0.35	34.3	18.1	15.4	3077	2624	0.0	0.60
B2	----	16.2	1.546	0.35	32.2	26.4	22.8	4488	3879	0.0	0.50
B3	----	18.4	1.558	0.35	29.2	39.3	34.7	6681	5894	0.0	0.50
C1+C2	----	17.1	1.175	0.33	35.4	68.2	57.8	11594	9821	0.0	0.65

(i) c_u*= c_u/Λ, where Λ is the reduction coefficient proposed by Jimenez, *et al.* (1981) (see Table VI.16).

Table VII.6 – Parameters and values considered for the soil foundation of Dike No.3, using *Mohr-Coulomb* model with method A, in the simulation analysis

Soils	γ_h [kN/m^3]	γ_{sat} [kN/m^3]	e_0	v	IP [%]	c_u [kN/m^2]	c_u*$^{(i)}$ [kN/m^2]	E_{ref}=75c_u [kN/m^2]	E_{ref}*=75c_u* [kN/m^2]	E_{ref}=f(Eoed) [kN/m^2]	c' [kN/m^2]	φ' [º]	K_0
B'	14.6	16.2	1.621	0.35	48.9	34.5	27.2	2588	2040	1475	11.8	19.3	1.00
B1	----	17.0	1.508	0.35	29.2	17.3	15.3	1298	1145	819	13.8	23.3	0.60
B2	----	16.2	1.521	0.35	41.3	21.3	17.4	1598	1308	477	18.3	18.7	0.60
B3	----	16.5	1.475	0.35	61.8	31.6	23.6	2370	1171	1568	11.8	16.7	0.70
C2	----	17.9	1.175	0.33	18.5	60.0	60.0	4500	4340	------	41.2	18.1	0.80

(i) c_u*= c_u/Λ, where Λ is the reduction coefficient proposed by Jimenez, *et al.* (1981) (see Table VI.17).

Table VII.7 – Parameters and values considered for the soil foundation of Dike No.3, using *Mohr-Coulomb* model with method B, in the simulation analysis

Soils	γ_h [kN/m^3]	γ_{sat} [kN/m^3]	e_0	v	IP [%]	c_u [kN/m^2]	c_u*[(i)] [kN/m^2]	E_{ref} [kN/m^2]	E_{ref}* [kN/m^2]	φ_u [º]	K_0
B'	14.6	16.2	1.621	0.35	48.9	34.5	27.2	5865	4625	0.0	1.00
B1	----	17.0	1.508	0.35	29.2	17.3	15.3	2941	2595	0.0	0.60
B2	----	16.2	1.521	0.35	41.3	21.3	17.4	3621	2965	0.0	0.60
B3	----	16.5	1.475	0.35	61.8	31.6	23.6	5372	4014	0.0	0.70
C2	----	17.9	1.175	0.33	18.5	60.0	60.0	10200	9838	0.0	0.80

(i) c_u*= c_u/Λ, where Λ is the reduction coefficient proposed by Jimenez, *et al.* (1981) (see Table VI.17).

Considering the Soft-Soil and Soft-Soil Creep models, the values for the parameters are those outlined in tables VII.8 and VII.9, respectively, for Dike No.1 and Dike No.3. The value of the secondary compressibility index determined based on the oedometer tests is very low, as it was already been mentioned in the previous chapter. Consequently, it was decided to test and compared them against the values proposed by Terzaghi *et al*., (1996), according to the relation $C_\alpha=\vartheta C_c=0.045C_c$.

Table VII.8 – Parameters and values considered for the soil foundation of Dike No.1, using *Soft Soil* and *Soft Soil Creep* models in the simulation analysis

Soils	γ_h [kN/m^3]	γ_{sat} [kN/m^3]	e_0	C_c	$C_s=C_r$	$C\alpha$[(i)]	v_{ur}	c' [kN/m^2]	φ' [º]	OCR	K_0
B'	14.6	15.9	1.422	0.544	0.148	0.02448	0.15	10.8	12.4	4.0	1.25
B1	----	17.4	1.508	0.748	0.132	0.03366	0.15	13.8	23.3	2.0	0.60
B2	----	16.2	1.546	0.641	0.125	0.02885	0.15	18.3	18.7	1.1	0.50
B3	----	18.4	1.558	0.473	0.121	0.02129	0.15	11.8	16.7	1.3	0.50

(i) Only for *Soft Soil Creep* model. According to Terzaghi *et al*. (1996), $C\alpha=\vartheta Cc=(0.04\pm 0.01)Cc$ for inorganic clays and silts. It was adopted $C_\alpha=\vartheta C_c= 0.045C_c$.

Table VII.9 – Parameters and values considered for the soil foundation of Dike No.3, using *Soft Soil* and *Soft Soil Creep* models in the simulation analysis

Soils	γ_h [kN/m^3]	γ_{sat} [kN/m^3]	e_0	C_c	$C_s=C_r$	$C\alpha$[(i)]	v_{ur}	c' [kN/m^2]	φ' [º]	OCR	K_0
B'	14.6	16.2	1.621	0.558	0.181	0.02511	0.15	11.8	19.3	3.7	1.00
B1	----	17.0	1.508	0.748	0.132	0.03366	0.15	13.8	23.3	2.0	0.60
B2	----	16.2	1.521	0.550	0.118	0.02475	0.15	18.3	18.7	1.0	0.60
B3	----	16.5	1.475	0.573	0.166	0.02579	0.15	11.8	16.7	2.0	0.70

(i) Only for *Soft Soil Creep* model. According to Terzaghi *et al*. (1996), $C\alpha=\vartheta Cc=(0.04\pm 0.01)Cc$ for inorganic clays and silts. It was adopted $C_\alpha=\vartheta C_c= 0.045C_c$.

With respect to the soil foundation permeability, two situations may occur. If the foundation was not improved with band-shaped drains, then the values will be those presented in tables VI.6 and VI.13 of chapter VI, for Dikes No.1 and No.3. In the areas where the band-shaped drains were installed, new horizontal permeability coefficients will be determined, taking in consideration the transition from an axisymmetric to a plane strain analysis, the smear effect and the limitation of the discharge capacity of the drains (hydraulic resistance).

The horizontal permeability coefficients in plane strain (K_{hPD}) were determined according to the Indraratna & Redana (1997) analytical solution, for three distinct scenarios, namely:

a) Considering smear and drain resistance, in both systems (axisymmetric and plane strain);
b) Not considering the smear diameter around the drain, in the plane strain geometry model, even though it was considered in axisymmetric, and drain hydraulic resistance in both systems (comparable to the solution of Hird *et al*. (1992);
c) Without considering the smear and without drain resistance;

allowing, for the first two scenarios listed above, the hypothesis of smear discriminated below:

a) $K_{hsAx}=0.10K_{h0}$ and $ds=2d_w$; $K_{hsAx}=0.10K_{h0}$ and $ds=3d_w$; $K_{hsAx}=0.10K_{h0}$ and $ds=4d_w$;
b) $K_{hsAx}=0.33K_{h0}$ and $ds=2d_w$; $K_{hsAx}=0.33K_{h0}$ and $ds=3d_w$; $K_{hsAx}=0.33K_{h0}$ and $ds=4d_w$;
c) $K_{hsAx}=0.66K_{h0}$ and $ds=2d_w$; $K_{hsAx}=0.66K_{h0}$ and $ds=3d_w$; $K_{hsAx}=0.66K_{h0}$ and $ds=4d_w$;

and considering that:

a) The drains characteristics are the ones defined in table VII.2;
b) The drains are placed in a triangular pattern: ($d_e=1.05S$), and spaced (S) of 2.0m in Dike No.3 and of 1.5m, 1.75m and 2.0m in Dike No.1;
c) The distance between the drains in plane strain analysis (S*) is always of 3.0m;
d) The geotextile filter permeability of the band-shaped drain is the one limiting the discharge capacity of the drains, thus $k_{wAx}=k_{geotextile}=0.07m/s$;
e) The drains permeability is the same in both systems, i.e., $k_{wAx}=k_{wPD}=0.07m/s$;
f) The horizontal permeability coefficient in the disturbed zone is equal, both in axisymmetric and in plane strain analysis ($k_{hsAx}=k_{hsPD}$);
g) The determination of b_s and b_w follows the same equivalence criterion between systems, therefore if $b_w=(B.d_w^2)/d_{and}^2$, then $b_s=(B.d_s^2)/d_e^2$;

then the values of K_{hPD} for Dike No.1, can be determined. These are indicated in tables VII.10 and VII.12. Looking at these results, it can be seen that:

a) The values obtained for the horizontal permeability coefficient K_{hPD} are very similar, whether considering the delimitation of the smear diameter (d_s) in both systems, or just in the axisymmetric state. The maximum difference is only of 4%, and in many cases varies between 0% and 2%. Therefore, due to the simplicity of modelling the improved zone of the dikes based on the second scenario, the same was adopted, without affecting significantly the final result of the simulations;

b) The ratio K_{hsPD}/K_{v0} is very low for K_{hsPD} =0.10K_{h0}, varying between 0.26 and 0.39, and very high for K_{hsPD} =0.66K_{h0}, as they range between 1.72 and 2.59. In an intermediate situation, i.e., for K_{hsPD} =0.33K_{h0}, this ratio is closer to the values proposed by several researchers, since they range from 0.78 to 1.17. According to them, as a general rule, the ratio K_{hs}/K_{v0} varies between 0.9 and 1.4 (see subchapter V.3);

c) Another important ratio is the one given between parameters K_{hPD} and K_{v0}. This is affected by a great variety of factors, as a consequence this relation suffers more significant fluctuations, as it is showed bellow:

K_{hsAx}=0.10K_{h0} and d_s=2d_w: S=1.5m $\Rightarrow$ 0.73 $\leq K_{hPD}/K_{v0} \leq$ 1.09;
S=1.75m $\Rightarrow$ 0.53 $\leq K_{hPD}/K_{v0} \leq$ 0.79;
S=2.0m $\Rightarrow$ 0.40 $\leq K_{hPD}/K_{v0} \leq$ 0.60;

K_{hsAx}=0.10K_{h0} and d_s=3d_w: S=1.5m $\Rightarrow$ 0.51 $\leq K_{hPD}/K_{v0} \leq$ 0.77;
S=1.75m $\Rightarrow$ 0.37 $\leq K_{hPD}/K_{v0} \leq$ 0.56;
S=2.0m $\Rightarrow$ 0.28 $\leq K_{hPD}/K_{v0} \leq$ 0.42;

K_{hsAx}=0.10K_{h0} and d_s=4d_w: S=1.5m $\Rightarrow$ 0.42 $\leq K_{hPD}/K_{v0} \leq$ 0.64;
S=1.75m $\Rightarrow$ 0.31 $\leq K_{hPD}/K_{v0} \leq$ 0.46;
S=2.0m $\Rightarrow$ 0.23 $\leq K_{hPD}/K_{v0} \leq$ 0.35;

K_{hsAx}=0.33K_{h0} and d_s=2d_w: S=1.5m $\Rightarrow$ 1.65 $\leq K_{hPD}/K_{v0} \leq$ 2.47;
S=1.75m $\Rightarrow$ 1.17 $\leq K_{hPD}/K_{v0} \leq$ 1.75;
S=2.0m $\Rightarrow$ 0.86 $\leq K_{hPD}/K_{v0} \leq$ 1.29;

K_{hsAx}=0.33K_{h0} and d_s=3d_w: S=1.5m $\Rightarrow$ 1.36 $\leq K_{hPD}/K_{v0} \leq$ 2.04;
S=1.75m $\Rightarrow$ 0.97 $\leq K_{hPD}/K_{v0} \leq$ 1.45;
S=2.0m $\Rightarrow$ 0.72 $\leq K_{hPD}/K_{v0} \leq$ 1.08;

K_{hsAx}=0.33K_{h0} and d_s=4d_w: S=1.5m $\Rightarrow$ 1.21 $\leq K_{hPD}/K_{v0} \leq$ 1.81;
S=1.75m $\Rightarrow$ 0.86 $\leq K_{hPD}/K_{v0} \leq$ 1.29;
S=2.0m $\Rightarrow$ 0.64 $\leq K_{hPD}/K_{v0} \leq$ 0.97;

K_{hsAx}=0.66K_{h0} and d_s=2d_w: S=1.5m $\Rightarrow$ 2.27 $\leq K_{hPD}/K_{v0} \leq$ 3.41;
S=1.75m $\Rightarrow$ 1.58$\leq K_{hPD}/K_{v0} \leq$ 2.37;
S=2.0m $\Rightarrow$ 1.16 $\leq K_{hPD}/K_{v0} \leq$ 1.74;

K_{hsAx}=0.66K_{h0} and d_s=3d_w: S=1.5m $\Rightarrow$ 2.11 $\leq K_{hPD}/K_{v0} \leq$ 3.17;
S=1.75m $\Rightarrow$ 1.48 $\leq K_{hPD}/K_{v0} \leq$ 2.22;
S=2.0m $\Rightarrow$ 1.09 $\leq K_{hPD}/K_{v0} \leq$ 1.63;

K_{hsAx}=0.66K_{h0} and d_s=4d_w: S=1.5m $\Rightarrow$ 2.01 $\leq K_{hPD}/K_{v0} \leq$ 3.02;
S=1.75m $\Rightarrow$ 1.41 $\leq K_{hPD}/K_{v0} \leq$ 2.12;
S=2.0m $\Rightarrow$ 1.04 $\leq K_{hPD}/K_{v0} \leq$ 1.56;

Table VII.10 – Dike No.1: Horizontal permeability coefficients in the improved area with drains (K_{hPD}), considering Indraratna & Redana (1997) analytical solution and K_{hsAx}= K_{hsPD} =0.10K_{h0}

	$K_{h0}=K_{hAx}$ [m/day]	K_{V0} [m/day]	$K_{hPD}^{(1)}$ [m/day]	$K_{hPD}^{(2)}$ [m/day]	$K_{hPD}^{(3)}$ [m/day]	$K_{hPD}^{(i)}/K_{h0}$			$K_{hPD}^{(i)}/K_{v0}$	$K_{hsPD}^{(i)}/K_{v0}$
						i=1	i=2	i=3	i=2	i=2
Soils	$K_{hsAx}=K_{hsPD}=0.10K_{h0}$; $d_s=2d_w$									
$B'_{(S=1.5m)}$	$6.06x10^{-5}$	$2.32x10^{-5}$	$1.66x10^{-5}$	$1.69x10^{-5}$	$6.05x10^{-5}$	0.27	0.28	1.00	0.73	0.26
$B1_{(S=1.5m)}$	$6.19x10^{-5}$	$1.58x10^{-5}$	$1.69x10^{-5}$	$1.73x10^{-5}$	$6.19x10^{-5}$	0.27	0.28	1.00	1.09	0.39
$B2_{(S=1.5m)}$	$1.04x10^{-4}$	$3.53x10^{-5}$	$2.85x10^{-5}$	$2.91x10^{-5}$	$1.04x10^{-4}$	0.27	0.28	1.00	0.83	0.30
$B3_{(S=1.5m)}$	$5.00x10^{-5}$	$1.29x10^{-5}$	$1.37x10^{-5}$	$1.40x10^{-5}$	$5.00x10^{-5}$	0.27	0.28	1.00	1.09	0.39
$B'_{(S=1.75m)}$	$6.06x10^{-5}$	$2.32x10^{-5}$	$1.20x10^{-5}$	$1.22x10^{-5}$	$4.18x10^{-5}$	0.20	0.20	0.69	0.53	0.26
$B1_{(S=1.75m)}$	$6.19x10^{-5}$	$1.58x10^{-5}$	$1.23x10^{-5}$	$1.25x10^{-5}$	$4.27x10^{-5}$	0.20	0.20	0.69	0.79	0.39
$B2_{(S=1.75m)}$	$1.04x10^{-4}$	$3.53x10^{-5}$	$2.07x10^{-5}$	$2.10x10^{-5}$	$7.20x10^{-5}$	0.20	0.20	0.69	0.60	0.30
$B3_{(S=1.75m)}$	$5.00x10^{-5}$	$1.29x10^{-5}$	$9.93x10^{-6}$	$1.01x10^{-5}$	$3.45x10^{-5}$	0.20	0.20	0.69	0.78	0.39
$B'_{(S=2.0m)}$	$6.06x10^{-5}$	$2.32x10^{-5}$	$9.10x10^{-6}$	$9.21x10^{-6}$	$3.04x10^{-5}$	0.15	0.15	0.50	0.40	0.26
$B1_{(S=2.0m))}$	$6.19x10^{-5}$	$1.58x10^{-5}$	$9.30x10^{-6}$	$9.42x10^{-6}$	$3.11x10^{-5}$	0.15	0.15	0.50	0.60	0.39
$B2_{(S=2.0m)}$	$1.04x10^{-4}$	$3.53x10^{-5}$	$1.57x10^{-5}$	$1.58x10^{-5}$	$5.24x10^{-5}$	0.15	0.15	0.50	0.45	0.30
$B3_{(S=2.0m)}$	$5.00x10^{-5}$	$1.29x10^{-5}$	$7.52x10^{-6}$	$7.61x10^{-6}$	$2.51x10^{-5}$	0.15	0.15	0.50	0.59	0.39
Soils	$K_{hsAx}=K_{hsPD}=0.10K_{h0}$; $d_s=3d_w$									
$B'_{(S=1.5m)}$	$6.06x10^{-5}$	$2.32x10^{-5}$	$1.13x10^{-5}$	$1.19x10^{-5}$	$6.05x10^{-5}$	0.19	0.20	1.00	0.51	0.26
$B1_{(S=1.5m)}$	$6.19x10^{-5}$	$1.58x10^{-5}$	$1.16x10^{-5}$	$1.22x10^{-5}$	$6.19x10^{-5}$	0.19	0.20	1.00	0.77	0.39
$B2_{(S=1.5m)}$	$1.04x10^{-4}$	$3.53x10^{-5}$	$1.95\ x10^{-5}$	$2.05\ x10^{-5}$	$1.04x10^{-4}$	0.19	0.20	1.00	0.58	0.30
$B3_{(S=1.5m)}$	$5.00x10^{-5}$	$1.29x10^{-5}$	$9.38x10^{-6}$	$9.83x10^{-6}$	$5.00x10^{-5}$	0.19	0.20	1.00	0.76	0.39
$B'_{(S=1.75m)}$	$6.06x10^{-5}$	$2.32x10^{-5}$	$8.34x10^{-6}$	$8.63x10^{-6}$	$4.18x10^{-5}$	0.14	0.14	0.69	0.37	0.26
$B1_{(S=1.75m)}$	$6.19x10^{-5}$	$1.58x10^{-5}$	$8.52x10^{-6}$	$8.83x10^{-6}$	$4.27x10^{-5}$	0.14	0.14	0.69	0.56	0.39
$B2_{(S=1.75m)}$	$1.04x10^{-4}$	$3.53x10^{-5}$	$1.43x10^{-5}$	$1.49x10^{-5}$	$7.20x10^{-5}$	0.14	0.14	0.69	0.42	0.30
$B3_{(S=1.75m)}$	$5.00x10^{-5}$	$1.29x10^{-5}$	$6.89x10^{-6}$	$7.13x10^{-6}$	$3.45x10^{-5}$	0.14	0.14	0.69	0.55	0.39
$B'_{(S=2.0m)}$	$6.06x10^{-5}$	$2.32x10^{-5}$	$6.37x10^{-6}$	$6.54x10^{-6}$	$3.04x10^{-5}$	0.11	0.11	0.50	0.28	0.26
$B1_{(S=2.0m))}$	$6.19x10^{-5}$	$1.58x10^{-5}$	$6.51x10^{-6}$	$6.69x10^{-6}$	$3.11x10^{-5}$	0.11	0.11	0.50	0.42	0.39
$B2_{(S=2.0m)}$	$1.04x10^{-4}$	$3.53x10^{-5}$	$1.10x10^{-5}$	$1.13x10^{-5}$	$5.24x10^{-5}$	0.11	0.11	0.50	0.32	0.30
$B3_{(S=2.0m)}$	$5.00x10^{-5}$	$1.29x10^{-5}$	$5.26x10^{-6}$	$5.40x10^{-6}$	$2.51x10^{-5}$	0.11	0.11	0.50	0.42	0.39
Soils	$K_{hsAx}=K_{hsPD}=0.10K_{h0}$; $d_s=4d_w$									
$B'_{(S=1.5m)}$	$6.06x10^{-5}$	$2.32x10^{-5}$	$9.04x10^{-6}$	$9.83x10^{-6}$	$6.05x10^{-5}$	0.15	0.16	1.00	0.42	0.26
$B1_{(S=1.5m)}$	$6.19x10^{-5}$	$1.58x10^{-5}$	$9.24x10^{-6}$	$1.01x10^{-5}$	$6.19x10^{-5}$	0.15	0.16	1.00	0.64	0.39
$B2_{(S=1.5m)}$	$1.04x10^{-4}$	$3.53x10^{-5}$	$1.56x10^{-5}$	$1.69x10^{-5}$	$1.04x10^{-4}$	0.15	0.16	1.00	0.48	0.30
$B3_{(S=1.5m)}$	$5.00x10^{-5}$	$1.29x10^{-5}$	$7.47x10^{-6}$	$8.12x10^{-6}$	$5.00x10^{-5}$	0.15	0.16	1.00	0.63	0.39
$B'_{(S=1.75m)}$	$6.06x10^{-5}$	$2.32x10^{-5}$	$6.72x10^{-6}$	$7.15x10^{-6}$	$4.18x10^{-5}$	0.11	0.12	0.69	0.31	0.26
$B1_{(S=1.75m)}$	$6.19x10^{-5}$	$1.58x10^{-5}$	$6.87x10^{-6}$	$7.31x10^{-6}$	$4.27x10^{-5}$	0.11	0.12	0.69	0.46	0.39
$B2_{(S=1.75m)}$	$1.04x10^{-4}$	$3.53x10^{-5}$	$1.16x10^{-5}$	$1.23x10^{-5}$	$7.20x10^{-5}$	0.11	0.12	0.69	0.35	0.30
$B3_{(S=1.75m)}$	$5.00x10^{-5}$	$1.29x10^{-5}$	$5.55x10^{-6}$	$5.91x10^{-6}$	$3.45x10^{-5}$	0.11	0.12	0.69	0.46	0.39
$B'_{(S=2.0m)}$	$6.06x10^{-5}$	$2.32x10^{-5}$	$5.17x10^{-6}$	$5.43x10^{-6}$	$3.04x10^{-5}$	0.09	0.09	0.50	0.23	0.26
$B1_{(S=2.0m))}$	$6.19x10^{-5}$	$1.58x10^{-5}$	$5.29x10^{-6}$	$5.55x10^{-6}$	$3.11x10^{-5}$	0.09	0.09	0.50	0.35	0.39
$B2_{(S=2.0m)}$	$1.04x10^{-4}$	$3.53x10^{-5}$	$8.90x10^{-6}$	$9.34x10^{-6}$	$5.24x10^{-5}$	0.09	0.09	0.50	0.26	0.30
$B3_{(S=2.0m)}$	$5.00x10^{-5}$	$1.29x10^{-5}$	$4.27x10^{-6}$	$4.48x10^{-6}$	$2.51x10^{-5}$	0.09	0.09	0.50	0.35	0.39

(1) Considering the smear diameter and reduced permeability on this zone, as well as drain resistance in both systems;

(2) There is no delimitation of smear in plane strain, even though it exists in axisymmetric, being considered drain resistance in both systems (comparable to the solution of Hird *et al*. (1992);

(3) Without considering smear and without drain resistance.

Table VII.11 – Dike No.1: Horizontal permeability coefficients in the improved area with drains (K_{hPD}), considering Indraratna & Redana (1997) analytical solution and K_{hsAx}= K_{hsPD} =0.33K_{h0}

	$K_{h0}=K_{hAx}$ [m/day]	K_{V0} [m/day]	$K_{hPD}^{(1)}$ [m/day]	$K_{hPD}^{(2)}$ [m/day]	$K_{hPD}^{(3)}$ [m/day]	$K_{hPD}^{(i)}/K_{h0}$			$K_{hPD}^{(i)}/K_{v0}$	$K_{hsPD}^{(i)}/K_{v0}$
						i=1	i=2	i=3	i=2	i=2
Soils	$K_{hsAx}=K_{hsPD}=0.33K_{h0}$; $d_s=2d_w$									
$B'_{(S=1.5m)}$	$6.06x10^{-5}$	$2.32x10^{-5}$	$3.75x10^{-5}$	$3.83x10^{-5}$	$6.05x10^{-5}$	0.62	0.63	1.00	1.65	0.78
$B1_{(S=1.5m)}$	$6.19x10^{-5}$	$1.58x10^{-5}$	$3.83x10^{-5}$	$3.91x10^{-5}$	$6.19x10^{-5}$	0.62	0.63	1.00	2.47	1.17
$B2_{(S=1.5m)}$	$1.04x10^{-4}$	$3.53x10^{-5}$	$6.45x10^{-5}$	$6.59x10^{-5}$	$1.04x10^{-4}$	0.62	0.63	1.00	1.87	0.89
$B3_{(S=1.5m)}$	$5.00x10^{-5}$	$1.29x10^{-5}$	$3.10x10^{-5}$	$3.16x10^{-5}$	$5.00x10^{-5}$	0.62	0.63	1.00	2.46	1.17
$B'_{(S=1.75m)}$	$6.06x10^{-5}$	$2.32x10^{-5}$	$2.66x10^{-5}$	$2.70x10^{-5}$	$4.18x10^{-5}$	0.44	0.45	0.69	1.17	0.78
$B1_{(S=1.75m)}$	$6.19x10^{-5}$	$1.58x10^{-5}$	$2.72x10^{-5}$	$2.76x10^{-5}$	$4.27x10^{-5}$	0.44	0.45	0.69	1.75	1.17
$B2_{(S=1.75m)}$	$1.04x10^{-4}$	$3.53x10^{-5}$	$4.58x10^{-5}$	$4.65x10^{-5}$	$7.20x10^{-5}$	0.44	0.45	0.69	1.32	0.89
$B3_{(S=1.75m)}$	$5.00x10^{-5}$	$1.29x10^{-5}$	$2.20x10^{-5}$	$2.23x10^{-5}$	$3.45x10^{-5}$	0.44	0.45	0.69	1.73	1.17
$B'_{(S=2.0m)}$	$6.06x10^{-5}$	$2.32x10^{-5}$	$1.98x10^{-5}$	$2.00x10^{-5}$	$3.04x10^{-5}$	0.33	0.33	0.50	0.86	0.78
$B1_{(S=2.0m))}$	$6.19x10^{-5}$	$1.58x10^{-5}$	$2.02x10^{-5}$	$2.05x10^{-5}$	$3.11x10^{-5}$	0.33	0.33	0.50	1.29	1.17
$B2_{(S=2.0m)}$	$1.04x10^{-4}$	$3.53x10^{-5}$	$3.40x10^{-5}$	$3.45x10^{-5}$	$5.24x10^{-5}$	0.33	0.33	0.50	0.98	0.89
$B3_{(S=2.0m)}$	$5.00x10^{-5}$	$1.29x10^{-5}$	$1.63x10^{-5}$	$1.65x10^{-5}$	$2.51x10^{-5}$	0.33	0.33	0.50	1.28	1.17
Soils	$K_{hsAx}=K_{hsPD}=0.33K_{h0}$; $d_s=3d_w$									
$B'_{(S=1.5m)}$	$6.06x10^{-5}$	$2.32x10^{-5}$	$3.00x10^{-5}$	$3.15x10^{-5}$	$6.05x10^{-5}$	0.50	0.52	1.00	1.36	0.78
$B1_{(S=1.5m)}$	$6.19x10^{-5}$	$1.58x10^{-5}$	$3.07x10^{-5}$	$3.22x10^{-5}$	$6.19x10^{-5}$	0.50	0.52	1.00	2.04	1.17
$B2_{(S=1.5m)}$	$1.04x10^{-4}$	$3.53x10^{-5}$	$5.17x10^{-5}$	$5.42x10^{-5}$	$1.04x10^{-4}$	0.50	0.52	1.00	1.54	0.89
$B3_{(S=1.5m)}$	$5.00x10^{-5}$	$1.29x10^{-5}$	$2.48x10^{-5}$	$2.60x10^{-5}$	$5.00x10^{-5}$	0.50	0.52	1.00	2.02	1.17
$B'_{(S=1.75m)}$	$6.06x10^{-5}$	$2.32x10^{-5}$	$2.16x10^{-5}$	$2.24x10^{-5}$	$4.18x10^{-5}$	0.36	0.37	0.69	0.97	0.78
$B1_{(S=1.75m)}$	$6.19x10^{-5}$	$1.58x10^{-5}$	$2.21x10^{-5}$	$2.29x10^{-5}$	$4.27x10^{-5}$	0.36	0.37	0.69	1.45	1.17
$B2_{(S=1.75m)}$	$1.04x10^{-4}$	$3.53x10^{-5}$	$3.72x10^{-5}$	$3.85x10^{-5}$	$7.20x10^{-5}$	0.36	0.37	0.69	1.09	0.89
$B3_{(S=1.75m)}$	$5.00x10^{-5}$	$1.29x10^{-5}$	$1.79x10^{-5}$	$1.85x10^{-5}$	$3.45x10^{-5}$	0.36	0.37	0.69	1.44	1.17
$B'_{(S=2.0m)}$	$6.06x10^{-5}$	$2.32x10^{-5}$	$1.62x10^{-5}$	$1.67x10^{-5}$	$3.04x10^{-5}$	0.27	0.28	0.50	0.72	0.78
$B1_{(S=2.0m))}$	$6.19x10^{-5}$	$1.58x10^{-5}$	$1.66x10^{-5}$	$1.71x10^{-5}$	$3.11x10^{-5}$	0.27	0.28	0.50	1.08	1.17
$B2_{(S=2.0m)}$	$1.04x10^{-4}$	$3.53x10^{-5}$	$2.80x10^{-5}$	$2.87x10^{-5}$	$5.24x10^{-5}$	0.27	0.28	0.50	0.81	0.89
$B3_{(S=2.0m)}$	$5.00x10^{-5}$	$1.29x10^{-5}$	$1.34x10^{-5}$	$1.38x10^{-5}$	$2.51x10^{-5}$	0.27	0.28	0.50	1.07	1.17
Soils	$K_{hsAx}=K_{hsPD}=0.33K_{h0}$; $d_s=4d_w$									
$B'_{(S=1.5m)}$	$6.06x10^{-5}$	$2.32x10^{-5}$	$2.57x10^{-5}$	$2.80x10^{-5}$	$6.05x10^{-5}$	0.42	0.46	1.00	1.21	0.78
$B1_{(S=1.5m)}$	$6.19x10^{-5}$	$1.58x10^{-5}$	$2.63x10^{-5}$	$2.86x10^{-5}$	$6.19x10^{-5}$	0.42	0.46	1.00	1.81	1.17
$B2_{(S=1.5m)}$	$1.04x10^{-4}$	$3.53x10^{-5}$	$4.44x10^{-5}$	$4.83x10^{-5}$	$1.04x10^{-4}$	0.43	0.46	1.00	1.37	0.89
$B3_{(S=1.5m)}$	$5.00x10^{-5}$	$1.29x10^{-5}$	$2.12x10^{-5}$	$2.31x10^{-5}$	$5.00x10^{-5}$	0.42	0.46	1.00	1.80	1.17
$B'_{(S=1.75m)}$	$6.06x10^{-5}$	$2.32x10^{-5}$	$1.88x10^{-5}$	$2.00x10^{-5}$	$4.18x10^{-5}$	0.31	0.33	0.69	0.86	0.78
$B1_{(S=1.75m)}$	$6.19x10^{-5}$	$1.58x10^{-5}$	$1.92x10^{-5}$	$2.04x10^{-5}$	$4.27x10^{-5}$	0.31	0.33	0.69	1.29	1.17
$B2_{(S=1.75m)}$	$1.04x10^{-4}$	$3.53x10^{-5}$	$3.24x10^{-5}$	$3.45x10^{-5}$	$7.20x10^{-5}$	0.31	0.33	0.69	0.98	0.89
$B3_{(S=1.75m)}$	$5.00x10^{-5}$	$1.29x10^{-5}$	$1.55x10^{-5}$	$1.65x10^{-5}$	$3.45x10^{-5}$	0.31	0.33	0.69	1.28	1.17
$B'_{(S=2.0m)}$	$6.06x10^{-5}$	$2.32x10^{-5}$	$1.42x10^{-5}$	$1.49x10^{-5}$	$3.04x10^{-5}$	0.23	0.25	0.50	0.64	0.78
$B1_{(S=2.0m))}$	$6.19x10^{-5}$	$1.58x10^{-5}$	$1.45x10^{-5}$	$1.53x10^{-5}$	$3.11x10^{-5}$	0.23	0.25	0.50	0.97	1.17
$B2_{(S=2.0m)}$	$1.04x10^{-4}$	$3.53x10^{-5}$	$2.46x10^{-5}$	$2.58x10^{-5}$	$5.24x10^{-5}$	0.24	0.25	0.50	0.73	0.89
$B3_{(S=2.0m)}$	$5.00x10^{-5}$	$1.29x10^{-5}$	$1.17x10^{-5}$	$1.23x10^{-5}$	$2.51x10^{-5}$	0.23	0.25	0.50	0.96	1.17

(1) Considering the smear diameter and reduced permeability on this zone, as well as drain resistance in both systems;

(2) There is no delimitation of smear in plane strain, even though it exists in axisymmetric, being considered drain resistance in both systems (comparable to the solution of Hird *et al*. (1992);

(3) Without considering smear and without drain resistance.

Table VII.12 – Dike No.1: Horizontal permeability coefficients in the improved area with drains (K_{hPD}), considering Indraratna & Redana (1997) analytical solution and K_{hsAx}= K_{hsPD} =0.66K_{h0}

	$K_{h0}=K_{hAx}$ [m/day]	K_{v0} [m/day]	$K_{hPD}^{(1)}$ [m/day]	$K_{hPD}^{(2)}$ [m/day]	$K_{hPD}^{(3)}$ [m/day]	$K_{hPD}^{(i)}/K_{h0}$ i=1	i=2	i=3	$K_{hPD}^{(i)}/K_{v0}$ i=2	$K_{hsPD}^{(i)}/K_{v0}$ i=2
Soils	$K_{hsAx}=K_{hsPD}=0.66K_{h0}$; $d_s=2d_w$									
$B'_{(S=1.5m)}$	$6.06x10^{-5}$	$2.32x10^{-5}$	$5.15x10^{-5}$	$5.27x10^{-5}$	$6.05x10^{-5}$	0.85	0.87	1.00	2.27	1.72
$B1_{(S=1.5m)}$	$6.19x10^{-5}$	$1.58x10^{-5}$	$5.28x10^{-5}$	$5.39x10^{-5}$	$6.19x10^{-5}$	0.85	0.87	1.00	3.41	2.59
$B2_{(S=1.5m)}$	$1.04x10^{-4}$	$3.53x10^{-5}$	$8.89x10^{-5}$	$9.08x10^{-5}$	$1.04x10^{-4}$	0.85	0.87	1.00	2.57	1.96
$B3_{(S=1.5m)}$	$5.00x10^{-5}$	$1.29x10^{-5}$	$4.27x10^{-5}$	$4.36x10^{-5}$	$5.00x10^{-5}$	0.85	0.87	1.00	3.38	2.56
$B'_{(S=1.75m)}$	$6.06x10^{-5}$	$2.32x10^{-5}$	$3.61x10^{-5}$	$3.67x10^{-5}$	$4.18x10^{-5}$	0.60	0.61	0.69	1.58	1.72
$B1_{(S=1.75m)}$	$6.19x10^{-5}$	$1.58x10^{-5}$	$3.70x10^{-5}$	$3.75x10^{-5}$	$4.27x10^{-5}$	0.60	0.61	0.69	2.37	2.59
$B2_{(S=1.75m)}$	$1.04x10^{-4}$	$3.53x10^{-5}$	$6.22x10^{-5}$	$6.32x10^{-5}$	$7.20x10^{-5}$	0.60	0.61	0.69	1.79	1.96
$B3_{(S=1.75m)}$	$5.00x10^{-5}$	$1.29x10^{-5}$	$2.99x10^{-5}$	$3.03x10^{-5}$	$3.45x10^{-5}$	0.60	0.61	0.69	2.36	2.56
$B'_{(S=2.0m)}$	$6.06x10^{-5}$	$2.32x10^{-5}$	$2.66x10^{-5}$	$2.69x10^{-5}$	$3.04x10^{-5}$	0.44	0.44	0.50	1.16	1.72
$B1_{(S=2.0m))}$	$6.19x10^{-5}$	$1.58x10^{-5}$	$2.72x10^{-5}$	$2.75x10^{-5}$	$3.11x10^{-5}$	0.44	0.44	0.50	1.74	2.59
$B2_{(S=2.0m)}$	$1.04x10^{-4}$	$3.53x10^{-5}$	$4.59x10^{-5}$	$4.64x10^{-5}$	$5.24x10^{-5}$	0.44	0.45	0.50	1.32	1.96
$B3_{(S=2.0m)}$	$5.00x10^{-5}$	$1.29x10^{-5}$	$2.19x10^{-5}$	$2.22x10^{-5}$	$2.51x10^{-5}$	0.44	0.44	0.50	1.73	2.56
Soils	$K_{hsAx}=K_{hsPD}=0.66K_{h0}$; $d_s=3d_w$									
$B'_{(S=1.5m)}$	$6.06x10^{-5}$	$2.32x10^{-5}$	$4.68x10^{-5}$	$4.91x10^{-5}$	$6.05x10^{-5}$	0.77	0.81	1.00	2.11	1.72
$B1_{(S=1.5m)}$	$6.19x10^{-5}$	$1.58x10^{-5}$	$4.78x10^{-5}$	$5.02x10^{-5}$	$6.19x10^{-5}$	0.77	0.81	1.00	3.17	2.59
$B2_{(S=1.5m)}$	$1.04x10^{-4}$	$3.53x10^{-5}$	$8.07x10^{-5}$	$8.47x10^{-5}$	$1.04x10^{-4}$	0.77	0.81	1.00	2.40	1.96
$B3_{(S=1.5m)}$	$5.00x10^{-5}$	$1.29x10^{-5}$	$3.86x10^{-5}$	$4.05x10^{-5}$	$5.00x10^{-5}$	0.77	0.81	1.00	3.15	2.56
$B'_{(S=1.75m)}$	$6.06x10^{-5}$	$2.32x10^{-5}$	$3.31x10^{-5}$	$3.43x10^{-5}$	$4.18x10^{-5}$	0.55	0.57	0.69	1.48	1.72
$B1_{(S=1.75m)}$	$6.19x10^{-5}$	$1.58x10^{-5}$	$3.38x10^{-5}$	$3.51x10^{-5}$	$4.27x10^{-5}$	0.55	0.57	0.69	2.22	2.59
$B2_{(S=1.75m)}$	$1.04x10^{-4}$	$3.53x10^{-5}$	$5.71x10^{-5}$	$5.92x10^{-5}$	$7.20x10^{-5}$	0.55	0.57	0.69	1.68	1.96
$B3_{(S=1.75m)}$	$5.00x10^{-5}$	$1.29x10^{-5}$	$2.73x10^{-5}$	$2.83x10^{-5}$	$3.45x10^{-5}$	0.55	0.57	0.69	2.20	2.56
$B'_{(S=2.0m)}$	$6.06x10^{-5}$	$2.32x10^{-5}$	$2.45x10^{-5}$	$2.52x10^{-5}$	$3.04x10^{-5}$	0.40	0.42	0.50	1.09	1.72
$B1_{(S=2.0m))}$	$6.19x10^{-5}$	$1.58x10^{-5}$	$2.51x10^{-5}$	$2.57x10^{-5}$	$3.11x10^{-5}$	0.40	0.42	0.50	1.63	2.59
$B2_{(S=2.0m)}$	$1.04x10^{-4}$	$3.53x10^{-5}$	$4.23x10^{-5}$	$4.34x10^{-5}$	$5.24x10^{-5}$	0.41	0.42	0.50	1.23	1.96
$B3_{(S=2.0m)}$	$5.00x10^{-5}$	$1.29x10^{-5}$	$2.02x10^{-5}$	$2.08x10^{-5}$	$2.51x10^{-5}$	0.40	0.42	0.50	1.61	2.56
Soils	$K_{hsAx}=K_{hsPD}=0.66K_{h0}$; $d_s=4d_w$									
$B'_{(S=1.5m)}$	$6.06x10^{-5}$	$2.32x10^{-5}$	$4.29x10^{-5}$	$4.67x10^{-5}$	$6.05x10^{-5}$	0.71	0.77	1.00	2.01	1.72
$B1_{(S=1.5m)}$	$6.19x10^{-5}$	$1.58x10^{-5}$	$4.39x10^{-5}$	$4.78x10^{-5}$	$6.19x10^{-5}$	0.71	0.77	1.00	3.02	2.59
$B2_{(S=1.5m)}$	$1.04x10^{-4}$	$3.53x10^{-5}$	$7.41x10^{-5}$	$8.07x10^{-5}$	$1.04x10^{-4}$	0.71	0.77	1.00	2.29	1.96
$B3_{(S=1.5m)}$	$5.00x10^{-5}$	$1.29x10^{-5}$	$3.55x10^{-5}$	$3.86x10^{-5}$	$5.00x10^{-5}$	0.71	0.77	1.00	3.00	2.56
$B'_{(S=1.75m)}$	$6.06x10^{-5}$	$2.32x10^{-5}$	$3.07x10^{-5}$	$3.27x10^{-5}$	$4.18x10^{-5}$	0.51	0.54	0.69	1.41	1.72
$B1_{(S=1.75m)}$	$6.19x10^{-5}$	$1.58x10^{-5}$	$3.14x10^{-5}$	$3.35x10^{-5}$	$4.27x10^{-5}$	0.51	0.54	0.69	2.12	2.59
$B2_{(S=1.75m)}$	$1.04x10^{-4}$	$3.53x10^{-5}$	$5.31x10^{-5}$	$5.65x10^{-5}$	$7.20x10^{-5}$	0.51	0.54	0.69	1.60	1.96
$B3_{(S=1.75m)}$	$5.00x10^{-5}$	$1.29x10^{-5}$	$2.54x10^{-5}$	$2.70x10^{-5}$	$3.45x10^{-5}$	0.51	0.54	0.69	2.10	2.56
$B'_{(S=2.0m)}$	$6.06x10^{-5}$	$2.32x10^{-5}$	$2.30x10^{-5}$	$2.41x10^{-5}$	$3.04x10^{-5}$	0.38	0.40	0.50	1.04	1.72
$B1_{(S=2.0m))}$	$6.19x10^{-5}$	$1.58x10^{-5}$	$2.35x10^{-5}$	$2.46x10^{-5}$	$3.11x10^{-5}$	0.38	0.40	0.50	1.56	2.59
$B2_{(S=2.0m)}$	$1.04x10^{-4}$	$3.53x10^{-5}$	$3.96x10^{-5}$	$4.16x10^{-5}$	$5.24x10^{-5}$	0.38	0.40	0.50	1.18	1.96
$B3_{(S=2.0m)}$	$5.00x10^{-5}$	$1.29x10^{-5}$	$1.90x10^{-5}$	$1.99x10^{-5}$	$2.51x10^{-5}$	0.38	0.40	0.50	1.55	2.56

(1) Considering the smear diameter and reduced permeability on this zone, as well as drain resistance in both systems;
(2) There is no delimitation of smear in plane strain, even though it exists in axisymmetric, being considered drain resistance in both systems (comparable to the solution of Hird *et al*. (1992);
(3) Without considering smear and without drain resistance.

In light of results and observations mentioned for Dike No.1, concerning this issue, it was decided to reduce the scenarios for Dike No.3. In this case, the horizontal permeability coefficients in plane strain (K_{hPD}) were determined according to the Indraratna & Redana (1997) analytical solution, only for the scenarios:

a) Not considering the smear diameter around the drain, in the plane strain geometry model, even though it was considered in axisymmetric, and drain hydraulic resistance in both systems (comparable to the solution of Hird *et al*. (1992);

b) Without considering smear and without drain resistance.

The remaining conditions are the same for Dike No.3, with the results of K_{hPD} being indicated in tables VII.13 and VII.15. Analysing the values obtained, it can be seen:

a) For B' and B1 soils, the ratio K_{hsPD}/K_{v0} is very low for K_{hsPD} =0.10K_{h0}, ranging between 0.28 and 0.39, and very high for K_{hsPD} =0.66K_{h0}, as it varies from 1.82 to 2.58. For K_{hsPD}=0.33K_{h0} the results obtained are comprehended between 0.91 and 1.29. These results are identical to those found for Dike No.1; however there is an exception for the B2 soil, as the value for the ratio K_{hsPD}/K_{v0} range from 0.97 to 6.41. This is due to the fact that ratio K_{h0}/K_{v0} for this soils, is approximately three times greater than the others (see Table VI.13 of chapter VI);

b) For the ratio K_{hPD}/K_{v0} the soil B2 presents, once more, bigger results than the others. For soils B' and B1 the values are similar to those obtained for Dike No.1, being:

K_{hsAx}=0.10K_{h0} and d_s=2d_w: B' and B1 $\Rightarrow$ 0.42 $\leq K_{hPD}/K_{v0} \leq$ 0.60; B2 $\Rightarrow K_{hPD}/K_{v0}$=1.48;

K_{hsAx}=0.10K_{h0} and d_s=3d_w: B' and B1 $\Rightarrow$ 0.30 $\leq K_{hPD}/K_{v0} \leq$ 0.42; B2 $\Rightarrow K_{hPD}/K_{v0}$=1.05;

K_{hsAx}=0.10K_{h0} and d_s=4d_w: B' and B1 $\Rightarrow$ 0.25 $\leq K_{hPD}/K_{v0} \leq$ 0.35; B2 $\Rightarrow K_{hPD}/K_{v0}$=0.87;

K_{hsAx}=0.33K_{h0} and d_s=2d_w: B' and B1 $\Rightarrow$ 0.91 $\leq K_{hPD}/K_{v0} \leq$ 1.29; B2 $\Rightarrow K_{hPD}/K_{v0}$=3.21;

K_{hsAx}=0.33K_{h0} and d_s=3d_w: B' and B1 $\Rightarrow$ 0.76 $\leq K_{hPD}/K_{v0} \leq$ 1.08; B2 $\Rightarrow K_{hPD}/K_{v0}$=2.68;

K_{hsAx}=0.33K_{h0} and d_s=4d_w: B' and B1 $\Rightarrow$ 0.68 $\leq K_{hPD}/K_{v0} \leq$ 0.96; B2 $\Rightarrow K_{hPD}/K_{v0}$=2.39;

K_{hsAx}=0.66K_{h0} and d_s=2d_w: B' and B1 $\Rightarrow$ 1.22 $\leq K_{hPD}/K_{v0} \leq$ 1.74; B2 $\Rightarrow K_{hPD}/K_{v0}$=4.31;

K_{hsAx}=0.66K_{h0} and d_s=3d_w: B' and B1 $\Rightarrow$ 1.15 $\leq K_{hPD}/K_{v0} \leq$ 1.63; B2 $\Rightarrow K_{hPD}/K_{v0}$=4.04;

K_{hsAx}=0.66K_{h0} and d_s=4d_w: B' and B1 $\Rightarrow$ 1.10 $\leq K_{hPD}/K_{v0} \leq$ 1.56; B2 $\Rightarrow K_{hPD}/K_{v0}$=3.86.

Of all the smear possibilities studied, and based on the ratios presented, it can be immediately point it out that the influence of reducing the horizontal permeability coefficient in the smear zone is greater than the increment of the smear diameter, as it was already been seen in the analyses performed in subchapter V.4. In addition to this, the new horizontal permeability coefficients for the plane strain (K_{hPD}) analysis, in the improved zone with drains, are very low when K_{hsPD}=0.10K_{h0} and very high for K_{hsPD}=0.66K_{h0}. According to the suggestions made by various researchers, the situation which would be, probably, the most appropriate, is the one which corresponds to the scenario where K_{hsPD}=0.33K_{h0}. However, this conclusion can only be drawn after observing the results from the numerical simulations.

Table VII.13 – Dike No.3: Horizontal permeability coefficients in the improved area with drains (K_{hPD}), considering Indraratna & Redana (1997) analytical solution and K_{hsAx}= K_{hsPD} =0.10K_{h0}

	$K_{h0}=K_{hAx}$ [m/day]	K_{V0} [m/day]	$K_{hPD}^{(2)}$ [m/day]	$K_{hPD}^{(3)}$ [m/day]	$K_{hPD}^{(i)}/K_{h0}$ i=2	$K_{hPD}^{(i)}/K_{h0}$ i=3	$K_{hPD}^{(i)}/K_{v0}$ i=2	$K_{hsPD}^{(i)}/K_{v0}$ i=2
Soils	$K_{hsAx}=K_{hsPD}=0.10K_{h0}$; $d_s=2d_w$							
B'$_{(S=2.0m)}$	4.31×10^{-5}	1.56×10^{-5}	6.55×10^{-6}	2.17×10^{-5}	0.15	0.50	0.42	0.28
B1$_{(S=2.0m))}$	6.19×10^{-5}	1.58×10^{-5}	9.42×10^{-6}	3.11×10^{-5}	0.15	0.50	0.60	0.39
B2$_{(S=2.0m)}$	1.49×10^{-4}	1.54×10^{-5}	2.27×10^{-5}	7.51×10^{-5}	0.15	0.50	1.48	0.97
Soils	$K_{hsAx}=K_{hsPD}=0.10K_{h0}$; $d_s=3d_w$							
B'$_{(S=2.0m)}$	4.31×10^{-5}	1.56×10^{-5}	4.65×10^{-6}	2.17×10^{-5}	0.11	0.50	0.30	0.28
B1$_{(S=2.0m))}$	6.19×10^{-5}	1.58×10^{-5}	6.69×10^{-6}	3.11×10^{-5}	0.11	0.50	0.42	0.39
B2$_{(S=2.0m)}$	1.49×10^{-4}	1.54×10^{-5}	1.61×10^{-5}	7.51×10^{-5}	0.11	0.50	1.05	0.97
Soils	$K_{hsAx}=K_{hsPD}=0.10K_{h0}$; $d_s=4d_w$							
B'$_{(S=2.0m)}$	4.31×10^{-5}	1.56×10^{-5}	3.86×10^{-6}	2.17×10^{-5}	0.09	0.50	0.25	0.28
B1$_{(S=2.0m))}$	6.19×10^{-5}	1.58×10^{-5}	5.55×10^{-6}	3.11×10^{-5}	0.09	0.50	0.35	0.39
B2$_{(S=2.0m)}$	1.49×10^{-4}	1.54×10^{-5}	1.34×10^{-5}	7.51×10^{-5}	0.09	0.50	0.87	0.97

(2) There is no delimitation of smear in plane strain, even though it exists in axisymmetric, being considered drain resistance in both systems (comparable to the solution of Hird *et al*. (1992);

(3) Without considering smear and without drain resistance.

Table VII.14 – Dike No.3: Horizontal permeability coefficients in the improved area with drains (K_{hPD}), considering Indraratna & Redana (1997) analytical solution and K_{hsAx}= K_{hsPD} =0.33K_{h0}

	$K_{h0}=K_{hAx}$ [m/day]	K_{V0} [m/day]	$K_{hPD}^{(2)}$ [m/day]	$K_{hPD}^{(3)}$ [m/day]	$K_{hPD}^{(i)}/K_{h0}$ i=2	$K_{hPD}^{(i)}/K_{h0}$ i=3	$K_{hPD}^{(i)}/K_{v0}$ i=2	$K_{hsPD}^{(i)}/K_{v0}$ i=2
Soils	$K_{hsAx}=K_{hsPD}=0.33K_{h0}$; $d_s=2d_w$							
B'$_{(S=2.0m)}$	4.31×10^{-5}	1.56×10^{-5}	1.42×10^{-6}	2.17×10^{-5}	0.33	0.50	0.91	0.91
B1$_{(S=2.0m))}$	6.19×10^{-5}	1.58×10^{-5}	2.05×10^{-6}	3.11×10^{-5}	0.33	0.50	1.29	1.29
B2$_{(S=2.0m)}$	1.49×10^{-4}	1.54×10^{-5}	4.94×10^{-5}	7.51×10^{-5}	0.33	0.50	3.21	3.21
Soils	$K_{hsAx}=K_{hsPD}=0.33K_{h0}$; $d_s=3d_w$							
B'$_{(S=2.0m)}$	4.31×10^{-5}	1.56×10^{-5}	1.19×10^{-6}	2.17×10^{-5}	0.28	0.50	0.76	0.91
B1$_{(S=2.0m))}$	6.19×10^{-5}	1.58×10^{-5}	1.71×10^{-6}	3.11×10^{-5}	0.28	0.50	1.08	1.29
B2$_{(S=2.0m)}$	1.49×10^{-4}	1.54×10^{-5}	4.12×10^{-5}	7.51×10^{-5}	0.28	0.50	2.68	3.21
Soils	$K_{hsAx}=K_{hsPD}=0.33K_{h0}$; $d_s=4d_w$							
B'$_{(S=2.0m)}$	4.31×10^{-5}	1.56×10^{-5}	1.06×10^{-6}	2.17×10^{-5}	0.25	0.50	0.68	0.91
B1$_{(S=2.0m))}$	6.19×10^{-5}	1.58×10^{-5}	1.53×10^{-6}	3.11×10^{-5}	0.25	0.50	0.96	1.29
B2$_{(S=2.0m)}$	1.49×10^{-4}	1.54×10^{-5}	3.68×10^{-5}	7.51×10^{-5}	0.25	0.50	2.39	3.21

(2) There is no delimitation of smear in plane strain, even though it exists in axisymmetric, being considered drain resistance in both systems (comparable to the solution of Hird *et al*. (1992);

(3) Without considering smear and without drain resistance.

Table VII.15 – Dike No.3: Horizontal permeability coefficients in the improved area with drains (K_{hPD}), considering Indraratna & Redana (1997) solution and K_{hsAx}= K_{hsPD} =0.66K_{h0}

	$K_{h0}=K_{hAx}$ [m/day]	K_{V0} [m/day]	$K_{hPD}^{(2)}$ [m/day]	$K_{hPD}^{(3)}$ [m/day]	$K_{hPD}^{(i)}/K_{h0}$ i=2	$K_{hPD}^{(i)}/K_{h0}$ i=3	$K_{hPD}^{(i)}/K_{v0}$ i=2	$K_{hsPD}^{(i)}/K_{v0}$ i=2
Soils	$K_{hsAx}=K_{hsPD}=0.66K_{h0}$; $d_s=2d_w$							
B'$_{(S=2.0m)}$	4.31×10^{-5}	1.56×10^{-5}	1.91×10^{-6}	2.17×10^{-5}	0.44	0.50	1.22	1.82
B1$_{(S=2.0m))}$	6.19×10^{-5}	1.58×10^{-5}	2.75×10^{-6}	3.11×10^{-5}	0.44	0.50	1.74	2.58
B2$_{(S=2.0m)}$	1.49×10^{-4}	1.54×10^{-5}	6.63×10^{-5}	7.51×10^{-5}	0.44	0.50	4.31	6.41
Soils	$K_{hsAx}=K_{hsPD}=0.66K_{h0}$; $d_s=3d_w$							
B'$_{(S=2.0m)}$	4.31×10^{-5}	1.56×10^{-5}	1.79×10^{-6}	2.17×10^{-5}	0.42	0.50	1.15	1.82
B1$_{(S=2.0m))}$	6.19×10^{-5}	1.58×10^{-5}	2.57×10^{-6}	3.11×10^{-5}	0.42	0.50	1.63	2.58
B2$_{(S=2.0m)}$	1.49×10^{-4}	1.54×10^{-5}	6.21×10^{-5}	7.51×10^{-5}	0.42	0.50	4.04	6.41
Soils	$K_{hsAx}=K_{hsPD}=0.66K_{h0}$; $d_s=4d_w$							
B'$_{(S=2.0m)}$	4.31×10^{-5}	1.56×10^{-5}	1.71×10^{-6}	2.17×10^{-5}	0.40	0.50	1.10	1.82
B1$_{(S=2.0m))}$	6.19×10^{-5}	1.58×10^{-5}	2.46×10^{-6}	3.11×10^{-5}	0.40	0.50	1.56	2.58
B2$_{(S=2.0m)}$	1.49×10^{-4}	1.54×10^{-5}	5.94×10^{-5}	7.51×10^{-5}	0.40	0.50	3.86	6.41

(2) There is no delimitation of smear in plane strain, even though it exists in axisymmetric, being considered drain resistance in both systems (comparable to the solution of Hird *et al*. (1992);

(3) Without considering smear and without drain resistance.

VII.2.3. DEFINITION OF THE INITIAL STRESS STATE AND INITIAL HYDROSTATIC PRESSURES

The initial stress state and the initial hydrostatic pressures are generated in the first step of the calculation procedure, with no time being associated to it. For the case studied, the initial vertical and horizontal stresses are calculated based on the lateral earth pressure coefficient at rest (K0 procedure). In this phase, the geometry of the model corresponds only to the initial ground level and to the soil layers of the foundation, as can be seen in figure VII.10. Simultaneously with the definition of the initial stress state, the initial hydrostatic pressures must be also generated (Generate by phreatic level). For the latter step, the initial water table is defined, as well as the boundary conditions associated to permeability (Figure VII.12). Figures VII.11 and VII.13 represents the total stresses (σ_0) and the initial hydrostatic pressures (u_0) for section PK0+240 of Dike No.1. For profiles PK0+140, Pk0+170, PK0+180 and PK0+200 of Dike No.3, the same procedure was performed. The effective stresses are calculated by Terzaghi's expressions for saturated soils ($\sigma'=\sigma- u$).

After this initial procedure, the following calculation steps are defined according to the construction rate and phases, being also necessary to indicate the timeline associated to the installation of the instrumentation, as well as their level and starting date of readings, and finally the raise up of the water level in the pond. However, between the K0 procedure and the subsequent steps, a plastic "*Nil-step*" calculation is advisable, in order to re-establish the equilibrium of the field stress, and then all stresses will obey the failure condition. In this phase, no additional load is applied, and time is only necessary for the Soft Soil Creep model, although very small. The geometry remains identical to the initial situation, as does the position of the water table, and the plastic calculation option should be considered (Plastic calculation).

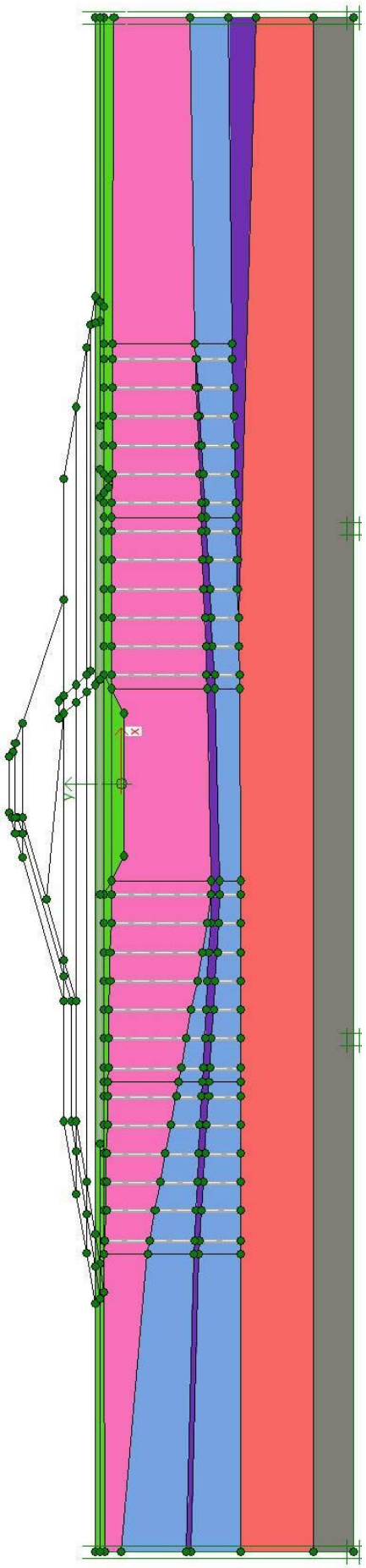

Figure VII.10 – Geometry used on the generation of the initial stress state - PK0+240 of Dike No.1

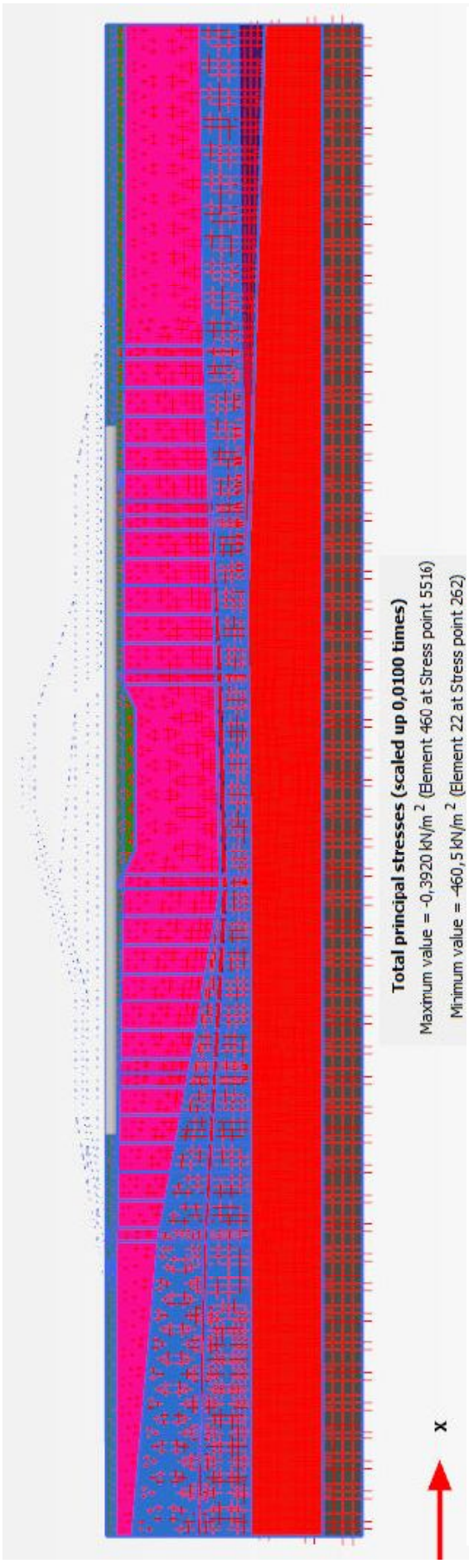

Figure VII.11 – Initial horizontal and vertical stresses on PK0+240 of Dike No.1

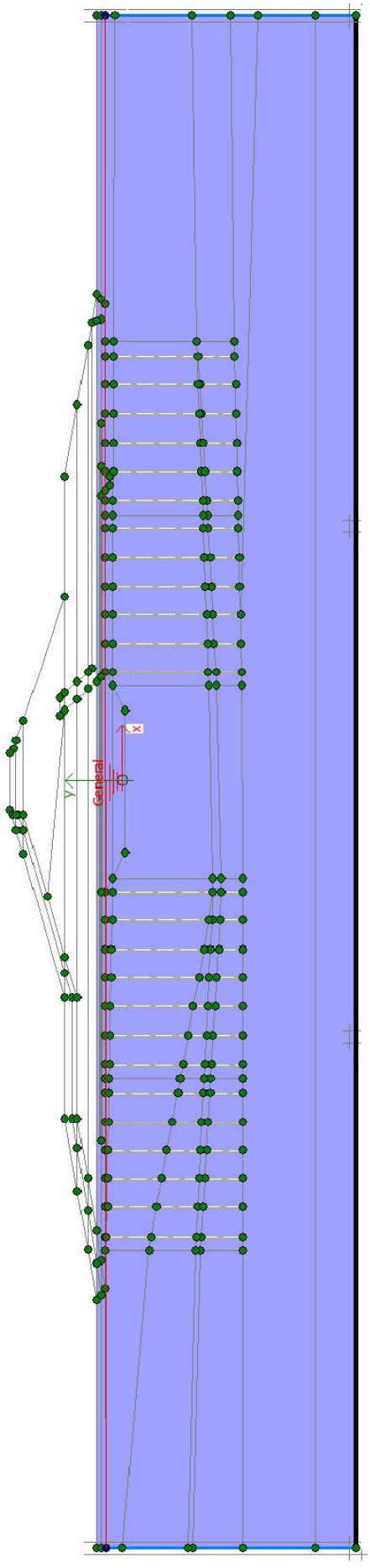

Figure VII.12 – Initial position of the water table on the ground foundation - PK0+240 of Dike No.1

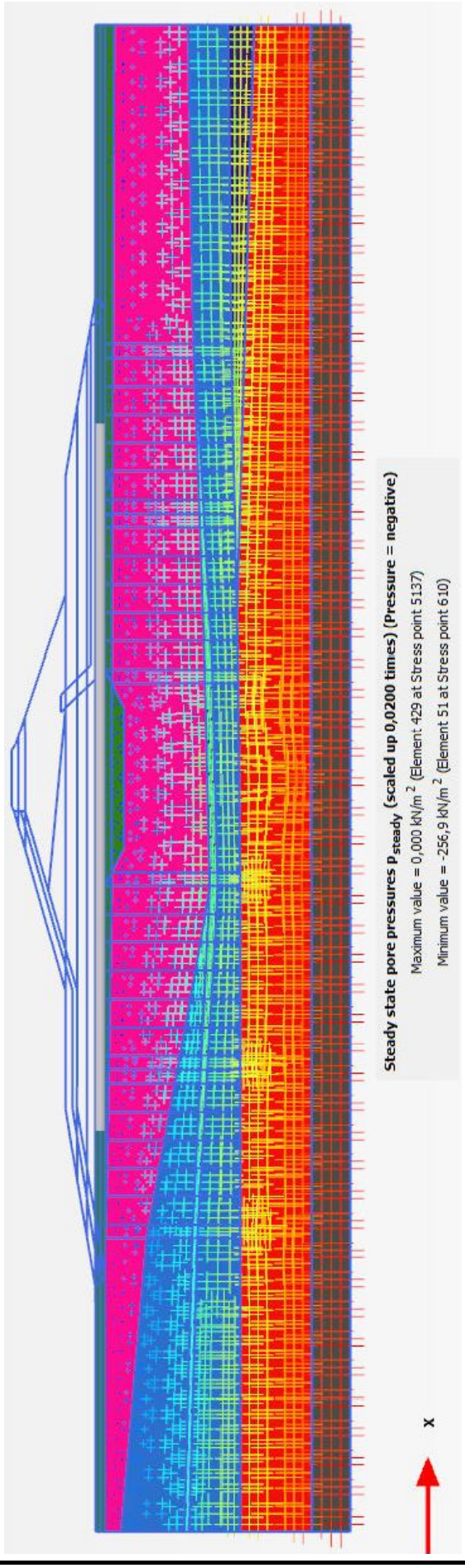

Figure VII.13 – Initial pore pressures on PK0+240 of Dike No.1

VII.2.4. DEFINITION OF THE CONSTRUCTION STAGES

Once the initial conditions of the problem are generated, and the "*nil-step*" performed, the displacements are set to zero. From this moment on, all the stages associated with to the case study can be discriminated, including:

a) Ground excavation;

b) Cut-off compaction;

c) Activation of the band-shaped drains and modification of the horizontal permeability coefficients in the zones where the drains are installed (when applicable);

d) Activation of the geotextile reinforcement (when applicable);

e) Application of all monitoring devices associated with each cross-section;

f) Embankment compaction over time;

g) Rising of reservoir water level over time.

In all these phases, the time associated to each step must be indicated, since the consolidation phenomenon of the soil is in question (Consolidation). The chronological order of construction and the timelines associated to each steps were defined previously in subchapter VI.5. So, it is advisable to consult table VI.29 for the cross-section PK0+240 of Dike No.1, and tables VI.30 to VI.33 for the four cross-sections of Dike No.3. It should be remembered that, in addition to the properties of the material and the geometry, the correct definition of the construction stages and their chronological order, is also fundamental to achieve good results on the simulations analysis. Some of these phases are represented in figures VII.14 to VII.21 for section PK0+240 of Dike No.1. The procedure for the other three profiles of Dike No.3 is identical to that listed for Dike No.1 with the exception of the activation of the geotextile reinforcement. In addition to this, the section Pk0+200 of Dike No.3 have no drains installed on the ground foundation.

In addition to the consolidation analyses, the safety factors correspondent to the conclusion of the dikes constructions, and to the last readings of the monitoring devices, after the water in the reservoir stabilised at level 7.80m. These calculations were only performed after the consolidation analyses were concluded, and to perform it, a new step was created, being chosen the option "Safety".

Since this is a geotechnical problem facing extremely high displacements, then the finite element mesh is updated at the end of each calculation stage (Update mesh), as is the water pressure (Update water pressure).

When not flow is not considered, the pore pressures are determined based on the position of the water level at each stage, considering also the excess pore pressure associated to the surcharge of the embankment dike, for the saturated clayed and silty soils. The pressures calculated at each new step take into account the previous values (From previous calculated step).

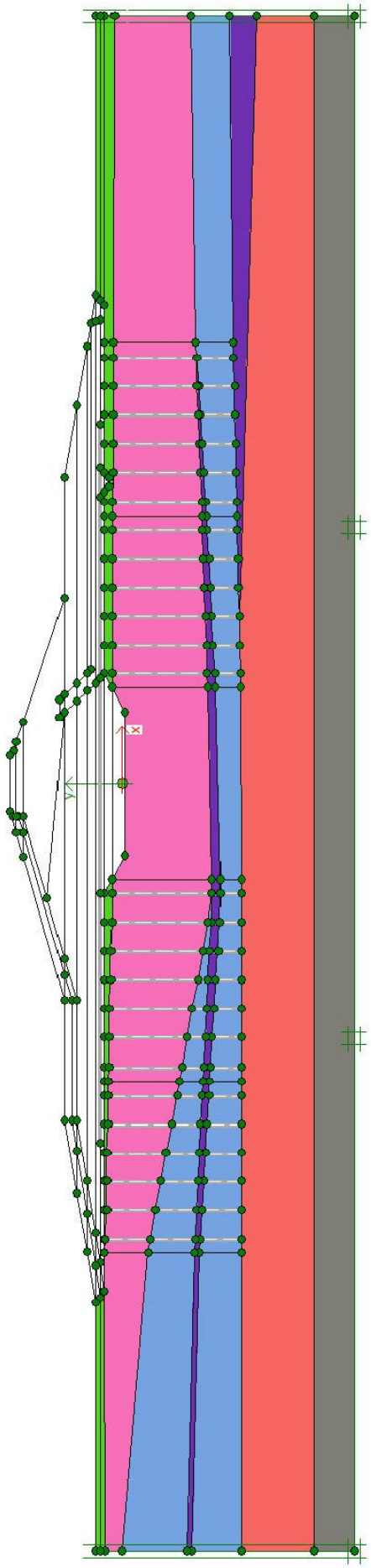

Figure VII.14 – Ground excavation up to the level of the embankment foundation and cut–off - PK0+240 of Dike No.1

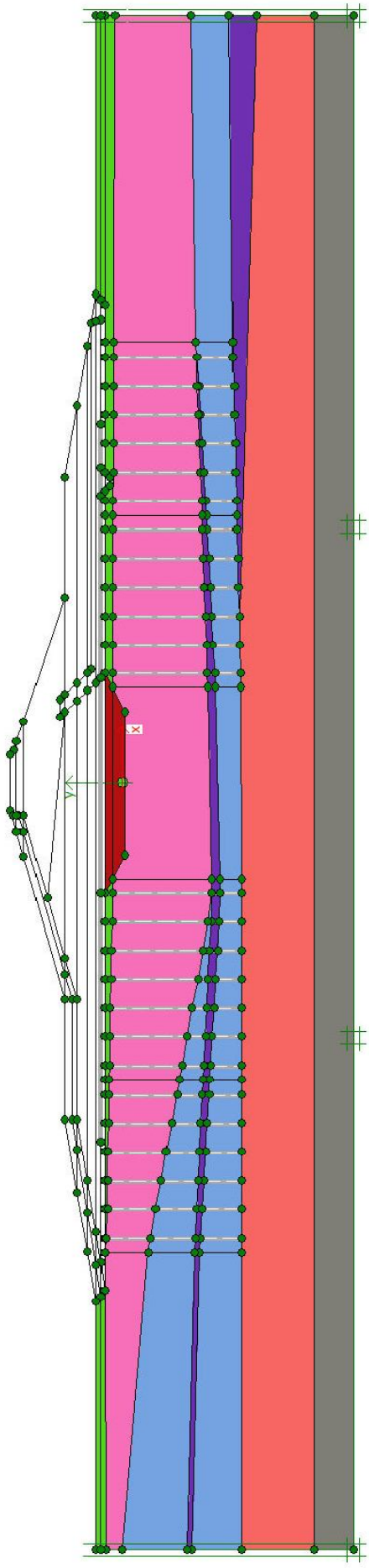

Figure VII.15 – Cut–off compaction - PK0+240 of Dike No.1

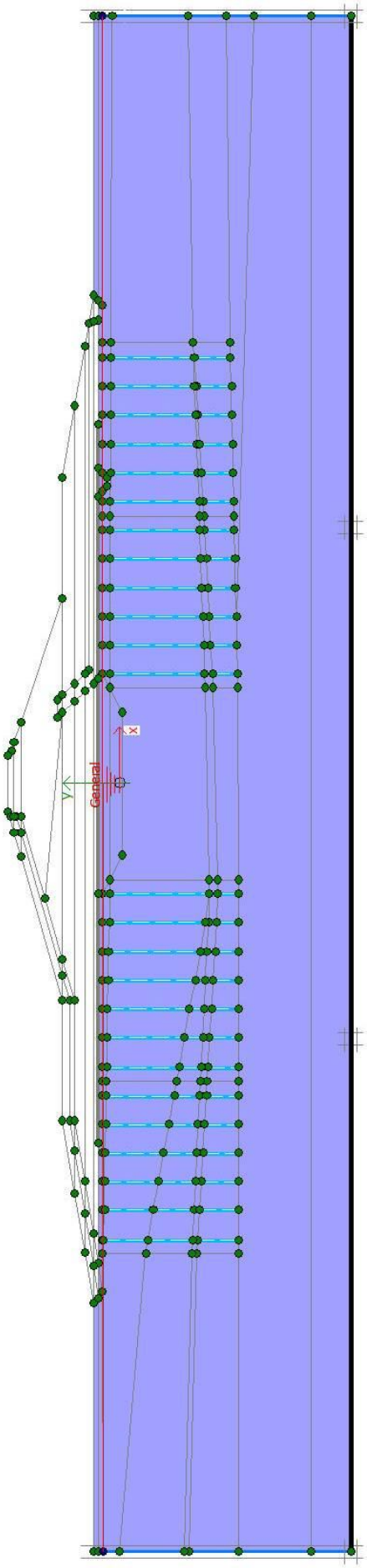

Figure VII.16– Drains activation - PK0+240 of Dike No.1

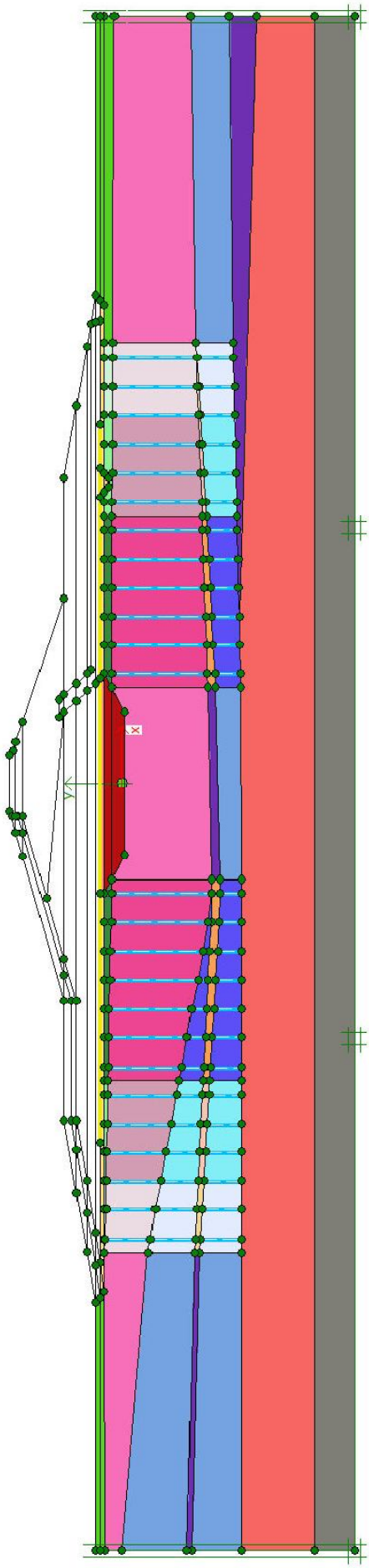

Figure VII.17 – Change of the horizontal permeability coefficients in the parallel drainage screens. Geotextile activation - PK0+240 of Dike No.1

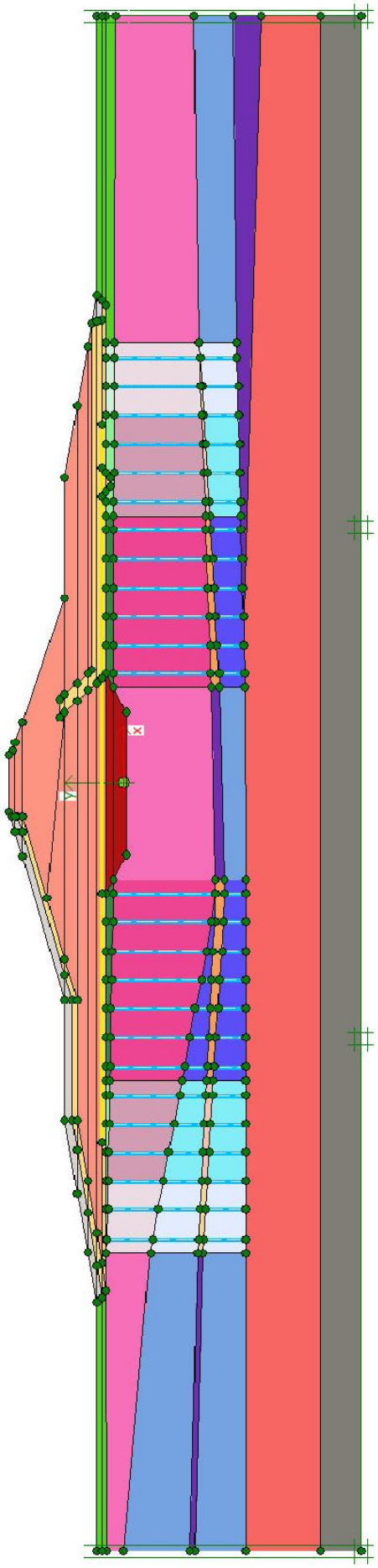

Figure VII.18 – Conclusion of embankment construction - PK0+240 of Dike No.1

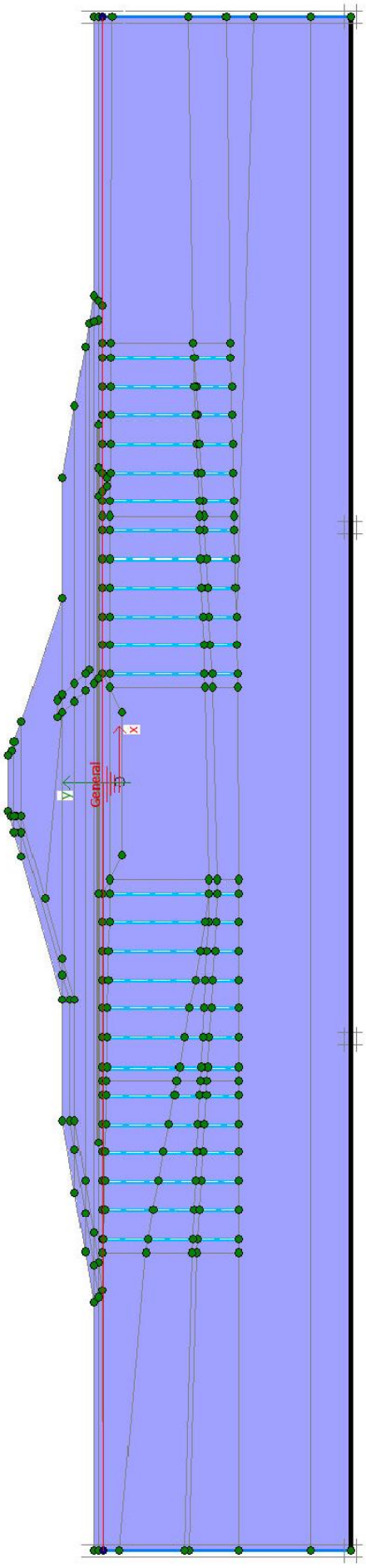

Figure VII.19 – Position of the water table on the ground foundation before water raise up in reservoir - PK0+240 of Dike No.1

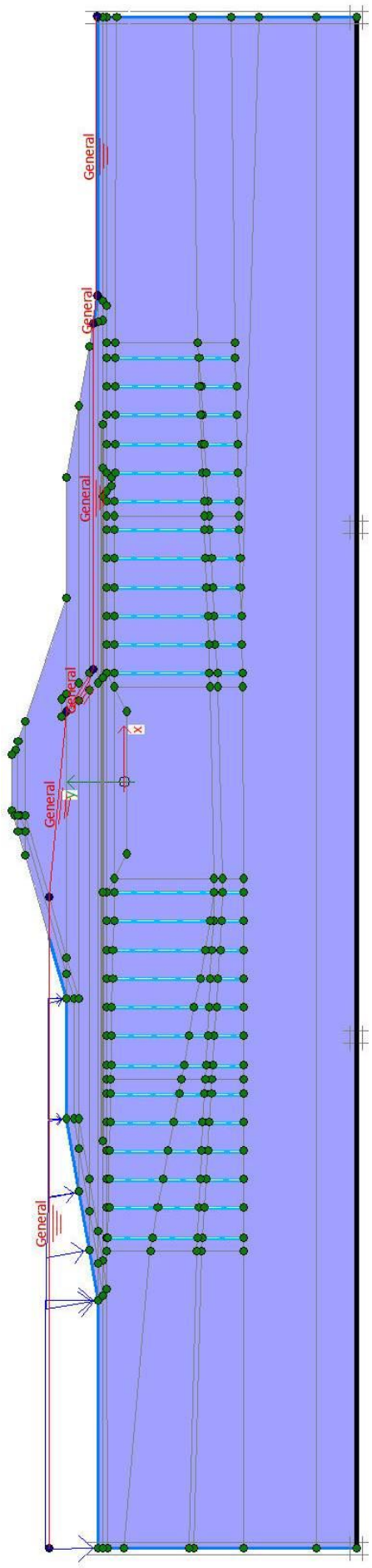

Figure VII.20 – Final water level in reservoir - PK0+240 of Dike No.1

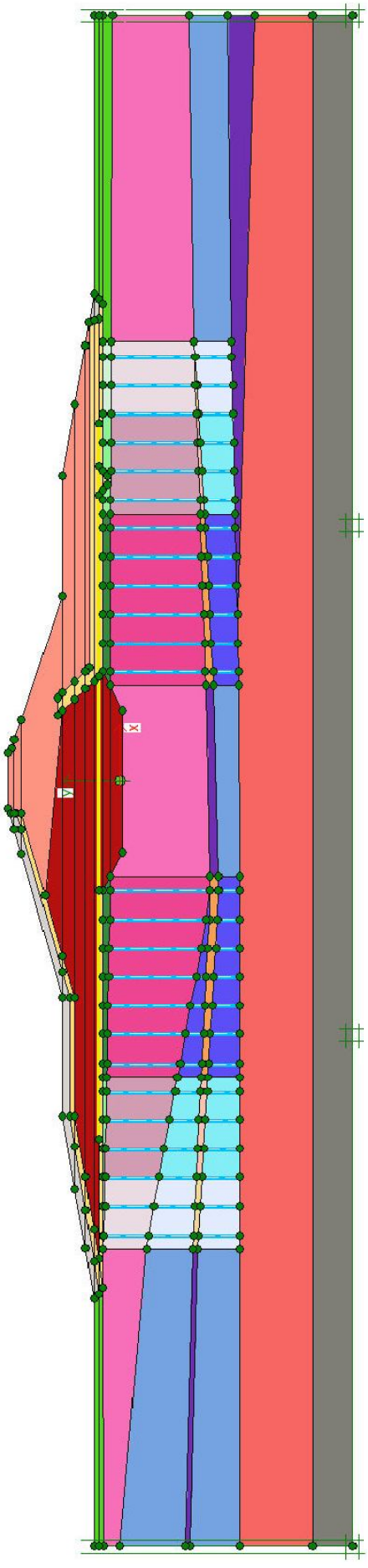

Figure VII.21 – Modification of the conditions in the embankment soils due to water raise up in reservoir - PK0+240 of Dike No.1

When the flow is considered in the analysis, two conditions can be chosen, namely:

a) When the water table is horizontal, the stationary flow option is adopted (Groundwater flow steady state);

b) If there is a difference between the upstream and downstream water levels, then a transient flow is adopted (Transient flow).

The flow net generated, in the foundation and in the embankment depends on the horizontal and vertical permeability coefficients of the soils, the flow boundary conditions, the hydraulic head and also with time. The saturation line is determined by the PLAXIS programme, using the variables listed above. Soil below this line is saturated, and soil above it, is partially saturated.

Although the study of partially saturated soil is not the aim of this thesis, the theme cannot be put apart in the analysis of these type of geotechnical structures, due its considerable relevance on the final results. Consequently, a brief introduction to this subject is essential, in order to understand the main differences between saturated and unsaturated soils or partially saturated soils.

The properties of partially saturated soils depend on the saturated characteristics and also of the Soil-Water Characteristic Curve (SWCC), which must be determined in laboratory (Fredlund, 2005). This curve defines the relation between the water content of soil and the suction, being used successfully in estimating all the properties of partially saturated soil, i.e., water and air permeability coefficients, shear strength, flow, as well as in the soils stiffness (Fredlund *et al*. 1994; Vanapalli *et al*., 1996a; Vanapalli *et al*., 1999; Fredlund, 2005). Several researchers have developed mathematical expressions to describe the SWCC curve, including Brooks & Corey (1964), van Guenuchten (1980) and Fredlund & Xing (1994). PLAXIS uses the van Guenuchten (1980) equation to describe the relation of the water content and saturation degree with suction (equation VII.4 and VII.5).

$$S_e = \frac{1}{\left[1+(\alpha.\psi)^n\right]^m}, \qquad m = 1-\frac{2}{n} \tag{VII.4}$$

where: $$S_e = \frac{\theta-\theta_r}{\theta_s-\theta_r} \tag{VII.5}$$

with: S_e – Effective degree of saturation;

θ_r – Residual water content of the soil, measured or adjusted by regression;

θ_s – Saturated water content;

$\theta=\omega$ – Water content;

ψ – Suction in the soil;

m, n and α – Model adjustment parameters.

The empirical parameters m and n can be estimated based on a non-linear regression analysis, using the minimum square method, and computational resources (van Genuchten, 1980).

In the meantime, the permeability of the soil will also be lower in function of the soil suction. Several models were proposed to estimate permeability, all based on the SWCC curve. Among the most referred in the literature, are the Childs & Collis-George (1950), Burdine (1953) and Mualem (1976) models.

Figure VII.22 represents the evolution of the water content with suction (SWCC curve) and Figure VII.23 the permeability with suction according to the various researchers (Fredlund, 2005).

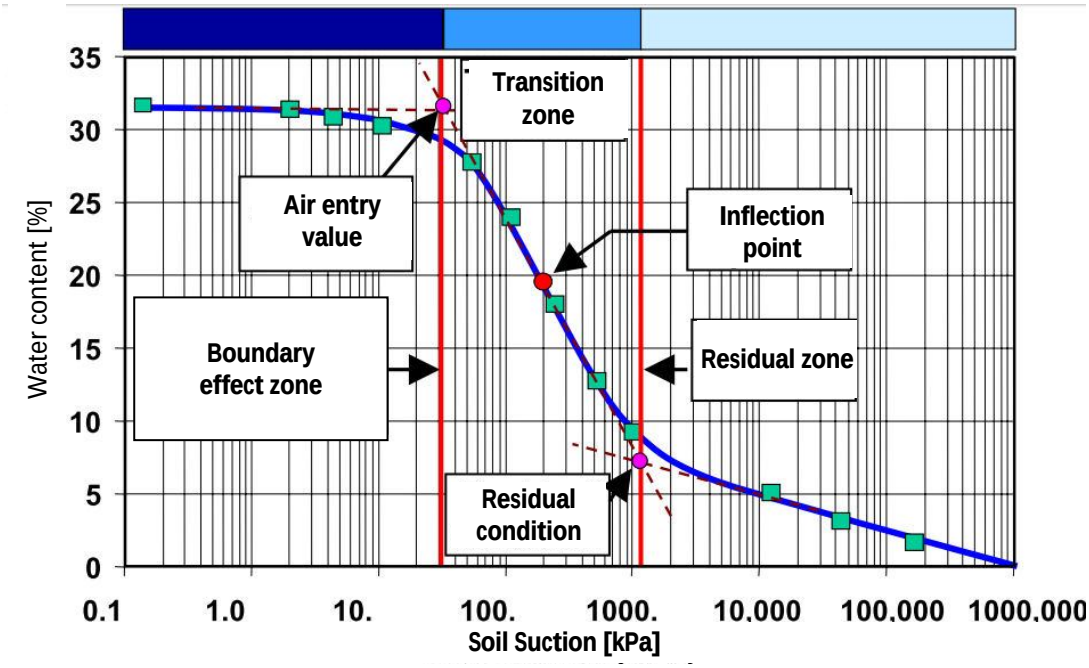

Figure VII.22 – Soil-water Characteristic Curve (SWCC) (Fredlund, 2005)

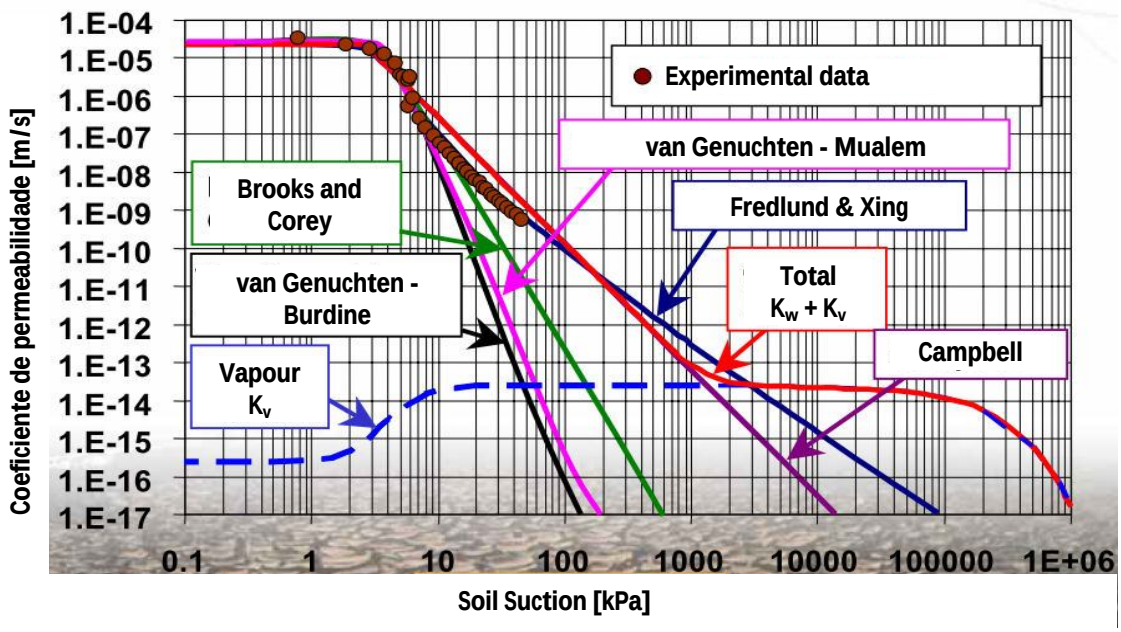

Figure VII.23 – Permeability decrease on partly saturated soils due to suction (Fredlund, 2005)

The reduction in the permeability coefficient $k_r(\psi)$, defined by Burdine in 1953, and applied on the SWCC van Guenuchten expression (1980), is given in equation VII.6.

$$k_r(\psi) = \frac{1-(\alpha.\psi)^{n-2}\left[1+(\alpha.\psi)^n\right]^{-m}}{\left[1+(\alpha.\psi)^n\right]^{2n}} \quad , \qquad m = 1-\frac{2}{n} \tag{VII.6}$$

The permeability coefficient for partially saturated soil, $k_w(\psi)$, will be calculated by the product of the permeability coefficient in the saturated conditions (k_s) and the reduction factor $k_r(\psi)$, i.e.:

$$k_w(\psi) = k_r(\psi).k_s \tag{VII.7}$$

In the absence of laboratory tests which could define these characteristics for the soils of Dikes No.1 and No.3 of the *Lebrija* Pond, it was adopted one the soils available on PLAXIS, taking in consideration the grain-size distribution, its initial saturated permeability, as well as identical compressibility properties (clay soil with high compressibility).

In order to determine the effective stresses, PLAXIS considers Bishop's definition, which is given by expression VII.8.

$$\sigma' = (\sigma - u_a) + \chi_f (u_a - u_w) \tag{VII.8}$$

with: u_a – Air pressure;
u_w – Water pressure;
χ_f – Function related to the saturation degree of the soil; being 0 for dry soils, and 1 when saturated;

The shear strength equation is also modified, since the effective stresses changes. In 1959, Bishop proposed the equation VII.9.

$$\tau_f = c' + (\sigma_n - u_a)\,tg\varphi' + \chi_f (u_a - u_w)\,tg\varphi' \tag{VII.9}$$

Later, in 1978, Fredlund, Morgenstern & Widger proposed a linear extension of the Mohr-Coulomb shear strength. Although it has been proven that this variation is not linear for high values of suction, the same continues to be used, as long as this aspect is taken into account. Since then, other proposals have been made to introduced the non-linear increment in the shear strength with suction, such as Escario & Saez (1986), Gan & Fredlund (1988), Escario & Juca (1989), Vanapalli *et al*. (1996b), Fredlund *et al*. (1996) and Vanapalli & Fredlund (1999), among others.

In turn, these constitutive relations need to be incorporated in the soil material models and behaviour. Concerning this aspect, elasto-plastic models have been modified in order to take suction into consideration, and so far good results were obtained (Alonso *et al*., 1990; Kohgo *et al*., 1993; Wheeler & Sivakumar, 1995; Maâtouk *et al*., 1995; Cui & Delage, 1996 ; Karube, 1997 ; Geiser *et al.*, 2000; Vaunat *et al*., 2000; Sun *et al*., 2000; Tang & Graham, 2002). The base of these models considerers the relations between two distinct types of parameters, according to:

a) (q-p-s) stress versus constitutive stress relation, for the stress state;

b) (e-p-s) stress versus constitutive volume-mass ratio (Figure VII.24), for the change of volume and mass.

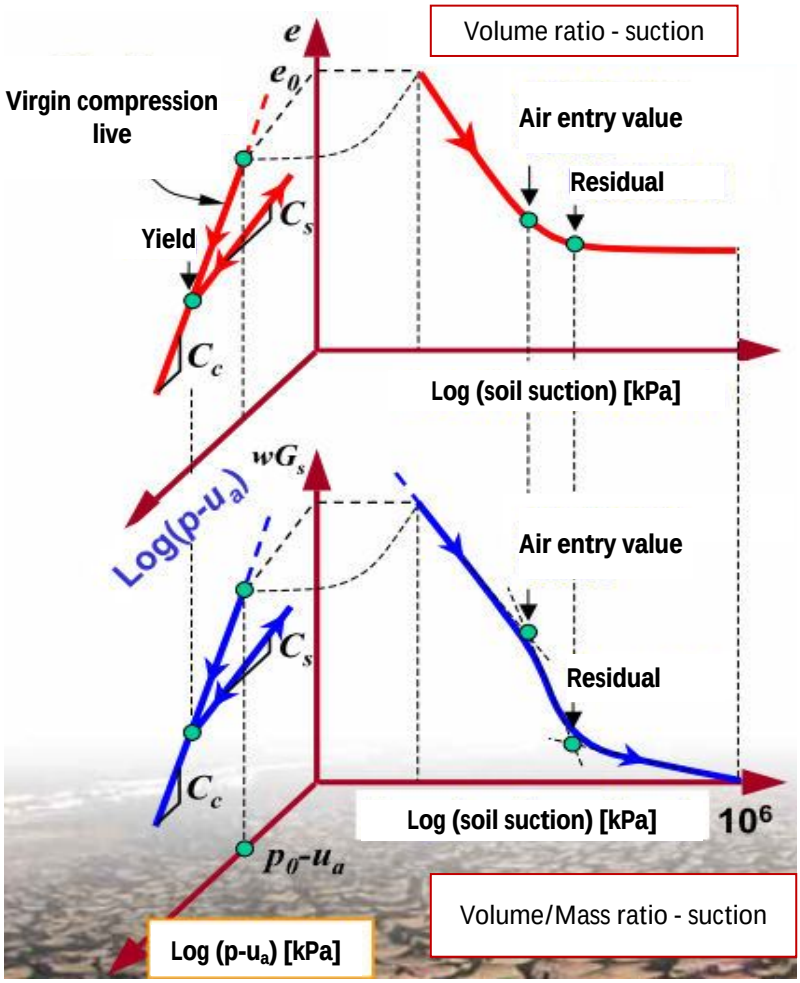

Figure VII.24 – Relationship between stress and volume-mass ratio for partly saturated soils (Fredlund, 2005)

VII.2.5. DEFINITION OF THE CONTROL POINTS

When pretending to obtain results for a specific parameter, in a specific point, during the calculation, in order to trace curves, then nodes or stress points which are located closer to them must be selected (Select points for curves). Those are defined in the "Calculations" sub-programme before starting the numerical calculation. However, these results are only viewed in the "Output" sub-programme once the analyses have been concluded.

The selection of these control points in the cross-sections modelled, were carefully chosen, since the simulation results will be compared with the monitoring results. Therefore, for the control of the settlement plates and the topographic stake marks, the nodes which were located closer to the position of these devices were selected. Regarding the pore pressures, the control points selected correspond to stress points located inside the triangular element, the nearest possible to the piezometers position.

Figure VII.25 shows the nodes chosen for profile PK0+240 of Dike No.1, including the two settlement plates located inside the embankment of the dike and all the topographic stake marks. The stress points for the pore pressures are either located in the embankment or in the foundation (Figure VII.26).

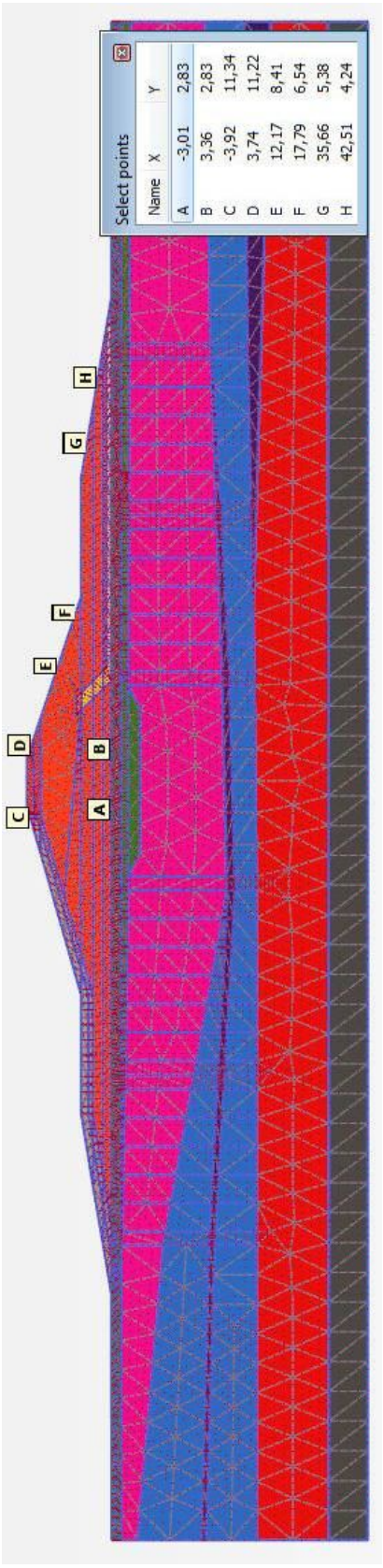

Figure VII.25 – Nodes used on the control of the settlements during simulation analysis - PK0+240 of Dike No.1

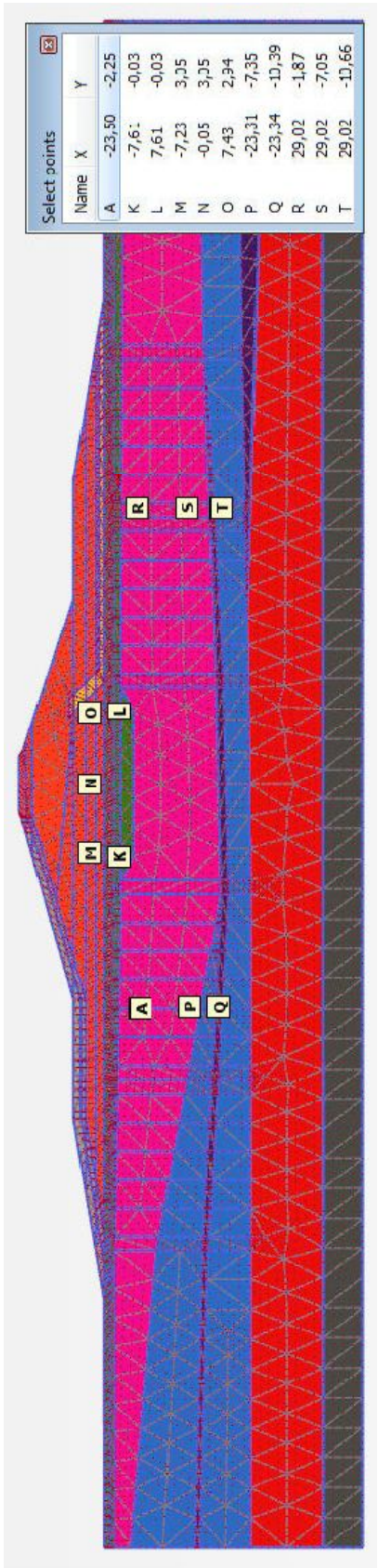

Figure VII.26 – Stress points used to control the pore pressures during simulation analysis - PK0+240 of Dike No.1

The control nodes correspondent to the settlement plates and topographic stake marks of profiles PK0+140, PK0+170 and PK0+200 of Dike No.3 are represented in figures VII.27, VII.28 and VII.29. The only two stress points of the pore pressures of Dike No.3 are located in section PK0+180, in the foundation below the upstream berm (Figure VII.30). In this case, stress point of PZ 180-1A was placed at level 0.50m and PZ 180-1B at level -4.50m, considering a difference of only 4 metres between them (see subchapter VI.6.2).

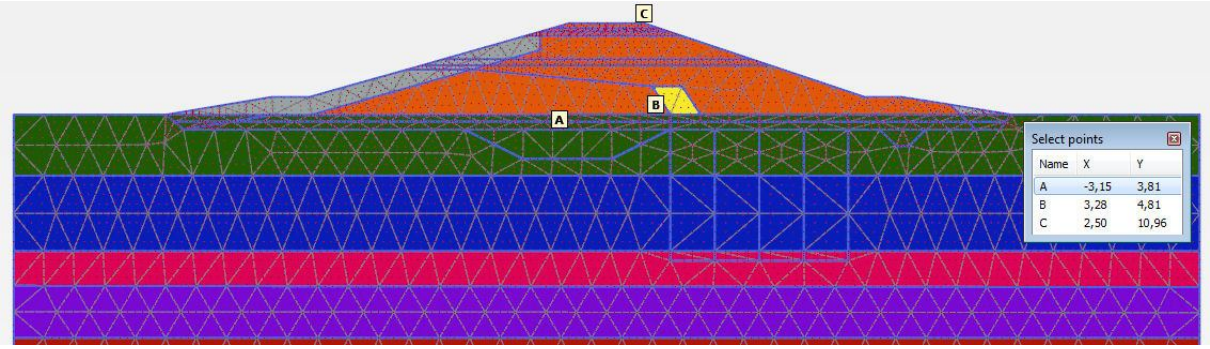

Figure VII.27 – Nodes used on the control of the settlements in PK0+140 of Dike No.3

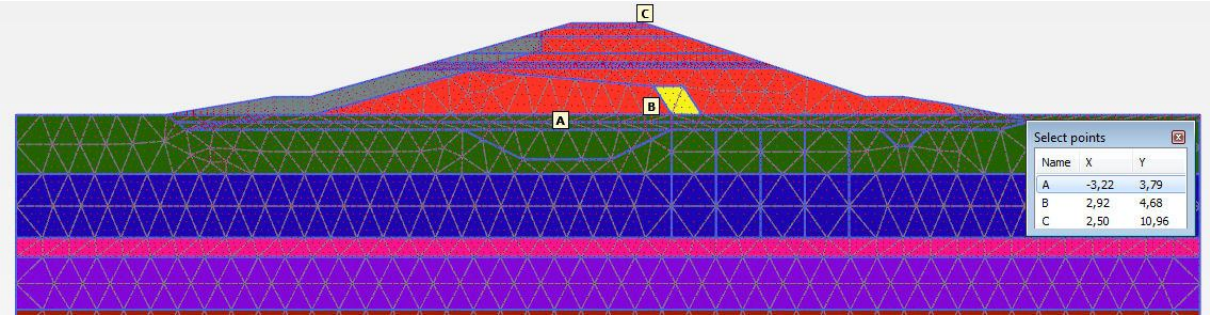

Figure VII.28 – Nodes used on the control of the settlements in PK0+170 of Dike No.3

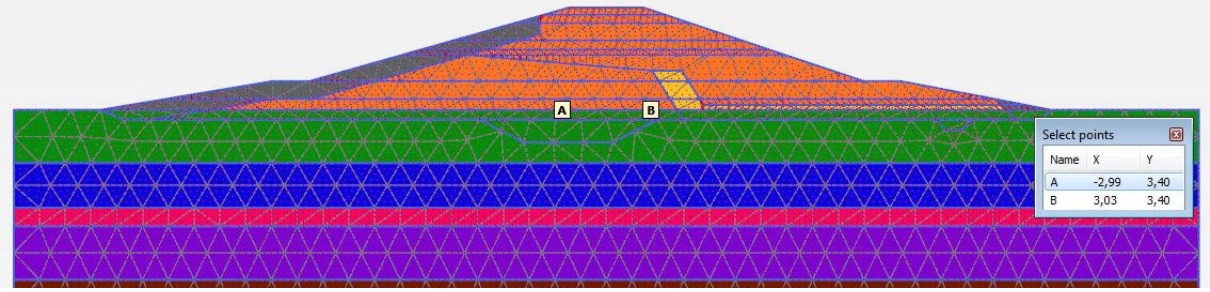

Figure VII.29 – Nodes used on the control of the settlements in PK0+200 of Dike No.3

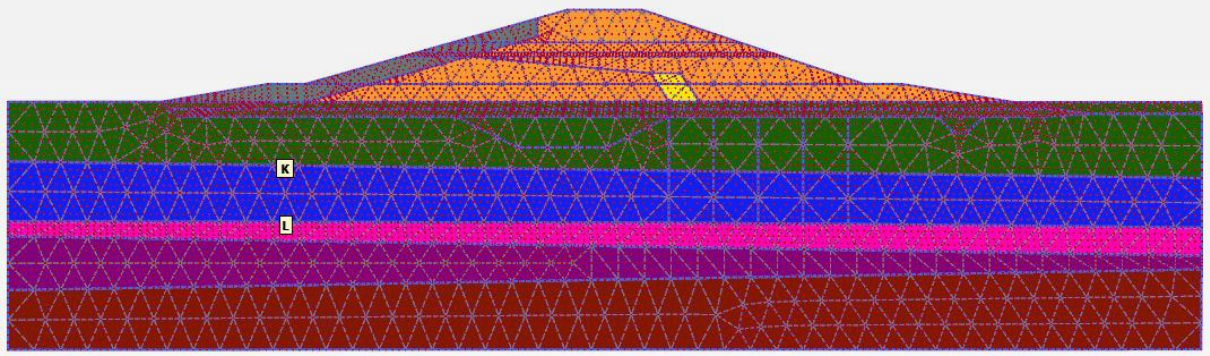

Figure VII.30 – Stress points used to control the pore pressures in PK0+180 of Dike No.3

Finally, when all the procedures, conditions and steps have been defined, the numerical calculation is initiated (Calculate current project). The results associated with each of the stages can be viewed once the simulations have been concluded.

VII.3. RESULTS OF THE NUMERICAL SIMULATION AND COMPARISON WITH MONITORING

After the numerical calculations are completed, for any of the calculation steps, the following results can be plotted in the "Output" sub-programme of PLAXIS:

a) Deformed mesh;
b) Vertical, horizontal or combined displacements;
c) Vertical, horizontal or combined strains;
d) Vertical, horizontal or combined total stress;
e) Vertical, horizontal or combined effective stress;
f) Pore pressures;
g) Pore pressures considering suction, if the flow is considered;
h) Excess pore pressures;
i) Percolated flow through the foundation and dike, if the flow is considered;
j) Groundwater head;
k) Saturated zones;
l) Zones with suction and the correspondent value, if the flow is considered;
m) The stress points that are in a plastic state (Plastic points). In PLAXIS, the red squares, called the "Mohr-Coulomb points", indicates that the stress state is located on the surface of Mohr-Coulomb failure envelope. These points are also useful to check whether the size of the mesh is sufficient. When these appear near the mesh boundaries, it means the mesh is too small and must, if possible, be enlarged. The blue inverted triangle, designated as "Cap points", represents a state of normal consolidation (primary compression), where the actual stress state is equal to the pre-consolidation stress.

The evolution of some of these results can also be analysed in depth, if the "Cross section" option is used. Additionally, the programme also allows plotting curves for the control points defined, when using the "Curves" option. It was based on this option, that the settlement and pore pressure curves associated to the control points selected before were outlined.

In an initial phase, the simulations for all the sections of Dikes No.1 and No.3 of the *Lebrija* Pond were performed without considering the flow. Due to the reduced computational time associated to the calculations without taking the flow in consideration, when compared with the simulations with flow, some sensibility analyses were performed in this phase. Later, in the modelling of the dikes considering the flow, the number of simulations was substantially reduced and only those considered most appropriate to the problem were performed.

In this chapter, the order followed for the presentation of the numerical simulations results will be different of the monitoring results, already discussed in chapter VI. In this case, the settlements precede the pore pressures results, being the latter useful to understand some of the settlement values obtained in the numerical analysis. Additionally, firstly will be presented the graphs for the PK0+240 of Dike No.1, and secondly the graphs for the cross-sections of Dike No.3.

VII.3.1. NUMERICAL ANALYSIS WITHOUT FLOW

Since the cross-section PK0+240 of Dike No.1 is the more instrumented, the quantity of data associated with the monitoring results is higher. In addition to this, geotextile reinforcement at the base of the foundation was installed, and the ground foundation was improved with band-shaped drains, both upstream and downstream of the cut-off trench. Consequently, a larger number of distinct analyses can be performed, allowing to observe the importance of these elements in the settlements, and compared them to the readings of the monitoring equipments.

For the smear values, the Indraratna & Redana (1997) solution was considered, although without the delimitation of the disturbed zone in the geometric modelling of the dikes. If this zone were discredited in the modelling, elements with extremely small dimensions would appear next to the drains leading to numerical problems in the calculation phase. In light of this, the horizontal permeability coefficients between the drains, in plane strain correspond to the values of $K_{hPD}^{(2)}$ indicated in tables VII.10 to VII.12 for Dike No.1, and in tables VII.13 to VII.15 for Dike No.3. When the smear effect is not considered, then the values $K_{hPD}^{(3)}$ are applied.

Therefore, the simulations performed for profile PK0+240 in Dike No.1 include the following analyses:

a) Consideration of the Mohr-Coulomb (MC) model for the soil foundation in undrained conditions, applying both method A and method B. In method A the stiffness modulus E_{ref} was determined either based on the oedometer modulus, on the initial undrained cohesion or on the reduced undrained cohesion (Table VII.4). In method B, only these two last hypotheses were used (Table VII.5). The smear conditions adopted were $K_{hsAx}=K_{hsPD}=0.33K_{h0}$ and $d_s=3d_w$. In this case, the ratio K_{hs}/K_{v0} varies between 0.78 and 1.17 and the value of K_{hPD} ranges between:

   $K_{hsAx}=0.33K_{h0}$ and $d_s=3d_w$: $S=1.5m \Rightarrow 1.36K_{v0} \leq K_{hPD} \leq 2.04K_{v0}$;
   $S=1.75m \Rightarrow 0.97K_{v0} \leq K_{hPD} \leq 1.45K_{v0}$;
   $S=2.0m \Rightarrow 0.72K_{v0} \leq K_{hPD} \leq 1.08K_{v0}$;

b) Consideration of the Soft Soil (SS) and Soft Soil Creep (SSC) models, in which the secondary compressibility index used in the SSC model was the one given by the Terzaghi *et al.* (1996) relation (Table VII.8). For these models, a sensitivity analysis was simultaneously performed for the horizontal permeability coefficient in the area with drains (K_{hPD}).

In a first phase, the influence of the variation of the smear diameter was studied, ($d_s=2d_w$; $d_s=3d_w$; $d_s=4d_w$), and the smear horizontal permeability coefficient was kept constant and equal to $K_{hsAx}=K_{hsPD}=0.33K_{h0}$. In addition to the values of K_{hPD} already presented, with $K_{hs}=0.33K_{h0}$ and $d_s=3d_w$, the others range between:

$K_{hsAx}=0.33K_{h0}$ and $d_s=2d_w$: $S=1.5m \Rightarrow 1.65K_{v0} \leq K_{hPD} \leq 2.47K_{v0}$;

$S=1.75m \Rightarrow 1.17K_{v0} \leq K_{hPD} \leq 1.75K_{v0}$;

$S=2.0m \Rightarrow 0.86K_{v0} \leq K_{hPD} \leq 1.29K_{v0}$;

$K_{hsAx}=0.33K_{h0}$ and $d_s=4d_w$: $S=1.5m \Rightarrow 1.21K_{v0} \leq K_{hPD} \leq 1.81K_{v0}$;

$S=1.75m \Rightarrow 0.86K_{v0} \leq K_{hPD} \leq 1.29K_{v0}$;

$S=2.0m \Rightarrow 0.64K_{v0} \leq K_{hPD} \leq 0.97K_{v0}$.

In a second phase, it was analysed the effect of the variation of the smear horizontal permeability coefficient ($K_{hs}=0.10K_{h0}$; $K_{hs}=0.33K_{h0}$; $K_{hs}=0.66K_{h0}$), maintaining the smear diameter around the drain constant and equal to $d_s=3d_w$. The values of K_{hPD} associated with the two new smear situations are:

$K_{hsAx}=0.10K_{h0}$ and $d_s=3d_w$: $S=1.5m \Rightarrow 0.51K_{v0} \leq K_{hPD} \leq 0.77K_{v0}$;

$S=1.75m \Rightarrow 0.37K_{v0} \leq K_{hPD} \leq 0.56K_{v0}$;

$S=2.0m \Rightarrow 0.28K_{v0} \leq K_{hPD} \leq 0.42K_{v0}$;

$K_{hsAx}=0.66K_{h0}$ and $d_s=3d_w$: $S=1.5m \Rightarrow 2.11K_{v0} \leq K_{hPD} \leq 3.17K_{v0}$;

$S=1.75m \Rightarrow 1.48K_{v0} \leq K_{hPD} \leq 2.22K_{v0}$;

$S=2.0m \Rightarrow 1.09K_{v0} \leq K_{hPD} \leq 1.63K_{v0}$;

In these analyses, some previously calculated smear conditions were excluded, since they were not relevant for the parametric study.

c) The influence of the geotextile reinforcement, as well as the band-shaped drains, on the settlements, having simulated several scenarios, including:
   - Foundation soil without drains and without geotextile reinforcement;
   - Foundation soil without drains and with geotextile reinforcement;
   - Foundation soil with drains, but without smear, and without geotextile reinforcement;
   - Foundation soil with drains, but without smear, and with geotextile reinforcement;

   In these analyses, only the SS and SSC models were used. Once again, the secondary compressibility index used in this last model was estimated according Terzaghi *et al.* (1996) expression;

d) Sensitivity study associated to the secondary compressibility index (C_α), which can only be performed when the SSC material model is adopted. Three distinct values were used for this parameter, namely for foundation soils B', B1, B2 and B3.

In the first hypothesis, C_α correspond to the values obtained directly from the oedometer test, secondly, C_α were estimated by the expression of the Terzaghi *et al.* (1996), and lastly, these indices were calculated based on the ratios λ^*/μ^* proposed in the PLAXIS manual (PLAXIS 2D-V11.02, 2012). Calculating λ^*/μ^* from the laboratory results, extraordinarily high values are obtained, while for C_α/C_c=0.045 proposed by Terzaghi *et al*. (1996) this ratio is reduced to 22.2. According to the PLAXIS manual, the ratio between λ^*/μ^* should be between 15 and 25. As 22.2 is close to the upper limit indicated by PLAXIS, then the third value of C_α used for the parametric analysis corresponds to the lower limit, i.e. λ^*/μ^*=15. Using this limit, higher values are obtained for this index (Table VII.16), implying higher creep settlements. The ratio between the parameters λ^* and μ^*, with the compressibility indexes C_c, C_r and C_α, are indicated in subchapters III.3.1 and III.3.2 (MATERIAL MODELS). For the smear effect it was considered $K_{hsAx}=K_{hsPD}=0.33K_{h0}$ and $d_s=3d_w$.

Table VII.16 – Dike No.1: Values tested in the sensitivity analysis for the secondary compressibility index (C_α)

		Cα (Oedometer)			**Cα (*Terzaghi*)**			**Cα (PLAXIS)**		
Soils	**λ***	**Cα**	**μ***	**λ*/μ***	**Cα**	**μ***	**λ*/μ***	**Cα**	**μ***	**λ*/μ***
B'	0,0975	0.00476	0,00214	45.5	0.02511	0.00439	22.2	0.03627	0.00650	15.0
B1	0,1295	0.00694	0,00163	79.7	0.03366	0.00583	22.2	0.04987	0.00864	15.0
B2	0,1094	0.00400	0,00067	164.3	0.02475	0.00492	22.2	0.04273	0.00729	15.0
B3	0,0803	0.00766	0,00218	36.9	0.02579	0.00361	22.2	0.03153	0.00535	15.0

e) Finally, it was performed a simulation combining the SSC model with the secondary compressibility index estimated from the PLAXIS relations, and with smear corresponding to $K_{hsAx}=K_{hsPD}=0.10K_{h0}$ and $d_s=3d_w$.

The simulations for the various profiles of dike No.3 were performed after the analysis of the results from Dike No.1. Therefore, it was considered unnecessary to repeat all the parametric analyses. Hence, in Dike No.3, the simulations for each section are restricted to the conditions and hypotheses which are considered reasonable to traduce the soil behaviour. Thus, only the Soft Soil Creep model was used with the secondary compressibility index (C_α) being estimated according to Terzaghi *et al.* (1996) and PLAXIS (Table VII.7).

Table VII.17 – Dike No.3: Values tested in the sensitivity analysis for the secondary compressibility index (C_α)

		Cα (Terzaghi)			**Cα (PLAXIS)**		
Soils	**λ***	**Cα**	**μ***	**λ*/μ***	**Cα**	**μ***	**λ*/μ***
B'	0.0925	0.02511	0.00416	22.2	0.03720	0.006164	15.0
B1	0,1295	0.03366	0.00583	22.2	0.04987	0.00864	15.0
B2	0.0947	0.02475	0.00426	22.2	0.03667	0.00632	15.0
B3	0.1005	0.02579	0.00452	22.2	0.03820	0.00670	15.0

In sections PK0+140, PK0+170 and PK0+180 of Dike No.3, where drains were installed to the foundation soil, it was assumed the following smear conditions: $K_{hsAx}=K_{hsPD}=0.10K_{h0}$ and $d_s=3d_w$. Associated to them, the value K_{hPD} varied between:

- $0.30K_{v0} \leq K_{hPD} \leq 0.42K_{v0}$ for B' and B1 ;
- $K_{hPD}=1.05K_{v0}$ for B2

The ratio K_{hsPD}/K_{v0} for soils B' and B1 is also low, ranging between 0.28 and 0.39. Soil B2 is the exception as the value obtained for this ratio is 0.97. This is due to the fact that ratio K_{h0}/K_{v0} is approximately three times bigger than the others, as previously mentioned. In light of this, an additional analysis was performed, where the horizontal permeability coefficient value of Dike No.1 was applied to soil B2 of Dike No.3. This analysis was extended to section PK0+200 of Dike No.3.

Once the conditions associated with the different simulations conducted for Dikes No.1 and No.3 of the *Lebrija* Pond have been indicated, the results and the graphs obtained for the different scenarios can be presented, without considering the flow.

In the graphs, for simplicity, the horizontal permeability coefficient in the disturbed zone is indicated only as K_{hs}, instead of K_{hsAx} or K_{hsPD}, as the value is always the same. Also, the initial horizontal permeability coefficient k_{h0} becomes K_h.

VII.3.1.1. SENSITIVITY ANALYSIS AND DIKE NO.1 SETTLEMENTS

In the next graphs, the curves of the numerical simulation results, for the several sensitivity analyses performed, without considering the flow, are plotted. These are always compared to the values measured in plates PL 240-1 and PL 240-2, or in the topographic stake marks TS 240-1 and TS 240-2.

a) Results considering the Mohr-Coulomb (MC) model for the soil foundation, in undrained conditions, applying both method A and method B:

Based on the curves shown in graphs VII.1 and VII.2, it is observed that the Mohr-Coulomb model cannot translate the response of the soil foundation reasonably. The model permits to obtain just an order of magnitude for the settlements, since it is not a model adequate neither to consolidation analysis nor to this type of clayed soils. The numerical settlements during the construction phase are bigger than the measured, decreasing a little after the conclusion of the dike with method A, and then increasing just a little during the reservoir filling phase. In method B, and since this cannot traduce the increment of shear strength associated to the soil consolidation, the curves are almost flat after the conclusion of the embankment. The settlements with the stiffness estimated based on the oedometer modulus gave extremely high values, being more reasonable to use the undrained shear strength empirical relations of Justo *et al.* (2006). Besides, the settlements calculated with the initial undrained shear strength are smaller, since the stiffness modulus is bigger. Nevertheless, none of the results correspondent to the settlements observed, being the curves far below of the real values, once the construction is concluded.

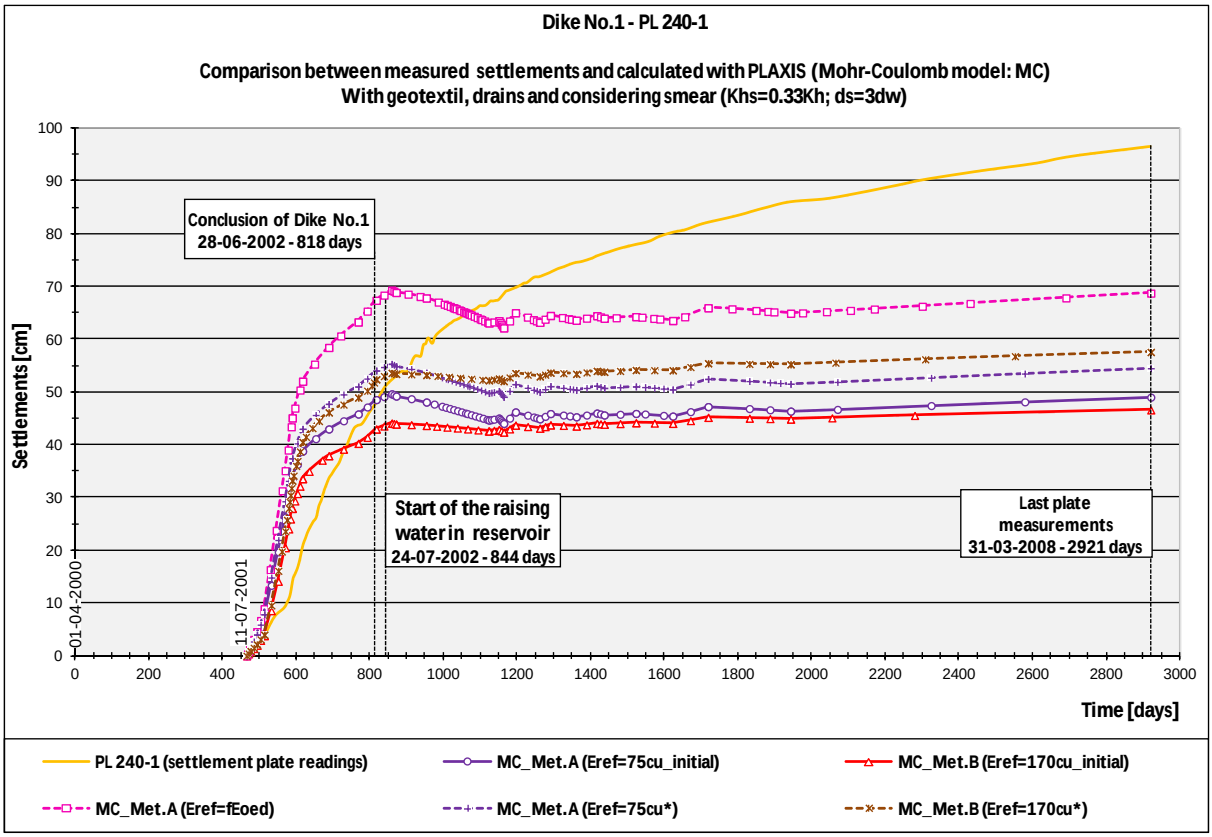

Graph VII.1 – PL 240-1 of Dike No.1: Settlements calculated with the *Morh-Coulomb* model for the soil foundation, in undrained conditions (Method A and B)

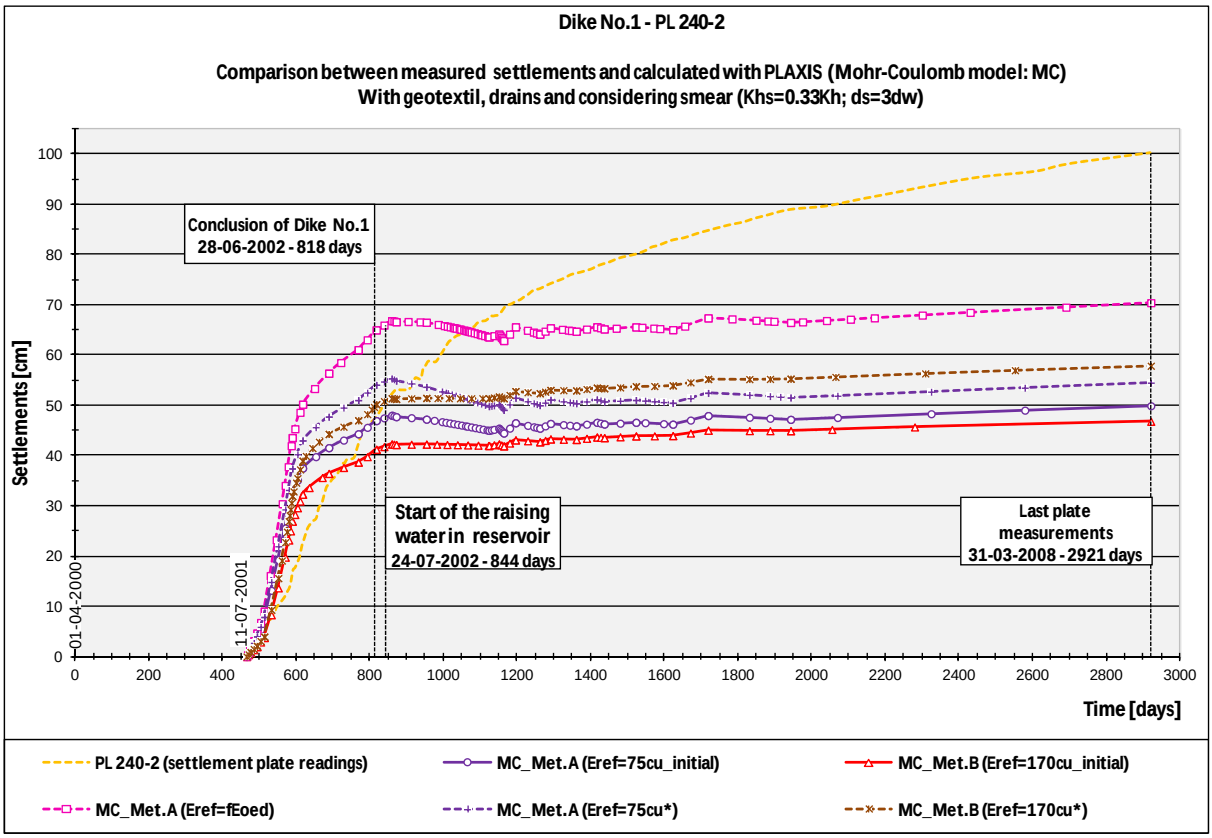

Graph VII.2 – PL 240-2 of Dike No.1: Settlements calculated with the *Morh-Coulomb* model for the soils foundation, in undrained conditions (Method A and B)

b) Results considering the Soft Soil and Soft Soil Creep models for the soil foundation, including sensitivity analysis of the smear effect:

- Varying diameter of the smear zone (d_s), and keeping smear horizontal permeability coefficient (K_{hs}) constant and equal to $0.33K_{h0}$.

- Varying smear horizontal permeability coefficient (K_{hs}), and keeping diameter of the zone (d_s) constant and equal to $3d_w$.

According to results plotted from graphs VII.3 to VII.6, the following statements may be made:

- The Soft Soil and Soft Soil Creep models settlements curves are quite similar the construction phase; however, in the post-construction phase and in the filling of the pond, only the SSC model can traduced relatively well the settlements increments with time. This is precisely the expected result, as this last model can calculate the settlements associated with secondary consolidation, which are quite significant in soft soils, such as the case of B1, B2 and B3;

- The variation of the diameter of the disturbed zone around the drains, known as smear diameter (d_s), has smaller influence on the settlements, when compared with the variation of the disturbed horizontal permeability coefficient or smear permeability coefficient (K_{hs}). Again, these results are consistent with the parametric analyses already performed in subchapters V.4 and V.5. The values of the horizontal permeability coefficient for plane strain analysis (K_{hPD}), in the zones with band-shaped drains, determined with the Indraratna & Redana (1997) analytical solution, gives exactly these same indication. Therefore, the graphical numerical results of these two sensitivity studies reinforce the analytical results obtained before.

- In addition, greater reduction in the horizontal permeability coefficient in the disturbed zone, implicates smaller settlement values. However, this does not mean that the drains are not working properly, just indicating that the drainage will take longer, which is why the greatest difference in the numerical results occurs precisely in the initial phase. Analysing graphs VI.5 and VII.6, it can be seen that the difference between the settlements for the different values of K_{hs} smooth out with time;

- From the various scenarios considered for the smear, the curves correspondent to the smear conditions $K_{hsAx}=0.10K_{h0}$ and $d_s=3d_w$, are almost coincident with the measured in the plates, especially for the construction phase. In fact, although this hypothesis presents relatively low values for the ratio K_{hsPD}/K_{v0}, it is the one which traduces the progress of the settlements fairly well, although in the post-construction phase they are still slightly below the values measured. This is already a reasonable approximation to the monitoring data, and the result is common to both settlement plates. It is important to indicate that the statement above can only be applied for the SSC model.

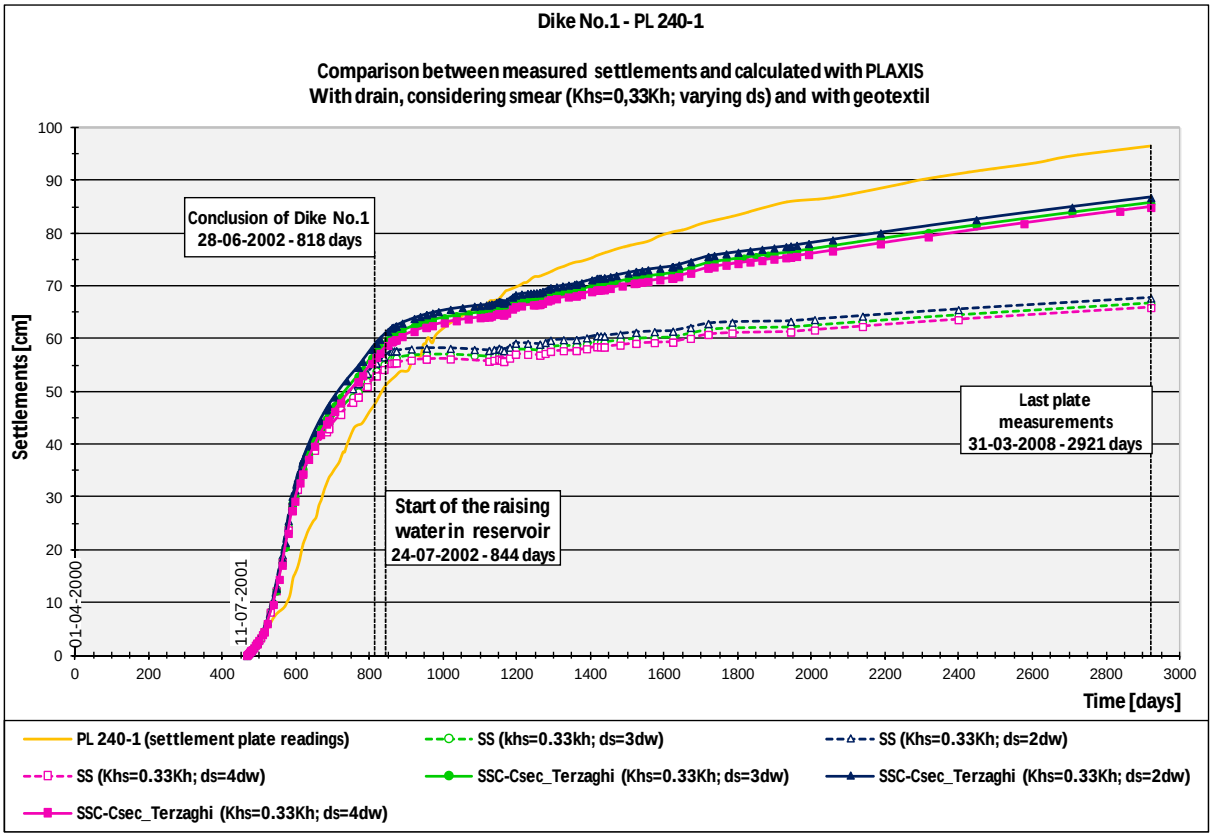

Graph VII.3 – PL 240-1 of Dike No.1: Settlements calculated with the *SS* and *SSC* models, considering several diameters for (d_s), keeping permeability in smear zone constant and equal to K_{hs}=0.33K_h

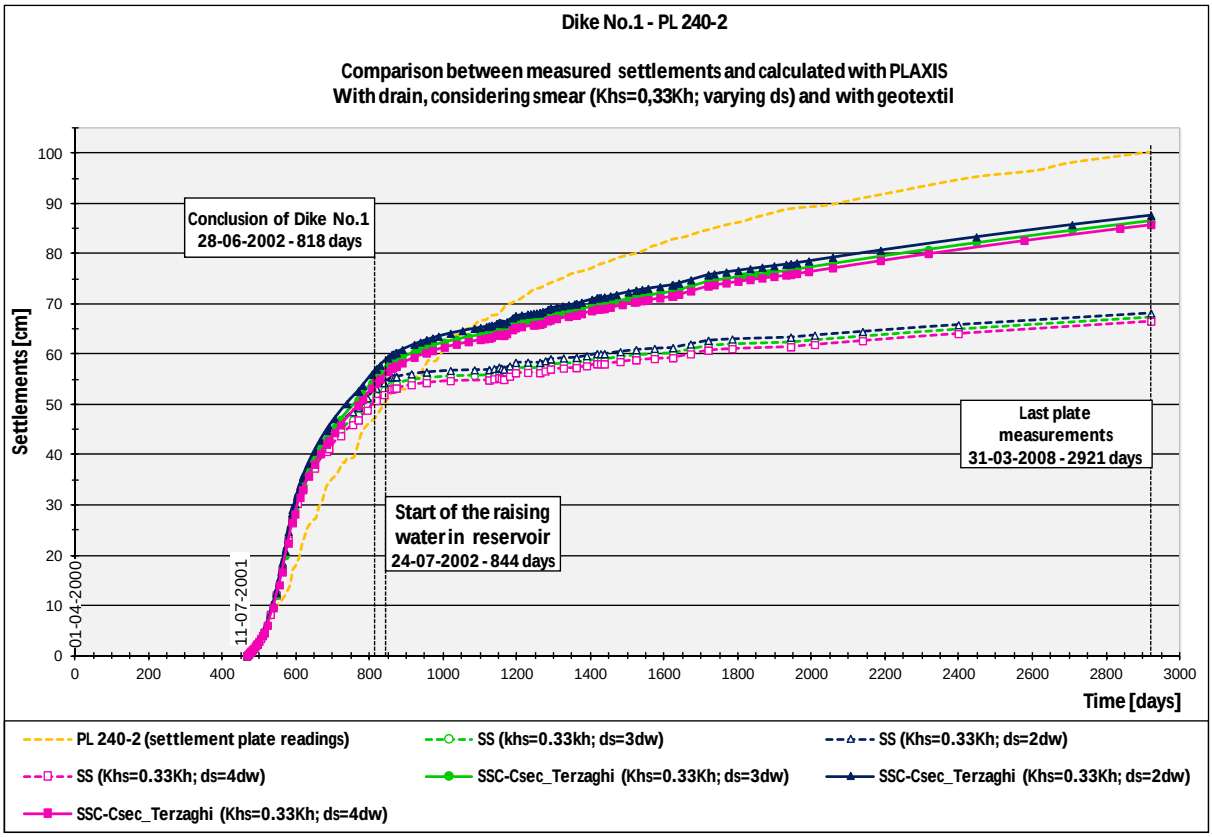

Graph VII.4 – PL 240-2 of Dike No.1: Settlements calculated with the *SS* and *SSC* models, considering several diameters for (d_s), keeping permeability in smear zone constant and equal to K_{hs}=0.33K_h

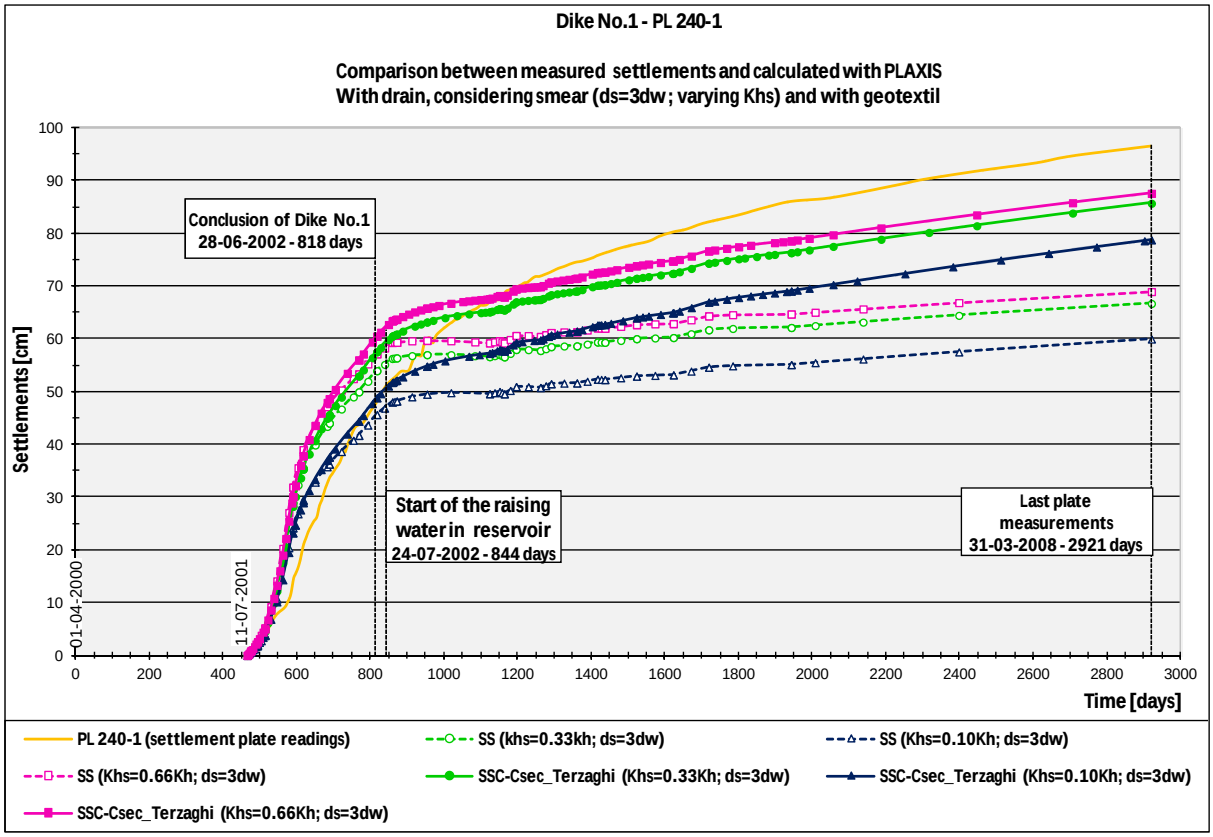

Graph VII.5 – PL 240-1 of Dike No.1: Settlements calculated with the *SS* and *SSC* models, considering several permeabilities in smear zone (K_{hs}), keeping diameter constant and equal to $d_s=3d_w$

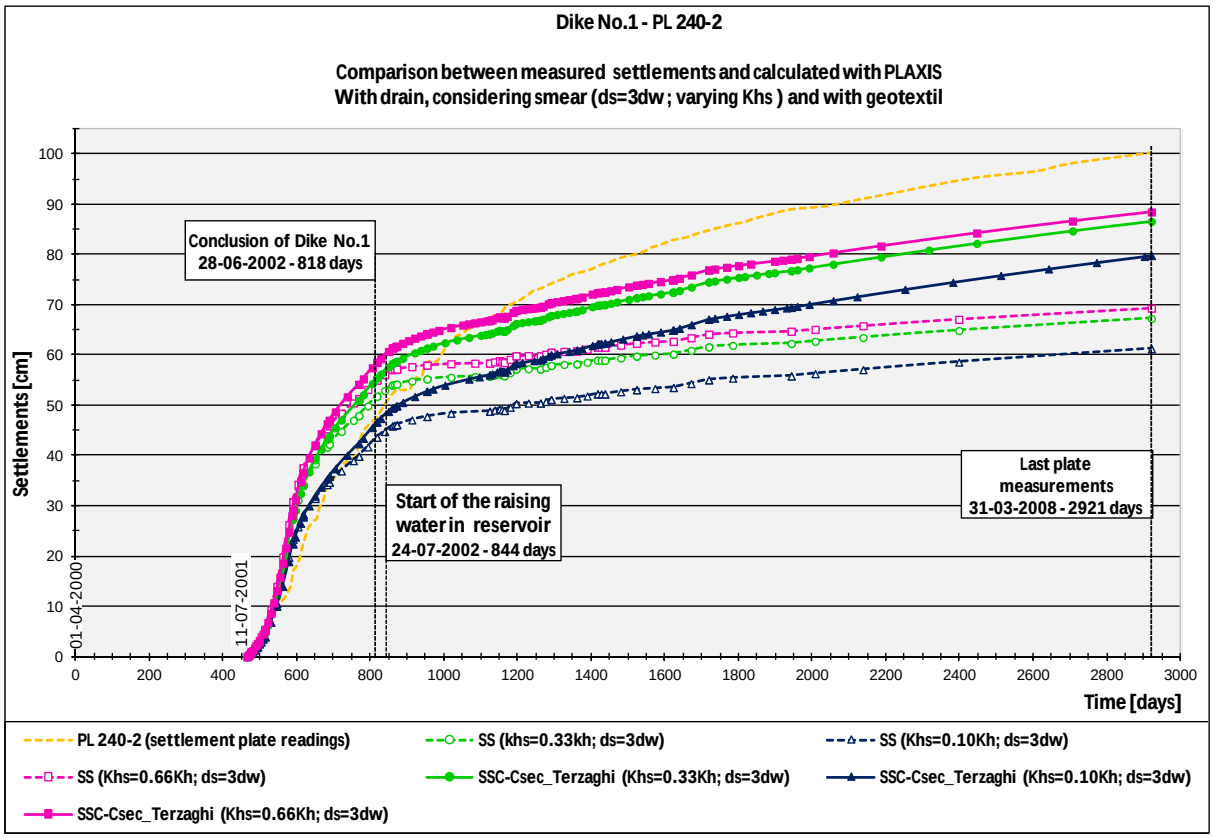

Graph VII.6 – PL 240-2 of Dike No.1: Settlements calculated with the *SS* and *SSC* models, considering several permeabilities in smear zone (K_{hs}), keeping diameter constant and equal to $d_s=3d_w$

c) Results associated with the influence of the geotextile reinforcement, as well as the soil improvement with the band-shaped drains:

In light of the results from the numerical simulations, when compared to the values from the measurements at the plates (Graph VII.7 and VII.8), it is observed that:

- The contribution of the geotextile reinforcement at the base of the dike is minimal; Even though there is a slight reduction in the settlement values, this element was applied with the objective of increasing the stability of the dike. Therefore, its influence will be more visible when analysing the safety factors associated with the slope stability, rather than in the settlement values;

- When the band-shaped drains are not considered, the settlements are extraordinarily low, although in a very early stage of the dyke construction they almost coincide with the values measured. After this initial phase, there is a huge detachment between the values calculated and measured. This means that without the drains it is impossible to attain the readings of the settlement plates. Regardless the mentioned above, another very interesting finding, taken from the similarity of the settlement curves without drains to the plates readings, at an early stage, is the indication of a strongly disturbance of the soil due to the drain installation. In fact, the soil permeability is very affected, and so will be the drainage around the drain. These results are in accordance with the anterior sensitivity analysis, that gave a high smear effect, i.e., horizontal smear permeability extremely low (K_{hsAx}=0.10K_{h0});

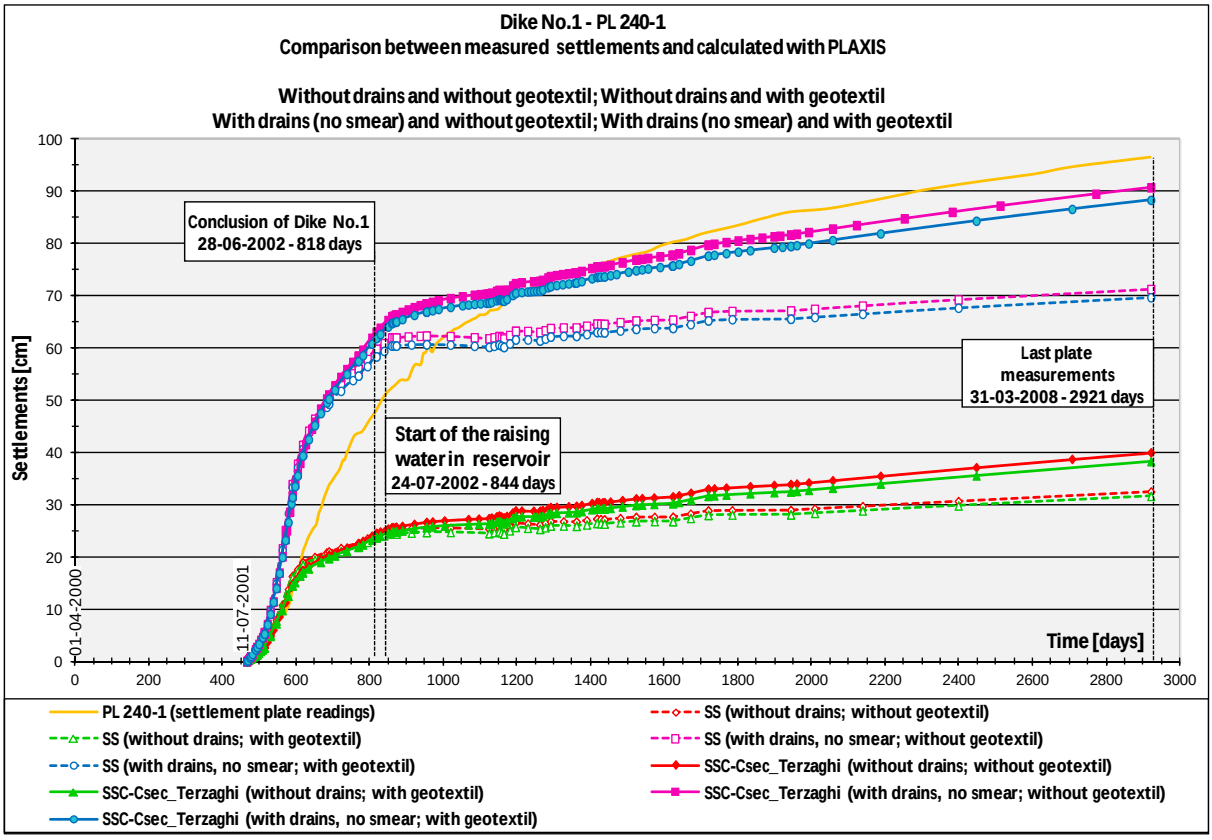

Graph VII.7 – PL 240-1 of Dike No.1: Settlements calculated with the *SS* and *SSC* models, with and without geotextile or band-shaped drains.

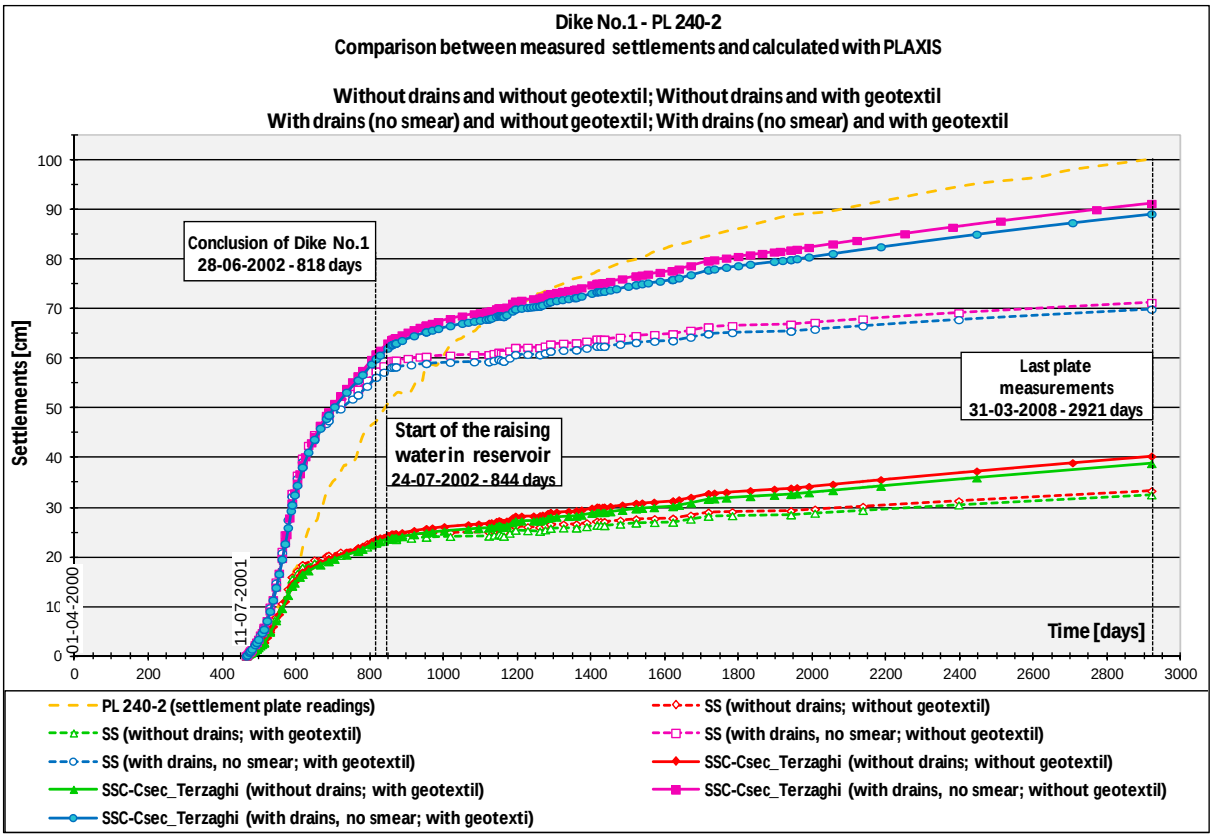

Graph VII.8 – PL 240-2 of Dike No.1: Settlements calculated with the *SS* and *SSC* models, with and without geotextile or band-shaped drains.

- When considering the existence of the drains on the ground foundation, but without taking the smear into account, the corresponding numerical curves are located well above the monitoring results, especially in the construction phase. The direct consequence taken from this result is that the smear effect must always be considered in the simulations. Once more, the Soft Soil Creep model is the most suitable to model the behaviour of the soil foundation, since it accompanies the evolution of the settlements over time.

d) Results associated with the sensitivity analysis of the secondary compressibility index (C_α):

From the results displayed on graphs VII.9 and VII.10, there is no doubt that the secondary compressibility index (C_α) reveals huge influence on the settlements rate, starting from the beginning of the construction phase, though it increases over time. In addition to this, the values of C_α estimated from the relation proposed by the PLAXIS manual ($\lambda^*/\mu^*=15$), provides better results with respect of final settlements, as they are closer to those registered in the plates. These results indicate that the creep compressibility of these soft soils is considerably higher than the one given by the oedometer tests.

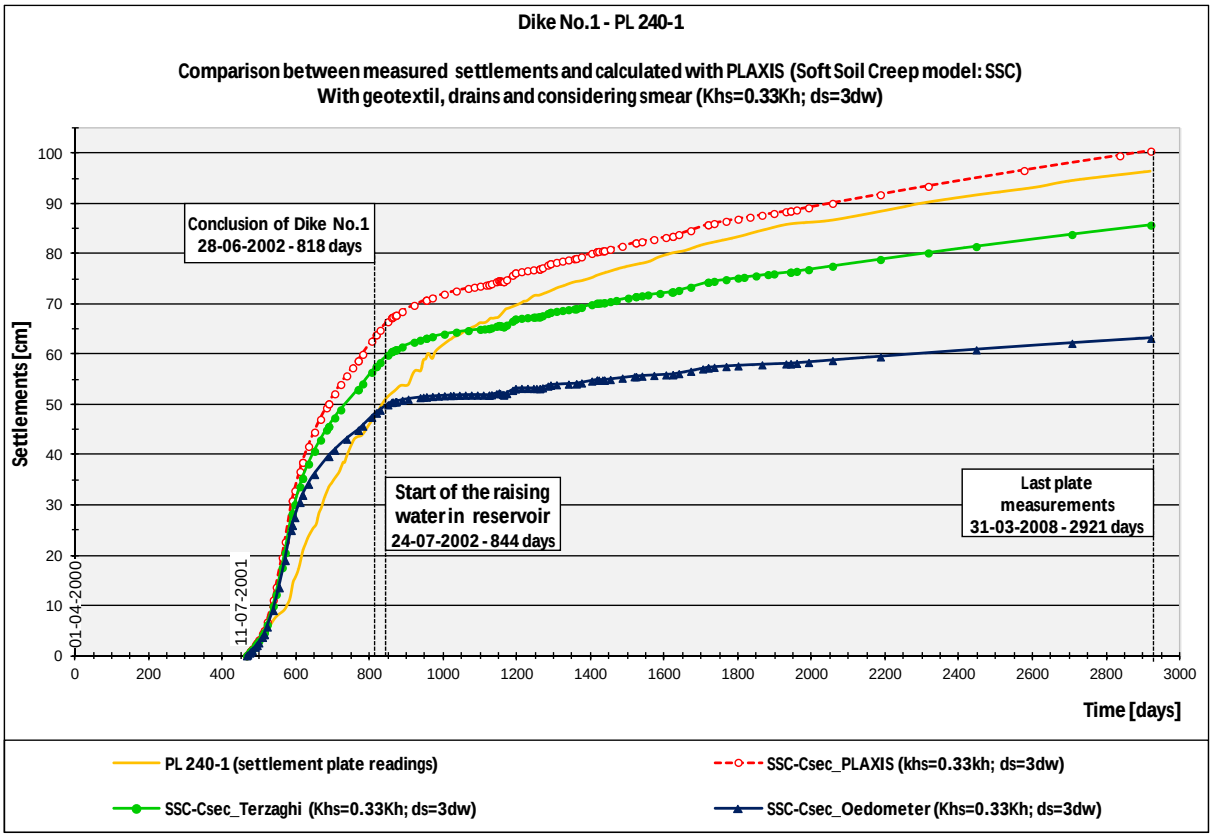

Graph VII.9 – PL 240-1 of Dike No.1: Settlements calculated with the *SSC* model considering several values for the secondary compressibility index (C_α)

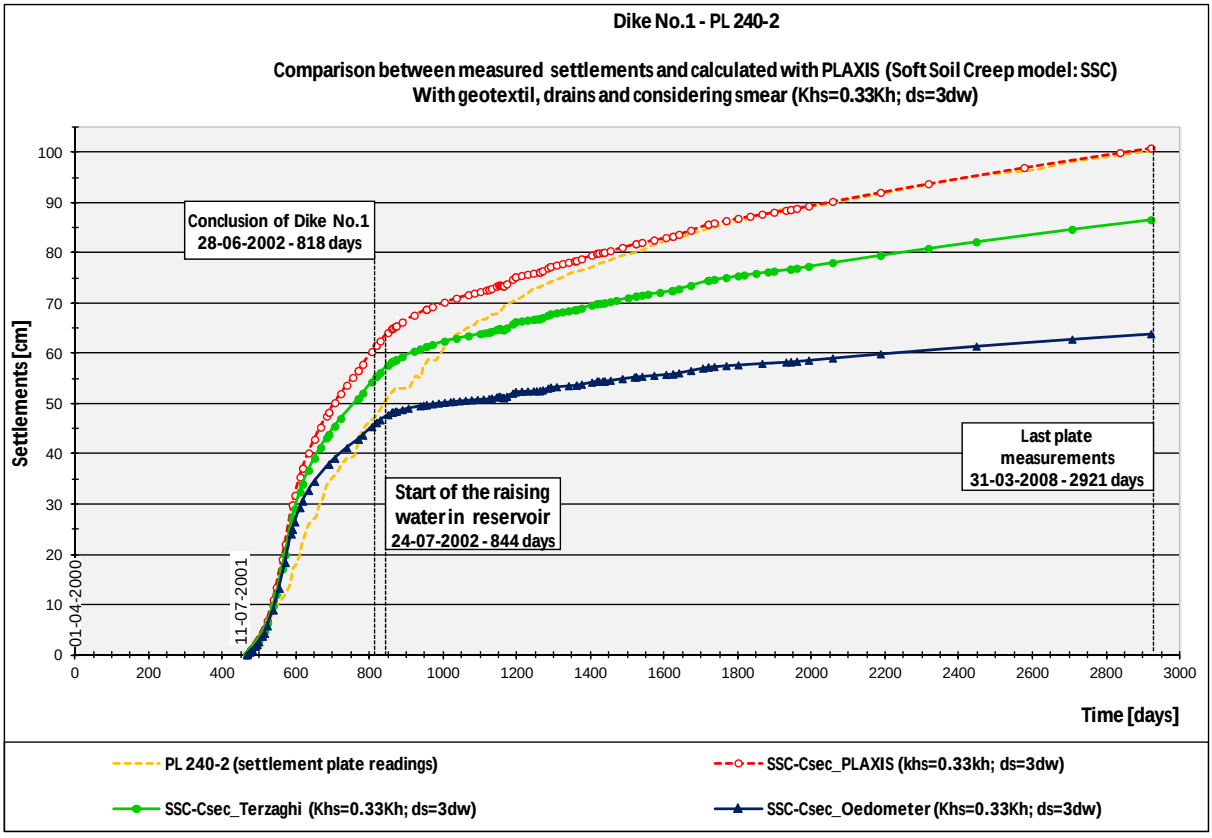

Graph VII.10 – PL 240-2 of Dike No.1: Settlements calculated with the *SSC* model considering several values for the secondary compressibility index (C_α)

e) Results of combining the SSC model, with the secondary compressibility index estimated accordingly to the PLAXIS relation, and smear corresponding to $K_{hsAx}=K_{hsPD}=0.10K_{h0}$ and $d_s=3d_w$:

Given the results of the parametric analyses performed thus far, it can be seen that the most significant parameters affecting the numerical calculations are, the horizontal permeability coefficient in the disturbed zone, the secondary compressibility index and the model behaviour adopted for the foundation soil.

So, in order to obtain a numerical result which adjusts, as well as possible, to the settlements of plates PL 240-1 and PL0240-2, all these parameters need to be combined. Based on the results and considerations already presented, the following possibilities were analysed:

- Soft Soil Creep model with secondary compressibility index (C_α) obtained from the Terzaghi *et al*. (1996) expression and smear corresponding to $K_{hsAx}=0.10K_{h0}$ and $d_s=3d_w$;
- Soft Soil Creep model with a secondary compressibility index (C_α) based on the relations suggested in PLAXIS and smear corresponding to $K_{hsAx}=0.10K_{h0}$ and $d_s=3d_w$;

The curves associated to these two scenarios can be found in graphs VII.11 and VII.12, being possible to observe a rather reasonable approximation between the settlements measured and calculated when the second hypothesis is adopted. In fact, considering the SSC model with the secondary compressibility index (C_α) calculated with the PLAXIS relations, and smear corresponding to $K_{hsAx}=0.10K_{h0}$ and $d_s=3d_w$, the results practically coincident, with major emphasis to the topographic stakes TS 240-1 and TS 240-2.

The results from the numerical calculations, associated to these second conditions, also adjust quite well to the settlements values for plates PL 240-1 and PL 240-2. The final values obtained are very similar, although during the construction phase they were still a little above the settlements measured.

Even though the topographic stake marks TS 205 and TS 270 are not located in section PK0+240, they are relatively close to it, and so it was decided to include them, for comparison purposes between the settlements calculated and registered. In this case, there is only a similarity in the evolution of the settlements for the topographic stake mark TS 205, and only for the conditions associated with the second scenario.

The deformed mesh and the vertical displacements (settlements) which correspond to the final stage of the calculations, for these last conditions, are represented in figures VII.31 and VII.32.

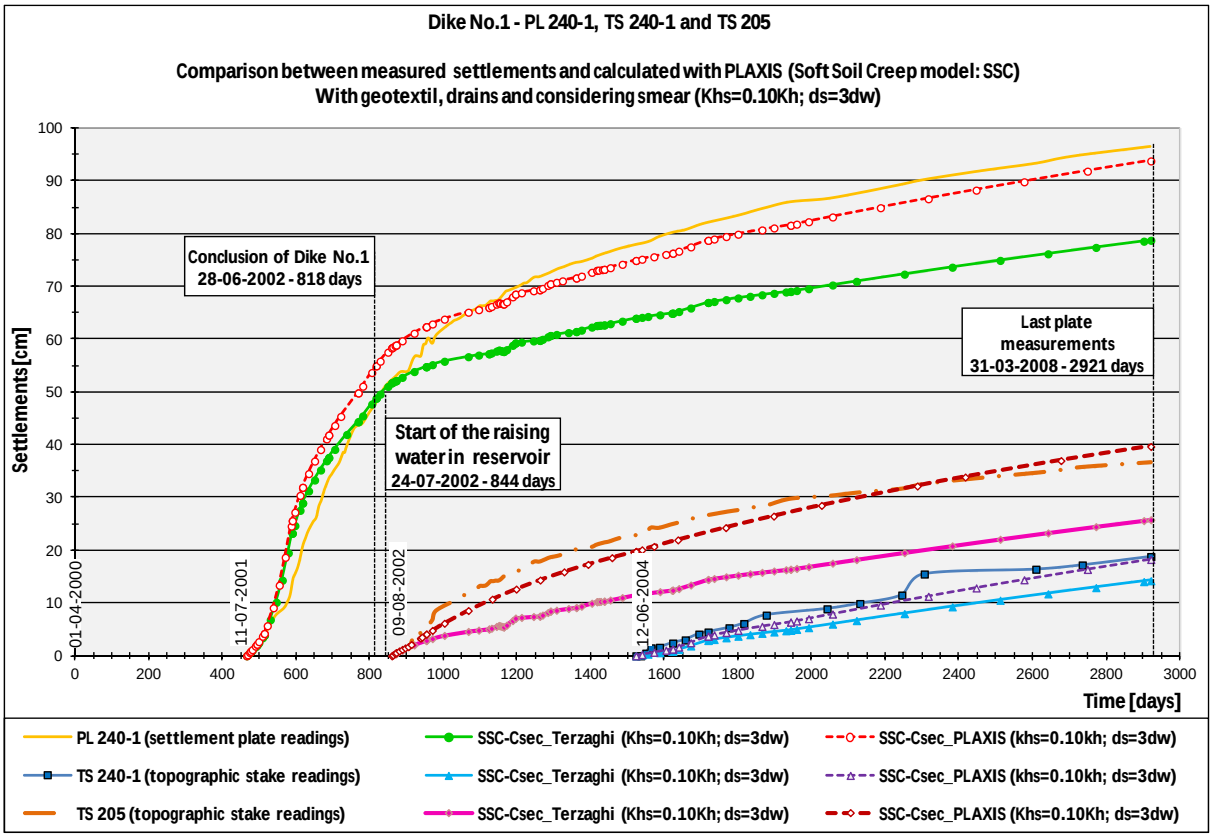

Graph VII.11 – Dike No.1: PL 240-1, TS 240-1 and TS 205 settlements, calculated with the *SSC* model, considering different secondary compressibility index (C_α) and smear given by $K_{hsAx}=0.10K_{h0}$ and $d_s=3d_w$

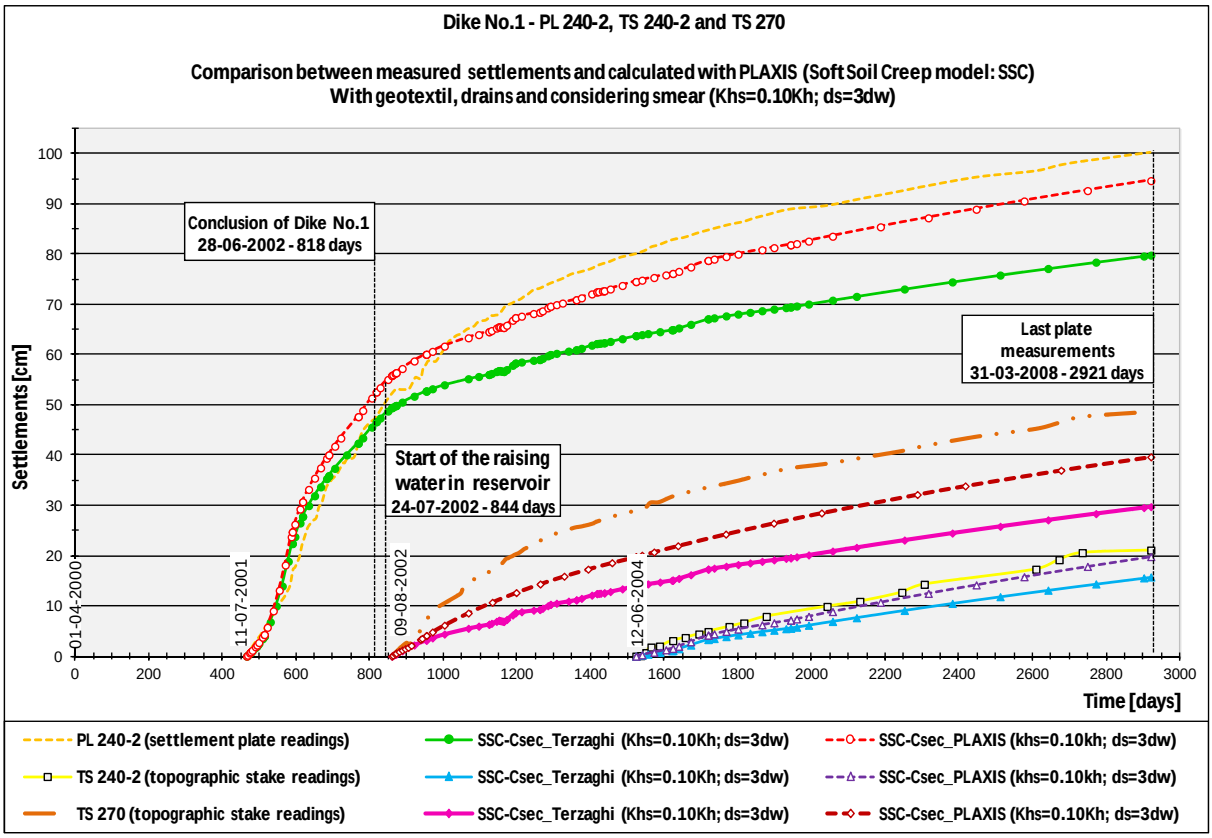

Graph VII.12 – Dike No.1: PL 240-2, TS 240-2 and TS 270 settlements calculated with the *SSC* model, considering different secondary compressibility index (C_α) and smear given by $K_{hsAx}=0.10K_{h0}$ and $d_s=3d_w$

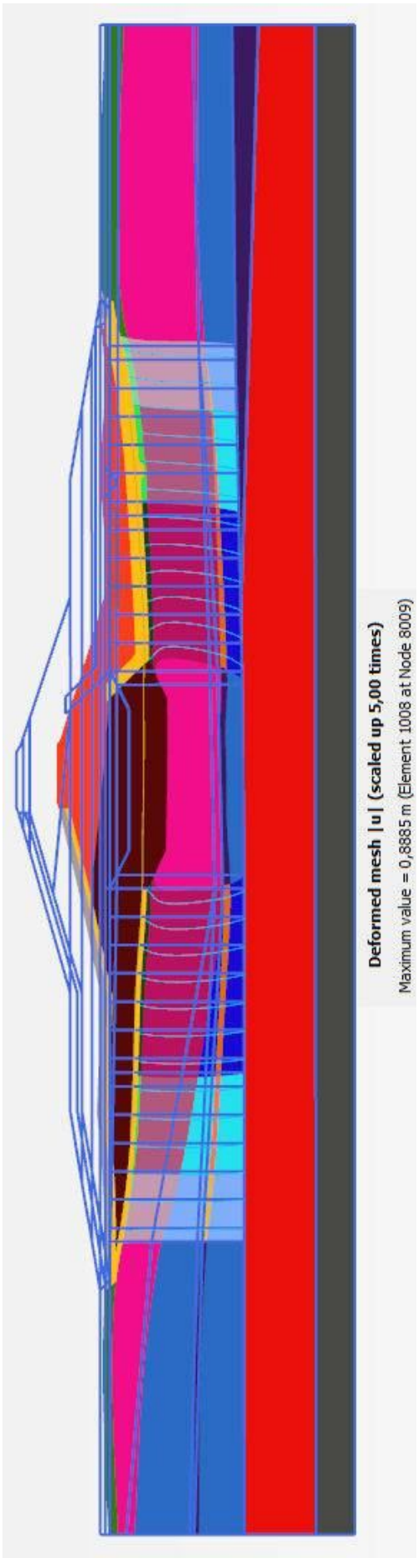

Figure VII.31 – PK0+240 of Dike No.1: Deformed mesh associated to the final calculation step, using the SSC model, and smear given by K_{hsAx}=0.10K_{h0} and d_s=3d_w

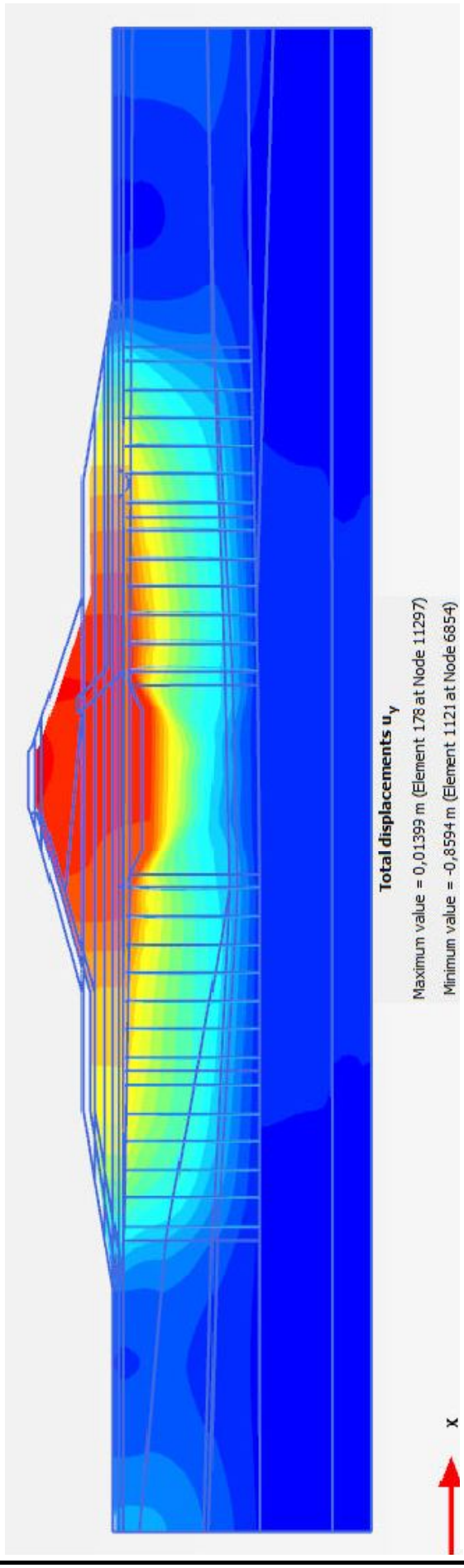

Figure VII.32 – PK0+240 of Dike No.1: Settlements associated to the final calculation step, using the SSC model, and smear given by K_{hsAx}=0.10K_{h0} and d_s=3d_w

VII.3.1.2. DIKE NO.3 SETTLEMENTS

In Dike No.3, and concerning the settlements analysis, the number of cross-sections modelled and studied is superior then Dike No.1. The study of the profiles PK0+140, PK0+170 and PK0+200 of Dike No.3 are of great interest, as it allows the comparison of the numerical results with and without drains. While no drains were applied to section PK0+200, the other sections of the foundation soil were treated with drains, although only downstream of the cut-off trench. By contrast, in Dike No.1, drains were applied both upstream and downstream of the cut-off trench. These differences allow the analyses to be diversified and the influence of these elements in the evolution of the consolidation and the settlements to be determined.

The analysis of the settlements readings have been already conducted in subchapter VI.6.4, however some of the results were difficult to interpret. In this chapter an effort will be made in order to understand the differences of the measured results, by comparing them to the numerical results. This can be done, since Dike No.1 gave an extremely good match between both results, and so, an order of the magnitude of the smear effect, as well as the secondary compressibility index, for the ground foundation, is already expected.

Thus, and due to the considerations taken for Dike No.1, for the analysis performed in Dike No.3 only the Soft Soil Creep model will be considered to simulate the behaviour of the soil foundation, with C_α being estimated based on the Terzaghi *et al.* (1996) expression or on the relations proposed by PLAXIS. With respect to the smear, two analyses are held, one ignoring the smear effect and the other with smear equal to $K_{hsAx}=0.10K_{h0}$ and $d_s=3d_w$. The analysis without smear permits to attain an idea of the maximum settlements for each cross-section, thought this is not a credible hypothesis.
Graphs VII.13 to VII.20 represent the settlement curves associated with the simulations for Dike No.3, and respective profiles. From comparing the results of the calculated and measured settlements, it is difficult to find a reasonable concordance for all the sections of Dike No.3. In fact:

- When the final settlements calculated come close to those measured, there is a significant difference in the initial phase;
- When the settlements have similar agreement in the construction phase, then the numerical results of the pos-constructive stage are relatively lower than the readings from the plates.

Looking at the different sections individually, it can be seen that:

> In section PK0+140, both the plates present settlements substantially lower than those calculated, not only on the construction phase but also on the filling of the reservoir. This result occurs even when considering C_α estimated with the PLAXIS relations, and for smear conditions given by $K_{hsAx}=0.10K_{h0}$ and $d_s=3d_w$. The difference between the results is more significant in plate PL 140-2 as the curves come closer 3 years (1175 days = 3.2 years) after the dike construction was concluded. This time is reduced to 1 year and 3 months (475 days =1.3 years) for plate PL 140-1. Additionally, while very good concordance of the settlements in the post-construction phase is observed for the latter, on the other plate these are always slightly above the values measured (Graphs VII.13 and VII.14);

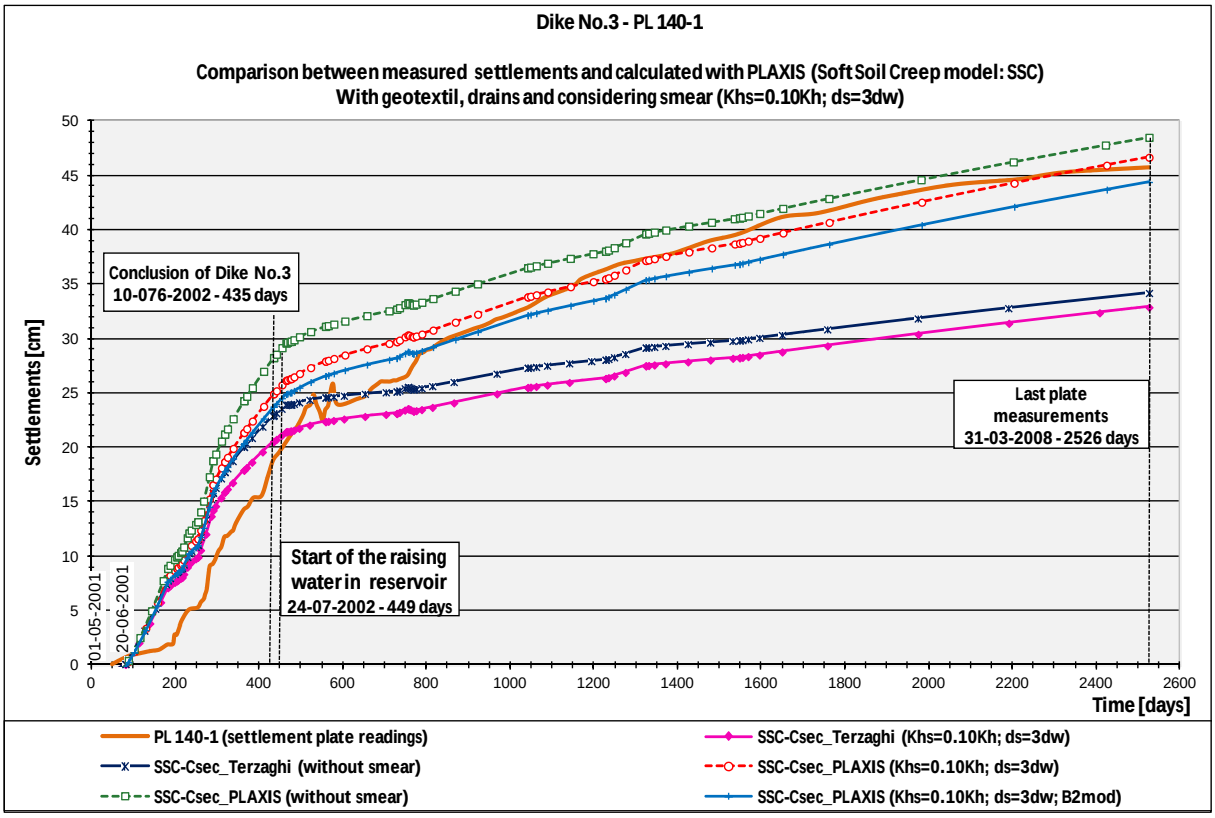

Graph VII.13 – PL 140-1 of Dike No.3: Settlements calculated with the *SSC* model, considering two different values for the secondary compressibility index (C_α), with and without smear effect

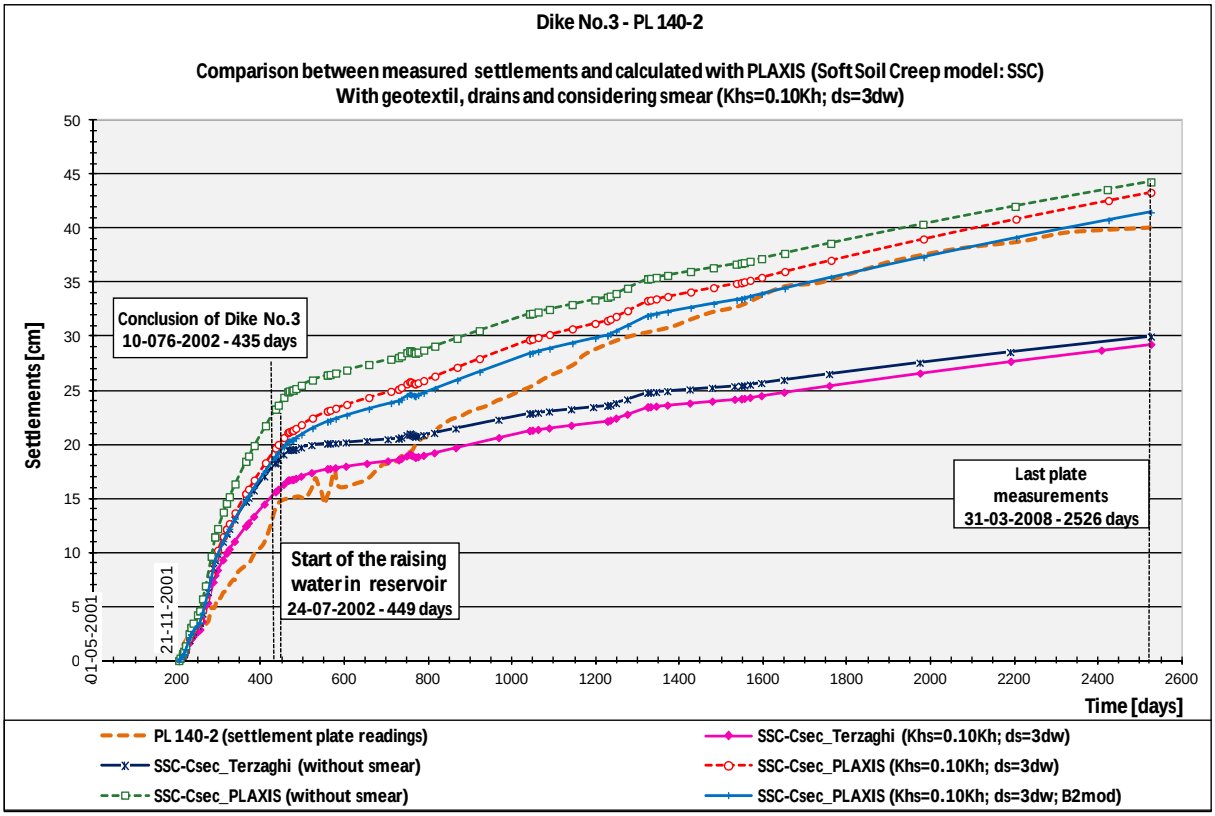

Graph VII.14 – PL 140-2 of Dike No.3: Settlements calculated with the *SSC* model, considering two different values for the secondary compressibility index (C_α), with and without smear effect

- In section PK0+170, the results from the simulations are coincident in the construction phase for plate PL 170-1, being much lower than the values measured in the post-construction phase. In turn, in plate PL 170-2 , it is observed precisely the opposite, meaning that there is concordance in the progress of the settlements for the post-construction phase, but in the initial phase the values calculated slightly exceed the real values. Discarding the simulation in which the smear effect is not considered, then, in general, the results which are closer to the plates readings correspond to C_α based on PLAXIS and smear equal to $K_{hsAx}=0.10K_{h0}$ and $d_s=3d_w$ (Graphs VII.15 and VII.16);
- In section PK0+200, excellent concordance is once again seen between the settlements calculated and measured for plate PL200-1 in the construction phase, although they are unable to traduce the evolution of the real settlements afterwards. In plate PL 200-2, again the settlements calculated are greater than those monitored in the construction phase, although this difference tends to decrease over time (Graphs VII.17 and VII.18).

From the comparison of the plate settlements numerical results, the fact that they present identical behaviour for plates PL170-1 and PL200-1 stands out, with the same occurring with plates PL 140-2, PL 170-2 and PL 200-2, although some slight differences are noted for these last plates. This would not be surprising, as long as these remarks were similar in all the plates, allowing conclusions to be withdrawn regarding to the parameters of the soils foundation in Dike No.3. As this is not the case, the following questions are immediately raised:

a) Are these plates exactly placed in the coordinates indicated before, which were considered in the simulations?

b) Are the compressibility parameters and permeability coefficients adopted for the foundation soil of Dike No.3 the most suitable?

These doubts are related more to plates PL 140-2, PL 170-2 and PL 200-2, which are located near the chimney drain and the horizontal downstream drain, and near the area improved with band-shaped drains. Looking at the results from the simulations, it is noticed that for these plates they always exceed the plate's readings, unlike to what happens with the other plates. This means, that the drainage in the simulation is occurring much faster than it happens in reality, or that the compressibility estimated for the soil foundation is too high. This second hypothesis is set aside, since the settlements for the plates located in the centre of the cut-off are quite good in the construction phase. Consequently, there is still the issue of the location of these plates and the soil horizontal permeability. To clarify the last issue, and since the horizontal permeability coefficient for stratum B2 of Dike No.3 is three times higher than the one adopted for Dike No.1, an additional calculation was made. For this calculation, the same horizontal permeability of Dike No.1 was considered for B2. The results obtained are shown in graphs VII.13 to VII.18. From their analysis and comparison, it can be seen that the decrease of settlements is of little significance for the sections treated with drains, and even less in the PK0+200, where there is no drains. Thus, given the results, it seems that these differences can be related to the location of the plates. If this is the case, they should be at a higher level and farther from the draining elements. In any case, it is very premature to take conclusions at this moment, as the results with the flow are yet to be analysed.

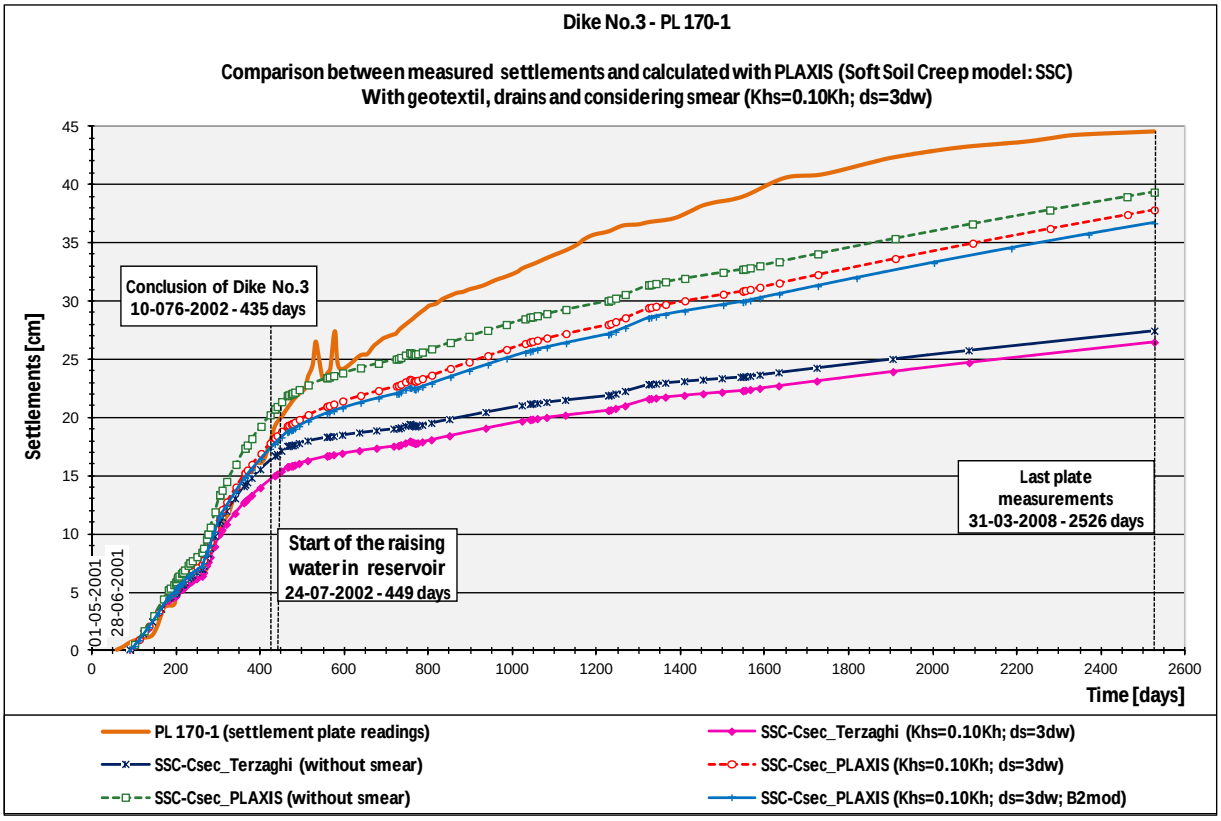

Graph VII.15 – PL 170-1 of Dike No.3: Settlements calculated with the *SSC* model, considering two different values for the secondary compressibility index (C_α), with and without smear effect

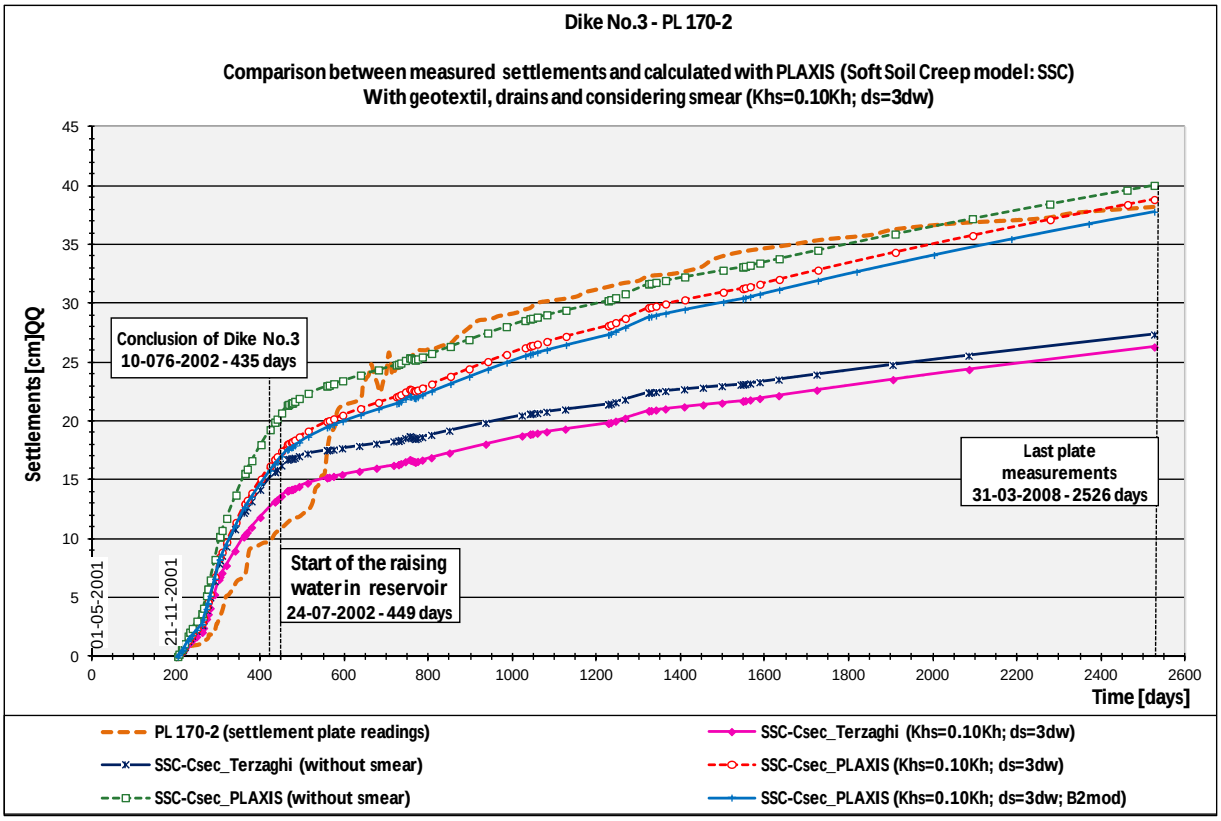

Graph VII.16 – PL 170-2 of Dike No.3: Settlements calculated with the *SSC* model, considering two different values for the secondary compressibility index (C_α), with and without smear effect

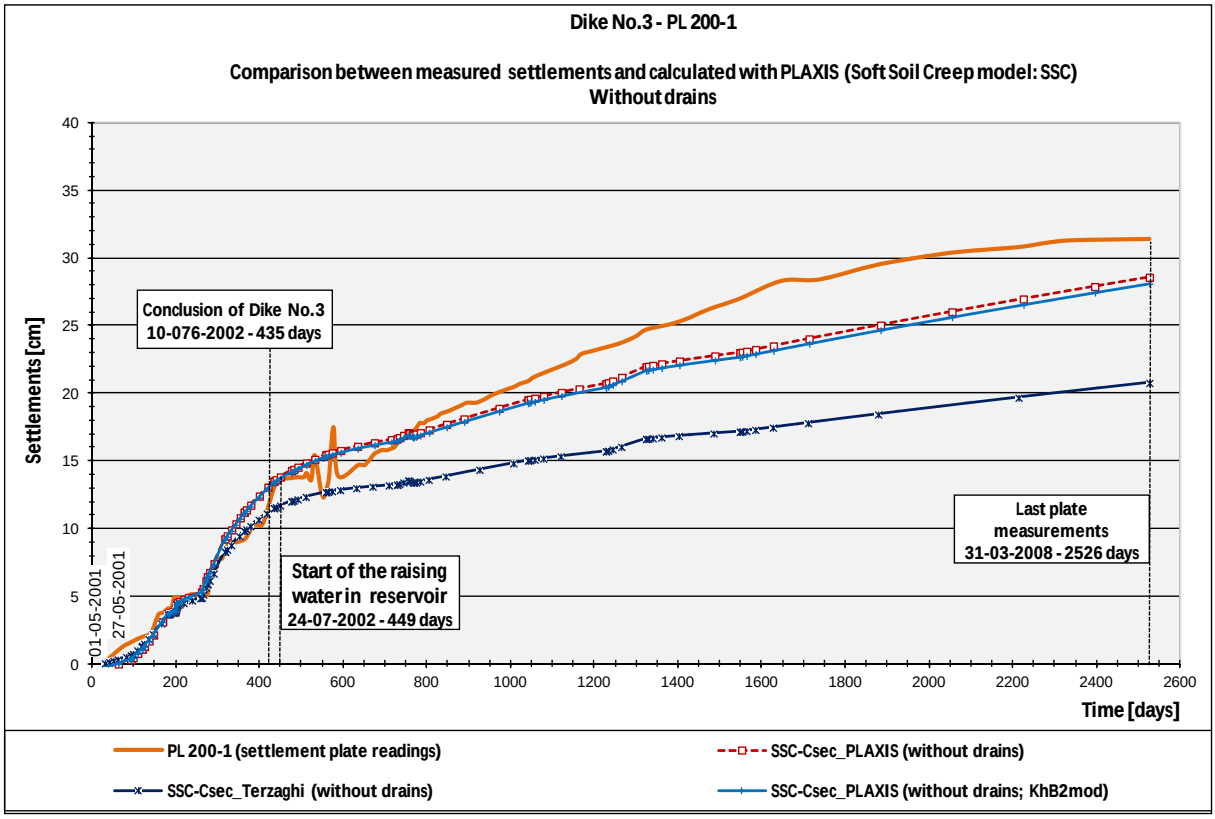

Graph VII.17 – PL 200-1 of Dike No.3: Settlements calculated with the *SSC* model, considering two different values for the secondary compressibility index (C_α)

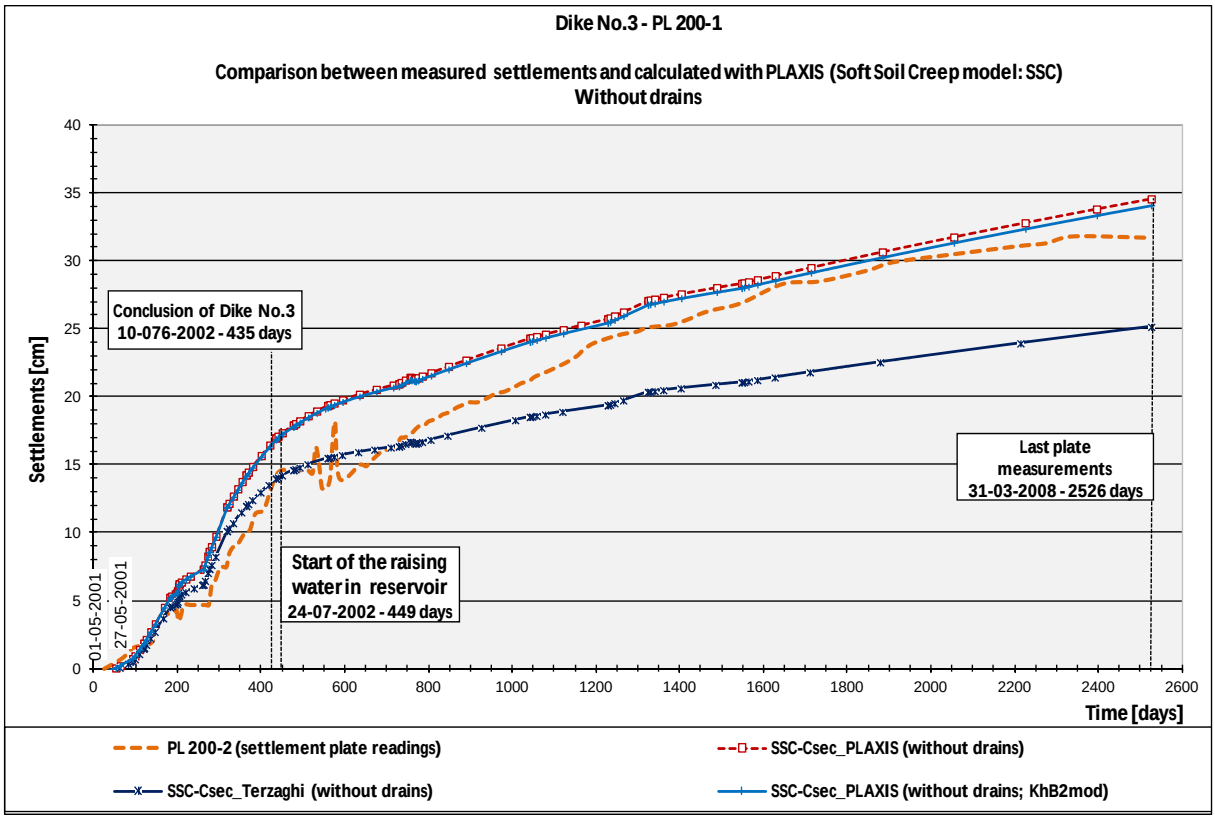

Graph VII.18 – PL 200-2 of Dike No.3: Settlements calculated with the *SSC* model, considering two different values for the secondary compressibility index (C_α)

Concerning the results obtained for the topographic stake marks TS 135 and TS 170, and for all the simulations performed they are lower than the measured values. However, once again, the result closest to the registered readings, corresponds to C_α estimated with PLAXIS and for the smear conditions $K_{hsAx}=0.10K_{h0}$ and $d_s=3d_w$ (Graphs VII.19 and VII.20).

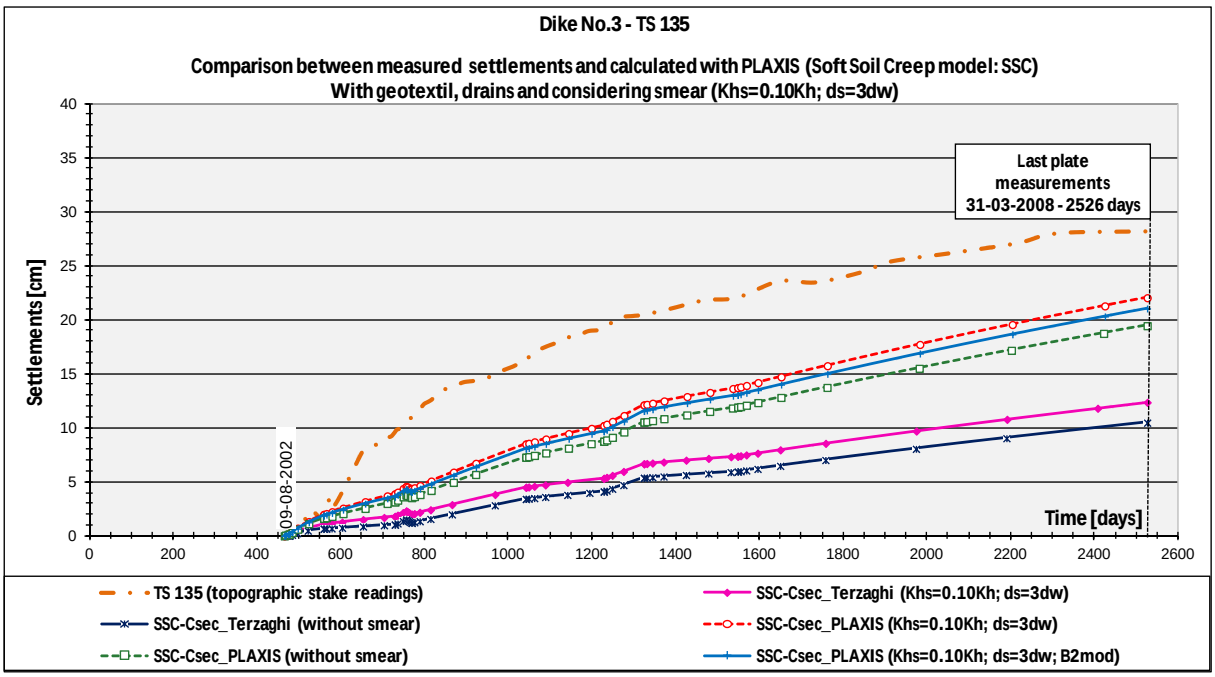

Graph VII.19 – TS 135 of Dike No.3: Settlements calculated with the *SSC* model, considering two different values for the secondary compressibility index (C_α), with and without smear effect

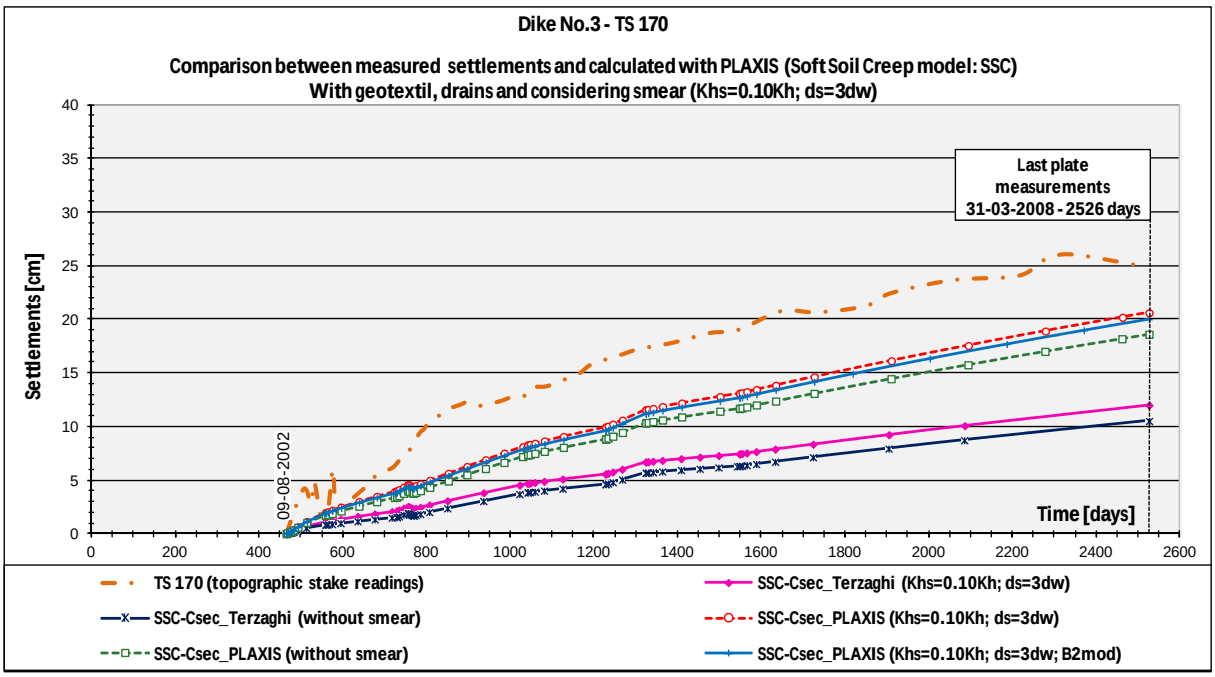

Graph VII.20 – TS 170 of Dike No.3: Settlements calculated with the *SSC* model, considering two different values for the secondary compressibility index (C_α), with and without smear effect

The final vertical displacements (settlements) for sections PK0+140, PK0+170 and PK0+200 of Dike No.3, corresponding to the Soft Soil Creep model with smear given by $K_{hsAx}=0.10K_{h0}$ and $d_s=3d_w$, are represented in figures VII.33, VII.34 and VII.35, respectively.

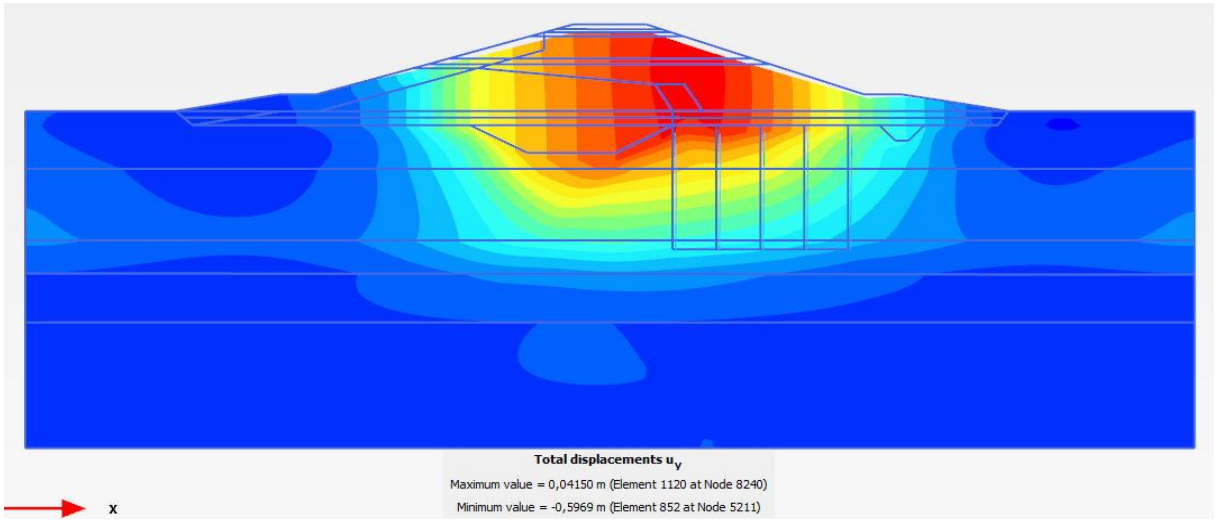

Figure VII.33 – PK0+140 of Dike No.3: Settlements associated to the final calculation step, using the *SSC* model, and smear effect given by $K_{hsAx}=0.10K_{h0}$ and $d_s=3d_w$

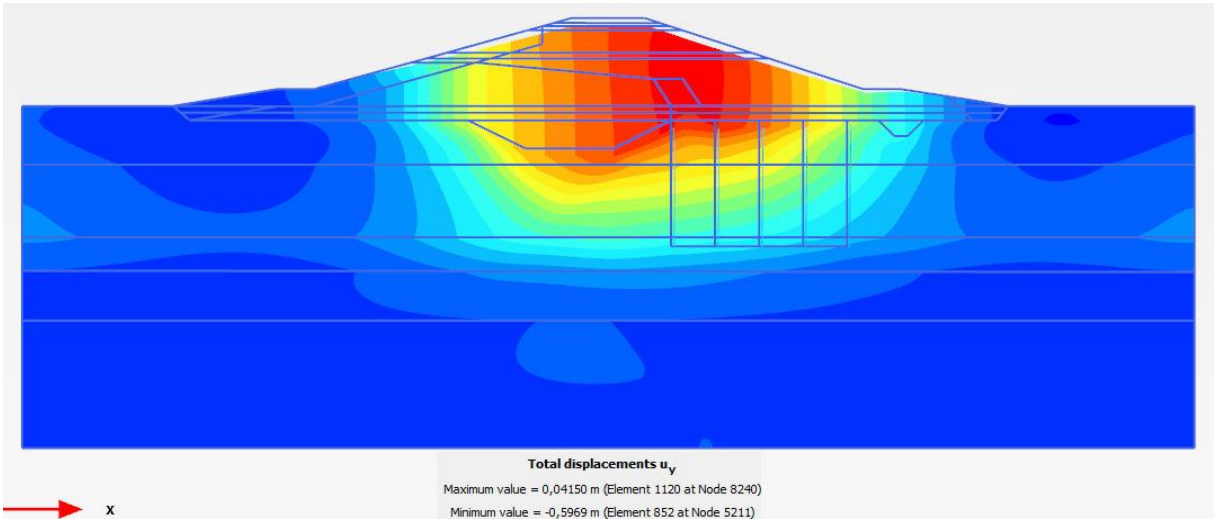

Figure VII.34 – PK0+170 of Dike No.3: Settlements associated to the final calculation step, using the *SSC* model, and smear effect given by $K_{hsAx}=0.10K_{h0}$ and $d_s=3d_w$

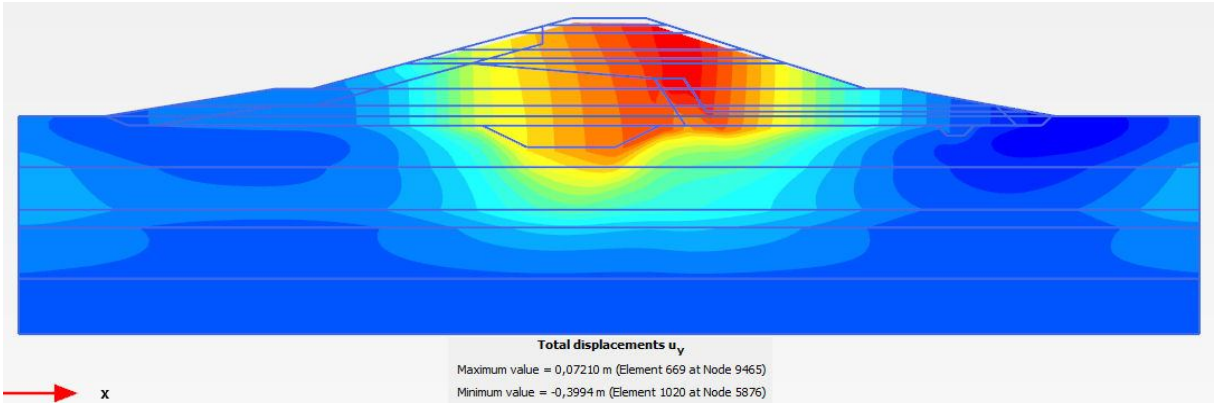

Figure VII.35 – PK0+200 of Dike No.3: Settlements associated to the final calculation step, using the *SSC* model, and smear effect given by $K_{hsAx}=0.10K_{h0}$ and $d_s=3d_w$

VII.3.1.3. PORE PRESSURES IN DIKE NO.1

From the 11 stress points where the pore pressures were controlled in the profile PK0+240 of Dike No.1, 5 are located inside the embankment, at the level of the cut-off, and 6 in the foundation in the areas improved with band-shaped drains (3 upstream and 3 downstream). In light of the high number of points to be controlled and compared, it was decided to concentrate the results of the analyses in order to reduce the number of graphs. As such, two distinct graphs, for each of the piezometers, are displayed, being:

a) In the first one, the curves associated with the following models are represented:
   - Mohr-Coulomb for methods A and B, with the stiffness modulus calculated according to the reduced value of the undrained cohesion (E_{ref}*=f(c_u*));
   - *Soft Soil*;
   - Soft Soil Creep, with C_α calculated by the Terzaghi *et al.* (1996) expression and PLAXIS relations;

   Adopting a smear effect constant and equal to $K_{hsAx}=0.33K_{h0}$ and $d_s=3d_w$.

b) In the second graph are represented the curves obtained only for the Soft Soil Creep model, with the value of C_α proposed by PLAXIS, with a constant smear diameter ($d_s=3d_w$), but considering different disturbed horizontal permeability coefficient (K_{hs}).

Additionally, and since evolution of the curves for the piezometers aligned beneath the upstream and downstream berm, are identical, it was decided to plot only the numerical results of the upper and lower piezometer, namely piezometers PZ 240-6A, PZ 240-6C, PZ 240-7A and PZ 240-7C are presented. However, and although the simulation results for PZ 240-6A were calculated, they will not be presented, as there is are no monitoring results for this piezometer. Regarding the piezometers placed in the dike, all the simulations results associated them will be shown. The exception is applied to PZ 240-4, as this is located mid-way between the PZ 240-3 and PZ0240-5.

On graphs VII.21 to VII.27 the pore pressures curves associated to the abovementioned piezometers, and corresponding to the first type analysis, are plotted. On the other hand, graphs VII.28 to VII.33 shows the curves of the remaining analysis. Excess pore pressure curves were not added, to avoid an overload of data in the graphs, thereby making it easier to read and understand them.

a) Results associated with the smear effect given by $K_{hsAx}=0.33K_{h0}$ and $d_s=3d_w$, adopting different material models for the soil foundation, as well as different values of C_α:

In general, based on the curves represented in graphs VII.21 to VII.27, it is observed that the numerical results are considerably different depending on their location. Therefore, based on them, the following remarks can be point out:

- The pore pressures for the Mohr-Coulomb model are always lower than those obtained with the SS and SSC models. This difference is more accentuated in the piezometers located at the base of the cut-off and inside the dike, and is minimal for the piezometers located in the foundation, since these are inserted between the drains;

- The pore pressures from the Soft Soil Creep model, with C_α determined with the PLAXIS relations, are always higher. However, during the construction phase, the results for the SS and SSC are practically the same. This is the reason why the settlements for these models and with the same conditions also coincide during almost the entire construction phase;
- The variations in the overloads, due both to the construction of the embankment and the reservoir filling, have an immediate effect on the simulations results. However, based on the interpretation of the results from the piezometers readings, performed in chapter VI, it is known that, in reality, there is a time lag between the application of the loads and the effect on the piezometers. The major consequence and difference associated with this effect is that, in the results from the simulations, any change of the construction level or in the water level in the pond leads to an immediate change in pore pressures.

Analysing the results for each of the piezometers, it can be added that:

- In piezometers PZ 240-1 and PZ 240-2, located at the base of the cut-off, the pore pressures calculated using the MC model are much lower than those registered, being the SSC model the one which is able to better describe the pore pressure over time. However, while for PZ 240-1 a reasonable adjustment between the results can be observed, this is not the case with PZ 240-2 (Graphs VII.21 and VI.22), thought the simulation results at these control points are identical. This significant discrepancy between measured and calculated results for the PZ 240-2, are in fact due to the higher and unexpected values measured in this piezometer, which are much greater than those from PZ 240-1;
- In piezometers PZ 240-3 and PZ 240-5, located 3 metres above the previous piezometers, already inside the dike and at foundation level, the model that give better results when compared with the readings, is the MC model. All the other models present much higher results. This difference between the results occurs during the construction phase and continues over time (Graphs VII.23 and VI.24). Due to the comparison of these numerical results with the real ones, without taking into account the flow net, this analysis is considered unsuitable to traduce the soil response inside the body of the embankment;
- In piezometer PZ 2406C, which is inserted in the upstream zone where the drains were installed, there is a reasonable adjustment between the results after the reservoir filling. Yet, in the initial phase, which corresponds to the construction of the embankment, there is a difference between the calculated and measured pore pressures. While the simulation results gradually decrease after a first initial value, indicating dissipation of excess pore pressure, the measures show a peak more or less half way through this phase, followed by a reduction. This difference leads to a discrepancy between the results in question. This peak corresponds approximately to the time when the embankment practically reaches its maximum height, followed by an interruption in the construction works, and only afterwards does the reservoir filling begins. However, the numerical calculation apparently considers only the overload associated to the embankment construction up to the level of the berm, and does not traduces the influence of the construction works above the berm level, and thus creating this discrepancy between on the constructing phase.

Another interesting aspect of these piezometers is related to the immediately increase in pore pressure with the reservoir filling. The rise up of the water level in the pond is felt instantaneously by the piezometers. This phenomenon occurs because, in this case, there is contact between the water in the pond and the drains, throughout the rip-rap upstream slope protection and the upstream drainage blanket (Graph VII.25);

- In piezometers PZ 240-7A and PZ 240-7C, there is a good approximation between the simulations results and the readings, for the SSC model with C_α determined from PLAXIS relations, especially from the moment correspondent to the pond filling. These piezometers are located in the zone with band-shaped drains, but in this case placed below the downstream berm. For these piezometers, once more the phenomenon described above occurs during the construction phase, although the increase of pore pressures measurements are smaller at depth, and so there is greater similarity between the real and numerical results (Graphs VII.26 and VI.27). As these piezometers are located in the downstream zone, there is no record of significant increments in pressure when the water starts to rise in the pond; instead, only a slight increase is seen, corresponding to the beginning of this phase, followed by a reduction. This result indicates that the drains are working and fulfilling their mission, since the excess pore pressure is dissipated over time.

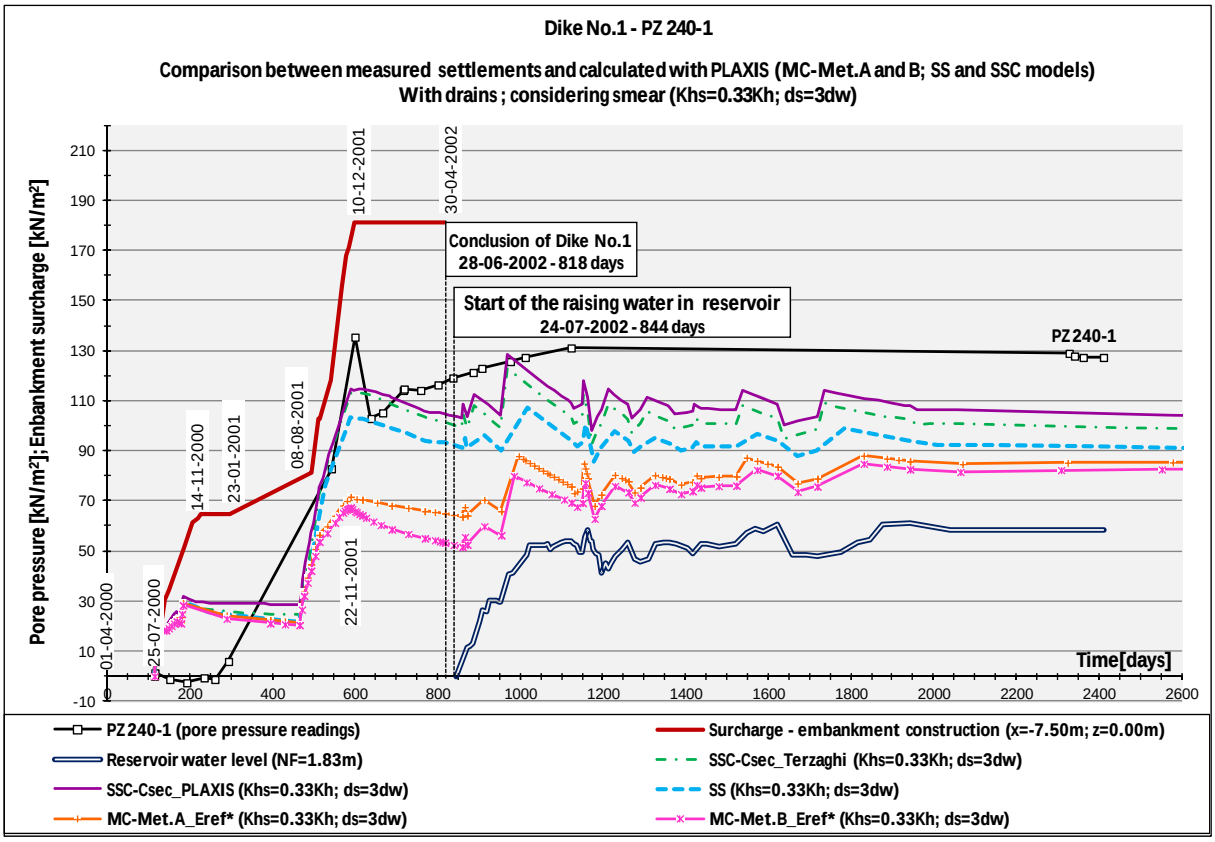

Graph VII.21 – PZ 240-1 of Dike No.1: Pore pressures calculated with MC, SS and SSC models, for various values of secondary compressibility index (C_α), and smear effect given by $K_{hsAx}=0.33K_{h0}$ and $d_s=3d_w$

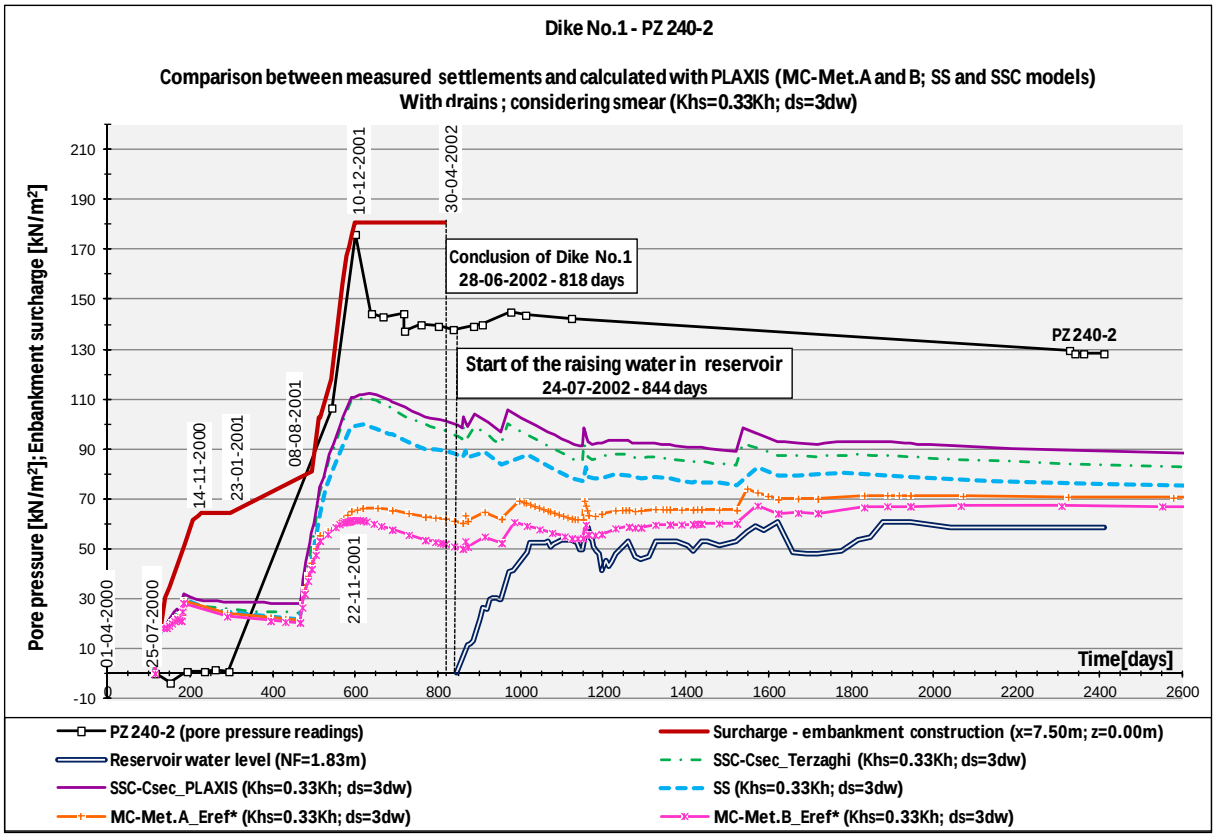

Graph VII.22 – PZ 240-2 of Dike No.1: Pore pressures calculated with MC, SS and SSC models, for various values of secondary compressibility index (C_α), and smear effect given by $K_{hsAx}=0.33K_{h0}$ and $d_s=3d_w$

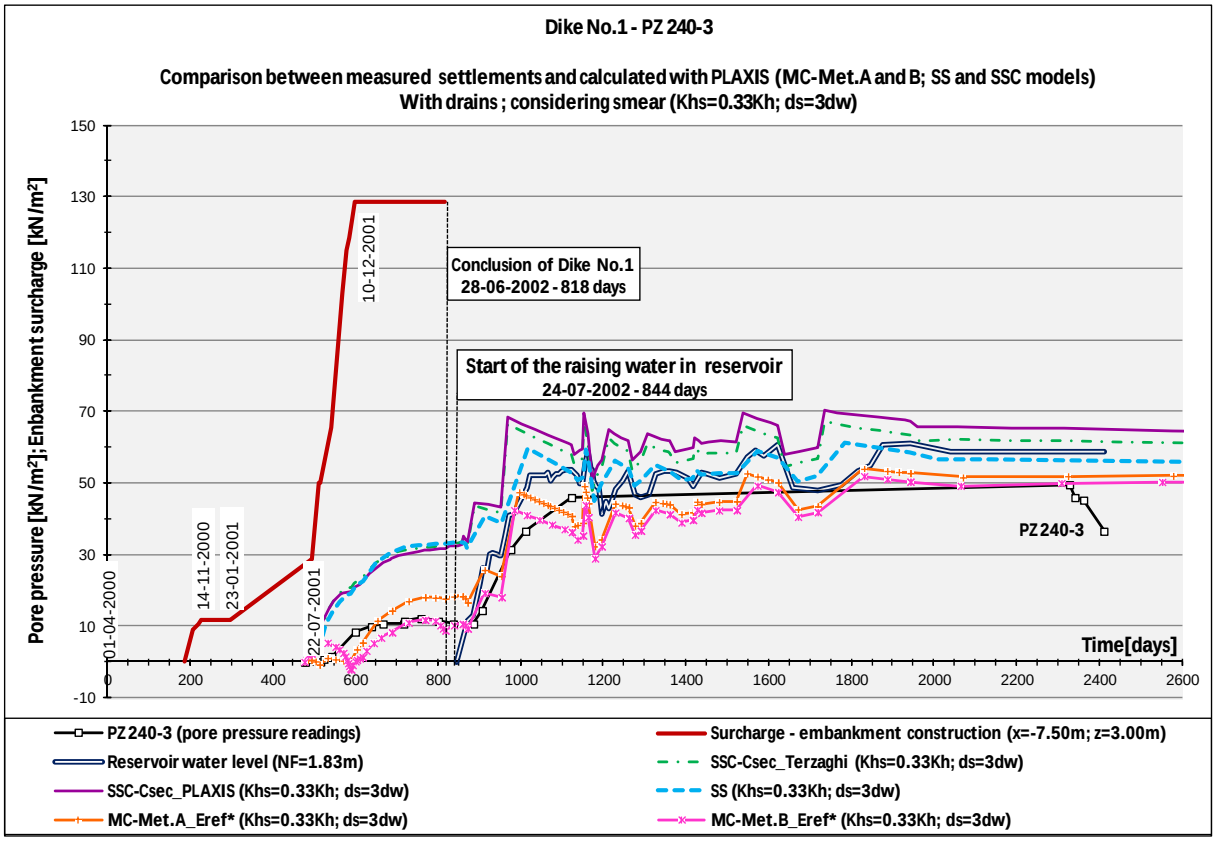

Graph VII.23 – PZ 240-3 of Dike No.1: Pore pressures calculated with MC, SS and SSC models, for various values of secondary compressibility index (C_α), and smear effect given by $K_{hsAx}=0.33K_{h0}$ and $d_s=3d_w$

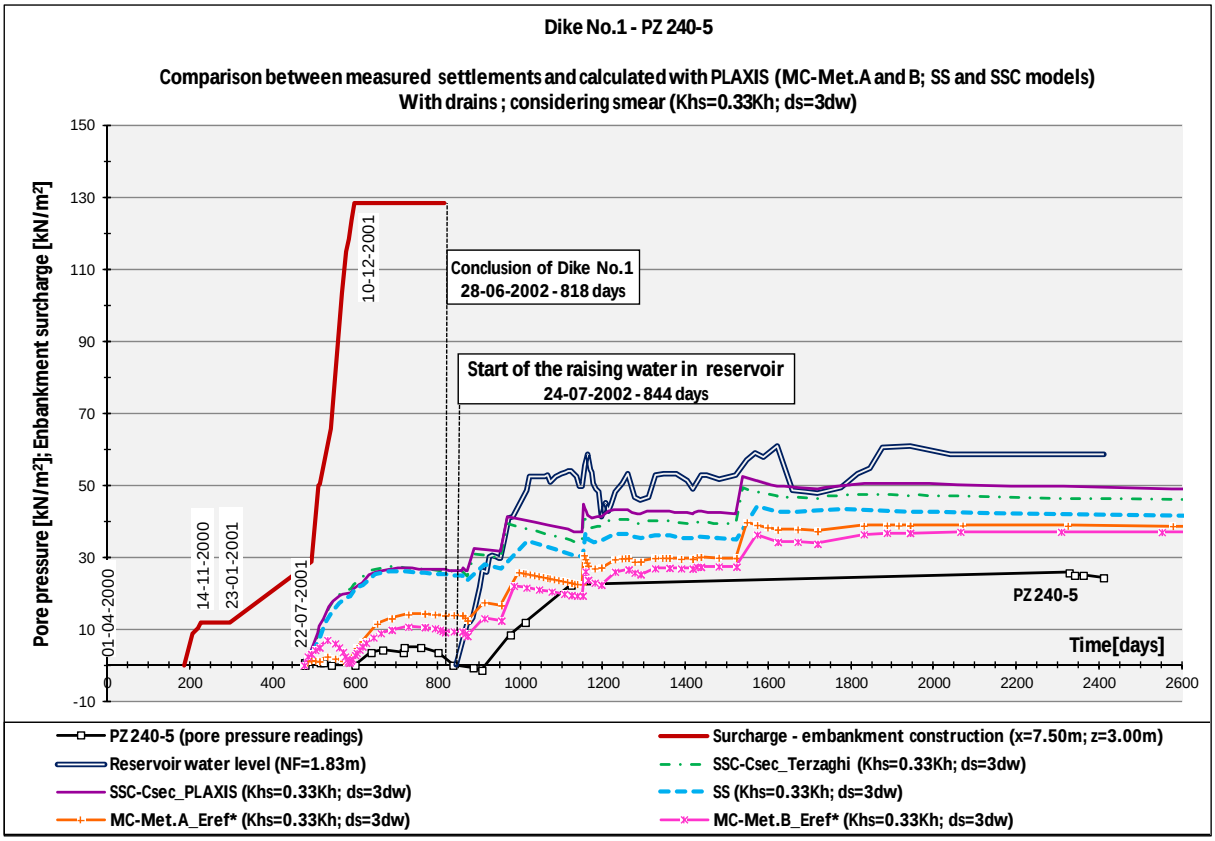

Graph VII.24 – PZ 240-5 of Dike No.1: Pore pressures calculated with MC, SS and SSC models, for various values of secondary compressibility index (C_α), and smear effect given by $K_{hsAx}=0.33K_{h0}$ and $d_s=3d_w$

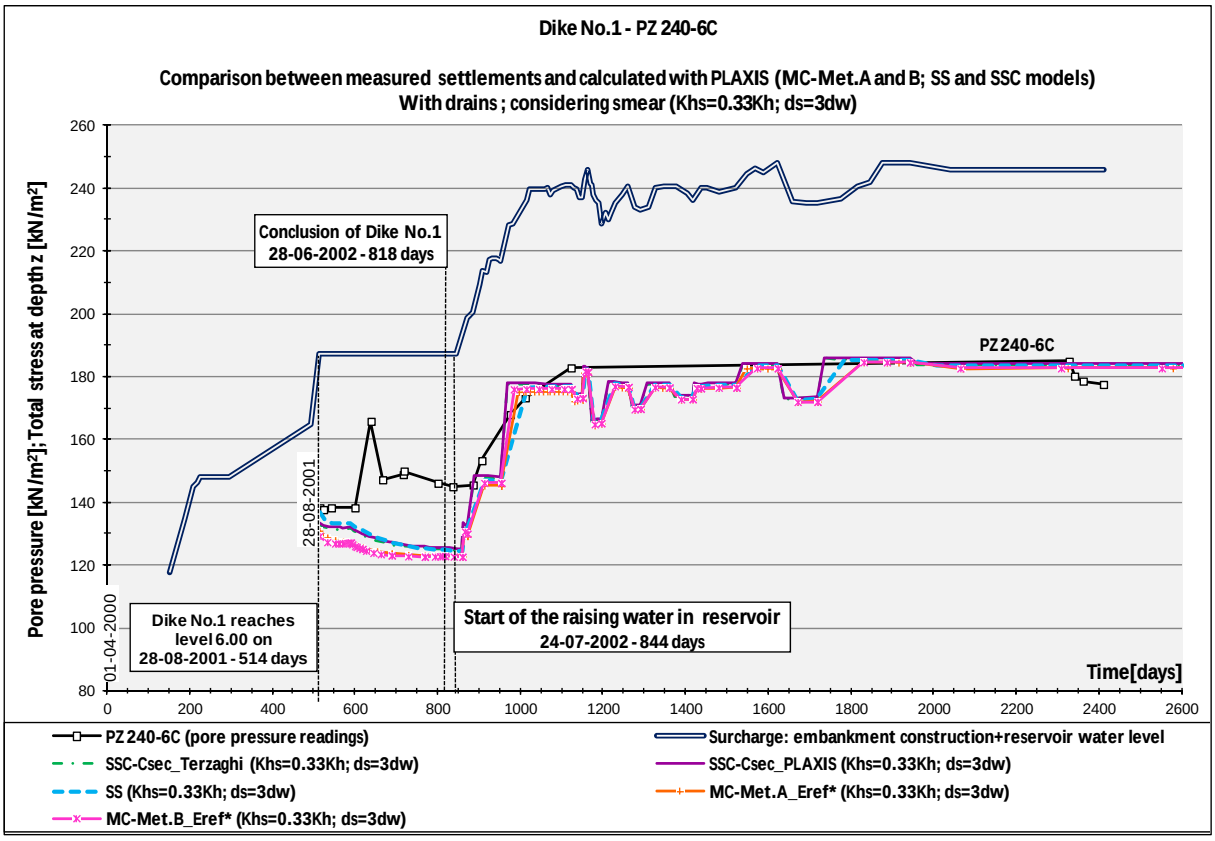

Graph VII.25 – PZ 240-6C of Dike No.1: Pore pressures calculated with MC, SS and SSC models, for various values of secondary compressibility index (C_α), and smear effect given by $K_{hsAx}=0.33K_{h0}$ and $d_s=3d_w$

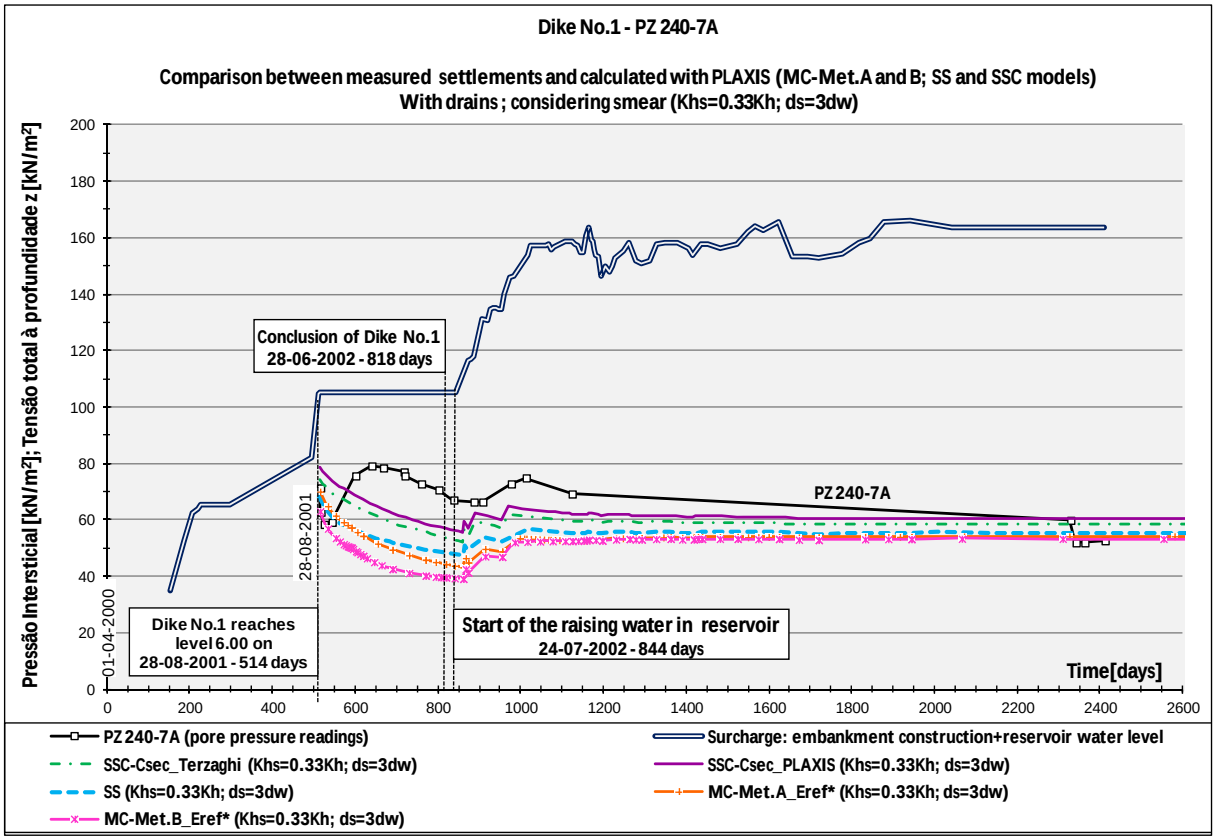

Graph VII.26 – PZ 240-7A of Dike No.1: Pore pressures calculated with MC, SS and SSC models, for various values of secondary compressibility index (C_α), and smear effect given by $K_{hsAx}=0.33K_{h0}$ and $d_s=3d_w$

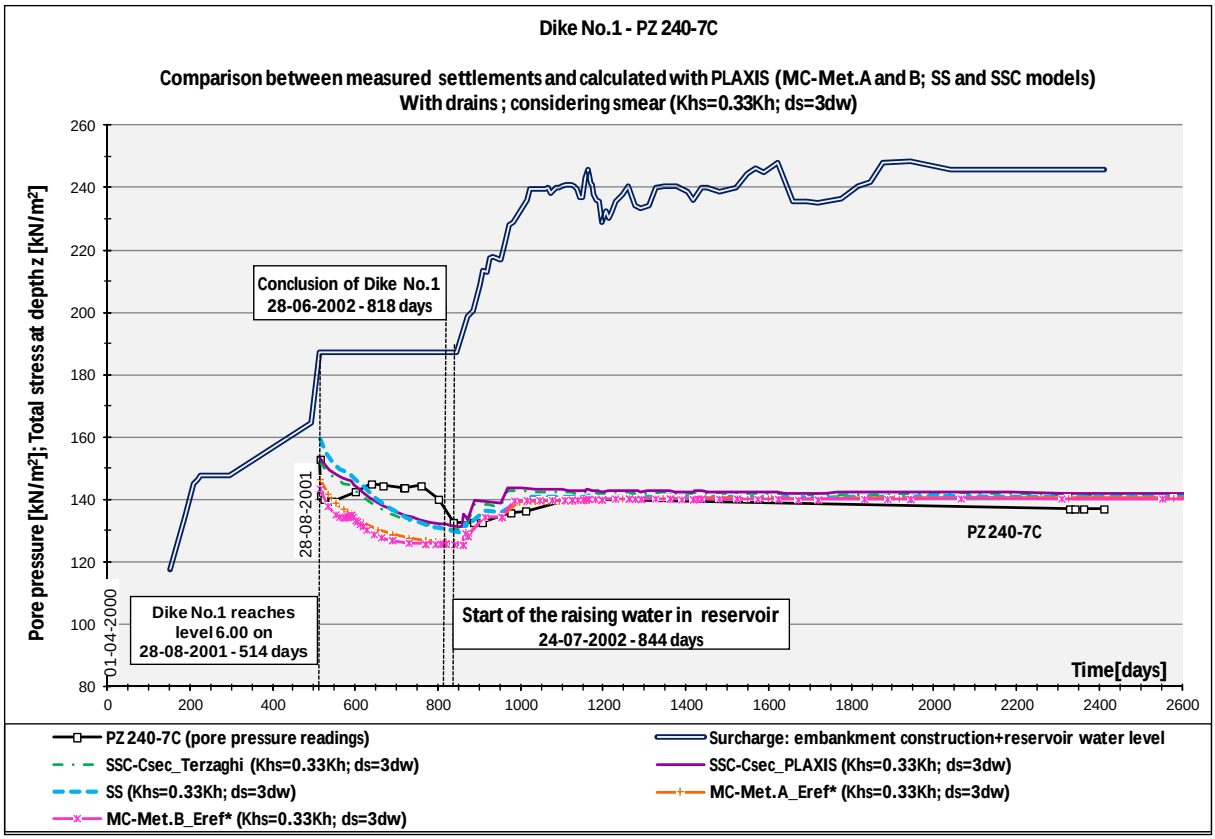

Graph VII.27 – PZ 240-7C of Dike No.1: Pore pressures calculated with MC, SS and SSC models, for various values of secondary compressibility index (C_α), and smear effect given by $K_{hsAx}=0.33K_{h0}$ and $d_s=3d_w$

b) Results associated with the Soft Soil Creep model for the soil foundation, including parametric analysis of the disturbed horizontal permeability coefficient K_{hsAx}

Based on graphs VII.28 to VII.33, it is seen that, in general, the curve which is closest to the measured results in the piezometers is, again, given by the smear condition $K_{hsAx}=0.10K_{h0}$ and $d_s=3d_w$, although the differences for the pore pressure curves with the three values of K_{hs} is almost insignificant, when compared with the settlements curves for the same simulation conditions. As expected, the higher values of pore pressure correspond to the lowest permeability of the soils foundation, since the drainage takes longer and so the same will happen to the dissipation of the pore pressure excess.

Once again, for piezometers PZ 240-3 and PZ 240-5, the simulations results are far superior to pressures measured, indicating that the drainage in the dike, i.e., "*in-situ*", takes place faster (Graphs VII. 30 and VII. 31). Consequently the settlements based on the simulations should be lower than the observed and measured in the plates. However, analyzing the values obtained on plates PL 240-1 and PL 240-2, which are situated near these piezometers, such does not occur. In fact, there is a good approach between the measured and calculated settlements at an early stage, but to higher permeability values the settlement attained are also higher (Graphs VII. 5 and VII. 6). However, relatively to the pore pressure curves associated to the variations of the horizontal permeability coefficient in the disturbed zone, for the piezometers that are placed inside the dyke, they remain constant until just before the reservoir filling. Up to the time of the dike conclusion, the coincidence between the curves is nearly complete for the several values of k_{hs}. So, apparently the discrepancy in terms of settlements, is not only due to the values of permeability, but also to the influence of secondary compressibility, starting to be felt in an early stage of the dike construction (Graphs VII. 9 and VII. 10).

Another interesting difference observed in the numerical values of the pore pressures, are the following:

- On the control stress points located inside of the dike, these are virtually coincident during the constructive phase of the dike, suffering only slight separation from each other during the filling of the reservoir;
- On the control stress points place in the ground foundation, either upstream or downstream of the cut-off trench, occurs precisely the reverse. In this case, the pore pressures are more distanced from each other on the constructive phase, converging to the same value during the filling phase.

This phenomenon is associated to the fact the that only the soils foundation, comprehended in the improved area, suffer variation on the horizontal permeability coefficients (k_{hPD}); in the embankment the permeability remains the same, and as such, the small variations observed in the post-construction phase takes place almost exclusively in the piezometers installed at the base of the cut-off trench, due to the influence of the soils foundation that are immediately below.

The hydraulic load associated with the end of construction and the final stage of the calculation is represented in figures VII.36 to VII.37. In turn, the corresponding pore pressures and the excess pore pressure, for the above conditions, are represented in figures VII.38 to VII.41.

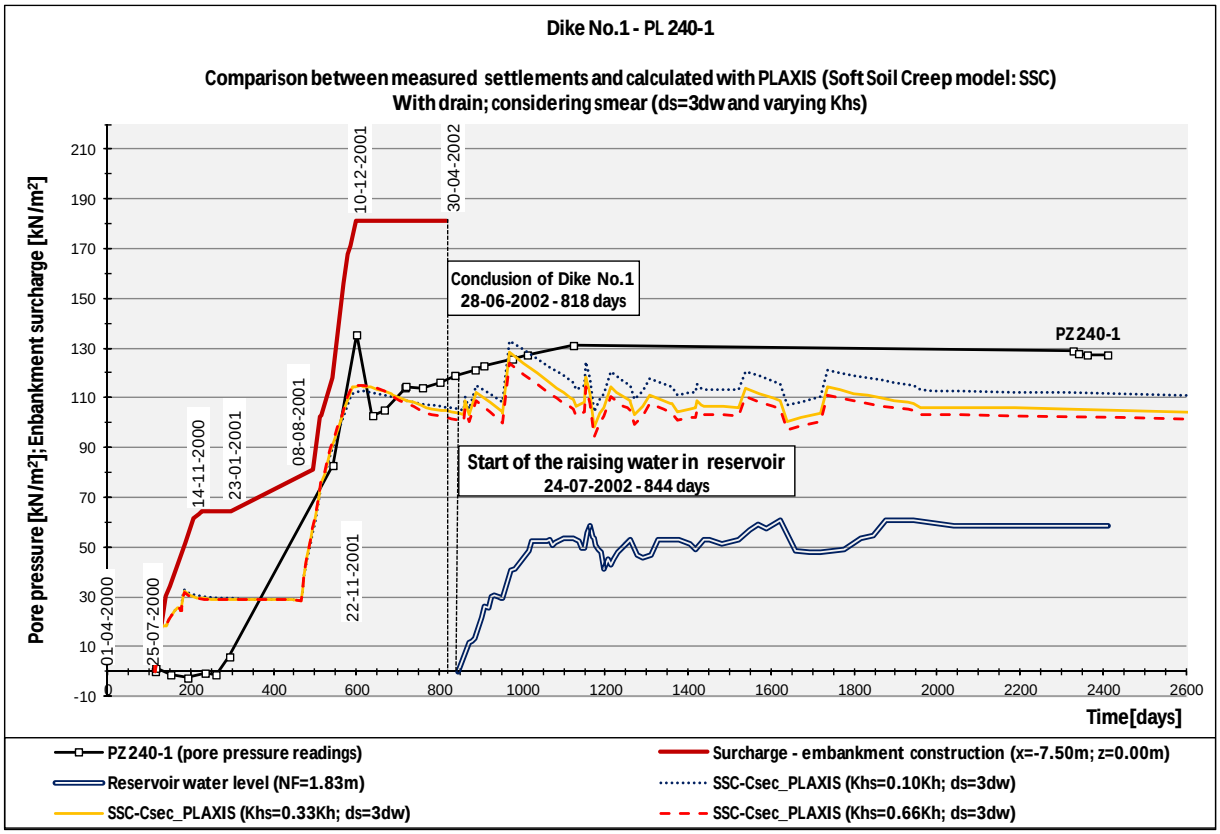

Graph VII.28 – PZ 240-1 of Dike No.1: Pore pressures calculated with the *SSC* models, considering several permeabilities in smear zone (K_{hs}), keeping diameter constant and equal to $d_s=3d_w$

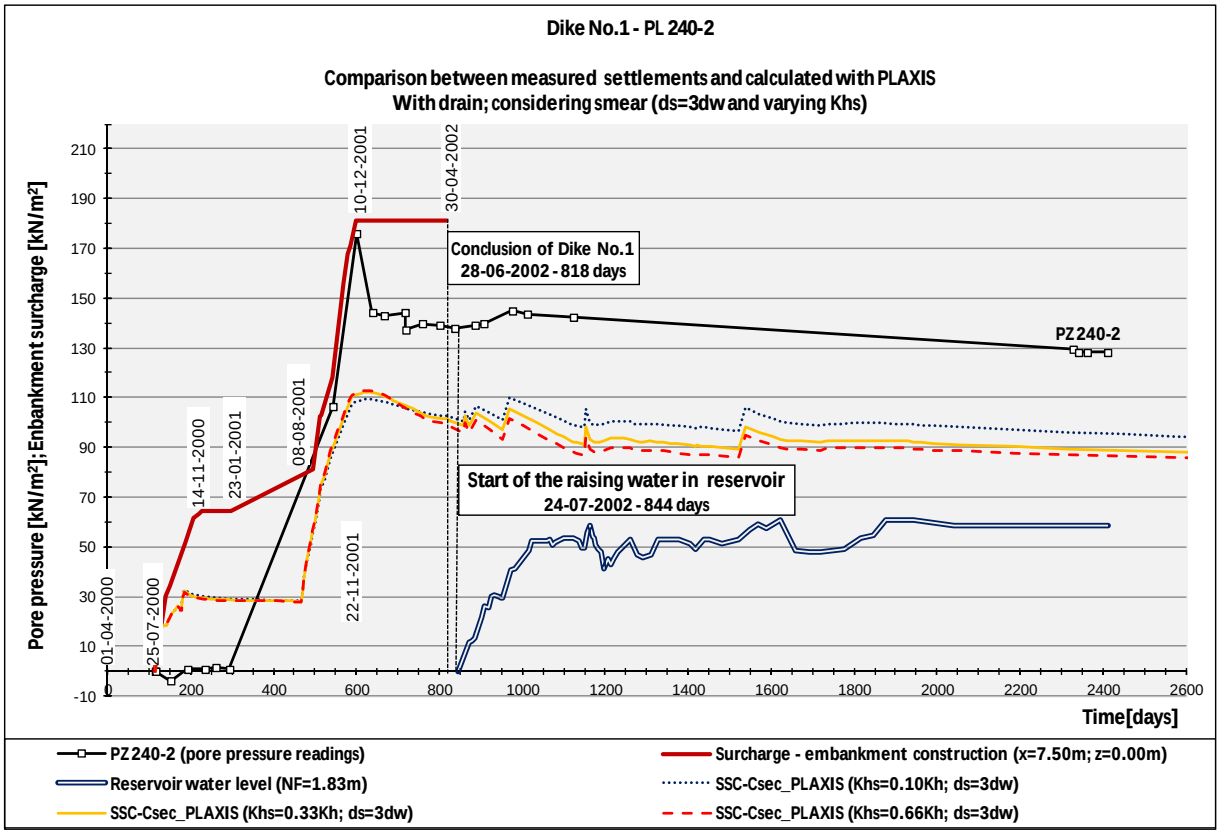

Graph VII.29 – PZ 240-2 of Dike No.1: Pore pressures calculated with the *SSC* models, considering several permeabilities in smear zone (K_{hs}), keeping diameter constant and equal to $d_s=3d_w$

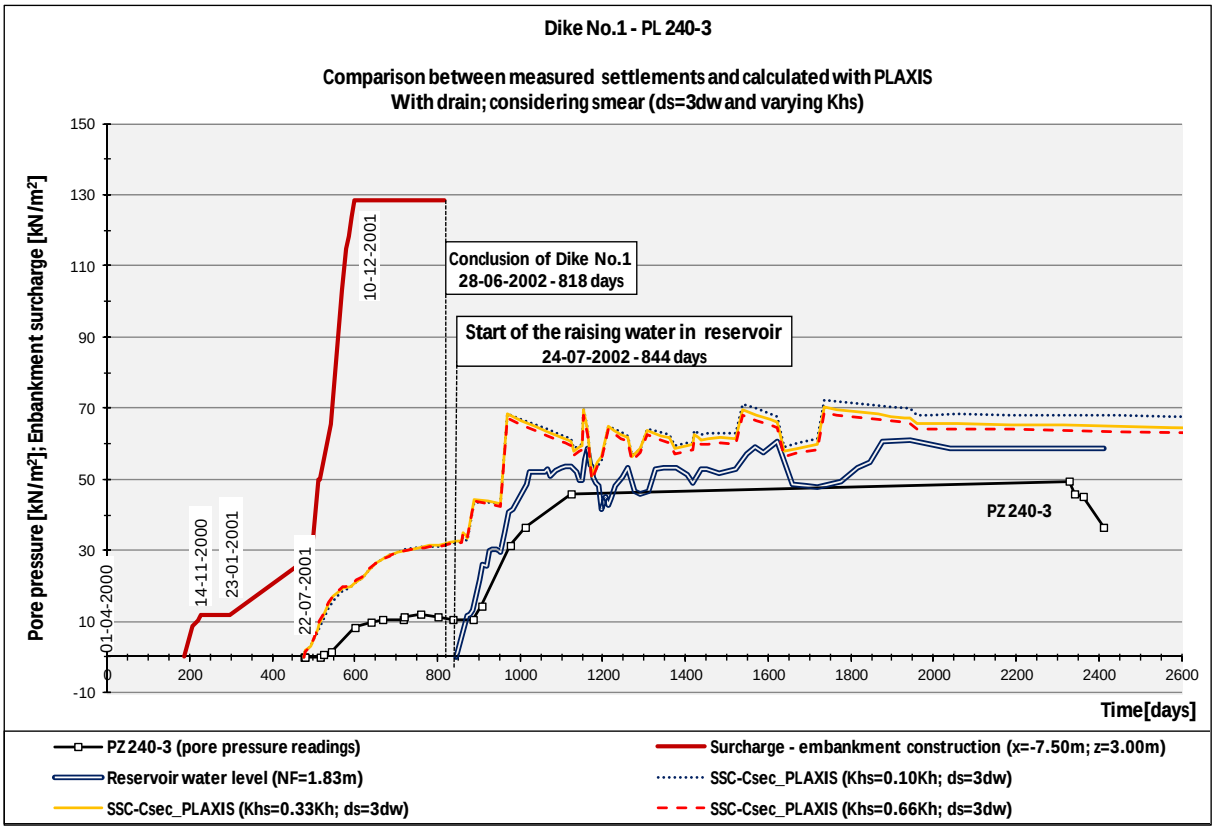

Graph VII.30 – PZ 240-3 of Dike No.1: Pore pressures calculated with the *SSC* models, considering several permeabilities in smear zone (K_{hs}), keeping diameter constant and equal to $d_s=3d_w$

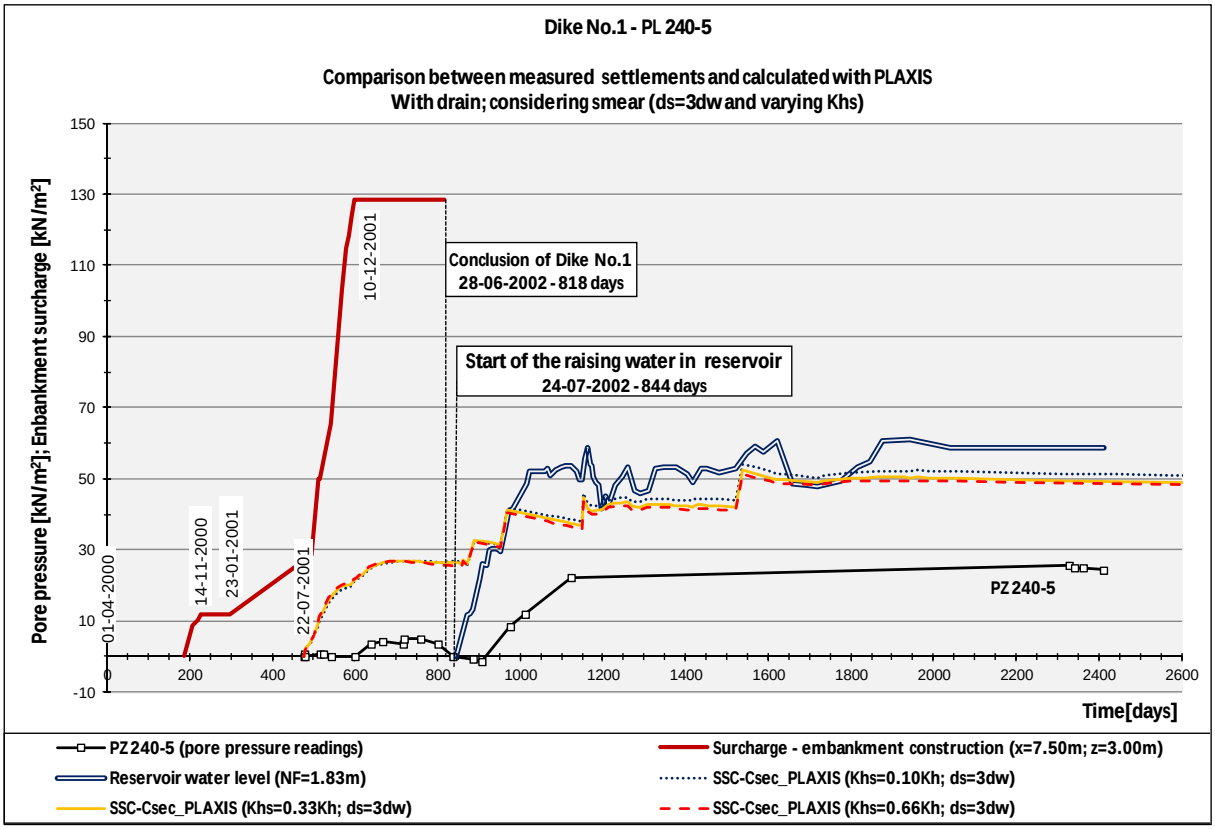

Graph VII.31 – PZ 240-5 of Dike No.1: Pore pressures calculated with the *SSC* models, considering several permeabilities in smear zone (K_{hs}), keeping diameter constant and equal to $d_s=3d_w$

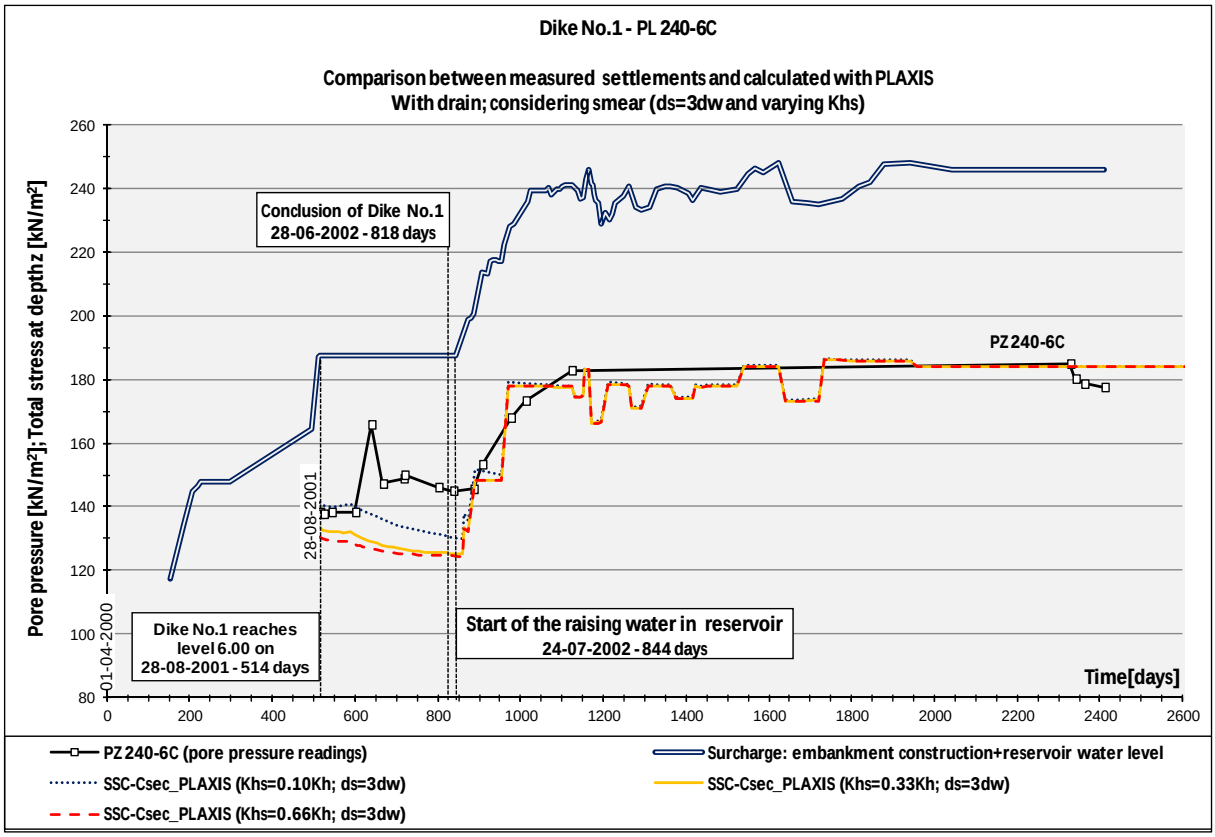

Graph VII.32 – PZ 240-6C of Dike No.1: Pore pressures calculated with the *SSC* models, considering several permeabilities in smear zone (K_{hs}), keeping diameter constant and equal to $d_s=3d_w$

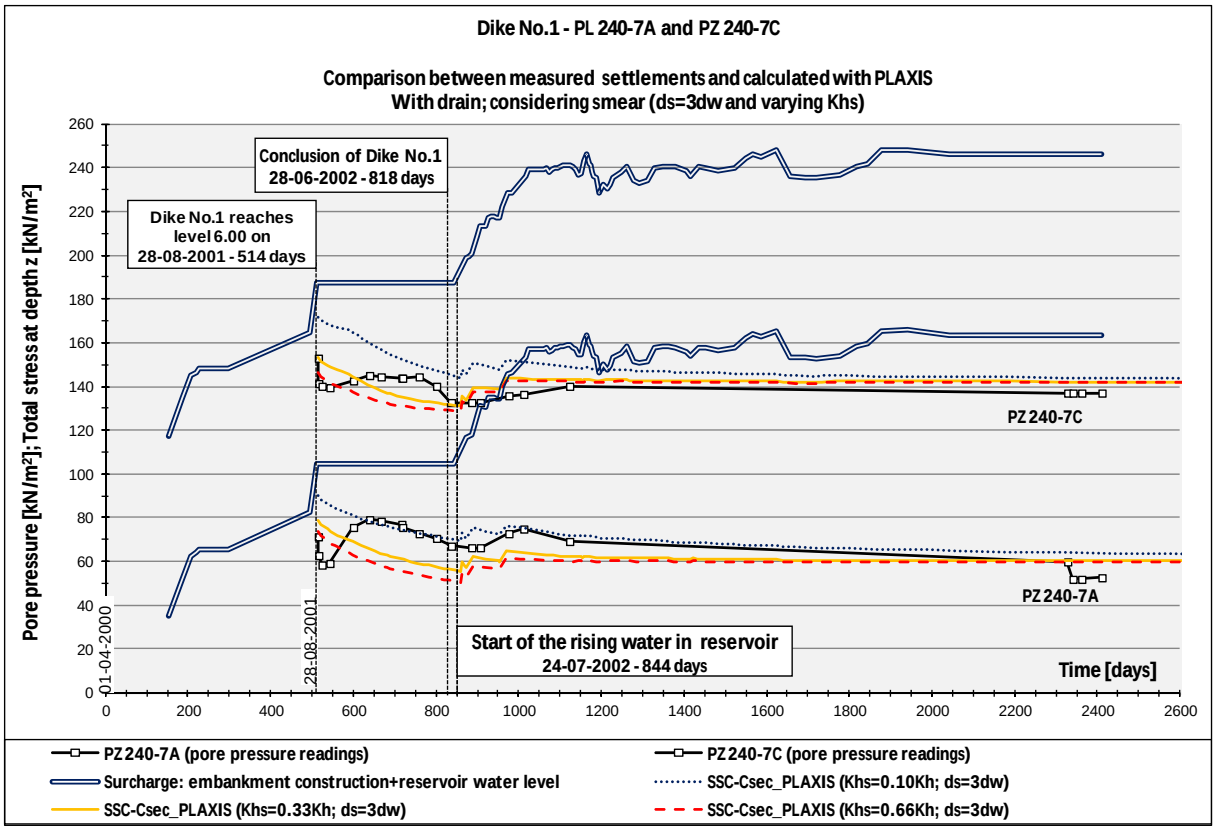

Graph VII.33 – PZ 240-7A and PZ 240-7C of Dike No.1: Pore pressures calculated with the *SSC* models, considering several permeabilities in smear zone (K_{hs}), keeping diameter constant and equal to $d_s=3d_w$

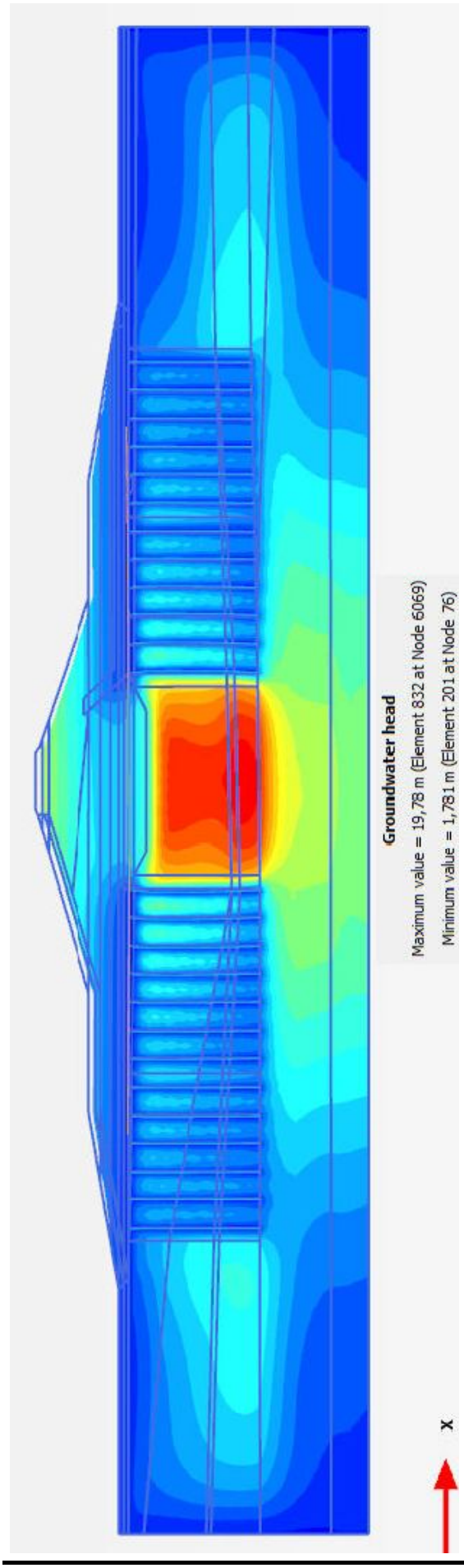

Figure VII.36 – PK0+240 of Dike No.1: Groundwater head associated to the conclusion of dike, using the SSC model, and smear given by K_{hsAx}=0.10K_{h0} and d_s=3d_w

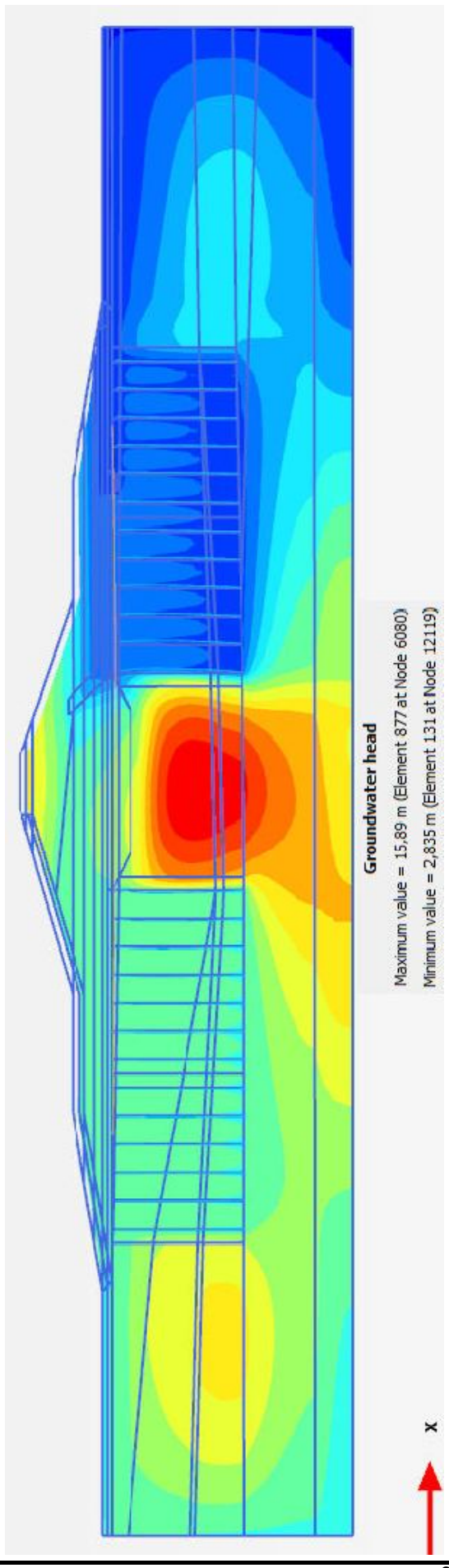

Figure VII.37 – PK0+240 of Dike No.1: Groundwater head associated to the final calculation step, using the SSC model, and smear given by K_{hsAx}=0.10K_{h0} and d_s=3d_w

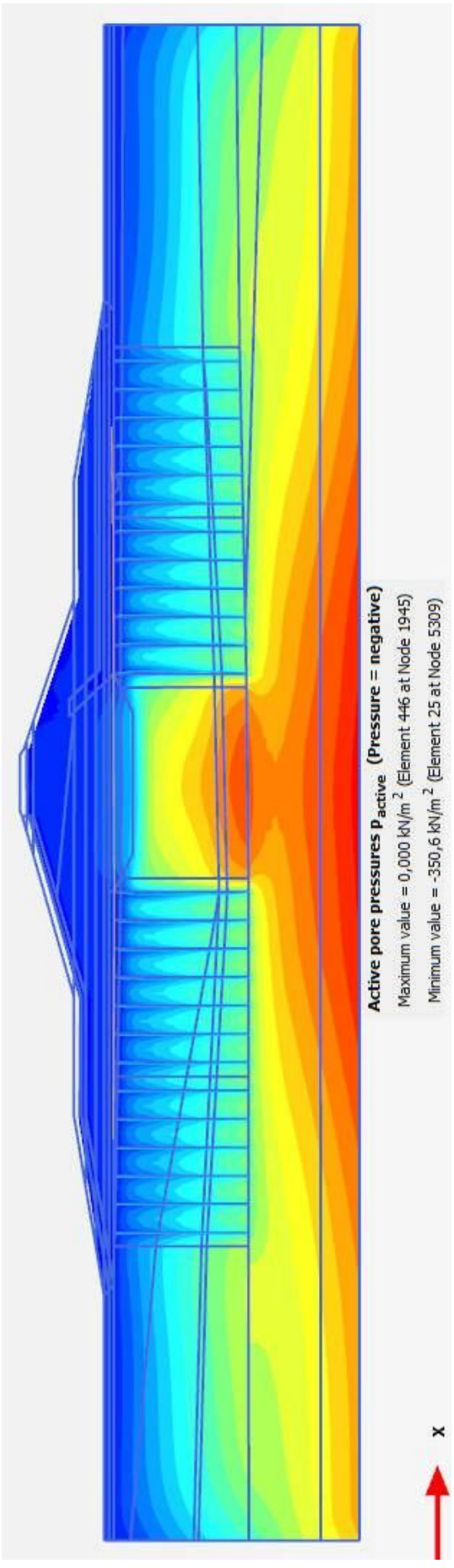

Figure VII.38 – PK0+240 of Dike No.1: Pore pressures associated to the conclusion of dike, using the SSC model, and smear given by K_{hsAx}=0.10K_{h0} and d_s=3d_w

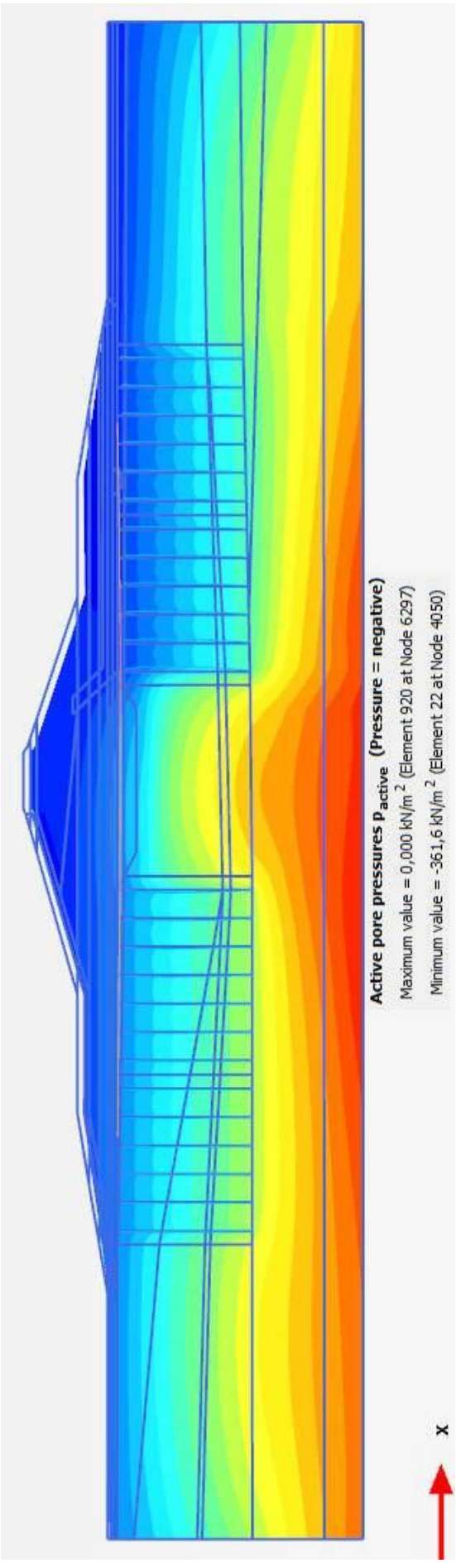

Figure VII.39 – PK0+240 of Dike No.1: Pore pressures associated to the final calculation step, using the SSC model, and smear given by K_{hsAx}=0.10K_{h0} and d_s=3d_w

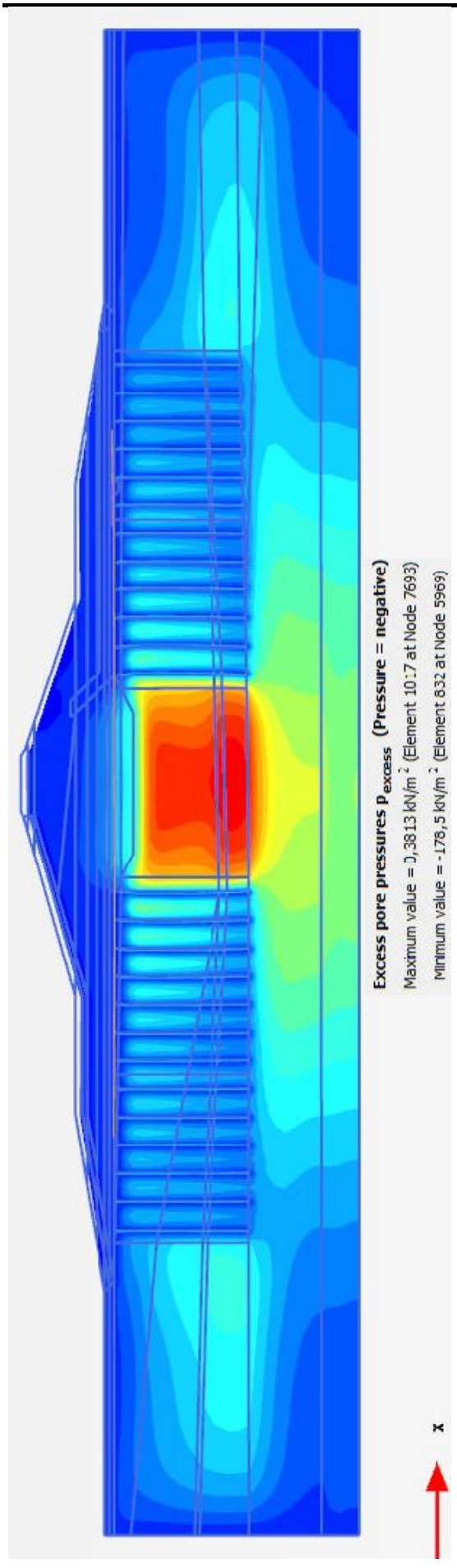

Figure VII.40 – PK0+240 of Dike No.1: Excess pore pressures associated to the conclusion of dike, using the SSC model, and smear given by K_{hsAx}=0.10K_{h0} and d_s=3d_w

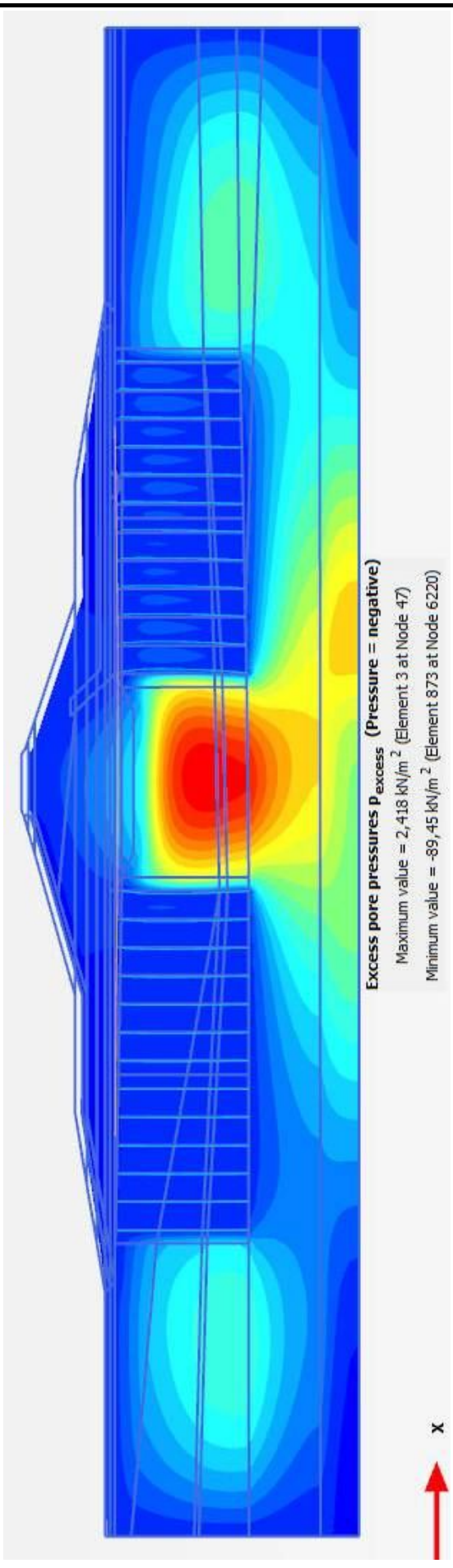

Figure VII.41 – PK0+240 of Dike No.1: Excess pore pressures associated to the final calculation step, using the SSC model, and smear given by K_{hsAx}=0.10K_{h0} and d_s=3d_w

VII.3.1.4. PORE PRESSURES IN DIKE NO.3

In Dike No.3, there are only 2 piezometers, both located in section PK0+180, below the upstream berm, in a zone not improved with drains. However, downstream of the cut-off trench, band-shaped drains were inserted in the ground foundation.

In light of the reduced number of points to be controlled and compared, in this case, the excess pore pressure curves were also included in the graphs. In addition to this, and owing to the conclusions obtained for Dike No.1, the simulations were restricted only the Soft Soil Creep model, with smear conditions equal to $K_{hsAx}=0.10K_{h0}$ and $d_s=3d_w$. Considering the conditions just mentioned, two distinct analyses were performed, varying both the secondary compressibility index (C_α) and the value of the horizontal permeability of soil B2. The results are displayed in graphs VII.34 and VII.35. Based on them, it is difficult to determine the most adequate compressibility conditions for the soils, since:

- When the final pore pressures calculated get closer to the piezometer readings, there is a significant difference in the initial phase;
- When the results are quite coincident in the construction phase, then the final values obtained in the numerical analysis are relatively higher than the measured ones.

The differences between the numerical and measured results show that the dissipation of the pore pressure excess, on the ground foundation, is occurring faster than expected. Although these piezometers are placed in a zone without drains, the foundation soil downstream has drains, thus these elements will have some influence in the drainage of the ground. As such, more considerations about the results can only be made when the flow is taken into account in the calculations.

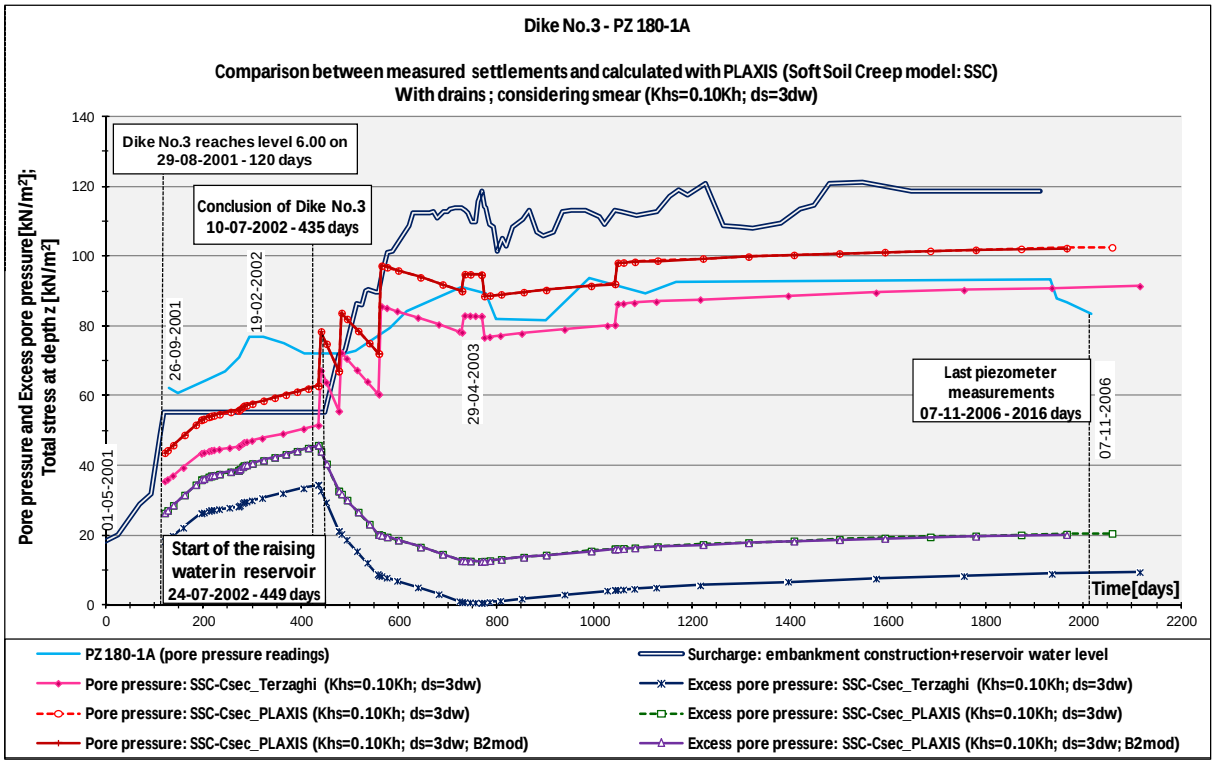

Graph VII.34 – PZ 180-1A of Dike No.3: Pore pressures and excess pore pressures calculated with SSC model,, for various values of secondary compressibility index (C_α), and smear effect given by $K_{hsAx}=0.10K_{h0}$ and $d_s=3d_w$

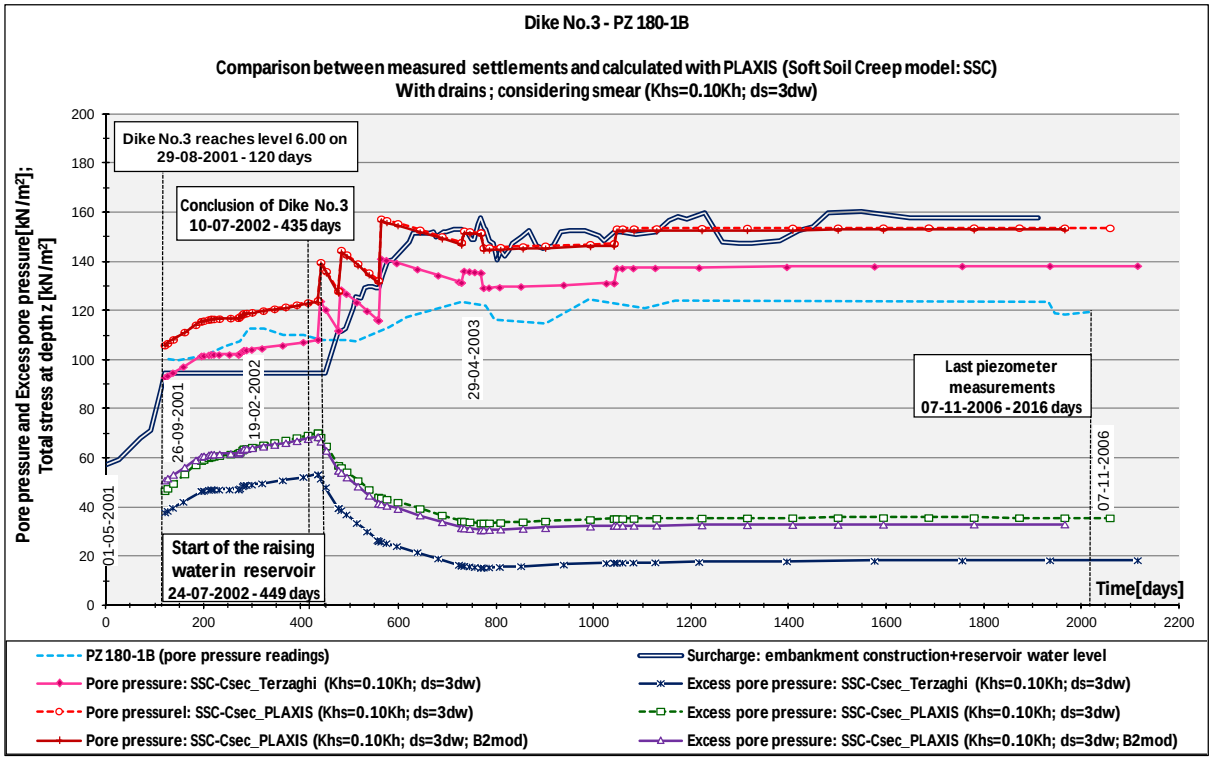

Graph VII.35 – PZ 180-1B of Dike No.3: Pore pressures and excess pore pressures calculated with SSC model, for various values of secondary compressibility index (C_α), and smear effect given by $K_{hsAx}=0.10K_{h0}$ and $d_s=3d_w$

Therefore, the only considerations which can be taken from the analysis of the simulations results, in this moment, are:

- The consideration of a higher value for the horizontal permeability of soil B2, does not lead to a significant increase on the excess pore pressure dissipation of the zone where the piezometers are located;
- The pore pressure and the excess pore pressure obtained with a higher secondary compressibility index are greater, as had already been seen in Dike No.1. However, the pore pressure curves do not match the readings in the piezometers, especially after the filling of the pond;
- There is a significant excess of pore pressure during the construction phase, followed by a dissipation of the pore pressure, even with rising of water in the reservoir, stabilising approximately at the same time as the water level in the pond also stabilised. This behaviour traduces the response of this type of soil, when saturated.

VII.3.2. RESULTS FROM NUMERICAL SIMULATION CONSIDERING THE FLOW

To take into consideration the creation of a flow net, and the percolation of the water, is necessary to introduce on the calculations procedures this aspect. Thus, the options “Groundwater flow steady state” or “Transient flow” must be adopted, as already explained in the beginning of this chapter.

In this case, the results of the settlements of Dike No.1 and Dike No.3 are displayed simultaneously. The same procedure is followed for the interpretation of the pore pressure results. The adoption of this procedure allows observing the similarities and discrepancies in both dikes, depending of the scenarios and conditions considered. Dike No.1 has drains upstream and downstream; on the other hand Dike No.3 only has drains downstream in the cross-sections PK0+140, PK0+170 and PK0+180, and no drains at all in PK0+200. As a consequence of the conclusions obtained thus far, only the numerical calculation for the Soft Soil Creep model will be presented, with C_α defined by the PLAXIS relation and the smear given by $K_{hsAx}=0.10K_{h0}$ and $d_s=3d_w$.

VII.3.2.1. DIKE NO.1 AND DIKE NO.3 SETTLEMENTS WITH FLOW

In graphs VII.36 to VII.43, are presented the results from the numerical calculations considering the flow, for section PK0+240 of Dike No.1 and sections PK0+140, PK0+170 and Pk0+200 of Dike No.3 of the *Lebrija* Pond. Based on them, it is noticed that:

- The simulations settlement results with flow always give higher values than those without flow, which means that the consolidation phenomenon occurs faster; this is associated with the fact that drainage is considered at any moment of the calculation;
- Another interesting aspect is the difference between the settlements from the simulations with and without the flow. While in Dike No.1, where there are bad-shaped drains upstream and downstream, this augmentation in settlement is small, on sections PK0+140 and Pk0+170 of Dike No.3, where the foundation has only been treated downstream, the difference between the settlements is greater. In turn, in plates PL 200-1 and PL 200-2, located in a section without drains, the difference between the settlements from the simulations with and without flow is significantly greater than the other cross-sections, corresponding to the maximum difference between the numerical results. This behaviour is directly associated with the drains installed on the ground foundation. Therefore, the difference between the results is smaller when there are drains because they perform their drainage function even without imposing the flow, allowing the dissipation of the excess pore pressure. If there are no drains in the foundation, in an analysis without flow, the water is stationary. So, in this last situation, in order to occur drainage on the ground foundations, the flow needs to be considered in the simulation, and this the reason why the biggest difference occurs in section PK0+200;
- In section PK0+240 of Dike No.1, there is a very good adjustment between the final settlements with flow and the readings from the plates, as well as an identical progress of both curves (Graphs VII.36 and VII.37). In the results without flow, the agreement of the monitoring curves with the values obtained numerically was already quite reasonable, but with the flow the approximation to the real results is even better. This means that the characterization of Dike No.1, both embankment and soil foundation, are adequate, if at the same time the conditions associated with flow simulations are taken into account;
- In the case of Dike No.3, and regarding the settlement analysis, the difficulty of getting a general conclusion for all the plates still applies, as it had already been mentioned in the results without the flow.

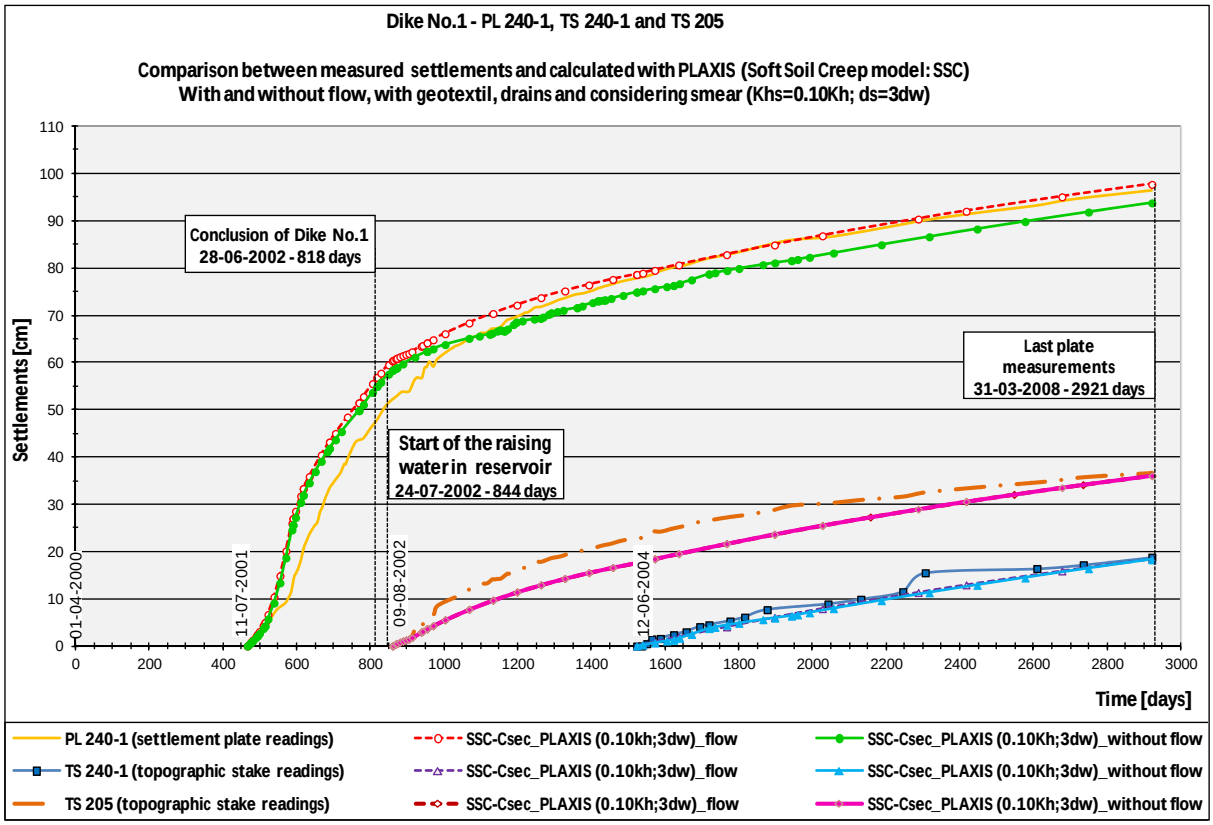

Graph VII.36 – PL 240-1, TS 240-1 and TS 205 of Dike No.1: Settlements obtained incorporating flow, calculated with SSC model, with $C_{\alpha PLAXIS}$, and smear effect given by $K_{hsAx}=0.10K_{h0}$ and $d_s=3d_w$

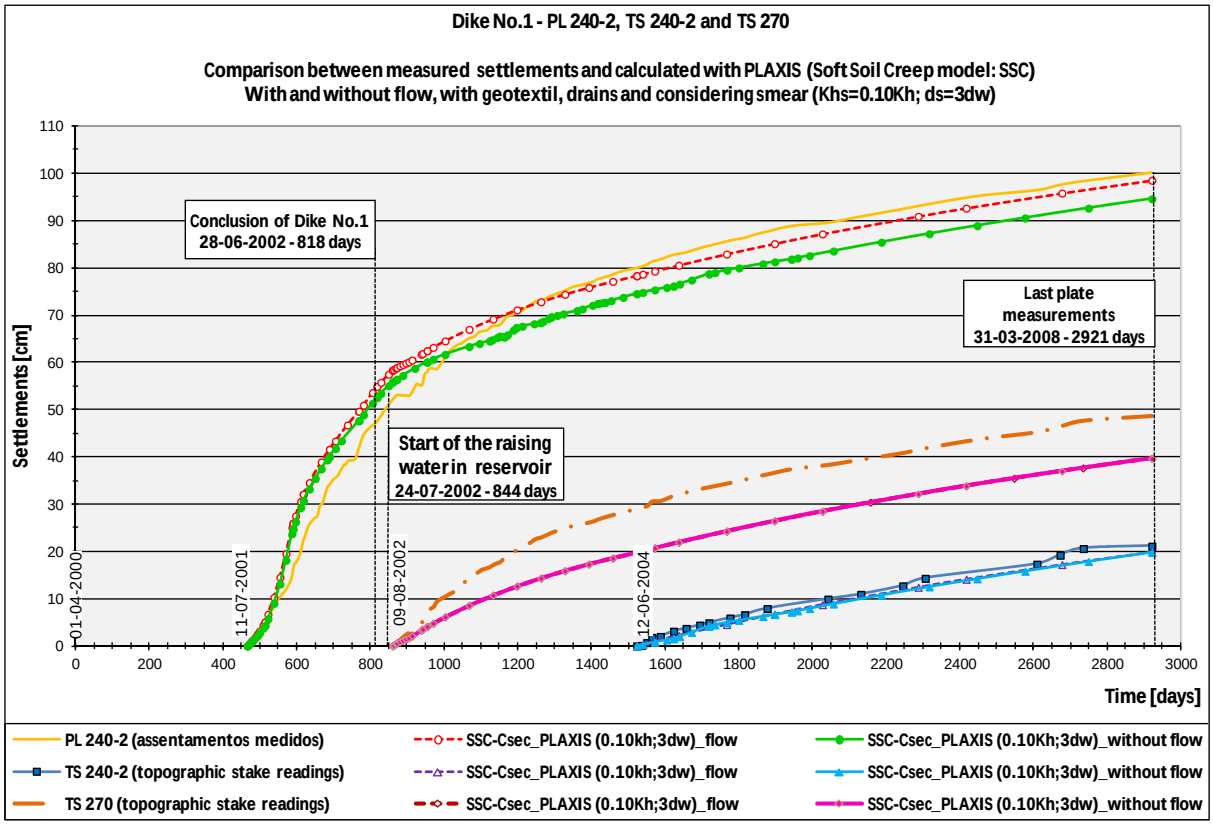

Graph VII.37 – PL 240-2, TS 240-2 and TS 270 of Dike No.1: Settlements obtained incorporating flow, calculated with SSC model, with $C_{\alpha PLAXIS}$, and smear effect given by $K_{hsAx}=0.10K_{h0}$ and $d_s=3d_w$

In plates PL 140-1 and PL 140-2, the settlements considering the flow move apart further more from those monitored (Graphs VII.38 and VII.39). In the simulations without flow, the results were already above the readings during the construction phase, although they got closer in the reservoir filling phase, but with the flow these differences are amplified. It is believed that the explanation for this difference lies in a combination of two factors, namely:

a) That section PK0+140 is in the limit of the improved zone with the band-shaped drains;
b) That in this section, unlike to what happens on the other profiles, the drains reach stratum B2, which has a horizontal permeability three times higher than the others soils.

To analyse this second factor, it was performed an additional simulation, where the drains did not attained layer B2. These results are also represented in graphs VII.40 and VII.41. It can be seen that the values obtained are very close to the simulations without flow, giving an idea of the influence of the horizontal permeability of the layers crossed by the drains. In any case, this reduction is felt mostly after the construction of the embankment, being the settlement results still very high during the construction phase. Therefore, even though there is an improvement in the global behaviour, this is not the reason why there is a marked difference between the simulated values and those measured from the plates.

So, going back to the first factor, it will be remembered that, in Dike No.3, the zone treated with drains is comprehended between the cross-section section PK0+140 and PK0+180. Therefore, in these two profiles, the drainage on the left side will be distinct to the right side, being faster in the zone where the drains were installed, and slower on the other. Consequently, the consolidation will also be distinct in these zones. In this case, the tri-dimensional effect is important. However, when modelling each of these cross-sections in a two-dimensional space, the drainage is considered the same on both sides. Consequently, the consolidation phenomena in the simulations will occur more rapidly, and so associated the settlement will be higher. This is an aspect which cannot be avoided when using the 2D modelling, being necessary to perform a 3D analysis to withdrawn some conclusions.

In plates PL 170-1 and PL 170-2, the results with flow show some concordance with those monitored (Graphs VII.40 and VII.41), obtaining final settlements which are closer to those registered. In plate PL 170-2, the concordance between the settlements is quite acceptable during the construction and post-construction phase, while in plate PL 170-1 they are still below those measured in the post-construction phase. This cross-section is located in a zone treated with drains on both sides, so the previous aspect has not been raised; this is also why there is a better adjustment of the simulations results with flow to those monitored in the plates.

In plates PL 200-1 and PL 200-2, where there is a greater increment in the settlement associated with the simulations with flow, it is noticed a good approximation between the monitored result for plate PL 200-1 and the calculated value (Graph VII.42). By contrast, in plate PL 240-2, the settlements which correspond to the monitoring results are much lower than any of the numerical results obtained, including from simulations without flow (Graph VII.43). This is the only case where, apparently, there is no plausible explanation. Given this disparity between the results, and recalling what was said in the analyses without flow, it is probable that plate PL 200-2 is located at another point inside the dike.

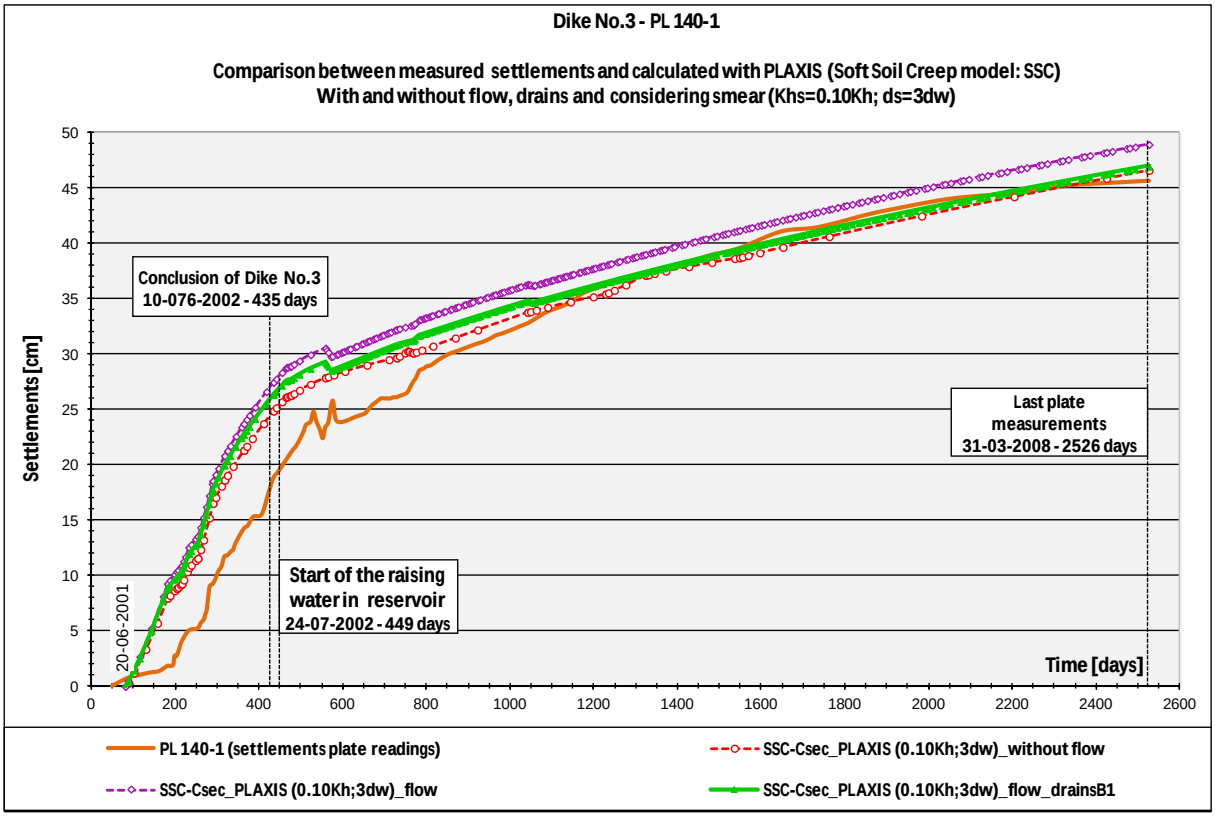

Graph VII.38 – PL 140-1 of Dike No.3: Settlements obtained incorporating flow, calculated with SSC model, with $C_{\alpha PLAXIS}$, and smear effect given by $K_{hsAx}=0.10K_{h0}$ and $d_s=3d_w$

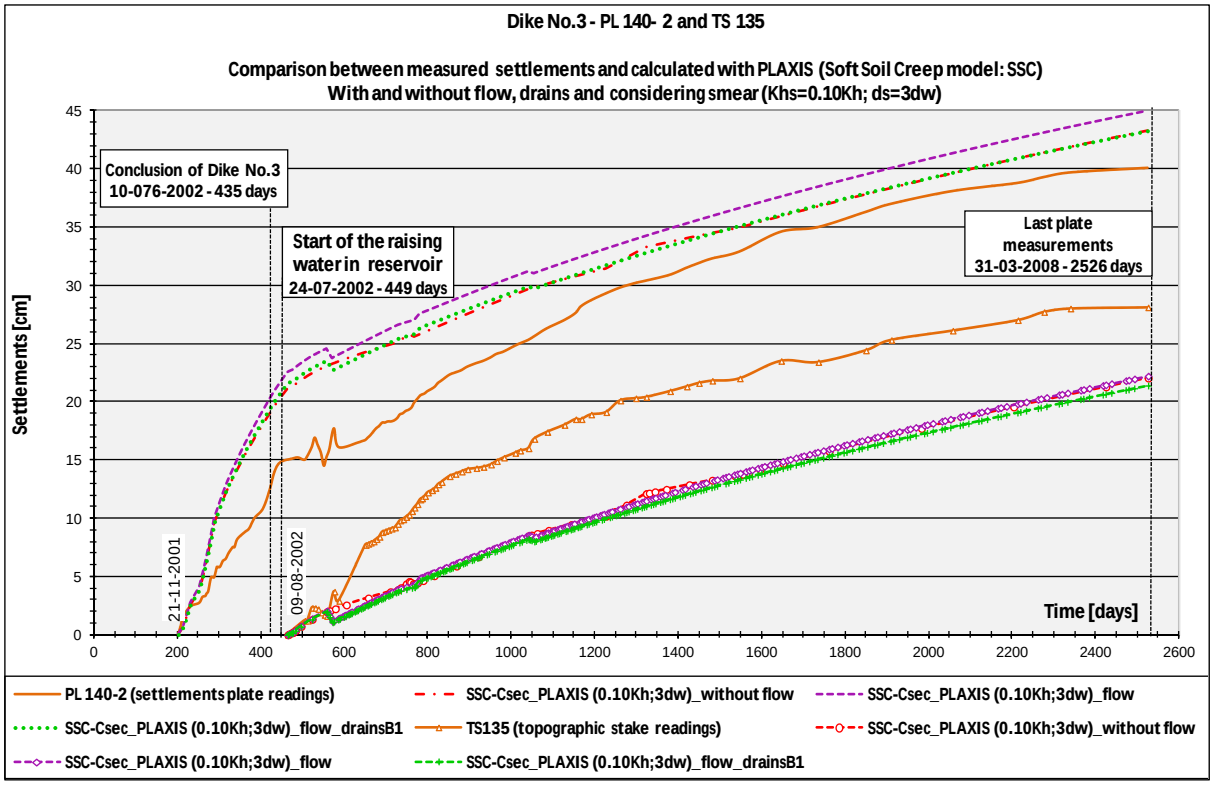

Graph VII.39 – PL 140-2 and TS 135 of Dike No.3: Settlements obtained incorporating flow, calculated with SSC model, with $C_{\alpha PLAXIS}$, and smear effect given by $K_{hsAx}=0.10K_{h0}$ and $d_s=3d_w$

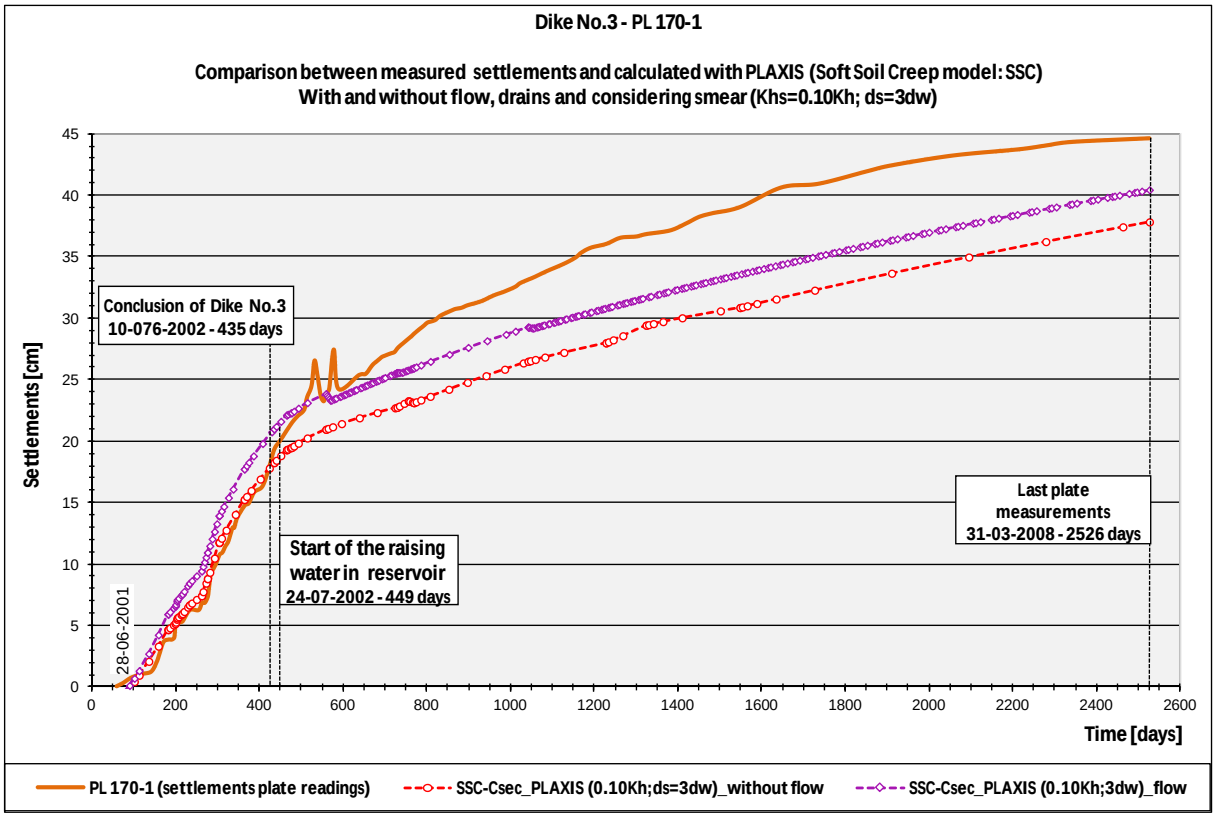

Graph VII.40 – PL 170-1 of Dike No.3: Settlements obtained incorporating flow, calculated with SSC model, with $C_{\alpha PLAXIS}$, and smear effect given by $K_{hsAx}=0.10K_{h0}$ and $d_s=3d_w$

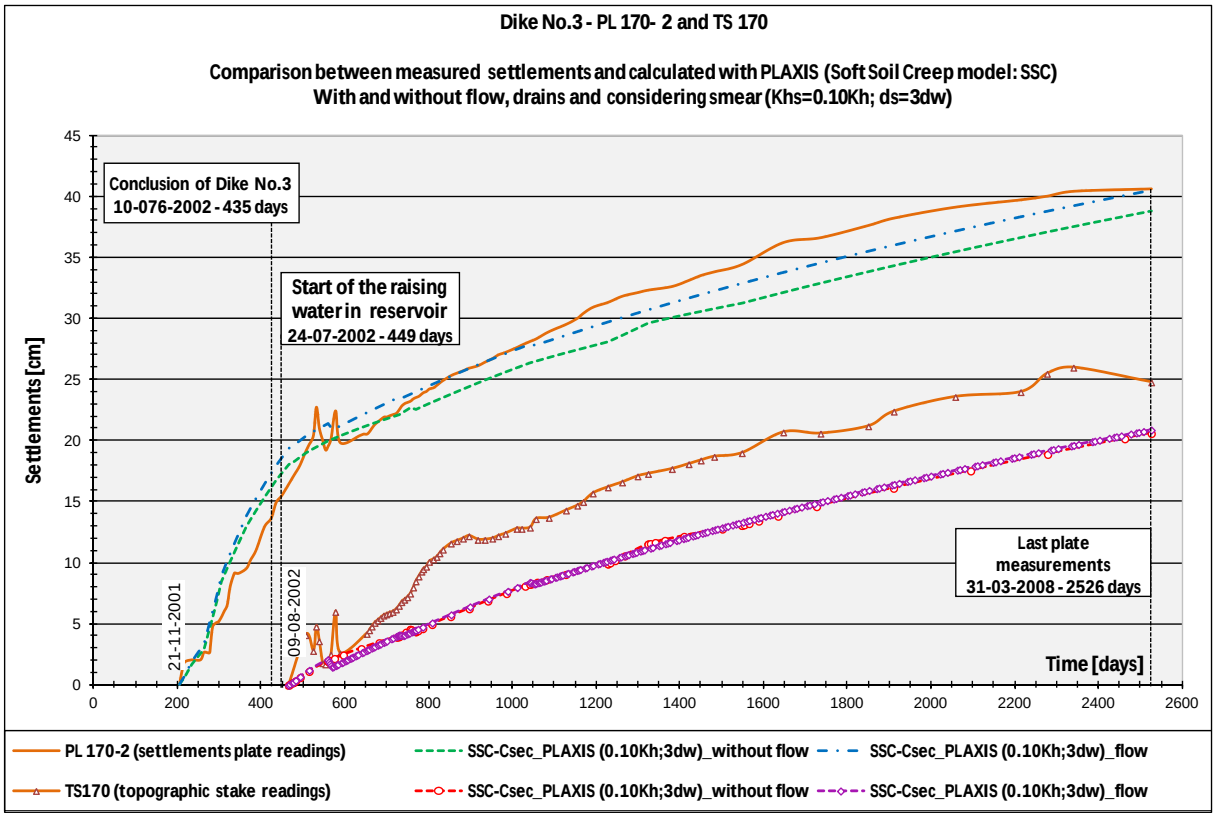

Graph VII.41 – PL 170-2 and TS 170 of Dike No.3: Settlements obtained incorporating flow, calculated with SSC model, with $C_{\alpha PLAXIS}$, and smear effect given by $K_{hsAx}=0.10K_{h0}$ and $d_s=3d_w$

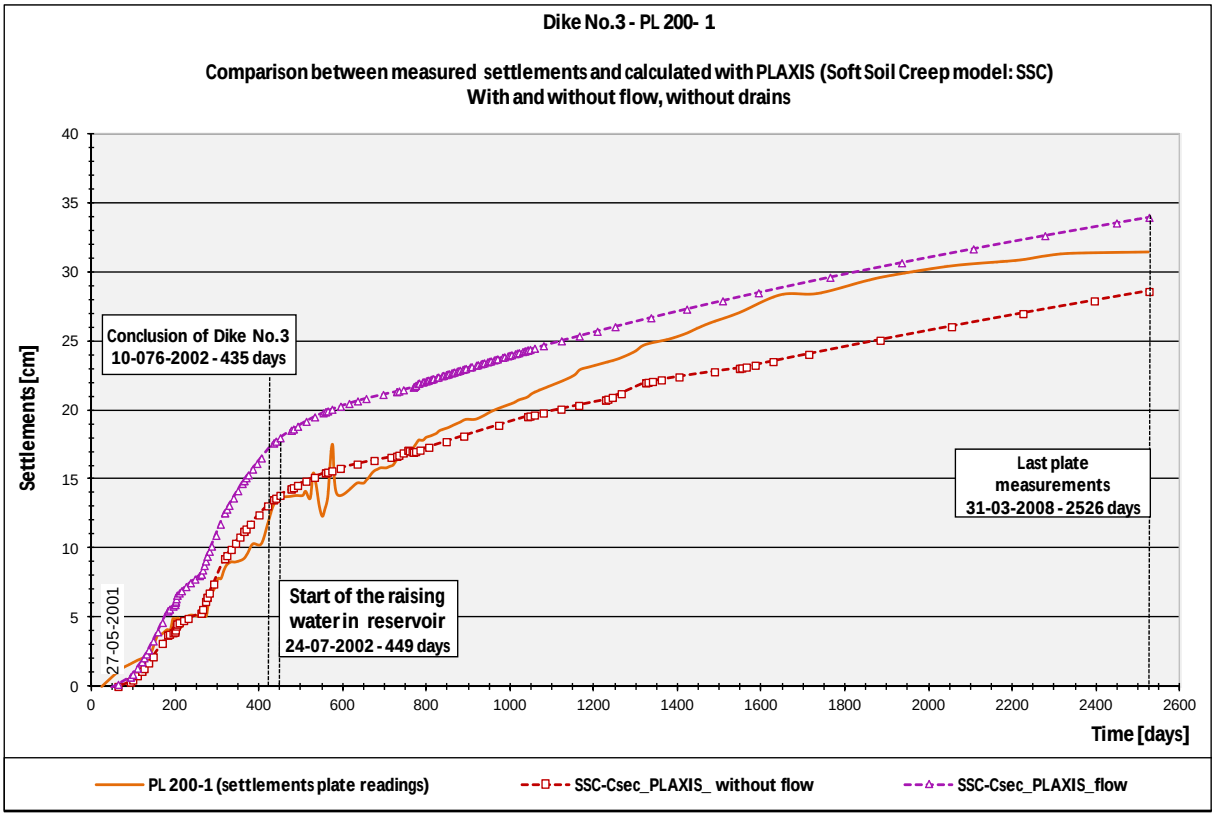

Graph VII.42 – PL 200-1 of Dike No.3: Settlements obtained incorporating flow, calculated with SSC model, with $C_{\alpha PLAXIS}$, and smear effect given by $K_{hsAx}=0.10K_{h0}$ and $d_s=3d_w$

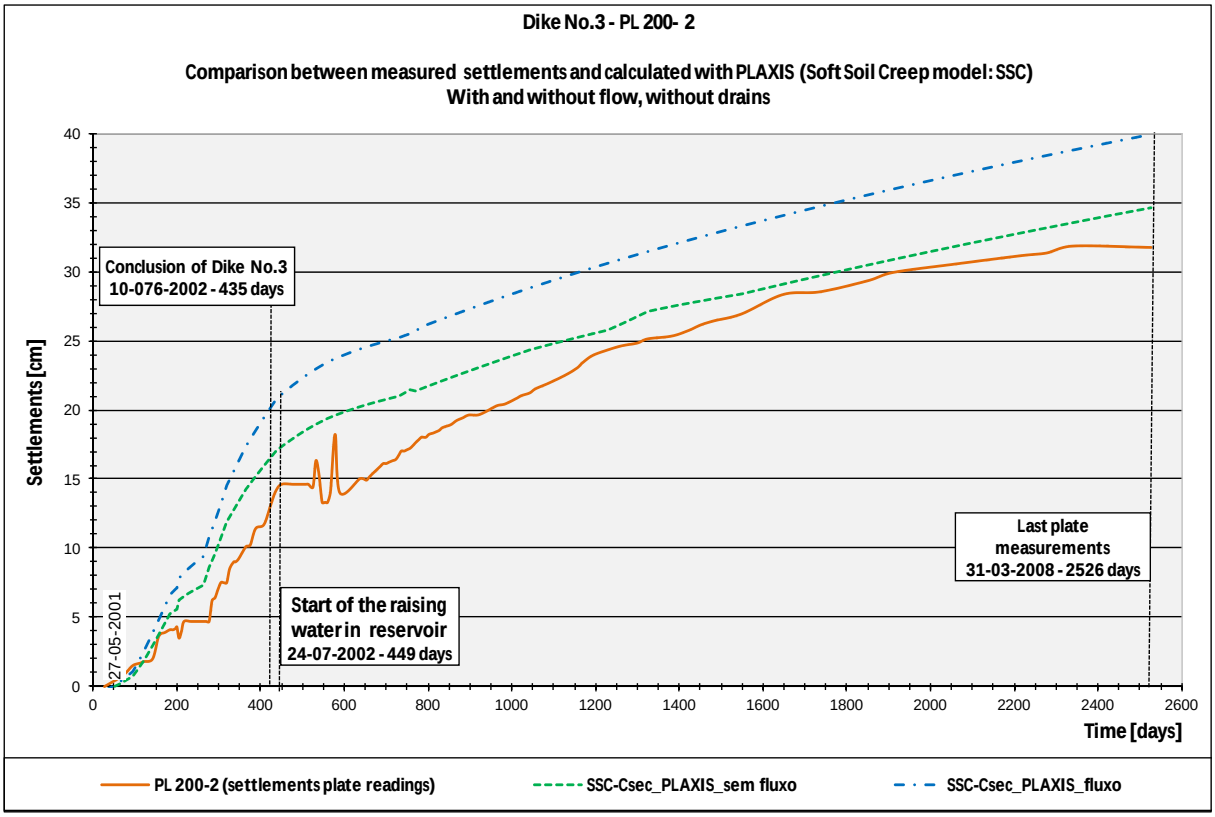

Graph VII.43 – PL 200-2 of Dike No.3: Settlements obtained incorporating flow, calculated with SSC model, with $C_{\alpha PLAXIS}$, and smear effect given by $K_{hsAx}=0.10K_{h0}$ and $d_s=3d_w$

Concerning the curves plotted for the topographic stake marks, though they overlap for the analyses with and without flow, this does not mean that the numerical settlements are the same. The curves are obtained using the settlements of the installation date as the initial value and as a reference. Since the curves from the numerical simulations are relatively parallel from these dates forward, the difference remains equal and so there is a match for these settlements.

The final settlements taking into consideration the flow are shown in figures VII.42 to VII.45.

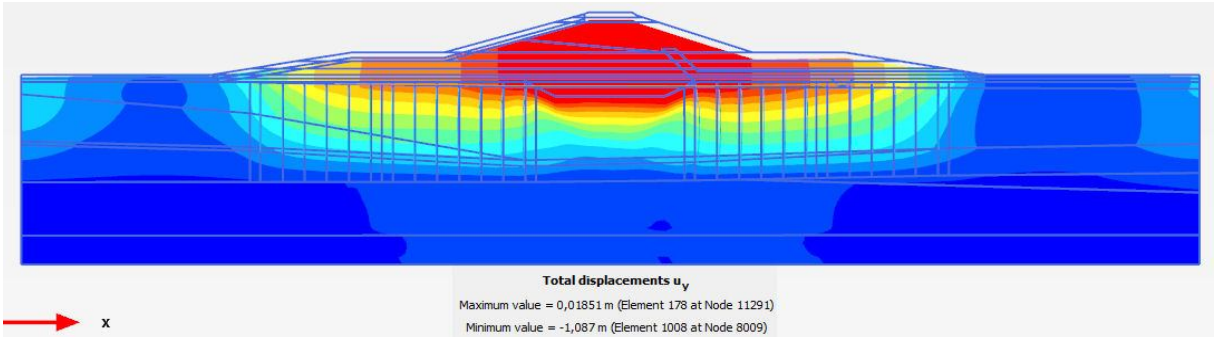

Figure VII.42 – PK0+240 of Dike No.1: Final settlements obtained incorporating flow, calculated with SSC model, with $C_{\alpha PLAXIS}$, and smear effect given by $K_{hsAx}=0.10K_{h0}$ and $d_s=3d_w$

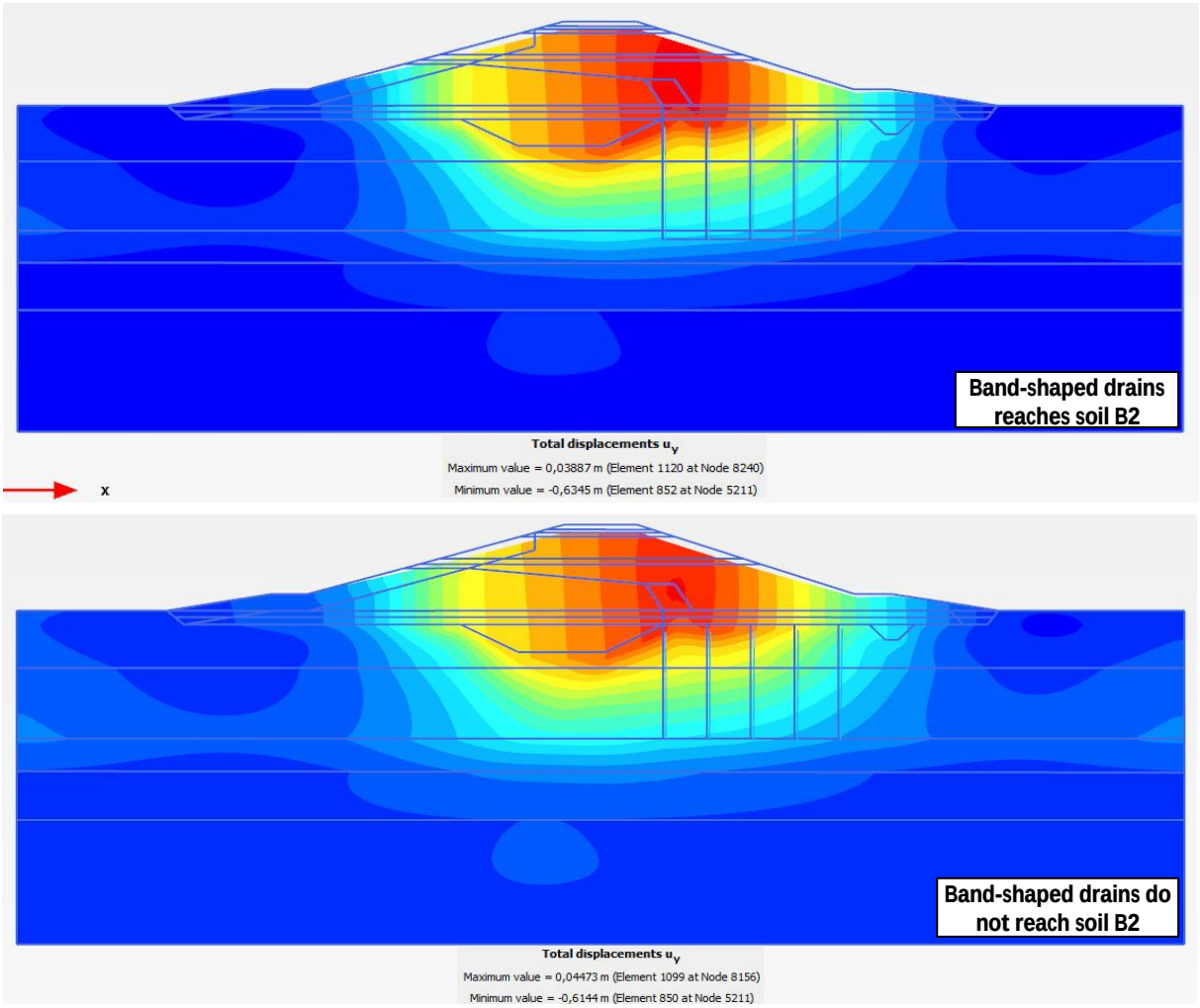

Figure VII.43 – PK0+140 of Dike No.3: Final settlements obtained incorporating flow, calculated with SSC model, with $C_{\alpha PLAXIS}$, and smear effect given by $K_{hsAx}=0.10K_{h0}$ and $d_s=3d_w$

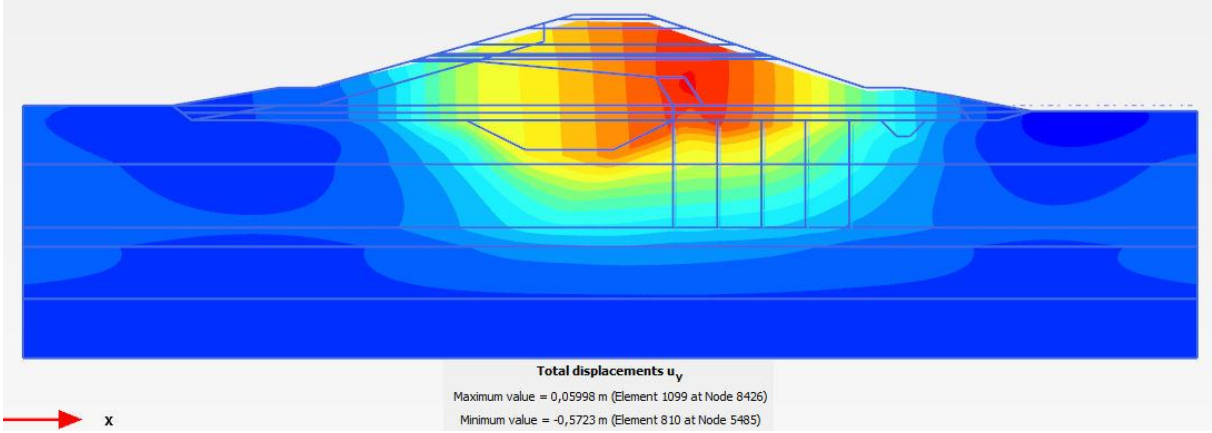

Figure VII.44 – PK0+170 of Dike No.3: Final settlements obtained incorporating flow, calculated with SSC model, with $C_{\alpha PLAXIS}$, and smear effect given by $K_{hsAx}=0.10K_{h0}$ and $d_s=3d_w$

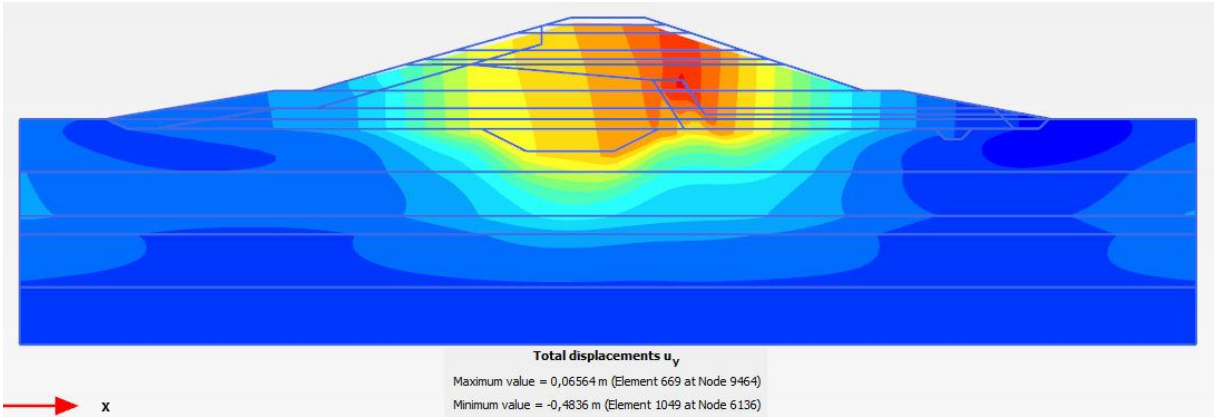

Figure VII.45 – PK0+200 of Dike No.3: Final settlements obtained incorporating flow, calculated with SSC model, with $C_{\alpha PLAXIS}$, and smear effect given by $K_{hsAx}=0.10K_{h0}$ and $d_s=3d_w$

From these figures one can observe that the settlement of Dike No.1 is practically symmetrical to its axis in section PK0+240; this is due to the existence of drains both upstream and downstream of the cut-off tranche. The same is observed in the deformed mesh plotted in Appendix III. In Dike No.3, and with regard to sections PK0+140 and Pk0+170, the maximum settlements are located downstream of the axis, right at the beginning of the band-shaped drains. Also in section PK0+200 of this dike, the maximum settlements take place in the zone of the chimney drain, since the water in the embankment converges to this element, leading the water away from the dike and also allowing the dissipation of the pore pressure excess. As a direct consequence, the consolidation of the embankment accelerates. This is also the reason why the settlement obtained from the numerical calculation for plate PL 200-2 (0.39m) are superior to those of plate PL 200-1 (0.33m), and why there is a significant difference between the simulations and the monitoring results for plate PL200-2 (0.32m).

VII.3.2.2. PORE PRESSURES IN DIKE NO.1 AND DIKE NO.3 WITH FLOW

The procedure adopted for these analyses was analogous to the one used for the settlements. In this case, the excess pore pressure curves were added to the pore pressure results, in order to get a better understanding of the effect associated with the flow and of the pore pressures.

In the profile PK0+240 of Dike No.1, 11 stress points were controlled, while in section PK0+180 of Dike No.3 only 2 stress points were followed. From all of them, just some of the results will be displayed, namely PZ 240-1, PZ 240-2, PZ 240-3, PZ 240-5, PZ 240-6C, PZ 240-7A and PZ 240-7C to Dike No.1, and PZ 180-1A and PZ 180-1B to Dike No.3. Based upon them, it is verified that:

- The main differences between the pore pressures with and without flow occur in the piezometers which are located inside the embankment. In fact, when considering the flow, it is registered an inversion of the results in relation to the analyses without flow. The explanation for this occurrence will be given in the following paragraph.
- In the analyses with flow, the pore pressures from the simulation almost matches the values measured in piezometers PZ 240-3 and PZ 240-5, on the contrary to what had been seen in the analysis without flow (Graphs VII.46 and VII.47). This is due to the fact that, in this case, there was no increase in the pore pressure excess on the embankment, in contrast to what happened before. Even though the embankment soil continues to be considered as having an undrained behaviour, by admitting the existence of the flow net, the water can circulate within the dike and moves towards to the drainage elements which are nearby, allowing the dissipation of the excess pore pressure very rapidly. So, it is not observed an increase in the pore pressure due to the embankment construction, although this effect occurs later, during the filling of the pond. In this last stage, the pore pressures calculated are close to the measured values, especially for the PZ 240-3, which is place on the upstream side, and very close to the upstream drainage blanket. As one can see the correspondence between the pressures due to water level in the reservoir of the readings in this piezometer is significant, giving to the aspect just mentioned. In the case of piezometer PZ 240-5, which is located near the chimney drain and downstream horizontal drain, although the behaviour observed is identical, the values of the pore pressure are lower since the drops of the potential lines, from the upstream to its position inside the dike, much be taken into account. The excess pore pressure results, for the simulations with and without flow, associated to the end of the dike construction, are represented in figures VII.46 and VII.47. In figures VII.48 and VII.49, the results correspond to the final step of the calculations, after the water in the reservoir is already stabilised. These figures attested that the increase in pore pressure is null in any zone of the dike, during the construction phase for the calculation with flow. In the filling phase, this value increases slightly in the interior of the dike, but is insignificant.
- For the reasons mentioned above, the pore pressures associated to the piezometers PZ 240-1 and PZ 240-2 are also extraordinarily lower than the measured (Graphs VII.44 and VII.45). This explains why the settlements of the plates PL 240-1 and PL 240-2, with the flow, are higher than the settlements without flow.
- In the piezometers located in the foundation, between the drains, either upstream or downstream of the cut-off trench, the differences on the results with or without flow are minimum and negligible (Graphs VII.46 and VII.47). This happens because the drains already allowed the drainage and dissipation of the excess pore pressure even in the analyses without flow, as can be seen in figures VII.46 to VII.49. Moreover, the pore pressures calculated are well-adjusted to the measured values, especially in the post-construction phase. In the construction phase, the agreement is not so good right after the piezometer installation. This may be associated with a stabilisation of pressure in the devices.

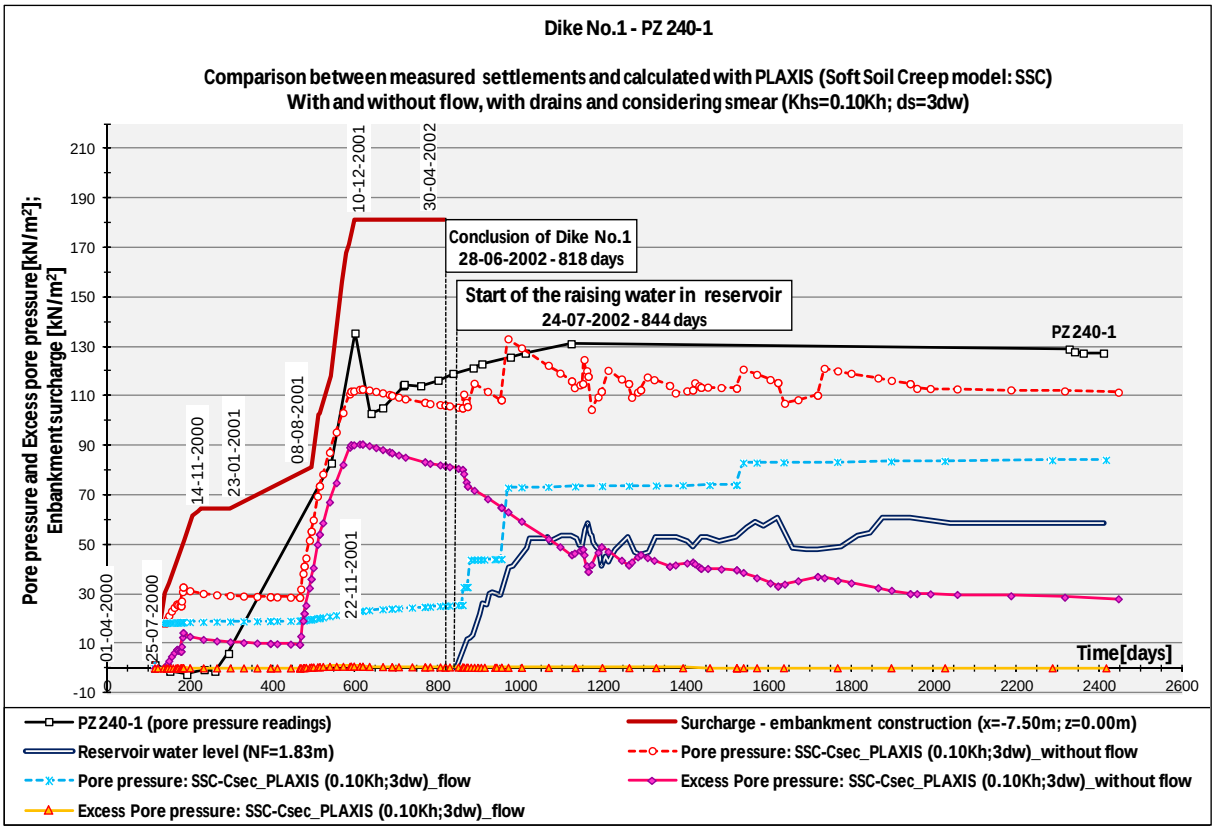

Graph VII.44 – PZ 240-1 of Dike No.1: Pore pressures and excess pore pressures considering flow, calculated with SSC model, with $C_{\alpha PLAXIS}$, and smear effect given by $K_{hsAx}=0.10K_{h0}$ and $d_s=3d_w$

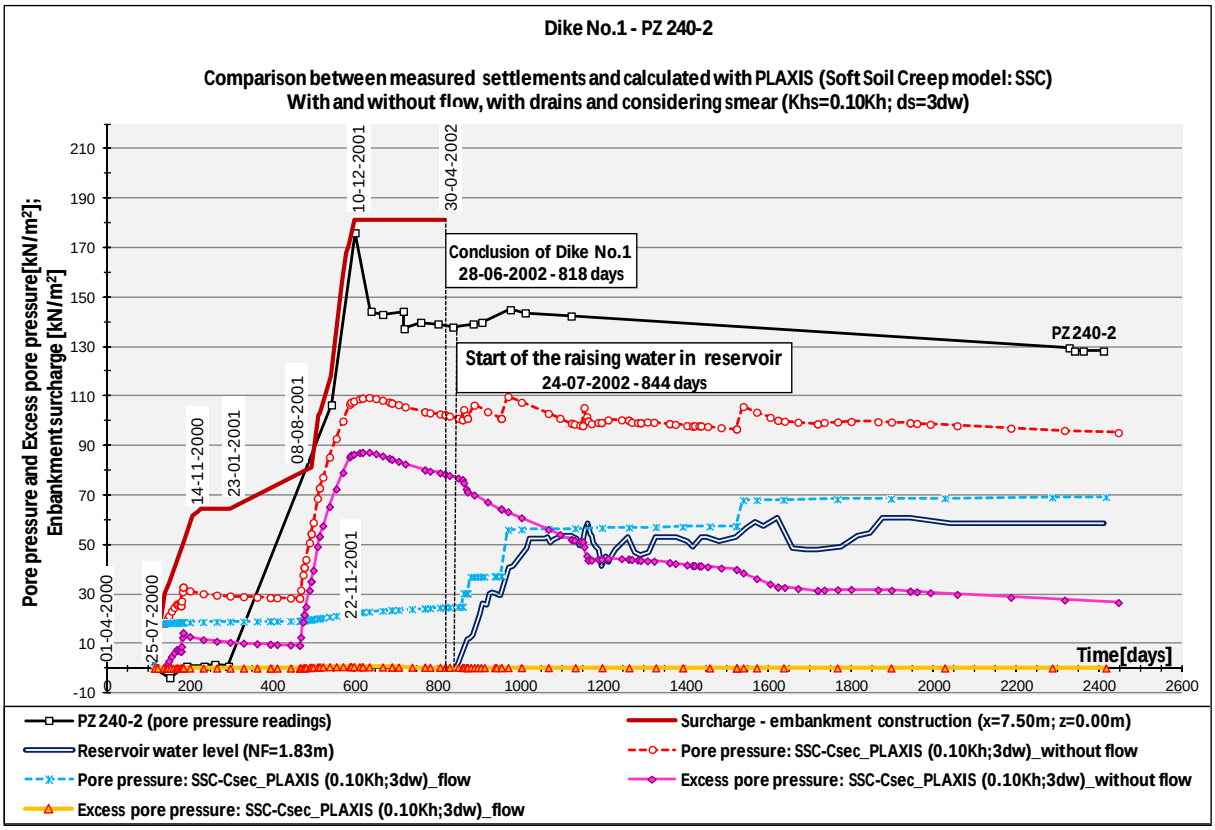

Graph VII.45 – PZ 240-2 of Dike No.1: Pore pressures and excess pore pressures considering flow, calculated with SSC model, with $C_{\alpha PLAXIS}$, and smear effect given by $K_{hsAx}=0.10K_{h0}$ and $d_s=3d_w$

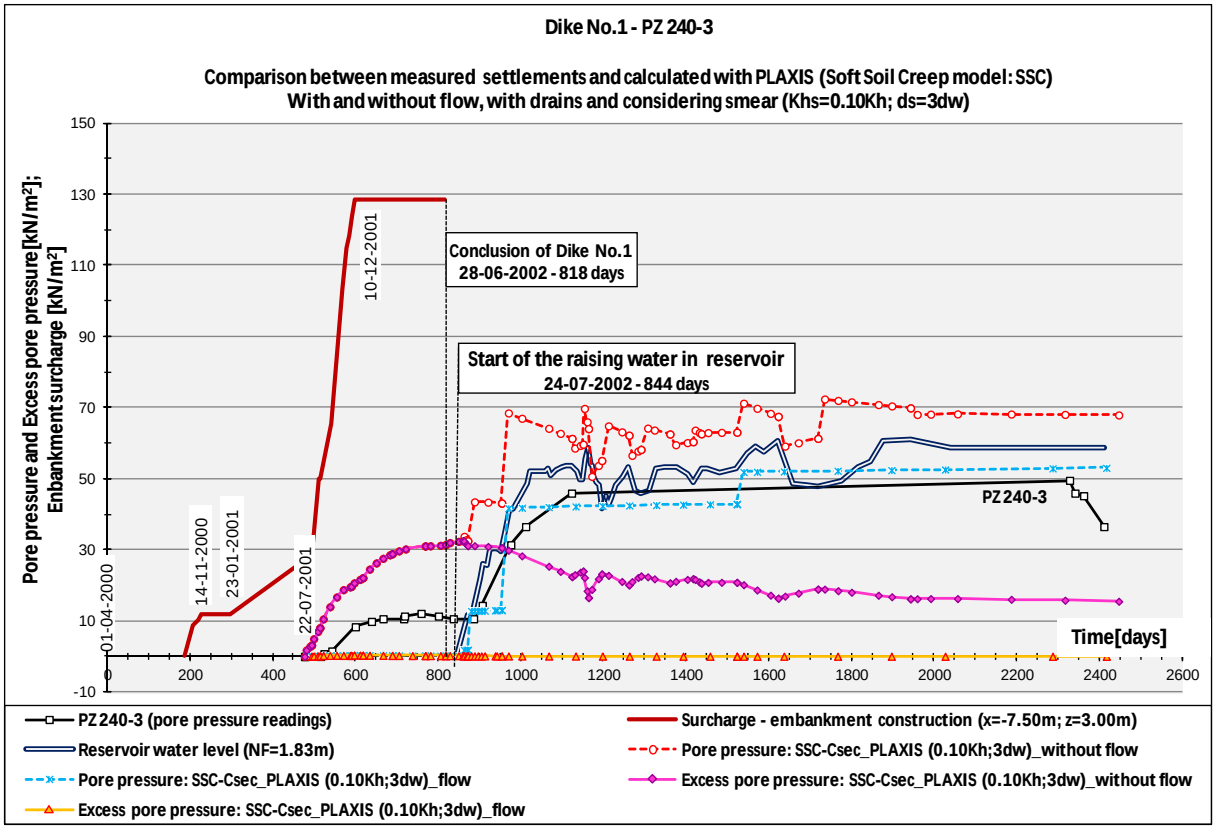

Graph VII.46 – PZ 240-3 of Dike No.1: Pore pressures and excess pore pressures considering flow, calculated with SSC model, with $C_{\alpha PLAXIS}$, and smear effect given by $K_{hsAx}=0.10K_{h0}$ and $d_s=3d_w$

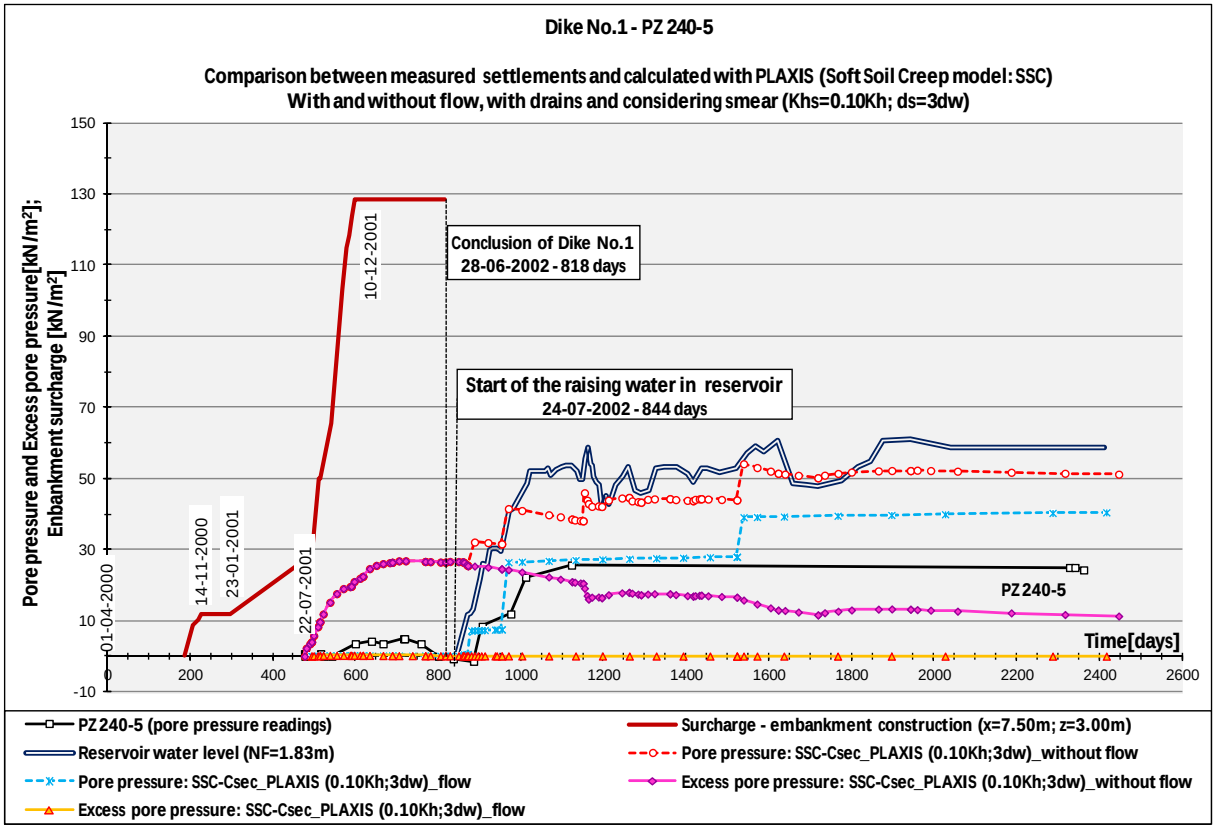

Graph VII.47 – PZ 240-5 of Dike No.1: Pore pressures and excess pore pressures considering flow, calculated with SSC model, with $C_{\alpha PLAXIS}$, and smear effect given by $K_{hsAx}=0.10K_{h0}$ and $d_s=3d_w$

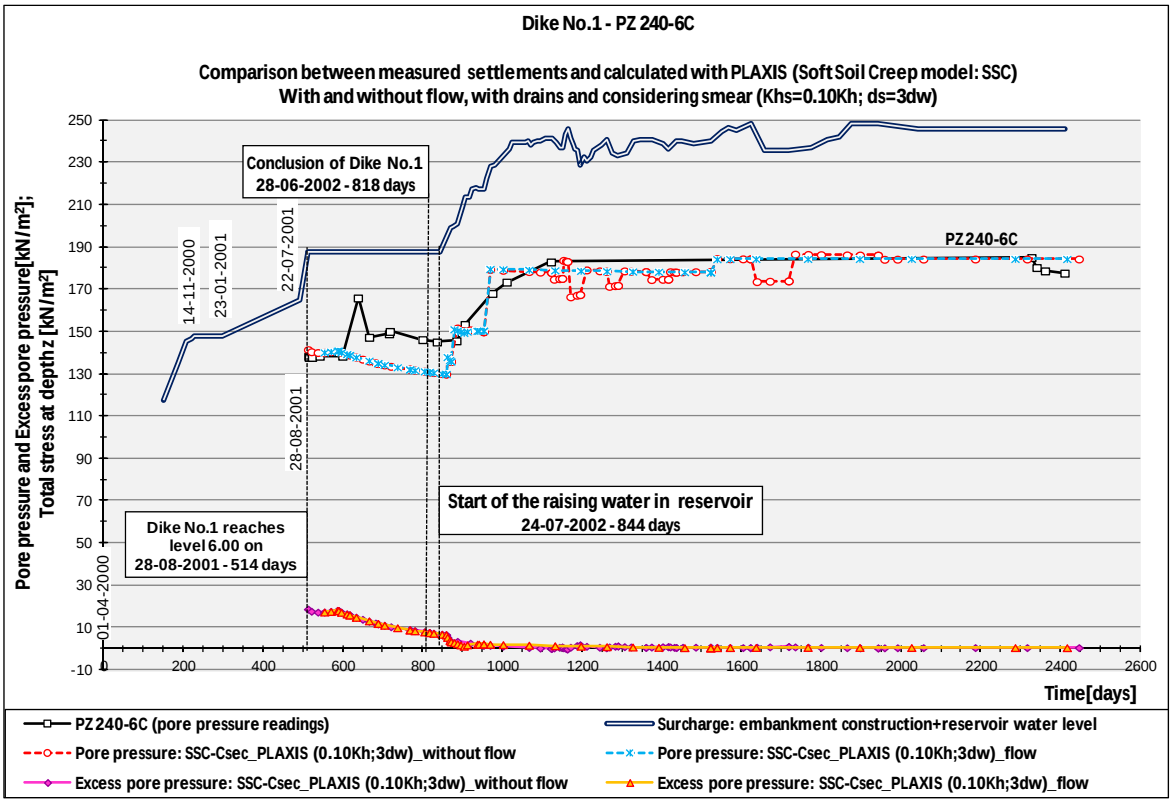

Graph VII.48 – PZ 240-6C of Dike No.1: Pore pressures and excess pore pressures considering flow, calculated with SSC model, with $C_{\alpha PLAXIS}$, and smear effect given by $K_{hsAx}=0.10K_{h0}$ and $d_s=3d_w$

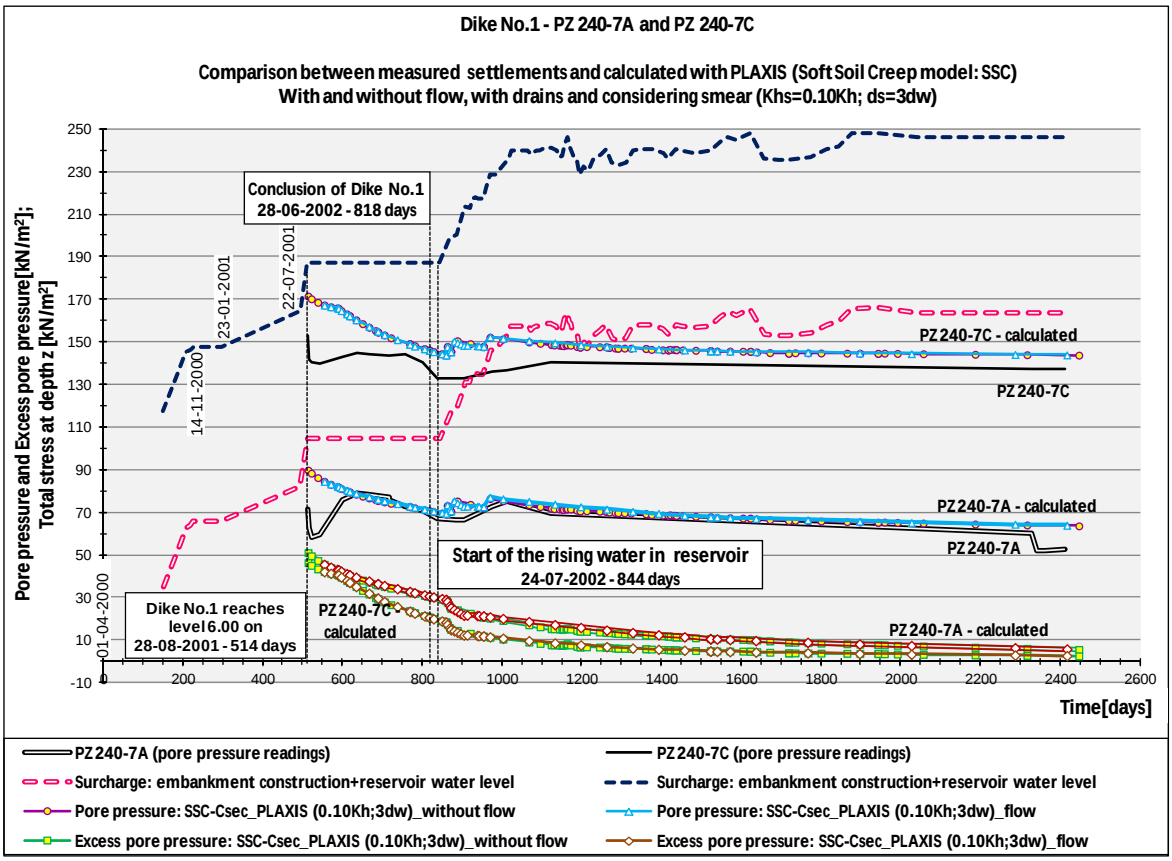

Graph VII.49 – PZ 240-7A and PZ 240-7C of Dike No.1: Pore pressures and excess pore pressures considering flow, calculated with SSC model, with $C_{\alpha PLAXIS}$, and smear effect given by $K_{hsAx}=0.10K_{h0}$ and $d_s=3d_w$

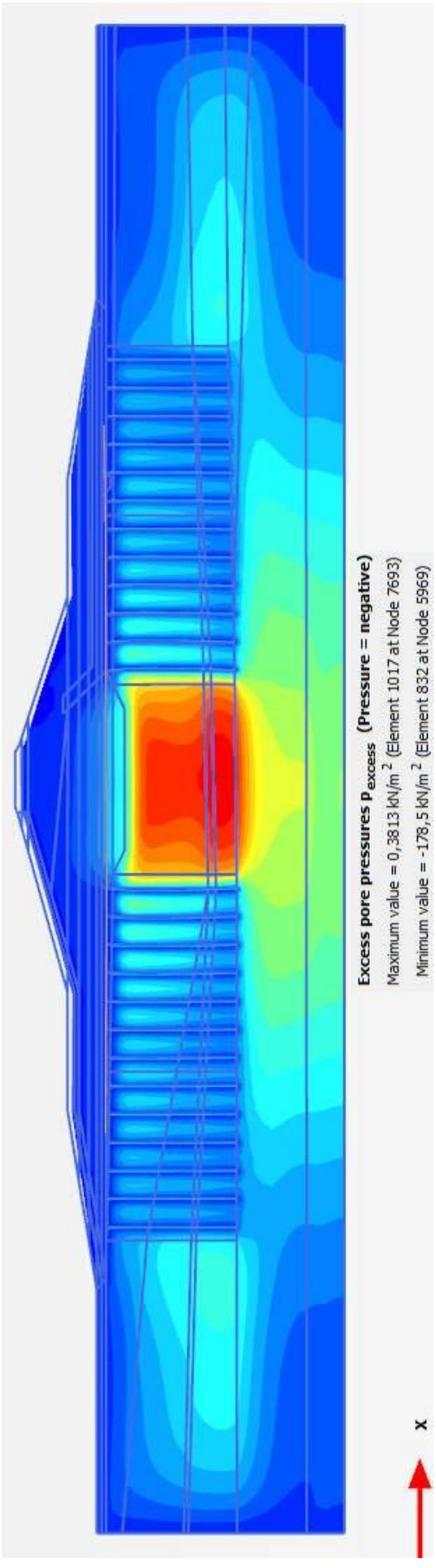

Figure VII.46 – PK0+240 of Dike No.1: Excess pore pressures, without flow, associated to the dike conclusion, with the SSC model, and smear (K_{hsAx}=0.10K_{h0} + ds=3d_w)

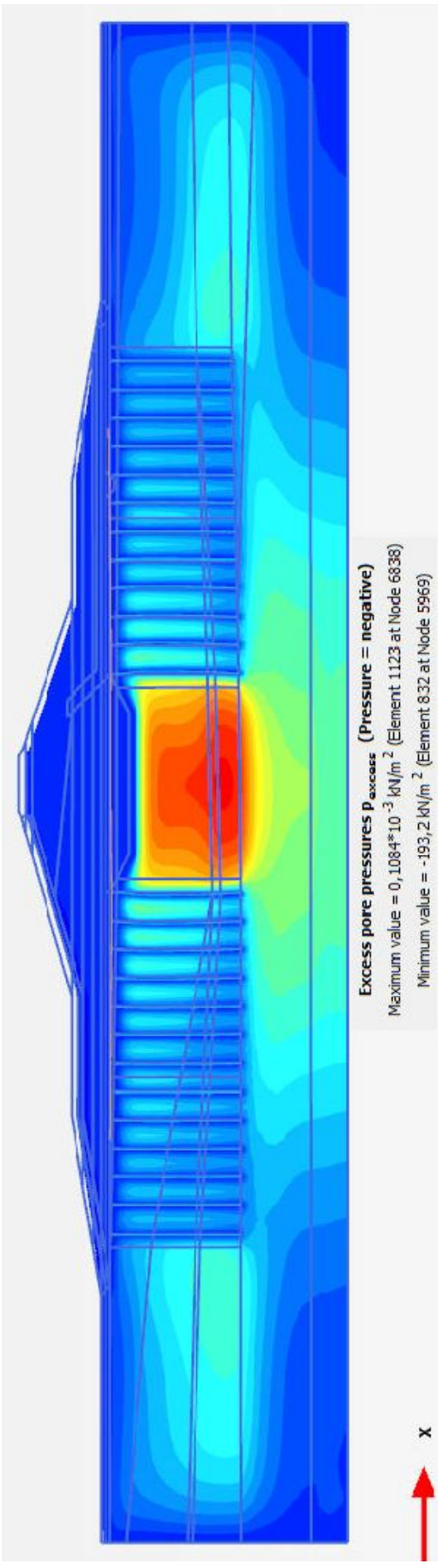

Figure VII.47– PK0+240 of Dike No.1: Excess pore pressures, with flow, associated to the dike conclusion, with the SSC model, and smear (K_{hsAx}=0.10K_{h0} + ds=3d_w)

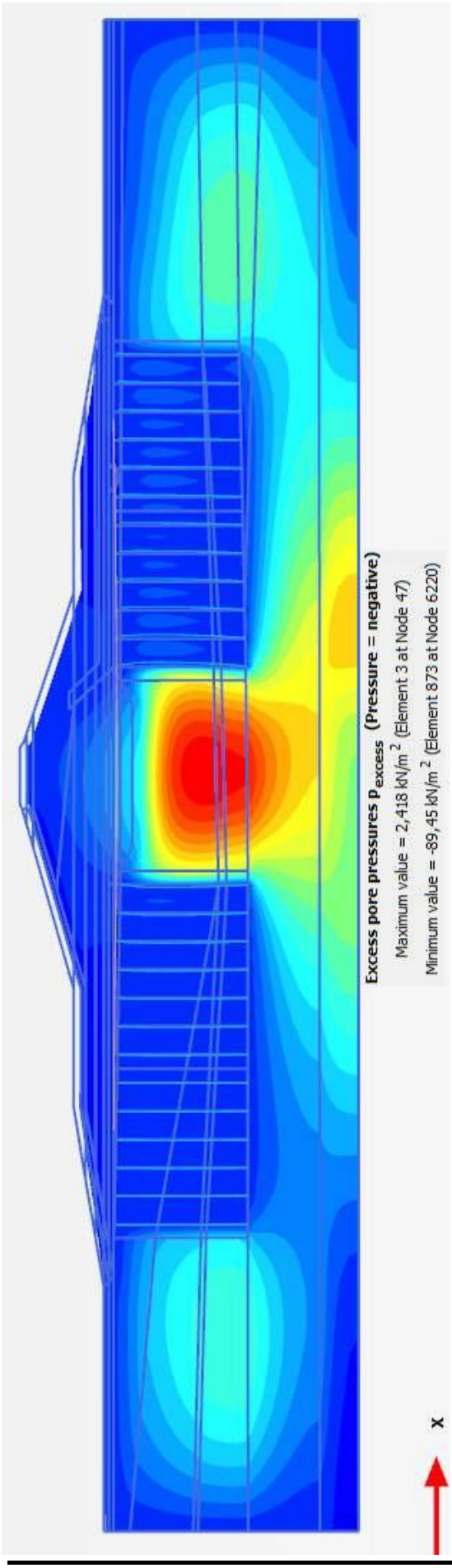

Figure VII.48 – PK0+240 of Dike No.1: Excess pore pressures, without flow, associated to the final step, with the SSC model, and smear (K_{hsAx}=0.10K_{h0} + ds=3d_w)

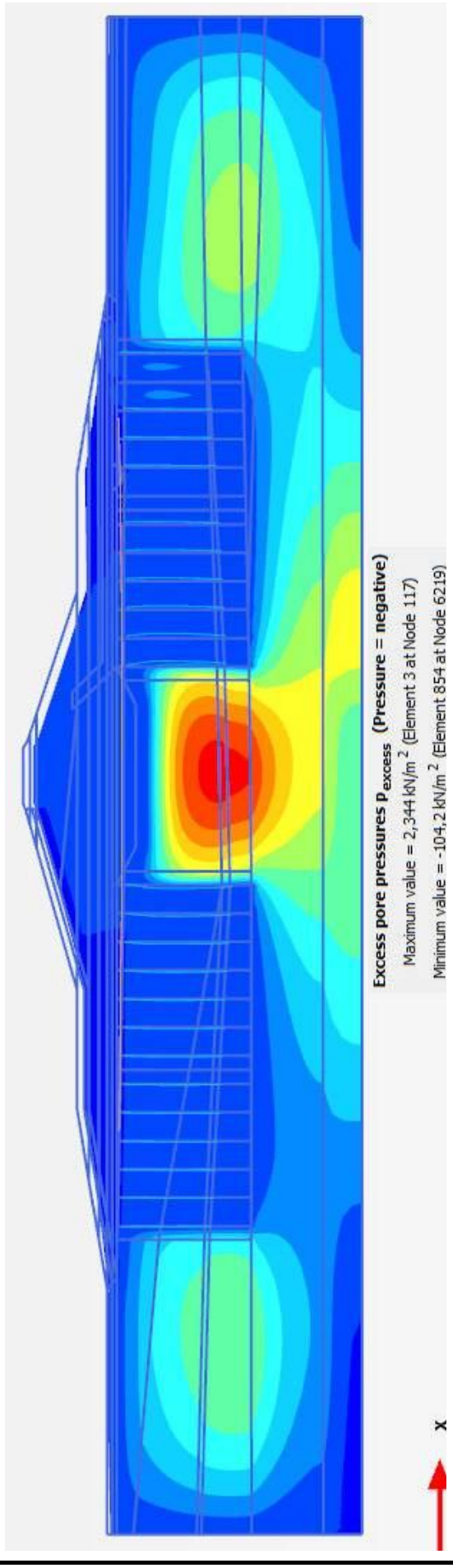

Figure VII.49 – PK0+240 of Dike No.1: Excess pore pressures, with flow, associated to the final step, with the SSC model, and smear (K_{hsAx}=0.10K_{h0} + ds=3d_w)

Figures VII.50 and VII.51 shows, respectively, the pore pressure associated to the construction conclusion of Dike No.1, and also to the final calculation step. The results proves that the pressure upstream is slightly higher than downstream, especially after the reservoir filling, since there is a connection between the drains and the pond through the upstream draining blanket.

The zones where suction occurs correspond to the zones where the soils are partially saturated. During the construction phase, although the water table is located just below the ground surface, the soil between the drains, and around them, is partially saturated as these elements capture the water in these areas (Figure VII.52). With the filling of the pond, the upstream side of the dike begins to saturate, as well as the soil foundation, and there is considerable increment of the saturated zones, even between the drains (Figure VII.53). In any case, the suction values are very low, around 0.001 to 0.002 kPa. Given the lack of tests performed in partially saturated conditions for these soils, is difficult to make further comments concerning the magnitudes in question.

- In piezometers PZ 180-1A and PZ 180-1B of Dike No.3, placed in the foundations, upstream of the cut-off trench, on a area without drains, it is seen that the pore pressure calculated, with and without flow, are quite similar. It is believed that this is a result of the reduced permeability of the soils foundation, associated to the fact that the drains in this cross-section are placed downstream of the cut-off trench, and relatively far away from the piezometers. Hence, the influence of the flow in zone of the foundations is insignificant. Besides, in the case of piezometer PZ 180-1B the simulation results always exceed the values measured, though relatively similar in PZ 180-1A after the reservoir filling (Graph VII.50). However, in this last piezometer, located near the surface, the inverse takes place during the construction phase, since the simulation results are smaller than the real values. This means that the dissipation of the excess pore pressure is higher in the numerical simulation during this phase of the works.

- With respect to the piezometer PZ 180-B and in accordance with the monitoring data, the soil foundation is dissipating the excess pore pressure more quickly than expected. Taking the flow in consideration, it was expected an increment in the dissipation of the pore pressure excess, especially in this piezometer, given the fact that he is placed in the more pervious layer of the foundations stratum of the foundation. If that case, the pore pressure would suffer a decrease and would get closer to the monitored results.

Figure VII.54 represents the excess pore pressure for the simulations with and without the flow, being possible to realise that the greatest difference in excess pore pressure occurs near the cut-off. The same result is confirmed by figure VII.55, as the difference in the pore pressure is insignificant in the zone where the piezometers are placed, due to distance from the downstream drains. Once more, with the flow, the circulation of the water is permitted, both in the foundation and in the dike, resulting in the appearance of partially saturated zones. The associated suction is represented in figure VII.56.

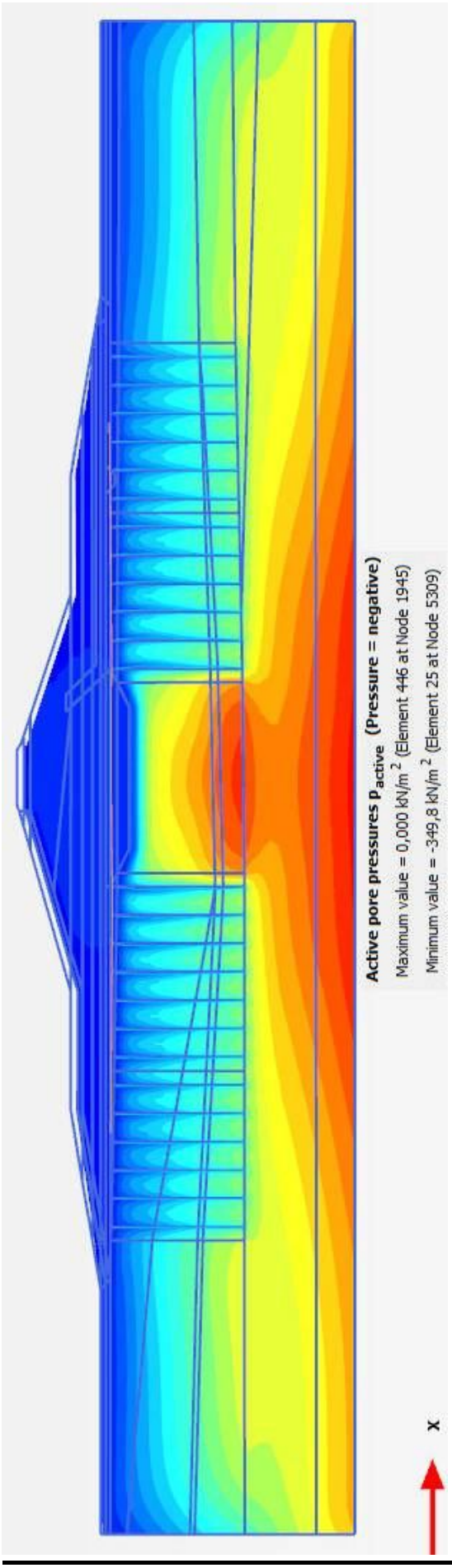

Figure VII.50 – PK0+240 of Dike No.1: Pore pressures, with flow, associated to the dike conclusion, with the SSC model, and smear (K_{hsAx}=0.10K_{h0} + ds=3d_w)

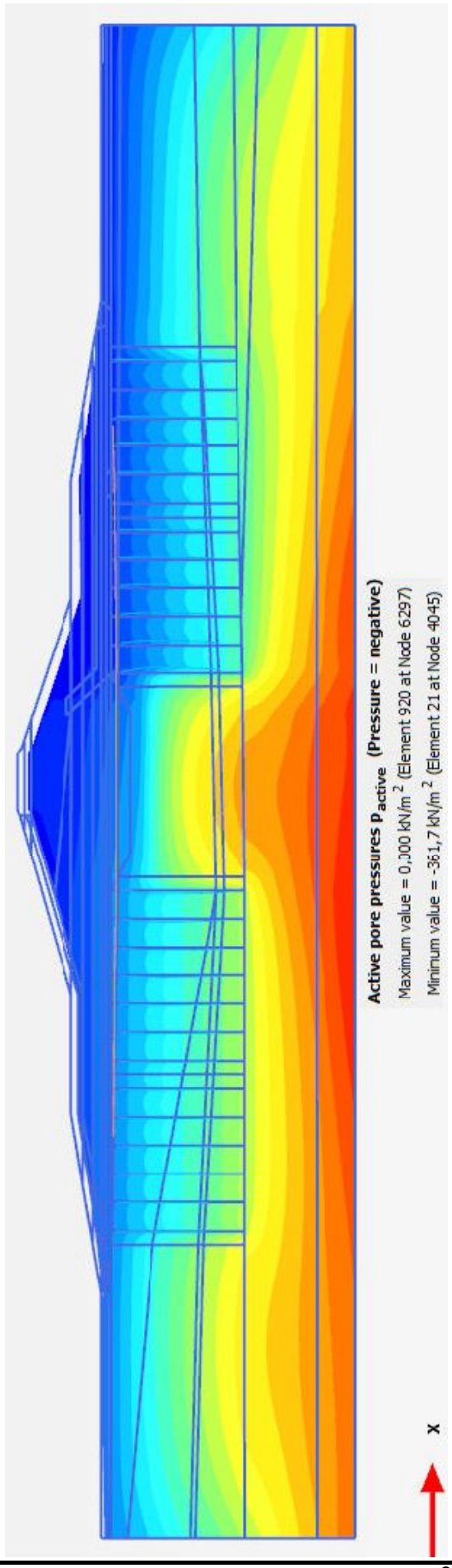

Figure VII.51 – PK0+240 of Dike No.1: Pore pressures, with flow, associated to the final step, with the SSC model, and smear (K_{hsAx}=0.10K_{h0} + ds=3d_w)

Figure VII.52 – PK0+240 of Dike No.1: Soil suction associated to the dike conclusion. with the SSC model. and smear (K_{hsAx}=0.10K_{h0} + ds=3d_w)

Figure VII.53 – PK0+240 of Dike No.1: Soil suction associated to the final step, with the SSC model, and smear (K_{hsAx}=0.10K_{h0} + ds=3d_w)

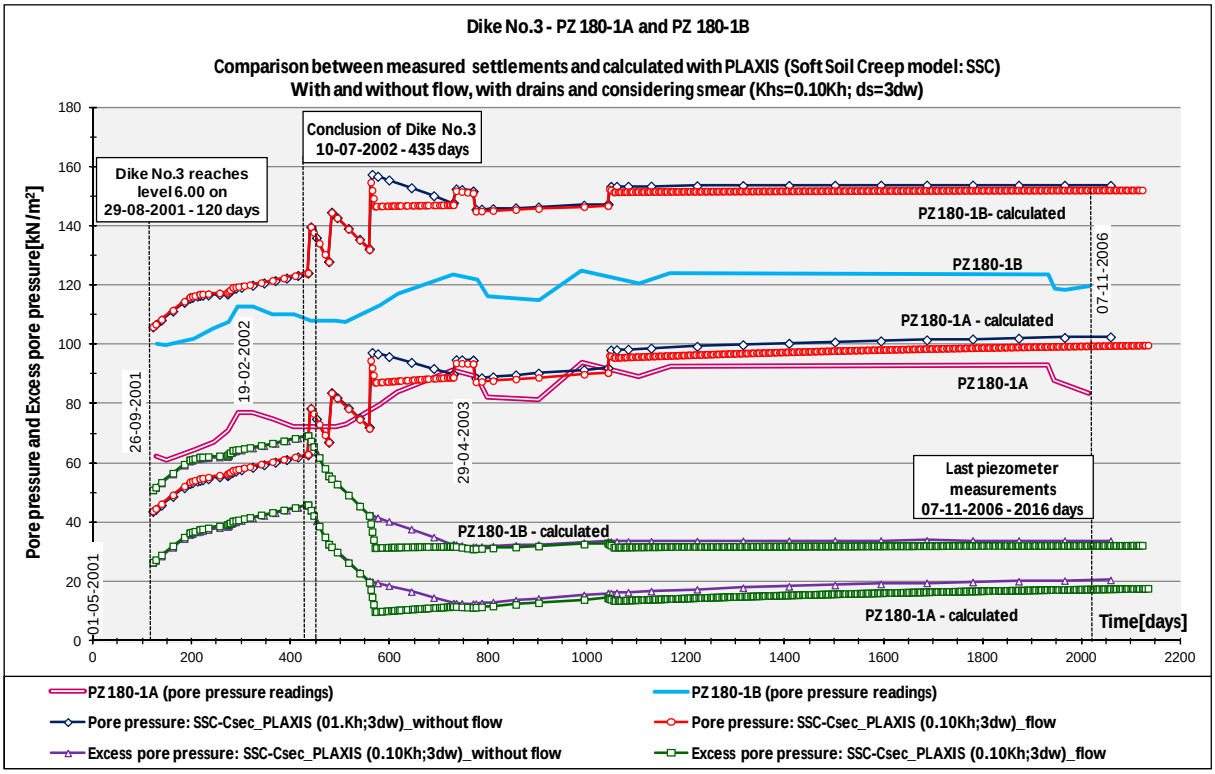

Graph VII.50 – PZ 180-1A and PZ 180-1B of Dike No.3: Pore pressures and excess pore pressures considering flow, calculated with SSC model, with $C_{\alpha PLAXIS}$, and smear effect given by K_{hsAx}=0.10K_{h0} and d_s=3d_w

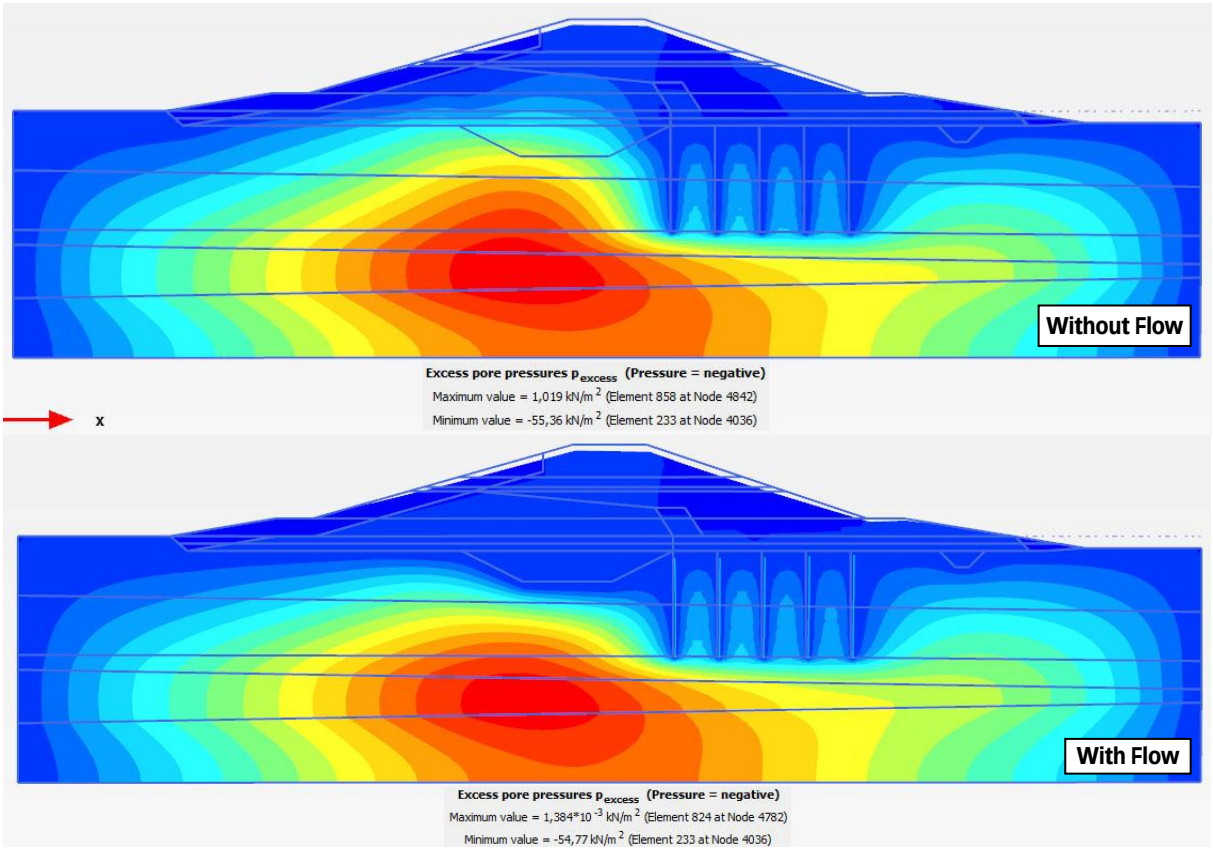

Figure VII.54 – PK0+180 of Dike No.3: Excess p**ore pressures, with and without flow, associated to the final calculation step, using the *SSC* model, and smear given by K_{hsAx}=0.10K_{h0} and d_s=3d_w**

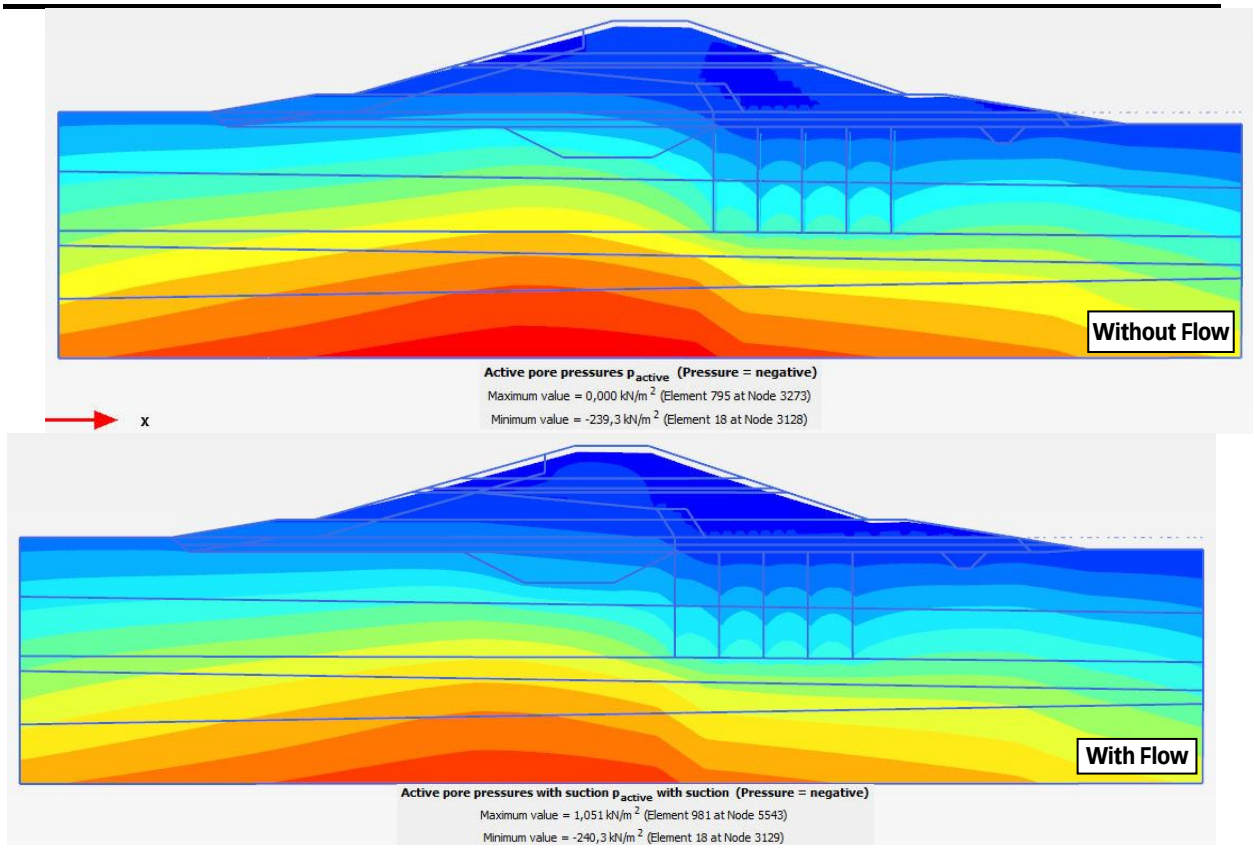

Figure VII.55 – PK0+180 of Dike No.3: Pore pressures, with and without flow, associated to the final calculation step, using the *SSC* model, and smear given by $K_{hsAx}=0.10K_{h0}$ and $d_s=3d_w$

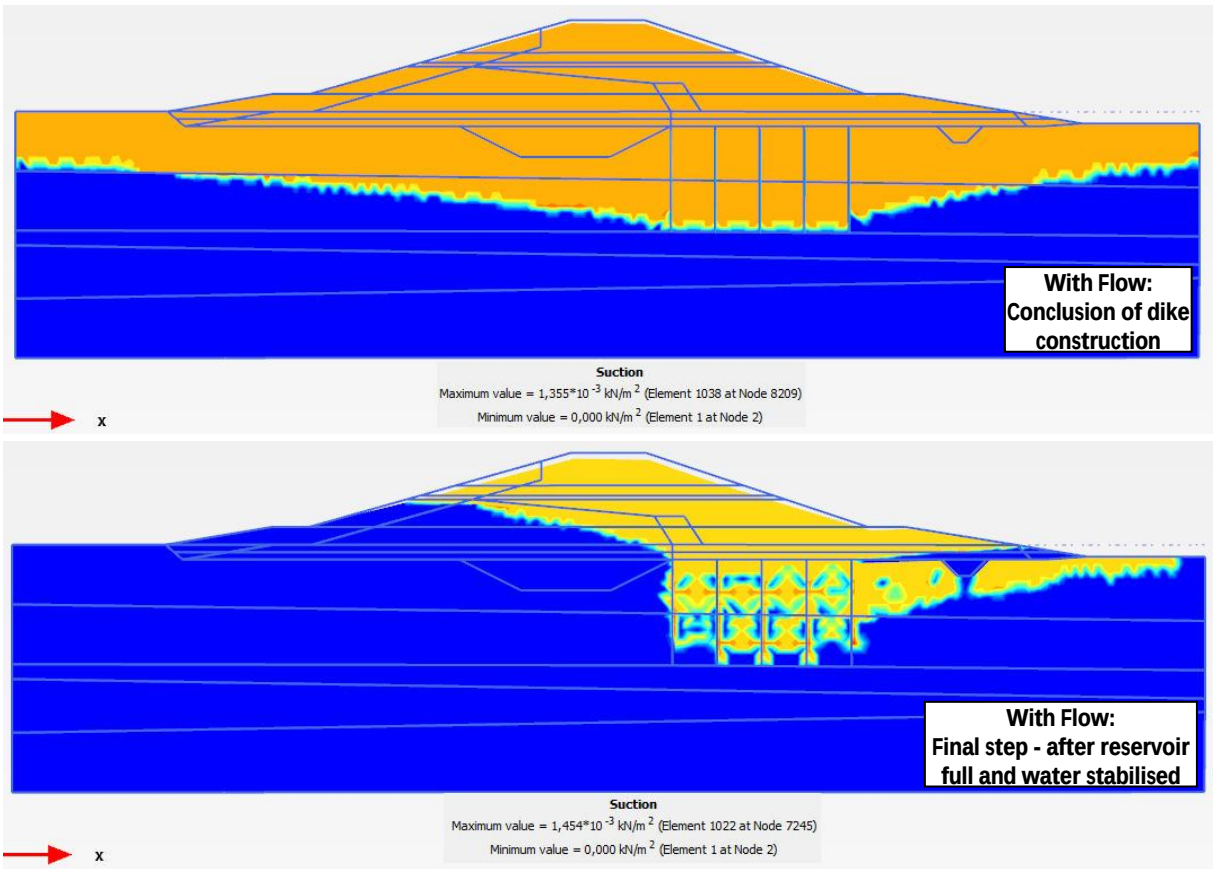

Figure VII.56 – PK0+180 of Dike No.3: Soil suction correspondent to the conclusion of the dike and to the final calculation step, using the *SSC* model, and smear given by $K_{hsAx}=0.10K_{h0}$ and $d_s=3d_w$

The results of the pore pressure and excess pore pressure, as well as the suction, for section PK0+200 are presented in the following figures, for the analysis with and without flow. These can also be compared to the previous results, and observe the differences associated to the drains.

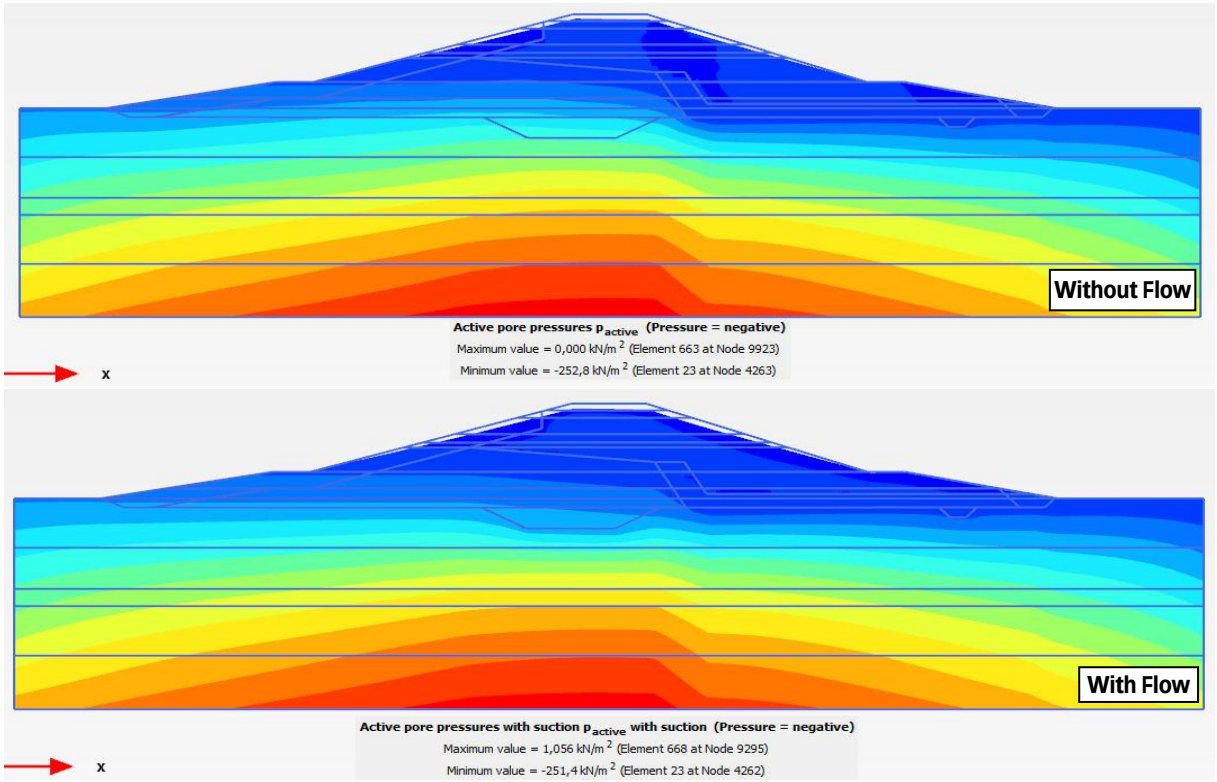

Figure VII.57 – PK0+200 of Dike No.3: Pore pressures, with and without flow, associated to the final calculation step, using the *SSC* model, and smear given by $K_{hsAx}=0.10K_{h0}$ and $d_s=3d_w$

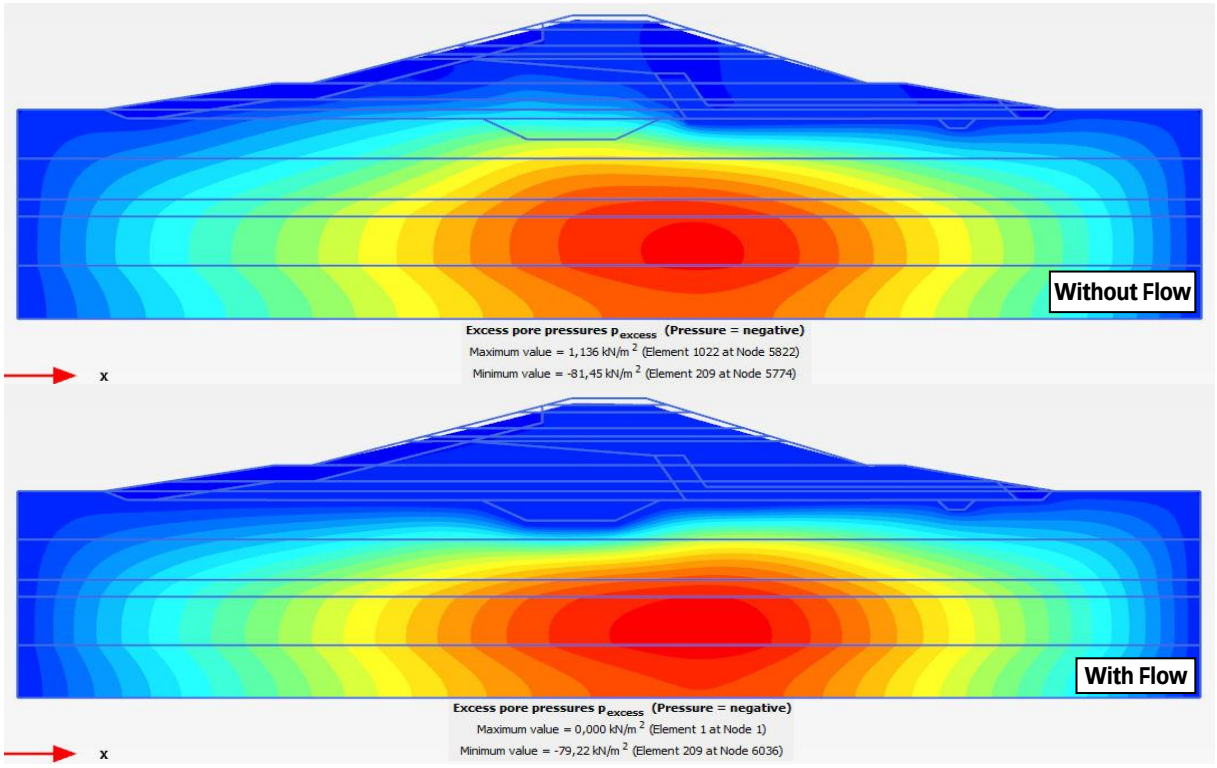

Figure VII.58 – PK0+200 of Dike No.3: Excess pore pressures, with and without flow, associated to the final calculation step, using the *SSC* model, and smear given by $K_{hsAx}=0.10K_{h0}$ and $d_s=3d_w$

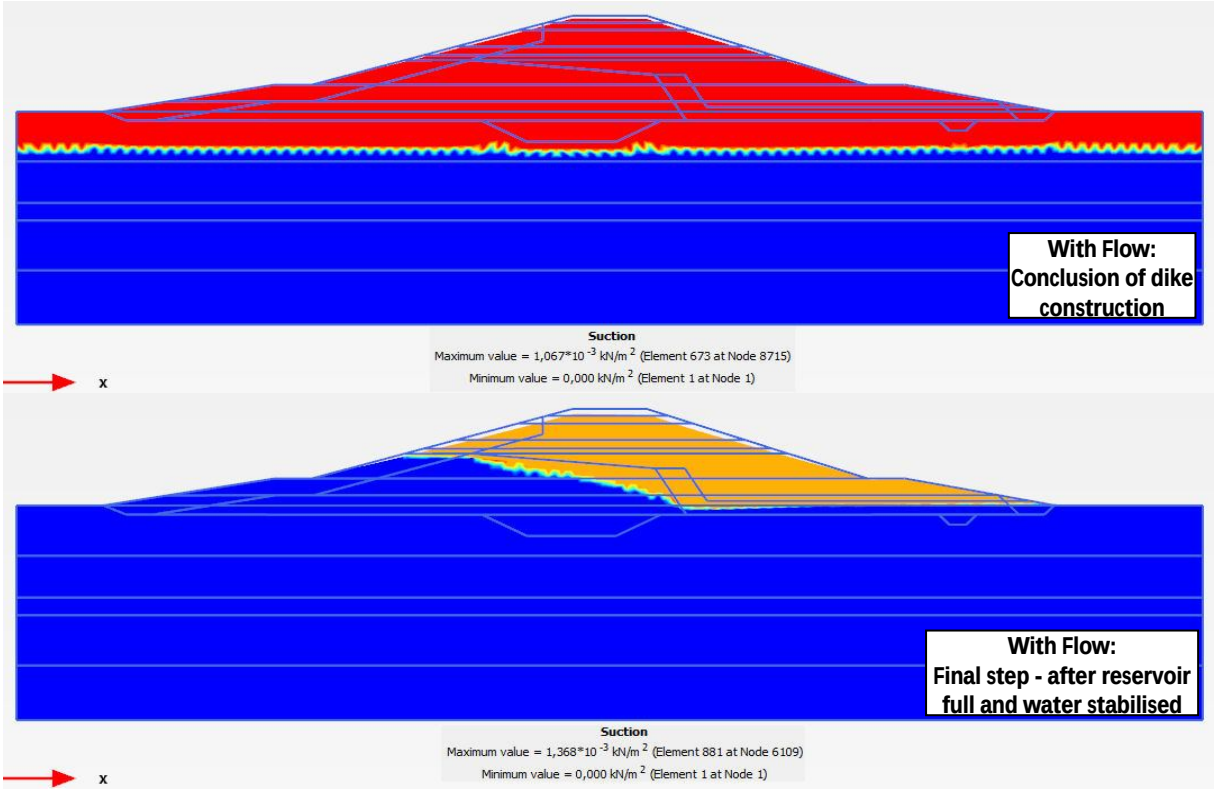

Figure VII.59 – PK0+200 of Dike No.3: Soil suction associated to the final calculation step, using the *SSC* model, and smear given by $K_{hsAx}=0.10K_{h0}$ and $d_s=3d_w$

From figures VII.57 to VII.59, it is confirmed that the excess pore pressure in the embankment is substantially reduced, when flow is considered, being in fact practically null. In the section PK0+200 the zone where the soils are partly saturated is perfectly define; before the rising of the water in the pond, the water table is positioned near the ground surface, and all the soil beneath are saturated; once the water level in the reservoir is stabilised, and the flow net in the dike is established, then the soil above the saturation flow line are partly saturated. The influence of the band-shaped drains on the flow net is clearly perceptible when comparing the previous cross-sections with this one, even though the values calculated for this parameter are relatively small. The flow rates associated either to the conclusion of the embankment construction and to the final calculation step, are plotted in Appendices III and IV. In addition, the groundwater head results will also be provided, for both the phases and sections studied.

In order to conclude the comparative analyses between the simulation and monitoring results, it remains the analyses of the horizontal displacements.

VII.3.3 HORIZONTAL DISPLACEMENTS IN DIKE NO.1 WITH FLOW

Given the extremely reduced measured of the inclinometers placed in Dike No.3, they will not be taken in considerations, and so, the analyses will be focused on the inclinometer I 240-1 of Dike No.1, since this was the only cross-section modelled. In graph VII.51, the horizontal displacements measured in I 240-1, for 801 days, 838 days and 1563 days are showed, being this final date the last reading available for this device. The other two dates correspondent to the time interval when the embankment dike was concluded.

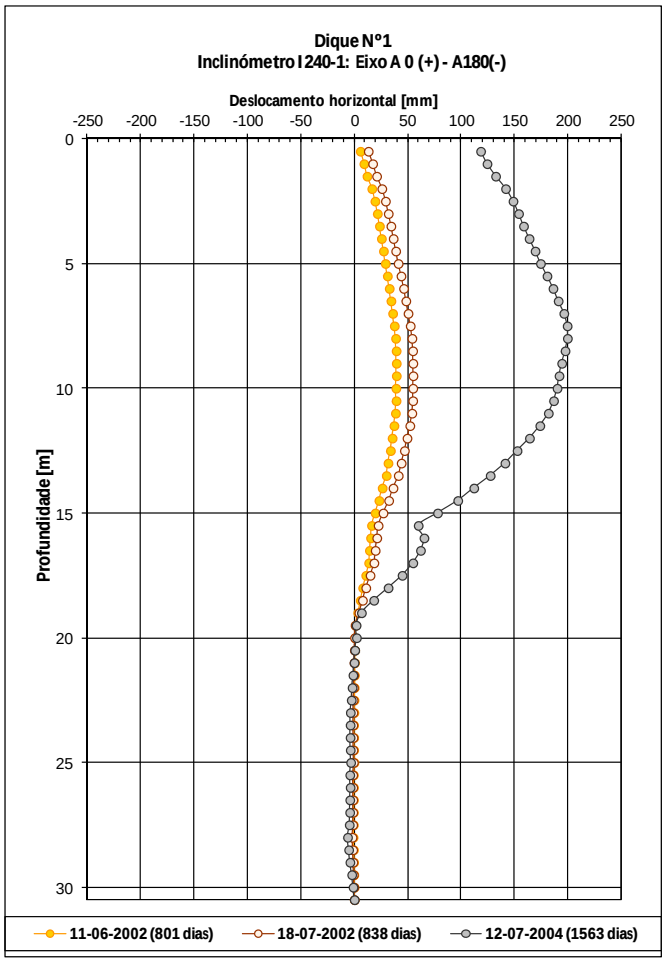

Graph VII.51 – PK0+240 of Dike No.1: Horizontal displacements on I 240-1 for the dates indicated

The horizontal displacements for the analyses without flow are shown in figures VII.60a to VII.60c and the results with flow are displayed in figures VII.61a to VII.61c.

From the comparison between the simulations results, the values are lower when considering the flow, in contrast to what was seen with the vertical displacements. So, according to these values the slope stability will be greater if the flow is considered, since the dissipation of the pore pressure excess is superior, as well as the consolidation rate, and therefore the shear strength of the soil increases. This conclusion will be proven by the results of the safety factors obtained in the stability analysis, perform in the following subchapter, as the horizontal displacements are closely associated to the slope stability.

In turn, the maximum horizontal displacements measured are much lower in comparison to those calculated with flow. The ratios between them are approximately 20% and 60%, respectively, for the conclusion of the dike construction and for the final reading on the inclinometer, which means that the stability in place is higher than the design. Despite this difference, the maximum displacements occurs more or less at the same depth, indicating that the slope surface in the numerical simulations agree with the observed in "loco".

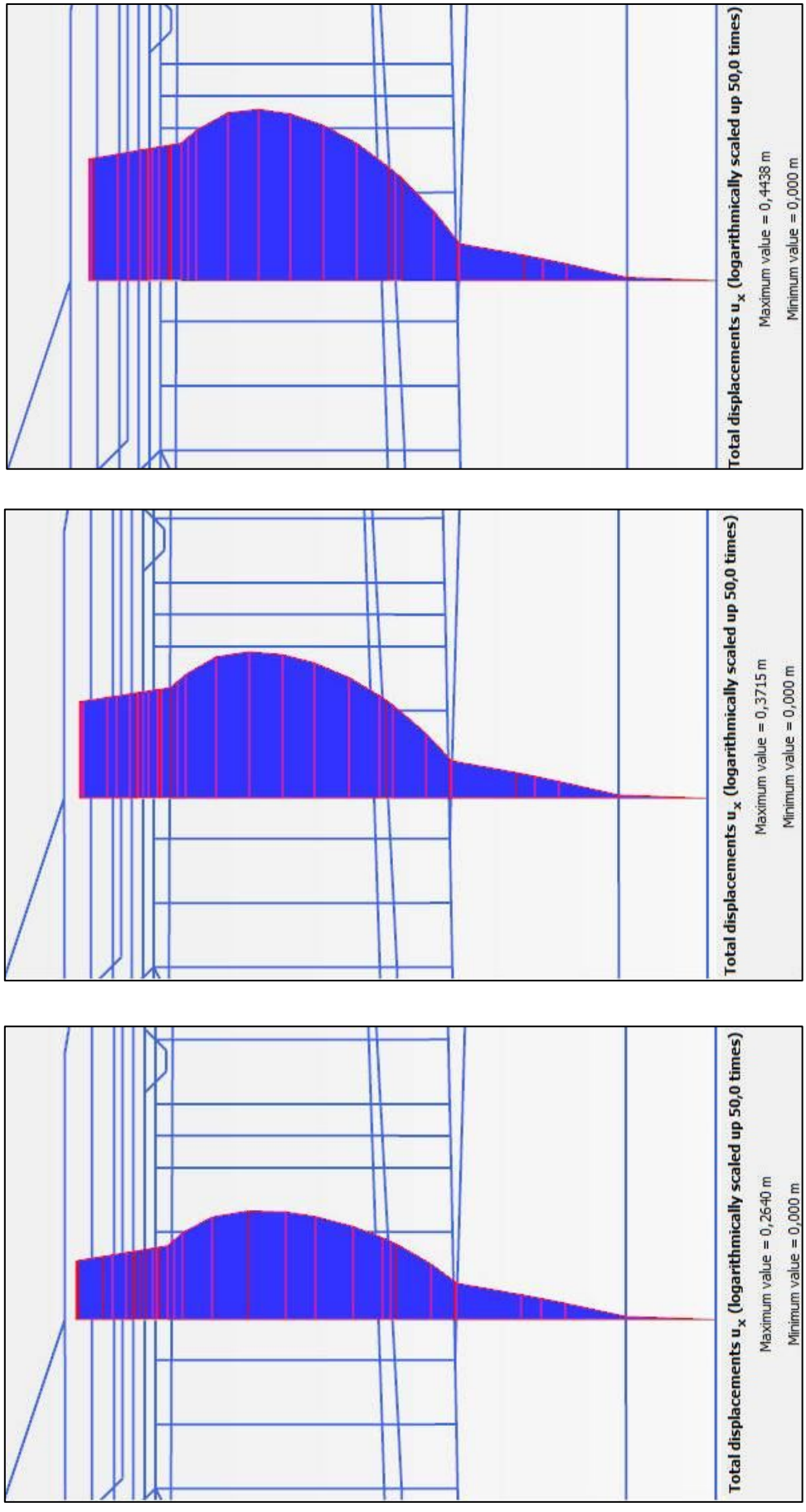

a) End of construction works (818 days) b) 1523 after the start of construction works c) Last calculation step (2921 days)

Figure VII.60 – PK0+240 of Dike No.1: Horizontal displacements. without flow. using the SSC model. and smear given by K_{hsh}=0.10K_{hp} and d_e=3d_w

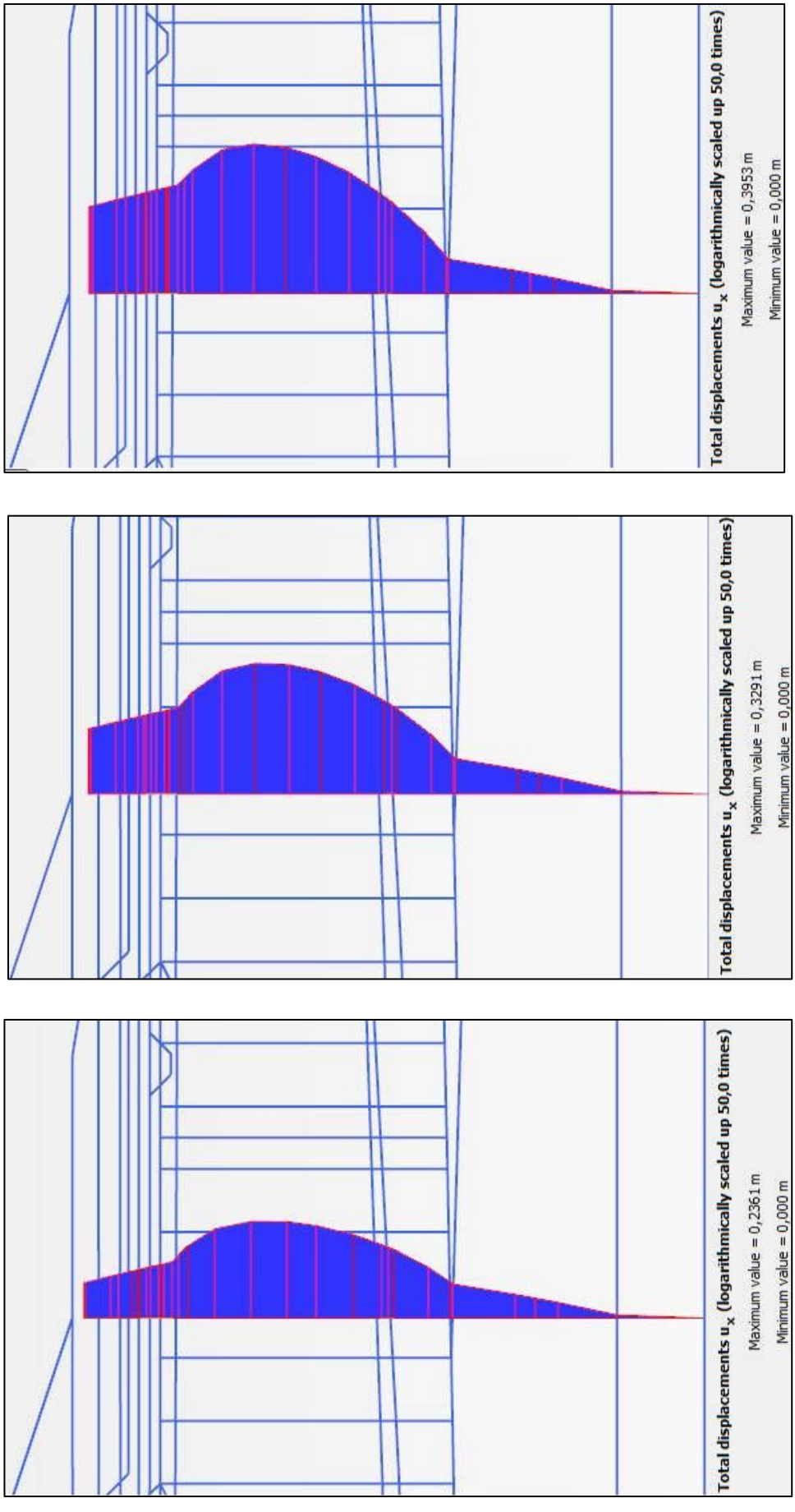

c) Last calculation step (2921 days)

b) 1523 after the start of construction works

a) End of construction works (818 days)

Figure VII.61 – PK0+240 of Dike No.1: Horizontal displacements, with flow, using the SSC model, and smear given by $K_{hsAx}=0.10K_{h0}$ and $d_s=3d_w$

VII.4. SLOPE STABILITY ANALYSIS FOR DIKES NO.1 AND NO.3

With the objective of analysing the influence of the reinforcement geotextile, the band-shaped drains, the smear effect, the soil material models, the secondary compressibility index and the flow, in the overall stability of the dikes, the safety factor was determined for several and different kind of scenarios. These were calculated for two distinct steps of the calculation procedure, one being associated to the final phase of the dikes construction and the other to the final step, with the reservoir completely full and the water level stabilized in the pond.

The results attained, namely for PK0+240 of Dike No.1, PK0+140, PK0+170 and PK0+200 of Dike No.3, can be consulted in tables VII.18 and VII.19. Based on them, it is remarked that the safety factor associated to the end of the embankment construction, prior to the reservoir filling, is slightly lower than that obtained for the last step of the calculation. This result is due to the increase in the shear strength of the soil, as the consolidation of the soil foundation takes place. Moreover, it can be seen that:

- The application of the geotextile reinforcement allows an increase in the factor of safety, which varies from 31% and 41% with respect to the initial situation, where the ground foundation did not received any improvement. When considering only the band-shaped drains but not the smear effect, this value is slightly lower, ranging between 10% and 28%. Considering both the geotextile and the drains, once more without the smear effect, the highest increment is produced, from 72% to 100%. In this last scenario, not only the geotextile contributes to safety, but also the drains are helping, as they allow a faster dissipation of the excess pore pressure. The consideration of the smear effect in the areas improved with the drains is another factor that considerably influences the stability. Therefore, for the worst scenario of smear, the stability safety factor falls, but they are still far above the initial values, varying between 52% and 69%. This comparisons were made for the models SS and SSC_$C_{\alpha(Terzaghi)}$;
- By considering the flow, the safety factors increase slightly for the same smear, resistance and compressibility conditions;
- For all the cross-sections analysed, the safety factors obtained with the *Soft Soil* and *Soft Soil Creep* models are identical, though slightly lower in the latter;
- The safety factors obtained with the *Mohr-Coulomb* model using method A are much higher than those for method B. Also, the values given by the *Mohr-Coulomb* model using method A, are quite close to those calculated with the *Soft Soil* and *Soft Soil Creep* models, as they all consider the same shear strength for the soil foundation, and all of them takes in consideration the increase of shear strength with the consolidation;
- In the *Mohr-Coulomb* model, when the reduced shear strength parameters are used, than the safety factors are lower, although with greater expression in method B. This result is justified by the fact that this method does not allow the increase of the shear strength with the consolidation.

Table VII.18 – Dike No.1: Safety factors correspondent to the slope stability analysis

	Conclusion of dike construction	**Raise up of reservoir: Last calculation step**
Model	Safety factor	Safety factor
Without geotextile; Without drains		
SS	1.818	1.907
SSC_$C_{\alpha(Terzaghi)}$	1.495	1.575
With geotextile; Without drains		
SS	2.466	2.509
SSC_$C_{\alpha(Terzaghi)}$	2.090	2.221
Without geotextile; With drains (without smear)		
SS	2.332	2.446
SSC_$C_{\alpha(Terzaghi)}$	1.890	2.017
With geotextile; With drains (without smear)		
SS	3.128	3.250
SSC_$C_{\alpha(Terzaghi)}$	3.002	3.148
With geotextile; With drains and smear (k_{hs}=0.10K_h; d_s=3d_w)		
SS	2.895	2.910
SSC_$C_{\alpha(Terzaghi)}$	2.529	2.544
SSC_$C_{\alpha(PLAXIS)}$	2.609	2.676
SSC_$C_{\alpha(PLAXIS)}$ +Flow	2.625	2.706
With geotextile; With drains and smear (k_{hs}=0.33K_h; d_s=3d_w)		
MC-Met.A (Eref=75c_u; c'; φ')	2.986	3.168
MC-Met.Ared (Eref*=75c_u*; c'; φ')	2.977	3.155
MC-Met.B (Eref=170c_u; c_u; φ_u)	1.803	1.912
MC-Met.Bred (Eref*=170c_u; c_u; φ_u)	1.610	1.691
SS	2.988	3.043
SSC_$C_{\alpha(Terzaghi)}$	2.601	2.634
SSC_$C_{\alpha(PLAXIS)}$	2.779	2.801
With geotextile; With drains and smear (k_{hs}=0.66K_h; d_s=3d_w)		
SS	3.024	3.106
SSC_$C_{\alpha(Terzaghi)}$	2.935	2.975

Table VII.19 – Dike No.3: Safety factors correspondent to the slope stability analysis

	Conclusion of dike construction			**Raise up of reservoir: Last calculation step**		
	Safety factor			Safety factor		
	PK0+140	PK0+170	PK0+200	PK0+140	PK0+170	PK0+200
Model	**With drains (without smear)**		**Without drains**	**With drains (without smear)**		**Without drains**
SSC_$C_{\alpha(Terzaghi)}$	2.256	2.102	1.663	2.306	2.127	1.782
Model	**With drains and smear (k_{hs}=0.10K_h; d_s=3d_w)**		**Without drains**	**With drains and smear (k_{hs}=0.10K_h; d_s=3d_w)**		**Without drains**
SSC_$C_{\alpha(Terzaghi)}$	2.246	2.095	1.663	2.355	2.120	1.782
SSC_$C_{\alpha(PLAXIS)}$	2.031	1.920	1.588	2.194	1.969	1.592
SSC_$C_{\alpha(PLAXIS)}$ +Flow	2.054	1.944	1.655	2.242	2.010	1.655

With respect to the slope stability surfaces, associated to the dikes conclusion, it is observed, that:

- For Dike No.3, in the cross-sections PK0+140 and PK0+170, where the drains were installed only downstream of the cut-off trench, the surface is located on the upstream side (Figure VII.62). This result is directly associated to the contribution of the drains on the right side of the cut-off, helping on the dissipation of the excess pore pressure, and thereby leading to a gain in the shear strength;
- When the foundation is not treated with drains (PK0+200), the rupture surface is not as well defined as the others in this phase (Figure VII.64);
- For Dike No.1, where the foundation is treated with drains both upstream and downstream, the rupture surface is located on the downstream side (Figure VII.66).

In turn, after the reservoir is full and the water level stabilised in the pond, the surface is always located on the downstream side (Figures VII.63, VII.65 and VII.67).

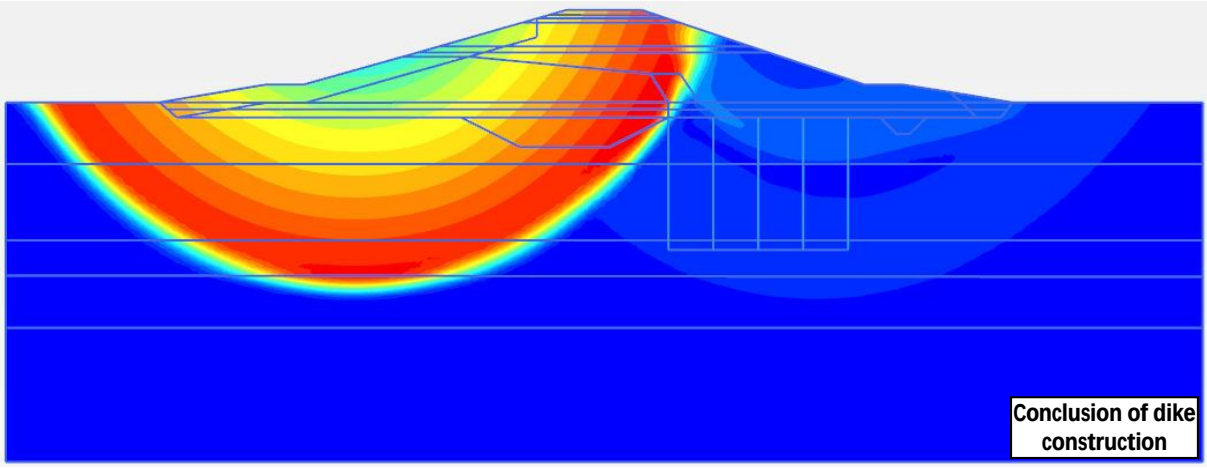

Figure VII.62 – PK0+140 of Dike No.3: Slope stability surface at the end of dike construction, with SSC model and smear given by $K_{hsAx}=0.10K_{h0}$ + $d_s=3d_w$ (with PVD drains downstream of the cut-off trench)

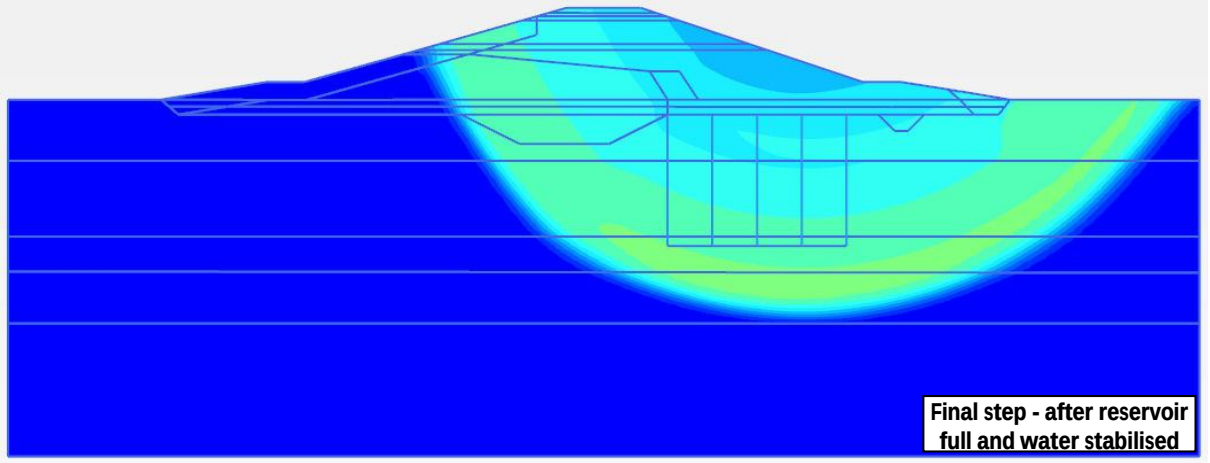

Figure VII.63 – PK0+140 of Dike No.3: Slope stability surface for the final calculation step, with SSC model and smear given by $K_{hsAx}=0.10K_{h0}$ + $d_s=3d_w$ (with PVD drains downstream of the cut-off trench)

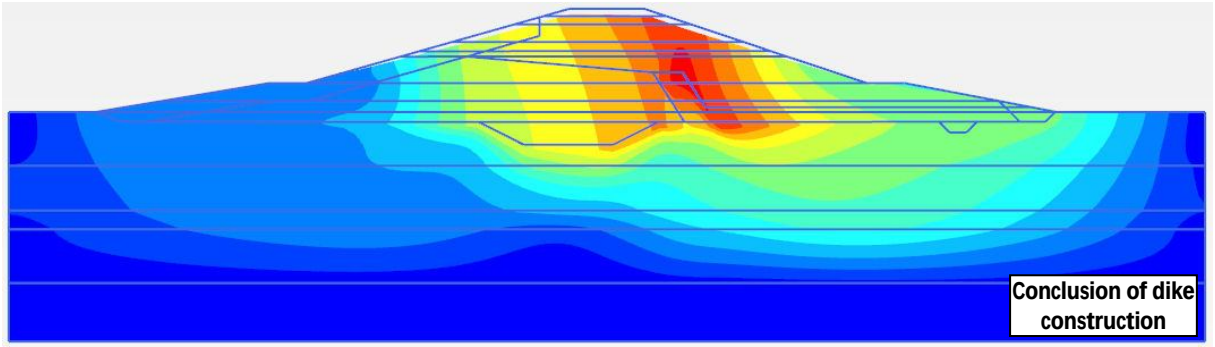

Figure VII.64 – PK0+200 of Dike No.3: Slope stability surface at the end of dike construction, with SSC model and smear given by $K_{hsAx}=0.10K_{h0}$ + $d_s=3d_w$ (without PVD drains)

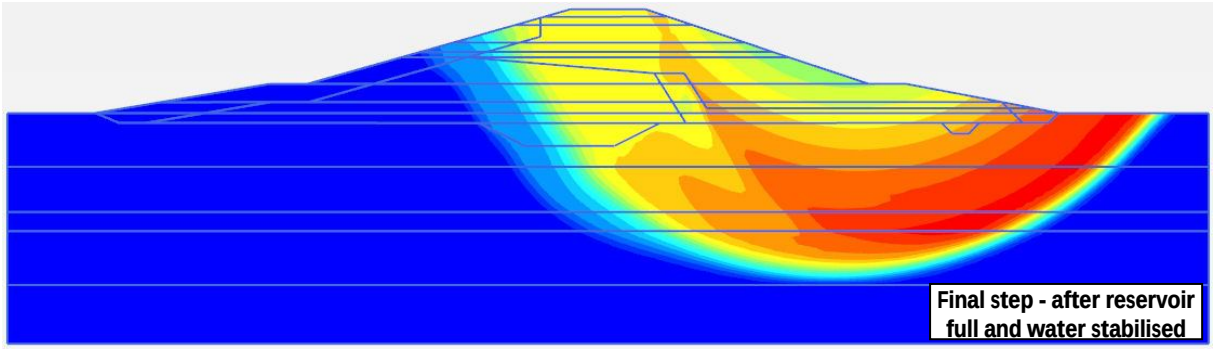

Figure VII.65 – PK0+200 of Dike No.3: Slope stability surface for the final calculation step, with SSC model and smear given by $K_{hsAx}=0.10K_{h0}$ + $d_s=3d_w$ (without PVD drains)

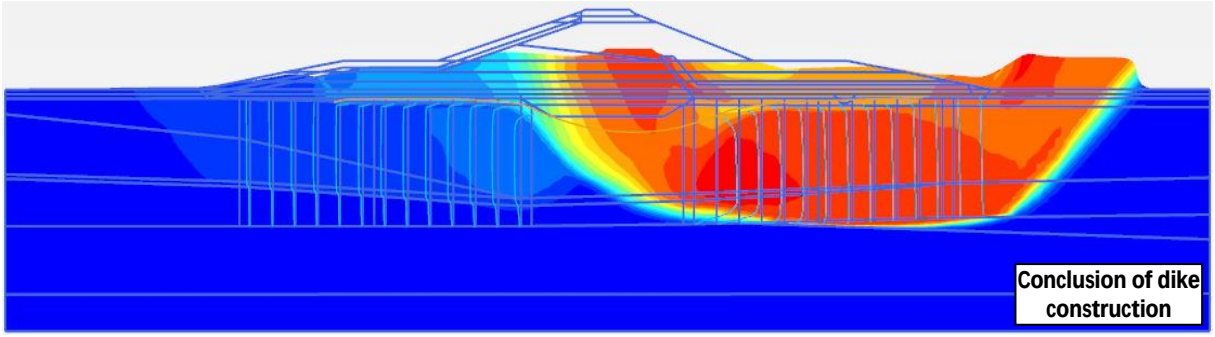

Figure VII.66 – PK0+240 of Dike No.1: Slope stability surface at the end of dike construction, with SSC model and smear given by $K_{hsAx}=0.10K_{h0}$ + $d_s=3d_w$ (with PVD drains on both sides of the cut-off trench)

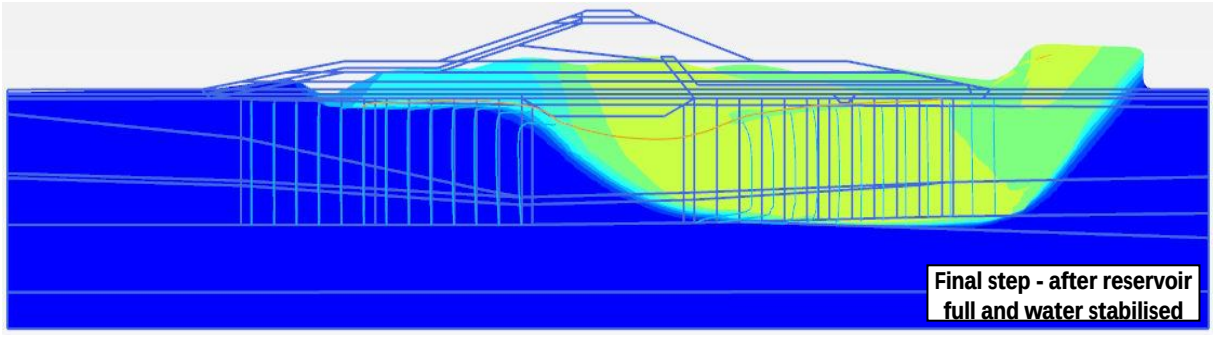

Figure VII.67 – PK0+240 of Dike No.1: Slope stability surface for the final calculation step, with SSC model and smear given by $K_{hsAx}=0.10K_{h0}$ + $d_s=3d_w$ (with PVD drains on both sides of the cut-off trench)

This chapter is the culmination of the practical work developed in the thesis, where the entire procedure associated to the modeling of the most relevant cross-sections of the case study, namely the Dykes No.1 and No.3 of the *Lebrija* Pond, is presented, as well as the results of the simulations for several conditions, confronting the numerical results with the real ones. These made it possible to prove the theoretical concepts that are described in chapters II to V, to validate the characteristics of the soils foundation, as well as the construction stages and timelines associated to the each of the dikes and sections, being these information given in chapter VI. In the latter, an analysis of all the monitoring results obtained for these two dykes was also included.

In light of the above, chapter VIII will present the main conclusions of the study performed, thereby concluding the research regarding the consolidation of soft soil in the presence of band-shaped drains.

VIII. CONCLUSIONS AND FUTURE DEVELOPMENTS

The consolidation of soft soil treated with vertical band-shaped drains is the central core of this thesis, which involved a good deal of research, balanced by theoretical and experimental aspects, but standing on a plateau of predominantly practical nature. The theoretical component is essential to understand the phenomena covered on the research study, which is manly oriented for the analysis of test results, monitoring data and numerical simulations.

The experimental component is associated with the study and analysis of Dikes No.1 and No.3 of the *Lebrija* Pond, being this an interesting work case and worthy of a more in-depth study, not only because these dikes are founded in soft soil improved with vertical band-shaped drains, but mostly because of the abundance and diversity of information available. This information includes the results of site investigation, field and laboratory tests, in order to characterize the soils foundation, as well as a significant quantity of monitoring data. In fact, these dikes are controlled since the beginning of their construction, in mid-2000.

For the numerical modelling of the dikes, a well-known software was used, namely PLAXIS. With this program, several scenarios were simulated for the smear effect in the zones improved with the drains, for the creep of the soft soil and for the flow. Additionally, three different material models were considered for the soil foundation, being two more adequate to traduce the behaviour of compressible soils, and one of these last models specially indicated for highly compressible soils. The numerical results obtained were compared with the monitoring data, and interesting conclusions were able to be drawn with respect to the topics under study, regarding Dikes No.1 and No.3 of the *Lebrija* Pond. This diversity of scenarios led to the need of checking and counter-checking the data and results, originating substantial volumes of information, which had to be carefully structured and graphically systematised, in order to be able to obtain the conclusions which will be presented in this chapter.

For systematization purposes, and given the amount of results analysed, it seems appropriate to divide the conclusions into three distinct groups. In the first group, the conclusions presented are those drawn from the monitoring results of Dikes No.1 and No.3 of the *Lebrija* Pond. The second group presents the conclusions associated with the parametric and sensitivity analyses, conducted analytically and numerically. Lastly, in the third group, the numerical simulations are compared with the monitoring results for the cross-sections modelled. The combination of these conclusions will allow answering the two questions rose in the introduction of this thesis.

VIII.1. CONCLUSIONS

Before listing the conclusions concerning the research work undertaken, a series of aspects will be highlighted, which should always be bear in mind, when results from site investigations, numerical simulations and the monitoring of geotechnical structures, are involved, namely:

- Ground foundations, including the soils that make part of them, are usually heterogeneous and anisotropic media, since they have its origins in the decomposition and alteration of rock massifs, suffering several natural processes until their actual state. As a result, the soils present a complex behaviour and not easy to fully predict, especially high compressibility soils, such as soft soils. In addition to its non-linear behaviour, this type of soil also suffers significant deformation under constant pressure (viscous or creep phenomenon);

- The mathematical models used in the numerical simulations to describe the behaviour of the soil must be adequate to the type of soil analysed, otherwise, the answer obtained will not be able to traduce with accuracy the phenomena involved. These models should call upon simple and easy to determine parameters to characterize the soil, based on current, both field and laboratory geotechnical tests. In the absence of data to allow the characterization of soils, it is always possible to use empirical correlations, but they must be chosen carefully, based on the type of soils;

- Not always the conditions of the samples used in the laboratory tests, notably for the oedometer and triaxial tests, which should be unaltered, are in fact in good conditions, i.e., their initial stress state, water content, or volumetric conditions do not correspondent to the reality. Consequently, the characteristics and parameters thus determined, do not translate with precision the state and behaviour of the soil. However, it is based on these same tests results that the soils properties are given, and later on used for the design of geotechnical problems;

- The readings from the devices installed in the soil to monitor and control its behaviour and response, may present anomalies or irregularities due to problems during installation, during the construction phase, or even after the construction has been concluded;

- When comparing and confronting the readings from the monitoring devices, or even from the laboratory test curves, with the results from numerical simulations, one cannot expect an exact match between these results; instead, one should observe them from a critical point a view, and try to achieve a reasonable agreement between these values, as well as a good trend of the numerical and measured curves, thereby giving a better understanding of the soil tendency and behaviour.

Taken into consideration the abovementioned aspects, the most relevant conclusions will be immediately presented.

VIII.1.1. CONCLUSIONS REGARDING THE MONITORING RESULTS OF DIKES NO.1 AND NO.3 OF THE *LEBRIJA* POND

The main conclusions withdrawn from the monitoring results of Dikes No.1 and No.3 of the *Lebrija* Pond, presented in subchapter VI.6 (MONITORING RESULTS FROM DIKES NO.1 AND NO.3), are the following:

- The drains enable a faster dissipation of the excess pore pressure as well as the consolidation phenomenon, since the settlements in the sections of the dikes improved with band-shaped drains, are much higher for the same period of time. Moreover, the stabilisation of the settlements begins to occur more or less one year after the conclusion of the dikes, in these same sections, confirming the efficiency of the drains. These settlements, although high, are coherent with the very weak characteristics of layers B1 and B2 of the foundation soil;

- The settlements estimated in the design phase for the highest cross-section of Dike No.1 (PK0+240), where band-shaped drains were installed upstream and downstream of the cut-off trench, were underestimated, as they correspond to 75% of those observed until now. The maximum values reach 100.2cm, against the 72.0cm estimated in the design phase. Expressed as a percentage, these settlements correspond, approximately, to 11.3% of the total height of the embankment, although this value reached 5.4%; at the end of the dike construction. This last result is almost half of the maximum value measured in this section;

- In Dike No.3, in the profiles where drains were installed on the downstream side of the cut-off trench, the maximum settlement is 46.0cm (6.5% of the total height of the dike), while in the unimproved zone, it is about 31.5cm (4.2%). In the phase corresponding to the end of the construction of Dike No.3, the values attained only 2.8% and 1.7%, respectively. Despite of the differences in height between these two dikes (approximately 2.6m), these results show the influence of the drains on the acceleration of the consolidation process of the foundation soils, and consequently on the settlements;

- The vertical displacements on the surface of the dikes, measured from the topographic stake marks, are mainly due to the consolidation of the soil foundation, since the settlements curves obtained for this devices are parallel to the settlements curves associated to the plates placed inside the dikes;

- In Dike No.1, the maximum horizontal displacements were registered in the inclinometers placed in the downstream berm (I 240-1) and near the downstream toe drain (I 260-2), ranging 20.0cm for I 240-1 and 22.7cm for I 260-2. These values were observed more or less at a similar level (between -1.00 and -2.00), located in the B1 soil layer. As the displacements drops substantially from this point on, until they reach the C soil layer, it can be concluded that there is a well-defined slope surface in this dike and on these cross-sections. In Dike No.3 the horizontal displacements measured in the only two inclinometers, placed in a cross-section without drains (PK0+220), are relatively small and insignificant, leading to the conclusion that the stability in this section is not an issue of concern;

- As a general rule, the pore pressure increases in all piezometers, during the construction phase of the embankment, and reducing during the time in which construction is interrupted for several months. With the filling of the pond, once again, an increment of pressure on the piezometers is observed, although the values vary substantially, depending of their position and installation date. After a phase during which the water level stabilises in the reservoir, the pore pressures starts to decrease in almost all of the piezometers which are located on

the downstream side of the cut-off and in the embankment body at lower levels. Such oscillation in the piezometers measurements indicates that, thought the soils presents an undrained behaviour and the pore pressures suffer the effect associated to the overload of the embankment and the reservoir filling, the drains are performing their role adequately, since they allow the dissipation of the excess pressure and an acceleration in the consolidation process;

- The band-shaped drains installed upstream of the cut-off accelerates the hydrodynamic consolidation phenomenon mainly during the construction phase, since the drainage of the soil foundation is ensured by the drainage blanket placed above the drains. However, this same drainage blanket is interconnected to the rip-rap upstream protection, so when the water level rises in the pond de drainage conditions changes;

- The values measured in piezometers PZ 240-1 and PZ 240-2 of Dike No.1 are much higher than expected, since the values are almost matching the overload due to the embankment construction, unlike the others, indicating that the dissipation of the excess pore pressure in these locations is not occurring as quickly as in other zones, mainly in the construction phase. Therefore, this fact must be taken into consideration in future comparisons with these results and also in further conclusions. Also, in Dike No.3, an initial difference of 40kN/m^2 is noted in the pore pressure readings, between PZ 180-1A and PZ 180-1B. This difference remains practically constant during the construction and post-construction phases, so, in reality, the piezometers shall be placed at levels with a difference of only 4 meters, instead of 5 meters.

VIII.1.2. CONCLUSIONS REGARDING THE PARAMETRIC AND SENSITIVITY ANALYSIS

Based on the sensitivity analyses performed in sub-chapters V.4 (SENSITIVITY ANALYSIS ON THE HORIZONTAL PERMEABILITY IN THE DISTURBED ZONE) and V.5 (SENSITIVITY ANALYSIS OF THE CONSOLIDATION DEGREE WITH PREFABRICATED VERTICAL DRAINS), regarding the determining of the permeability in plane strain, considering the smear effect and the limitation of the discharge capacity of the band-shaped drains used in the *Lebrija* Pond, the principal conclusions are:

- The smear effect is expressed by a significant reduction in the horizontal permeability in plane strain analysis (K_{hPD}), having the reduction in permeability in the disturbed zone (K_{hsAx}) a greater impact than the diameter of this zone (d_s). This result proves that the influence due to the installation procedure of the band-shaped drain on the soil surrounding, substantially delays the consolidation rate as well as the time to attain the complete primary consolidation. Additionally, the distance between the parallel drainage screens which is considered in the geometry of the bidimensional problem (S*), is also highly significant in the result of the progress of the consolidation degree, and should not be very different from the real value. Besides, the bigger the distance between the drains in the bidimensional analysis in plane strain (S*), or the diameter of the disturbed zone (d_s), or the reduction of the horizontal permeability (k_{hsAx}), the smaller is the consolidation degree for the same time elapsed;

- The horizontal permeability in plane strain, determined considering the geometric delimitation of the smear zone in both systems (axisymmetric and plane strain), are slightly lower than those calculated while admitting the delimitation of the smear diameter only in the axisymmetric state. For the case study, in light of the smear hypotheses adopted, these differences vary between 0% and 6%, the latter corresponding to the extreme situation in which k_{hsAx}/k_{h0}=0.66 and d_s/d_w=4 are adopted. For the most common smear conditions, defined by several researchers has been given by k_{hsAx}/k_{h0}=0.33 and d_s/d_w=3, the difference in the results between both solutions is of only 2%. In light of these results, it can be concluded that the analytical formulation, without considering the delimitation of the smear zone in plane strain, was the best solution to be applied in the numerical modelling of the *Lebrija* Pond dikes. This decision is reflected on a substantial simplification of the geometric modelling in the zone with band-shaped drains, and on the finite element mesh quality, as well as a quicker calculation, without loss of accuracy in the final results;

- The consolidation degree curves obtained numerically with the PLAXIS programme coincide with those calculated by the analytical expressions, in axisymmetric strain, for the same conditions.

In addition to these conclusions, those withdrawn from the sensitivity and parametric analyses performed and presented in sub-chapter VII.3, based on the numerical simulations with the PLAXIS, are added, namely:

- When considering materials models, which do not consider the creep, for the foundation soft soil, the settlement curves are relatively flat in the post-construction phase, meaning that they are unable to translate the evolution of the settlements over time. Therefore, these models are not suitable for characterising the behaviour of this type of soil;
- The larger the reduction of the horizontal permeability coefficient in the disturbed zone, the smaller the corresponding settlement. This does not mean that the drains are not working properly, but instead that the drainage takes longer, hence the greater difference between the numerical results occurs precisely in the initial phase. The variation of the diameter of the disturbed zone (d_s), have less influence on the settlement results, in contrast to the disturbed horizontal permeability coefficient (K_{hs});
- The value of the secondary compressibility index (C_α) presents a huge importance in the progress of the settlements, being its effect felt already in the construction phase. High values for this parameter, implicates higher settlements obtained from the numerical analysis;
- The effect of the band-shaped drains improvement on the soil foundation is, without any doubt, the solution that conducts to the greatest difference in the consolidation rate and on the settlements results. When the drains technique is considered, the settlements are extraordinarily higher. In turn, the contribution of the geotextile reinforcement at the base of the dike, regarding its effect on the settlements, is almost insignificant. However, in the following conclusions it will be seen that regarding the slope stability, the geotextile is extremely important.

VIII.1.3. CONCLUSIONS REGARDING THE COMPARISON OF NUMERICAL AND MONITORING RESULTS

The conclusions presented in the following paragraphs complement the previous ones and allows the closure of the research study undertaken in this thesis. They summarise a significant quantity of information resulting from the interconnection of the monitoring data with the results from the numerical simulations, provided in sub-chapter VII.3 (RESULTS OF THE NUMERICAL SIMULATION AND COMPARISON WITH MONITORING). Therefore, the final conclusions are:

- The magnitude of the soil disturbance in the vicinity of the drains (*smear effect*) is very high for the soil foundation of the *Lebrija* Pond dikes, with 90% reduction in the horizontal permeability with respect to the initial value, in a distance 3 times superior to the drain diameter, i.e., $K_{hsAx}=0.10K_{h0}$ and $d_s=3d_w$. The horizontal permeability coefficients in plane strain, obtained with these conditions and for a drain spacing of 3 meters in the plane strain modelling, are very low, with the ratio K_{hsPD}/K_{v0} varying between 0.26 and 0.39. In turn, the ratio K_{hPD}/K_{v0} varies between 0.28 and 0.77 for the foundation soil of Dike No.1 and between 0.30 and 1.05 for Dike No.3. These values are, in general, considered low; but in light of the high plasticity and reduced stiffness of the soil crossed by the drains, i.e. B', B1 and B2, they are acceptable;
- The *Mohr-Coulomb* model is inappropriate for traducing the behaviour of the compressible soils of the foundation of the *Lebrija* Pond dikes, as the settlements progress does not continues with time, especially in the post-construction phase, staying far below of the values measured. The *Soft Soil* and *Soft Soil Creep* models presents relatively similar settlements in the construction phase; however, in the post-construction phase and during the filling of the dam, only the latter can keep up with the increment of the settlements over time. Therefore, the *Soft Soil Creep* model is considered to be the most suitable to characterise the behaviour of the foundation soils B', B1, B2 and B3;
- The secondary compressibility indexes (C_α) for soil B', B1, B2 and B3, obtained using the oedometer laboratory tests are very low, making it impossible to achieved the same monitored settlements. Estimating this parameter using the expression $C_\alpha/C_c=0.045$, proposed by Terzaghi *et al*. (1996), the numerically calculated settlements come closer to those registered in the plates, yet they are still a little lower than the desired. Only when the secondary compressibility index is estimated based on the relation $\lambda^*/\mu^*=15$, proposed by PLAXIS, a relatively good match is observed between the numerical and monitored results. Hence, it can be concluded that the secondary consolidation is much higher than the expected tanking in consideration the oedometer results. The values associated to C_α indexes, in order to achieved a reasonable agreement with the simulations results for the settlements, range from 0.032 to 0.050 for the soft soil of Dike No.1 and from 0.037 to 0.050 for Dike No.3;
- Considering the flow in the numerical analyses, the adjustment between the calculated and monitored settlements is higher, leading to the conclusion that their inclusion in the simulations of this type of geotechnical structures is essential. Considering the water seepage, the adjustment between the numerical and monitored settlement curves ranges between excellent to very reasonable, not only in the plates installed in the improved areas

with the bad-shaped drains, but also in the zones without drains. The major impact of the flow on the results occurs in the sections without drains, and is lower in the sections where the drains were installed, since the dissipation of the excess pore pressure in these last areas already occurred much faster in the analyses without the flow, due to the existence of drains. By allowing the flow at every step of the calculation, drainage occurs even in zones which do not have drains, being that the reason why it is noticed a large difference in the numerical results with and without flow, in these zones. In the plates located in the border or on the limit of the areas with drains, the calculated settlements exceed those measured, as there is a boundary effect that the analysis in plane strain is unable to avoid or eliminate. Drainage will be distinct on the left and on the right of this cross-section, occurring faster on one side and slower on the other, affecting consolidation as well as the settlements in the peripheral area. Therefore, the bidimensional analysis is not suitable enough in these sections, and a tridimensional analysis should be performed;

- The conclusions from the previous paragraph are also supported by the analysis of the pore pressure results when considering the flow, as the numerical values are quite close to those monitored. Based on these, it is concluded that, in the body of the dike embankment, drainage occurs relatively quickly, and there are almost no excess pore pressure associated with the construction stages, owing to its partly saturated condition. Besides, the pore pressure in the piezometers installed in the areas with drains, is relatively similar in both analyses, confirming the conclusion that the dissipation of the excess pore pressure does not undergo significant alterations in these zone due to the flow consideration;
- In Dike No.1, the combination of the application of a geotextile reinforcement at the base and the treatment of the foundation with the drains, upstream and downstream of the cut-off trench, represented a significant increase in the safety factor, namely from 1.5 to 2.5, in the final phase of construction. This result is obtained when considering the analyses without flow, for the *Soft Soil Creep* model, for $K_{hsAx}=0.10K_{h0}$ and $d_s=3d_w$. These are the conditions with a lower associated safety factor. For all the others conditions studied the safety coefficients gave higher values. In the case of Dike No.3, where no geotextile was installed, on the final phase of construction, and for the sections improved with drains the safety factor is approximately 1.9, while in the untreated section it is reduced to 1.6. Lastly, it is concluded that the band-shaped drains allowed the consolidation of the soil foundation to be accelerated, leading to an increase of their shear strength in the construction and pos-construction phase, thereby ensuring the stability of DikesNo.1 andNo.3 of the *Lebrija* Pond.

Given the results and conclusions withdrawn from this research, and as a closure of the thesis, the two questions raised in the introduction can be finally answered. So, the first question posed was:

"What is the interest in combining such diverse phenomena, as the smear, the creep and the flow, in the consolidation of soft soil in the presence of band-shaped drains?"

The answer will be:

Highly compressible soils, such as soft soil, are mainly located in flooded lowlands areas, as well as in coastal regions near the mouth of rivers, where the sediments transported by the river

deposit and generates large extensions of fine soils, sometimes with considerable thickness, with phreatic levels close to the surface. Generally, these soils are underconsolidated, normally consolidated or slightly overconsolidated, and thus present considerable settlements when charged. These settlements are associated not only to the phenomenon of primary or hydrodynamic consolidation but also secondary or creep consolidation, the latter being extraordinarily significant in this type of soil, as it was concluded in this thesis.

Since ancient times, man has favoured the above mentioned regions, with easy access to the water and relatively plan, to live and settle, therefore obliging them, inevitably, to deal with soils of this nature. With evolution, man has transformed these zones and adapted them to his needs. The evolution of science and technology has allowed large cities to develop in these zones, thereby creating new demands and requiring new levels of performance in terms of the bearing capacity and stiffness of the soils. So, the solutions pass through the study of these natural materials, in order to deepen the knowledge about them and understand their behaviour, and in the search for new foundation solutions. Using this last solution, man cleverly tried to avoid or circumvent the disadvantages associated with this type of soils.

Deep or indirect foundations are a good alternative in certain types of construction work; however, in other situations, the same are not viable, consequently alternative solutions were studied and tested. The improvement with vertical band-shaped drains is one of the solutions currently applied to these types of soils, since it is an efficient, economic and versatile method. The drains accelerates the consolidation phenomenon, as the time associated with the dissipation of the excess pore pressure is shortened, also leading to an increase in the shear strength of the soil. However, the disturbance caused by installation process of the drains into the ground, designated as smear effect, implicates a decrease in the horizontal permeability of the soil in the vicinity of the drains, especially in soft soil. This aspect must be taken into consideration in the design of geotechnical works with band-shaped drains, as it was shown throughout this study.

Despite the considerable amount of research already conducted on this theme, it is still not possible to precisely define the magnitude of this effect on the soil prior to their installation, since it depends on several aspects. In the design project, it is usual to admit values for the horizontal permeability and for the diameter of the disturbed area, searching for the spacing between drains and pattern which will be more appropriate to the problem in question. To confirm or optimize the solution attained in design, experimental embankment field test are preformed, considering several improvement scenarios for the foundation. Nevertheless this requires a high initial investment, plus time, which is not always possible. Consequently, validation of the smear effect based on the back-analysis of the settlements results, both numerical and measured "*in situ*", allows the increase of knowledge concerning this subject.

As the consolidation phenomenon is associated to the dissipation of the excess pore pressure of the saturated clay soil, and the vertical band-shaped drains constitute an adequate solution for achieving it faster, then the flow of water is another important aspect to be considered in

these studies. As a result, in the design project of structures founded on soft soils, where this type of treatment is used, it is essential to considered a material model which is able to traduce the soil behaviour adequately, taking into account not only the primary consolidation but also the secondary consolidation (creep), the effect of the disturbed zone around the drain (smear effect) and the establishment of the water seepage in the soil, i.e., the flow net.

Concerning the second question, namely:

"Why is it so important to incorporate a real case study on the research?"

The answer will be:

Case studies are always extremely important and useful in the development of research work as they allow the theoretical concepts applied to be proven, to verify the data obtained experimentally by confrontation of the results, and most of all to conclude about the soil behaviour. Notwithstanding, it is also necessary to ensure that the experimental data is reliable and of a high quality.

VIII.2. FUTURE DEVELOPMENTS

The themes covered in this thesis are extremely vast, and so, does not end here. There are developments which may launch other ideas for continuing the research, namely:

- Characterise the unsaturated properties of the soft soil by laboratory test results, so as to apply them to the PLAXIS programme, since it allows the users to define these properties;
- Review the parameters of the secondary compressibility index, obtained in the oedometer test, as they are much lower than the ones considered reasonable for the soils in question;
- Adapt the calculation programme, in order to consider the variation of the horizontal permeability coefficient in the disturbed zone, which is significantly lower in the zone adjacent to the drain and augmenting with the distance, until it equals the initial horizontal permeability value at the end of the smear zone;
- The installation of measuring devices in the reinforcement geotextile, in order to compare and check the measured results with the calculated;
- Lastly, performing a three-dimensional analysis, with the aim of studying the influence of transforming a radial flow into a horizontal and bidimensional flow, as well as the effect on the drainage and consolidation of the soils, in the sections located at the boundary of the improved areas.

BIBLIOGRAPHY

Aboshi, H. & Inoue, T. (1986). "Prediction of Consolidation Settlement of Clay Layers, Especially in the Case of Soil Stabilization by Vertical Drain". *Proceedings of the IEM-JSSMFE joint Symposium on Geotechnical Problems*, pp.31-40. Japan.

Abrantes, A.C.L.S. (2008). "Problemas de Consolidação na Construção de Aterros sobre Solos Moles". *Dissertação para obtenção do grau de Mestre*. Universidade de Aveiro, Portugal.

Adachi, T., Mimura, M. & Oka, F. (1985). "Descriptive Accuracy of Several Existing Constitutive Models for Normally Consolidated Clays". *Fifth International Conference on Numerical Methods in Geomechanics*, pp.259-266. Nagoya.

Akagi, T. (1979). "Consolidation Caused by Mandrel-Driven Sand Drains". *Proceedings of the 6thAsian Regional Conference Soil Mechanics and Foundation Engineering*, Vol.1, pp.125-128. Singapore.

Al Rechane, B. (1995). "Palliatifs Pour les Difficultés Expérimentales de L'appareil Triaxial – Comportement Type Pour les Sables et Argiles Remaniées". *Thèse de Docteur Ingénieur*. Ecole Centrale Paris-France.

Alonso, E.E., Gens A. & Josa A. (1990). "A Constitutive Model for Partially Saturated Soils". *Géotechnique*, Vol.40, Issue 3, pp.405–430.

Alves, R.M.M. (2011). "Estudo de Modelação da Consolidação Acelerada por Drenos Verticais Tomando em Consideração a Fluência Do Terreno". *Dissertação para obtenção do grau de Mestre*. Faculdade de Ciências e Tecnologia da Universidade Nova de Lisboa. Lisboa, Portugal.

ASTM D 4751. "Standard Testing Method for Determining Apparent Opening Size of a Geotextile". *ASTM, American Society for Testing and Materials,* Philadelphia, Pennsylvania, USA.

Atkinson, M.S. & Eldred, P. J. L. (1981). "Consolidation of Soils Using Vertical Drains". *Géotechnique* 31, No.1, pp.33-43.

Balasubramaniam, A.S., Bergado, D.T., Nopadol, P., Long, P.V. & Ahamad, M.(1997). "Performance of Test Embankments with Prefabricated Vertical Drains in Soft Bangkok Clay". *Proceedings of the 14th International Conference on Soil Mechanics and Foundation Engineering*, Vol.3 pp.1723-1726.

Baligh, M.M., Azzouz, A.S., Wissa, A.Z.E, Martin, R.T & Morrison, M.J. (1981). "The Piezocone Penetometer". *Cone Penetration Testing and Experience, American Society of Civil Engineering*. St. Louis. USA.

Bardet, J-P. (1997). "Experimental Soil Mechanics". *Prentice-Hall*. New Jersey-USA.

Barron, R. (1944). "The Influence of Drain Wells on the Consolidation of Fine Grained Soils". *Dissertation, U.S. Engineering Office*. Providence, USA.

Barron, R. (1948). "Consolidation of Fine Grained Soils by Drain Wells". *Transactions of ASCE.*, Vol.113, pp.718-724. Virginia, USA.

Basu, D. & Madhav, M.R (2000). "Effect of Prefabricated Vertical Drain Clogging on the Rate of Consolidation: A Numerical Study". *Geosynthetics International*, Vol.7 No.3 pp.189-215.

Basu, D. & Prezzi, M. (2007). "Effect of the Smear and Transition Zones around Prefabricated Vertical Drains Installed in a Triangular Pattern on the Rate of Soil Consolidation". *International Journal Geomechanics*, Vol.7, No.1, pp.34-43.

Bell, F. (2004). "Engineering Geology and Construction". Spon Press. London-United Kingdom.

Bergado, D.T. & Long, P.V. (1994b). "Numerical Analysis of Embankment on Subsiding Ground Improved by Vertical Drains and Granular Piles". *Proceedings of the 13th International Conference on Soil Mechanics and Foundation Engineering*, Vol.4 pp.1361-1366.

Bergado, D.T., Alfaro, M. C. & Balasubramaniam, A.S. (1993a). "Improvement of Soft Bangkok Clay Using Vertical Drains". *Geotextiles and Geomembranes*, Vol.12, No.7, pp.615-663.

Bergado, D.T., Alfaro, M. C. & Chan, E.H.C. (1992). "Filtration and Drainage Characteristics of Vertical Drains ". *Proceedings of the Symposium on International Lowland Technology.* Institute of Lowland Technology, pp.181-188. Saga, Japan.

Bergado, D.T., Anderson, L.R., Miura, N. & Balasubramaniam, A.S. (1996a). "Prefabricated Vertical Drains (PVD)". *Soft Ground Improvement in Lowland and Other Environments. ASCE*. Reston, Va., Chapter 4, pp.88-185.

Bergado, D.T., Asakami, H., Alfaro, M.C. & Balasubramaniam, A. S. (1991). "Smear Effects of Vertical Drains on Soft Bangkok Clay". *Journal of Geotechnical Engineering, ASCE*, Vol. 117, No.10, pp.1509-1530.

Bergado, D.T., Balasubramaniam, A.S., Jonathan Fannin, R. & Holtz, R.D. (2002). "Prefabricated Vertical Drains (PVDs) in Soft Bangkok Clay: A Case Study of the New Bangkok International Airport Project". *Canadian Geotechnical Journal*, Vol.39 No.2 pp.304-315.

Bergado, D.T., Chai, J.C., Alfaro, M.C. & Balasubramaniam, A.S. (1994a). "Improvement Techniques of Soft Ground in Subsiding and Lowland Environment". Balkema. Netherlands.

Bergado, D.T., Manivannan, R. & Balasubramaniam, A.S. (1996b). "Proposed Criteria for Discharge Capacity of Prefabricated Vertical Drains". *Geotextiles and Geomembranes*, Vol.14, pp.481-505.

Bergado, D.T., Manivannan, R. & Balasubramaniam, A.S. (1996c). "Filtration Criteria for Prefabricated Vertical Drain Geotextile Filter Jackets in Soft Bangkok Clay". *Geosynthetics International*, Vol.3, No.1, pp.63-83.

Bergado, D.T., Mukherjee, K., Alfaro, M.C. & Balasubramaniam, A.S. (1993b). "Prediction of Vertical-Band-Drain Performance by the Finite-Element Method". *Geotextiles and Geomembranes*, Vol.12, No.6, pp.567-586.

Biarez, J. & Hicher, P-Y. (1989). "Lois de Comportement des Sols Remaniés et des Matériaux Granulaires". Notes de Cours pour le DEA " Mécanique des Sols et Structures " Tome2 : Modélisation Mécanique. École Centrale Paris-France.

Biarez, J. & Hicher, P-Y. (1994). "Elementary Mechanics of Soil Behaviour, Saturated, Remoulded Soils". A.A. Balkema. Rotterdam / Brookfield.

Bjerrum, L. (1967). "Engineering Geology of Norwegian Normally Consolidated Marine Clays as Related to Settlements of Buildings". *7th Ranking Lecture, Geotechnique* 17, pp.81-118.

Bjerrum, L. (1972). "Embankments on Soft Soil". *Proceedings of the specialty Conference, American Society of Civil Engineering,* Vol 2, pp.1-54.

Bo, M.W. (2004). "Discharge Capacity of Prefabricated Vertical Drain and their Field Measurements". *Geotextiles and Geomembranes*, Vol.22 pp.37-48.

Bowles, J.E. (1996). "Foundations Analysis and Design" - 5th edition. International Edition of the McGraw-Hill Companies.

Brinkgreve, R.B.J. (1994). "Geomaterial Models and Numerical Analysis of Softnening". *Dissertation*. Delft University of Technology. Netherlands.

Britto, A.M. & Gunn, M.J. (1987). "Critical State Soil Mechanics Via Finite Elements". Published by Ellis Horwood Limited, United Kingdom.

Brooks, R.H. & Corey, A.T. (1964). "Hydraulic Properties of Porous Media". Hydrologic papers #3, *Colorado State University*. Fort Collins, Colorado.

Buisman, K. (1936). "Results of Long Duration Settlements Test". *Proceedings of the 1st International Conference on Soil Mechanics and Foundation Engineering*. Vol.1, pp.103-107. Cambridge.

Burdine, N.T. (1953). "Relative Permeability Calculations from Pore Size Distribution Data". *Transactions AIME*, Vol.198, pp.71-77.

Burland, J.B. (1967). "Deformation of Soft Clay". *Dissertation*. Cambridge University. Cambridge, USA.

Butterfield, R. (1979). "A Natural Compression Law for Soils (an Advanced on e-logp')". *Geotechnique* 29, pp. 469-480.

Calderon, P.A. & Romana, M. (1997). "Improvement by Precharge and Prefabricated Vertical Drains at Tank Group No.3 Site, at the "Total Oil Storage Plant" at Valencia Harbor*". Proceedings of the 14th International Conference on Soil Mechanics and Foundation Engineering*, Vol. 3, pp.1577-1580. Hamburg.

Calderon, P.A. (1992). "Estudio Experimental de la Hinca de Drenes Verticales Prefabricados*".* Tésis Doctoral, Universidad Politécnica de Valencia, España.

Calhoun, C.C. (1972). "Development of Design Criteria and Acceptance Specifications for Plastic Filter Cloth*". Technical Report S -72-7 of U.S. Army Corps of Engineers.* Waterways Experimental Station, 105pp. Vicksburg, Mississippi, USA.

Campanella, R.G., Gillespie, D. & Robertson, P.K. (1982). " Pore Pressures During Cone Penetration Testing". *Second European Symposium on Penetration Testing's*, Vol.2. Amsterdam.

Carrillo, N. (1942). "Simple Two and Three Dimensional Cases in the Theory of Consolidation Soils". *Journal of Mathematics and Physics Mechanics*, Vol.21, pp.1-5.

Carroll, R.G. Jr. (1983). "Geotextile filter criteria". *Transportation Research Record*, No.916, pp.46-53. Washington D.C., USA.

Carvalho, A.T., Dias, T.M. & Pimentel, V. (2002). "Projecto e Observação de um Aterro sobre Solos Moles". *Atas do 8º Congresso Nacional de Geotecnia*, Vol. 3, Tema 6, Abril de 2002, pp. 539-1549. Laboratório Nacional de Engenharia Civil – LNEC. Lisboa, Portugal.

Cea Azañedo, J.C., Saura, J., Marcos, J.M., Justo, J.L. & Rendón. (2005). "Proyecto, Construcción y Comportamiento de los Diques de Cierre de la Balsa de Lebrija*". I Simposio Nacional Sobre Proyecto, Construcción e Impermeabilización de Balsas* – Volumen II (comunicaciones libres). Sevilla-España.

Cedergreen, H.R. (1989). "Seepage, Drainage and Flow Nets"- 3th edition. *John Wiley & Sons.* California, USA.

Chai, J., Hong, Z., & Shen, S. (2010). "Vacuum-Drain Consolidation Induced Pressure Distribution and Ground Deformation*". Geotextiles and Geomembranes*, Vol.28, pp. 525-535.

Chai, J.C. & Miura, N. (1999). "Investigation of Factor Affecting Vertical Drain Behavior". *Journal Geotechnical Geoenvironmental Engineering, ASCE*, Vol.125, No.3, pp.216-226.

Chai, J.C., Miura, N. & Bergado, D.T. (2008). "Preloading Clayey Deposit by Vacuum Pressure With Cap-Drain: Analyses Versus Performance". *Geotextiles and Geomembranes*, Vol.26 No.3 pp. 220-230.

Chai, J.C., Miura, N. & Nomura, T. (2004). "Effect of Hydraulic Radius on Long-Term Drainage Capacity of Geosynthetics Drains". *Geotextiles and Geomembranes*, Vol.22, No.1-2 pp.3-16.

Chai, J.C., Miura, N. & Sakajo, S. (1997). "A Theoretical Study on Smear Effect around Vertical Drain". *Proceedings of the 14th International Conference on Soil Mechanics and Foundation Engineering*, Vol.3, pp.1581-1584. Hamburg.

Chen, R.H. & Chen, C.N. (1986). "Permeability Characteristics of Prefabricated Vertical Drains". *Proceedings of the 3rd International Conference on Geotextiles*, Vol.1, pp.785-790. Vienna, Austria.

Cheung, Y.K., Lee, P.K.K. & Xie, K.H. (1991). "Some Remarks on Two and Three Dimensional Analysis of Sand-Grained Ground". *Computers and Geotechnics*, 12, pp.73-87.

Cheung, Y.K., Tsui, Y. & Lu, P.Y. (1990). "Consolidation Analysis of Soils by Elasto-plastic Constitutive Models". *International Journal of Rock Mechanics and Mining Sciences & Geomechanics Abstracts*, Vol.27, No.5, pp.273.

Chew, S., Karunaratne, G., Kuma, V., Lim, L., Toh, M. & Hee, A. (2004). "A Field Trial for Soft Clay Consolidation Using Electric Vertical Drains. *Geotextiles and Geomembranes*, Vol.22, No.1-2 pp.17-35.

Childs, E.C. & Collis-George, G.N. (1950). "The Permeability of Porous Materials". *Proceedings of Royal Society*, London, Ser. A, Vol.201, pp.392-405.

Christopher, B.R. & Holtz, R.D. (1985). "Geotextile Engineering Manual". *Report No. FHWA-TS-86/203 of U.S. Department of Transportation, pp.*1044. Federal Highway Administration, Washington-Dc, USA.

Chu, J., Bo, M.W. & Choa, V. (2004). "Practical Considerations for Using Vertical Drains in Soil Improvement Projects". *Geotextiles and Geomembranes*, Vol. 22, No.1-2, pp. 101-117.

Coelho, S. (1996). "Tecnologia de Fundações"- 1ª edição. Edições E.P.G.E. Lisboa-Portugal.

Cristóvão, A.J.F. (1997). "Tratamento de Lodos por Vibrosubstituição (Colunas de Brita) e Drenos Verticais na Regularização da Zona Sul da Frente Tejo – EXPO'98". *Atas do 6º Congresso Nacional de Geotecnia*, Vol.2, pp.715-725. Instituto Superior Técnico- IST. Lisboa-Portugal.

Cui, Y.J. & Delage, P. (1996). "Yielding and Plastic Behaviour of an Unsaturated Compacted Silt". *Geotechnique*, Vol.46, pp.291-311.

Dahlberg, R (1974). "Penetration Testing in Sweden". *Proceedings of the 1st European Symposium on Penetration Testing*, Vol.1, PP.115-131. Stockholm, Sweden.

Da Silva, E.M.J. (1999). "Uma Contribuição para a Interpretação do Ensaio Pressiométrico Autoperfurador em Argila". *Tese de Mestrado*. Faculdade de Ciências e Tecnologia da Universidade Nova de Lisboa. Portugal.

Da Silva, E.M.J. (2009). "Consolidación de Suelos Blandos en Presencia de Drenes de Banda. El Dique Nº 3 de Lebrija". *Trabajo de Investigación Tutelado.* Escuela Técnica Superior de Arquitectura de la Universidad de Sevilla. Sevilla-España.

Da Silva, E.M.J., Alpañés J.L.J. & Durand P.N. (2012). "Resultados da Monitorização do Dique Nº1 da Represa de Lebrija". *Atas do XIII Congresso Nacional de Geotecnia e do V Congresso Luso-Brasileiro de Geotecnia*, IST/LNEC, CD, pp.391. Lisboa, Portugal.

Da Silva E.M.J., Justo J.L., Soriano C.C. & Durand P.N. (2010a). "Análise dos Assentamentos do Dique Nº3 da Represa de Lebrija". *Atas do XII Congresso Nacional de Geotecnia*, Universidade do Minho, CD1, pp.1202-1218. Guimarães, Portugal.

Da Silva E.M.J., Justo J.L., Soriano C.C. & Durand P.N. (2010b). "Monitorização do comportamento de diques fundados em solos moles tratados com drenos verticais". *Atas do XII Congresso Nacional de Geotecnia*, Universidade do Minho, CD1, pp.1219-1228. Guimarães, Portugal.

Da Silva, E.M.J., Justo, J.L., Soriano C.C. & Durand P.N. (2010c). "Comportamento dos Diques da Represa de Lebrija. Um Exemplo de Melhoria e Reforço dos Solos de Fundação". *Atas do XV Congresso Brasileiro de Mecânica dos Solos e Engenharia Geotécnica e V Congresso Luso-Brasileiro de Geotecnia*, ID462 / CDU-624.131(063). Cidade de Gramado, São Paulo – Brasil.

Danziger, F.A.B. (1990). "Desenvolvimento de Equipamento para Realização de Ensaios de Piezocone: Aplicação a Argilas Moles". *Tese de Mestrado*, Universidade Federal do Rio de Janeiro, Brasil.

Das, B.M. (1999). "Principles of Foundation Engineering"- 4th edition. PWS Publishing. California-USA.

Davies, J.A. & Humpheson, C. (1981). "A Comparison Between the Performance of Two Types of Vertical Drain Beneath a Trial Embankment in Belfast". *Géotechnique* 31, No.1, pp.19-31.

De Melo, P.G. (2007). "Desemprenho de Geodrenos na Consolidação de Materiais Aluvionares do Tejo". *Atas do 2º Seminário Português sobre Geossintéticos*. Laboratório Nacional de Engenharia Civil – LNEC. Lisboa-Portugal.

De Santayanna & Fernando, P. (1997). "Análise do Comportamento da Área Tratada com Drenos Verticais na Expansão Este do Aterro Sanitários de Beirolas". *Laboratório Nacional de Engenharia Civil*, pp.1109-118. LNEC. Lisboa-Portugal.

Drucker, D.C. (1954). "A Definition of Stable Inelastic Material". *Journal Applied Mechanics, Transactions ASCE*, No.26, pp.101-106.

Drucker, D.C. (1966). "Concepts of Path Independence and Material Stability for Soils". *Proceedings IUTAM Symphosium.* pp.23-43. Springer, Berlin.

Dubin, B. & Moulin, G. (1986). "Influence of a Critical Gradient on the Consolidation of Clay". *Consolidation of Soils: Testing and Evaluation, ASTM.* STP 892: 354-377.

Escario, V. (1974). "Penetration Testing in Spain". *Proceedings of the 1st European Symposium on Penetration Testing*, Vol.1, PP.105-113. Stockholm, Sweden.

Escario, V. & Saez, J. (1986). "The Shear Strength of Partly Saturated Soils". *Geotechnique*, Vol.36 Issue 3, pp.453-456.

Escario, V. & Juca (1989). "Shear Strength and Deformation of Partly Saturated Soils". *Proceedings of the 12th International Conference on Soil Mechanics & Foundation Engineering*, Vol.2, pp.43-46. Rio de Janeiro.

FCG Consortium, P. (2004). "Análise das Terraplenagens". *Relatório Final. Elaborado por Parsons, FCG Consortium para a NAER, Novo Aeroporto, SA*. Lisboa, Portugal.

Fellenius, B.H. & Castonguay (1985). "The Efficiency of Band Shaped Drains". *Report of National Research Council of Canada*, University of Ottawa, pp.1-54. Ottawa.

Folque, J. (1987). "O Uso de Drenos Verticais para Acelerar a consolidação". *Laboratório Nacional de Engenharia Civil*, LNEC. Lisboa-Portugal.

Fox, E.N. (1948). "The Mathematical Solution for the Early Stages of Consolidation". 2nd edition. *Proceedings of International Conference on Soil Mechanics and Foundation Engineering*, Vol.1, pp.41-52.

Fox, P.J., Edil, T. & Lan, L. (1992). "C_a/C_c Concept Applied to Compression of Peat". *Journal of Geotechnical Engineering Division, ASCE*, Vol.118, GT8, pp.1256-1263.

Fredlund, D.G., Morgenstern, N.R. & Widger, R.A. (1978). "Shear Strength of Unsaturated Soils". *Canadian Geotechnical Journal*, Vol.15, pp.313-321.

Fredlund, D.G. & Xing, A. (1994). "Equations for the Soil-Water Characteristic Curve". *Canadian Geotechnical Journal*, Vol.31, pp.521-532.

Fredlund, D.G., Xing, A. & Huang, S. (1994). "Predicting the Permeability Function for Unsaturated Soils Using the Soil -Water Characteristic Curve". *Canadian Geotechnical Journal*, Vol.31, pp.533–546.

Fredlund. D.G., Xing. A., Fredlund. M.D. & Barbour, S.L. (1996). "The Relationship of the Unsaturated Soil Shear Strength to the Soil-Water Characteristic Curve. *Canadian Geotechnical Journal*, Vol.33, pp.440-448.

Fredlund, D.G. (2005). "Unsaturated Soil Mechanics in Engineering – Terzaghi Lecture". *GeoFrontriers, Geo-Institute, American Society of Civil Engineering*. Austin, Texas. January 23 to 26.

Furtado, R.J.A. (1995). "Aterros Sobre Solos Argilosos Moles. A Doca Nº4 do Porto de Leixões – Um Caso Típico". *Atas do 5º Congresso Nacional de Geotecnia*, Vol.3, pp.203-219. FCTUC, Universidade de Coimbra-Portugal.

Gan, J.K.M. & Fredlund, D.G. (1988). "Multistage Direct Shear Resting of Unsaturated Soils". American Society for Testing Materials. *Geotechnical Testing Journal*, Vol.2, pp.132-138.

Garlanger, J.E. (1972). "The Consolidation of Soils Exhibiting Creep Under Constant Effective Stress". *Geotechnique* 22, pp.71-78.

Geotest (2001). "Campana de Ensayos Vane-Test & Ensayos Dilatométricos de Marchetti DMT – Tramo Final del Canal del Bajo Guadalquivir (1ª fase)". Caracterización Geotécnica y Geoambiental In Situ. España.

Geiser, F., Laloui, L. & Vulliet L. (2000). "Modelling the Behaviour of Unsaturated Silt". *Experimental Evidence and Theoretical Approaches in Unsaturated Soils*, pp.155-175. A. Tarantino & C. Mancuso (eds.), Rotterdam. Balkema.

Gnanendran, C.T. (1993). "Observed and Calculated Behaviour of a Geotextile Reinforced Embankment on a Soft Compressible Soil". *Ph.D. thesis*, University of Western Ontario, London.

Hansbo, S. (1957). " A New Approach to the Determination of the Shear Strength of Clay by the Fall-Cone Test". *Swedish Geotechnical Instrumentation Proceedings*. pp.14.

Hansbo, S. (1960). "Consolidation of clay, with special reference to influence of vertical sand drains: A study made in connection with full-scale investigations at Ska-Edeby". *Doctoral Thesis*. Swedish Geotechnical Institute.

Hansbo, S. (1977). "Geodrains in theory and practice". *Geotechnical report from Terrafigo*-Stockholm.

Hansbo, S. (1979). "Consolidation of Clay by Bandshape Prefabricated Drains". *Ground Engineering*, Vol.12, No.5, pp.16-25. Great-Britain.

Hansbo, S. (1981a). "Consolidation of Fine Grained Soils by Prefabricated Drains". *Proceedings of the 10th International Conference on Soil Mechanics and Foundation Engineering*, Vol.3, pp.677-682. Stockholm, Sweden.

Hansbo, S. (1981b). "How to Evaluate the Properties of Prefabricated Drains". *Proceedings of the 8th European Conference on Soil Mechanics and Foundation Engineering*, Vol.2, pp.621-626. Helsinki.

Hansbo, S. (1987). "Facts and Fiction in the Field of Vertical Drainage". *International Symposium on Prediction and Performance in Geotechnical Engineering*, pp.61-72. Alberta-Canada.

Hansbo, S. (1997a). "Aspects of Vertical Drain Design : Darcian or non-Darcian Flow". Géotechnique 47, No.5, pp.983-992.

Hansbo, S. (1997b). "Practical Aspects of Vertical Drain Design". *Proceedings of the 14th International Conference on Soil Mechanics and Foundation Engineering*, Vol.3, pp.1749-1752. Hamburg.

Hansbo, S., Jamiolkowski, M. & Kok, L. (1981). "Consolidation by Vertical Drains". *Géotechnique* 31, No.1, pp.45-66.

Hawlader, B., Imai, G. & Muhunthan, B. (2002). "Numerical Study of the Factors Affecting the Consolidation of Clay with Vertical Drains". *Geotextiles and Geomembranes*, Vol. 20, No. 4, pp.213-239.

Hermann, L.R., Shen, C.K., Jafroudi, S., DeNatale, J.S. & Dafalias, Y.F. (1981). "A Verification Study for the Bounding Surface Plasticity Model for Cohesive Soils". *Final report to the Civil Engineering Laboratory,* Naval Construction Battalion Center, Port Hueneme, California.

Hinchberger, S.D. & Rowe, R.K. (1998). "Modelling the Rate-sensitive Characteristics of the Gloucester Foundation Soils". *Canadian Geotechnical Journal*, No.35, pp.769-789.

Hird, C.C. & Moseley, V.J. (2000). "Model Study of Seepage in Smear Zones Around Vertical Drains in Layered Soil". *Géotechnique* 50, No.1, pp.89-97.

Hird, C.C., Pyrah, I.C. & Russell, D. (1992). "Finite Element Modeling of Vertical Drains Beneath Embankments on Soft Ground". *Géotechnique* 42, No.3, pp.499-511. London-United Kingdom.

Hird, C.C., Pyrah, I.C., Russell, D. & Cinicioglu, F. **(1995).** "Modelling the Effect of Vertical Drains in Two-Dimensional Finite-Element Analyses of Embankments on Soft Ground". *Canadian Geotechnical Journal*, Vol.32, No.5, pp.795-807.

Holtz, R.D. & Christopher, B.R. (1987). "Characteristics of Prefabricated Drains for Accelerating Consolidation". *Proceedings of the 9th European Conference on Soil Mechanics and Foundation Engineering*, Balkema, Vol.2, pp.903-906.

Holtz, R.D. & Holm, G. (1973). "Excavation and Sampling Around Some Sand Drains at Ska-Edeby, Sweden". *Proceedings of the Nordic Geotechnical Meeting*. Trondheim, NGI-Oslo.

Holtz, R.D. (1987). "Preloading with Prefabricated Vertical Strip Drains". *Geotextiles and Geomembranes,* Vol.6, pp.109-131.

Holtz, R.D. (1991). "Prefabricated Vertical Drains: Design and Performance". *Butterworth-Heinemann PUBLISHER* - Oxford and Boston.

Holtz, R.D., Jamiolkowski, M., Lancellotta, R. & Pedroni, S. (1987). "Performance of Prefabricated Band-Shaped Drains". *Construction Industry Research and Information Association*. London, United Kingdom.

Holtz, R.D., Shang, J.Q. & Bergado, D.T. (2001). "Soil Improvement". *Geotechnical and Geoenvironment Engineering Handbook* (chapter-15). Academic Publisher, Norwel. USA.

Hughes, F.H. & Chalmers, A. (1972). "Small Diameter Sand Drains". *Civil Engineering Public Works Revue*. March 3-6.

Illán Ortega, S. (2002). "Auscultación, Dique Nº1 y Nº3, Balsa de Abastecimiento al Canal del Bajo Gualdalquivir – Informe de seguimiento de Piezómetros de Cuerda Vibrante y Tuberías Inclinométricas (Campaña Septiembre de 2002)". Informe técnico elaborado por Ingeniería de Instrumentación y Control, S.A -Grupo EP. Madrid – España.

Illán Ortega, S. (2003). "Auscultación, Dique Nº1 y Nº3, Balsa de Abastecimiento al Canal del Bajo Gualdalquivir – Informe de seguimiento de Piezómetros de Cuerda Vibrante y Tuberías Inclinométricas (Campaña 8 de Enero de 2003)". Informe técnico elaborado por Ingeniería de Instrumentación y Control, S.A -Grupo EP. Madrid – España.

Illán Ortega, S. (2004 a). "Auscultación, Dique Nº1 y Nº3, Balsa de Abastecimiento al Canal del Bajo Gualdalquivir – Informe de seguimiento de Piezómetros de Cuerda Vibrante y Tuberías Inclinométricas (Campaña 15 de Enero de 2004)". Informe técnico elaborado por Ingeniería de Instrumentación y Control, S.A -Grupo EP. Madrid – España.

Illán Ortega, S. (2004 b). "Auscultación, Dique Nº1 y Nº3, Balsa de Abastecimiento al Canal del Bajo Gualdalquivir – Informe de seguimiento de Piezómetros de Cuerda Vibrante y Tuberías Inclinométricas (Campaña 15 de Julio de 2004)". Informe técnico elaborado por Ingeniería de Instrumentación y Control, S.A -Grupo EP. Madrid – España.

Indraratna, B. & Redana, I.W. (1997). "Plane-Strain Modeling of Smear Effects Associated with Vertical Drains". *Journal of Geotechnical and Geoenvironmental Engineering*, Vol.123, No.5, pp.474-478.

Indraratna, B. & Redana, I.W. (1998). "Laboratory Determination of Smear Zone due to Vertical Drain Installation". *Journal of Geotechnical and Geoenvironmental Engineering*, Vol.124, No.2, pp.180-184.

Indraratna, B., Bamunawita, C. & Khabbaz, H. (2004). "Numerical Modeling of Vacuum Preloading and Field Applications". *Canadian Geotechnical Journal*, No.41, pp.1098-1110.

Indraratna, B., Bamunawita, C., Redana I.W. & McIntosh, G. (2003). "Modelling of Prefabricated Vertical Drains in Soft Clay And Evaluation of their Effectiveness in Practice". Ground Improvement, No.3, pp.127-137.

Indraratna, B., Rujikiatkamjorn, C. & Sathananthan, I. (2005). "Analytical and Numerical Solutions for a Single Vertical Drain Including the Effects of vacuum Preloading". *Canadian Geotechnical Journal*, No.42, pp.994-1014.

Jamiolkowski, M. & Lancellotta, R. (1981). "Consolidation by Vertical Drains: Uncertainties Involved in Prediction of Settlement Rates". *Proceedings of the 10th International Conference on Soil Mechanics and Foundation Engineering*, Vol.4, pp.593-595. Balkema. Rotterdam, Netherlands.

Jamiolkowski, M., Lancellotta, R. & Wolki, W. (1983). "Precompression and Speeding Up Consolidation*". Proceedings of the 8th International Conference on Soil Mechanics and Foundation Engineering*, Vol.3, pp.1201-1226. Helsinki**,** Finland.

Janbu, N. (1969). "The resistence concept applied to soils". *Proceedings of the 7th ICSMFE*, Vol.1, pp.191-196. Cidade do México. [Referido em Neher *et al*. (2000) e Manivannan (2005)].

Jiménez Salas, J.A., Justo, J.L. & Serrano, A. (1981). " Geotecnia y Cimientos II – 2ªEdition". Editorial Rueda. Madrid-España.

Justo, J.L. (1966). "A Review of Vertical Sand Drains". *Report for the degree of Master of Science in Engineering*. Department of Civil Engineering, Imperial College of Science and Technology. London, S.W.7.

Justo, J.L. (2000a). "Dictamen Sobre la Estabilidad del Dique de Lebrija". Cliente: Confederación Hidrográfica del Guadalquivir. *Informe técnico no publicado*. Escuela Técnica Superior de Arquitectura de la Universidad de Sevilla-España.

Justo, J.L. (2000b). "Informe sobre los Asientos, drenes, Filtros y Tuberías del Tramo Final del Canal del Bajo Guadalquivir". Cliente: Confederación Hidrográfica del Guadalquivir. *Informe técnico no publicado*. Escuela Técnica Superior de Arquitectura de la Universidad de Sevilla-España.

Justo, J.L. (2001). "Dictamen sobre la Modificación del Dique de Lebrija – Memoria y Anejos nº1 al 3". Cliente: Confederación Hidrográfica del Guadalquivir. *Informe técnico no publicado*. Escuela Técnica Superior de Arquitectura de la Universidad de Sevilla-España.

Justo, J.L. (2002). "Dictamen sobre el Llenado de la Balsa de Lebrija hasta Cota +6 – Memoria y Apéndices 1 a 3 y 7 a 14". Cliente: Confederación Hidrográfica del Guadalquivir. *Informe técnico no publicado*. Escuela Técnica Superior de Arquitectura de la Universidad de Sevilla-España.

Justo, J.L., Durand, P.N., Soriano, C., & Da Silva, E. (2009). "Monitoring of Performance in Four Dikes on Soft Soil*". Proceedings of the 17th International Conference on Soil Mechanics and Geotechnical Engineering,* Vol.3, pp.2008-2011. Alexandria, Egipt.

Justo, J.L., Durand, P.N., Soriano, C., Saura, J. & Marco, J.M. (2006). "Comportamiento de Cuatro Diques de Tierra sobre Suelo Blando: Mejora y Refuerzo del Terreno". *Revista de Ingeniería Civil* No.143, pp.79-83. España.

Justo, J.L., Soriano, C., Durand, P.N., Justo, E.M. & Romero, M.M. (2003). "Parámetros para Análisis sin Drenaje en Suelos Blandos". *Revista de Obras Públicas* No.3.431, pp.37-48. España.

Kabbaj, M., Oka, F., Leroueil, S. & Tavenas, F. (1986). "Consolidation of Natural Clays and Laboratory Testing". *Consolidation of Soils: Testing and Evaluation, ASTM.* STP 892: 378-404.

Kamon, M., Pradhan, B.S. & Suwa, S. (1984). "Laboratory Evaluation of the Prefabricated Band-Shaped Drains, Soil Improvement". *Current Japanese Materials Research*, Vol.9. Cambridge University Press. Cambridge, United Kingdom.

Karube, D. (1997). "Stress Analysis of Unsaturated Soil Based on the 'Driest' Curve". *Proceedings of the 14th International Conference on Soil Mechanics Foundation Engineering*, Hamburg, Germany, Vol.1, pp.333-336. Rotterdam. Balkema.

Kavazanjian, E. Jr. (1978). "A Generalized Approach to the Prediction of the Stress-strain-time Behaviour of Coft clay". *Ph.D. thesis*, University of California, Berkeley.

Kellner, L., Bally, R.T. & Matter, S. (1983). "Some Aspects Concerning Retaining Capacity of Geotextiles". *Proceedings of the Second International Conference on Geotextiles, IFAI*, Vol.1, pp.85-90.

Kjellman, W. (1948). *"*Accelerating consolidation of fine-grained soils by means of cardboard wicks*". Proceedings of the 2sd International Conference on Soil Mechanics and Geotechnical Engineering*. Vol.2, pp.302-305.

Kohgo, Y., Nakano, M. & Miyazaki, T. (1993). "Theoretical Aspects of Constitutive Modeling for Unsaturated Soils". *Soils and Foundations*, Vol.33, Issue 4, pp.49-63.

Kremer, R. (1983). Discussion to Specialty Session 6. *Proceedings of the 8th European Conference on Soil Mechanics and Foundation Engineering*, Helsinki, Vol.3, pp.1235-1237.

Kukamoto, N., Sumioka, N., Moriwaki, T. & Yoshikuni, H. (1988). "Settlement Behavior of Improved Ground With a Vertical Drain System". *Soils and Foundations - JSSMFE*, Vol.28, No.1, pp.77-88.

Kutter, B.L. & Sathialingam, N. (1992). "Elasto-Viscoplastic Modelling of the Rate-Dependent Behaviour of Clays". *Géotechnique* 42, No.3, pp.427-441.

Lawrence, C.A. & Koerner, R.M. (1988). "Flow Behaviour of Kinked Strip Drains Geosynthetics for Soil Improvement*". ASCE Geotechnical Special Publications,* No.18, pp.22-35.

Leo, C.J. (2004). "Quelques Considérations sur le Comportement des Argiles Sensibles". *Ph.D. Thesis*, Laval University, Québec, Canada.

Leroueil, S. (1977). "Quelques Considérations sur le Comportement des Argiles Sensibles". *Ph.D. Thesis*, Laval University, Québec, Canada.

Lo, D.O.K. (1991). "Equal Strain Consolidation by Vertical Drains". *Journal of Geotechnical and Geoenvironmental Engineering, ASCE.* pp.316-327.

Lorenzo, G.A., Bergado, D.T., Bunthai, W., Hormdee, D. & Phothiraksanon, P. (2004). "Innovations and Performances of PVD and Dual Function Geosynthetic Applications". *Geotextiles and Geomembranes*, Vol.22, pp.75-99.

Maâtouk, A., Leroueil, S. & La Rochelle, P. (1995). "Yielding and Critical State of a Collapsible Unsaturated Silty Soil". *Geotechnique,* Vol.45, Issue 3, pp.465-477.

Madhav, M.R., Park, Y-M. & Miura, N. (1993). "Modelling and Study of Smear Zones Around Vertical Drains". *Soils and Foundations,* Vol.33, No.4, pp.135-147.

Magnan, J.P. (1983a). "Théorie et Pratique des Drains Verticaux". *Technique et Documentation*, Lavoisier, Paris, France.

Magnan, J.P. (1983b). "Back-analysis of Soil Consolidation Around Vertical Drains". *Improvement of Ground,* No.2, pp.45-52.

Mayne, P.W. & Kemper, J.B. (1988). "Profiling OCR in Stiff Clays by CPT and SPT". *Geotechnical Testing Journal, American Society of Testing Materials*, Vol.11, No.2, pp. 139-147.

Manivannan, G. (2005). "Viscoplastic Modelling of Embankments on Soft Soils". *Ph.D. Thesis*, University of New South Wales Australian Defence Force Academy. School of Aerospace, Civil and Mechanical Engineering. Australia.

Maranha das Neves & Guedes de Melo (1975). "Mecânica dos Solos – Equilíbrios Limite e Estados Críticos". *Curso 110-2 do Laboratório Nacional de Engenharia Civil*, LNEC. Lisboa, Portugal.

Mateus da Silva, J.M.M. (1996). "Modelação do Colapso e da Fluência em Aterros". *Tese de Doutoramento.* Faculdade de Engenharia da Universidade do Porto. Porto, Portugal.

McDonald, P. (1985). "Settlement of Fills on Soft Clay with Vertical Drains". *Proceedings of the 11th International Conference on Soil Mechanics and Geotechnical Engineering*, Vol. 8/c/15, pp.2213-2216. San Francisco.

McGown, A. & Hughes, F.H. (1981). "Practical Aspects of the Design and Installation of Deep Vertical Drains". *Géotechnique 31,* No.1, pp.3-17.

Mendes, M.M.S.C.S. (2011). "Estudo de Modelação da Consolidação Acelerada por Drenos Verticais Tomando em Consideração a Fluência do Terreno". *Dissertação para obtenção do grau de Mestre.* Instituto Superior Técnico, Universidade Técnica de Lisboa. Lisboa, Portugal.

Mesri, G. & Godlewshi, P.M. (1977). "Time and Stress Compressibility Interrelationship". *Journal of Geotechnical Engineering Division - ASCE*, Vol.103, GT5, pp.417-430.

Mesri, G. (1973). "Coefficient of Secondary Consolidation". *Journal of the Soil Mechanics and Foundation Engineering Division - ASCE,* Vol.99, pp.122-137.

Mesri, G., Feng, T.W, All S. & Hayat T.M. (1994). "Permeability Characteristics of Soft Clays". *Proceedings of the 13th International Conference on Soil Mechanics and Geotechnical Engineering,* Vol.2, pp.187-192. New Delhi-India.

Mesri, G., Stark, T.D., Ajlouni, M.A. & Chen, C.S. (1997). "Secondary Compression of Peat with or without Surcharging". *Journal of Geotechnical and Geoenvironmental Engineering*, Vol. 123, No.5, pp. 411-421.

Miller, R.J. & Low, P.F. (1963). "Threshold Gradient for Water Flow in Clay Systems". *Soil Science Society of America Journal,* Vol.27 No.6, pp.605-609.

Miura, N., Chai, J.C. & Toyota, K. (1998). "Investigation on Some Factors Affecting Discharge Capacity of Prefabricated Vertical Drain". *Proceedings of the 6th International Conference on Geosynthetics*, pp. 845-850. International Geosynthetics Society. Atlanta.

Mohkam, M. (1983). "Contribution à l'Étude Expérimentales et Théorique du Comportement des Sables sous Chargements Cycliques". *Thèse de Docteur.* Université Scientifique et Médicale et Institut Polytechnique de Grenoble. France.

Moran, Proctor, Mueser & Rutledge (1958). "Study of Deep Soil Stabilization by Vertical Sand Drains". *Bureau of Yards and Docks*, Department of the Navy, Washington D.C., USA.

Morris, P.M. & Williams, D.T. (1994). "Effective Stress Vane Shera Strength Correction Factor Correlations". *Canadian Geotechnical Journal*, Vol.31, No.3, pp.335-342.

Mualem, Y. (1976). "A New Model for Predicting Hydraulic Conductivity of Unsaturated Porous Media". *Water Resources Research*, Vol.12, pp.513-522.

Murakami, Y. (1988). "Secondary Compression in the Stage of Primary Consolidation. Technical Note". *Soils and Foundations*, Vol.28, No.3, pp.169-174.

Nagaraj, T.S. & Miura, N. (2001). "Soft Clay Behavior – Analysis and Assessment". *A. A. Balkema Publishers.* Rotterdam/USA.

Naskos (1985). "Quelques Aspects du Comportement Mécanique de L'argile Saturée Consolidée Sous Fortes Pressions". *Thèse de Docteur Ingénieur*. Ecole Centrale Paris, France.

Naylor, D.J., Pande, G.N.; Simpson, B. & Tabb, R. (1981). "Finite Elements in Geotechnical Engineering". *Pineridge Press*, Swansea, United Kingdom.

Neher, H., Wehnert, M. & Bonnier, P. (2000). "An Evaluation of Soft Soil Models Based on Trial Embankments". *Computer Methods and Advances in Geomechanics.* A.A. Balkema. pp.373-379. Rotherdam.

Nicolson, D.P. & Jardine, R.J. (1981). "Performance of Vertical Drains at Queenborough Bypass". *Géotechnique* 31, No.1, pp.67-90.

Ogink, H.J.M. (1975). "Investigations on the Hydraulic Characteristics of Synthetic Fabrics". *Publication No. 146 of Delft Hydraulics Laboratory*. Delft, Netherlands.

Onoue, A. (1988). "Consolidation by Vertical Drains Taking Well Resistance and Smear into Consideration". *Soils and Foundations,* Vol.28, No.4, pp.165-174.

Onoue, A., Ting, N., Germaine, J.T. & Whitman, R.V. (1991). "Permeability of Disturbed Zone Around Vertical Drains". *Geotechnical Special Publication, ASCE,* No.27, pp.879-890.

Ortigão, J.A.R. (1993). "Introduçao à Mecânica dos Solos dos Estados Criticos". *Livros Técnicos e Cientificos Editora Lda.* Rio de Janeiro, Brasil.

Pilot, G. (1981). "Methods of Improving the Engineering Properties of Soft Clay". *In Soft Clay Engineering, Elsevier Publication Company.* pp. 637-691. New York, USA.

Pinto, S.L.D. & Da Silva, J.M.M.M. (2000). "Aterros Sobre Solos Lodosos. Caracterização Geotécnica. Caso Prático da Retenção Marginal na Zona da EXPO'URBE". *Atas do 7º Congresso Nacional de Geotecnia, Faculdade de Engenharia da Universidade do Porto*. Vol.1, pp.551-560. Porto, Portugal.

PLAXIS 2D-V11.02, Manual (2012). "Finite Element Code for Soil and Rock Analyses". *Edited by Brinkgreeve, R. B. J., Swolfs, W. M. & Engin, E. Delft University of Technology & PLAXIS bv*. Delft, Netherlands.

Port Experts Group-APEC 20th TPT-WG (2002). "Soft Seabed Ground Improvement Technology". *Report TPTWG20/PEG*. Republic of Korea.

Pothiraksanon, C., Bergado, D.T. & Abuel-Naga, H.M. (2010). "Full-scale embankment consolidation test using prefabricated vertical thermal drains". *Soils and Foundations*, Vol.50 pp.599-608.

Purushothama Raj, P. (1999). "Ground Improvement Techniques". *Laxmi Publications (P), Ltd.* New-Delhi, India.

Rankilor, P.R. (1981). "Membranes in Ground Engineering". *John Wiley & Sons*. Chichester, United Kingdom.

Rathmayer, H. & Saari, K. (1983). "Improvement of Ground". *Proceedings of the 8th European Conference on Soil Mechanics and Foundation Engineering Organized by the Finnish Geotechnical Society*. Vol.3, pp. 973-1399. A.A.Balkema. Helsínquia.

Rendulic, L. (1935). "Der Hydrodynamische Spannungsangleich in Zentral Entwasserten Tonzylindren". *Wasserwirt. Tech*. Vol.2. pp.250-253 and pp.269-273.

Rixner, J.J., Kraemer, S.R. & Smith, A.D. (1986). "Prefabricated Vertical Drains". Federal Highway Administration. *Report FHWA-RD-86/168*, Vol.1. Washington D.C., USA.

Roscoe, K.H. & Burland, J.B. (1968). "On the Generalized Stress-Strain Behaviour of Wet-Clays". *Engineering Plasticity, Cambridge University Press*. Cambridge, USA.

Roscoe, K.H., Schofield, A.N. & Wroth, C.P. (1958). "On the Yielding of Soils". *Géotechnique 8*, pp.22-53.

Rowe, R.K. & Hinchberger, S.D. (1998). "The Significance of Rate Effects in Modelling the Sackville Test Embankment". *Canadian Geotechnical Journal*, No.35, pp.500-516.

Rujikiatkamjorn, C. & Indraratna, B. (2007). "Analytical Solutions and Design Curves for Vacuum-Assisted Consolidation with Both Vertical and Horizontal Drainage". *Canadian Geotechnical Journal*, Vol.44, pp.188-200.

Runesson, K. (1978). "On Non-linear Consolidation of Soft Clay". *Doctoral Thesis* submitted at Chalmers University of Technology- Gothenburg, Publication 78:1.

Runesson, K., Hansbo, S. & Wiberg, N.E. (1985). "The Efficiency of Partially Penetrating Vertical Drains". *Géotechnique 35*, No.4, pp.511-516.

Saïm, R. (1996). "Difficultés Expérimentales et Palliatifs pour Utiliser au Mieux les Résultats Expérimentaux". *Document de travail pour la table ronde de 31 Mai* – École Centrale Paris, France.

Saïm, R. (1997). "Des Comportements Repères des Grains Sans Colle à Un Exemple de Sol Réel". *Thèse de Docteur Ingénieur*. Ecole Centrale Paris, France.

Sanchez, J.M., & Sagaseta, C. (1990). "Analysis of Stage Construction of Embankments on Soft Soil". *Proceedings of the 2th European Speciality Conference on Numerical Methods in Geotechnical Engineering*, pp.457-471. Santander, Spain.

Saowapakpiboon, J., Bergado, D.T., Youwai, S., Chai, J.C., Wanthong, P. & Voottipruex, P. (2010). "Measured and Predicted Performance of Prefabricated Vertical Drains (PVDs) with and Without Vacuum Preloading". *Geotextiles and Geomembranes*, Vol.28, No.1, pp.1-11.

Saura Martínez, J.F., Rodríguez, V.G., Cea Azañedo, J.C.; Justo, J.L. & Marcos, J.M. (2004). "Los Diques de Cierre de la Balsa de Lebrija. Un Ejemplo de Construcción sobre Suelos Blandos". *XXI Congreso Internacional de Grandes Presas. Revista de Obras Públicas* No.3.441, pp.119-130. España.

Saye, S. R. (2001). "Assessment of Soil Disturbance by the Installation of Displacement Sand Drains and Prefabricated Vertical Drains". *Soil Behaviour and Soft Ground Construction, ASCE Geotechnical Special Publication* No.119, pp.325-362. Reston, VA.

Schober, W. & Teindl, H. (1979). "Filter Criteria for Geotextiles". *Design of parameters in Geotechnical Engineering*, Vol.2, pp.121-129. BGS, London.

Schofield, A.N. & Wroth, C.P. (1968). "Critical State Soil Mechanics". *McGraw-Hill*. London, United Kingdom.

Sherard, J.L., Woodward, R.J., Gizienski, S.F. & Clevenger, W.A. (1963). "Earth and Earth-Rock Dams". *John Wiley & Sons*. New York, USA.

Shinsha, H., Hara, H., Abe, Y. & Tanaka, A. (1982). "Consolidation Settlement And Lateral Displacement of Soft Ground Improved by Sand Drains." *Tsuchi-to-Kiso, Japanese Society of Soil Mechanics Foundation Engineering*, Vol. 30, No.5, pp.7-12.

Silfverberg, L. (1947). "Report on the activities at the Swedish Geotechnical Institute during 1944-1948." *Swedish Geotechnical Institute* , Meddelande, No.2. Sweden.

Sivaram, B. & Swamee, P. (1977). "A Computational Method for Consolidation Coefficient". *Soils and Foundations*. Tokyo, Japan.

Soriano, C. (2005). "Validación de un Modelo Soft-Soil-Creep Mediante Ensayos de Laboratorio en Arcilla Blanda". *Trabajo de investigación*. Escuela Técnica Superior de Arquitectura de la Universidad de Sevilla. Sevilla-España.

Sridharan, A. & Prakash, K. (1985). "Improved Rectangular Hyperbola Method for the Determination of Coefficient of Consolidation". *Geotechnical Testing Journal, ASCE*, Vol.8, No.1, Mar, pp.37-40.

Sridharan, A. & Rao, S. (1981). "Rectangular Hyperbola Fitting Method for One Dimensional Consolidation". *Geotechnical Testing Journal, ASCE*, Vol.4, No.4, Dec, pp.161-168.

Stanton, T.E. (1948). "Vertical Sand Drains as a Means of Foundation Consolidation and Accelerating Settlement of Embankments over Marsh Land". *Proceedings of the 2nd International Conference on Soil Mechanics and Foundation Engineering,* Vol.V, pp.273-279. Rotterdam, Nederland.

Sun, D.A., Matsuoka, H., Yao, Y.-P. & Ichihara, W. (2000). "An Elasto-Plastic Model for Unsaturated Soil in Three-Dimensional Stresses". *Soils and Foundations*, Vol.40, Issue 3, pp.17-28.

Sweetland, D.B. (1977). "The Performance of Non-woven Fabrics as Drainage Screens in Subdrains". *M.Sc. Thesis*, University of Strathclyde, 207pp. Glasgow, United Kingdom.

Tavenas, F., Jean, P. & Leroueil, S. (1983). "The Permeability of Natural Soft Clays, Part 2: Permeability Characteristics". *Canadian Geotechnical Journal*, Vol. 20, November, pp. 645-660.

Tang, G.X. & Graham, J. (2002). "A Possible Elastic-Plastic Framework for Unsaturated Soils with High Plasticity. *Canadian Geotechnical Journal*, Vol.39, pp.894-907.

Taylor, D.W. (1948). "Fundamentals of Soil Mechanics". *John Wiley & Sons*. New York, USA.

Terzaghi, K. (1925). "Erdbaumechanick auf Bodenphsikalischer Grundlage". *Deuticke*. Vienna, Austria.

Terzaghi, K. (1943). "Theoretical soil mechanics". *John Wiley & Sons*. New York, USA.

Terzaghi, K., Peck, R. & Mesri, G. (1996). "Soil Mechanics in Engineering Practice" – *3rd Edition. Wiley Interscience.*

Tovar de Lemos, A.F. (1990). "Mecânica dos Meios Contínuos". *Instituto Superior Técnic*o. Lisboa, Portugal.

Vairinhos, A.M.C. (2013). "A Influência do Efeito Smearing na Consolidação de Solos Moles Tratados com Drenos Verticais Pré-Fabricados*". Tese de Mestrado*. Universidade de Évora.Évora, Portugal.

van Genuchten, M.Th. (1980). "A Closed-form Equation for Predicting the Hydraulic Conductivity of Unsaturated Soils". *Soil Science Society of America Journal*, Vol.44, pp.892–898.

Vanapalli, S.K., Fredlund. D.G. & Pufahl, D.E. (1996a). "The Relationship Between the Soil-Water Characteristic Curve and the Shear Strength of a Compacted Glacial Till". *Geotechnical Testing Journal*, GTJODJ. Vol.19, pp.259-268.

Vanapalli. S.K., Fredlund D.G., Pufahl, D.E. & Clifton, A.W. (1996b). "Model for the Prediction of Shear Strength With Respect to Soil Suction". *Canadian Geotechnical Journal*, Vol.33 pp.379-392.

Vanapalli, S. K. & Fredlund, D. G. (1999). "Empirical Procedures to Predict the Shear Strength of Unsaturated Soils." *Proceedings of the 11th Asian Regional Conference*, Seoul, Korea. pp.93-96.

Vanapalli, S. K., Pufahl, D. E. & Fredlund, D. G. (1999). "Interpretation of the Shear Strength of Unsaturated Soils in Undrained Loading Conditions." *Proceedings of the 52th Canadian Geotechnical Conference*, Regina, Saskatchewan. pp.643-650.

Van den Elzen, L.W.A. & Atkinson, M.S. (1980). "Accelerated Consolidation of Compressible, Low Permeability Subsoils by means of Colbond Drains". *Arnhem: Colbon b.v.*

Van Impe, W. (1989). "Soil Improvement Techniques and their Evolution". Rotterdam, Netherlands.

Vertematti, J.C., Oliveira, H.M. & Almeida, M.S.S. (2004). "Manual Brasileiro de Geossintéticos". *Editor Edgar Blucher*. Brasil.

Walker, R. & Indraratna, B. (2006). "Vertical Drain Consolidation with Parabolic Distribution of Permeability in Smear Zone". *Journal of Geotechnical and Geoenvironmental Engineering*, Vol.132, No.7, pp.937-941.

Walker, R. & Indraratna, B. (2007). "Vertical Drain Consolidation with Overlapping Smear Zones". *Géotechnique* 57, No.5, pp.463-467.

Wheeler, S.J. & Sivakumar, V. (1995). "An Elasto-Plastic Critical State Framework for Unsaturated Soil". *Geotechnique*, Vol.45, Issue 1, pp. 35-53.

Wood, D.M. (1990). "Soil Behaviour and Critical State Soil Mechanics". *Cambridge University Press.* Cambrigde, USA.

Xiao, D. (2001). "Consolidation of Soft Clay using Vertical Drains". *Ph.D. Thesis*, Nanyang Technological University, Singapore.

Yin, J.H. & Graham, J. (1989). "Viscous-elastic-plastic Modelling of One-dimensional Time Dependent Behavior of Clays". *Canadian Geotechnical Journal*, Vol.26, No.2, pp.199-209.

Yin, J.H. & Zhu, J.G. (1999a). "Elastic Viscoplastic Consolidation Modelling and Interpretation of Pore-water Pressure Responses in Clay Underneath Tarsiut Island". *Canadian Geotechnical Journal*, No.36, pp.708-717.

Yin, J.H. & Zhu, J.G. (1999b). "Measured and Predicted Time-dependent Stress-strain Behavior of Hong Kong marine deposits". *Canadian Geotechnical Journal*, No.36, pp.760-766.

Yoshikuni, H. & Nakanodo, H. (1974). "Consolidation of Soils by Vertical Drain Wells with Finite Permeability". *Soils and Foundations*, Vol.14, No.2, pp.35-46.

Yoshikuni, H. (1979). "Design and Construction Control of Vertical Drain Methods". Ghioto, Tokyo, Japan.

Zeng, G.X. & Xie, K.H. (1989). "New Development of the Vertical Drain Theories". *Proceedings of the International Conference on Soil Mechanics and Foundation Engineering*, Vol.2, pp.1435-1438.

Zeng, G.X., Xie, K.H. & Shi, Z.Y. (1987). "Consolidation Analysis of Sand-Grained Ground by FEM". *Proceedings of the ARCSMFE*, Vol.1, pp.139-142.

Zervoyannis, C. (1982). "Etude Synthétique des Propriétés Mécaniques des Argiles et des Sables sur Chemins Oedométrique et Triaxial de Révolution". *Thèse de Docteur Ingénieur*. Ecole Centrale Paris-France.

Zhu, G. & Yin, J-H. (2004). "Consolidation Analysis of Soil with Vertical and Horizontal Drainage Under Ramp Loading Considering Smear Effects". *Geotextiles and Geomembranes*, Vol.22 pp.63-74.

Zhu, G., Yin, J.H. & Graham, J. (2001). "Consolidation Modelling of Soils Under the Test Embankment at Chek Lap Kok International Airport in Hong Kong Using a Simplified Finite Element Method". *Canadian Geotechnical Journal*, No.36, pp.349-363.

APPENDIX I:

DATA REFERENT TO DIKE NO.1 AND DIKE NO.3 OF *LEBRIJA* POND

Band-shaped Drains

VT Vane-Test
DMT Marchetti Dilatometer
PZC Piezocone
DP Dynamic Probe
CD Pit Exploration
SD/SI Boreholes (SPT where made in some)

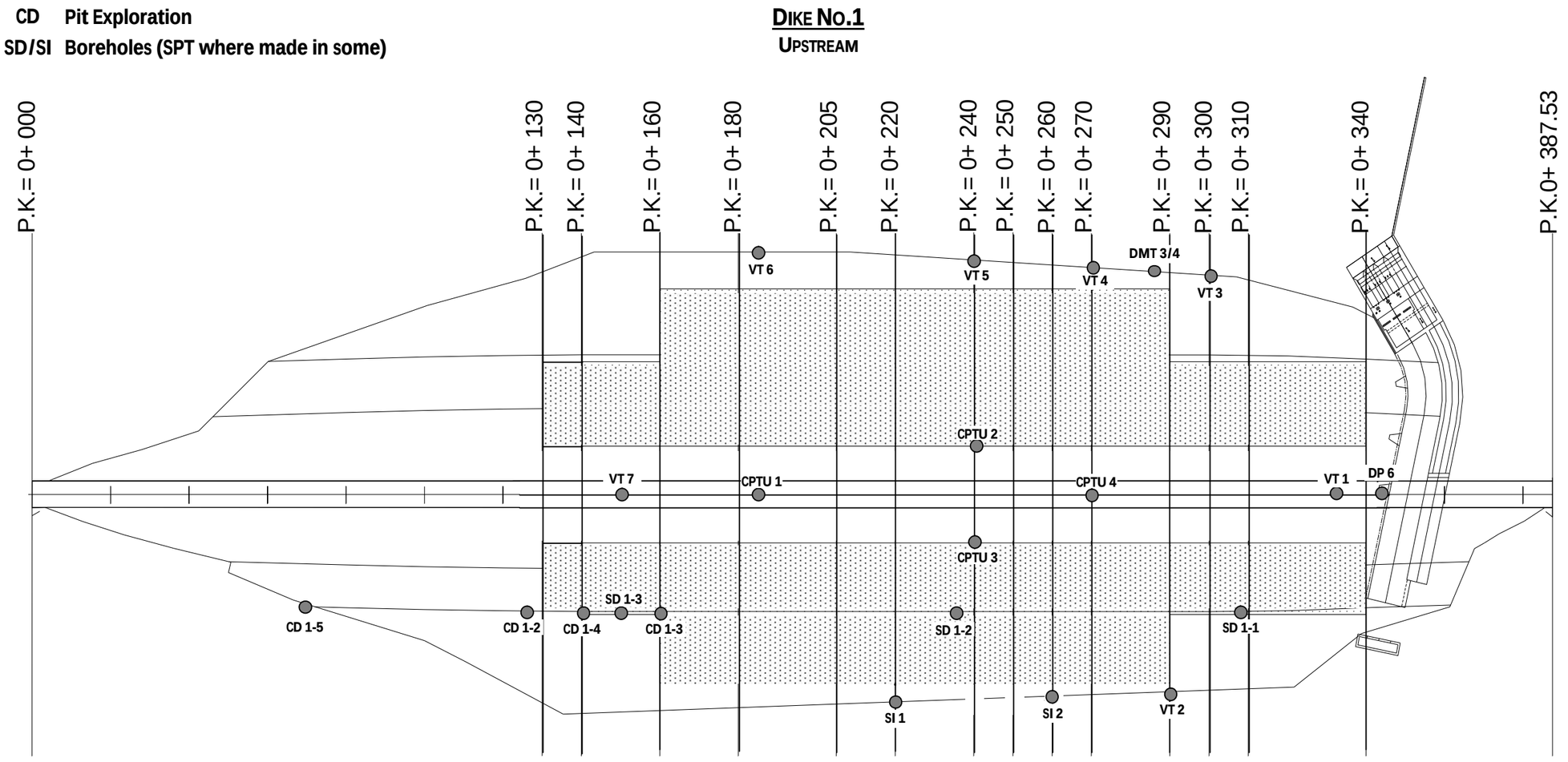

Figure AP I.1 – Plan showing the geotechnical prospecting made in Dike No.1.

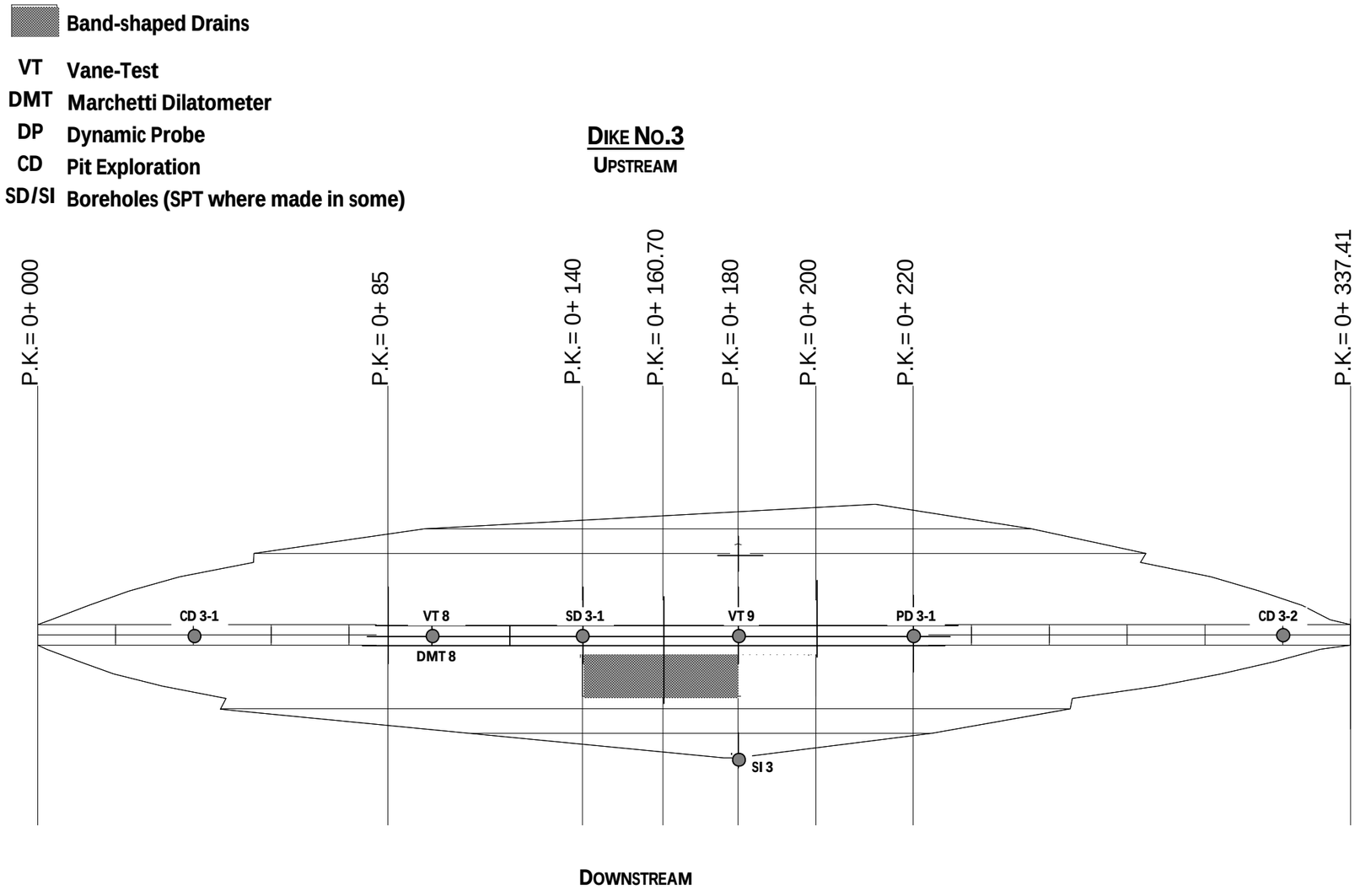

Figure AP I.2 – Plan showing the geotechnical prospecting made in Dike No.3.

Table AP I.1a) – Laboratory and field test results – Prospecting made on Dike No.1 subsoil of *Lebrija* Pond

Soils	Tests and boreholes	Dike No.1 Section	< #200 [%]	Atterberg Limits			γ_d	γ_t	Oedometer								Piezocone		Marchetti Dil.		Gs
				w_L [%]	w_P [%]	IP [%]	[kN/m^3]	[kN/m^3]	e_0	Cc	Cs	Ca	Ca_{mod}	s'_p [kN/m^2]	OCR	Cv 10^{-8}m^2/s	Ch 10^{-8}m^2/s	OCR	OCR	K0	
Soil A	VT 1	335																			
	VT 7	150																			
	SD 1-3	140	97,0	66,5	32,5	34,0	13,8	17,6	0,862	0,315	0,067	0,001861	0,003103	79,4	3,0	55,00					2,63
	DMT 7	150																			
	DMT 7	150																	>10	3,4 a 4	
	DMT 7	150																			
	DMT 3/4	290																			
Average			**97,0**	**66,5**	**32,5**	**34,0**	**13,8**	**17,6**	**0,86**	**0,32**	**0,07**	**0,001861**	**0,003103**		**3,0**	**55,00**			**> 10**	**3,4 a 4**	**2,63**
Soil B'	SD 1-2	235	99,3	88,5	31,0	57,5	11,7	16,2	1,364	0,518	0,158	0,004633	0,007821	77,0	4,6	2,70					2,82
	SD 1-1	307	98,8	73,5	30,3	43,2	10,5	15,7	1,48	0,57	0,137	0,004879	0,016073	68,0	3,4	3,00					2,65
	SI 1	220	99,6	82,5	28,7	53,8															
	SI 1	220		65,0	25,2	39,8															
	PZC 2	238																> 1			
	PZC 3	238						12,8 a 19,6										> 2			
	PZC 1	185					12,8											> 1			
	PZC 4	270					11,8											2			
	VT 5	240																	3,5 a 6	1,1 a 1,4	
	DMT 3/4	290																	3,5 a 6	1,1 a 1,4	
	DP 6	344,5																			
Average			**99,2**	**77,4**	**28,8**	**48,6**	**11,7**	**15,9**	**1,422**	**0,544**	**0,148**	**0,004756**	**0,011947**		**4,0**	**2,85**		**> 2**	**3,5 a 6**	**1,1 a 1,4**	**2,74**
Soil B1	SD 1-2	235	97,7	74,5	36,0	38,5	10,3	16,0	1,508	0,748	0,132	0,006944	0,009385	70,0	2,0	1,90					2,63
	SD 1-2	235	98,3	58,9	29,8	29,1	11,3	17,6													
	SI 1	220	99,1	53,0	21,0	32,0	10,9	17,0		0,523	0,130										
	SI 1	220	79,6	52,0	19,0	33,0	11,2	17,6		0,500	0,124										
	SI 1	220		64,3	27,4	36,9															
	SI 1	220		55,3	22,6	32,7															
	SI 1	220		57,9	24,2	33,7															
	SI 1	220		58,8	27,1	31,7															
	SI 1	220		49,7	24,0	25,7															
	SI 1	260		76,3	35,4	40,9															
	SI 1	260	99,2	67,1	28,0	39,1															
	SI 1	260		62,4	31,2	31,2															
	SI 1	260	99,7	66,7	25,4	41,3															
	SI 1	260	99,0	58,0	24,0	34,0	10,5	16,4													
	PZC 2	238						13,7 a 18,9									3,50	1			
	PZC 3	238						18,6									10,40 a 12,30	1			
	PZC 1	185						13,7 a 19,6									8,30	1,1 a 1,7			
	VT 5	240																			
	PZC 4	270						18,6									5,70 a 7,50	1			
	DMT 3/4	290																	1,2 a 1,8	0,65	
	DMT 3/4	290																	1	0,5 a 0,6	
Average			**96,1**	**61,1**	**26,8**	**34,3**	**10,8**	**17,4**	**1,508**	**0,748**	**0,132**	**0,006944**	**0,009385**		**2,0**	**1,90**	**7,44**	**1 a 1,7**	**1 a 1,8**	**0,5 a 0,65**	**2,63**

Table AP I.1b) – Laboratory and field test results – Prospecting made on Dike No.1 subsoil of *Lebrija* Pond

Soils	Tests and boreholes	Dike No.1 Section	N_{DP}	N_{SPT}	Unconfined Comp. Test		Piezocone	Marchetti Dilatometer			Direct Shear Test		Triaxial		Vane-Test			Soil classification	
					qu	c_u	c_u	c_u	E_{DMT}	j	c; c_{CU}	j';j_{cu}	c; c_{CU}	j';j_{cu}	$s_{u\,max.}$	$s_{u\,res.}$	St		
					[kN/m²]	[kN/m²]	[kN/m²]	[kN/m²]	[kN/m²]	(°)	[kN/m²]	(°)	[kN/m²]	(°)	[kN/m²]	[kN/m²]		USCS	AASTHO
Soil A	VT 1	335													182,8	51,1	3,58		
	VT 7	150													155,8	47,7	3,26		
	SD 1-3	140			274,7	137,4												MH	
	DMT 7	150							>7250	43a 46									
	DMT 7	150						160 a 180	17250 a 30850										
	DMT 7	150							18150 a 40000										
	DMT 3/4	290							>6800	42 a 44									
Average					**274,7**	**137,4**		**160 a 180**	**> 6800**	**42 a 46**					**169,3**	**49,4**	**3,42**	**MH**	
	SD 1-2	235			14,7	7,4												CH	
	SD 1-1	307									c´=10,79	j'=12,4						CH	
	SI 1	220													30,9	25,8	1,20	CH	A-7-6 (20)
	SI 1	220													29,4	21,7	1,35		
	PZC 2	238					35,3												
Soil B'	PZC 3	238					39,2												
	PZC 1	185					33,4												
	PZC 4	270					29,4												
	VT 5	240													31,7	19,9	1,60		
	DMT 3/4	290						10 a 24	3150 a 6350										
	DP 6	344,5	11																
Average			**11**		**14,7**	**7,4**	**34,3**	**10 a 24**	**3150 a 6350**		**c´=10,8**	**j'=12,4**			**30,7**	**22,5**	**1,37**	**CH**	
	SD 1-2	235		1									c_{cu}=8,8	j_{cu}=18,8				CH	
	SD 1-2	235		5	16,7	8,4												MH	
	SI 1	220											c´=12,9	j'=23,9				CH	A-7-6 (19)
	SI 1	220											c´=13,9	j'=24,1				CH	A-7-6 (18)
	SI 1	220													19,6	9,3	2,11		
	SI 1	220													19,6	19,0	1,03		
	SI 1	220													14,1	13,9	1,01		
	SI 1	220													16,6	-----	-----		
	SI 1	220													20,6	18,4	1,12		
	SI 1	260													21,1	15,5	1,36		
Soil B1	SI 1	260																CH	A-7-6 (20)
	SI 1	260													17,1	16,0	1,07		
	SI 1	260													14,8	-----	-----	CH	A-7-6 (20)
	SI 1	260											c´=14,6	j'=21,9				CH	A-7-6 (20)
	PZC 2	238					19,6												
	PZC 3	238					19,6												
	PZC 1	185					14,7												
	VT 5	240													19,1	9,2	2,07		
	PZC 4	270					16,7												
	DMT 3/4	290						16 a 20	1800 a 4550										
	DMT 3/4	290						18 a 24	1350 a 2700										
Average				**1 a 5**	**8,4**	**8,4**	**17,6**	**16 a 24**	**1350 a 4550**				**c´=13,8**	**j'=23,3**	**18,1**	**14,5**	**1,40**	**MH; CH**	

Table AP I.1c) – Laboratory and field test results – Prospecting made on Dike No.1 subsoil of *Lebrija* Pond

Soils	Tests and boreholes	Dike No.1 Section	< #200 [%]	Atterberg Limits			γ_d	γ_t	Oedometer								Piezocone		Marchetti Dil.		Gs
				w_L [%]	w_P [%]	IP [%]	[kN/m^3]	[kN/m^3]	e_0	Cc	Cs	Ca	Ca_{mod}	s'_p [kN/m^2]	OCR	Cv 10^{-8}m^2/s	Ch 10^{-8}m^2/s	OCR	OCR	K0	
Soil B2	SD 1-1	307	92,1	50,5	16,1	34,4	9,4	15,7	1,652	0,811	0,153	0,002165	0,001240	38,8	1,3	5,30					2,55
	SD 1-2	235	98,0	57,0	30,9	26,1	11,1	17,2	1,439	0,471	0,097	0,005828	0,006567	47,0	0,9	3,90					2,76
	SI 2	260		60,0	26,0	34,0															
	SI 2	260		57,9	25,2	32,7															
	SI 2	260		59,5	23,5	36,0															
	SI 2	260	99,1	52,0	22,0	30,0															
	PZC 2	238						15,7									13,60	1			
	PZC 3	238						13,7 a 18,6										1			
	VT 5	240																			
	VT 5	240																			
	DMT 3/4	290																	0,7 a 0,9	0,5	
	DMT 3/4	290																	0,75	0,45	
	DMT 3/4	290																	0,8	0,48	
	DMT 3/4	290																	1	0,5	
Average			**96,4**	**56,2**	**24,0**	**32,2**	**10,3**	**16,2**	**1,546**	**0,641**	**0,125**	**0,003996**	**0,003903**		**1,1**	**4,60**	**13,60**	**1,0**	**0,7 a 1**	**0,45 a 0,5**	**2,66**
Soil B3	SD 1-3	140	97,7	64,8	44,3	20,5	10,9	17,1	1,558	0,473	0,121	0,007658	0,012822	58,3	1,3	3,50					2,85
	SI 2	260		62,6	24,8	37,8															
	SI 2	260																			
	PZC 2	238						19,6									13,60	1			
	PZC 3	238						18,6										1,5			
	VT 1	335																			
	VT 5	240																			
	DMT 7	150																	<1,0	0,9	
	DMT 3/4	290																	0,6 a 0,8	0,38 a 0,45	
	DMT 3/4	290																	0,75 a 1	0,45 a 0,5	
	DP 6	344,5																			
Average			**97,7**	**63,7**	**34,6**	**29,2**	**10,9**	**18,4**	**1,558**	**0,473**	**0,121**	**0,007658**	**0,012822**		**1,3**	**3,50**	**13,60**	**1 a 1,5**	**0,6 a 1**	**0,38 a 0,5**	**2,85**
Soil C1	SD 1-1	307	91,6	58,1	11,3	46,8	10,2	15,9													
	SD 1-1	307	90,2	64,1	22,0	42,1	11,3	16,2													
	SD 1-1	307	90,7	68,3	21,5	46,8	11,9	16,8													
	VT 1	335																			
	PZC 2	238						15,7										1			
	PZC 3	238																2			
	PZC 4	270																2			
	DMT 3/4	290																	0,75 a 1	0,45 a 0,5	
	DP 6	344,5																			
Average			**90,8**	**63,5**	**18,3**	**45,2**	**11,1**	**16,1**										**1 a 2**	**0,75 a 1**	**0,45 a 0,5**	

Table AP I.1d) – Laboratory and field test results – Prospecting made on Dike No.1 subsoil of *Lebrija* Pond

Soils	Tests and boreholes	Dike No.1 Section	N_{DP}	N_{SPT}	Unconfined Comp. Test		Piezocone	Marchetti Dilatometer			Direct Shear Test		Triaxial		Vane-Test			Soil classification	
					qu [kN/m²]	c_u [kN/m²]	c_u [kN/m²]	c_u [kN/m²]	E_{DMT} [kN/m²]	j (º)	c; c_{CU} [kN/m²]	j';j_{cu} (º)	c; c_{CU} [kN/m²]	j';j_{cu} (º)	$s_{u\,max.}$ [kN/m²]	$s_{u\,res.}$ [kN/m²]	St	USCS	AASTHO
Soil B2	SD 1-1	307									c_{cu}=11,8	j_{cu}=23,7						CH	
	SD 1-2	235		0							c_{cu}=12,8	j_{cu}=12,1						MH-OH	
	SI 2	260													23,6	20,0	1,18		
	SI 2	260													31,5	29,4	1,07		
	SI 2	260													20,9	19,1	1,09		
	SI 2	260											c´=18,3	j'=18,7				CH	A-7-6 (18)
	PZC 2	238					29,4												
	PZC 3	238					24,5												
	VT 5	240													25,4	11,1	2,28		
	VT 5	240													30,5	9,4	3,24		
	DMT 3/4	290						21 a 23	1350										
	DMT 3/4	290						24	1150										
	DMT 3/4	290						24 a 30	1800										
	DMT 3/4	290						30 a 38	1800 a 2700										
Average							**27,0**	**21 a 38**	**1150 a 2700**		**c_{cu}=12,3**	**j_{cu}=17,9**	**c´=18,3**	**j'=18,7**	**26,4**	**17,8**	**1,48**	**MH-OH; CH**	
Soil B3	SD 1-3	140		3 a 6							c´=11,77	j'=16,7						MH	
	SI 2	260													48,1	45,6	1,05		
	SI 2	260													34,5	21,7	1,59		
	PZC 2	238					39,2												
	PZC 3	238					35,3												
	VT 1	335													34,6	26,9	1,29		
	VT 5	240													40,1	23,8	1,69		
	DMT 7	150						32	1800										
	DMT 3/4	290						28 a 38	----										
	DMT 3/4	290						40	4550 a 6800										
	DP 6	344,5	9																
Average			**9**	**3 a 6**			**37,3**	**28 a 40**	**1800 a 6800**		**c´=11,8**	**j'=16,7**			**39,3**	**29,5**	**1,33**	**MH**	
Soil C1	SD 1-1	307		13 a 17	90,3	45,2							c_{cu}=1,96	j_{cu}=28,8					
	SD 1-1	307		13 a 17	84,4	42,2													
	SD 1-1	307									c_{cu}=8,8	j_{cu}=26,7						CH	
	VT 1	335													52,9	7,7	6,83		
	PZC 2	238					54,9												
	PZC 3	238					49,1												
	PZC 4	270					49,1												
	DMT 3/4	290						40 a 46	7700 a 11800										
	DP 6	344,5	19																
Average			**19**	**13 a 17**	**87,4**	**43,7**	**51,0**	**40 a 46**	**7700 a 11800**		**c_{cu}=8,8**	**j_{cu}=26,7**	**c_{cu}=1,96**	**j_{cu}=28,8**	**52,9**	**7,7**	**6,83**	**CH**	

Table AP I.1e) – Laboratory and field test results – Prospecting made on Dike No.1 subsoil of *Lebrija* Pond

Soils	Tests and boreholes	Dike No.1 Section	< #200 [%]	Atterberg Limits			γ_d	γ_t	Oedometer								Piezocone		Marchetti Dil.		Gs
				w_L [%]	w_P [%]	IP [%]	[kN/m³]	[kN/m³]	e_0	Cc	Cs	Ca	Ca_{mod}	s'_p [kN/m²]	OCR	Cv $10^{-8}m^2/s$	Ch $10^{-8}m^2/s$	OCR	OCR	K0	
Soil C2	SD 1-3	140	98,9	65,1	38,1	27,0	12,3	17,2													
	SD 1-2	235	98,0	62,8	35,8	27,0	13,4	18,9													
	SD 1-2	235	90,3	53,4	30,6	22,8	12,8	18,1													
	VT 1	335																			
	DP 6	344,5																			
Average			**95,7**	**60,4**	**34,8**	**25,6**	**12,8**	**18,1**													
Soil D	SD 1-3	140	99,6	66,5	42,0	24,5	12,5	18,2													
	SD 1-3	140	98,0	51,9	32,6	19,3	15,9	19,5													
	SD 1-3	140	97,3	54,9	31,0	23,9	14,7	19,1													
	SD 1-3	307	96,7	59,0	34,9	24,1	13,8	17,8													
	SD 1-3	307	88,8	58,2	31,9	26,3	13,2	17,4													
	PZC 1	185						13,7 a 18,6									10,20	10			
	VT 1	335																			
	VT 7	150																			
	DMT 7	150																	15	2	
	DP 6	344,5																			
Average			**96,1**	**58,1**	**34,5**	**23,6**	**14,0**	**18,4**									**10,20**	**10**	**15**	**2**	

Table AP I.1f) – Laboratory and field test results – Prospecting made on Dike No.1 subsoil of *Lebrija* Pond

Soils	Tests and boreholes	Dike No.1 Section	N_{DP}	N_{SPT}	Unconfined Comp. Test		Piezocone	Marchetti Dilatometer			Direct Shear Test		Triaxial		Vane-Test			Soil classification	
					qu [kN/m²]	c_u [kN/m²]	c_u [kN/m²]	c_u [kN/m²]	E_{DMT} [kN/m²]	j (º)	c; c_{CU} [kN/m²]	j'; j_{cu} (º)	c; c_{CU} [kN/m²]	j'; j_{cu} (º)	$s_{u\,max.}$ [kN/m²]	$s_{u\,res.}$ [kN/m²]	St	USCS	AASTHO
Soil C2	SD 1-3	140			137,3	68,7												MH	
	SD 1-2	235		27							c´=41,2	j'=18,1						MH	
	SD 1-2	235		27	149,0	74,5												MH	
	VT 1	335													83,5	37,5	2,22		
	DP 6	344,5	57																
Average			**57**	**27**	**143,2**	**71,6**					**c´=41,2**	**j'=18,1**			**83,5**	**37,5**	**2,22**	**MH**	
Soil D	SD 1-3	140		36 a 40							c_{cu}=147,2	j_{cu}=24,6						MH	
	SD 1-3	140		36 a 40	306,1	153,1												MH	
	SD 1-3	140		Nega	353,2	176,6												MH	
	SD 1-3	307			479,7	239,9												MH	
	SD 1-3	307			438,5	219,3												MH	
	PZC 1	185					176,6												
	VT 1	335													170,7	87,1	1,96		
	VT 7	150													245,0				
	DMT 7	150						215 a 260	26300 a 30850										
	DP 6	344,5	82 a 136																
Average			**82 a 136**	**36 a 60**	**394,4**	**197,2**	**176,6**	**215 a 260**	**26300 a 30850**		**c_{cu}=147,2**	**j_{cu}=24,6**			**207,9**	**87,1**	**1,96**	**MH**	

Table AP I.2a) – Laboratory and field test results – Prospecting made on Dike No.3 subsoil of *Lebrija* Pond

Soils	Tests and boreholes	Dike No.3 Section	< #200 [%]	Atterberg Limits			γ_t	Oedometer							Marchetti Dilatometer		Gs
				w_L [%]	w_P [%]	IP [%]	[kN/m³]	e_0	Cc	Cs	Ca	Ca_{mod}	s'_p [kN/m²]	OCR	OCR	K0	
Soil A	SD 3-1	140	62,0	88,0	37,1	50,9	17,0	1,184	0,360	0,116	0,000770	0,001530	152,9	6,0			2,55
	DMT 8	100														4,5	
	DMT 8	100														1,6	
Average			**62,0**	**88,0**	**37,1**	**50,9**	**17,0**	**1,184**	**0,360**	**0,116**	**0,000770**	**0,001530**	**152,9**	**6,0**		**1,6 a 4,5**	**2,55**
Soil B'	SD 3-1	140															
	SD 3-1	140	98,8	96,0	47,1	48,9	16,2	1,621	0,558	0,181	0,004320	0,006200	147,1	3,7			2,56
	DMT 8	100													2,0 a 3,5	0,8 a 1,1	
	VT 8	100															
	VT 8	100															
	VT 9	180															
	VT 9	180															
	DP 3-1	220															
Average			**98,8**	**96,0**	**47,1**	**48,9**	**16,2**	**1,621**	**0,558**	**0,181**	**0,004320**	**0,006200**	**147,1**	**3,7**	**2,0 a 3,5**	**0,8 a 1,1**	**2,56**
Soil B1	SD 3-1	140															
	SD 3-1	140	98,8	62,0	32,8	29,2	17,0										
	SD 3-1	140															
	VT 9	180															
	DP 3-1	220															
Average			**98,8**	**62,0**	**32,8**	**29,2**	**17,0**										
Soil B2	SD 3-1	140	83,4	72,2	30,9	41,3	16,2	1,521	0,550	0,118	0,012590	0,018680	33,8	0,6			2,47
	DMT 8	100													1,0	0,6	
	VT 8	100															
	VT 9	180															
	DP 3-1	220															
Average			**83,4**	**72,2**	**30,9**	**41,3**	**16,2**	**1,521**	**0,550**	**0,118**	**0,012590**	**0,018680**	**33,8**	**0,6**	**1,0**	**0,6**	**2,47**
Soil B3	SD 3-1	140	99,6	107,5	45,7	61,8	16,5	1,475	0,573	0,166	0,001750	0,003230	171,6	2,0			2,60
	DMT 8	100													1,8	0,7	
	VT 9	180															
	DP 3-1	220															
Average			**99,6**	**107,5**	**45,7**	**61,8**	**16,5**	**1,475**	**0,573**	**0,166**	**0,001750**	**0,003230**	**171,6**	**2,0**	**1,8**	**0,7**	**2,60**
Soil C2	SD 3-1	140															
	SD 3-1	140	96,7	62,2	43,7	18,5	17,9										
	SD 3-1	140															
	DMT 8	100													2,1	0,8	
	DP 3-1	220															
Average			**96,7**	**62,2**	**43,7**	**18,5**	**17,9**								**2,1**	**0,8**	
Soil D	SD 3-1	140	98,6	65,5	46,0	19,5	17,5										
	SD 3-1	140	85,1	97,1	50,7	46,4	18,4										
	SD 3-1	140	82,1	89,0	46,5	42,5											
	DMT 8	100													4,5	1,2	
	DP 3-1	220															
Average			**88,6**	**83,9**	**47,7**	**36,1**	**18,0**								**4,5**	**1,2**	

Table AP I.2b) – Laboratory and field test results – Prospecting made on Dike No.3 subsoil of *Lebrija* Pond

Soils	Tests and boreholes	Dike No.3 Section	N_{DP}	N_{SPT}	Unconfined Comp. Test		Marchetti Dilatometer			Direct Shear Test		Vane-Test			Oedometer	Soil classification
					qu	c_u	c_u	E_{DMT}	j	c; c_{CU}	j';j_{cu}	$S_{u\,max.}$	$S_{u\,res.}$	St	Cv	
					[kN/m²]	[kN/m²]	[kN/m²]	[kN/m²]	(°)	[kN/m²]	(°)	[kN/m²]	[kN/m²]		$10^{-8}m^2/s$	USCS
Soil A	SD 3-1	140			202,0	101,0									1,80	CH
	DMT 8	100						16350	42 a 45							
	DMT 8	100						12700	36 a 38							
Average					**202,0**	**101,0**		**12700 a 16350**	**36 a 45**						**1,80**	**CH**
Soil B'	SD 3-1	140		5												
	SD 3-1	140			101,0	50,5				c´=11,8	j´=19,3				2,70	MH
	DMT 8	100					25 a 30	2250 a 4550								
	VT 8	100										36,3	14,7	2,47		
	VT 8	100										43,4	14,6	2,96		
	VT 9	180										54,0	20,4	2,65		
	VT 9	180										41,7	14,3	2,92		
	DP 3-1	220	4													
Average			**4**	**5**	**101,0**	**50,5**	**25 a 30**	**2250 a 4550**		**c´=11,8**	**j´=19,3**	**43,8**	**16,0**	**2,75**	**2,70**	**MH**
Soil B1	SD 3-1	140		2												
	SD 3-1	140								c_{cu}=14,7	j_{cu}=10,5					MH
	SD 3-1	140		2												
	VT 9	180										19,0	7,8	2,44		
	DP 3-1	220	2													
Average			**2**	**2**						**c_{cu}=14,7**	**j_{cu}=10,5**	**19,0**	**7,8**	**2,44**	**1,40**	**CH**
Soil B2	SD 3-1	140			17,6	8,8									1,40	CH
	DMT 8	100					22 a 26	1800								
	VT 8	100										28,1	11,8	2,39		
	VT 9	180										23,3	7,2	3,26		
	DP 3-1	220	9													
Average			**9**		**17,6**	**8,8**	**22 a 26**	**1800**				**25,7**	**9,5**	**2,82**	**1,40**	**CH**
Soil B3	SD 3-1	140			43,2	21,6									6,70	MH
	DMT 8	100					32 a 44	5450								
	VT 9	180										43,1				
	DP 3-1	220	22													
Average			**22**		**43,2**	**21,6**	**32 a 44**	**5450**				**43,1**				
Soil C2	SD 3-1	140		28												
	SD 3-1	140			51,0	25,5										MH
	SD 3-1	140		28												
	DMT 8	100					60	5450 a 14500								
	DP 3-1	220	46													
Average			**46**	**28**	**51,0**	**25,5**	**60**	**5450 a 14500**								**MH**
Soil D	SD 3-1	140			231,5	115,8										MH
	SD 3-1	140			218,8	109,4										MH
	SD 3-1	140														MH
	DMT 8	100					>100	29000								
	DP 3-1	220	62 a126													
Average			**62 a126**		**225,2**	**112,6**	**>100**	**29000**								**MH**

Table AP I.3a) - Subsoil laboratory and field test results – Prospecting made on Dike No.1 and No.3 of *Lebrija* Pond

Subsoils Dike No.1	< # 200 [%]	Gs	γ_t [kN/m³]	Atterberg Limits			Oedometer					N_{DP}	N_{SPT}
				w_L [%]	w_P [%]	IP [%]	e_0	Cc	Cs	OCR	Cv $10^{-8}m^2/s$		
A	97,0	2,63	17,6	66,5	32,5	34,0	0,862	0,315	0,067	3,0	55,00		
B'	99,2	2,74	15,9	77,4	28,8	48,6	1,422	0,544	0,148	4,0	2,85	11	
B1	96,1	2,63	17,4	61,1	26,8	34,3	1,508	0,748	0,132	1,8	1,90		1 a 5
B2	96,4	2,66	16,2	56,2	24,0	32,2	1,546	0,641	0,125	1,1	4,60		
B3	97,7	2,85	18,4	63,7	34,6	29,2	1,558	0,473	0,121	1,3	3,50	9	3 a 6
C1	90,8		16,1	63,5	18,3	45,2						19	13 a 17
C2	95,7		18,1	60,4	34,8	25,6						57	27
D	96,1		18,4	58,1	34,5	23,6						82 a 136	36 a 60

Subsoils Dike No.3	< # 200 [%]	Gs	γ_t [kN/m³]	Atterberg Limits			Oedometer					N_{DP}	N_{SPT}
				w_L [%]	w_P [%]	IP [%]	e_0	Cc	Cs	OCR	Cv $10^{-8}m^2/s$		
A	62,0	2,55	17,0	88,0	37,1	50,9	1,184	0,360	0,116	6,0	1,80		
B'	98,8	2,56	16,2	96,0	47,1	48,9	1,621	0,558	0,181	3,7	2,70	4	5
B1	98,8		17,0	62,0	32,8	29,2					1,40	2	2
B2	83,4	2,47	16,2	72,2	30,9	41,3	1,521	0,550	0,118	0,6	1,40	9	
B3	99,6	2,60	16,5	107,5	45,7	61,8	1,475	0,573	0,166	2,0			
C1												22	
C2	96,7		17,9	62,2	43,7	18,5						46	28
D	88,6		18,0	83,9	47,7	36,1						62 a 126	

Table AP I.3b) - Subsoil laboratory and field test results – Prospecting made on Dike No.1 and No.3 of *Lebrija* Pond

Subsoils Dike No.1	Piezocone			Ch/Cv	Unconfined Comp. Test		Vane-Test		
	c_u [kN/m²]	OCR	Ch $10^{-8}m^2/s$		qu [kN/m²]	c_u [kN/m²]	$S_{u\,max.}$ [kN/m²]	$S_{u\,res.}$ [kN/m²]	St
A					274,7	137,4	169,3	49,4	3,42
B'	34,3	> 2,0	7,44	2,61	14,7	7,4	30,7	22,5	1,37
B1	17,6	1,0 a 1,7	7,44	3,91	8,4	8,4	18,1	14,5	1,40
B2	27,0	1,0	13,60	2,96			26,4	17,8	1,48
B3	37,3	1,0 a 1,5	13,60	3,89			39,3	29,5	1,33
C1	51,0	1,0 a 2,0			87,4	43,7	52,9	7,7	6,83
C2					143,2	71,6	83,5	37,5	2,22
D	176,6	10,0	10,20		394,4	197,2	207,9	87,1	1,96

Subsoils Dike No.3	Piezocone			Ch/Cv	Unconfined Comp. Test		Vane-Test		
	c_u [kN/m²]	OCR	Ch $10^{-8}m^2/s$		qu [kN/m²]	c_u [kN/m²]	$S_{u\,max.}$ [kN/m²]	$S_{u\,res.}$ [kN/m²]	St
A					202,0	101,0			
B'					101,0	50,5	43,8	16,0	2,75
B1							19,0	7,8	2,44
B2					17,6	8,8	25,7	9,5	2,82
B3					43,2	21,6	43,1		
C1									
C2					51,0	25,5			
D					225,2	112,6			

Table AP I.3c) - Subsoil laboratory and field test results – Prospecting made on Dike No.1 and No.3 of *Lebrija* Pond

Subsoils Dike No.1	Marchetti Dilatometer						Soil classification
	c_u [kN/m²]	E_{DMT} [kN/m²]	j (º)	OCR	K0	Soil Description	USCS
A	160 a 180	> 6800	42 a 46	> 10,0	3,4 a 4,0	Silty sand; Sandy silt	MH
B'	10 a 24	3150 a 6350		3,5 a 6,0	1,1 a 1,4	Silt	CH
B1	16 a 24	1350 a 4550		1,0 a 1,8	0,5 a 0,65	Silty sand; Silty clay; Clay	MH; CH
B2	21 a 38	1150 a 2700		0,7 a 1,0	0,45 a 0,5	Clay; Silty clay; Organic soil	MH-OH; CH
B3	28 a 40	1800 a 6800		0,6 a 1,0	0,38 a 0,5	Clay; Silty clay; Clay and sandy silt	MH
C1	40 a 46	7700 a 11800		0,75 a 1,0	0,45 a 0,5	Silt; Clayed silt	CH
C2							MH
D	215 a 260	26300 a 30850		15,0	2,0	Clayed silt	MH

Subsoils Dike No.3	Marchetti Dilatometer						Soil classification
	c_u [kN/m²]	E_{DMT} [kN/m²]	j (º)	OCR	K0	Soil Description	USCS
A		12700 a 16350	36 a 45		1,6 a 4,5	Silty sand; Sandy silt; Clay	CH
B'	25 a 30	2250 a 4550		2,0 a 3,5	0,8 a 1,1	Silt; Clayed silt; Clay	MH
B1							CH
B2	22 a 26	1800		1,0	0,6	Clay	CH
B3	32 a 44	5450		1,8	0,7	Silty clay	
C1							
C2	60	5450 a 14500		2,1	0,8	Silt	MH
D	>100	29000		4,5	1,2	Clayed silt	MH

Table AP I.3d) - Subsoil laboratory and field test results – Prospecting made on Dike No.1 and No.3 of *Lebrija* Pond

Subsoils Dike No.1	Direct Shear Test				Triaxial			
	c' [kN/m²]	f' (º)	c_{cu} [kN/m²]	f_{cu} (º)	c' [kN/m²]	j' (º)	c_{cu} [kN/m²]	f_{cu} (º)
A								
B'	10,8	12,4						
B1					13,8	23,3	8,8	18,8
B2			12,3	17,9	18,3	18,7		
B3	11,8	16,7						
C1			8,8	26,7			1,96	28,8
C2	c´=41,2	18,1						
D			147,2	24,6				

Subsoils Dike No.3	Direct Shear Test				Triaxial			
	c' [kN/m²]	f' (º)	c_{cu} [kN/m²]	f_{cu} (º)	c' [kN/m²]	j' (º)	c_{cu} [kN/m²]	f_{cu} (º)
A								
B'	11,8	19,3						
B1			4,7	10,5				
B2								
B3								
C1								
C2								
D								

APPENDIX II:

PREFABRICATED COLBONDDRAIN CX1000 TECHNICAL DATA SHEET

COLBONDDRAIN ® CX 1000

Descripción del Producto

Colbonddrain es un compuesto de drenaje consistente en una estructura formada por un núcleo alveolar de poliolefinas recubierto por un geotextil no tejido de polipropileno termosoldado. El filtro y núcleo están soldados para producir un producto totalmente cerrado que previene la introducción de finos en la estructura de drenaje. Este compuesto tiene unos altos índices de descarga a profundidades de más de 50 m.

Colbonddrain es hincado en el terreno y usado normalmente en el drenaje vertical para asentamientos rápidos de terrenos saturados y consolidación de suelos. También es usado para el drenaje horizontal y vertical en bandas en vertederos, grandes superficies, túneles, bóvedas etc.

PROPIEDADES DE COLBONDDRAIN ®	UNIDAD	VALORES DE ENSAYO	NORMAS DE ENSAYO
Compuesto			
Peso	g/ml	80	EN ISO 9864
Peso	g/m^2	800	EN ISO 9864
Ancho	m	0.1	
Espesor	mm	4.0	EN ISO 9863-1
Resistencia a tracción	kN/m	2,5	EN ISO 10319
Deformación a 1.0 kN	%	3,0	EN ISO 10319
(1)Capacidad de flujo en el plano q_w(350, 0.1) 350 kPa i =0.1, f/f	m^2/s	140×10^{-6}	EN ISO 12958(1)
Permeabilidad, VI_{H50}	m/s	0.070	EN ISO 11058
Filtro			
Peso	gr/m^2	100	EN ISO 9864
Espesor	mm	0.6	EN ISO 9863-1
Resistencia a tracción	kN/m	6.2	EN ISO 10319
Deformación en rotura	%	≥50	EN ISO 10319
Resistencia punzonamiento estático	kN	1.0	EN ISO 12236
Ensayo perforación dinámica	mm	45	EN ISO 13433
Porometría	µm	<75	EN ISO 12956

(1) Ensayo entre dos capas de espuma(flexible/flexible)

TERRATEST CIMENTACIONES, S.L.

(Certificate No. 935136)

Colbond Geosynthetics
part of
Colbond bv
P.O. Box 9600
6800 TC Arnhem
the Netherlands
Phone +31 26 366 46 00
Fax +31 26 366 58 12

COLBONDDRAIN ® CX 1000

Dimensiones y pesos*

Tipo	Ancho	Largo	Diámetro	Rollos por paquete	Peso	Camión
CX1000	0.1 m	280 m	1.16 m	10 rollos CX1000/10	245 Kg.	134.400 ml

*valores indicativos

Cubrir como máximo en dos semanas después de su instalación. Previsto para una duración de un mínimo de 5 años en suelos naturales con 4<ph<9 y temperatura <25ºC.

Para evitar el daño por los rayos UV, recomendamos, una vez acopiado y desembalado el material se cubra con lonas o plásticos opacos que no permitan el paso de la luz.

Garantía de Calidad, fabricado de acuerdo a la norma de calidad ISO 9001. Marcado CE 0799-CPD-11

CE

0799-CPD

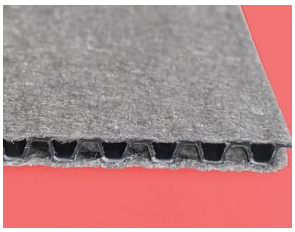

TERRATEST CIMENTACIONES, S.L.

(Certificate No. 935136)

Colbond Geosynthetics
part of
Colbond bv
P.O. Box 9600
6800 TC Arnhem
the Netherlands
Phone +31 26 366 46 00
Fax +31 26 366 58 12

APPENDIX III:

PLAXIS SIMULATION RESULTS OF *LEBRIJA* POND DIKE NO.1

In this Appendix some of the PLAXIS simulation results for Dike No.1, considering the flow, will be shown. This decision is due to the fact that the results for these conditions, give, in general, a better correspondence to the measured values on the monitoring devices, and also because most of the results, without taking the flow into account, are already presented in chapter VII. All the results correspondent to the simulation with the Soft Soil Creep model, secondary compressibility index estimated according to PLAXIS relation ($C_{\alpha PLAXIS}$), and smear given by $K_{hsAx}=0.10K_{h0}$ and $d_s=3d_w$.

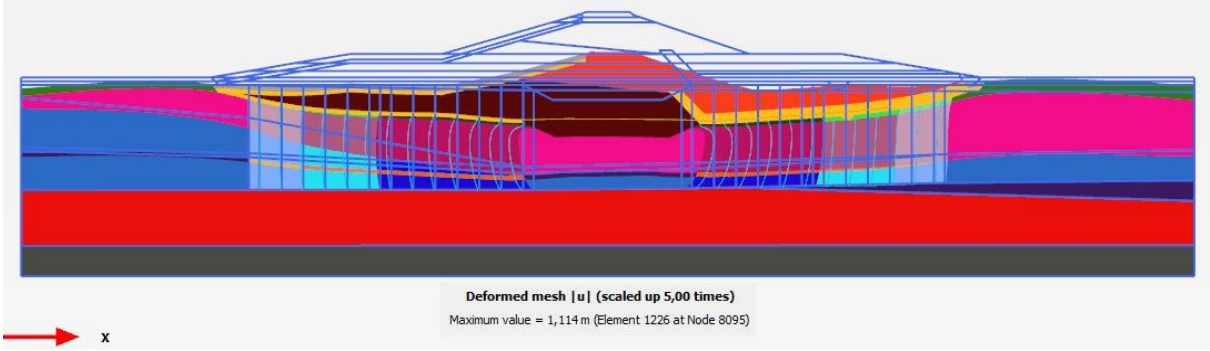

Figure AP III.1 – PK0+240 of Dike No.1: Deformed mesh at the final calculation step (considering flow)

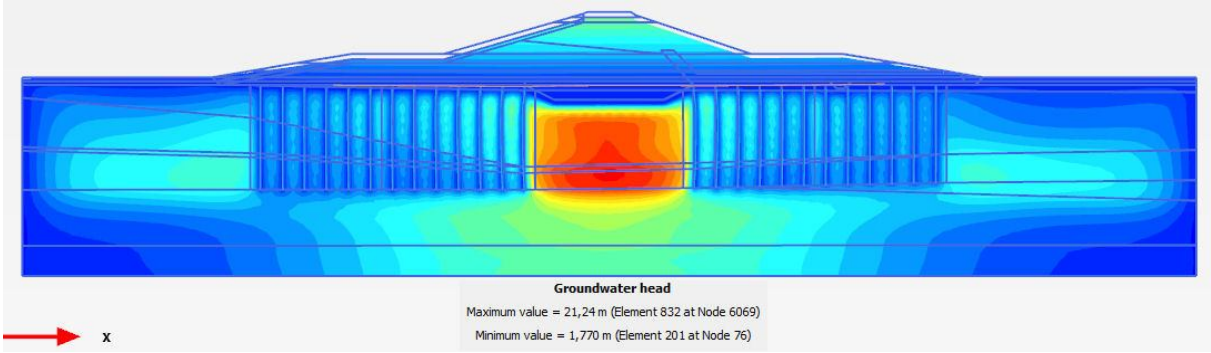

Figure AP III.2 – PK0+240 of Dike No.1: Groundwater head at the conclusion of the dike construction (considering flow)

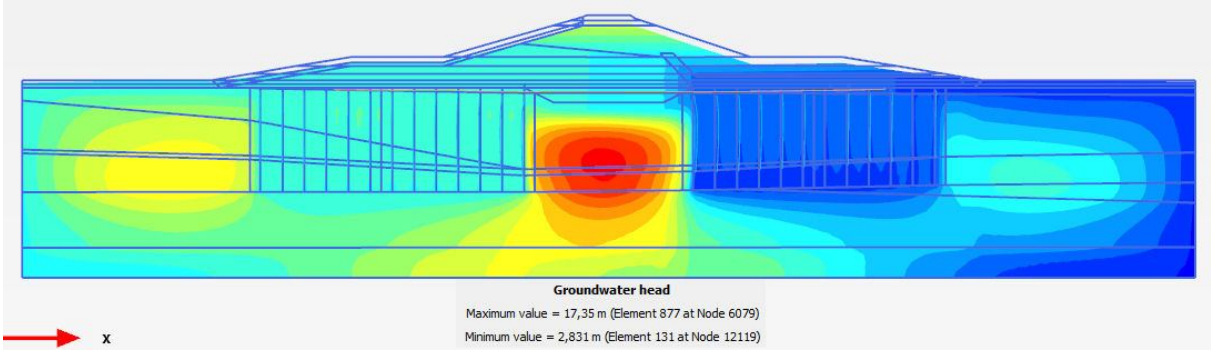

Figure AP III.3 – PK0+240 of Dike No.1: Groundwater head at the final calculation step (considering flow)

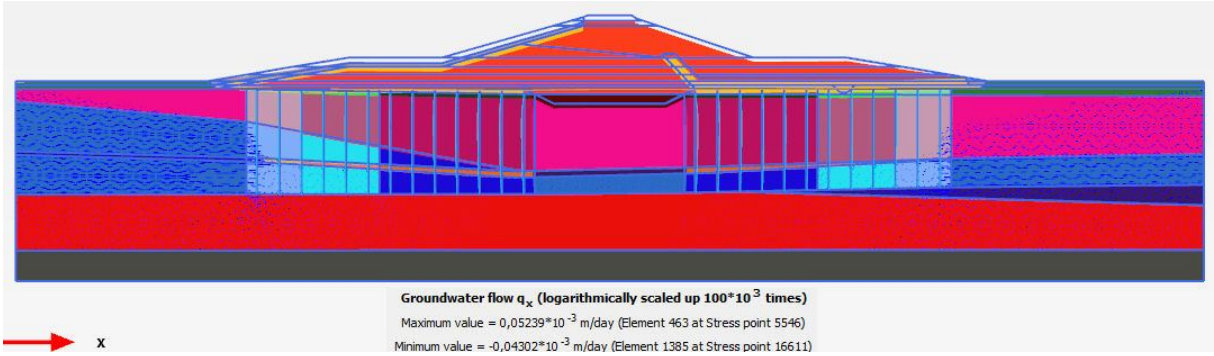

Figure AP III.4 – PK0+240 of Dike No.1: Horizontal groundwater flow at the conclusion of the dike construction

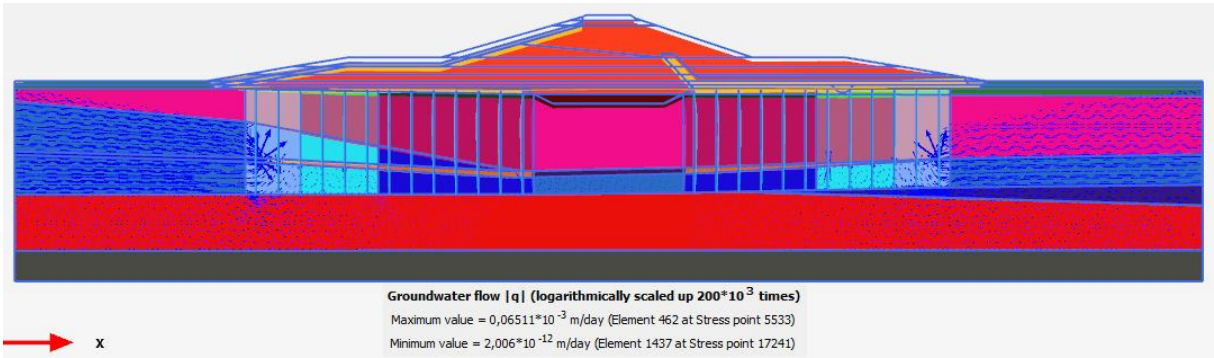

Figure AP III.5 – PK0+240 of Dike No.1: Combined groundwater flow at the conclusion of the dike construction

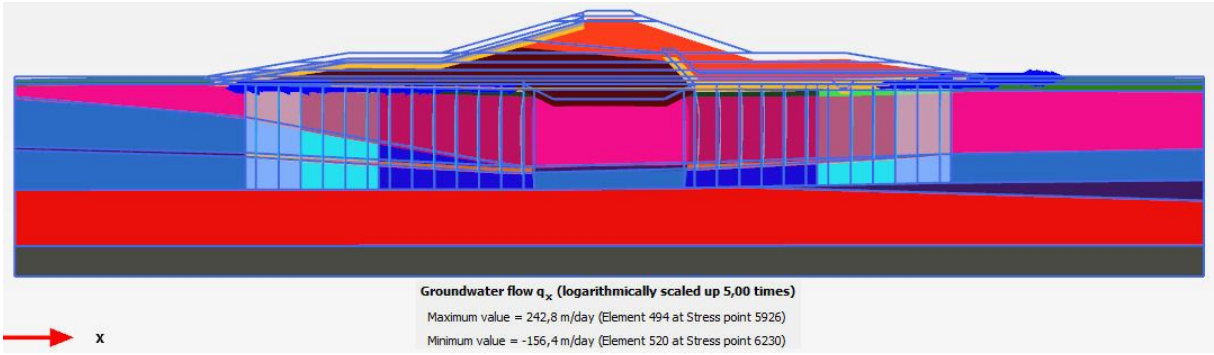

Figure AP III.6 – PK0+240 of Dike No.1: Horizontal groundwater flow at the final calculation step

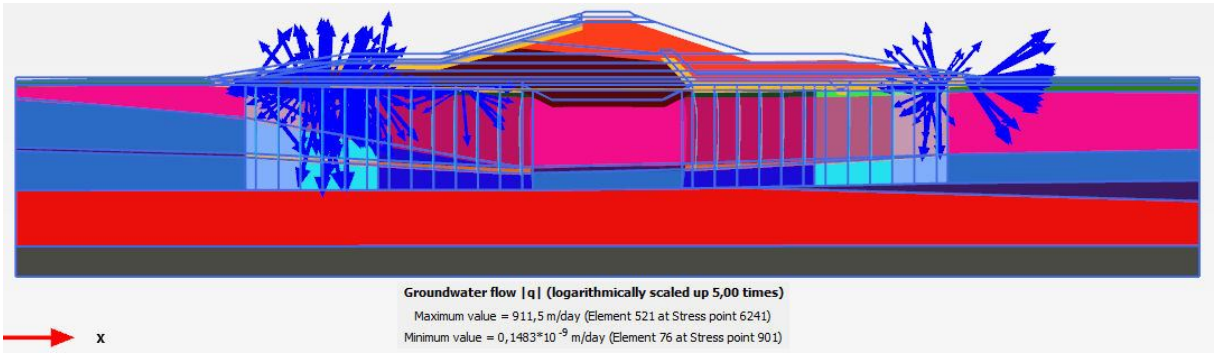

Figure AP III.7 – PK0+240 of Dike No.1: Combined groundwater flow at the final calculation step

APPENDIX IV:

PLAXIS SIMULATION RESULTS OF *LEBRIJA* POND DIKE NO.3

Once again, and following the same procedure as it was indicated in the previous Appendix, only the simulation results taking the flow into account will be presented here. All the results correspondent to the simulation with the Soft Soil Creep model, secondary compressibility index estimated according to PLAXIS relation ($C_{\alpha PLAXIS}$), and smear given by $K_{hsAx}=0.10K_{h0}$ and $d_s=3d_w$.

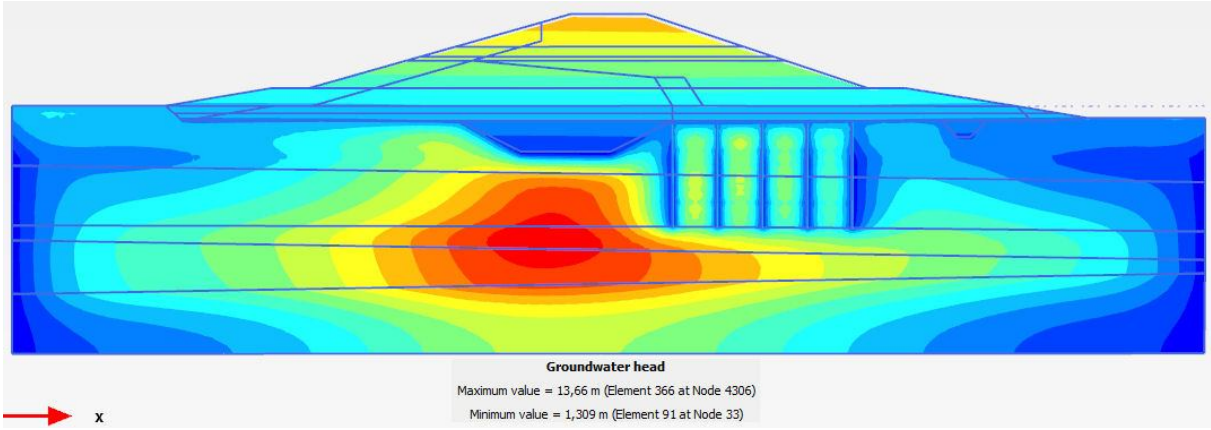

Figure AP IV.1 – PK0+180 of Dike No.3: Groundwater head at the conclusion of the dike construction (considering flow)

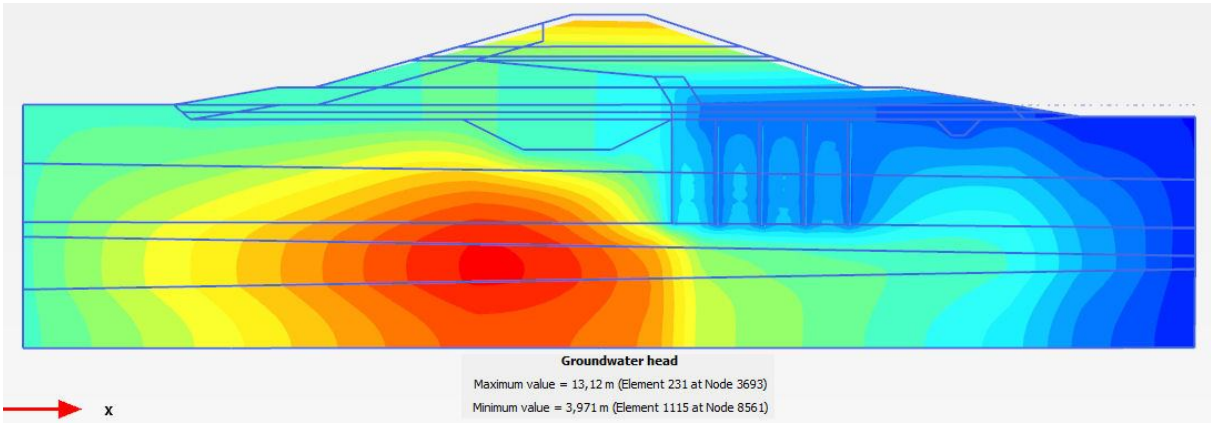

Figure AP IV.2 – PK0+180 of Dike No.3: Groundwater head at the final calculation step (considering flow)

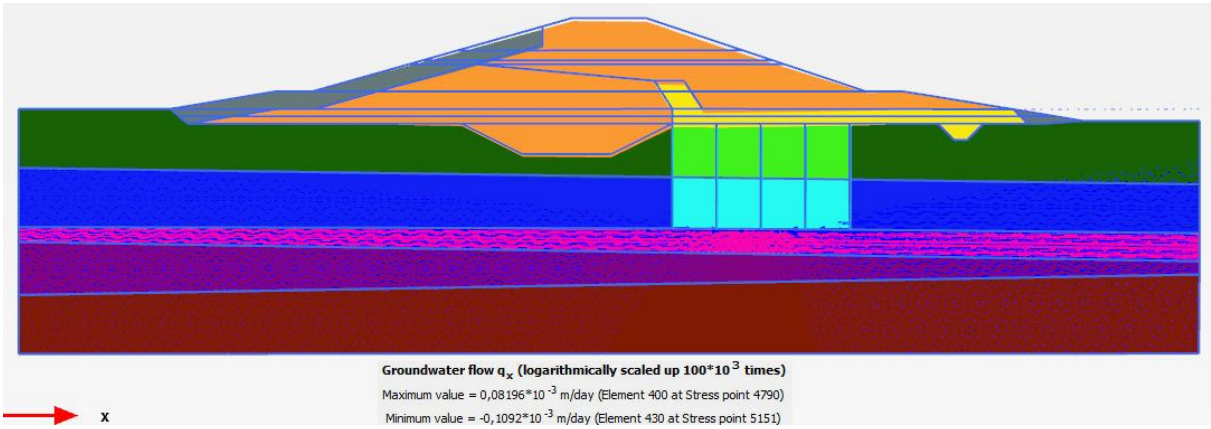

Figure AP IV.3 – PK0+180 of Dike No.3: Horizontal groundwater flow at the conclusion of the dike construction

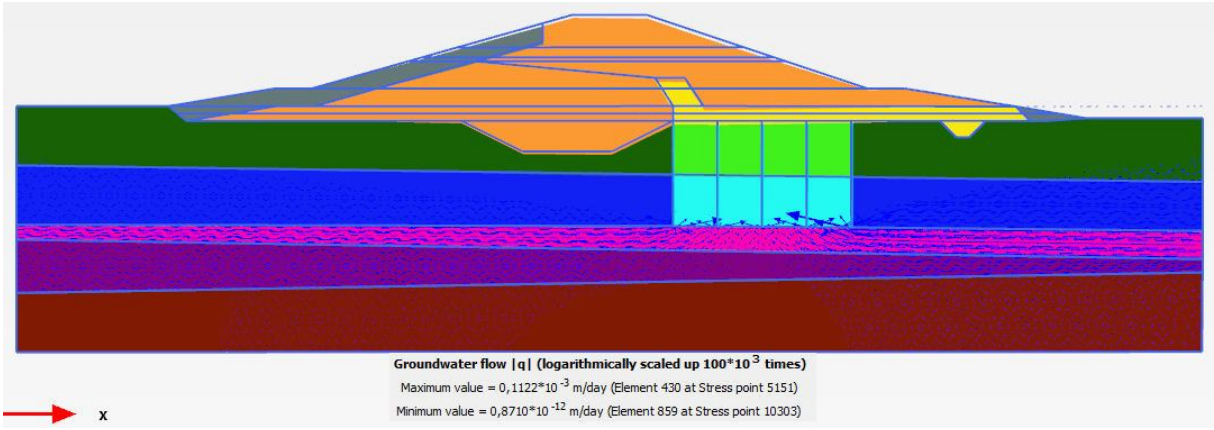

Figure AP IV.4 – PK0+180 of Dike No.3: Combined groundwater flow at the conclusion of the dike construction

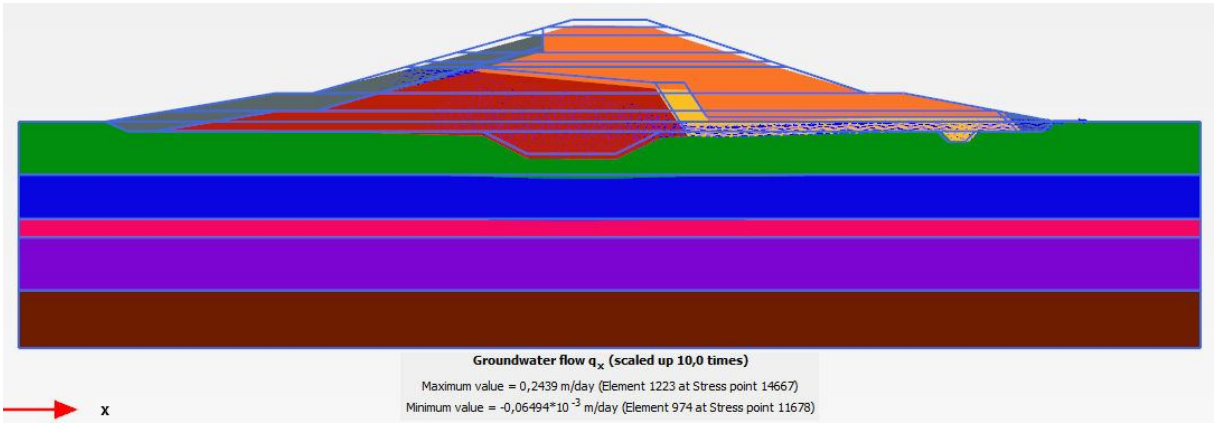

Figure AP IV.5 – PK0+180 of Dike No.3: Horizontal groundwater flow at the final calculation step

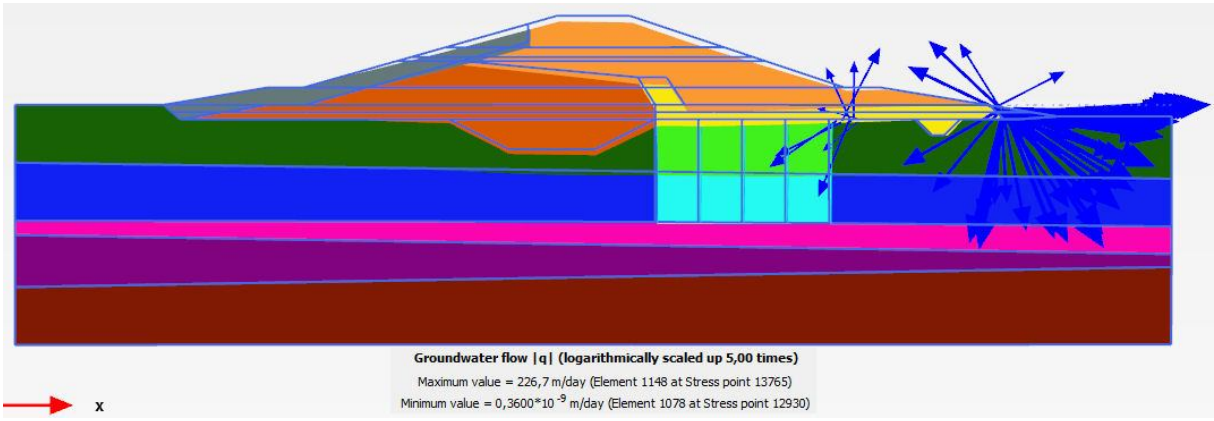

Figure AP IV.6 – PK0+180 of Dike No.3: Combined groundwater flow at the final calculation step

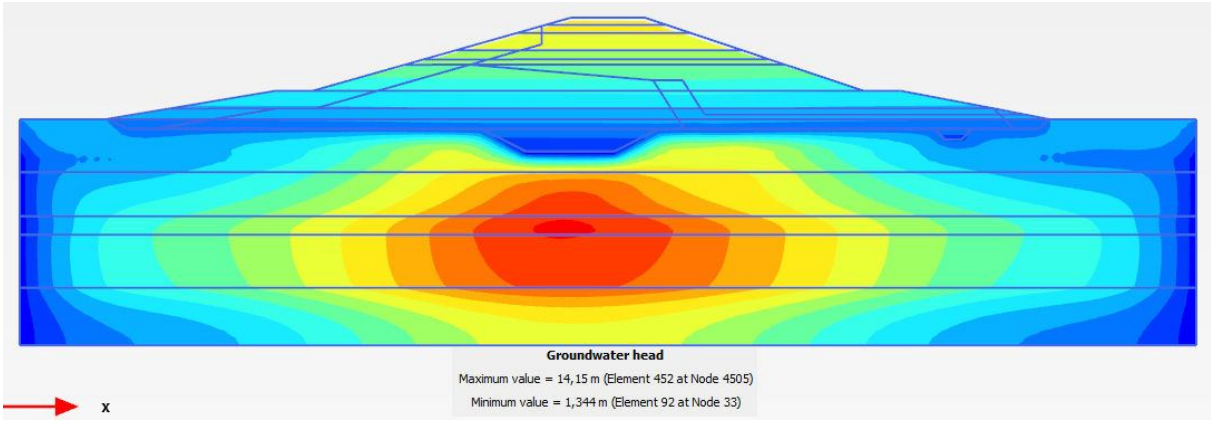

Figure AP IV.7 – PK0+200 of Dike No.3: Groundwater head at the conclusion of the dike construction (considering flow)

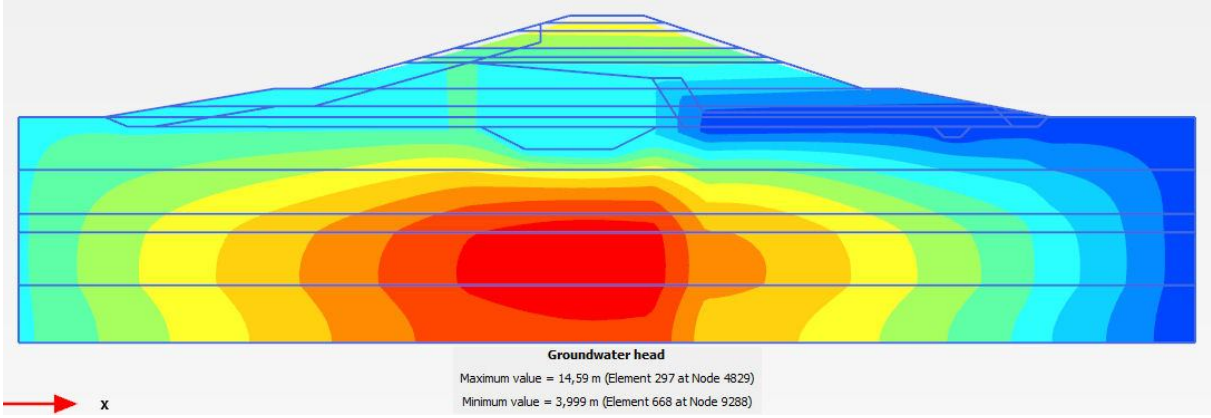

Figure AP IV.8 – PK0+200 of Dike No.3: Groundwater head at the final calculation step (considering flow)

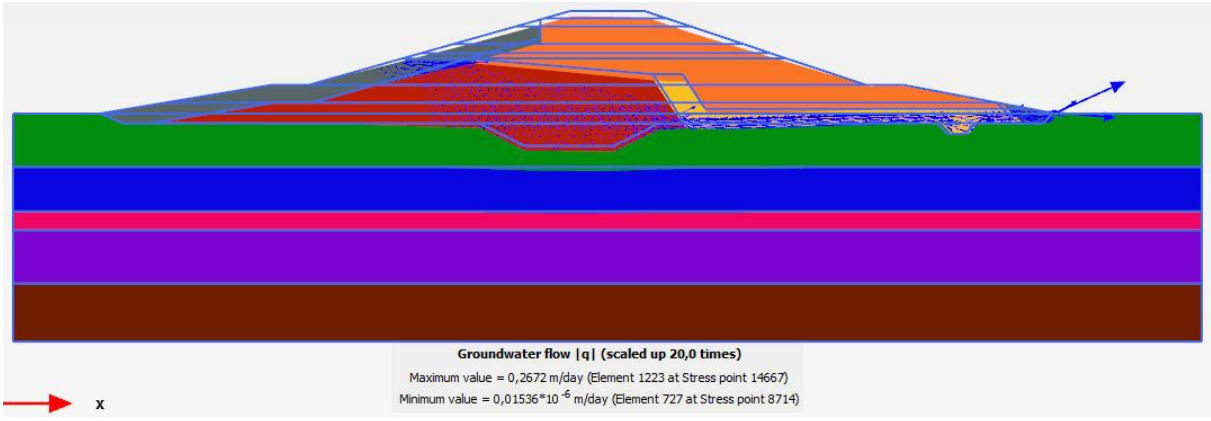

Figure AP IV.9 – PK0+200 of Dike No.3: Combined groundwater flow at the final calculation step